SSC-325

CORRELATION OF THEORETICAL AND MEASURED HYDRODYNAMIC PRESSURES FOR THE SL-7 CONTAINERSHIP AND THE GREAT LAKES BULK CARRIER S.J. CORT

SHIP STRUCTURE COMMITTEE

1984

5/8" TO TRIM

SHIP STRUCTURE COMMITTEE

THE SHIP STRUCTURE COMMITTEE is constituted to prosecute a research program to improve the hull structures of ships and other marine structures by an extension of knowledge pertaining to design, materials and methods of construction.

RADM C. T. Lusk, Jr., USCG (Chairman)
Chief, Office of Merchant Marine Safety
U. S. Coast Guard Headquarters

Mr. T. W. Pross
Associate Administrator for Shipbuilding, Operations & Research
Maritime Administration

Mr. P. M. Palermo
Executive Director
Ship Design & Integration Directorate
Naval Sea Systems Command

Mr. J. B. Gregory
Chief, Technology Assessment & Research Branch
Minerals Management Service

Mr. W. M. Hannan
Vice President
American Bureau of Shipping

Mr. T. W. Allen
Engineering Officer
Military Sealift Command

CDR D. B. Anderson, U. S. Coast Guard (Secretary)

SHIP STRUCTURE SUBCOMMITTEE

The SHIP STRUCTURE SUBCOMMITTEE acts for the Ship Structure Committee on technical matters by providing technical coordination for the determination of goals and objectives of the program, and by evaluating and interpreting the results in terms of structural design, construction and operation.

U. S. COAST GUARD

CAPT A. E. HENN
CAPT J. R. WALLACE
MR. J. S. SPENCER
MR. R. E. WILLIAMS

NAVAL SEA SYSTEMS COMMAND

MR. J. B. O'BRIEN (CHAIRMAN)
CDR R. BUBECK
MR. J. E. GAGORIK
MR. A. H. ENGLE
MR. S. G. ARNTSON (COTR)
MR. G. WOODS (COTR)

MARITIME ADMINISTRATION

MR. F. SEIBOLD
MR. N. O. HAMMER
DR. W. M. MACLEAN
MR. M. W. TOUMA

NATIONAL ACADEMY OF SCIENCES
COMMITTEE ON MARINE STRUCTURES

MR. A. DUDLEY HAFF - LIAISON
MR. R. W. RUMKE - LIAISON

SOCIETY OF NAVAL ARCHITECTS & MARINE ENGINEERS

MR. N. O. HAMMER - LIAISON
MR. F. SELLARS - LIAISON

WELDING RESEARCH COUNCIL

DR. G. W. OYLER - LIAISON

MILITARY SEALIFT COMMAND

MR. D. STEIN
MR. T. W. CHAPMAN
MR. A. ATTERMEYER
MR. A. B. STAVOVY

AMERICAN BUREAU OF SHIPPING

DR. D. LIU
MR. I. L. STERN
MR. B. NADALIN

MINERALS MANAGEMENT SERVICE

MR. R. GIANGERELLI
MR. R. C. E. SMITH

INTERNATIONAL SHIP STRUCTURES CONGRESS

MR. S. G. STIANSEN - LIAISON

AMERICAN IRON & STEEL INSTITUTE

MR. J. J. SCHMIDT - LIAISON

STATE UNIVERSITY OF NY MARITIME COLLEGE

DR. W. R. PORTER - LIAISON

U.S. COAST GUARD ACADEMY

LT J. TUTTLE - LIAISON

U.S. NAVAL ACADEMY

DR. R. BHATTACHARYYA - LIAISON

U.S. MERCHANT MARINE ACADEMY

DR. C. B. KIM - LIAISON

2" TO BIND

S/S 486-332 COV. 2

(1" To Trim)

Committee on Marine Structures
Marine Board
National Academy of Sciences - National Research Council

The Committee on Marine Structures has technical cognizance of the Interagency Ship Structure Committee's research program.

(1 1/8" To Bind)

Mr. A. D. Haff, Chairman, Annapolis, MD
Prof. A. H.-S. Ang, University of Illinois, Champaign, IL
Dr. K. A. Blenkarn, Amoco Production Company, Tulsa, OK
Mrs. Margaret Ochi, Gainesville, PA
Mr. D. Price, National Oceanic and Atmospheric Administration, Rockville, MD
Mr. D. A. Sarno, ARMCO Inc., Middletown, OH
Mr. J. E. Steele, Naval Architect, Quakertown, PA
Mr. R. W. Rumke, Executive Secretary, Committee on Marine Structures

LOADS ADVISORY GROUP

The Loads Advisory Group provided technical guidance and reviewed the report.

Mr. J. E. Steele, Chairman, Quakertown, PA
Prof. R. G. Davis, Texas A&M University, Galveston, TX
Mr. J. P. Fischer, American Steamship Company, Buffalo, NY
Mr. P. W. Marshall, Shell Oil Co., Houston, TX
Prof. Robert Plunkett, Univ. of Minnesota, Minneapolis, MN
Mr. C. B. Walburn, Bethlehem Steel Corp., Sparrows Point, MD

S/S 486-332 Cov 3

(1" To Trim)

SHIP STRUCTURE COMMITTEE PUBLICATIONS

SSC-316 Ship Structure Committee Long-Range Research Plan: Guidelines for Program Development by E.M. MacCutcheon, O.H. Oakley and R.D. Stout, 1983, AD-A140275

SSC-317 Determinsation of Strain Rates in Ship Hull Structures: A Feasibility Study by J. G. Giannotti and K. A. Stambaugh, 1984

SSC-318 Fatigue Characterization of Fabricated Ship Details for Design by W. H. Munse, T. W. Wilbur, M. L. Tellalian, K. Nicoll and K. Wilson, 1983, AD-A140338

SSC-319 Development of A Plan to Obtain In-Service Still-Water Bending Moment Information for Statistical Characterization by J. W. Boylston and K. A. Stambaugh, 1984

SSC-320 A Study of Extreme Waves and Their Effects on Ship Structures by W. H. Buckley, 1983, AD-A140317

SSC-321 Survey of Experience Using Reinforced Concrete in Floating Marine Structures by O.H. Burnside and D.J. Pomerening, 1984

SSC-322 Analysis and Assessment of Major Uncertainties Associated With Ship Hull Ultimate Failure by P. Kaplan, M. Benatar, J. Bentson and T.A. Achtarides, 1984

SSC-323 Updating of Fillet Weld Strength Parameters for Commercial Shipbuilding by R.P. Krumpen, Jr., and C.R. Jordan, 1984

SSC-324 Analytical Techniques for Predicting Grounded Ship Response by J.D. Porricelli and J.H. Boyd, 1984

SSC-325 Correlation of Theoretical and Measured Hydrodynamic Pressures for the SL-7 Containership and the Great Lakes Bulk Carrier S. J. Cort by H.H. Chen, Y.S. Shin & I.S. Aulakh, 1984

SSC-326 Long-Term Corrosion Fatigue of Welded Marine Steels by O.H. Burnside, S.J. Hudak, E. Oelkers, K. Chan, and R.J. Dexter, 1984

None Ship Structure Committee Publications - A Special Bibliography, AD-A140339

(1 1/4" To Bind)

S/S 486-332 Cov 4

TOP

SSC-325 CORRELATION OF HYDRODYNAMIC PRESSURES FOR THE SL-7 CONTAINERSHIP AND THE BULK CARRIER S.J. CORT 1984

CENTER ON SPINE

5/5 486-382 B/5

(1" TO TRIM)

(7/8" TO BIND)

Member Agencies:

United States Coast Guard
Naval Sea Systems Command
Maritime Administration
American Bureau of Shipping
Military Sealift Command
Minerals Management Service

Ship Structure Committee

Address Correspondence to:

Secretary, Ship Structure Committee
U.S. Coast Guard Headquarters, (G-M/TP 13)
Washington, D.C. 20593
(202) 426-2197

An Interagency Advisory Committee
Dedicated to the Improvement of Marine Structures SSC-325

For the past twenty years, the Ship Structure Committee has had many projects directed at gathering and analyzing the loads experienced by ships in an effort towards a more rational design process.

This volume shows the amount of correlation between theoretical calculations, model testing results and full scale data collection of hydrodynamic pressures on the SL-7 class of containership and the M/V STEWART J. CORT, a Great Lakes ore carrier.

CLYDE T. LUSK, Jr.
Rear Admiral, U.S. Coast Guard
Chairman, Ship Structure Committee

486-332 (1) 2 BLANK

Technical Report Documentation Page

1. Report No.	2. Government Accession No.	3. Recipient's Catalog No.
SSC- 325		

4. Title and Subtitle	5. Report Date
Correlation of Theoretical and Measured Hydrodynamic Pressures for the SL-7 Containership and the Great Lakes Bulk Carrier S.J.CORT	1983
	6. Performing Organization Code: RD-1/RD-3
7. Author(s): Hsao H. Chen, Yung S. Shin, & Inderjeet S. Aulakh	8. Performing Organization Report No.: OED-82018
9. Performing Organization Name and Address: American Bureau of Shipping, Ocean Engineering Division, Sixty-five Broadway, New York, N. Y. 10006	10. Work Unit No. (TRAIS)
	11. Contract or Grant No.
12. Sponsoring Agency Name and Address: U. S. Coast Guard, Office of Merchant Marine Safety, Washington, D. C. 20593	13. Type of Report and Period Covered: Final, March 1981--June 1983
	14. Sponsoring Agency Code: (G-MTH-4)

15. Supplementary Notes

The USCG acts as the contracting office for the Ship Structure Committee

16. Abstract

Calculated results from the ABS/SHIPMOTION computer program are compared with pressures obtained by experimental testing on scaled-down models of the SL-7 class containership and the S. J. CORT and with full-scale pressure measurements from the Great Lakes self-unloader, S. J. CORT. The degree of closeness in the correlations is different between the model-test and full-scale data. The correlation is also different between the SL-7 containership and the S.J.CORT. In general, the theoretical prediction has the same trend as measured values either from the model test or full-scale trial, with the model-test results showing a better correlation.

It is not the intention of this report to either identify factors in the theory which are responsible for the discrepancies in correlation, nor to suggest what direction further research must take.

17. Key Words	18. Distribution Statement
hydrodynamic pressure SHIPMOTION model tests full-scale pressure measurements	Document is available to the -U.S. Public through the National Technical Information Service, Springfield, VA 22161

19. Security Classif. (of this report)	20. Security Classif. (of this page)	21. No. of Pages	22. Price
UNCLASSIFIED	UNCLASSIFIED	300	

Form DOT F 1700.7 (8-72) Reproduction of completed page authorized

486-332 (3) 4 BLANK

METRIC CONVERSION FACTORS

Approximate Conversions to Metric Measures

Symbol	When You Know	Multiply by	To Find	Symbol
	LENGTH			
in	inches	*2.5	centimeters	cm
ft	feet	30	centimeters	cm
yd	yards	0.9	meters	m
mi	miles	1.6	kilometers	km
	AREA			
in^2	square inches	6.5	square centimeters	cm^2
ft^2	square feet	0.09	square meters	m^2
yd^2	square yards	0.8	square meters	m^2
mi^2	square miles	2.6	square kilometers	km^2
	acres	0.4	hectares	ha
	MASS (weight)			
oz	ounces	28	grams	g
lb	pounds	0.45	kilograms	kg
	short tons (2000 lb)	0.9	tonnes	t
	VOLUME			
tsp	teaspoons	5	milliliters	ml
Tbsp	tablespoons	15	milliliters	ml
fl oz	fluid ounces	30	milliliters	ml
c	cups	0.24	liters	l
pt	pints	0.47	liters	l
qt	quarts	0.95	liters	l
gal	gallons	3.8	liters	l
ft^3	cubic feet	0.03	cubic meters	m^3
yd^3	cubic yards	0.76	cubic meters	m^3
	TEMPERATURE (exact)			
°F	Fahrenheit temperature	5/9 (after subtracting 32)	Celsius temperature	°C

*1 in = 2.54 (exactly). For other exact conversions and more detailed tables, see NBS Misc. Publ. 286, Units of Weights and Measures, Price $2.25, SD Catalog No. C13.10:286.

Approximate Conversions from Metric Measures

Symbol	When You Know	Multiply by	To Find	Symbol
	LENGTH			
mm	millimeters	0.04	inches	in
cm	centimeters	0.4	inches	in
m	meters	3.3	feet	ft
m	meters	1.1	yards	yd
km	kilometers	0.6	miles	mi
	AREA			
cm^2	square centimeters	0.16	square inches	in^2
m^2	square meters	1.2	square yards	yd^2
km^2	square kilometers	0.4	square miles	mi^2
ha	hectares (10,000 m^2)	2.5	acres	
	MASS (weight)			
g	grams	0.035	ounces	oz
kg	kilograms	2.2	pounds	lb
t	tonnes (1000 kg)	1.1	short tons	
	VOLUME			
ml	milliliters	0.03	fluid ounces	fl oz
l	liters	2.1	pints	pt
l	liters	1.06	quarts	qt
l	liters	0.26	gallons	gal
m^3	cubic meters	35	cubic feet	ft^3
m^3	cubic meters	1.3	cubic yards	yd^3
	TEMPERATURE (exact)			
°C	Celsius temperature	9/5 (then add 32)	Fahrenheit temperature	°F

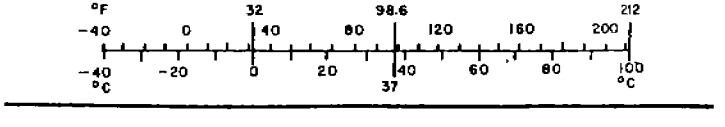

TABLE OF CONTENTS

1. INTRODUCTION

The accurate estimation of load acting on a ship structure is an important aspect of ship design. With current trends in ships now oriented towards longer and wider ships in the case of oil tankers and bulk carriers, and to longer ships for the container and LNG trade, local strength is an important structural consideration that must be adequately accounted for.

To evaluate and refine theoretical methods for calculating local loads on a ship hull, a study was initiated to compare calculated hydrodynamic pressures with pressures obtained by experimental testing on a scaled-down model of a ship, and with full - scale pressure measurements. Two vessels were chosen for this purpose - the SL-7 class containership, and the Great Lakes self-unloader STEWART J. CORT. These vessels represent nearly opposite combinations of hull form characteristics and speed.

The experimental pressure measurements were obtained on models of the two ships at the University of Michigan Towing Tank. Full-scale measurements were conducted on the S. J. CORT by the DWT Naval Ship Research and Development Center (DWTNSRDC). Both the model test and full-scale measurements of hydrodynamic pressure were sponsored by the Ship Structure Committee (SSC). Theoretical pressure calculation and comparison with measured pressure data were carried out by the American Bureau of Shipping (ABS).

This report presents the comparison study described above. Comparison plots are shown and conclusions are drawn regarding the quality of correlation between measured (model test and full-scale)

and theoretically calculated pressure. However, it is not the intention of this report to either identify factors in the theory which are responsible for the discrepancies in correlation, nor to suggest what direction further research must take.

In the subsequent chapters, model test and full-scale measured results are first discussed followed by a summary of mathematical formulations employed in the computer program ABS/SHIPMOTION for hydrodynamic pressure calculation. It should be noted that this program is one of several available in the industry to calculate the hydrodynamic pressures. Theories used in different programs are not identical, due to different assumptions embodied in their formulations. Therefore, the correlation of measured data with calculated results from the program ABS/SHIPMOTION provides only a qualitative indication as to the adequacy of the generally available theories for predicting the hydrodynamic pressures.

II. SUMMARY OF MODEL TEST AND FULL-SCALE MEASUREMENT RESULTS

II.1 Model Tests

Experimental measurements of hydrodynamic pressure acting on the model hulls of the SL-7 class containership and the S. J. CORT was conducted at the University of Michigan Towing Tank in Ann Arbor, Michigan.

Model testing procedures are described in detail in Reference [1]. The hydrodynamic pressure, which is comprised of pressure due to the incident and diffracted waves and that due to the ship motions, is measured by running the model in waves, free to heave and pitch. The pressure component due to the incident and diffracted waves is measured by restraining the model in both heave and pitch while operating in waves. Such a test is referred to as the "diffraction" or "scattering" experiment. The pressure component arising from ship motions is measured by forcibly oscillating the model in either heave or pitch while running at a steady forward speed in the absence of incident waves. This test is usually referred to as a "forced oscillation", or a "shaker test". The summation of pressure components due to the incident and diffracted waves and that due to ship motions, taking the phase angles into account, should equal the hydrodynamic pressure.

The SL-7 model was tested in the full load condition in head seas at Froude numbers 0.15, 0.23 and 0.32 over a range of ship length/wave length ratios from 0.65 to 1.65. Particulars of the ship and model for the full load condition are given in Table II-1(a), and pressure tap locations are given in Table II-1(b) and Figure II-1. For the SL-7, in addition to the hydrodynamic pressure, the components of the dynamic

pressures due to ship motions and wave excitation (incident and diffracted waves) were also measured at Froude number 0.23.

The S.J. CORT model was tested in the full load and in the ballast condition at Froude numbers 0.1 and 0.132 in head seas. Particulars of the ship and model for both loading conditions are given in Table II-1(c). The model was tested over a range of ship length/wave ratios from 1.00 to 6.54. The pressure tap locations are given in Table II-1(d) and in Figure II-2. In testing the S.J. CORT model, only the hydrodynamic pressure was measured.

The model tests results of motions and pressures are presented graphically in Reference 1 in non-dimensional form. The non-dimensional responses in Reference 1, as well as in the present report, are defined as follows:

(i) Heaving motion:

$$\text{Non-dimensional heave} = \frac{\text{Heave amplitude}}{\text{Wave amplitude}}$$

(ii) Pitching motion:

$$\text{Non-dimensional pitch} = \frac{\text{(amplitude of pitch in radians) x (LBP/2)}}{\text{Wave amplitude}}$$

(iii) Non-dimensional pressure for model in waves, free to heave and pitch:

$$\text{Non-dimensional total pressure} = \frac{\text{Pressure amplitude}}{\text{(water density) x (gravitation constant) x (incident wave amplitude)}}$$

(iv) Pressure for the model fixed in incident waves: The non-dimensional pressure is the same as that described in (iii).

(v) Pressure for the model in forced heave:

$$\text{Non-dimensional pressure due to heave} = \frac{\text{Pressure amplitude}}{\text{(water density) x (gravitation constant) x (heave amplitude)}}$$

(vi) Pressure for model in forced pitch:

$$\text{Non-dimensional pressure due to pitch} = \frac{\text{Pressure amplitude}}{\text{(water density) x (gravitation constant) x (vertical displacement)}}$$

(vii) Froude Number:

$$F_n = \frac{\text{Ship speed}}{\sqrt{\text{LBP x gravitation constant}}}$$

The vertical displacement in (vi) is the vertical amplitude of motion of the particular pressure tap in question when the model is forced to pitch. It is equal to the pitch rotation in radians multiplied by the longitudinal distance from the pressure tap to midship in the forced pitch test. Also, in the above non-dimensional response expressions heave is defined as the vertical displacement of the model measured at midship, and pitch as the angular rotation about an axis located at the intersection of the water plane and midship section.

II.2 Full-Scale Measurement

In addition to model testing at the University of Michigan, full-scale pressure measurements were conducted on the S. J. CORT by the DWT Naval Ship Research and Development Center. Data were collected from mid October through mid December 1979 as the CORT made round trip transits between Burns Harbor, Indiana and Burlington Ore Docks-Superior, Wisconsin, via Lakes Michigan and Superior. A description of the measurement procedure is presented in Reference 2

Reduced data, in the form of pressure power spectra and wave spectra, were supplied to ABS by DTNSRDC. These data were used to calculate the transfer functions of the hydrodynamic pressure. The transfer function of pressure is simply the pressure power spectra divided by the wave spectra and then square rooted.

The pressure correlation was performed for eight conditions. Each condition represents a different combination of loading condition, ship speed, ship-wave angle and wave height. The conditions under consideration are given in Table II-2(a). The pressure tap locations are given in Table II-2(b).

III. SUMMARY OF MATHEMATICAL FORMULATION FOR HYDRODYNAMIC PRESSURE CALCULATION

Theoretical calculation of pressure transfer function has been performed by using the program ABS/SHIPMOTION. The theory employed in this program is summarized subsequently.

III.1 General Formula of Dynamic Pressure Calculation

The dynamic pressure acting on ship's surface below the mean water line is approximated by the equation as follows (see Reference [ ] :

$$p = \left[P_T - \frac{V}{i\omega_e} \frac{\partial P_T}{\partial \bar{x}}\right] \exp(i\omega_e t) + \rho g z^* \exp(i\omega_e t) \qquad \text{(III-1)}$$

$$z^* = \tilde{z} + \bar{y}\phi - \bar{x}\theta \qquad \text{(III-2)}$$

where

P_T = two-dimensional hydrodynamic pressure,

$\tilde{z}$ = vertical displacement of the vessel,

$\bar{x}, \bar{y}$ = coordinates of the point under consideration. See Figure III-1.

ρ = density of water,

g = gravitational acceleration,

V = ship speed,

ω_e = frequency of encounter,

t = time,

i = imaginary unit.

The hydrodynamic pressure, P_T in equation (III-1), on the underwater surface of a ship consists of the following additive terms:

P_1: pressure due to the ship motions in still water;

P_2: pressure due to reflection of waves from the restrained body;

P_3: pressure due to incident waves.

Furthermore, P_1 may be decomposed into three components:

$$P_1 = P_V + P_L + P_R \qquad \text{(III-3)}$$

where

P_V = pressure due to vertical motion;

P_L = pressure due to lateral motion;

P_R = pressure due to rolling motion.

The term P_2 is associated with the action of waves on a restrained body and, therefore, has the components due to the orbital velocity and acceleration of wave particles. Thus, P_2 and P_3 may be combined into one term, P_W, the pressure due to wave actions.

Therefore, the hydrodynamic pressure acting on a point $(\bar{y}, \bar{z})$ of a ship section at a distance $\bar{x}$ from the center of gravity can be expressed as:

$$P_T = P_V + P_L + P_R + P_W$$

where

$$\begin{aligned}
P_V &= (\rho g/\omega_e^2) P_{aV} \ddot{z} + (\rho g/\omega_e) P_{dV} \dot{z} \\
P_L &= (\rho g/\omega_e^2) P_{aL} \ddot{y} + (\rho g/\omega_e) P_{dL} \dot{y} \\
P_R &= (\rho g/\omega_e^2) P_{aR} \ddot{\phi} + (\rho g/\omega_e) P_{dR} \dot{\phi} \\
P_W &= (\rho g/\omega_e^2)(P_{aV} \ddot{\zeta}_v + P_{aL} \ddot{\zeta}_L) \\
&\quad + (\rho g/\omega_e)(P_{dV} \dot{\zeta}_v + P_{dL} \dot{\zeta}_L) + \rho g \zeta
\end{aligned} \qquad \text{(III-4)}$$

$\left\{\begin{matrix} P_{aV} \\ P_{aL} \\ P_{aR} \end{matrix}\right\}$ = two-dimensional pressure component in phase with the $\left\{\begin{matrix} \text{vertical} \\ \text{lateral} \\ \text{rolling} \end{matrix}\right\}$ acceleration due to the added mass effect

$\left\{\begin{matrix} P_{dV} \\ P_{dL} \\ P_{dR} \end{matrix}\right\}$ = two-dimensional pressure component in phase with the $\left\{\begin{matrix} \text{vertical} \\ \text{lateral} \\ \text{rolling} \end{matrix}\right\}$ velocity due to the damping effect.

The two-dimensional pressure components in phase with accelerations and velocities are determined by solving a two-dimensional boundary value problem of a cylinder of a constant

ship-shaped section heaving, swaying and rolling in the free surface of the fluid.

In equation (III-4), $\dot{z}$, $\ddot{z}$, $\dot{y}$, $\ddot{y}$, $\dot{\phi}$ and $\ddot{\phi}$ are respectively the velocities and accelerations of vertical, lateral and rolling motions. For an arbitrary section at a distance $\bar{x}$ from the center of gravity of the ship, C.G., the displacement, velocity and acceleration in complex notation of the vertical motion are

$$\begin{aligned} z &= \tilde{z} - \bar{x}\theta, \\ \dot{z} &= \dot{\tilde{z}} + V\theta - \bar{x}\dot{\theta} = i\omega_e(\tilde{z} - \bar{x}\theta) + V\theta, \\ \ddot{z} &= \ddot{\tilde{z}} + 2V\dot{\theta} - \bar{x}\ddot{\theta} = -\omega_e^2(\tilde{z} - \bar{x}\theta) - 2i\omega_e V\theta. \end{aligned} \tag{III-5}$$

for the lateral motion,

$$\begin{aligned} y &= \tilde{y} + \bar{x}\psi - \overline{OG}\,\phi, \\ \dot{y} &= \dot{\tilde{y}} - V\psi + \bar{x}\dot{\psi} - \overline{OG}\dot{\phi} = i\omega_e(\tilde{y} + \bar{x}\psi - \overline{OG}\phi) - V\psi, \\ \ddot{y} &= \ddot{\tilde{y}} - 2V\dot{\psi} + \bar{x}\ddot{\psi} - \overline{OG}\ddot{\phi} = -\omega_e^2(\tilde{y} + \bar{x}\psi - \overline{OG}\phi) \\ &\quad + 2i\omega_e V\psi. \end{aligned} \tag{III-6}$$

and for the rolling motion,

$$\begin{aligned} \dot{\phi} &= i\omega_e\phi_o, \\ \ddot{\phi} &= -\omega_e^2\phi_o. \end{aligned} \tag{III-7}$$

The coordinate systems $\tilde{x}\tilde{y}\tilde{z}$ and $\bar{x}\bar{y}\bar{z}$, as well as the rotational motions, θ, ψ and ϕ of a ship, are defined in Figures III-1(a) and III-1(b). Furthermore,

$$\begin{aligned}
\tilde{z} &= z_o \sin(\omega_e t + \varepsilon_z) \quad , \text{ heave} \\
\theta &= \theta_o \sin(\omega_e t + \varepsilon_\theta) \quad , \text{ pitch} \\
\tilde{y} &= y_o \sin(\omega_e t + \varepsilon_y) \quad , \text{ sway} \\
\psi &= \psi_o \sin(\omega_e t + \varepsilon_\psi) \quad , \text{ yaw} \\
\phi &= \phi_o \sin(\omega_e t + \varepsilon_\phi) \quad , \text{ roll}
\end{aligned} \tag{III-8}$$

where z_o, θ_o,.... are the amplitudes of the respective motions;

ε_z, ε_θ,.... are the phase angles of the respective motions.

The wave elevation, ζ, vertical and lateral orbital accelerations and velocities of a wave, $\ddot{\zeta}_v$, $\ddot{\zeta}_L$, $\dot{\zeta}_v$ and $\dot{\zeta}_L$, involved in the pressure due to wave action, P_W, can be determined by considering a travelling simple wave in deep water. The surface profile of such a wave is

$$\zeta = \zeta_\omega \sin(-kx \cos\beta + ky \sin\beta + \omega_e t) \tag{III-9}$$

where

ζ_ω = wave amplitude,

k = wave number

$= 2\pi/\lambda = \omega^2/g = g/c^2$,

β = heading angle,

λ = wave length,

g = gravitational acceleration,

c = wave celerity,

ω = wave circular frequency,

ω_e = wave encounter frequency

$= \omega - kV \cos \beta$,

V = ship speed.

The wave velocity potential for the simple deep-water wave given in equation (III-9) is

$$\phi_\omega = -\zeta_\omega \frac{g}{\omega} e^{-k(z - \overline{OG})} \cos(-kx \cos \beta + ky \sin \beta + \omega_e t) \qquad \text{(III-10)}$$

where $\overline{OG}$ is the vertical distance of ship's C.G. from static waterline. $\overline{OG}$ should be negative for L.G. below waterline. The wave elevation for the subsurface of the deep water wave is

$$\zeta = \zeta_\omega e^{-k(z - \overline{OG})} \sin(-kx \cos \beta + ky \sin \beta + \omega_e t) \qquad \text{(III-11)}$$

The vertical orbital velocity and acceleration of the wave are

$$\dot{\zeta}_v = \omega\zeta_\omega e^{-k(z - \overline{OG})} \cos(-kx \cos \beta + ky \sin \beta + \omega_e t) = i\omega\zeta, \qquad \text{(III-12)}$$

$$\ddot{\zeta}_v = -\omega^2\zeta_\omega e^{-k(z - \overline{OG})} \sin(-kx \cos \beta + ky \sin \beta + \omega_e t) = -\omega^2\zeta,$$

and the lateral orbital velocity and acceleration of the wave are

$$\dot{\zeta} = -\omega\zeta_\omega \sin\beta\, e^{-k(z - \overline{OG})} \sin(-kx\cos\beta + ky\sin\beta + \omega_e t)$$

$$= \omega \sin(\beta)\zeta, \qquad \text{(III-13)}$$

$$\ddot{\zeta}_L = -\omega^2\zeta_\omega \sin\beta\, e^{-k(z - \overline{OG})} \cos(-kx\cos\beta + ky\sin\beta + \omega_e t)$$

$$= i\omega^2 \sin(\beta)\zeta.$$

III.2 Two-Dimensional Pressure Components

The two-dimensional pressure components, P_{aV}, P_{dV}, P_{aL}, P_{dL}, P_{aR} and P_{dR}, to be used for computing P_V, P_L P_R and P_W by equation (III-4), can be determined using two different methods: conformal mapping technique and Frank's close-fit method.

The conformal mapping technique involves the representations of a ship's section by a Fourier-like series whose coefficients are called mapping coefficients. Once the mapping coefficients are known, it is a relatively straight-forward procedure to obtain the hydrodynamic quantities; therefore, the basic problem is the mapping of the ship's section. Most normal ship sections can be adequately described by mapping coefficients, but certain sections, such as completely submerged sections and bulbous bows, cannot be mapped. For such sections where the mapping technique cannot be applied, the close-fit method is used.

In the close-fit technique the ship's sectional contour is represented by a number of straight line segments. The two-dimensional hydrodynamic pressure is then determined using a method of distributing source singularities over the submerged portion of the hull. Most sections can be handled using this analysis, but a drawback does exist. It can be shown that a set of discrete "irregular" frequencies fails to give a solution. As the beam/draft ratio becomes large, these irregular frequencies approach the operating frequencies and seriously affect the accuracy of the results.

III.2.a Conformal Mapping Technique

A more detailed description of conformal mapping in the two-dimensional pressure calculation is given by Reference 4. The formulations of pressure components are summarized as followed:

$$
\begin{aligned}
P_{aV} &= \delta_e (M_3 B_3 + N_3 A_3)/(A_3^2 + B_3^2) \\
P_{dv} &= \delta_e (M_3 A_3 - N_3 B_3)/(A_3^2 + B_3^2) \\
P_{aL} &= \delta_e (\tfrac{d}{b}) (M_2 B_2 + N_2 A_2)/(A_2^2 + B_2^2) \\
P_{dL} &= \delta_e (\tfrac{d}{b}) (M_2 A_2 - N_2 B_2)/(A_2^2 + B_2^2) \\
P_{aR} &= \delta_e b(\tfrac{d^2}{b^2} - 1) (M_4 B_4 + N_4 A_4)/(A_4^2 + B_4^2) \\
P_{dR} &= \delta_e b(\tfrac{d^2}{b^2} - 1) (M_4 A_4 - N_4 B_4)/(A_4^2 + B_4^2)
\end{aligned}
\qquad \text{(III-14)}
$$

where

δ_e = $\omega_e^2 b/g$, non-dimensional frequency of encounter

d = draft of the section

b = half-beam of the section

M_i = sine, N_i = cosine } component of an oscillating velocity potential at a point $(\bar{y}, \bar{z})$ on the section contour.

A_i = in phase with motion, B_i = 90° out of phase from motion } the conjugate stream function value

M_i, N_i, A_i and B_i are functions of coefficients of the conformal mapping which maps the cross-section of the ship under consideration onto a circle.

Subscripts 2, 3 and 4 are for sway, heave and roll, respectively. For a given ship section with a draft d and half-beam b, the mapping function can be written as follows:

$$y = y(\theta) = a_o \sin\theta - \sum_{m=1}^{N} a_{2m-1} \sin(2m-1)\theta$$

$$z = z(\theta) = a_o \cos\theta + \sum_{m=1}^{N} a_{2m-1} \cos(2m-1)\theta \qquad \text{(III-15)}$$

where a_o, a_1, $\cdots a_{2N-1}$ are the mapping coefficients; θ is the angle in the plane of the circle, with 0° corresponding to the centerline bottom of the ship section and $\pi/2$ located at the waterline on the section side. The coordinate system oyz is such that the origin o is on the waterline at centerline of the section, oy lies on the waterline, and oz on the centerline positive downward. As can be seen from equation (III-15), since the unknowns a_o, a_1, ..., a_{2N-1} and θ can not be solved analytically for $N > 2$ an iterative approach must be used.

With the mapping function given in equation (III-15), the following expressions for heaving motion can be derived:

$$A_3 = \psi_{cH}\left(\frac{\pi}{2}\right) + \sum_{m=1}^{\infty} P_{2mH}\ \psi_{2mH}\left(\frac{\pi}{2}\right)$$

$$B_3 = \psi_{sH}\left(\frac{\pi}{2}\right) + \sum_{m=1}^{\infty} q_{2mH}\ \psi_{2mH}\left(\frac{\pi}{2}\right)$$

(III-16)

$$M_3 = \phi_{sH}(\theta) + \sum_{m=1}^{\infty} q_{2mH}\ \phi_{2mH}(\theta)$$

$$N_3 = \phi_{cH}(\theta) + \sum_{m=1}^{\infty} P_{2mH}\ \phi_{2mH}(\theta)$$

The cosine component of the multiple potential P_{2mH} and sine component q_{2mH} are found by a least square fit involving the solution of the following matrix equation:

$$P_{2mH} = [X]^{-1} Y1$$

$$q_{2mH} = [X]^{-1} Y2 \qquad \text{(III-17)}$$

where

$$X = X_{ij} = \sum_{\theta} D_{iH}(\theta)\, D_{jH}(\theta)$$

$$Y1 = Y1_j = \sum_{\theta} D_{jH}(\theta)\, [\psi_{cH}(\theta) - (\tfrac{x}{b})\, \psi_{cH}(\tfrac{\pi}{2})]$$

$$Y2 = Y2_j = \sum_{\theta} D_{jH}(\theta)\, [\psi_{sH}(\theta) - (\tfrac{x}{b})\, \psi_{sH}(\tfrac{\pi}{2})]$$

$$D_{iH}(\theta) = (\tfrac{x}{b})\psi_{2iH}\,(\tfrac{\pi}{2}) - \psi_{2iH}(\theta) \qquad \text{(III-18)}$$

The remaining terms in equation (III-16) are as follows:

Stream Functions:

$$\psi_{cH}(\theta) = \pi e^{-kz} \sin(ky) \qquad \text{(III-19)}$$

$$\psi_{sH}(\theta) = \pi e^{kz} \cos(ky) + \int_o^{\infty} e^{-\beta y} \left[\frac{k \cos(\beta z) + \beta \sin(\beta z)}{\beta^2 + k^2}\right] d\beta$$

$$\psi_{2mH}(\theta) = \cos(2m\theta) - \sum_{n=1}^{N} \frac{k(2n-3)\, a_{2n-3} \cos(2m + 2n - 3)\theta}{2m + 2n - 3}$$

Velocity Potentials:

$$\phi_{cH}(\theta) = \pi e^{-kz} \cos(ky)$$

$$\phi_{sH}(\theta) = \pi e^{kz} \sin(ky) - \int_0^\infty e^{-\beta y} \left[\frac{\beta \cos(\beta z) - k \sin(\beta z)}{\beta^2 + k^2}\right] d\beta$$

$$\phi_{2mH}(\theta) = \sin(2m\theta) + \sum_{n=1}^{N} \frac{k(2n-3)\, a_{2n-3} \sin(2m + 2n - 3)\theta}{2m + 2n - 3} \qquad \text{(III-20)}$$

In the above equation, the term k is the wave number given in equation (III-9), and a_{2n-3} are the mapping coefficients.

For swaying and rolling motions, equations similar to (III-16) - (III-20) can also be obtained, and can be found in Reference 4.

III.2.b Close-Fit Method

The close-fit method for calculating two-dimensional pressure is described in detail in Reference 5.

The close-fit technique involves the determination of the two-dimensional hydrodynamic pressure due to vertical, lateral or rolling motion on a section's contour using a method of distributing source singularities over the submerged portion of the hull. Each of the sources has a density which can be determined from the kinematic boundary condition. The hydrodynamic pressure at point (y_i, z_i) along the section's contour is obtained by substituting the velocity potential, described by these piece-wise sources, into the linearized Bernoulli equation.

$$P^{(m)}(y_i,z_i,\omega;t) = \rho\phi_t{}^{(m)}(y_i,z_i,\omega;t) \qquad \text{(III-21)}$$

or

$$P^{(m)}(y_i,z_i,\omega) = P_a{}^{(m)}(y_i,z_i,\omega)\ \cos\omega t + P_v{}^{(m)}(y_i,z_i,\omega)\sin\omega t \qquad \text{(III-22)}$$

where the superscript m denotes the mode of motion. When m=2, 3 or 4, it represents the swaying, heaving or rolling motion. In equation (III-22), $P_a{}^{(m)}$ is the hydrodynamic pressure in phase with the displacement, and is 180 degrees out-of-phase with the acceleration. The term $P_v{}^{(m)}$ is the hydrodynamic pressure in phase with velocity.

In using the close-fit method, each ship's sections is described by N + 1 offset pairs (η_i, ζ_i) whose midpoint (y_i,z_i) can be determined from plane geometry.

In order to determine the pressure, the velocity potential $\phi^{(m)}$ is defined

$$\phi^{(m)}(y,z;t) = R_e \int_{C_o} Q(s)\ G(z,\zeta)e^{-i\omega t}ds$$

or as shown in Reference 5 for point i:

$$\phi_i^{(m)} = \left\{ \frac{1}{2\pi} \sum_{j=1}^{N} Q_j R_e\{G_{2ij}\} - \sum_{j=1}^{N} Q_{N+j} R_e \{G_{2ij}\} \right\} \cos\omega t$$

$$+ \left\{ \frac{1}{2\pi} \sum_{j=1}^{N} Q_{N+j} R_e \{G_{1ij}\} \right. \qquad \text{(III-24)}$$

$$\left. + \sum_{j=1}^{N} Q_j R_e \{G_{2ij}\} \right\} \sin\omega t$$

where Q_j is the density of the pulsating source at point j, G_{ij} is the point potential at i due to point j.

The density of the source potential is determined by applying the kinematic boundary condition which can be summarized as follows:

$$\sum_{j=1}^{N} Q_j^{(m)} I_{ij}^{(m)} + \sum_{j=1}^{N} Q_{N+j}^{(m)} J_{ij}^{(m)} = 0$$

$$\text{(III-25)}$$

$$- \sum_{j=1}^{N} Q_j^{(m)} J_{ij}^{(m)} + \sum_{j=1}^{N} Q_{N+j}^{(m)} I_{ij}^{(m)} = \omega A^{(m)} n_i^{(m)}$$

where $I_{ij}^{(m)}$ is the influence coefficient in phase with displacement of the i^{th} midpoint due to the j^{th} segment in the m^{th} mode of oscillation; $J_{ij}^{(m)}$ is the same as $I_{ij}^{(m)}$ but in phase with velocity; $n_i^{(m)}$ is the direction cosine of the normal velocity at i^{th} midpoint for the m^{th} mode of oscillation; $Q_j^{(m)}$ is the source strength in phase with displacement along j^{th} segment for the m^{th} mode of oscillation; $Q_{j+N}^{(m)}$ is the same as $Q_j^{(m)}$ but in phase with velocity; and $A^{(m)}$ is the oscillation of amplitude in the m^{th} mode.

The influence coefficients are defined in Appendix B of Reference 5. Equation (III-25) can be solved for source density, Q_j, by solving the two simultaneous equations.

IV. CORRELATION OF MOTIONS AND HYDRODYNAMIC PRESSURES

Theoretically determined transfer functions of the motion and hydrodynamic pressure are obtained from the program ABS/SHIPMOTION. Theory pertaining to the pressure calculation is given in Chapter III.

In correlating the theoretical motions and pressures with model test data, the same non-dimensional responses defined in Chapter II are used. For comparing the full-scale measured pressure, a dimensional form in terms of PSI per unit wave amplitude (RAO) is used.

Two sets of pressure calculation have been made. In one set, the speed effect term on pressure is not included. In this case, the second term in the square bracket of equation (III-1) is excluded. Pressures obtained in this manner are two-dimensional results, and are labelled as "Shipmotion results" in the graphs where the comparison of the calculated and measured pressures are shown.

The second set of pressure is calculated in accordance with equation (III-1), where the speed effect term on pressure is included. Results of this set are labelled as "speed corrected pressures" in the graphs of comparison.

In contrast to the pressure calculations in which two cases are considered, the motions are calculated only for the case where the speed effects are included.

The correlations of motions and pressures for the SL-7 model test are shown in Appendix A in graphical form. All the responses in the comparison are in the non-dimensional form previously described. The

correlations include plots of heave motion in Figures A-1 and A-2; pitch motion in Figures A-3 and A-4; pressure due to forced heave in Figures A-5 to A-15; pressure due to forced pitch in Figures A-16 to A-27; pressure due to incident wave in Figures A-28 to A-40; pressure for F_n = 0.15 in Figures A-41 to A-66; pressure for F_n = 0.23 in Figures A-67 to A-92; and pressure for F_n = 0.32 in Figures A-93 to A-118.

Appendix B contains the correlation plots for the S. J. CORT model-test measurements. These include plots of pressure in fully loaded condition, F_n = 0.1, in Figures B-1 to B-24; pressure in fully loaded condition, F_n = 0.13, Figures B-25 to B-48; pressure in ballast condition F_n = 0.1, in Figures B-49 to B-58; and pressure in ballast condition F_n = 0.13, in Figures B-59 to B-68. Pressure values in Appendix B are in non-dimensional form as defined in Chapter II.

The plots of correlation for S.J. CORT full-scale measurements are in Appendix C. Appendix C contains plots of wave and pressure spectra for different conditions (Figure C-1 - Figure C-23), and of pressure transfer functions (Figure C-24 - Figure C-73). The pressure transfer function is calculated by dividing the pressure spectral ordinate by the wave spectrum, and then taking the square root. While correlating the measured pressure with the theoretically calculated pressure, it should be noted that the measured pressures are for the vessel at headings from 0 to 23 degrees off the bow (See Table II-2(a)), while the theoretical presures are calculated for head seas only. The use of head seas in the calculation is to reduce the extensive utilization of computer time. The theoretical results obtained in the head sea condition would be able to provide

qualitative correlation with data measured at headings slightly off from the head seas.

From the graphs of pressure and wave spectra obtained during the full-scale trials, it is observed that for part of the frequency range plotted the pressure spectra ordinates are very small, and the accuracy of their measurement could be in doubt. As such, for this frequency range the pressure transfer functions have not been calculated. Correlation of the measured and calculated pressure transfer functions has been confined to the frequency range in which the wave and pressure spectrum values lie within the range of accuracy of the measuring instruments.

V. CONCLUDING REMARKS

From the comparisons shown in Appendices A, B and C, it can be seen that the correlation of theoretical calculations of motion and pressures, with both model-test and full-scale measurement, is very encouraging. However, the degree of closeness in the correlations is different between model-test and full-scale data. The correlation is also different between the SL-7 containership and the S. J. CORT. In general, the theoretical prediction has the same trend as measured values either from model test or full-scale trial. Also, the model test shows a better correlation than the full-scale measurement. A more detailed discussion on the comparison follows:

V.1. SL-7 Model Test

Measured heaving and pitching motions are compared with theoretical calculations for two ship speeds at Froude numbers 0.23 and 0.32, where the speed - effect terms are included in the calculations.

The measurements show the same trend as the computed results, but have smaller values in heave motion at lower wave frequencies. At very low wave frequencies, i.e. long waves, the non-dimensional heave which is defined in Chapter II should approach unity. The measured data of heaving motion as shown in Figures A-1 and A-2, especially at Froude number 0.23, are much smaller than unity at low wave frequencies and the results are, therefore, questionable.

Calculated pressure components for forced heave and forced pitch were obtained in two different manners: by first including and then not including the speed-effect term. As can be seen from Figures A-5

to A-27, the correlation is very striking, especially for the calculated pressures where the speed-effect terms are not included. Very good agreement is also obtained between measured pressure due to wave excitations and the calculations without taking the speed-effect terms into account.

Shown in Figures A-41 to A-118 are correlations of the non-dimensional pressure for Froude numbers of 0.15, 0.23 and 0.32. A general conclusion of the comparison is that except at the bow and stern regions of the vessel, good agreement is obtained between measured and calculated data. However, the peak frequency of the predicted pressure is somewhat (0.1 rad/sec) less than the measured. Within the scope of linear theory of ship motion, the pressure is the sum of pressure components due to the motion and wave excitation. Since good correlation is obtained for the pressure components, the discrepancy of the pressure peak frequency may be a result of the the calculated and measured phase angles of the pressure components. The comparison of phase angle, however, has not been carried out, due to the lack of measured data.

As described above, the pressure correlation in bow and stern regions is not as good as in the midlength of the vessel. The poorer agreement in the two ends is expected, because the three-dimensional effects and particularly the nonlinearity of waves in the bow region cannot be fully accounted for by linear theory and the strip method. The discrepancies of pressure in the bow region are also found by Kim [6] in his correlation with model-test pressure data measured by Japanese researchers.

Comparisons in Appendix A also show that the pressures calculated without the speed-effect term (i.e., two-dimensional pressures) have generally better correlation than those with the speed-effect term. This indicates that the speed-effect term used in the present study is not as effective as expected.

V.2 M/V S. J. CORT Model Test

The model tests of the M/V S. J. Cort were performed with the emphasis on short waves. For all the measurements in the two loading conditions, fully loaded and ballast, and two Froude numbers 0.1 and 0.13, correlation with theoretical total pressures is shown in Appendix B. In general, good agreement is shown with the exceptions subsequently discussed.

As with the SL-7 correlation, the pressure in the bow region of the vessel has larger discrepancies than other regions. This is probably due to the three-dimensional effects and the nonlinearity of bow waves which are not accounted for by linear theory and the strip method.

The inclusion of the speed-effect term in calculating the pressure has a mixed effect on the correlation. As a result, this term slightly improves the correlation in some cases and it has adverse effects to the correlation in other cases.

The theoretically predicted pressure exhibits a similar trend as the measured values. However, for pressure points on the ship's bottom, theoretical results show a diverging tendency in the region of high frequencies. This can be seen from Figures B-4, B-5, B-8, B-12, B-13, B-17, B-21 etc. Reasons causing this divergency can not be readily identified.

V.3 M/V S. J. CORT Full-Scale Measurement

From the plots in Appendix C, it is observed that the correlation of the pressures at Frames 30-31 is better than those at Frame 20-21. Again, this may be due to the pressure of the bow wave, a factor which linear theory and strip method do not take into consideration.

As observed in the model tests correlations, the inclusion of the speed-effect term in the pressure calculation has a mixed effect on the correlation.

In general, the correlation is reasonably good, except at pressure points 6 and 14. Pressure point 6 which is located close to the free surface between Frames 20 and 21, exhibits the largest discrepancy between measurement and calculation, with measured values as much as three times higher than calculated values at the higher speeds tested. This could be due to a defective pressure gauge, and Reference [2] has noted that gauges 6 and 14 should be considered unreliable for data analysis purposes. Therefore, the correlation of the pressures at these two gauges is uncertain and plots of pressure correlation at these two gauges are not included in this report.

VI. REFERENCES

1. Troesch, A.M. and Slocum, S., "Pressure Distribution on Models of the SL-7 Containership and Great Lakes Bulk Carrier S. J. Cort in Waves," Department of Naval Architecture and Marine Engineering, University of Michigan, March 1981.

2. Swanek, R.A. and Kihl, D.P., "Investigation of Springing Responses on the Great Lakes Ore Carrier M/V Stewart J. Cort.", DWTNSRDC Report 5602/39, February 1980.

3. Hoffman, D., Zielinski, T.E., and Hsuing, C.C., "Hydrodynamic Pressure Distribution on Ship Hulls in Waves," Webb Institute of Naval Architecture, January 1977.

4. Zielinski, T.E., "Program HYDRO2D Two-Dimensional Hydrodynamic Properties of Ship Sections," Webb Institute of Naval Architecture, November 1976.

5. Frank, W., "Oscillation of Cylinders in or Below the Free Surface of Deep Fluids," NSRDC Report 2375, October 1967.

6. Kim, C. H. "Hydrodynamic Loads on the Hull Surface of the Seagoing Vessel," SNAME Spring Meeting/STAR Symposium, Honolulu, 1982.

Table II-I(a) SL-7 Hull Particulars

	Ship		Model	
	(meters)	(feet)	(meters)	(feet)
Length over all (LOA)	288.500	946.60	2.60700	11.8300
Length between Perpendiculars (LBP)	268.400	880.50	3.35500	11.0100
Draft at Longitudanal Center of Flotation	9.940	32.60	0.12400	0.4080
Trim by Stern	0.043	0.14	0.00053	0.0018
Longitudanal Center of Gravity (Aft of Midship)	11.700	38.40	0.14600	0.4800

Ship Displacement : 48364 long tons
47500 metric tons

Model displacement : 0.0945 long tons
0.0928 metric tons

Note:

For both ship and model the Pitch Radius of Gyration = 0.21 * LBP

Table II-1(b) Pressure Tap Locations on SL-7
(Dimensions are for full-scale)

Tap Number	Station (Sta 20 = FP)	Distance above Base-line		Distance off Center-line	
		(meter)	(feet)	(meter)	(feet)
1	18	0.00	0.00	-	-
2	17	0.00	0.00	-	-
3	16	0.00	0.00	-	-
4	15	0.00	0.00	-	-
5	15	2.03	6.67	-	-
6	15	4.07	13.37	-	-
7	15	7.11	23.33	-	-
8	14	0.00	0.00	-	-
9	14	4.07	13.37	-	-
10	13	0.00	0.00	-	-
11	13	1.00	3.30	-	-
12	13	4.06	13.33	-	-
13	13	7.11	23.33	-	-
14	12	0.00	0.00	-	-
15	10	0.00	0.00	-	-
16	10	0.00	0.00	8.12	26.67
17	10	4.06	13.33	-	-
18	10	7.11	23.33	-	-
19	7	0.00	0.00	-	-
20	7	4.06	13.33	-	-
21	5	0.00	0.00	-	-
22	5	0.00	0.00	8.12	26.67
23	5	4.06	13.33	-	-
24	5	7.11	23.33	-	-
25	3	0.00	0.00	-	-
26	3	4.06	13.33	-	-

Table II-1(c) M/V S. J. Cort Hull Particulars

	Ship		Model	
	Full Load	Ballast	Full Load	Ballast
LOA m(ft)	304.8 (1000)	304.8 (1000)	4.57 (15.00)	4.57 (15.00)
LBP m(FT)	301.4 (989)	301.4 (989)	4.52 (14.83)	4.52 (14.83)
Displacement MT(LT)	69500 (68259)	38981 (38285)	.2346 (.2304)	.1316 (.1292)
LCG m(ft)	1.49 (4.9) (for'd of ⌀)	12.7 (41.8) (aft of ⌀)	.022 (.074) (for'd of ⌀)	.191 (.627) (aft of ⌀)
Draft at ⌀ m(ft)	7.85 (25.75)	4.52 (14.82)	.118 (.386)	.068 (.222)
Trim m(ft)	0.00	3.5 (11.4) (by stern)	0.00	.052 (.171) (by stern)
Pitch Radius Of Gyration	0.249 LOA	0.266 LOA	0.249 LOA	0.266 LOA

Note:

⌀ is at LOA/2

Table II-1(d) Pressure Tap Locations on M/V S. J. CORT

Tap Number	Distance Aft of Fore-peak		Distance above Base-line		Distance off Center-line	
	(meter)	(feet)	(meter)	(feet)	(meter)	(feet)
1	6.1	20.0	0.00	0.00	-	-
2	6.1	20.0	2.49	8.16	-	-
3	6.1	20.0	5.50	18.06	-	-
4	14.6	48.0	0.00	0.00	-	-
5	14.6	48.0	0.00	0.00	7.42	24.33
6	14.6	48.0	2.49	8.16	-	-
7	14.6	48.0	5.50	18.06	-	-
8	36.6	120.0	0.00	0.00	-	-
9	36.6	120.0	2.49	8.16	-	-
10	36.6	120.0	4.02	13.19	-	-
11	36.6	120.0	5.50	18.06	-	-
12	76.2	250.0	0.00	0.00	-	-
13	76.2	250.0	0.00	0.00	13.55	44.44
14	76.2	250.0	2.49	8.16	-	-
15	76.2	250.0	5.50	18.06	-	-
16	115.8	380.0	5.50	18.06	-	-
17	158.5	520.0	0.00	0.00	-	-
18	158.5	520.0	2.49	8.16	-	-
19	158.5	520.0	5.50	18.06	-	-
20	195.1	640.0	5.50	18.06	-	-
21	234.7	770.0	0.00	0.00	-	-
22	234.7	770.0	2.38	7.81	-	-
23	234.7	770.0	5.50	18.06	-	-
24	274.3	900.0	5.50	18.06	-	-

Notes: Distances are for full scale ship.

TABLE II - 2(a) Test Conditions of M/V S. J. CORT Full-Scale Trial

Run No.	Condi-tion	Speed (mph)	Froude Number	Draft			Ship-Wave Angle (deg)	Wave Height (ft)
				For,d (ft)	Mean (ft)	Aft (ft)		
82	1	14.4	.1184	19.92	20.58	22.00	6	6
80	2	14.4	.1184	19.92	20.58	22.00	11	0
89	3	14.7	.1208	27.00	27.00	27.00	6	3
119	4	14.2	.1167	27.00	27.00	27.00	9	3
116	5	13.5	.1100	27.00	27.00	27.00	23	4
117	6	13.5	.1100	27.00	27.00	27.00	10	3
41	6a	13.5	.1100	27.00	27.00	27.00	10	8
99	7	11.6	.095	18.0	19.92	21.25	0	5
102	8	11.6	.095	19.92	20.58	22.0	20	6

TABLE II-2(b): LOCATION OF POINTS FOR FULL SCALE PRESSURE MEASUREMENT ON M.V. S.J. CORT

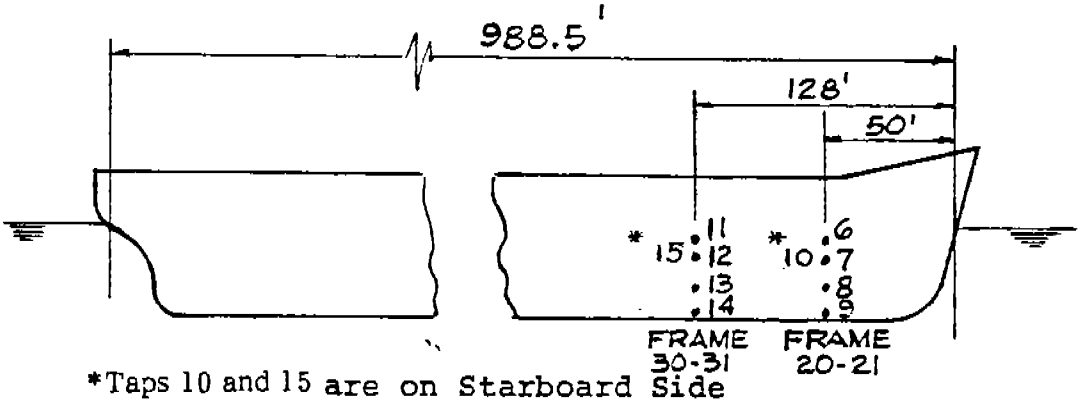

*Taps 10 and 15 are on Starboard Side

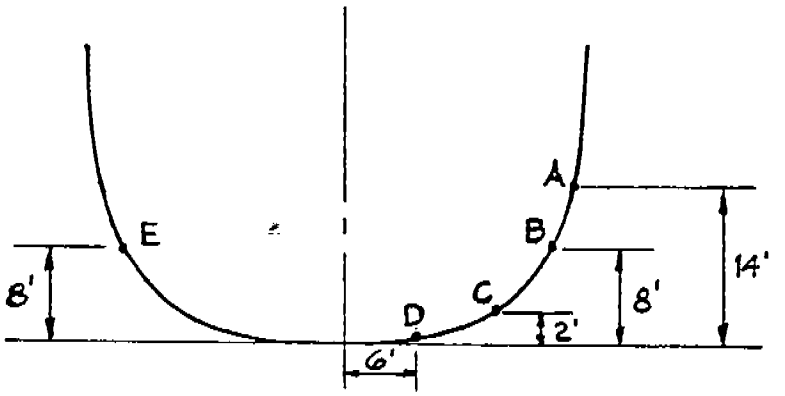

LOCATION	FR 20-21	FR 30-31
A	6	11
B	7	12
C	8	13
D	9	14
E	10	15

Notes: Station Spacing = 44'
*Points 16 and 22 are at a distance of 26' from ℄

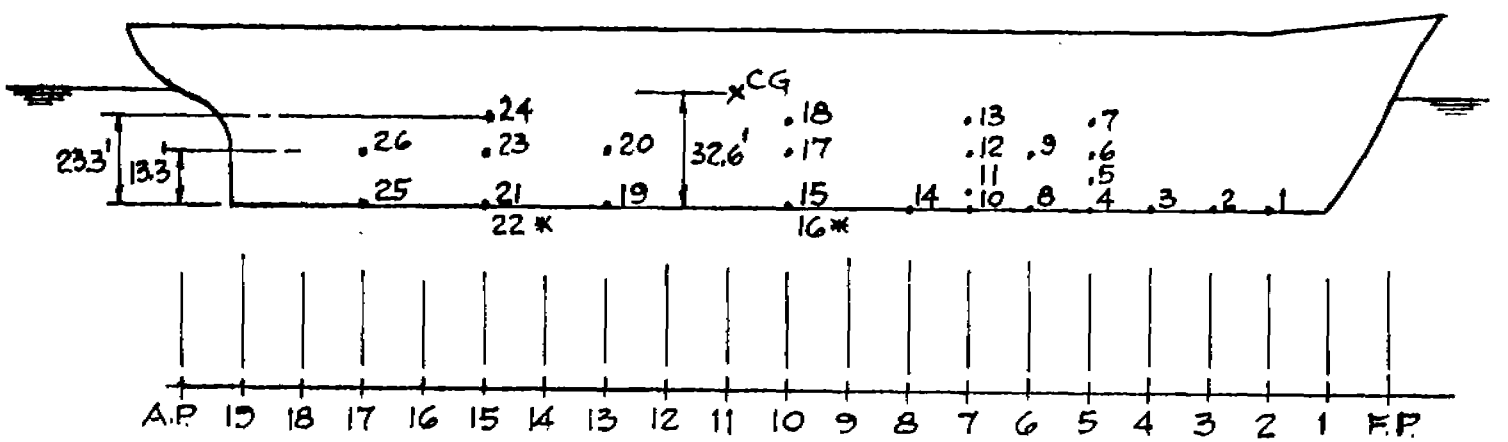

FIGURE II-1 SL-7 PRESSURE TAP LOCATIONS IN MODEL TEST

Notes: Station Spacing = 50'

*Point #5 is at a distance of 24.33 ft. from ℄
**Point #13 is at a distance of 44.44 ft. from ℄

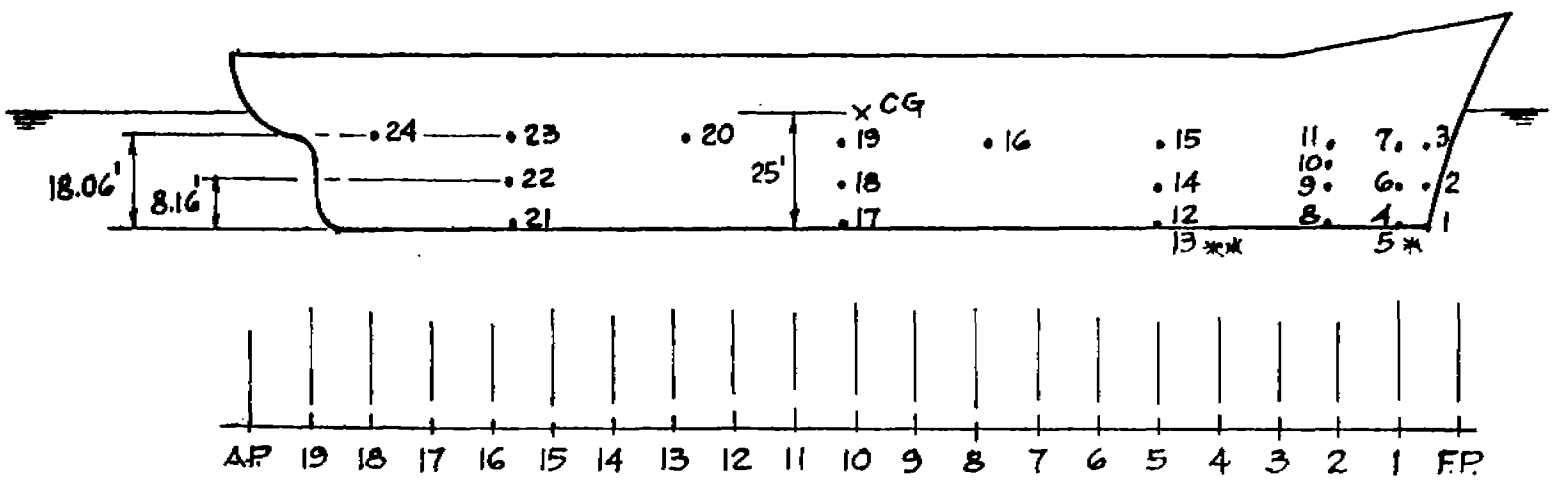

FIGURE II-2 M.V. S.J. CORT PRESSURE TAP LOCATIONS IN MODEL TEST

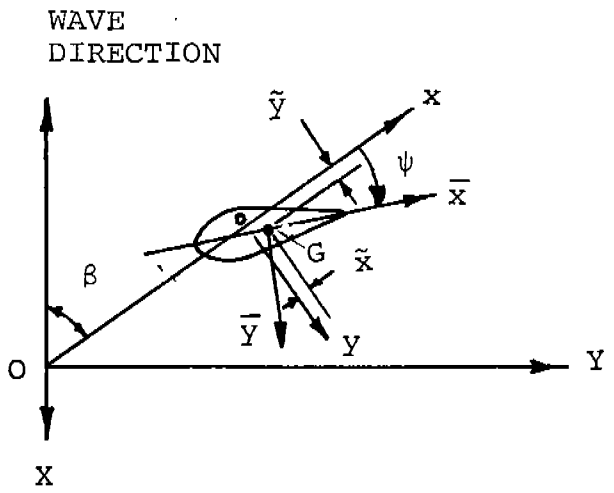
WAVE
DIRECTION
$\tilde{y}$
x
ψ
$\bar{x}$
G
$\tilde{x}$
β
$\bar{y}$
y
O
Y
X

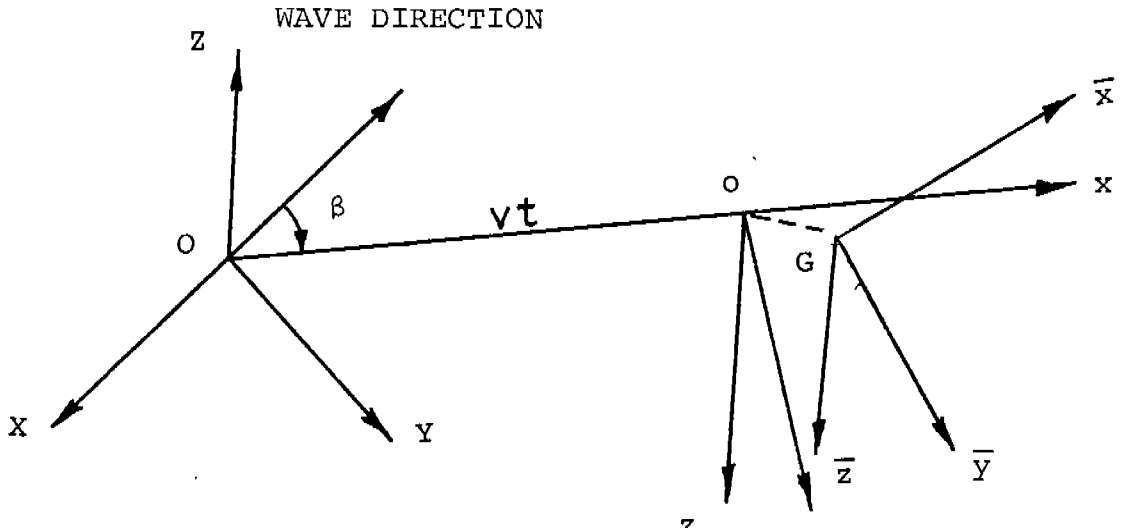
WAVE DIRECTION
Z
$\bar{x}$
x
β
vt
o
O
G
X
Y
$\bar{z}$
$\bar{y}$
z

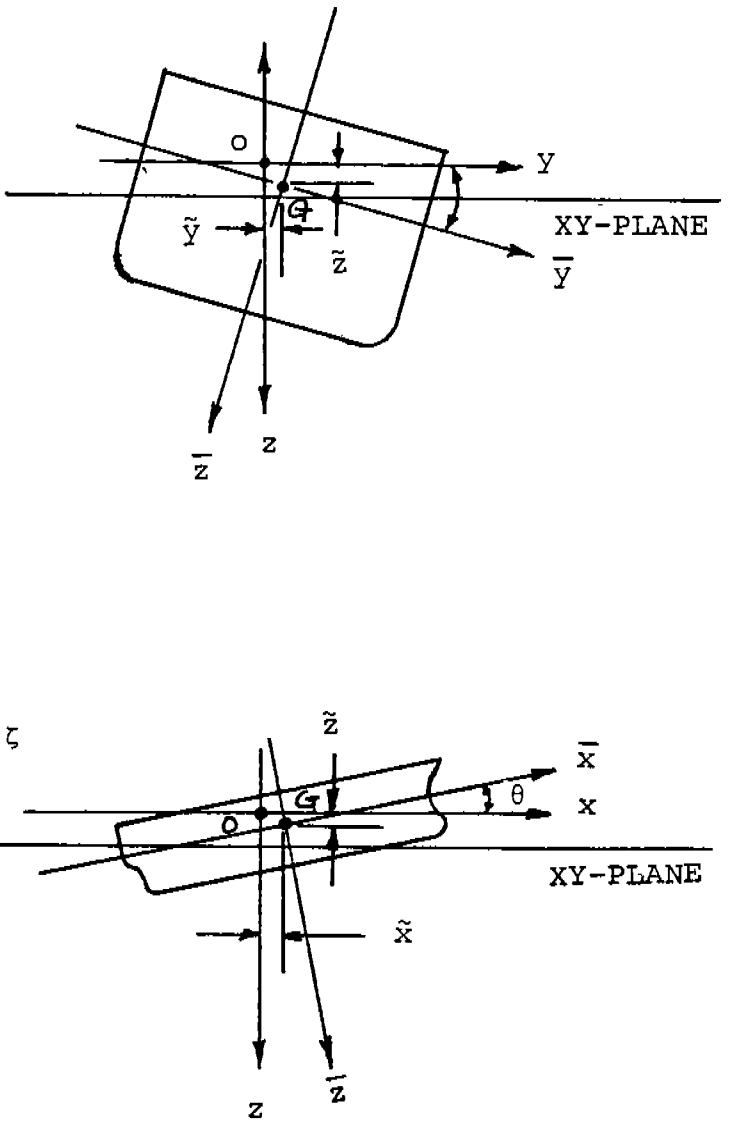

FIGURE III-1 (b) COORDINATE SYSTEM

(1/4" TO TRIM)

APPENDIX A

SL-7 MODEL TEST/THEORY CORRELATION PLOTS

Figs. A-1 and A-2:	SL-7 Non-dimensional Heave, $F_n = 0.23$
Figs. A-3 and A-4:	SL-7 Non-dimensional Pitch, $F_n = 0.23$
Figs. A-5 to A-15:	SL-7 Non-dimensional Pressure due to Forced Heave, $F_n = 0.23$
Figs. A-16 to A-27:	SL-7 Non-dimensional Pressure due to Forced Pitch, $F_n = 0.23$
Figs. A-28 to A-40:	SL-7 Non-dimensional Wave Pressure, $F_n = 0.23$
Figs. A-41 to A-66:	SL-7 Non-dimensional Pressure, $F_n = 0.15$
Figs. A-67 to A-92:	SL-7 Non-dimensional Pressure, $F_n = 0.23$
Figs. A-93 to A-118:	SL-7 Non-dimensional Pressure, $F_n = 0.32$

(1/2" TO BIND)

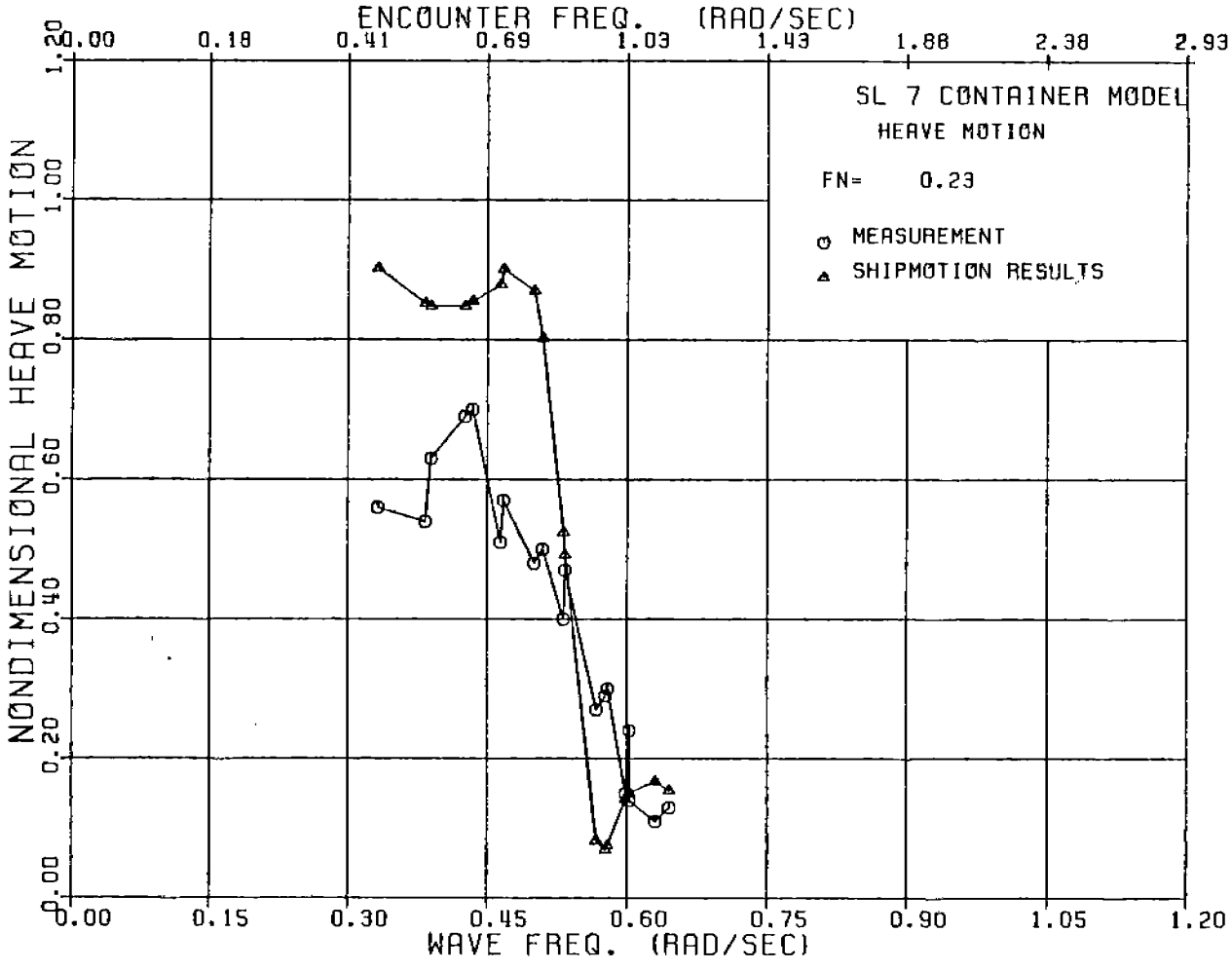

FIGURE A-1: SL-7 NONDIMENSIONAL HEAVE MOTION, F_n=0.23

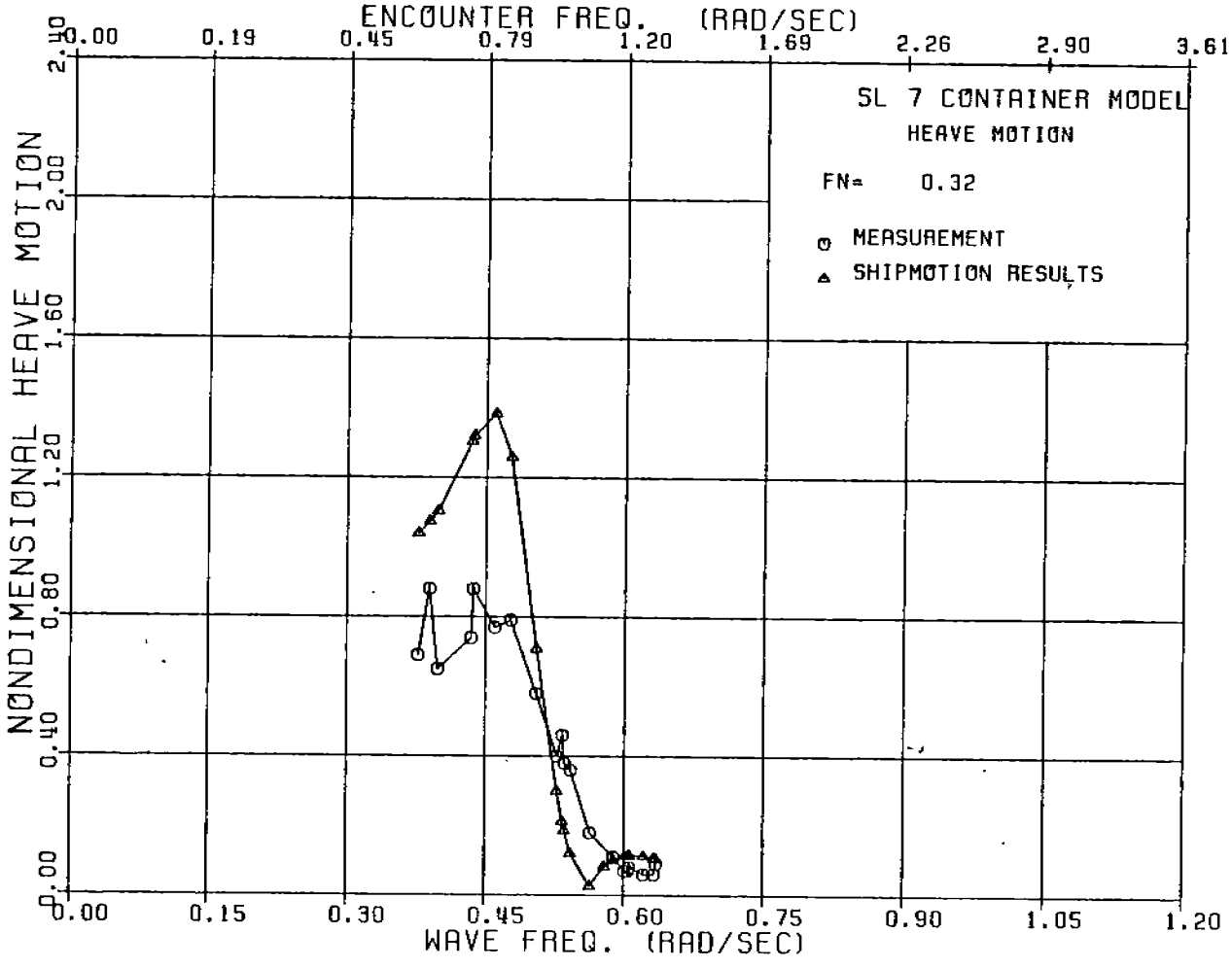

FIGURE A-2: SL-7 NONDIMENSIONAL HEAVE MOTION, F_n=0.32

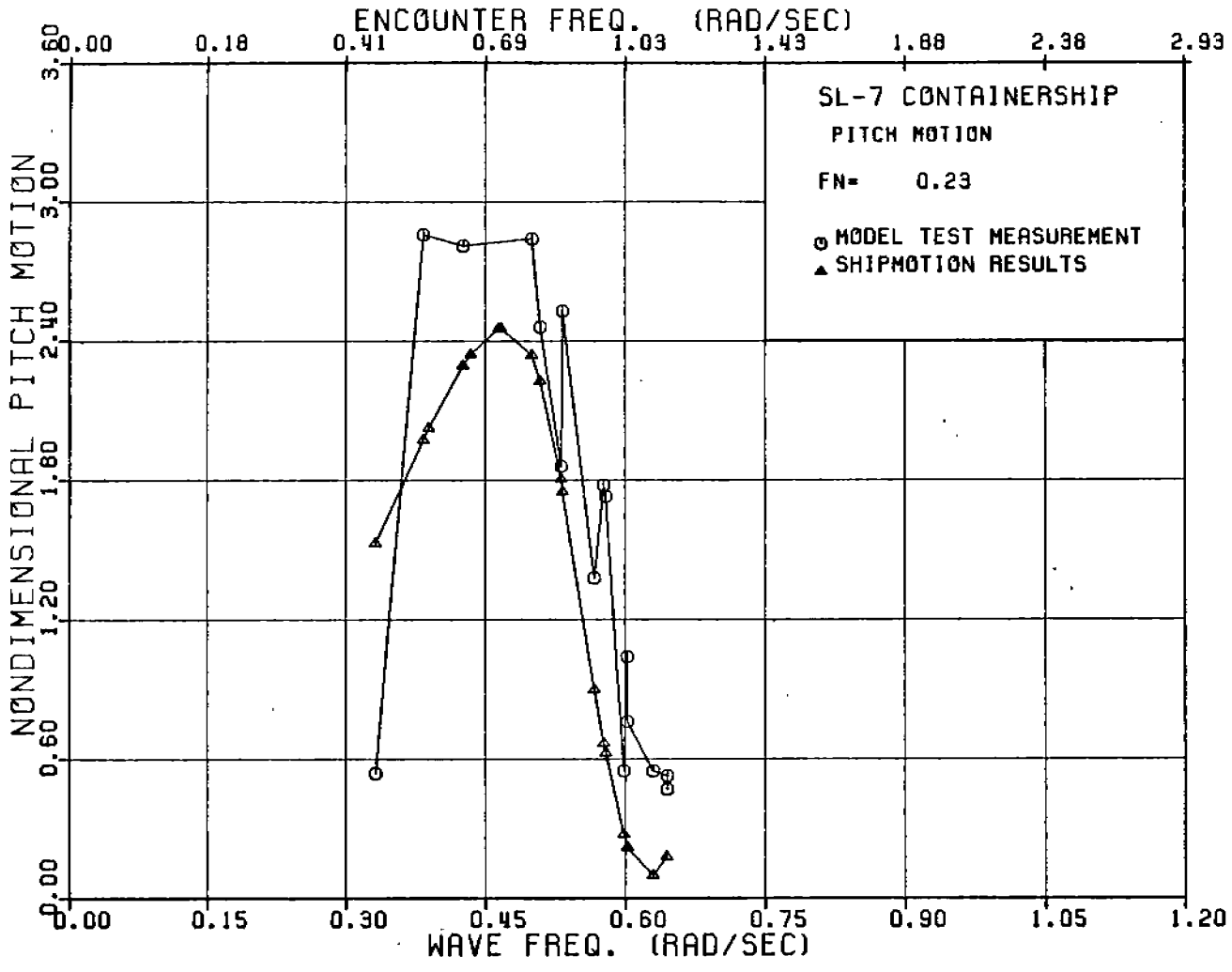

FIGURE A-3: SL-7 NONDIMENSIONAL PITCH MOTION, F_n=0.23

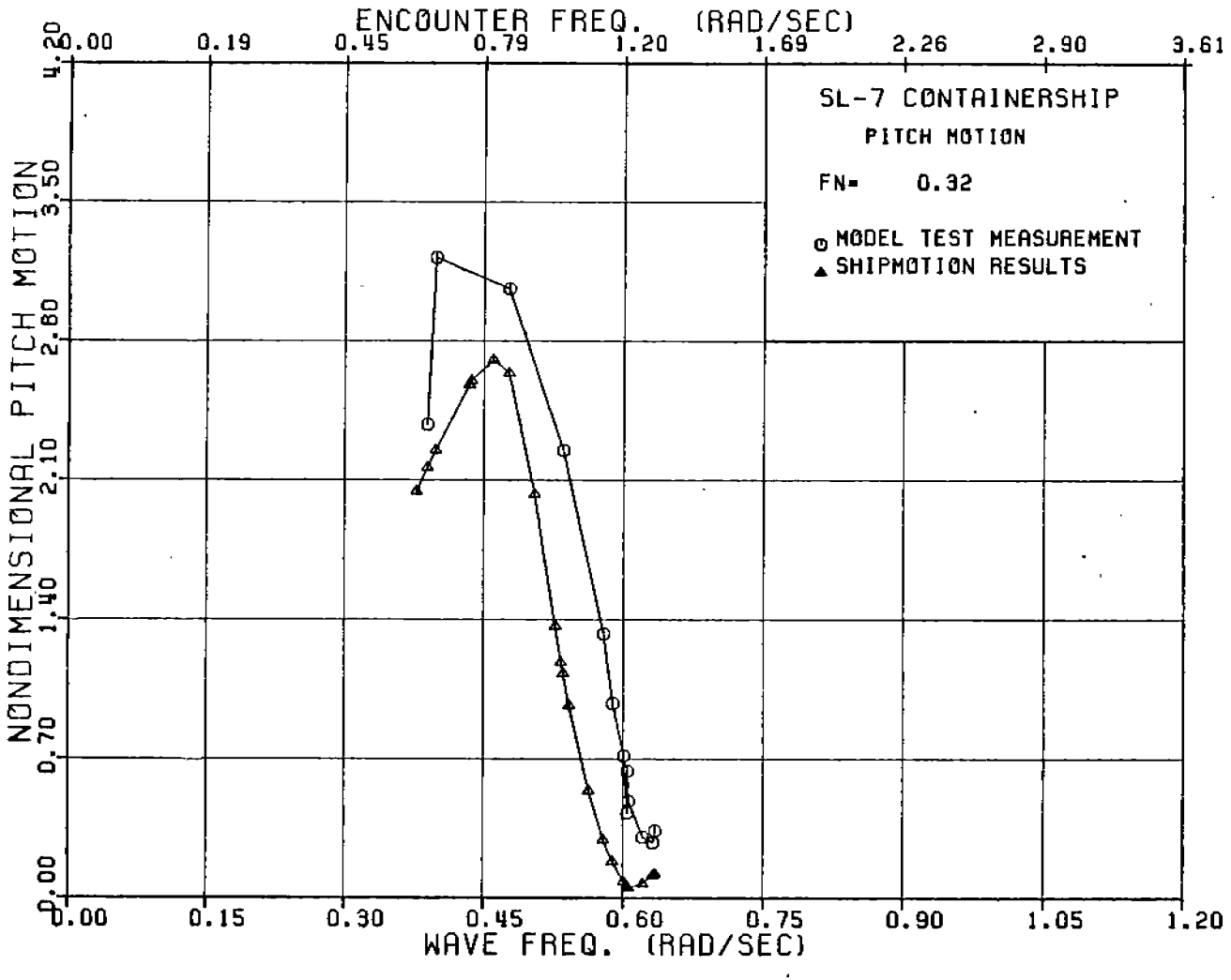

FIGURE A-4: SL-7 NONDIMENSIONAL PITCH MOTION, F_n=0.32

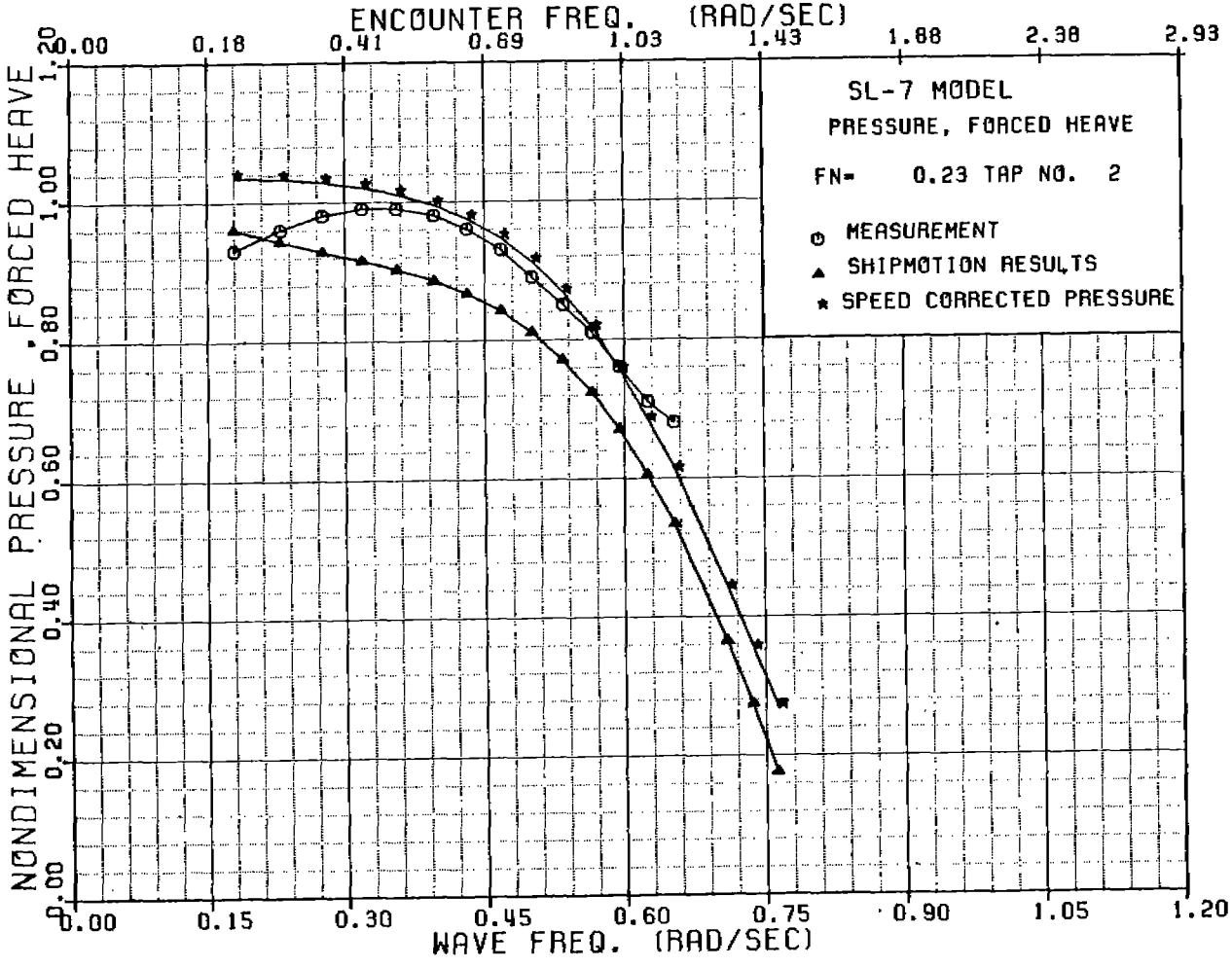

FIGURE A-5: SL-7 NONDIMENSIONAL PRESSURE AT TAP 2 DUE TO FORCED HEAVE, F_n=0.23

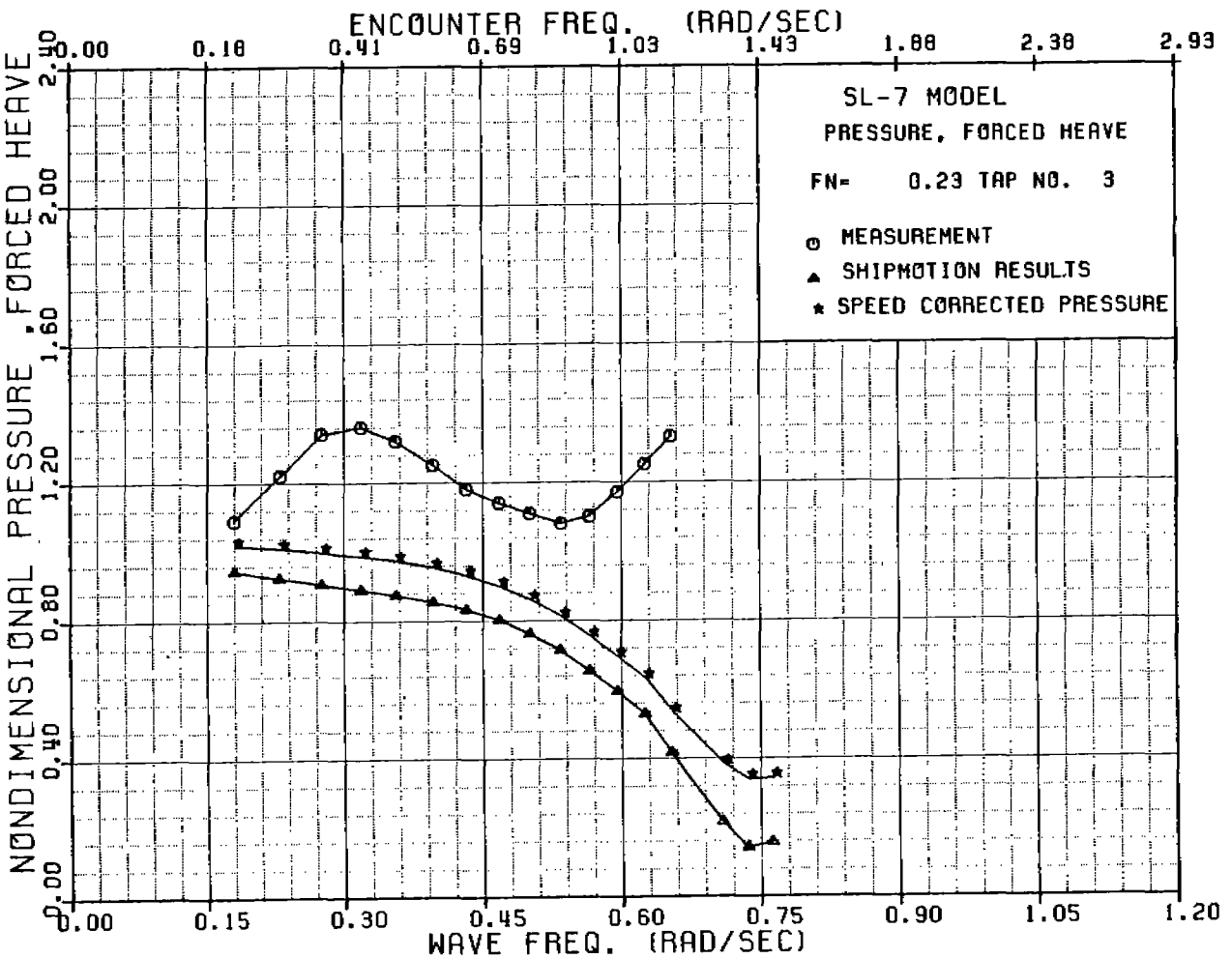

FIGURE A-6: SL-7 NONDIMENSIONAL PRESSURE AT TAP 3 DUE TO FORCED HEAVE, F_n=0.23

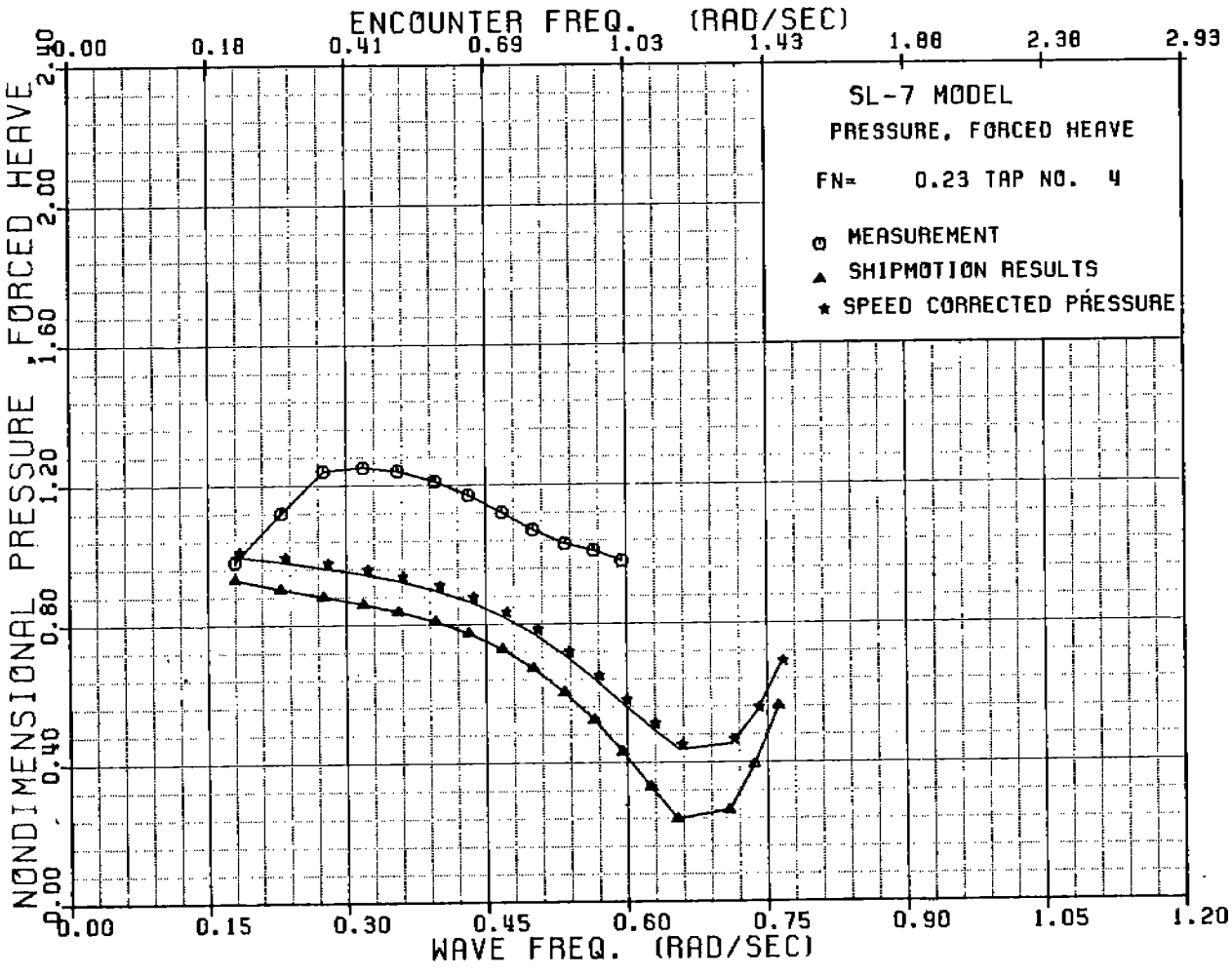

FIGURE A-7: SL-7 NONDIMENSIONAL PRESSURE AT TAP 4 DUE TO FORCED HEAVE, F_n=0.23

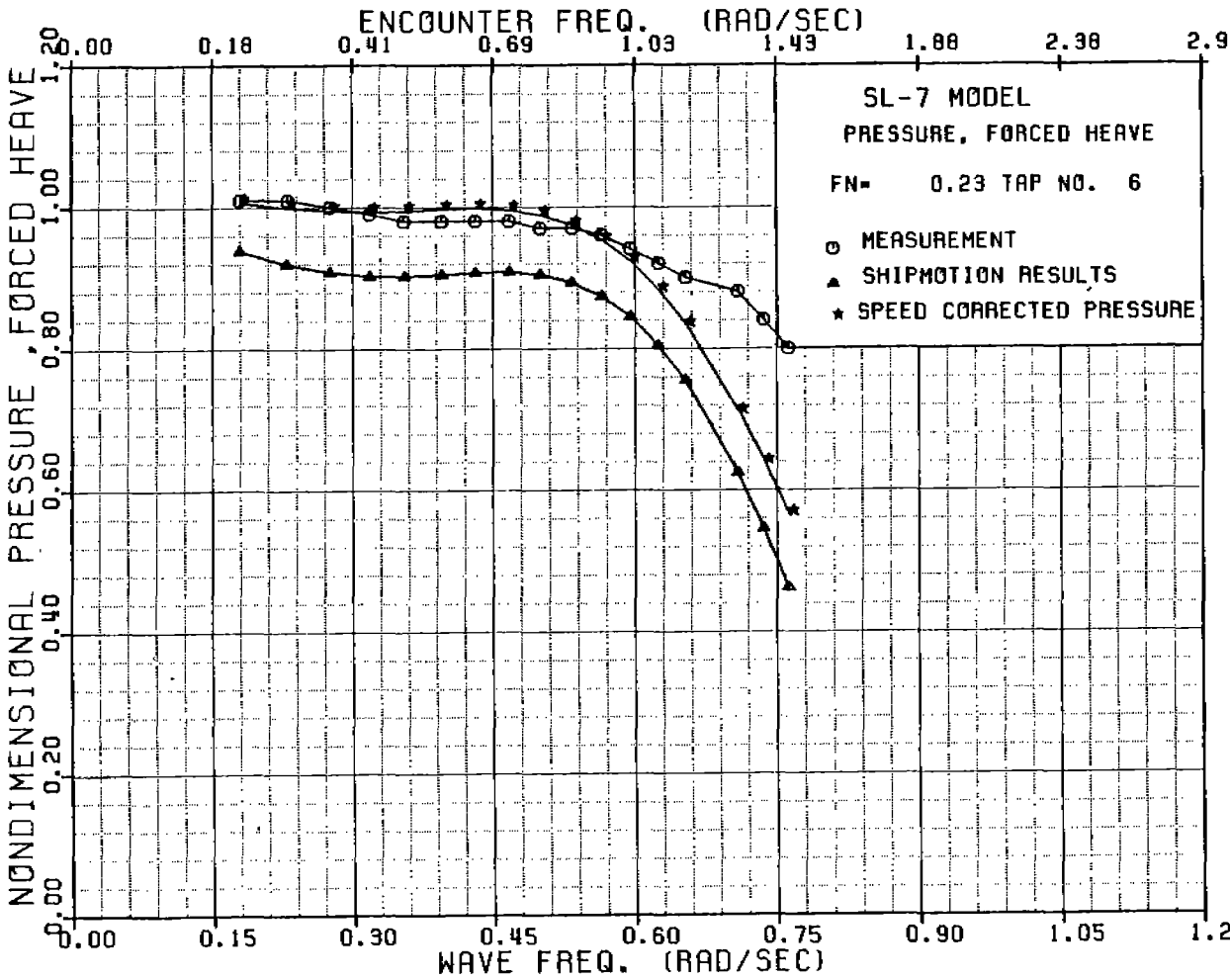

FIGURE A-8: SL-7 NONDIMENSIONAL PRESSURE AT TAP 6 DUE TO FORCED HEAVE, F_n=

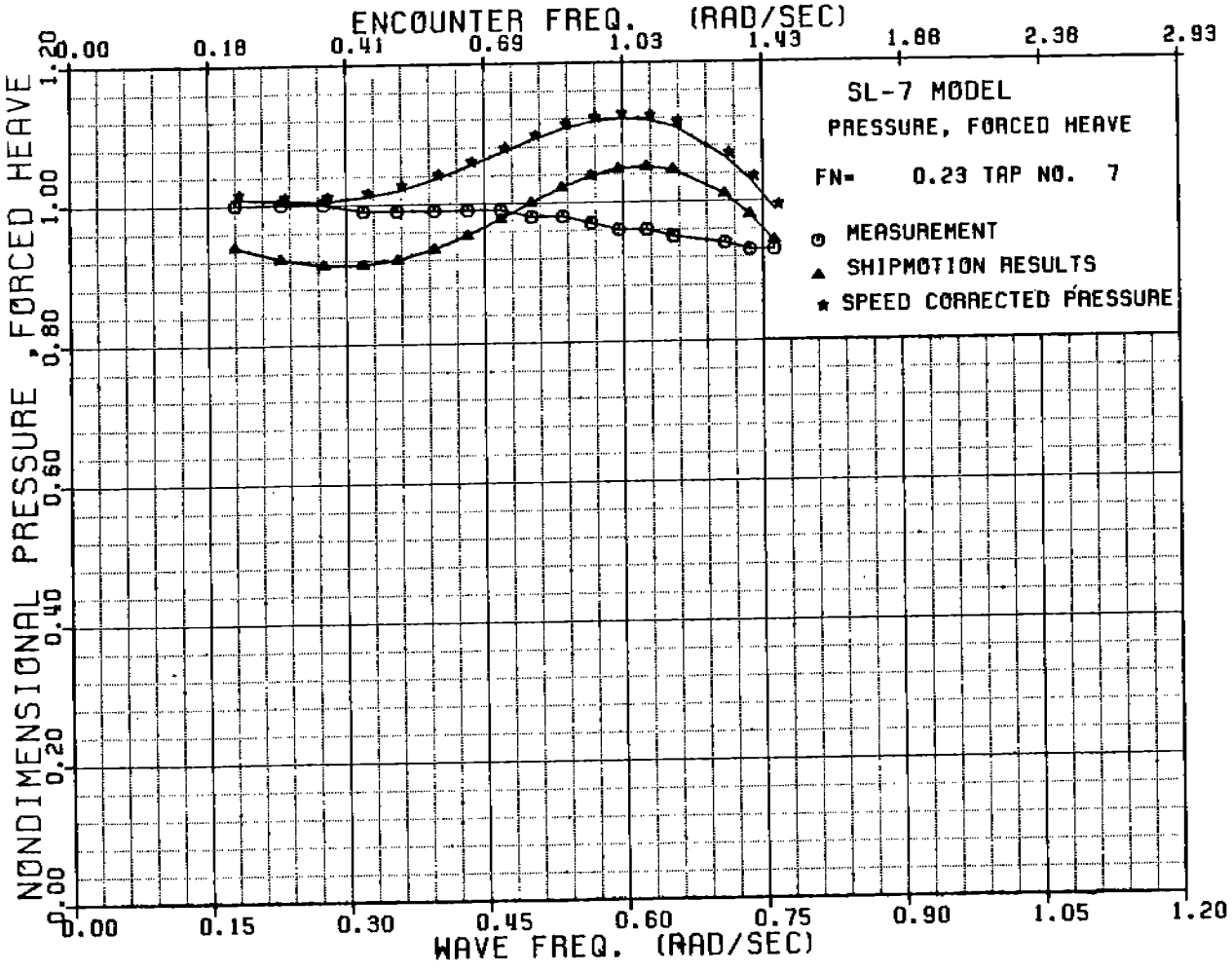

FIGURE A-9: SL-7 NONDIMENSIONAL PRESSURE DUE TO FORCED HEAVE AT TAP 7, F_n=0.23

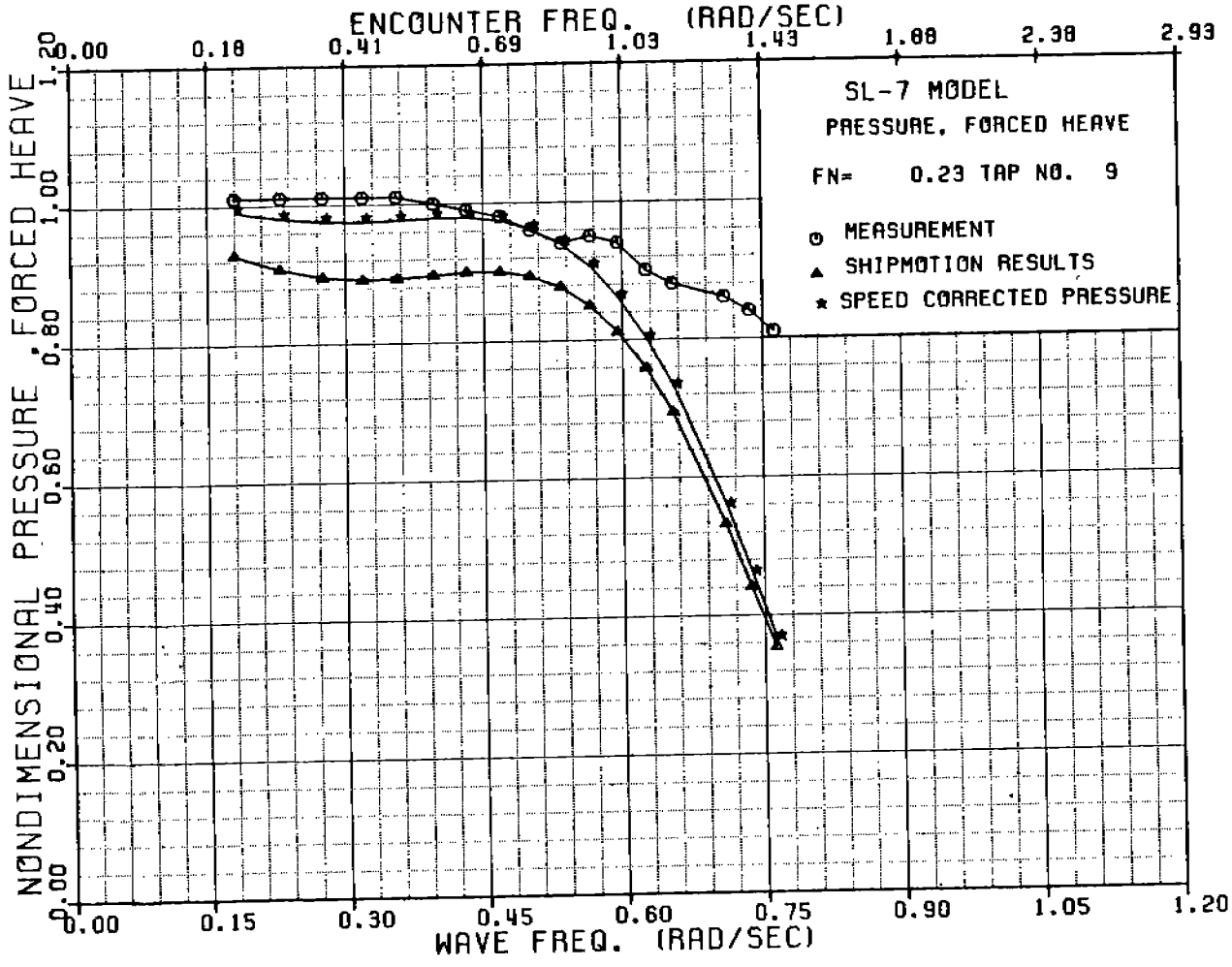

FIGURE A-10: SL-7 NONDIMENSIONAL PRESSURE DUE TO FORCED HEAVE AT TAP 9, F_n=0.23

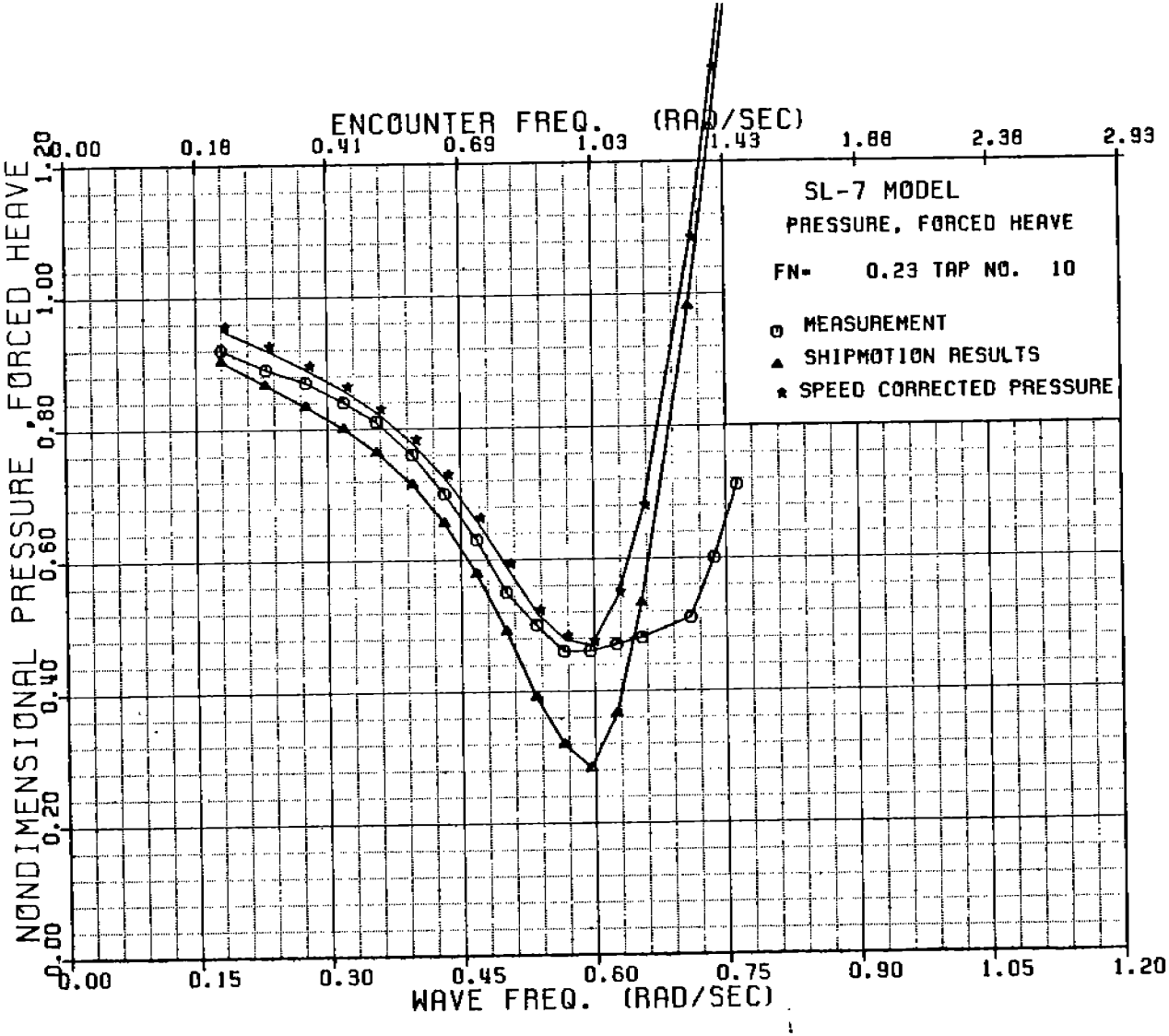

FIGURE A-11: SL-7 NONDIMENSIONAL PRESSURE DUE TO FORCED HEAVE AT TAP 10, F_n=0.23

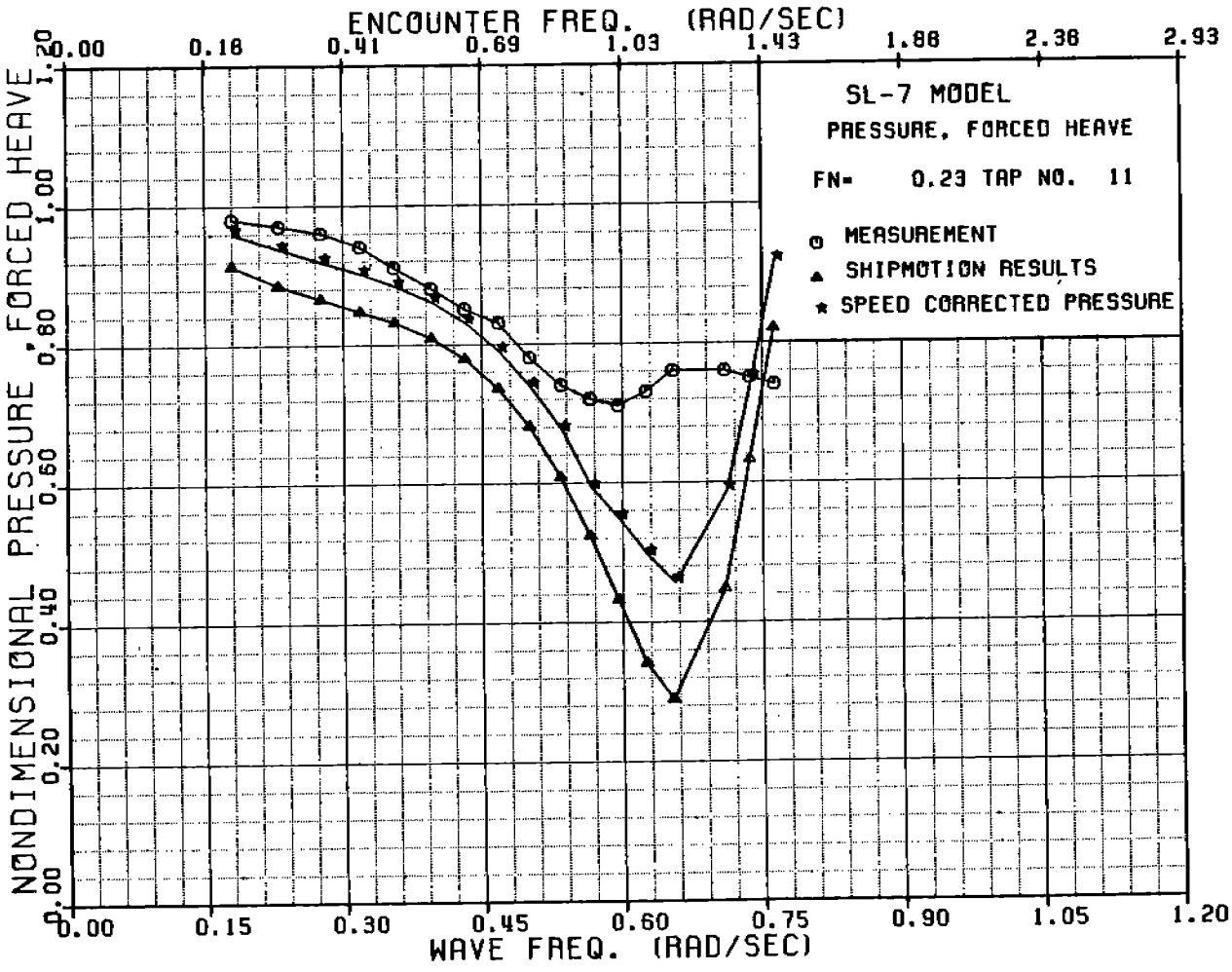

FIGURE A-12: SL-7 NONDIMENSIONAL PRESSURE DUE TO FORCED HEAVE AT TAP 11, F_n=0.23

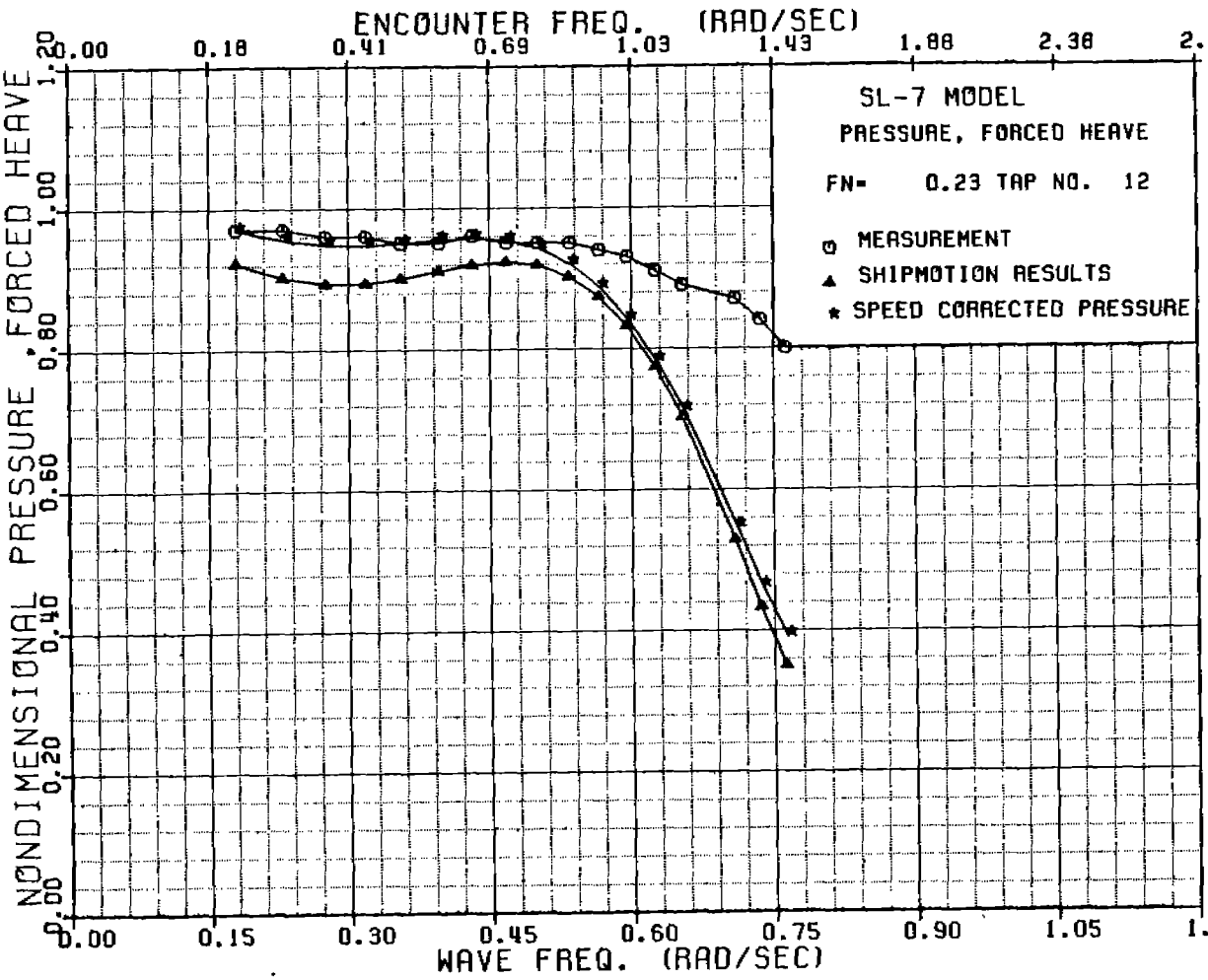

FIGURE A-13: SL-7 NONDIMENSIONAL PRESSURE DUE TO FORCED HEAVE AT TAP 12

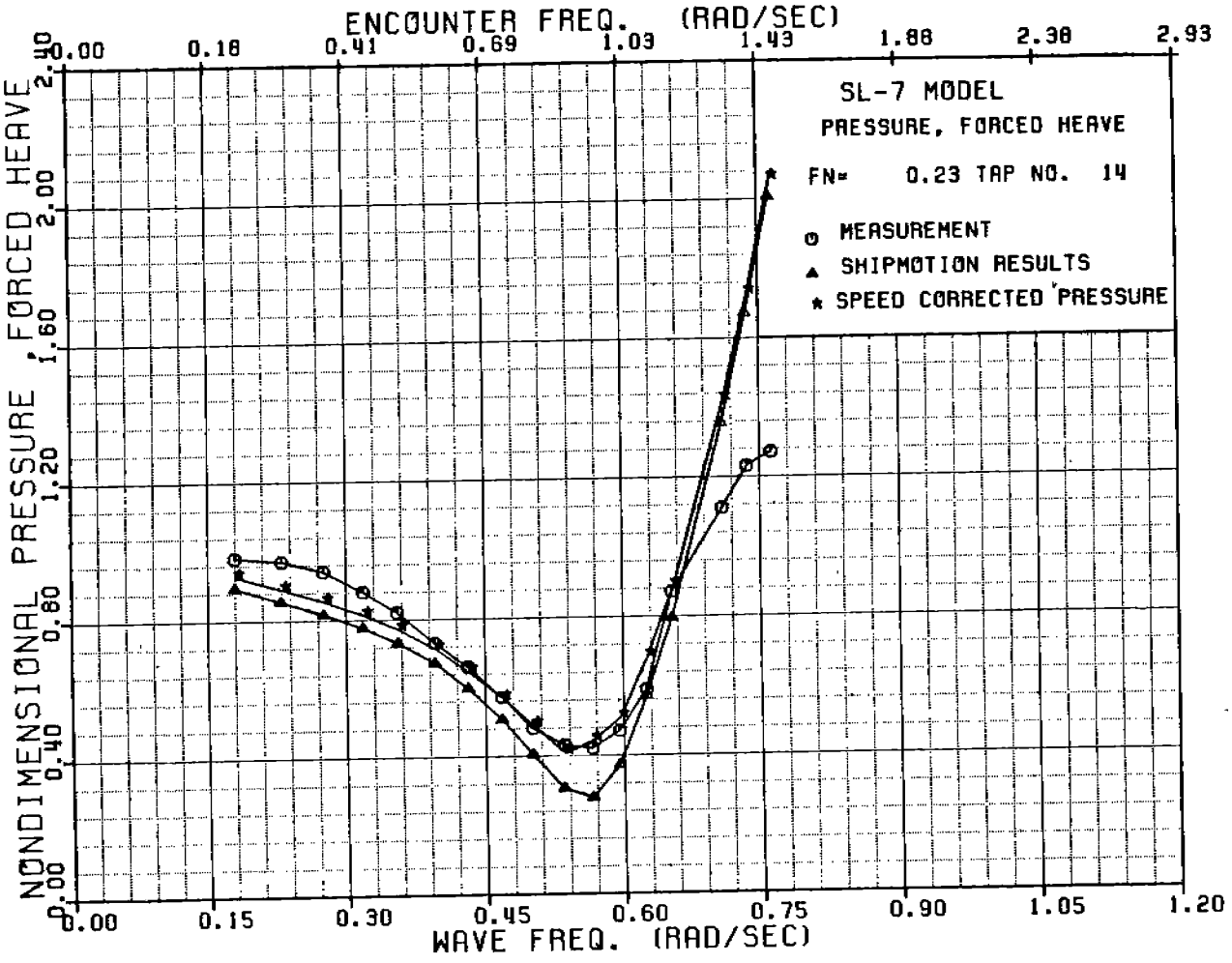

FIGURE A-14: SL-7 NONDIMENSIONAL PRESSURE DUE TO FORCED HEAVE AT TAP 14, F_n=0.23

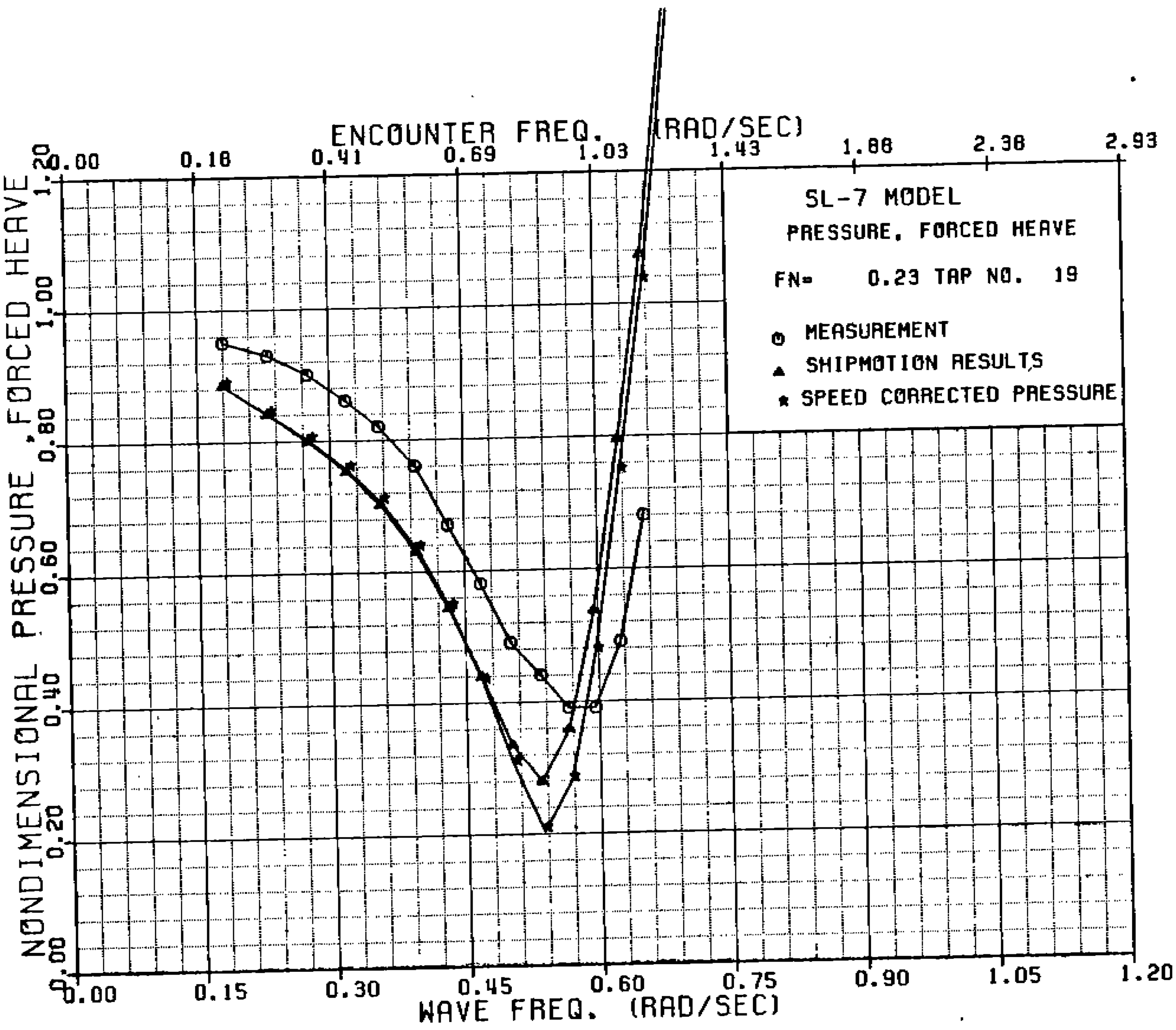

FIGURE A-15: SL-7 NONDIMENSIONAL PRESSURE DUE TO FORCED HEAVE AT TAP 19, F_n=0.23

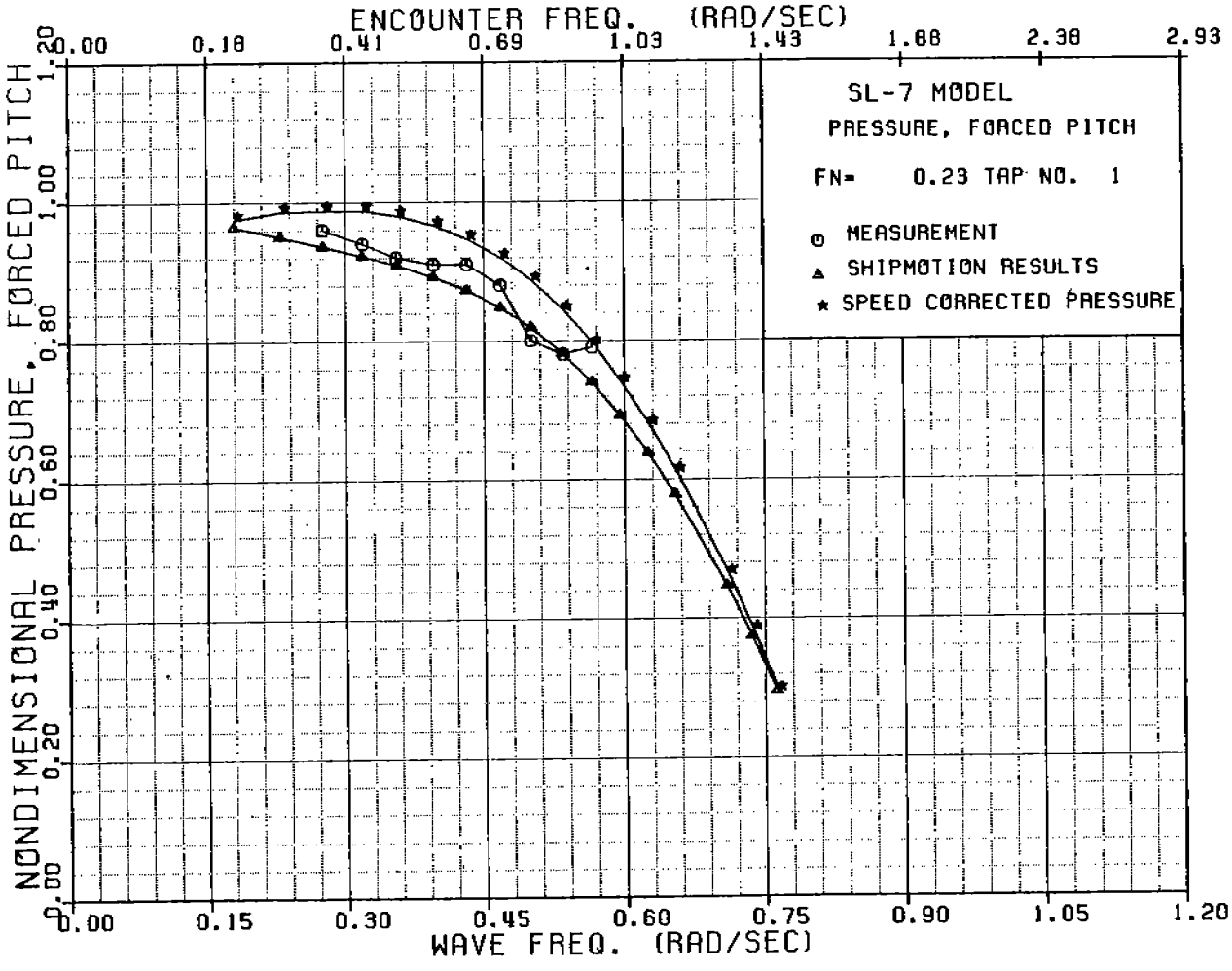

FIGURE A-16: SL-7 NONDIMENSIONAL PRESSURE DUE TO FORCED PITCH AT TAP 1, F_n=0.23

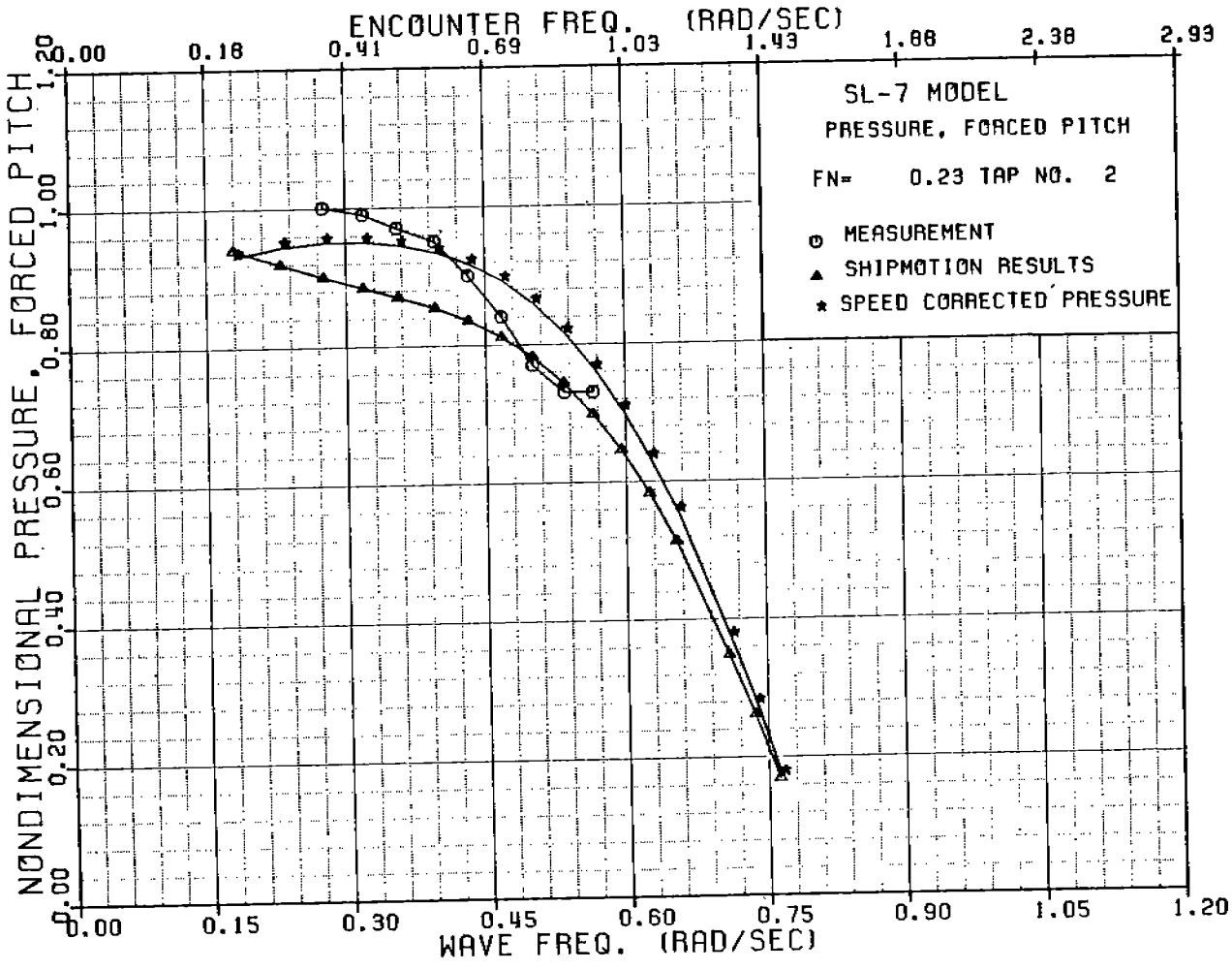

FIGURE A-17: SL-7 NONDIMENSIONAL PRESSURE DUE TO FORCED PITCH AT TAP 2, F_n=0.23

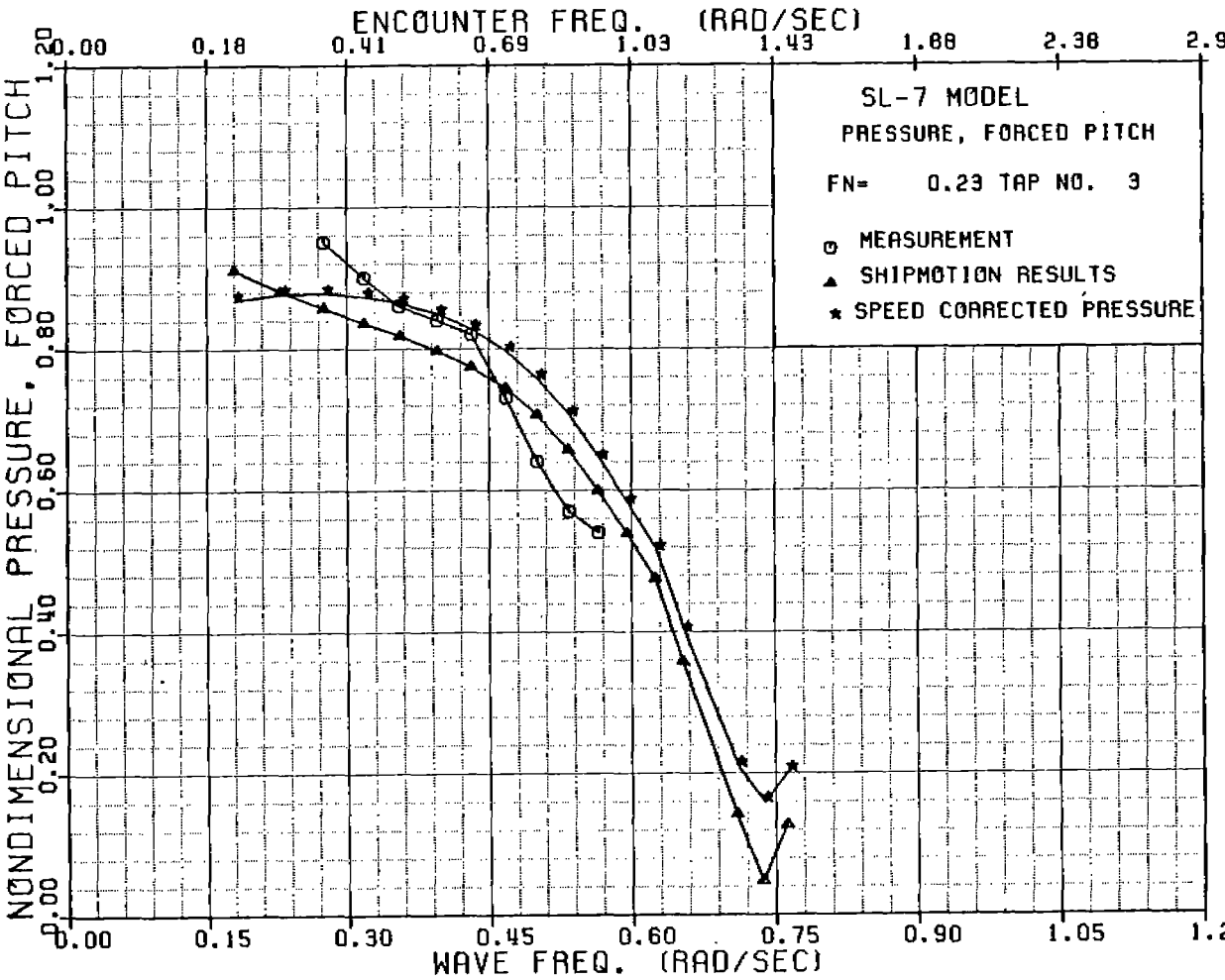

FIGURE A-18: SL-7 NONDIMENSIONAL PRESSURE DUE TO FORCED PITCH AT TAP 3, F

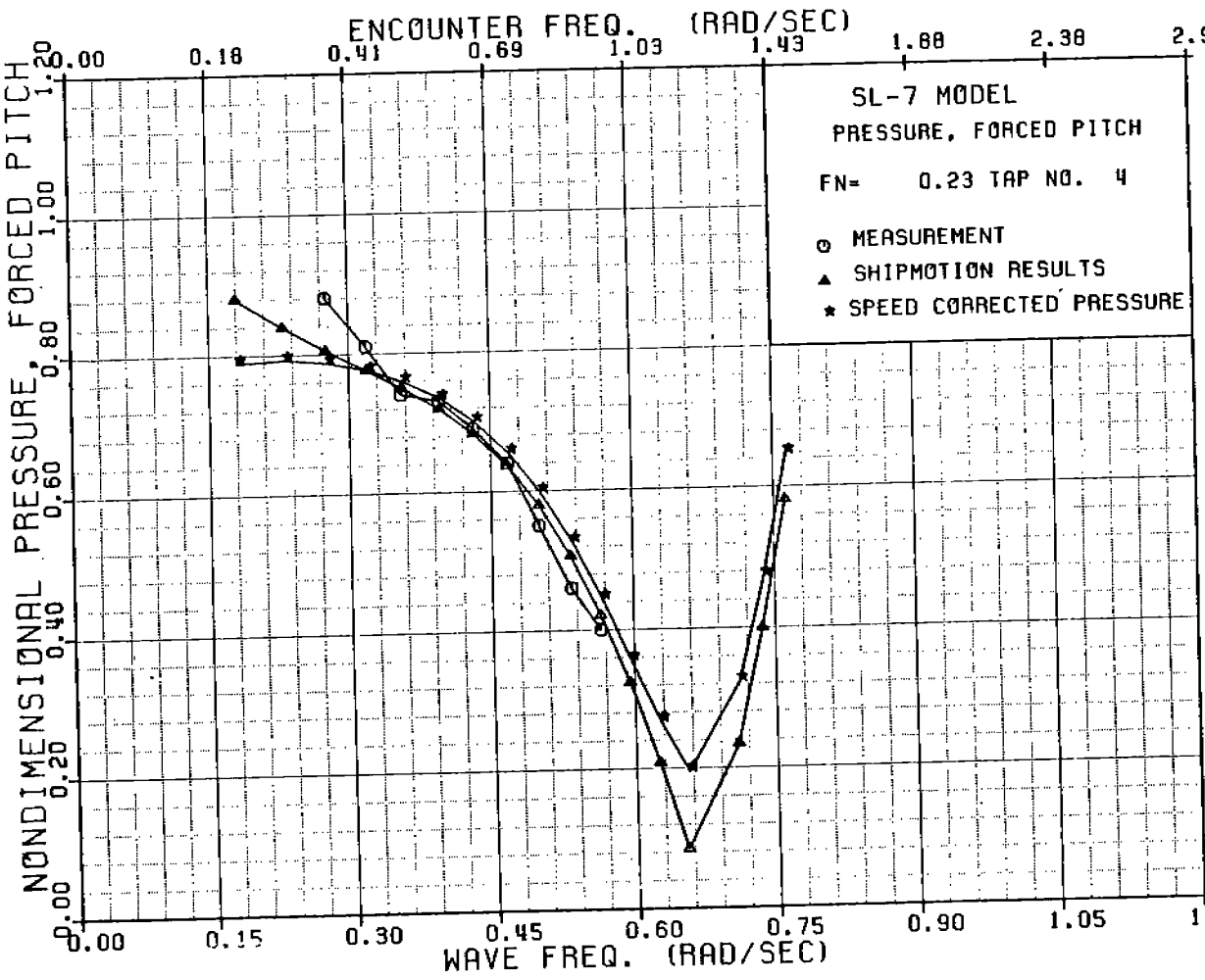

FIGURE A-19: SL-7 NONDIMENSIONAL PRESSURE DUE TO FORCED PITCH AT TAP 4, F

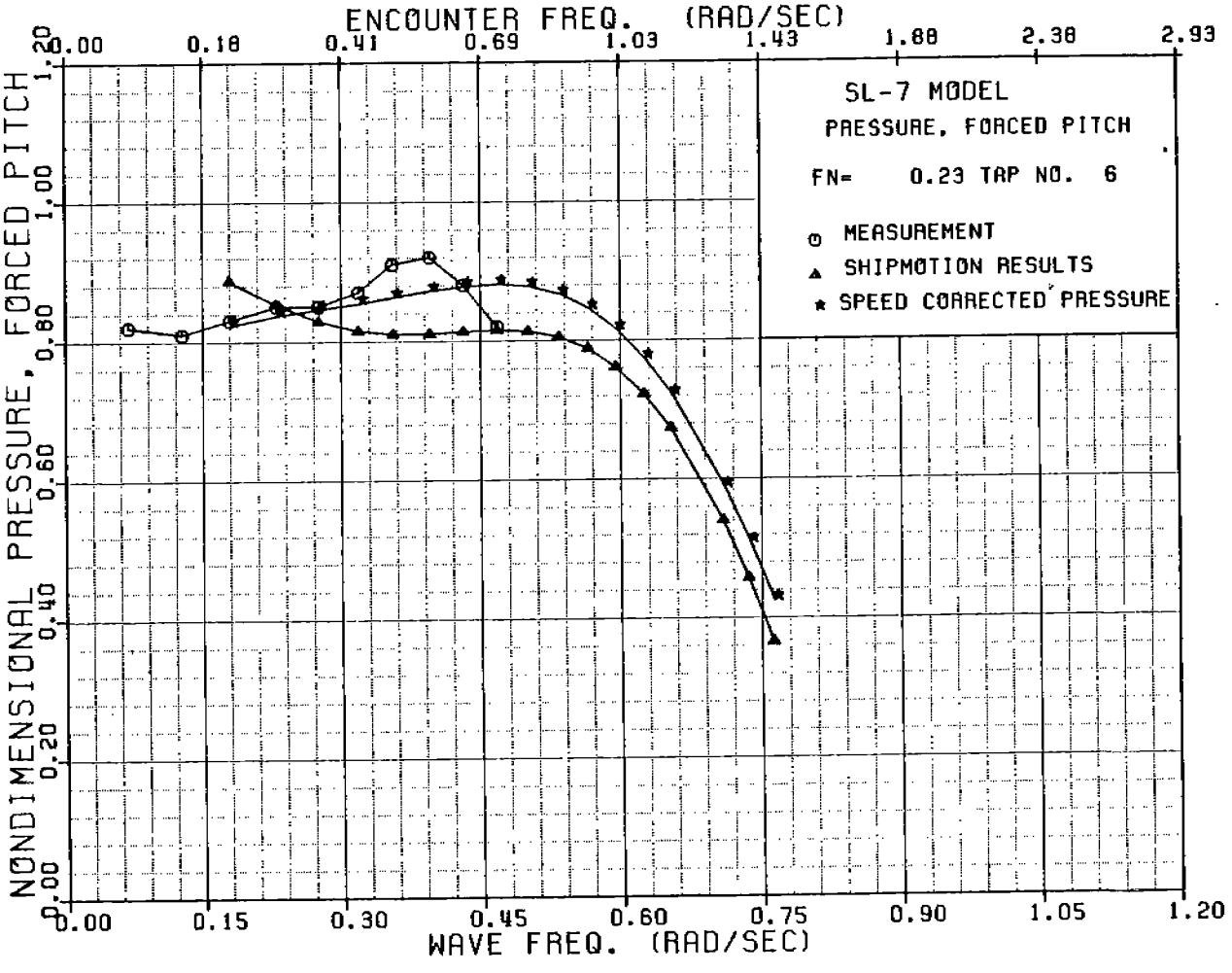

FIGURE A-20: SL-7 NONDIMENSIONAL PRESSURE DUE TO FORCED PITCH AT TAP 6, F_n=0.23

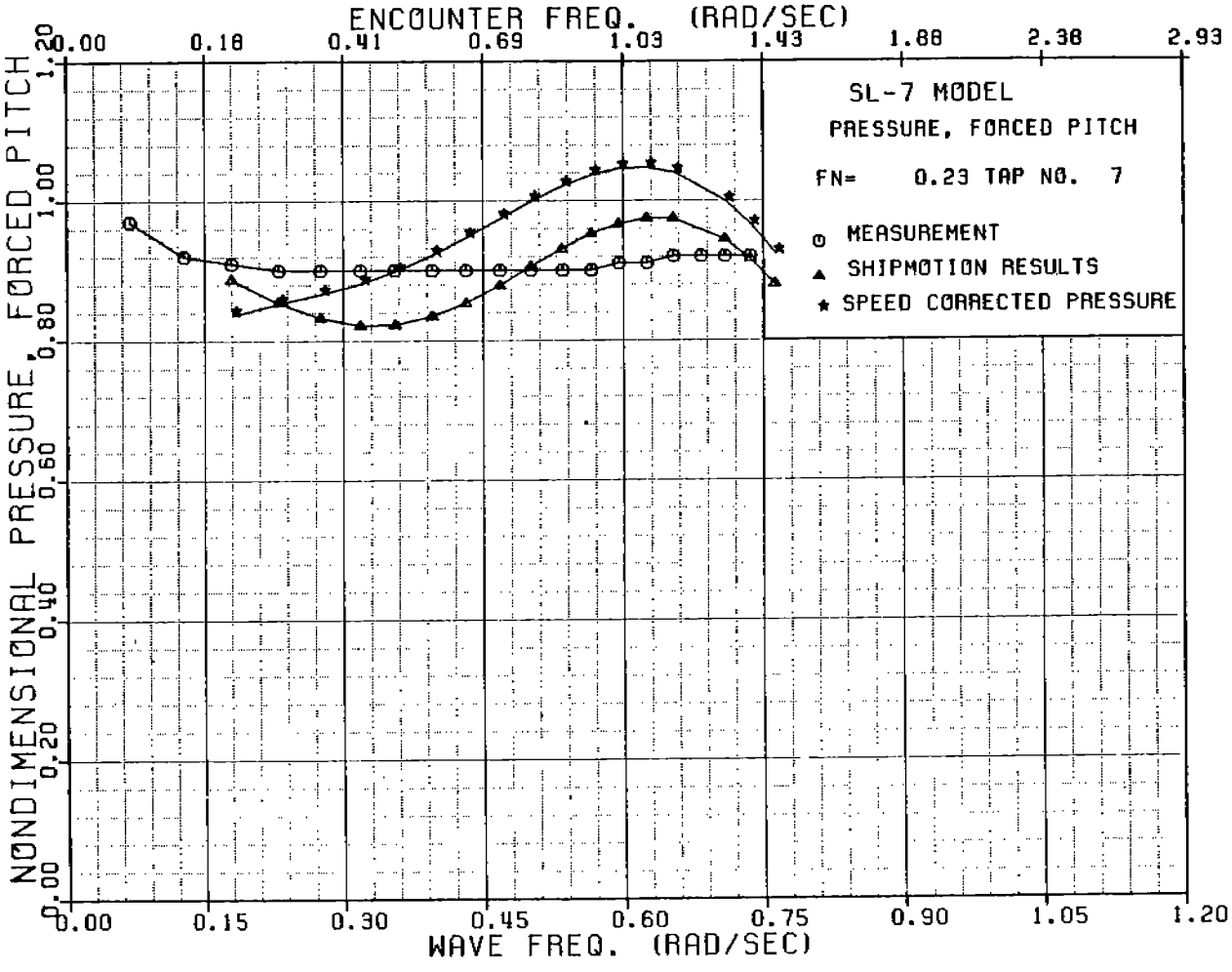

FIGURE A-21: SL-7 NONDIMENSIONAL PRESSURE DUE TO FORCED PITCH AT TAP 7, F_n=0.23

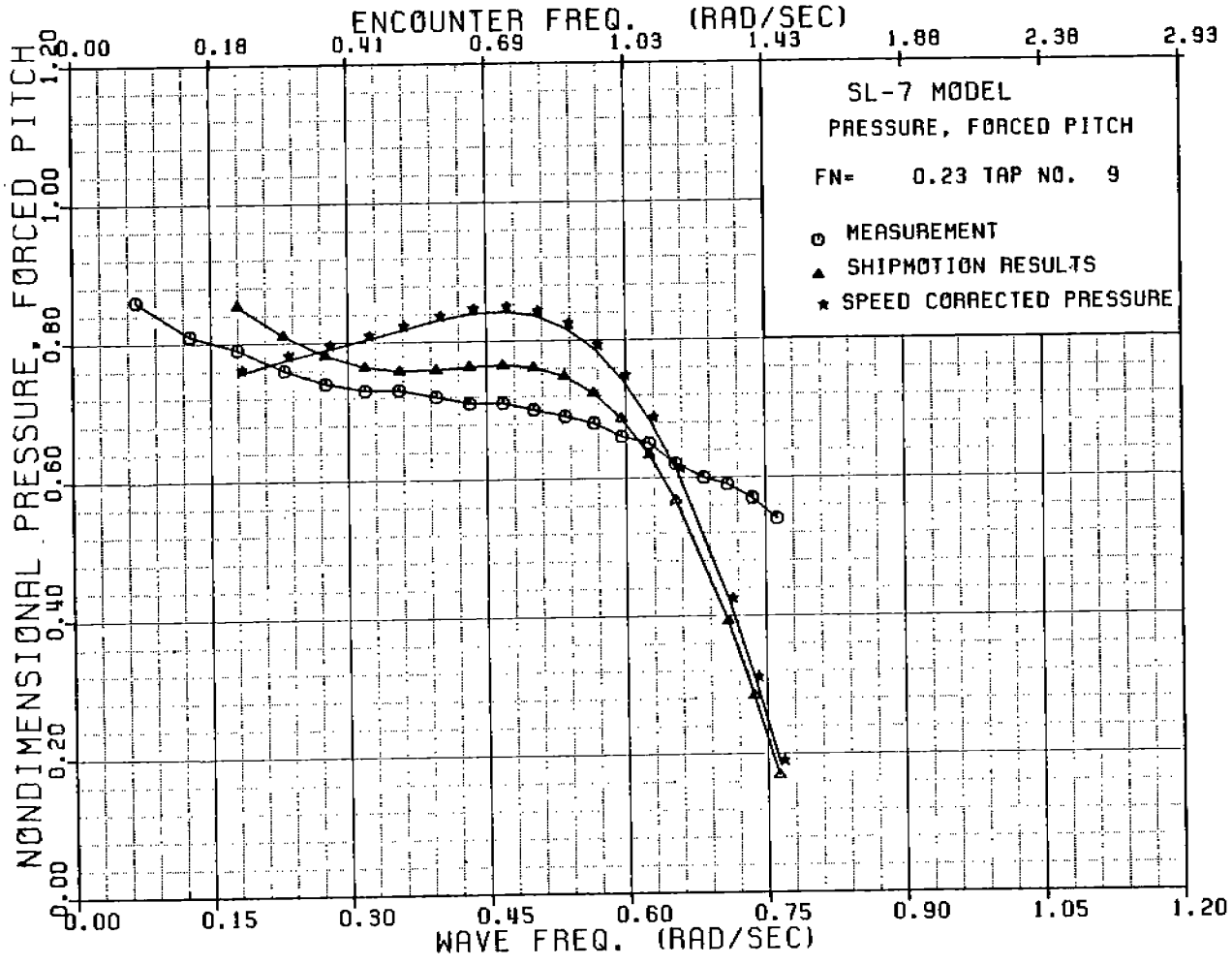

FIGURE A-22: SL-7 NONDIMENSIONAL PRESSURE DUE TO FORCED PITCH AT TAP 9, F_n=0.23

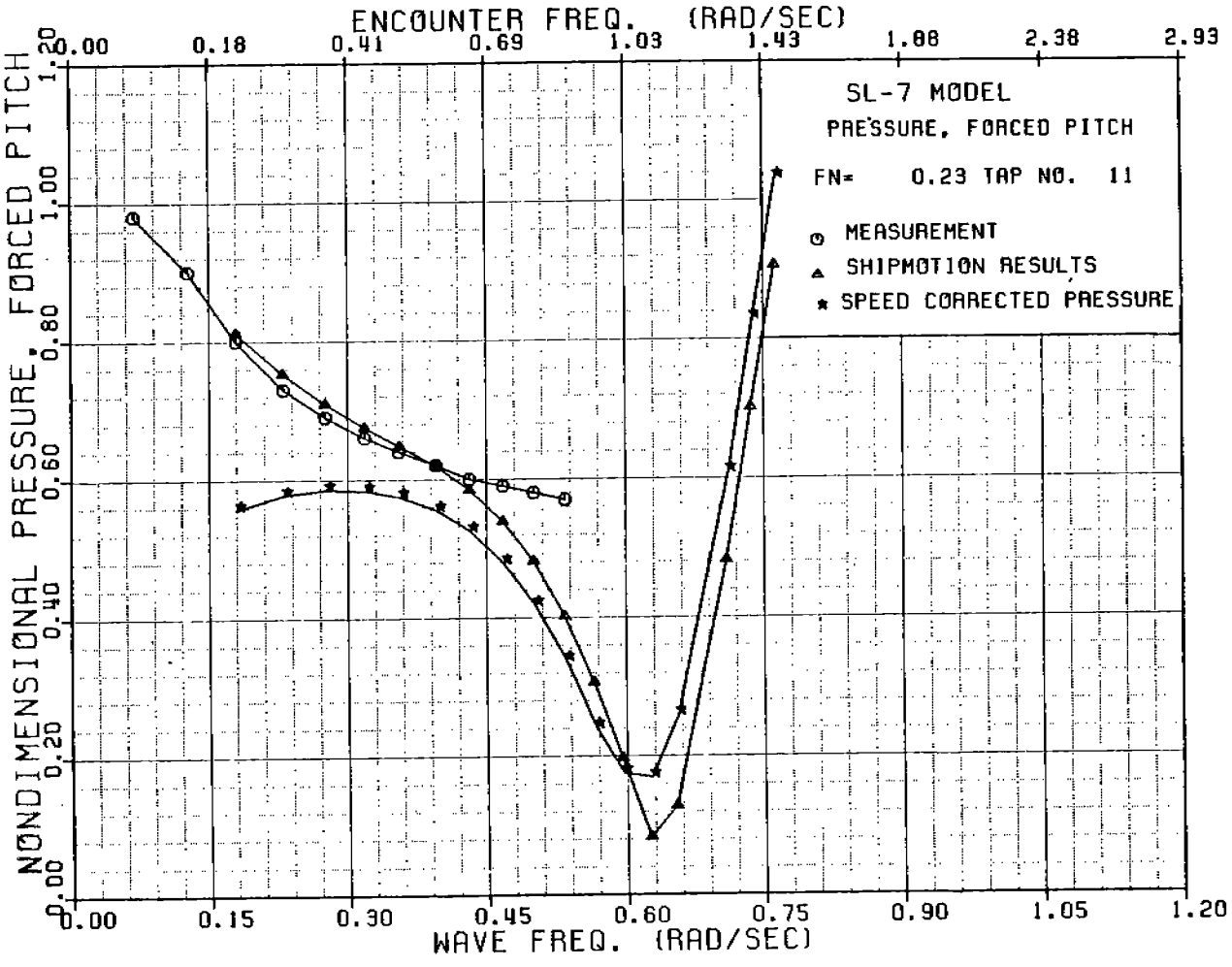

FIGURE A-23: SL-7 NONDIMENSIONAL PRESSURE DUE TO FORCED PITCH AT TAP 11, F_n=0.23

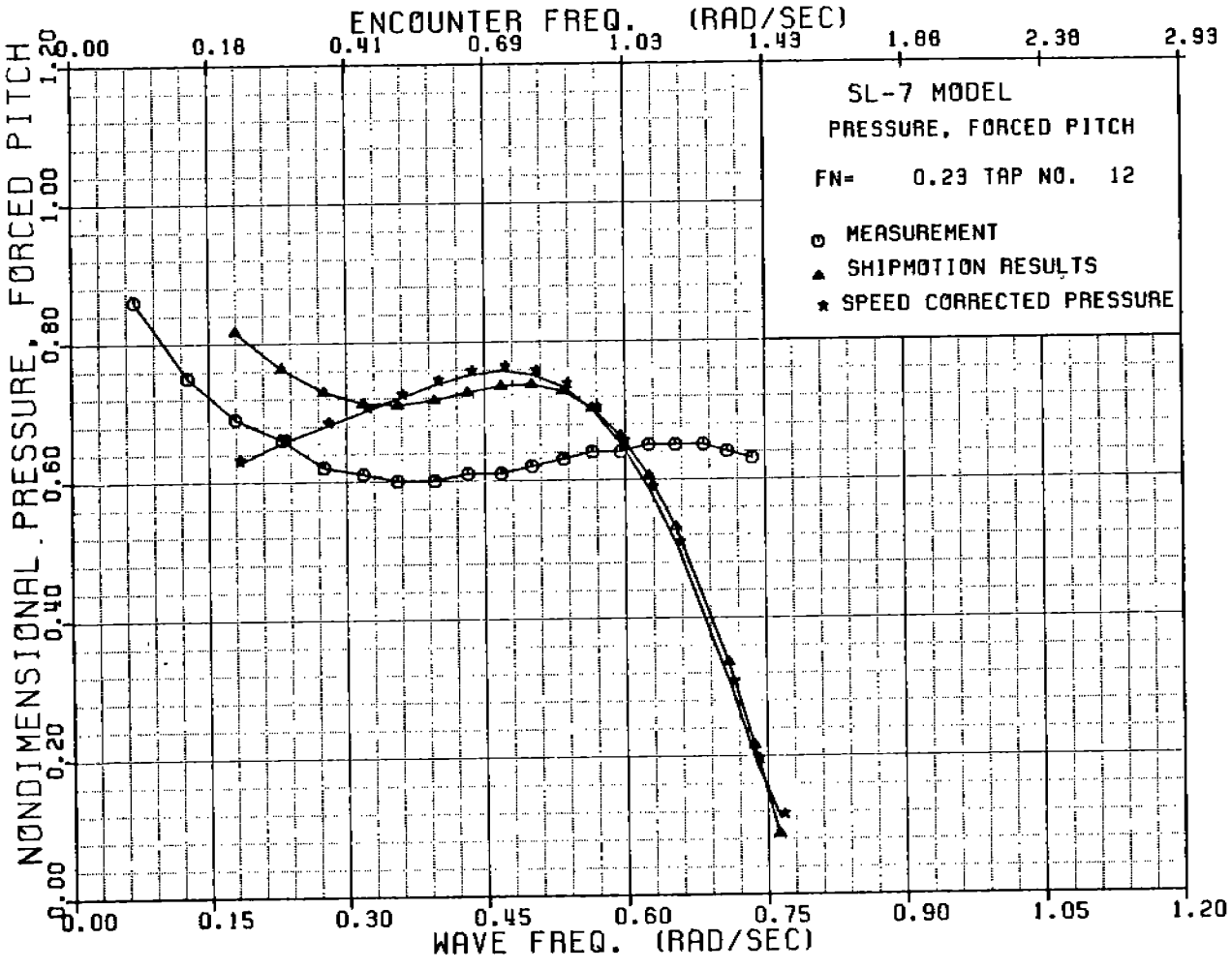

FIGURE A-24: SL-7 NONDIMENSIONAL PRESSURE DUE TO FORCED PITCH AT TAP 12, F_n=0.23

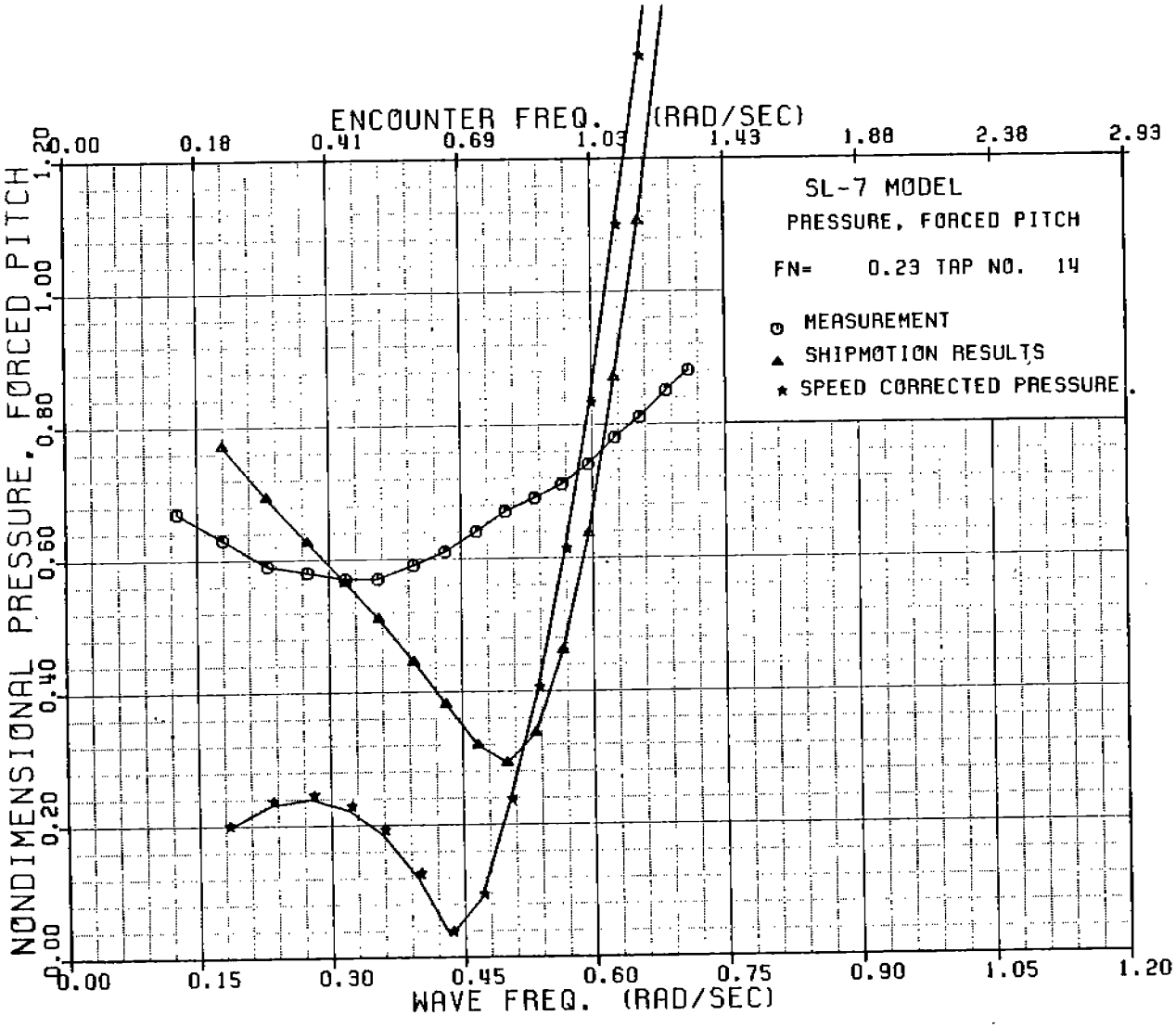

FIGURE A-25: SL-7 NONDIMENSIONAL PRESSURE DUE TO FORCED PITCH AT TAP 14, F_n=0.23

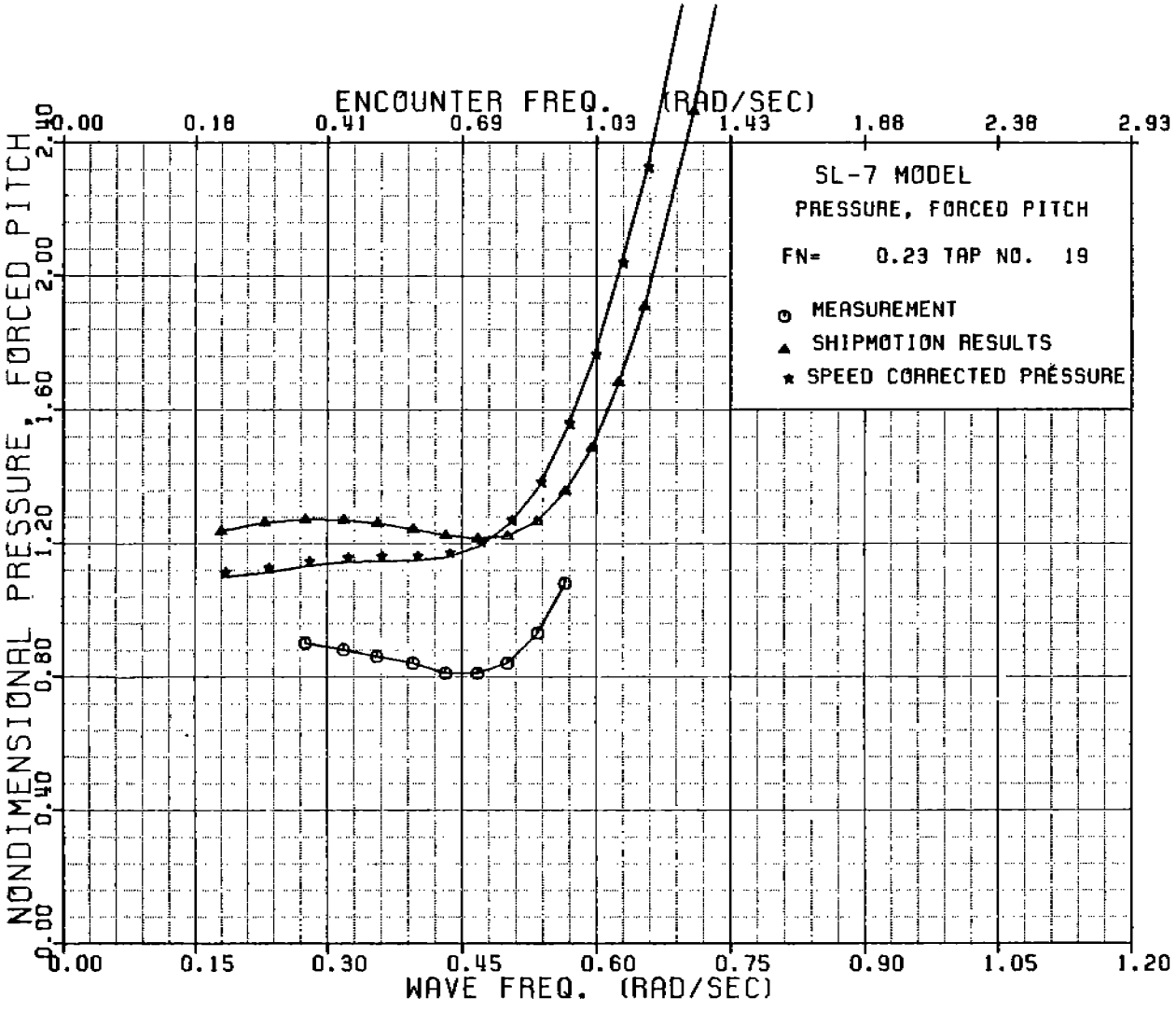

FIGURE A-26: SL-7 NONDIMENSIONAL PRESSURE DUE TO FORCED PITCH AT TAP 19, F_n=0.23

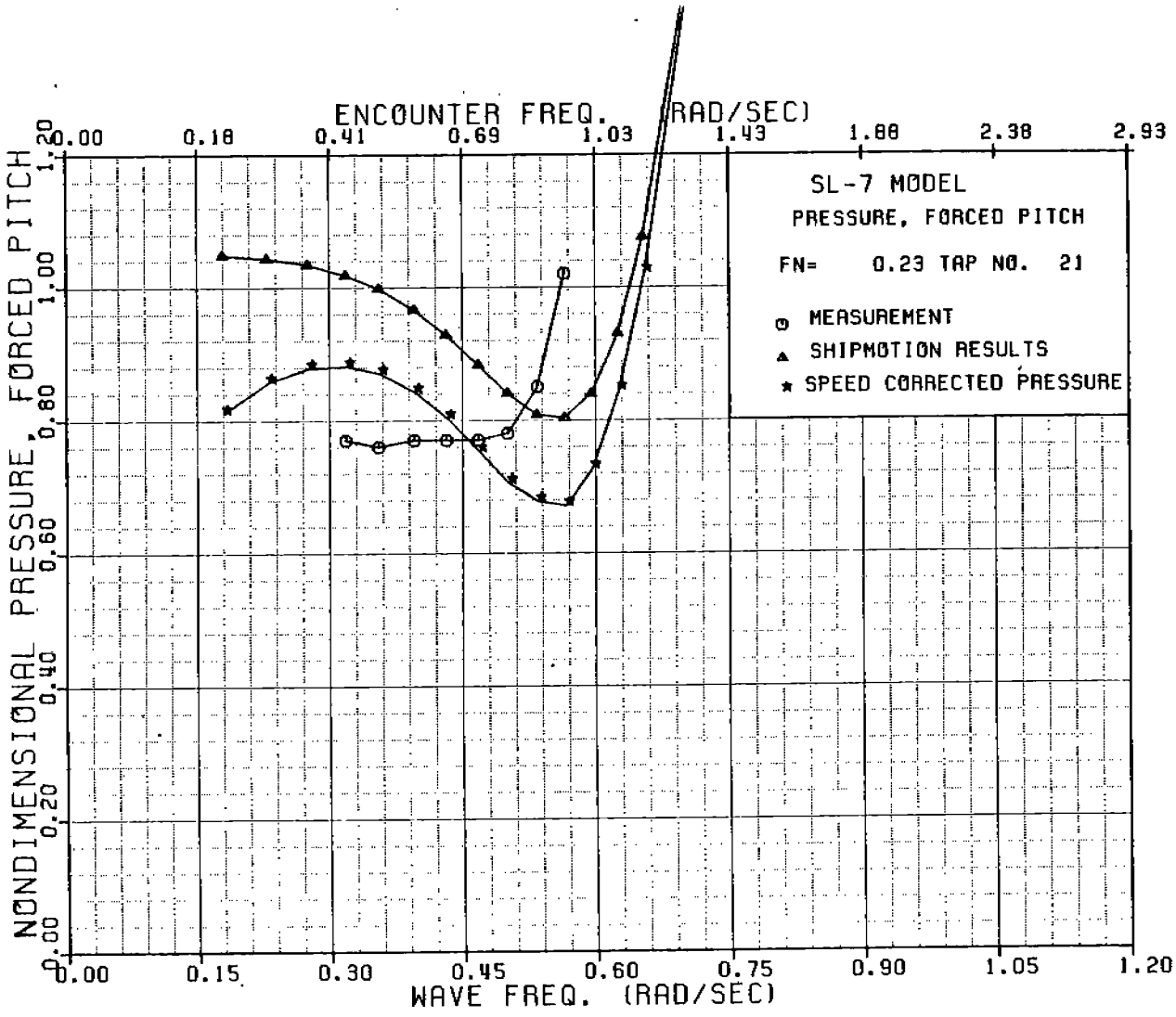

FIGURE A-27: SL-7 NONDIMENSIONAL PRESSURE DUE TO FORCED PITCH AT TAP 21, F_n=0.23

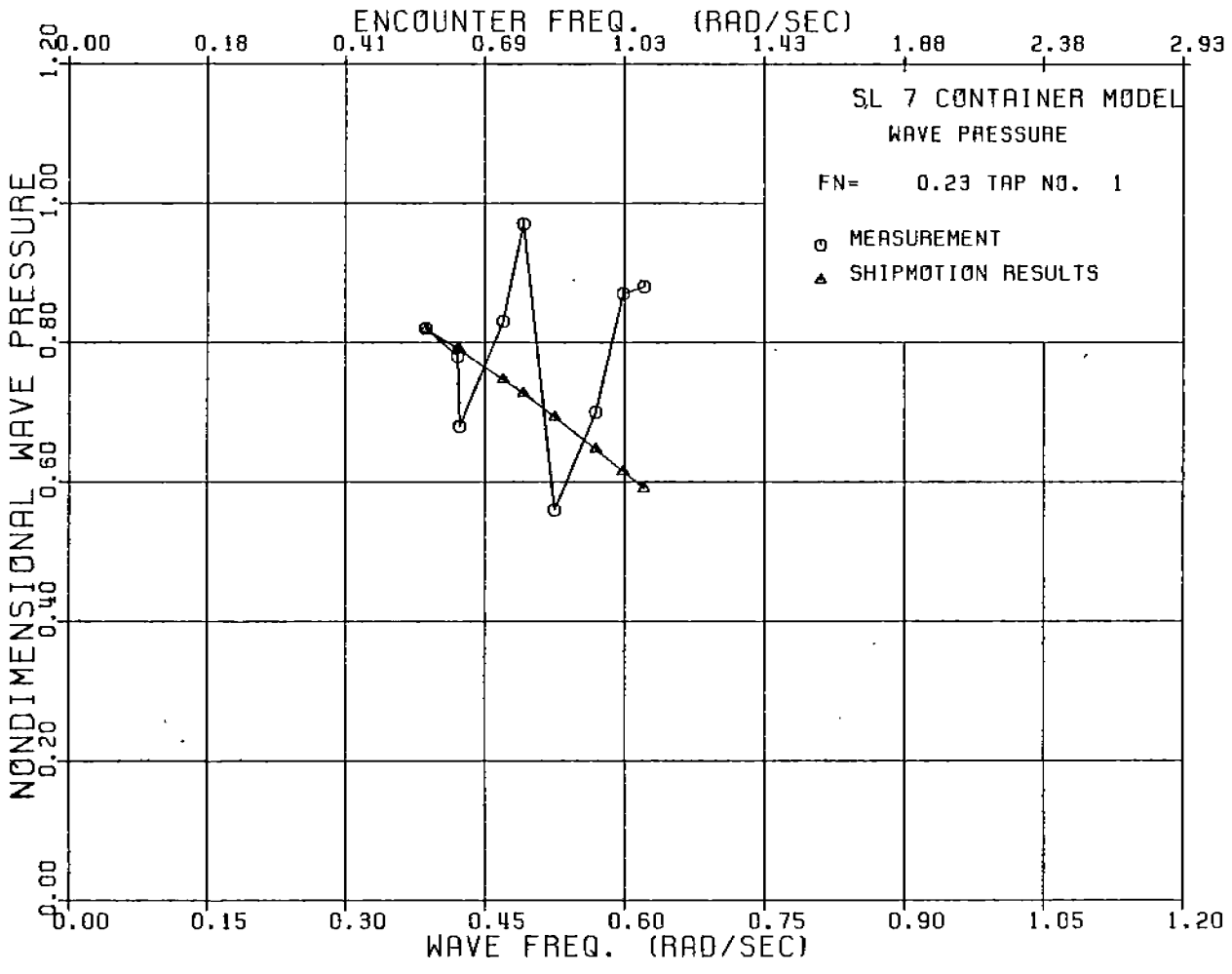

FIGURE A-28: SL-7 NONDIMENSIONAL WAVE PRESSURE AT TAP 1, F_n=0.23

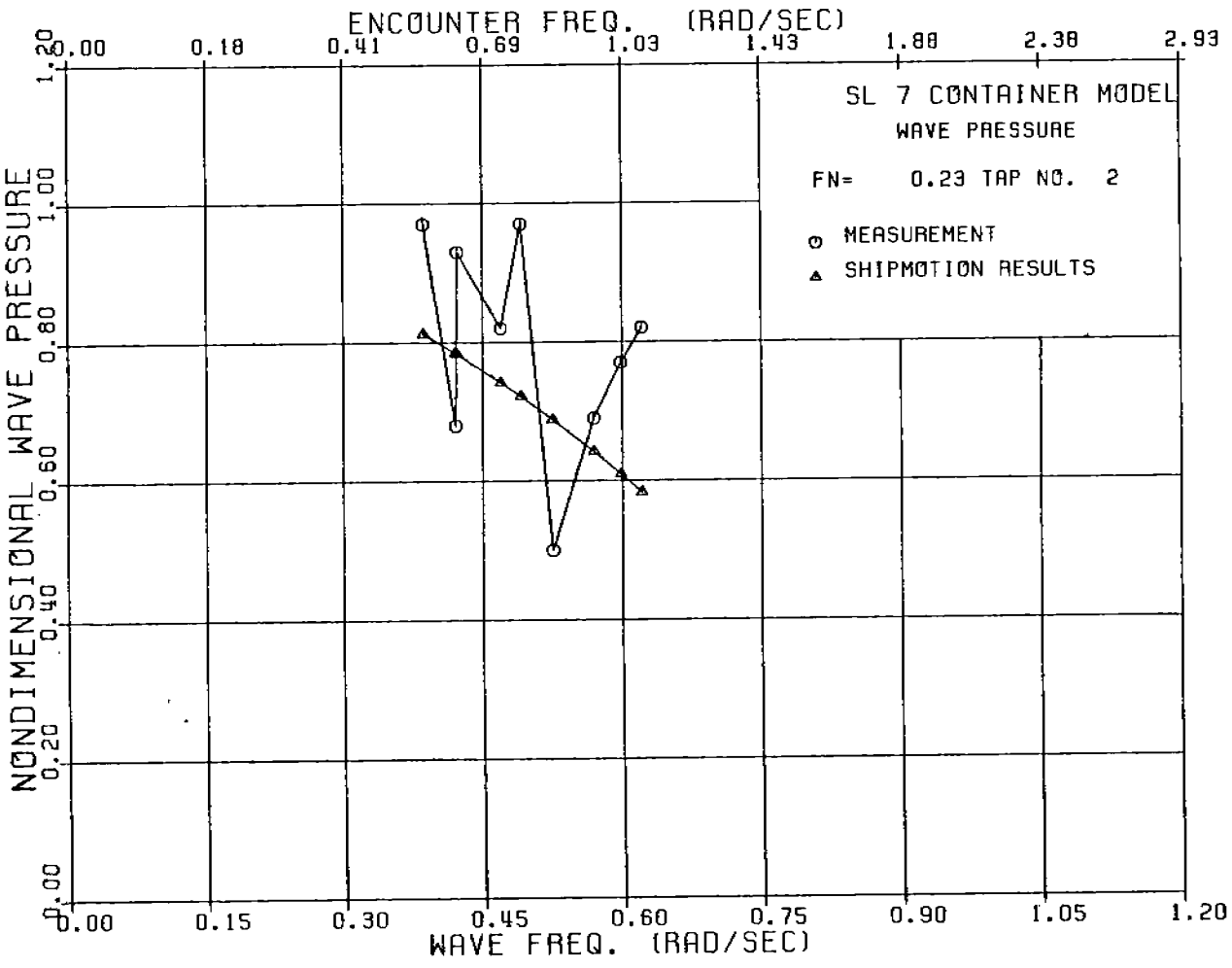

FIGURE A-29: SL-7 NONDIMENSIONAL WAVE PRESSURE AT TAP 2, F_n=0.23

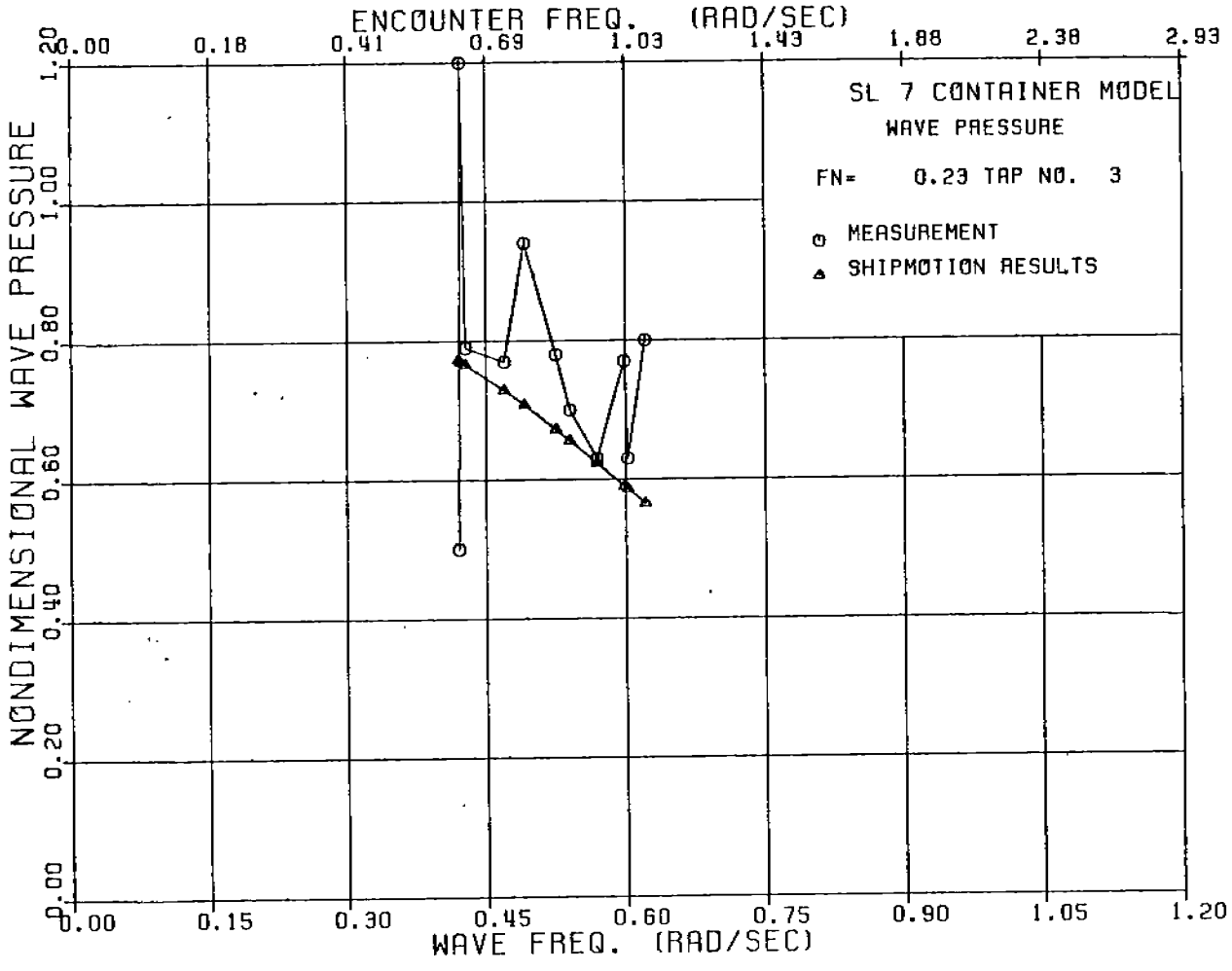

FIGURE A-30: SL-7 NONDIMENSIONAL WAVE PRESSURE AT TAP 3, F_n=0.23

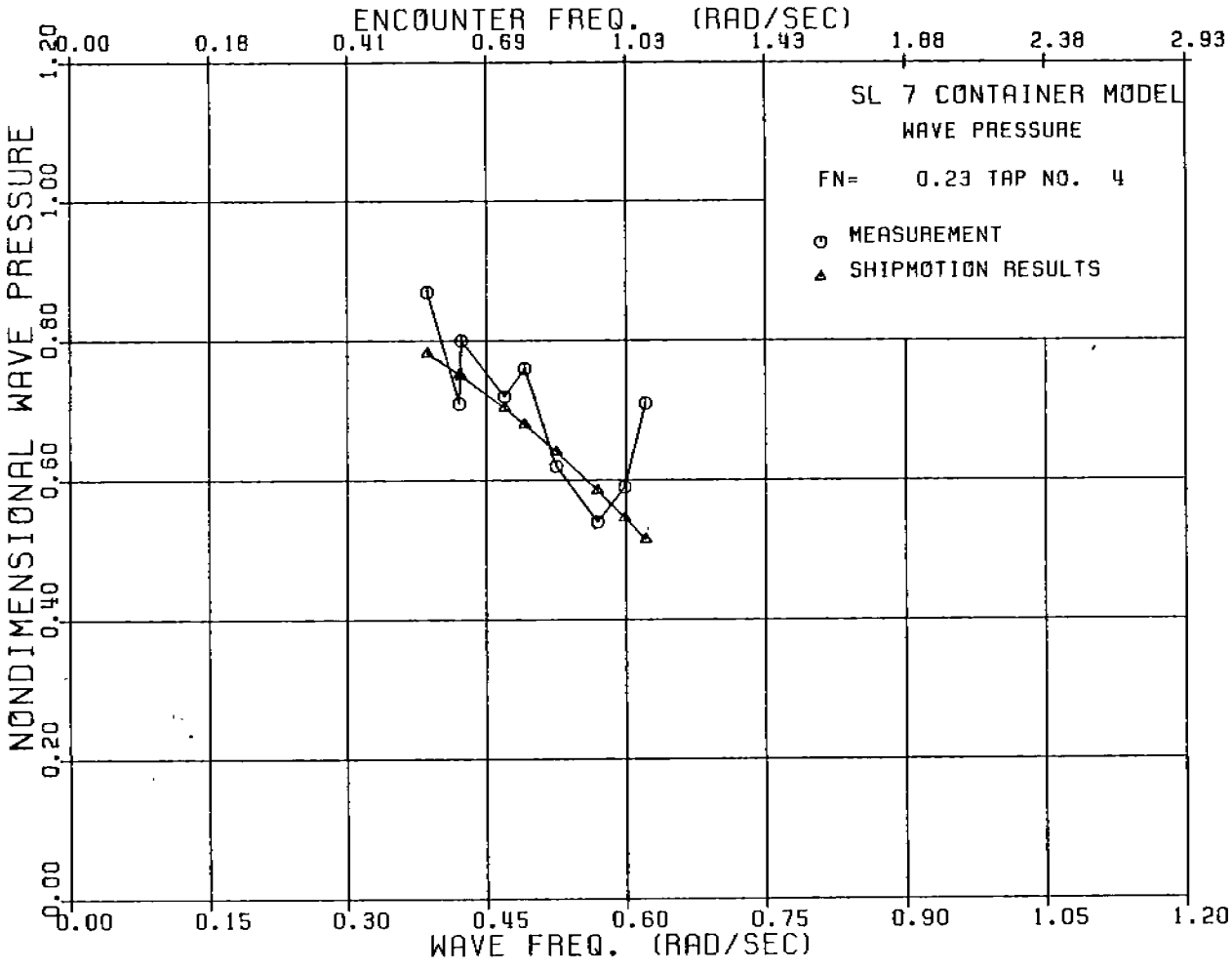

FIGURE A-31: SL-7 NONDIMENSIONAL WAVE PRESSURE AT TAP 4, F_n=0.23

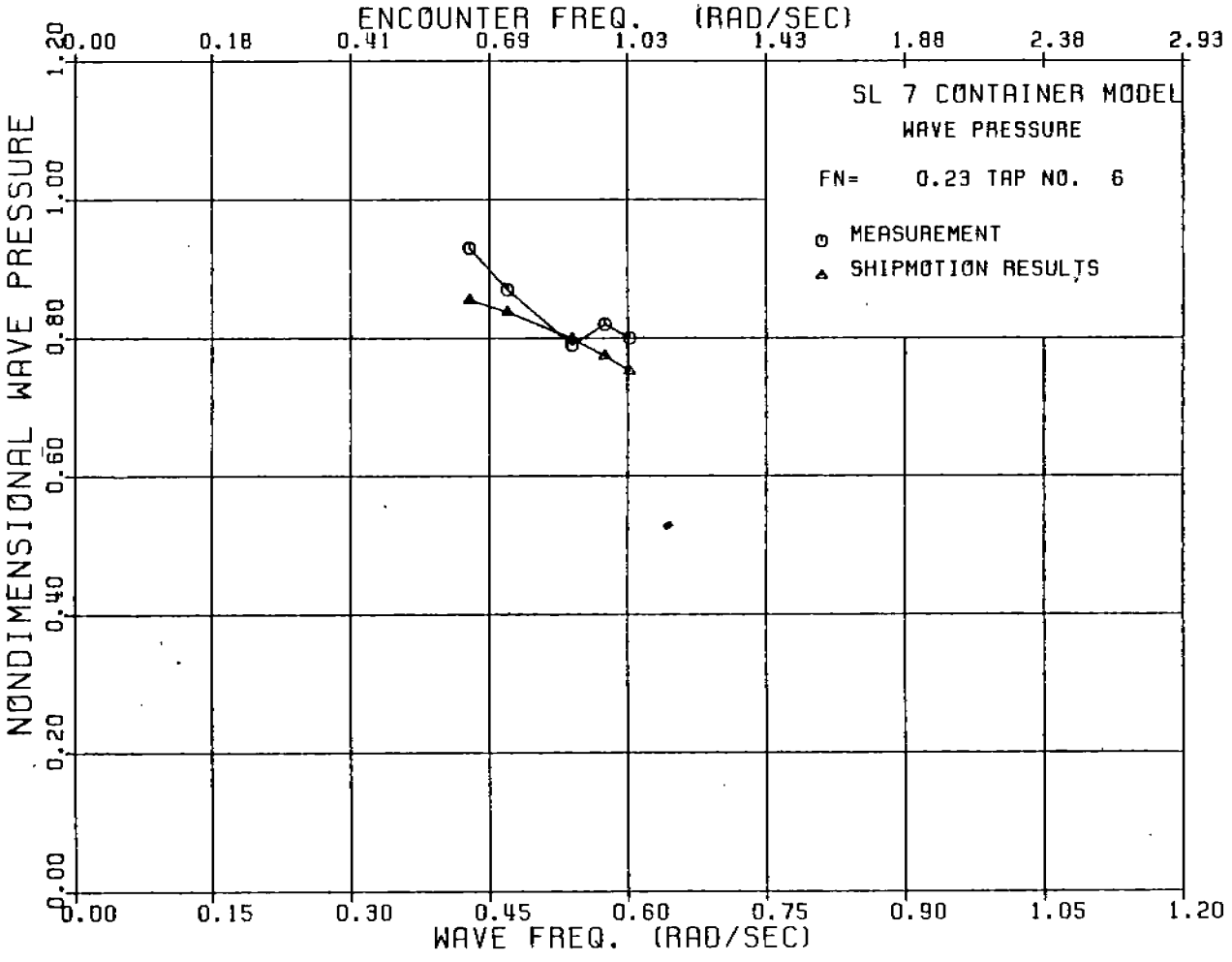

FIGURE A-32: SL-7 NONDIMENSIONAL WAVE PRESSURE AT TAP 6, F_n=0.23

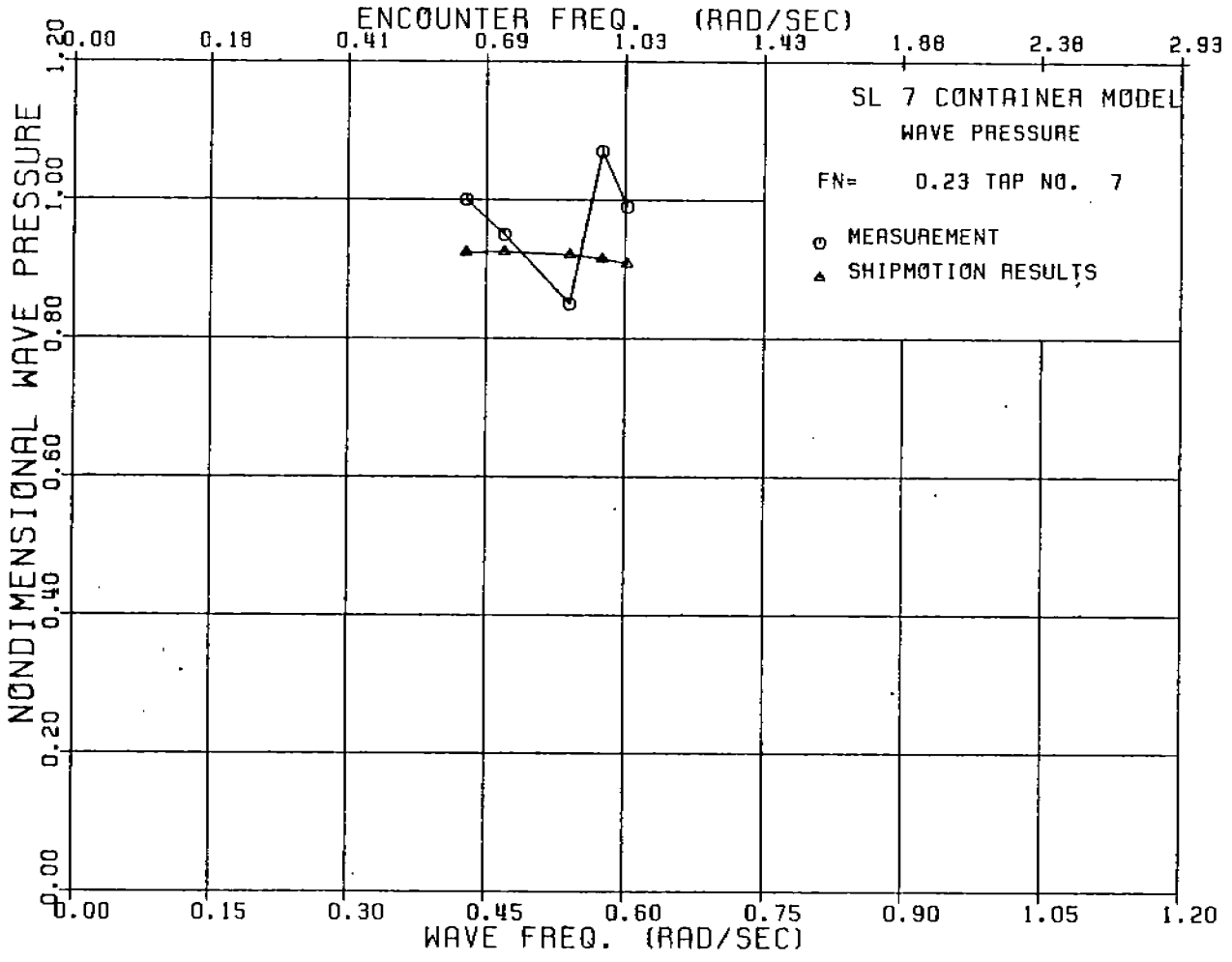

FIGURE A-33: SL-7 NONDIMENSIONAL WAVE PRESSURE AT TAP 7, F_n=0.23

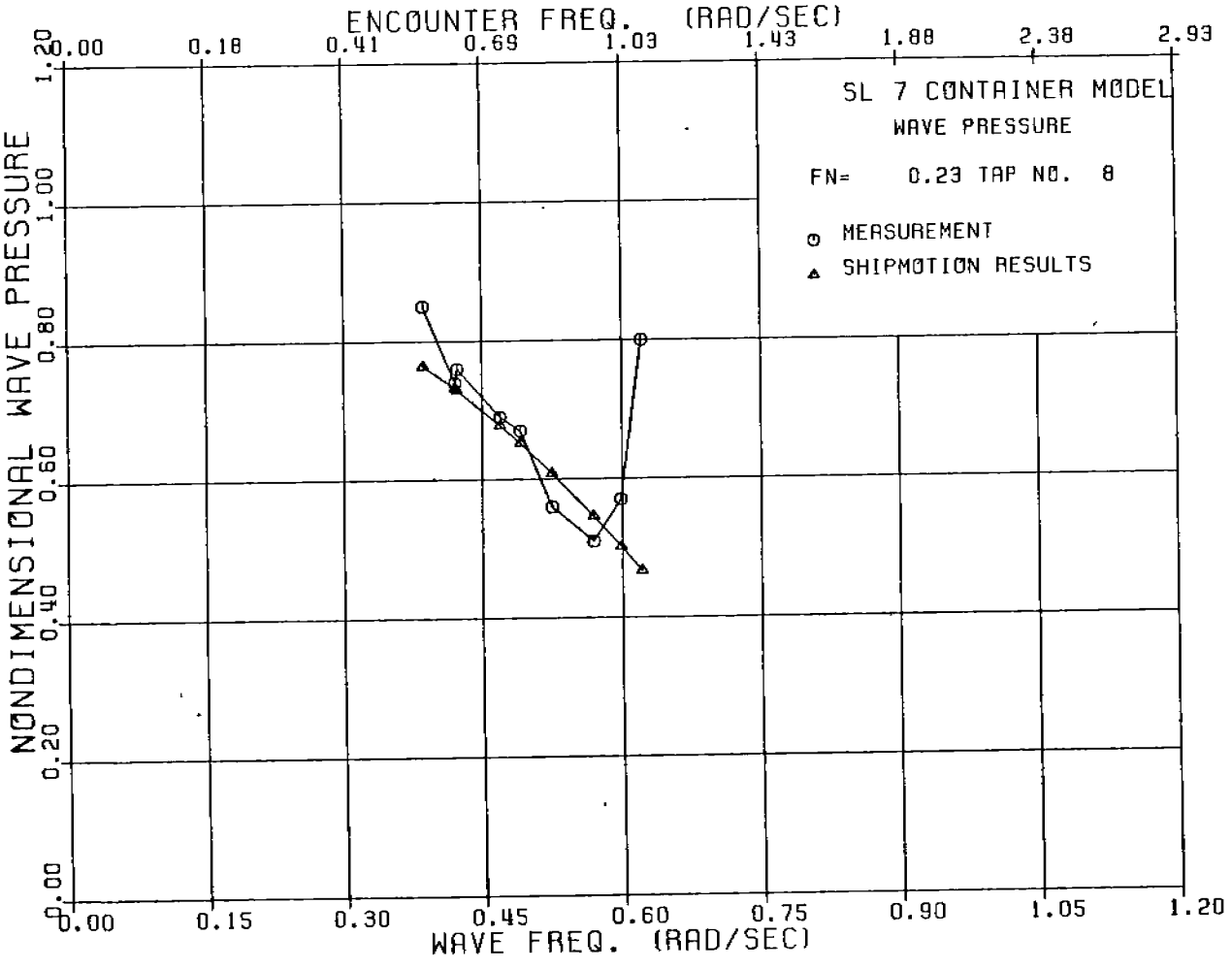

FIGURE A-34: SL-7 NONDIMENSIONAL WAVE PRESSURE AT TAP 8, F_n=0.23

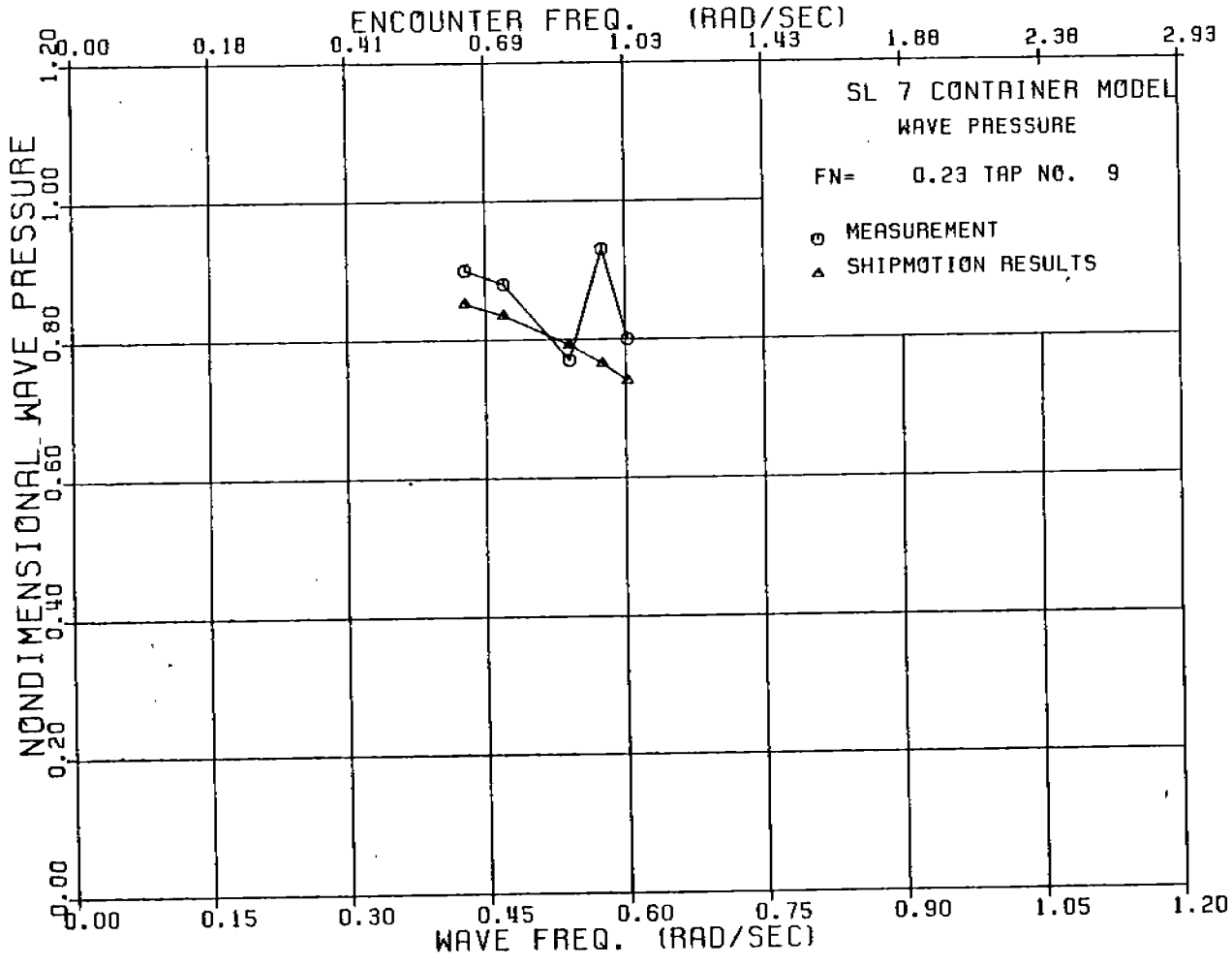

FIGURE A-35: SL-7 NONDIMENSIONAL WAVE PRESSURE AT TAP 9, F_n=0.23

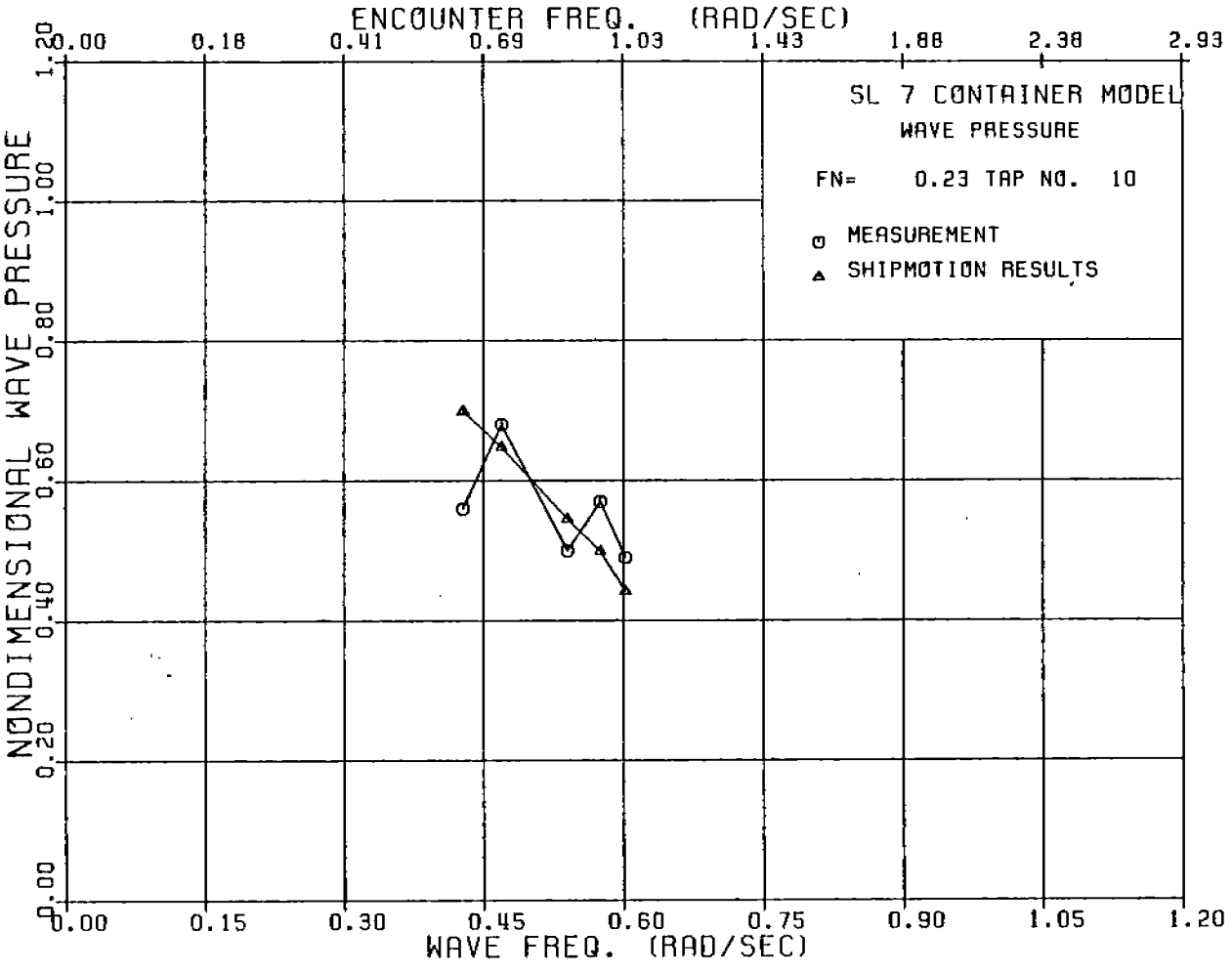

FIGURE A-36: SL-7 NONDIMENSIONAL WAVE PRESSURE AT TAP 10, F_n=0.23

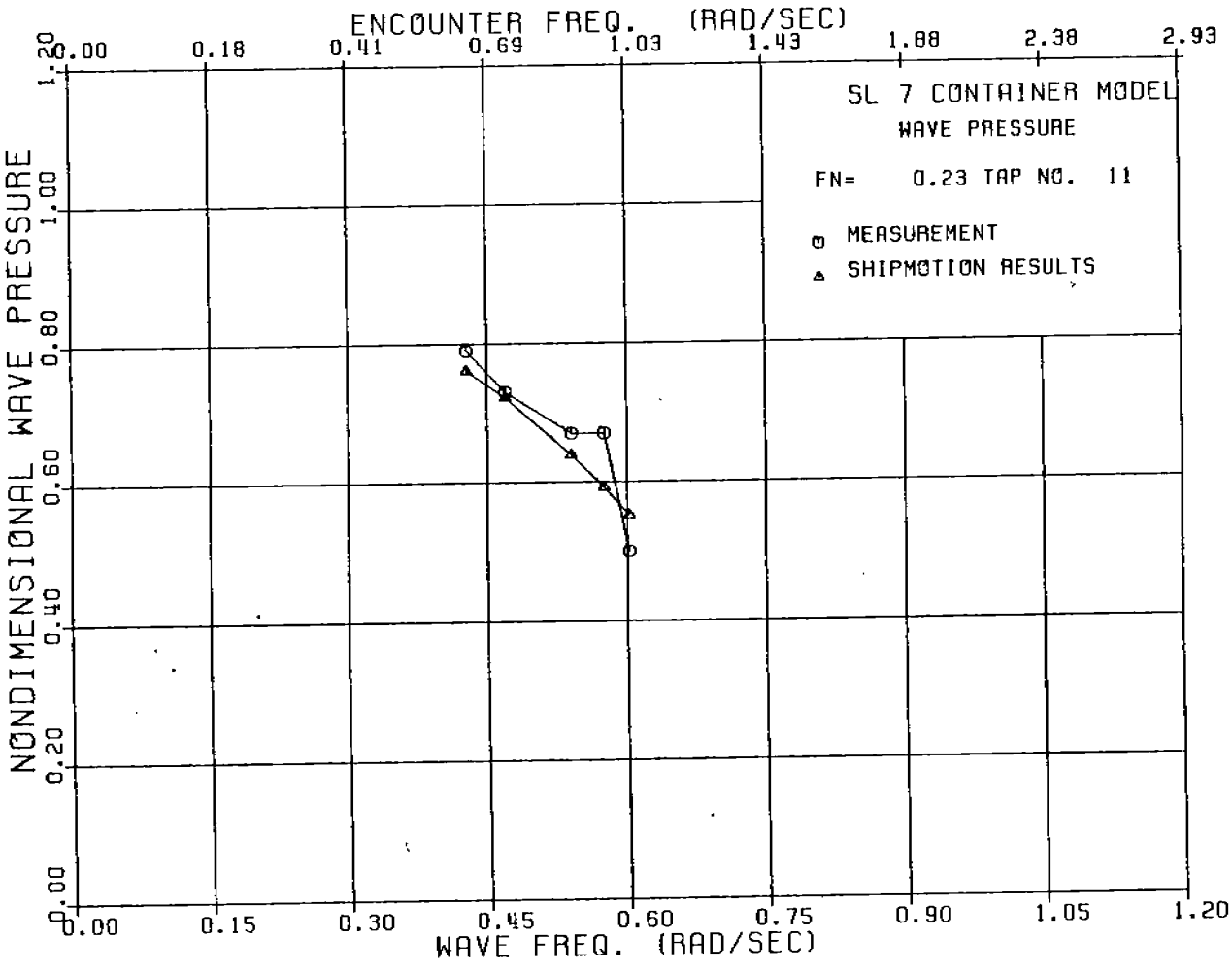

FIGURE A-37: SL-7 NONDIMENSIONAL WAVE PRESSURE AT TAP 11, F_n=0.23

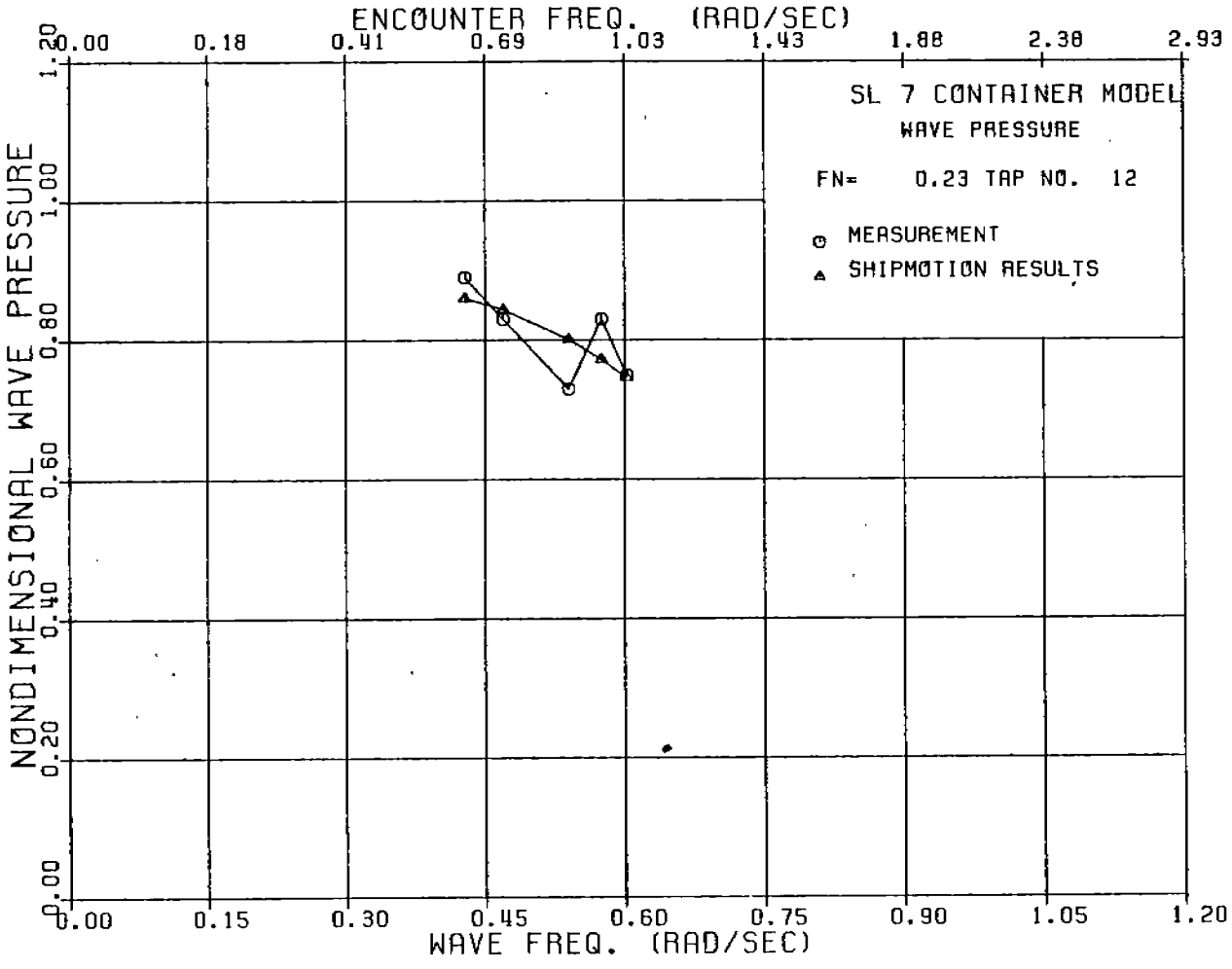

FIGURE A-38: SL-7 NONDIMENSIONAL WAVE PRESSURE AT TAP 12, F_n=0.23

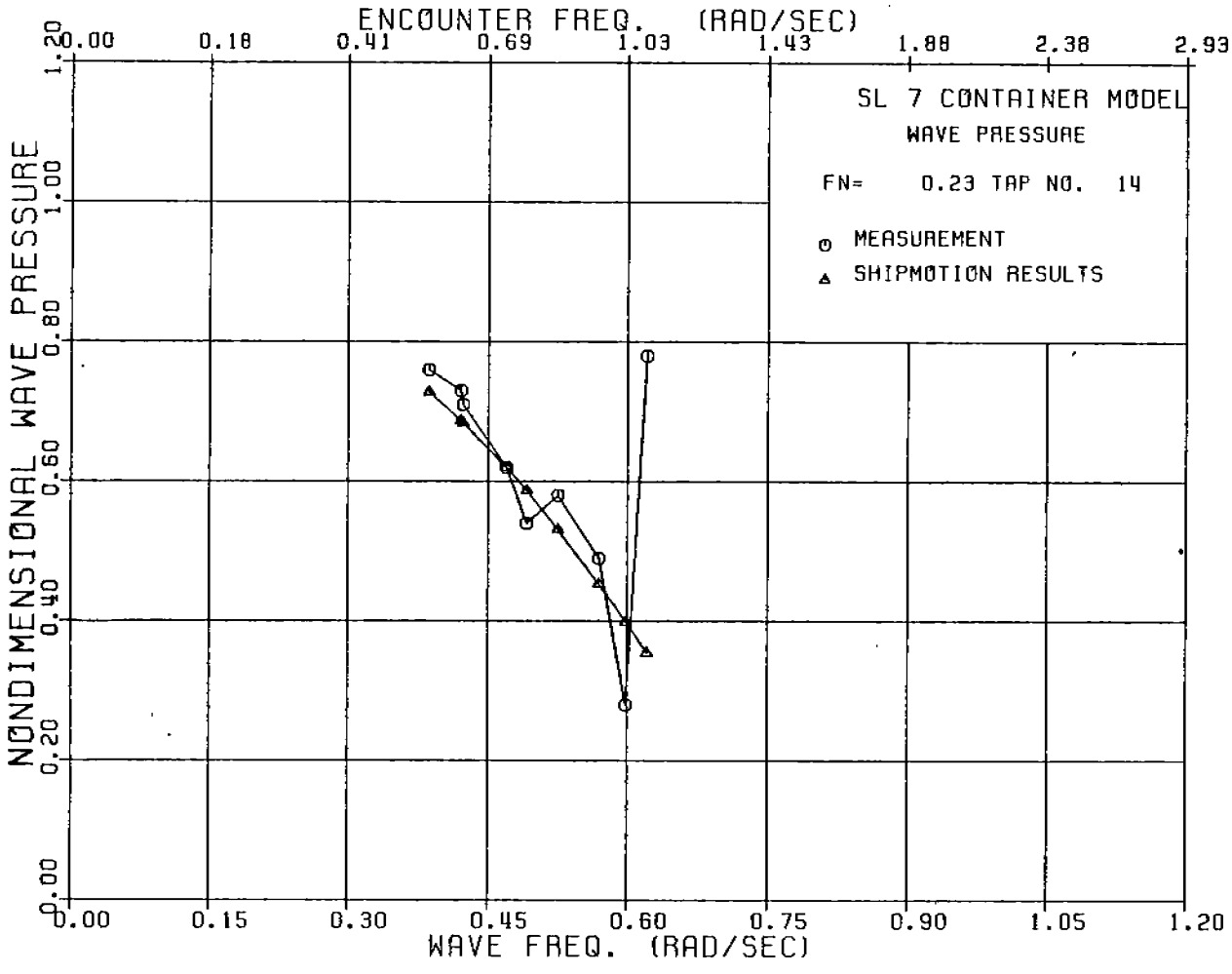

FIGURE A-39: SL-7 NONDIMENSIONAL WAVE PRESSURE AT TAP 14, F_n=0.23

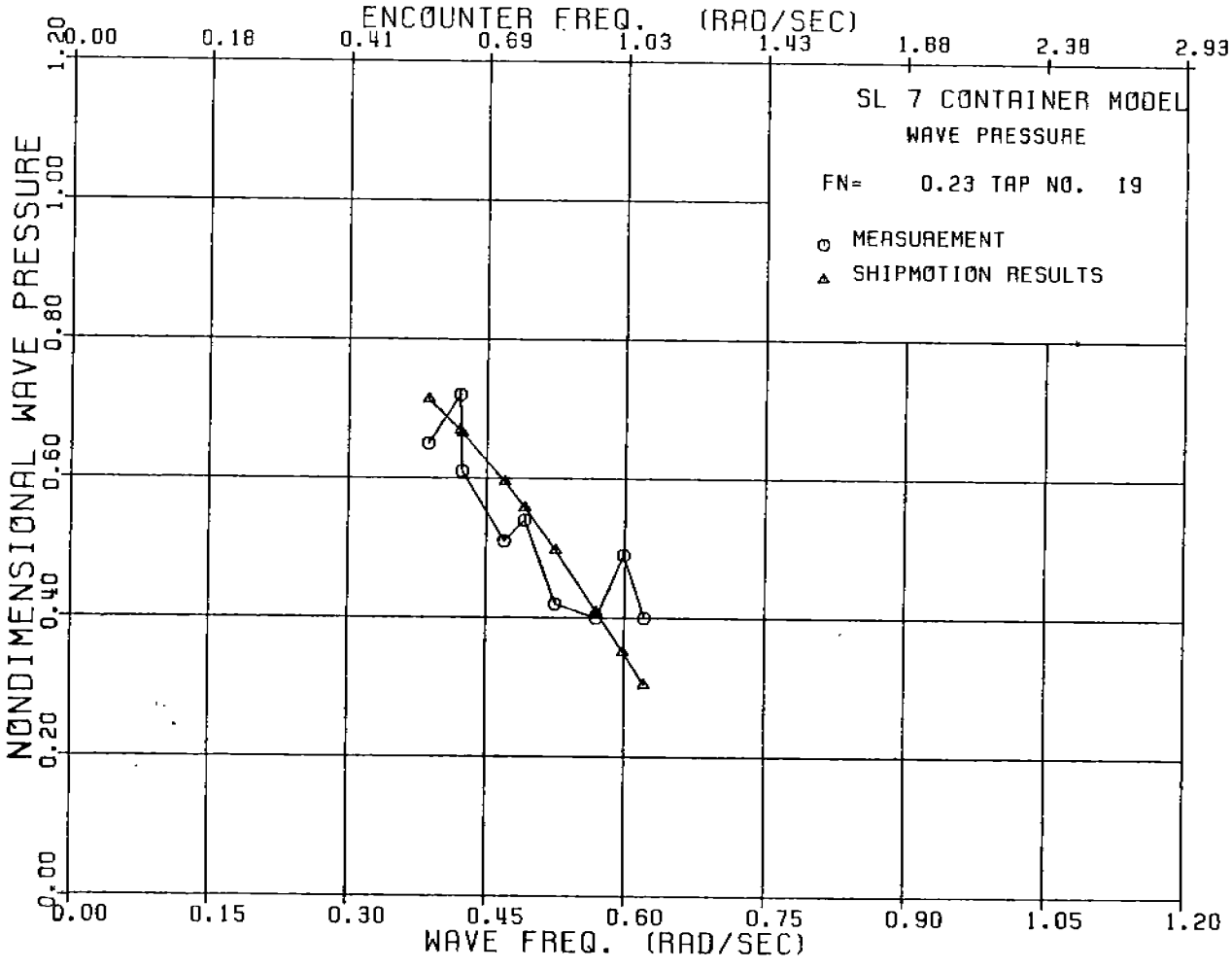

FIGURE A-40: SL-7 NONDIMENSIONAL WAVE PRESSURE AT TAP 19, F_n=0.23

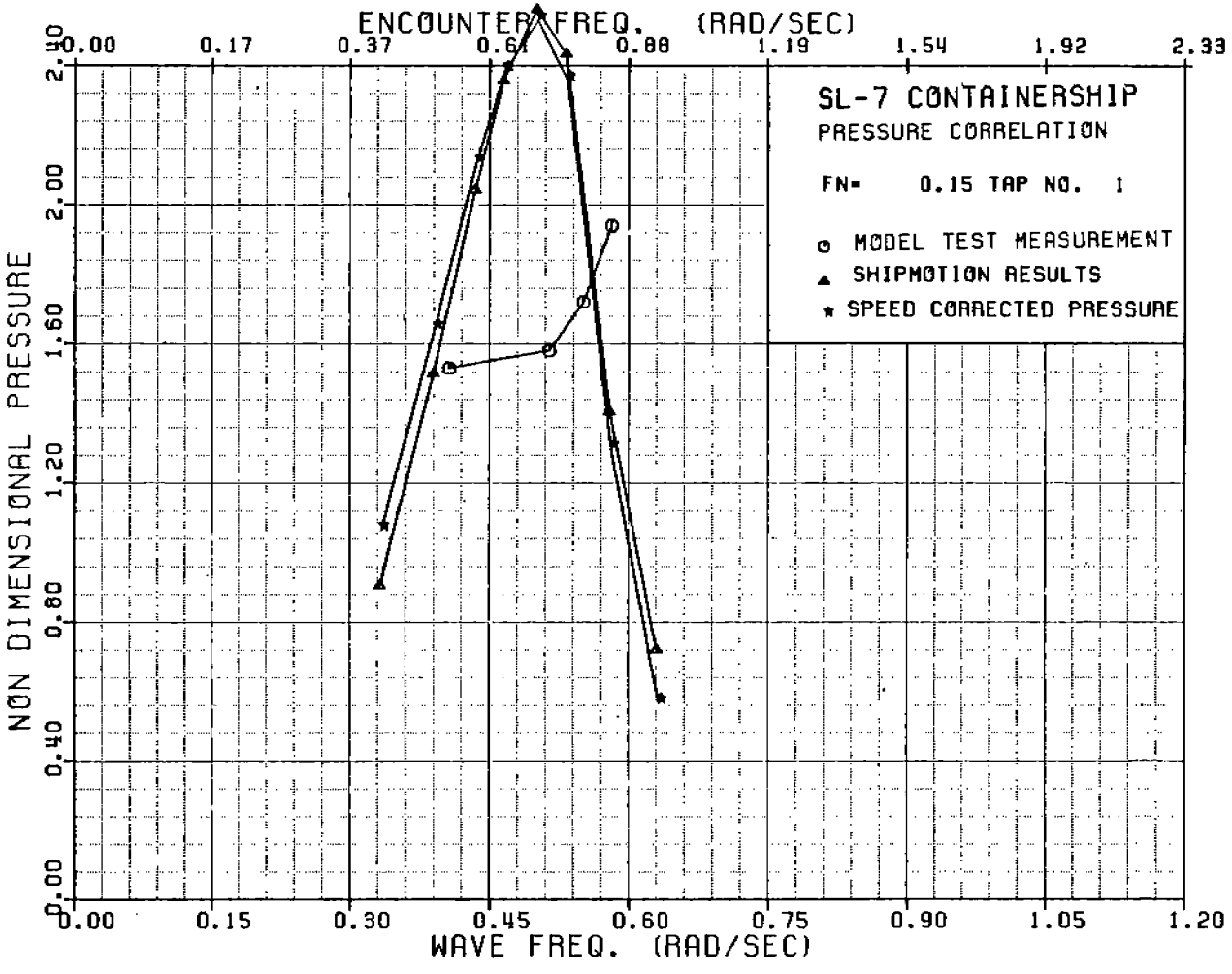

FIGURE A-41 SL-7 NONDIMENSIONAL PRESSURE AT TAP 1 , FN=0.15

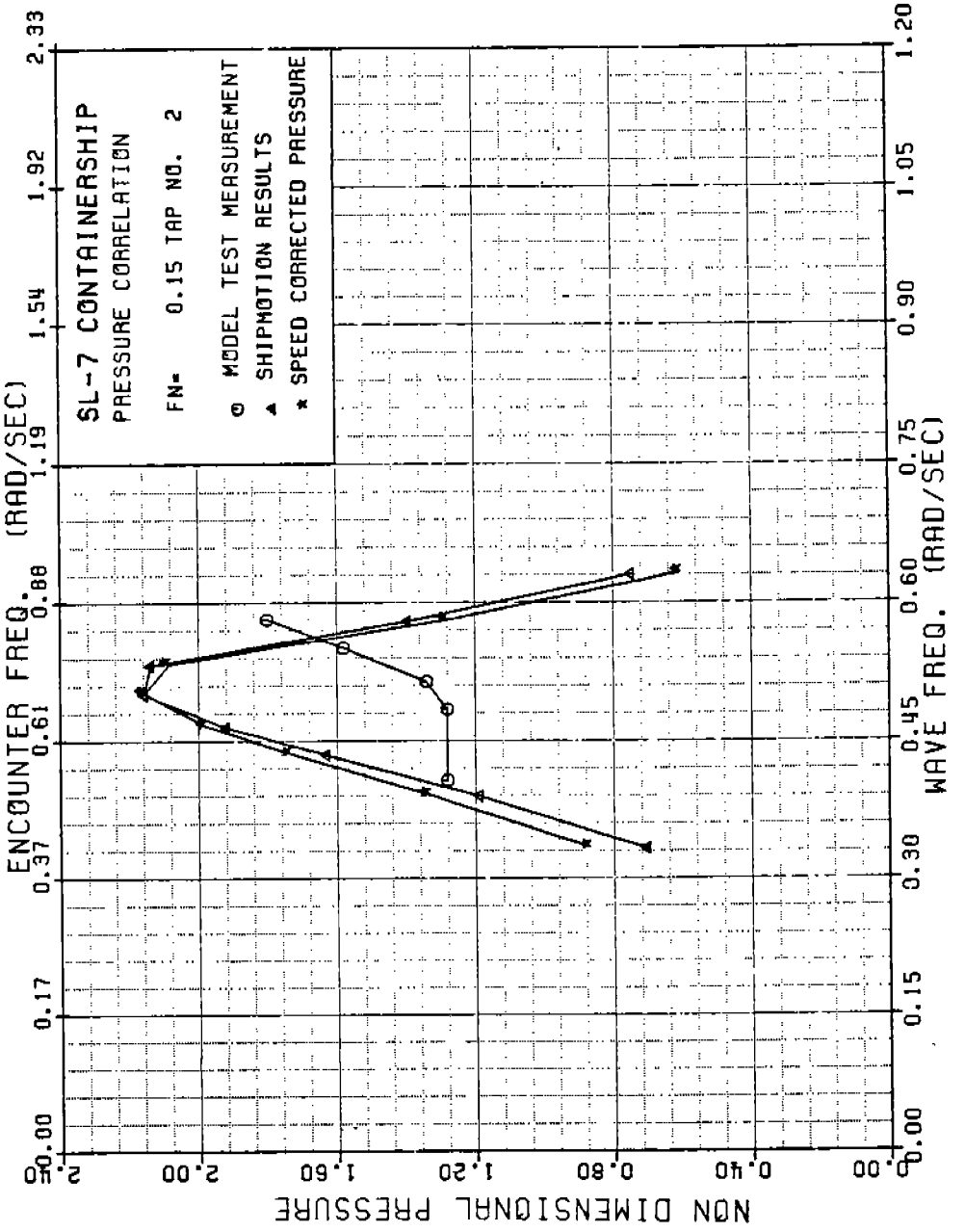

FIGURE A-42 SL-7 NONDIMENSIONAL PRESSURE AT TAP 2 , FN=0.15

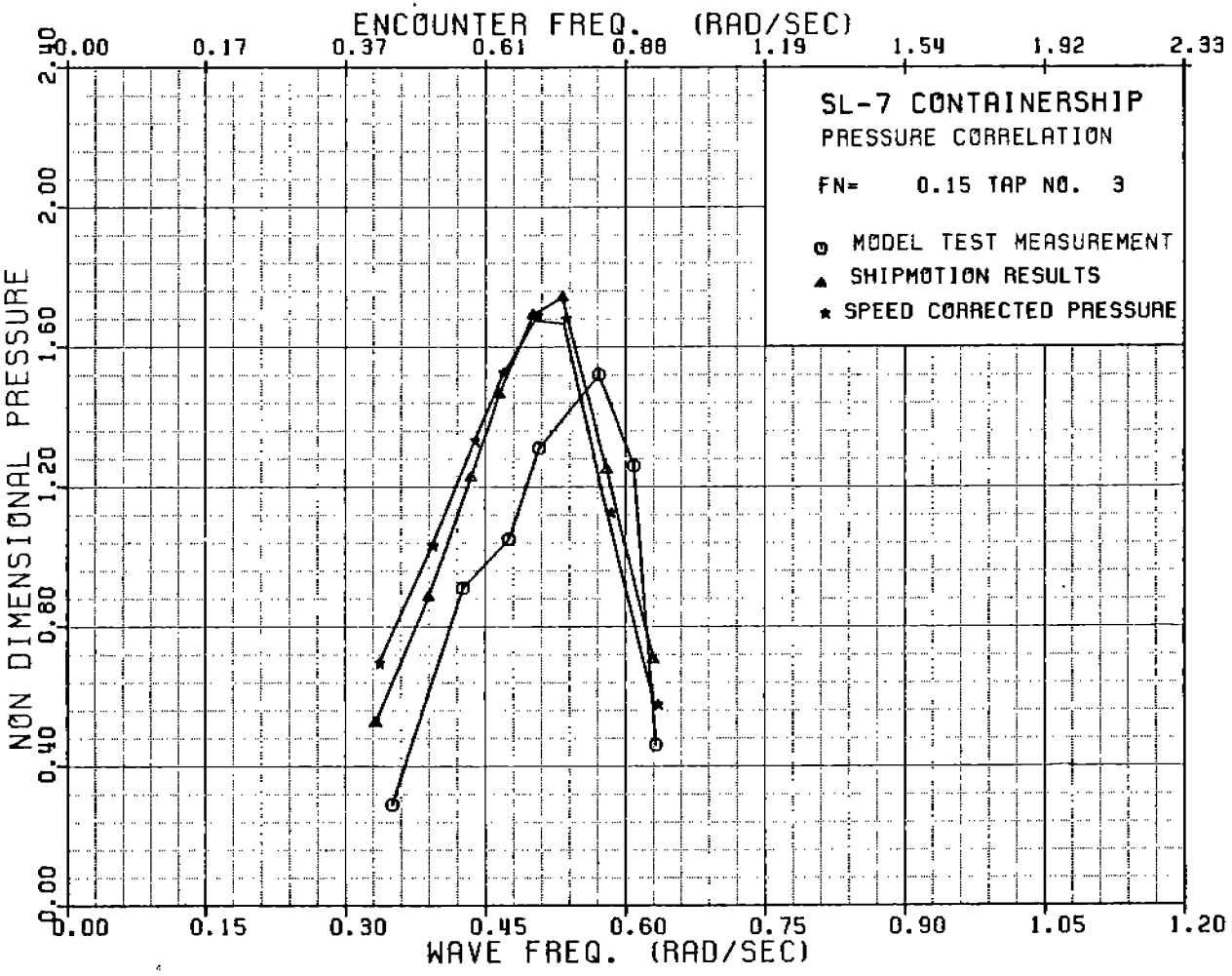

FIGURE A-43 SL-7 NONDIMENSIONAL PRESSURE AT TAP 3 , FN=0.15

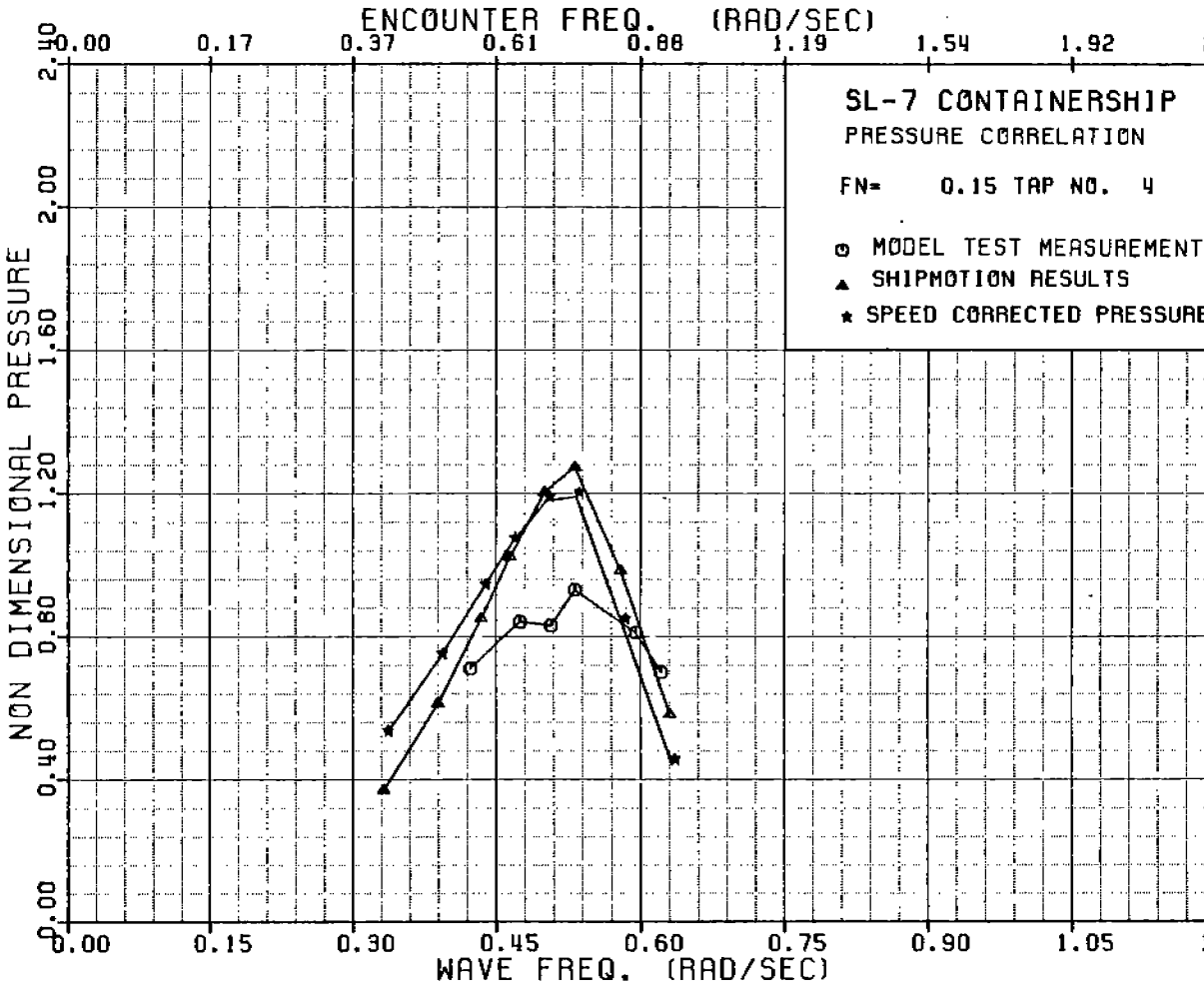

FIGURE A-44 SL-7 NONDIMENSIONAL PRESSURE AT TAP 4 , FN=

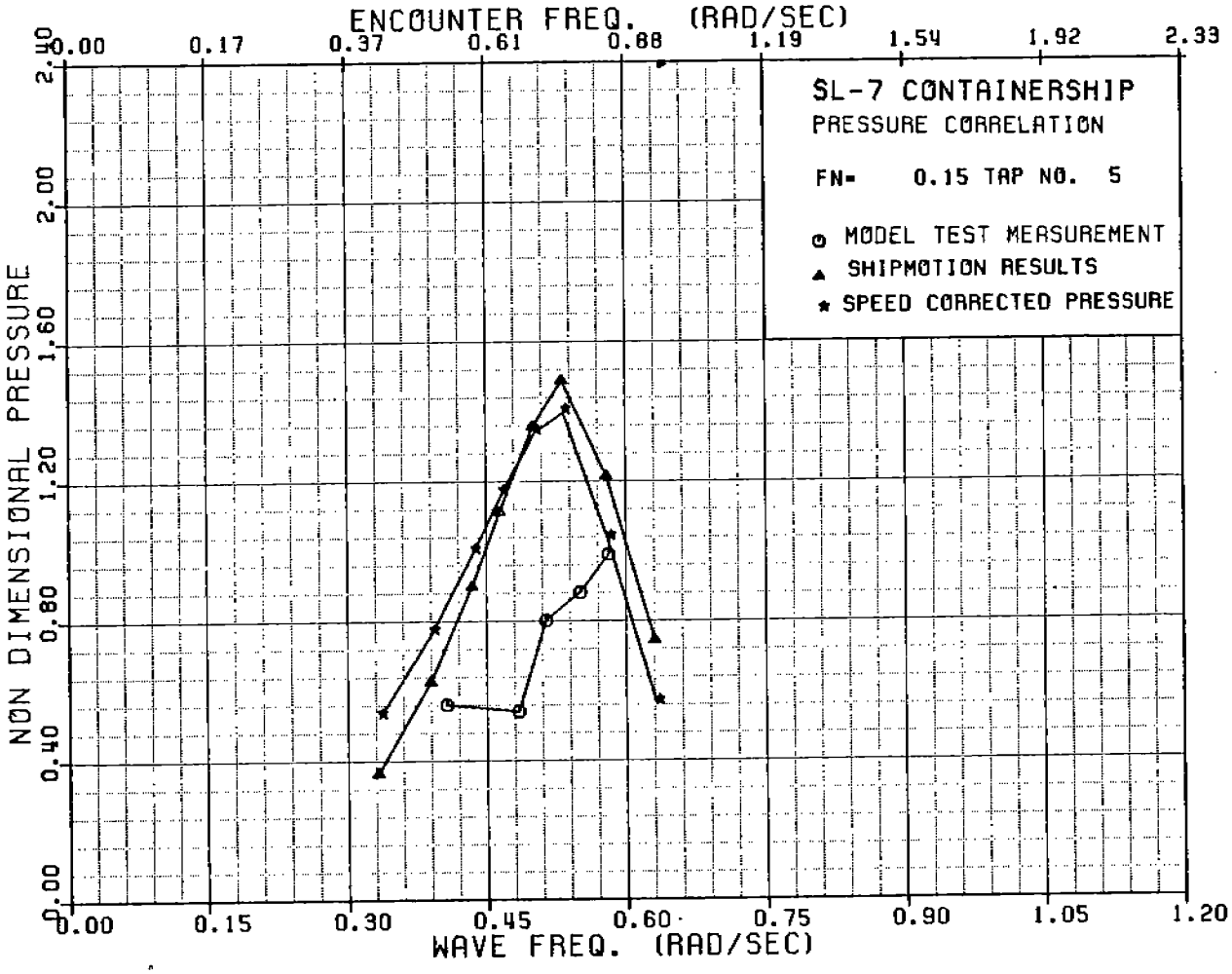

FIGURE A-45 SL-7 NONDIMENSIONAL PRESSURE AT TAP 5 , FN=0.15

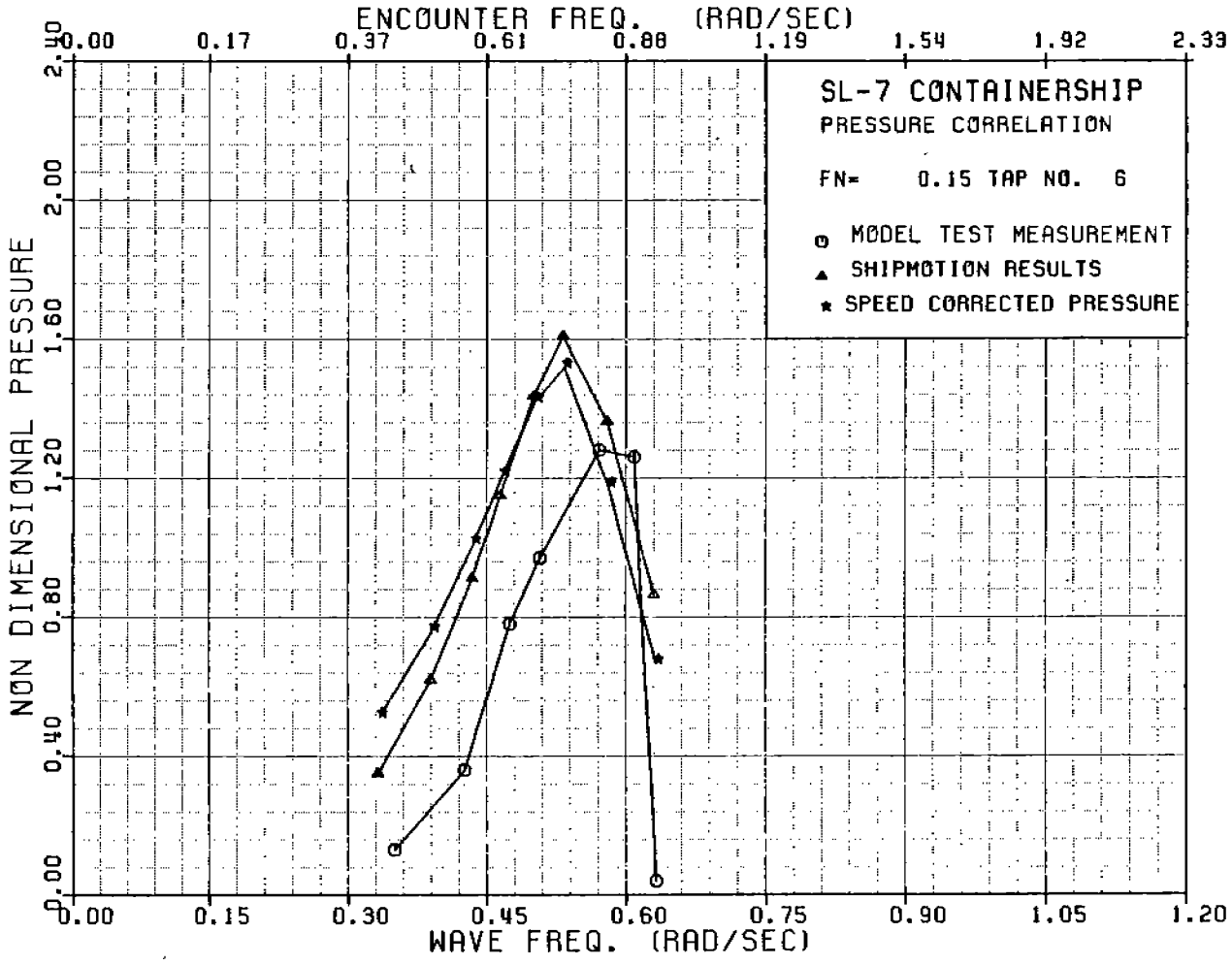

FIGURE A-46 SL-7 NONDIMENSIONAL PRESSURE AT TAP 6 , FN=0.15

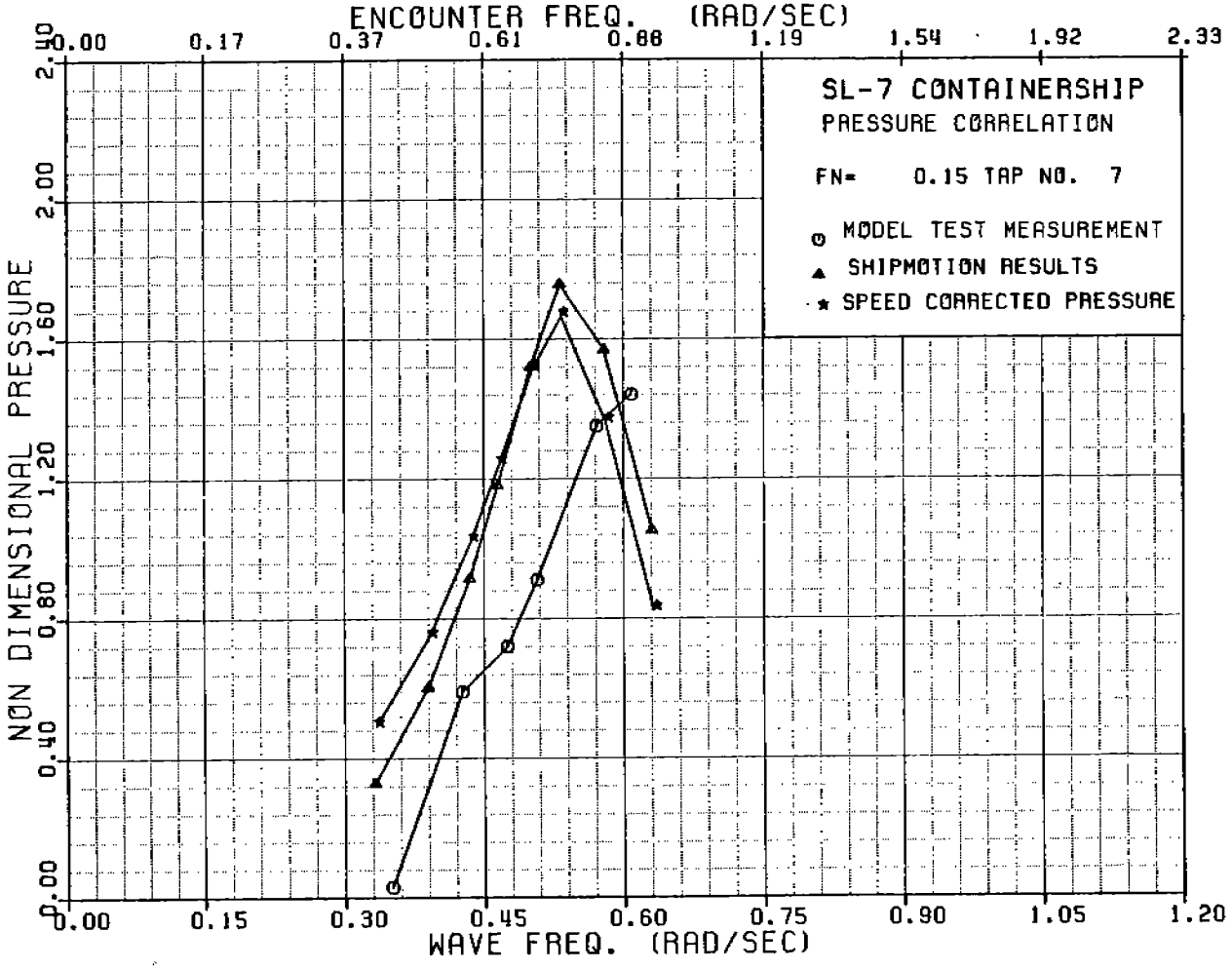

FIGURE A-47 SL-7 NONDIMENSIONAL PRESSURE AT TAP 7 , FN=0.15

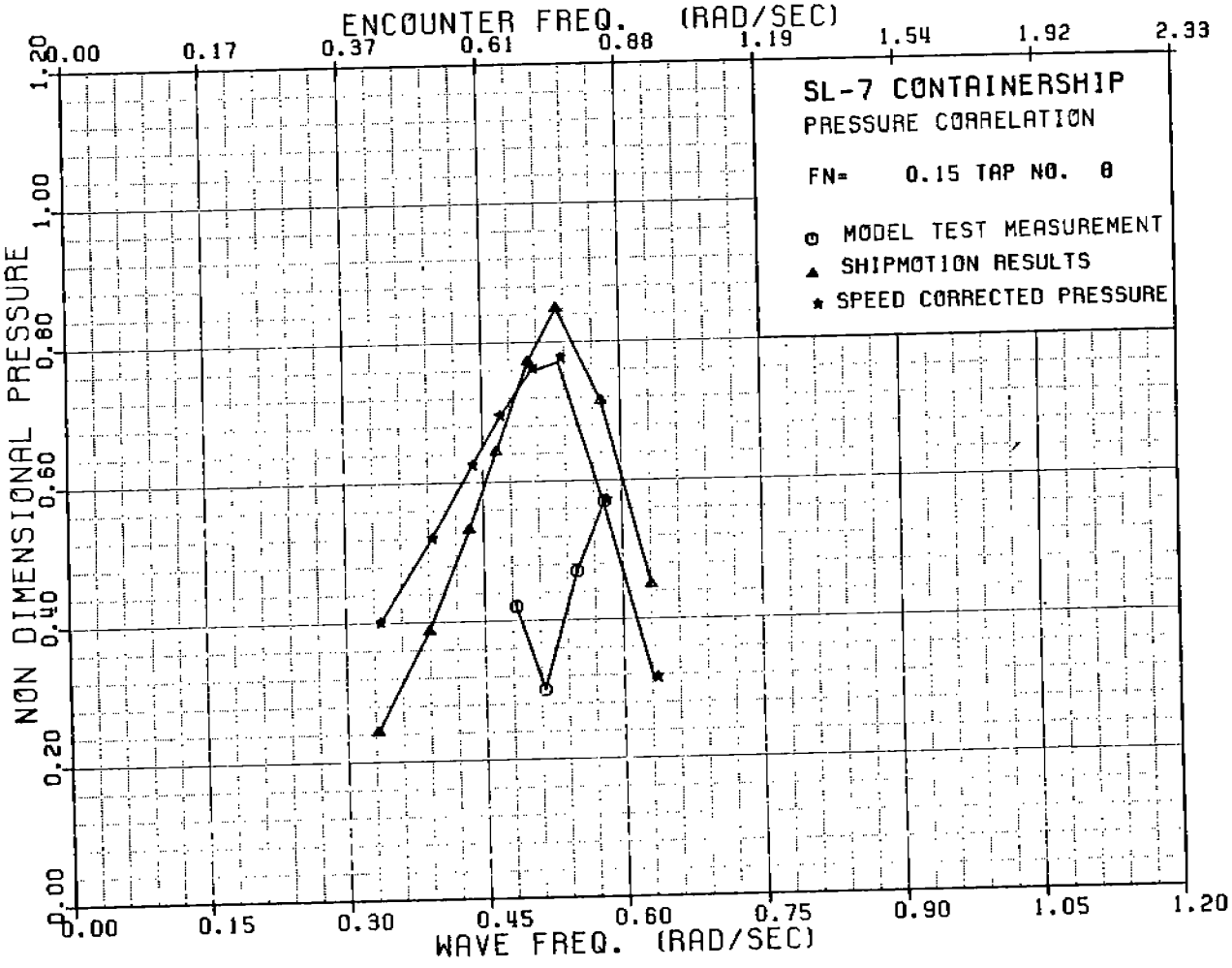

FIGURE A-48 SL-7 NONDIMENSIONAL PRESSURE AT TAP 8 , FN=0.15

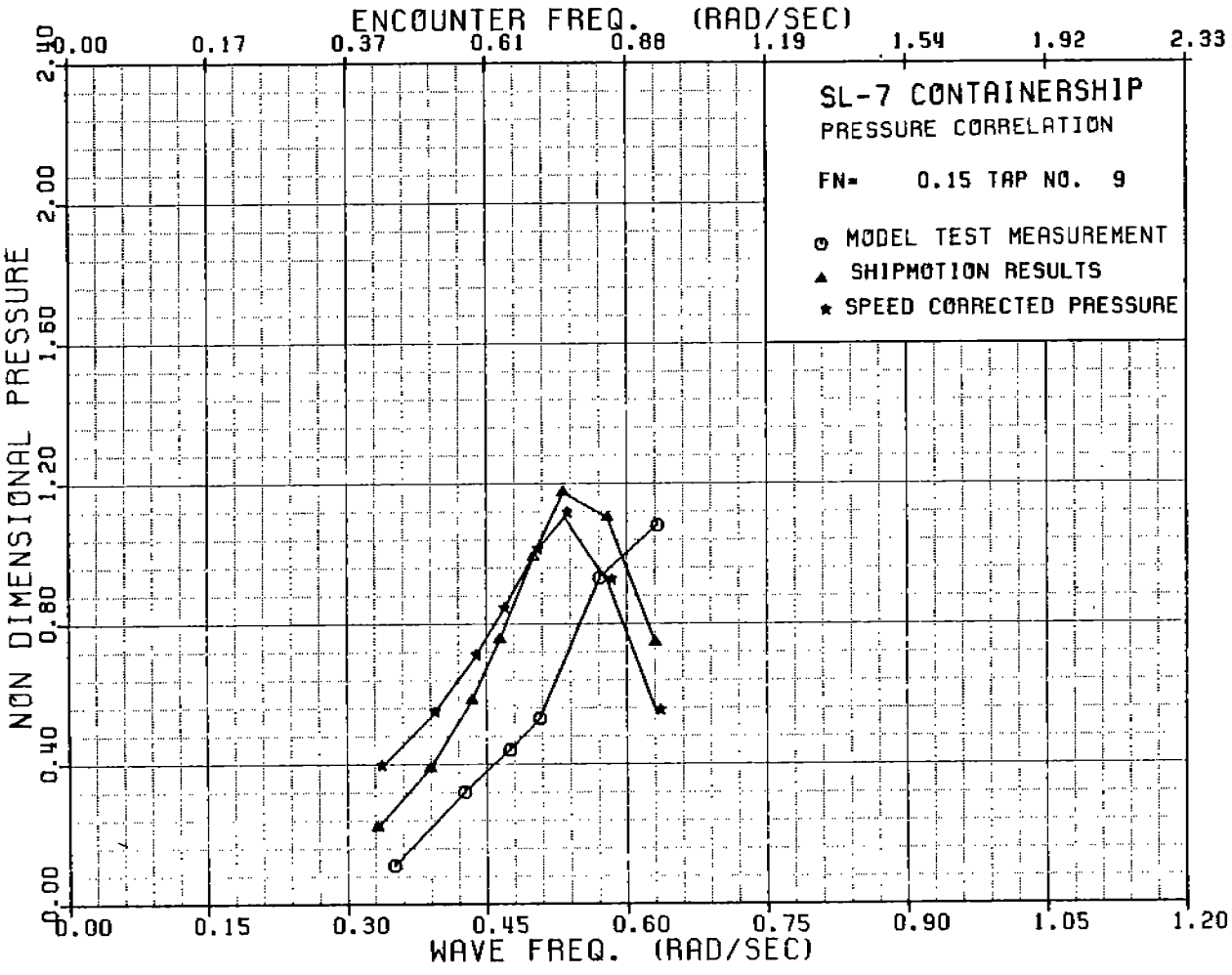

FIGURE A-49 SL-7 NONDIMENSIONAL PRESSURE AT TAP 9 , FN=0.15

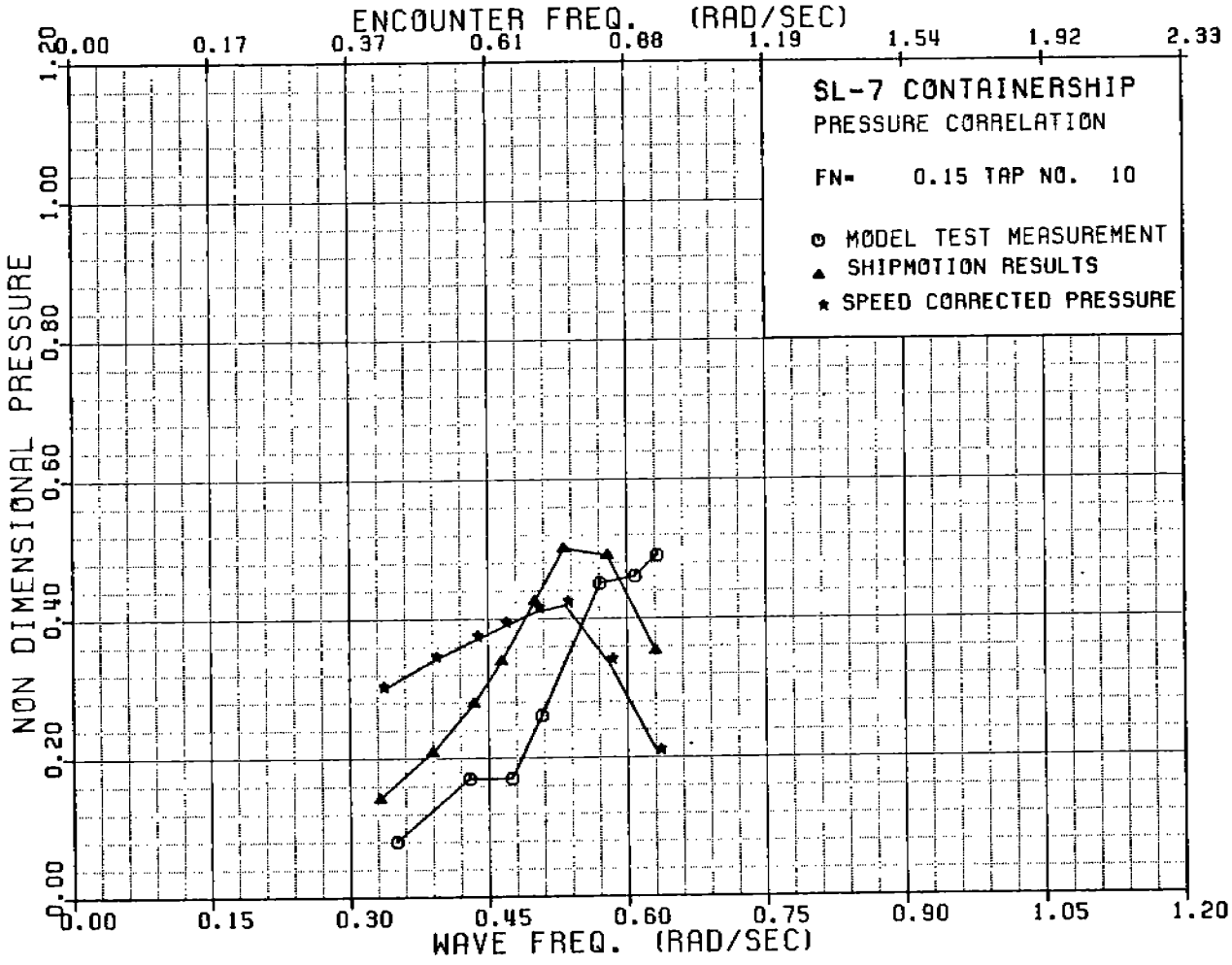

FIGURE A-50 SL-7 NONDIMENSIONAL PRESSURE AT TAP 10, FN=0.15

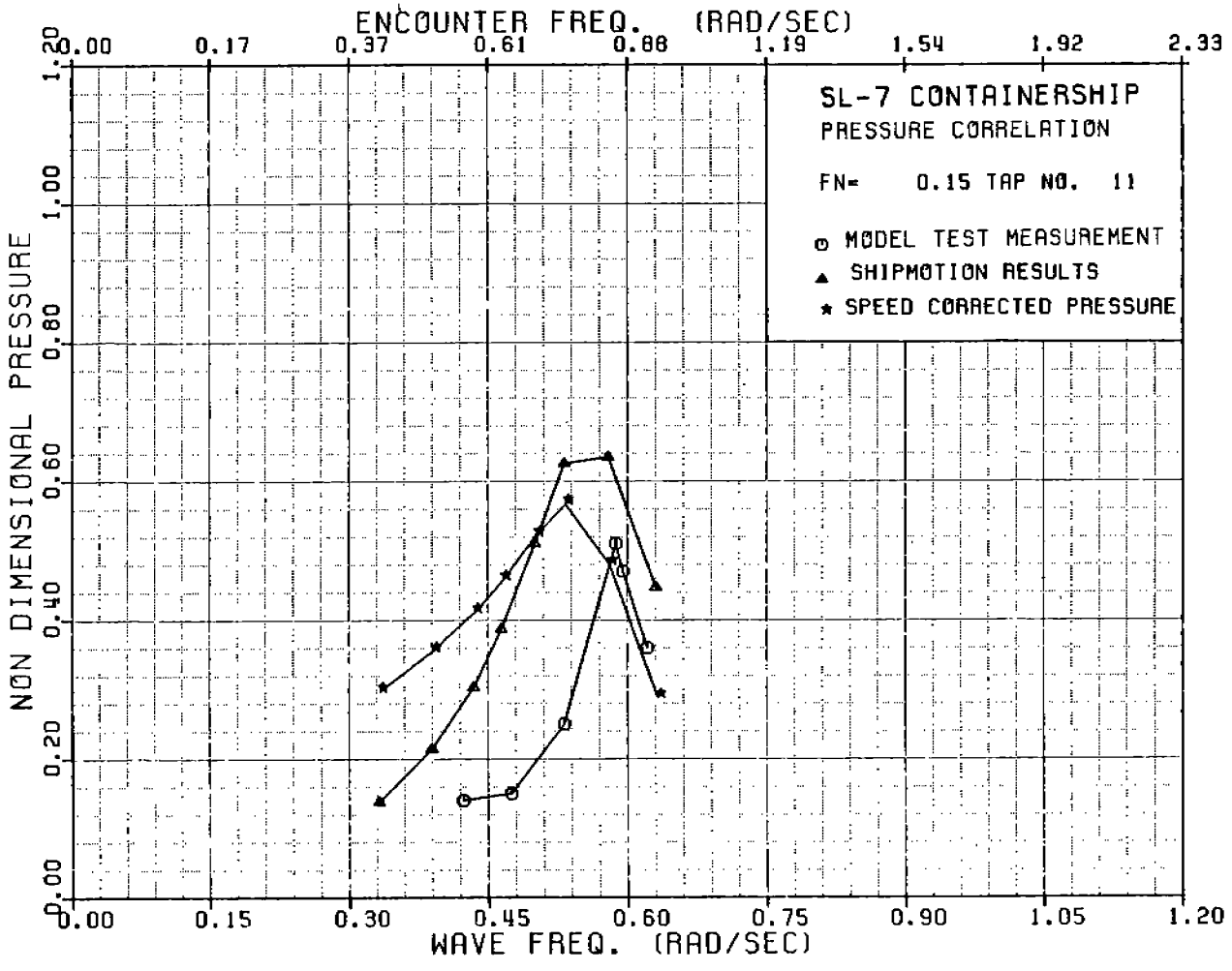

FIGURE A-51 SL-7 NONDIMENSIONAL PRESSURE AT TAP 11, FN=0.15

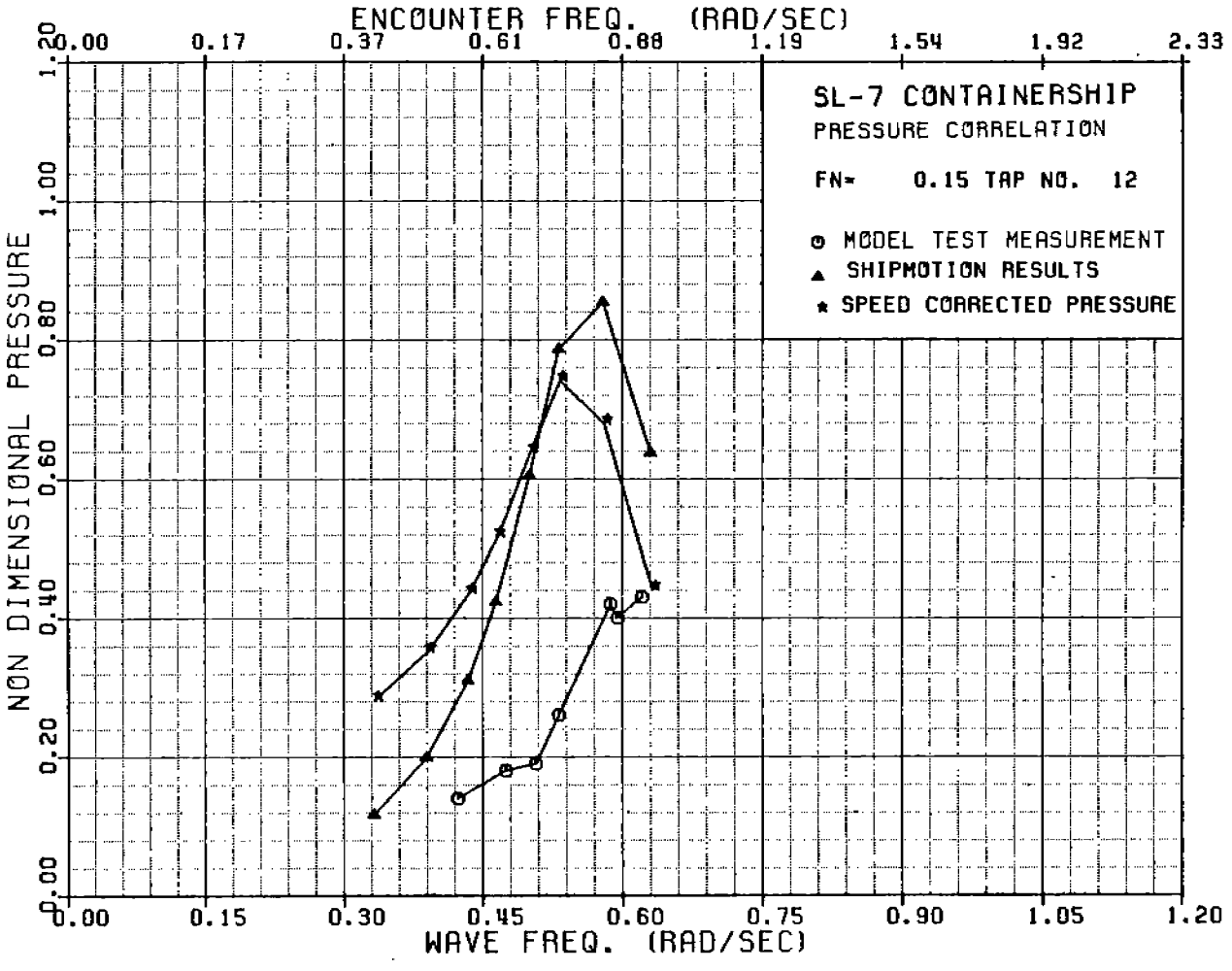

FIGURE A-52 SL-7 NONDIMENSIONAL PRESSURE AT TAP 12, FN=0.15

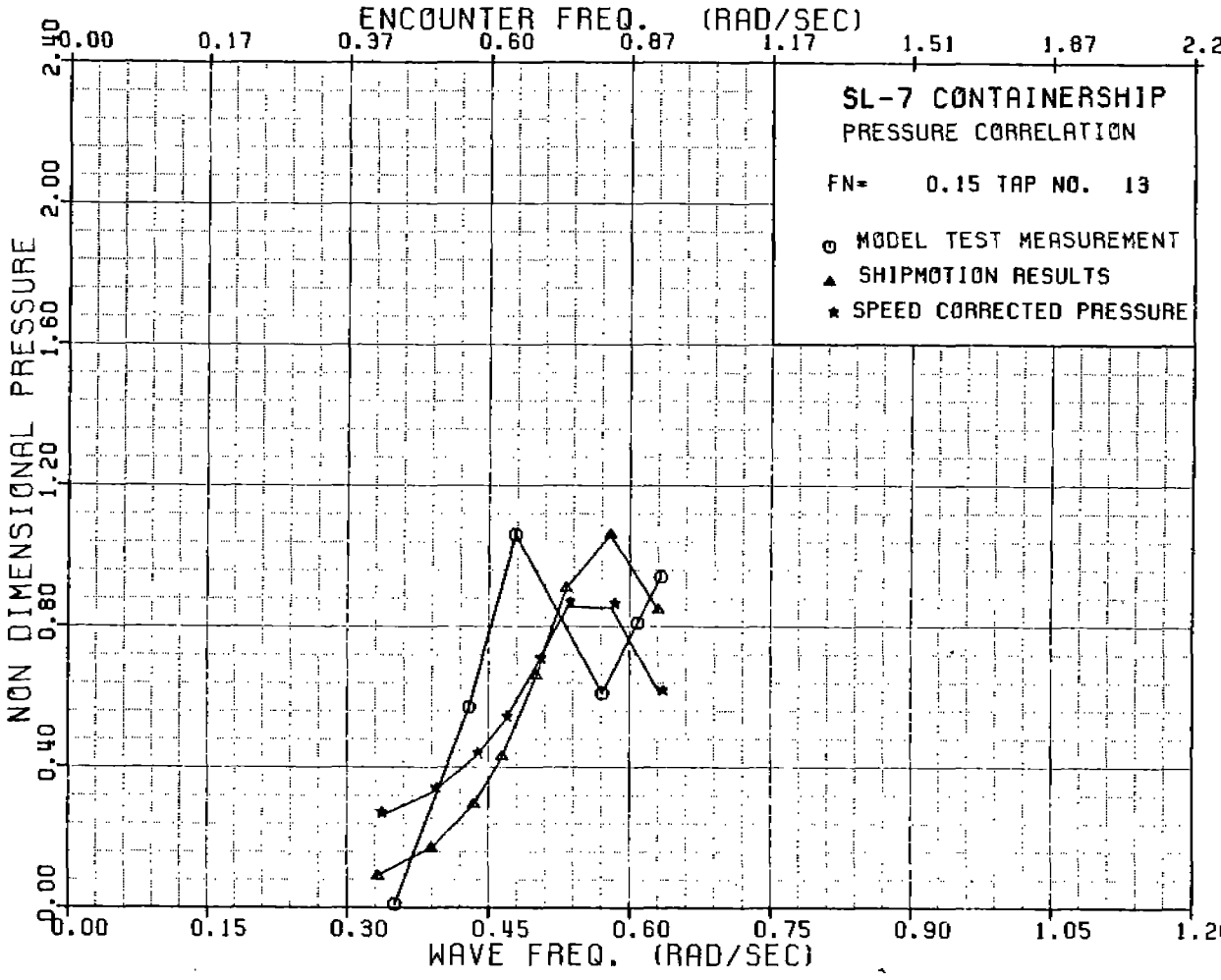

FIGURE A-53 SL-7 NONDIMENSIONAL PRESSURE AT TAP 13, FN=0

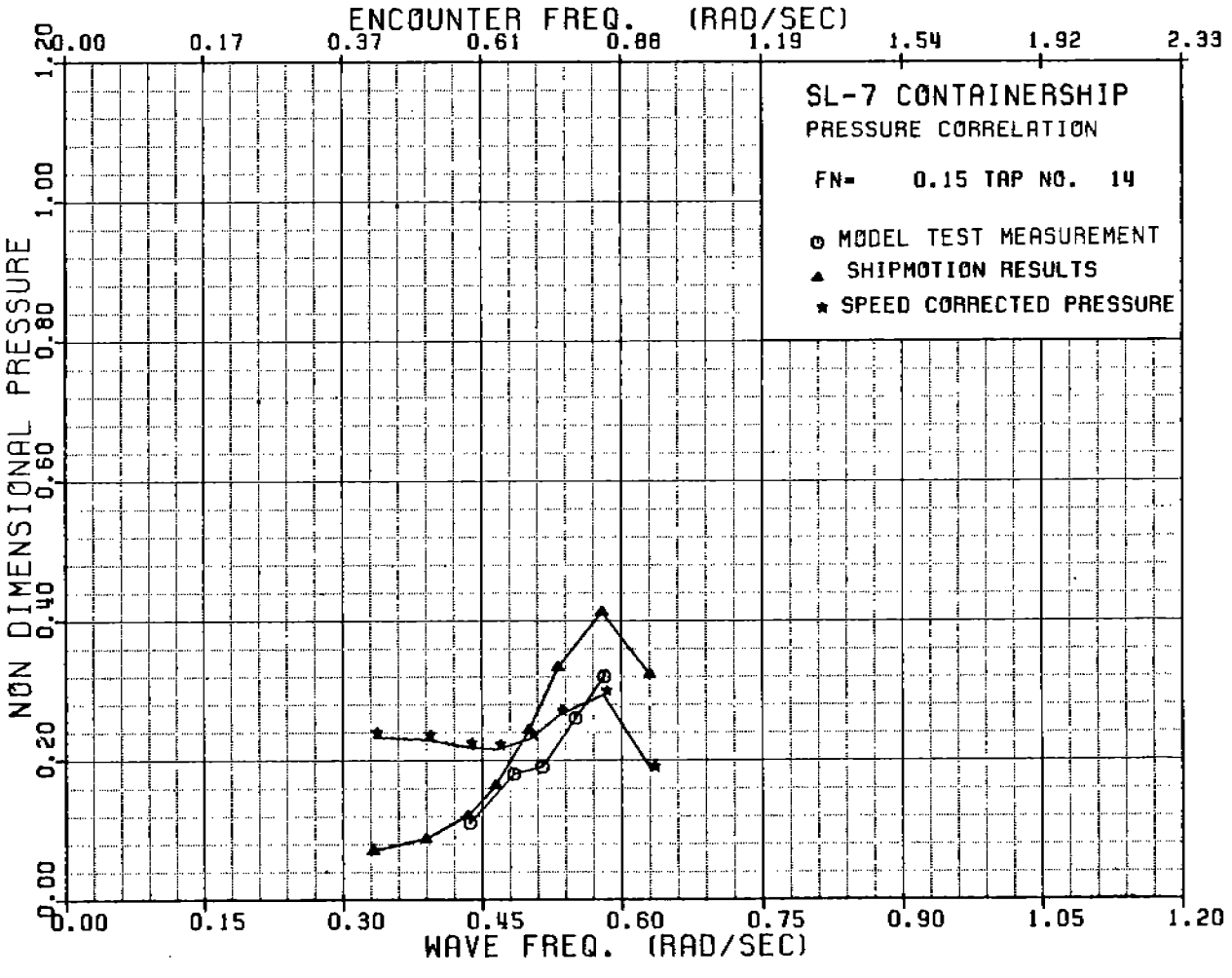

FIGURE A-54 SL-7 NONDIMENSIONAL PRESSURE AT TAP 14, FN=0.15

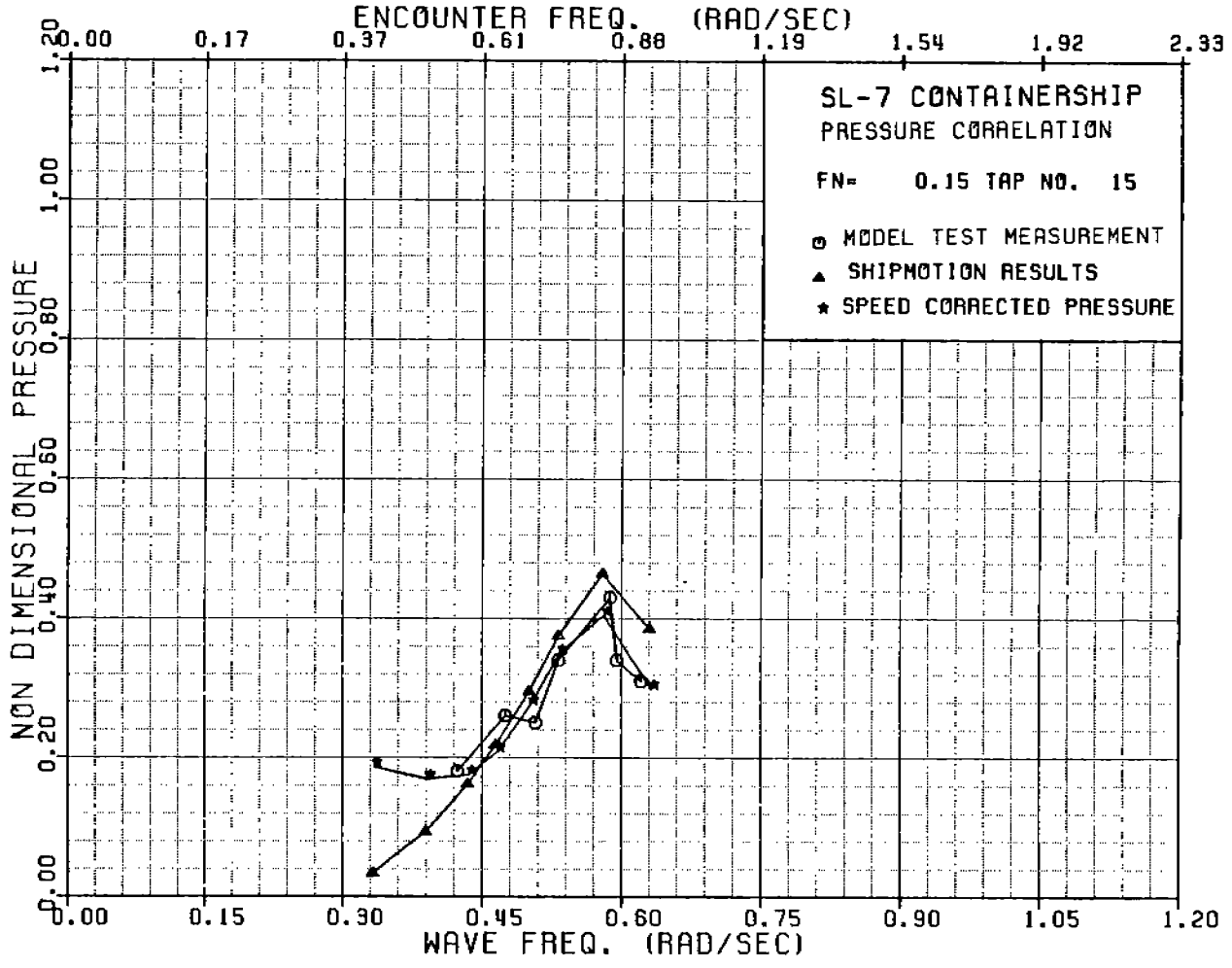

FIGURE A-55 SL-7 NONDIMENSIONAL PRESSURE AT TAP 15, FN=0.15

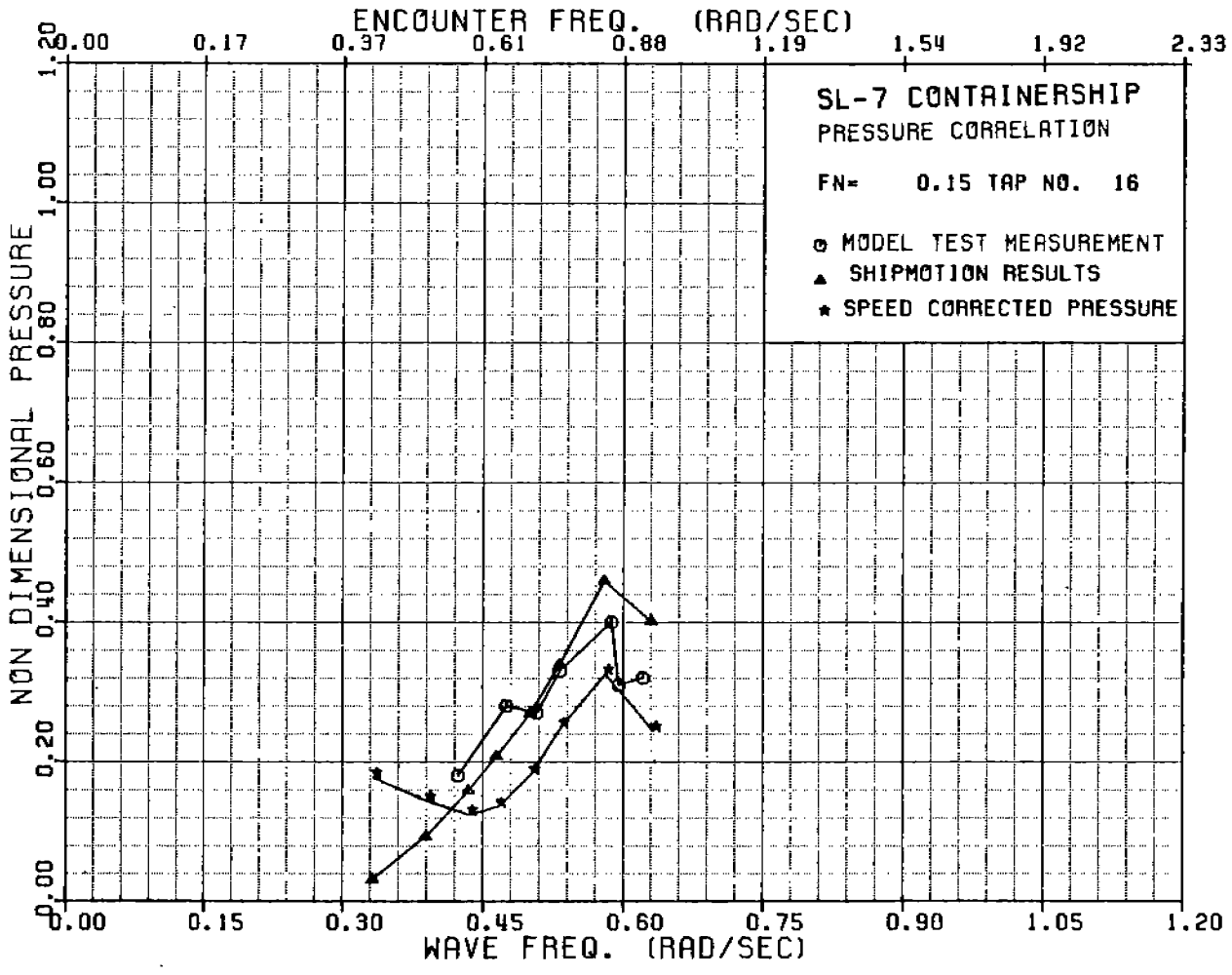

FIGURE A-56 SL-7 NONDIMENSIONAL PRESSURE AT TAP 16, FN=0.15

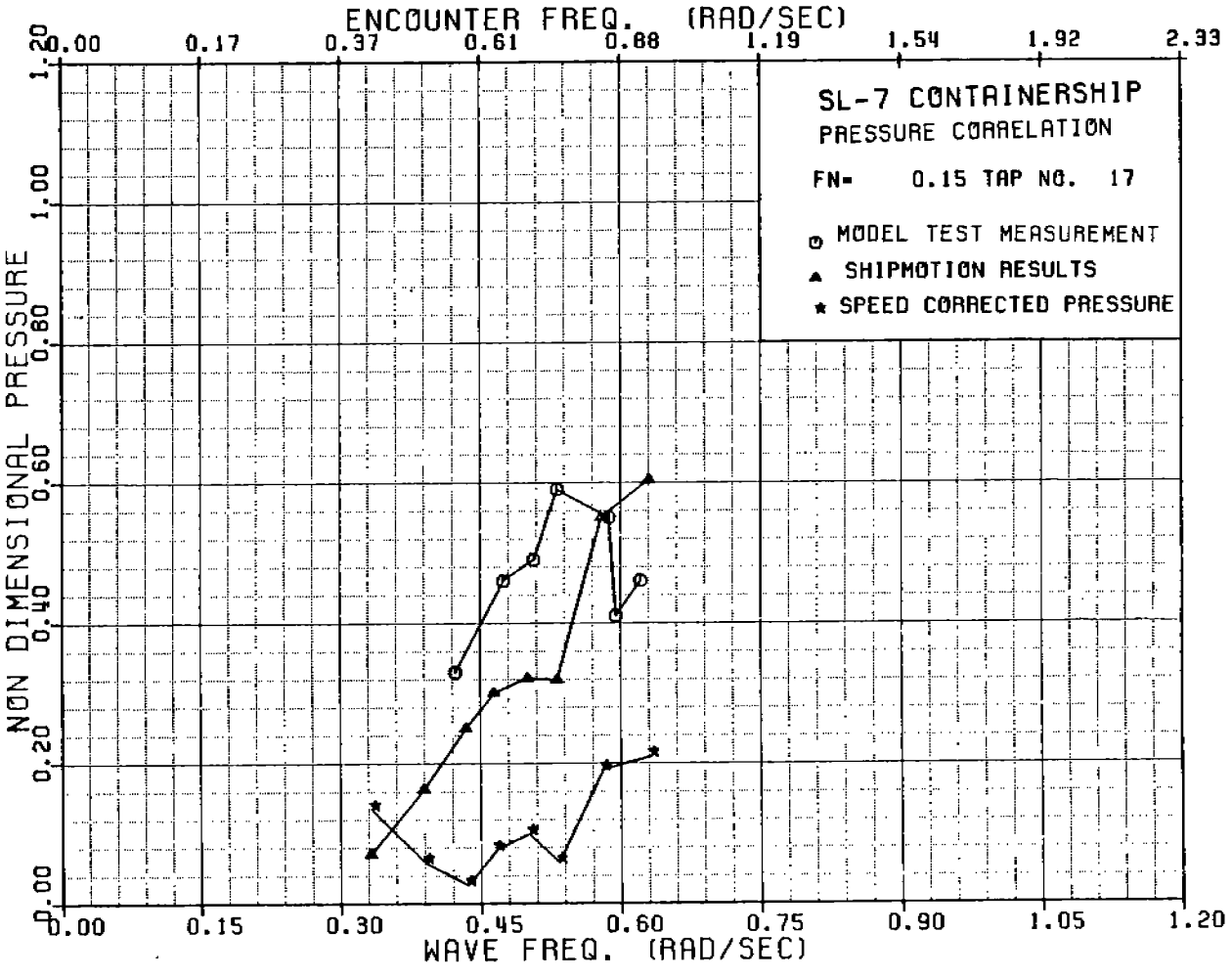

FIGURE A-57 SL-7 NONDIMENSIONAL PRESSURE AT TAP 17, FN=0.15

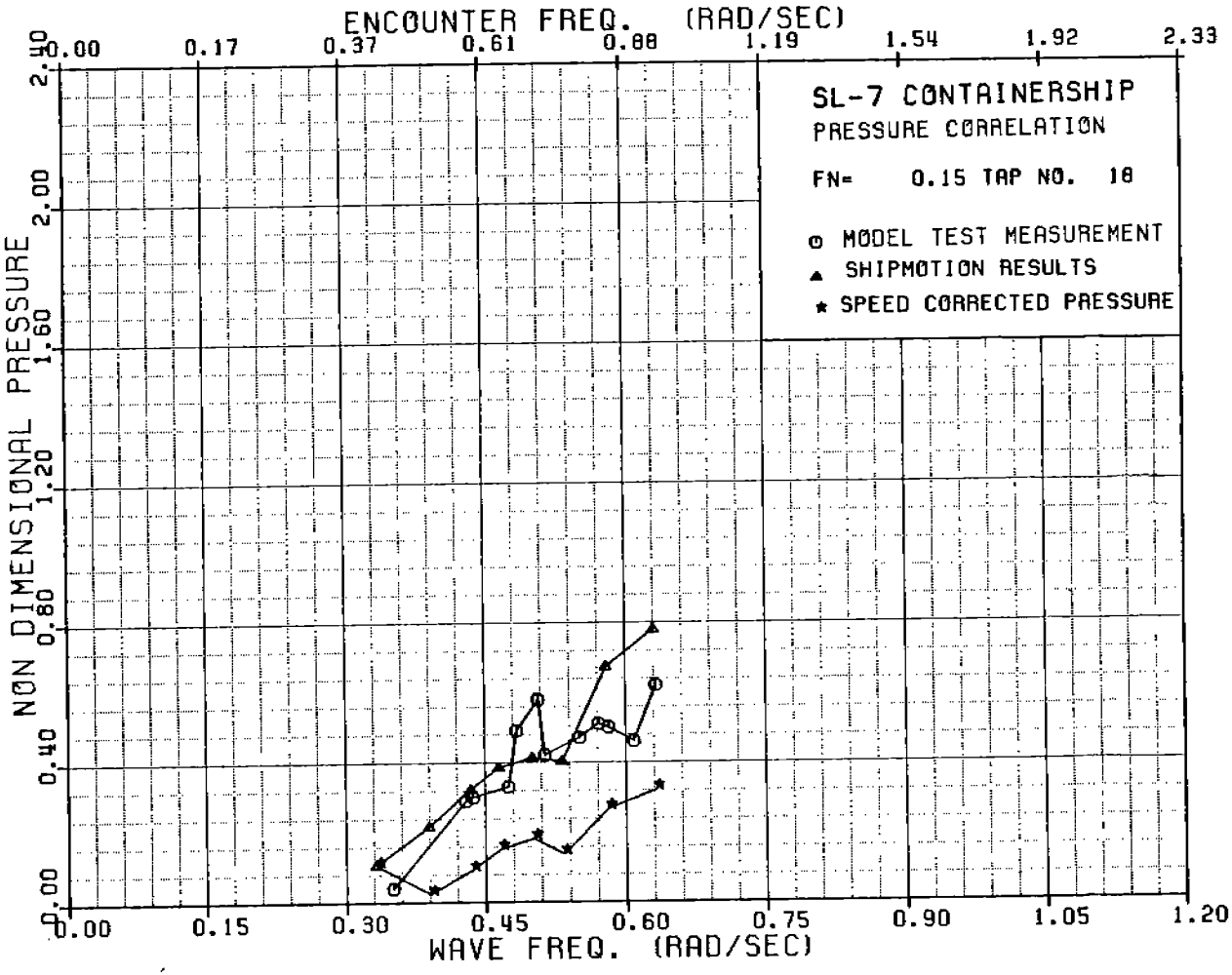

FIGURE A-58 SL-7 NONDIMENSIONAL PRESSURE AT TAP 18, FN=0.15

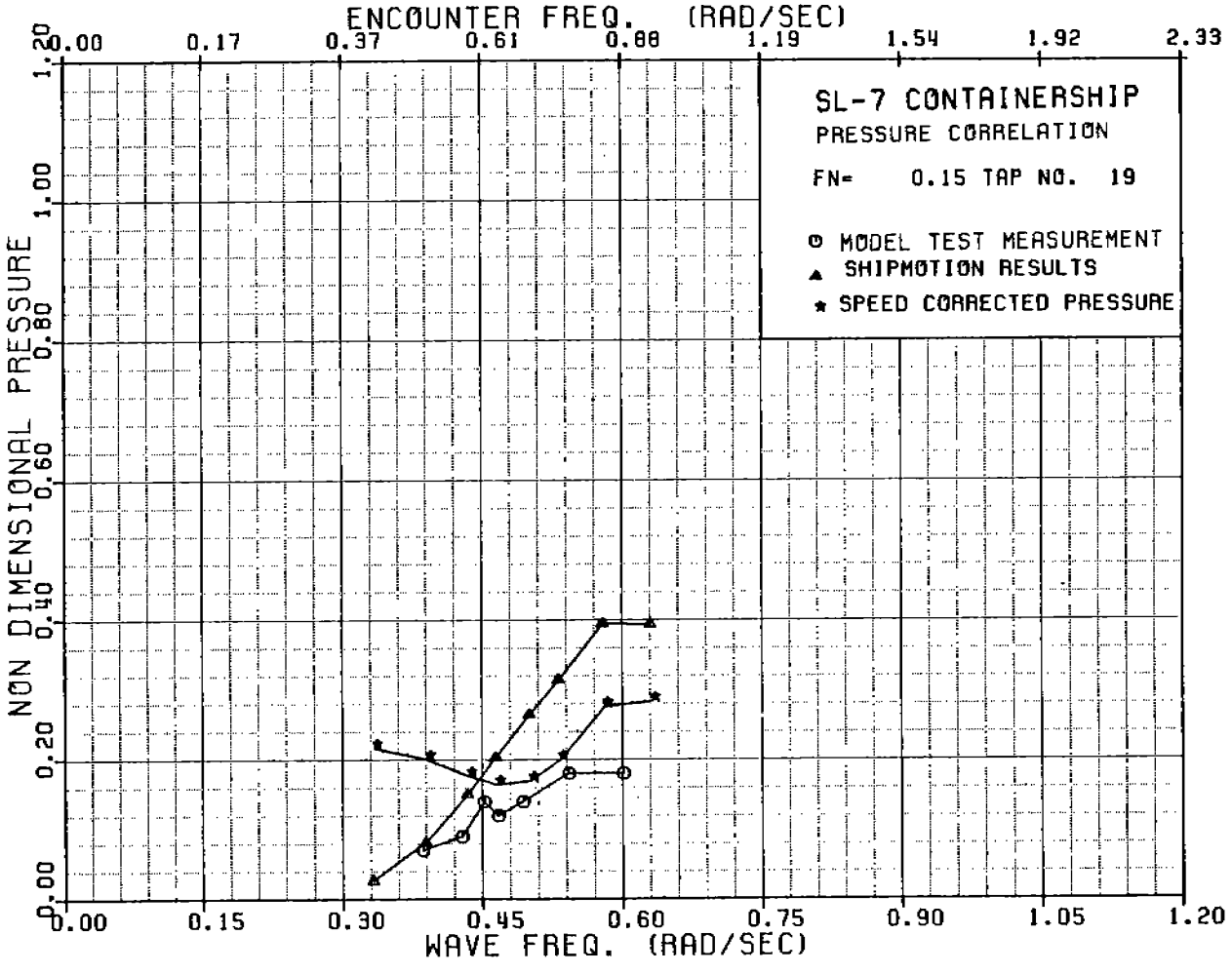

FIGURE A-59 SL-7 NONDIMENSIONAL PRESSURE AT TAP 19, FN 0.15

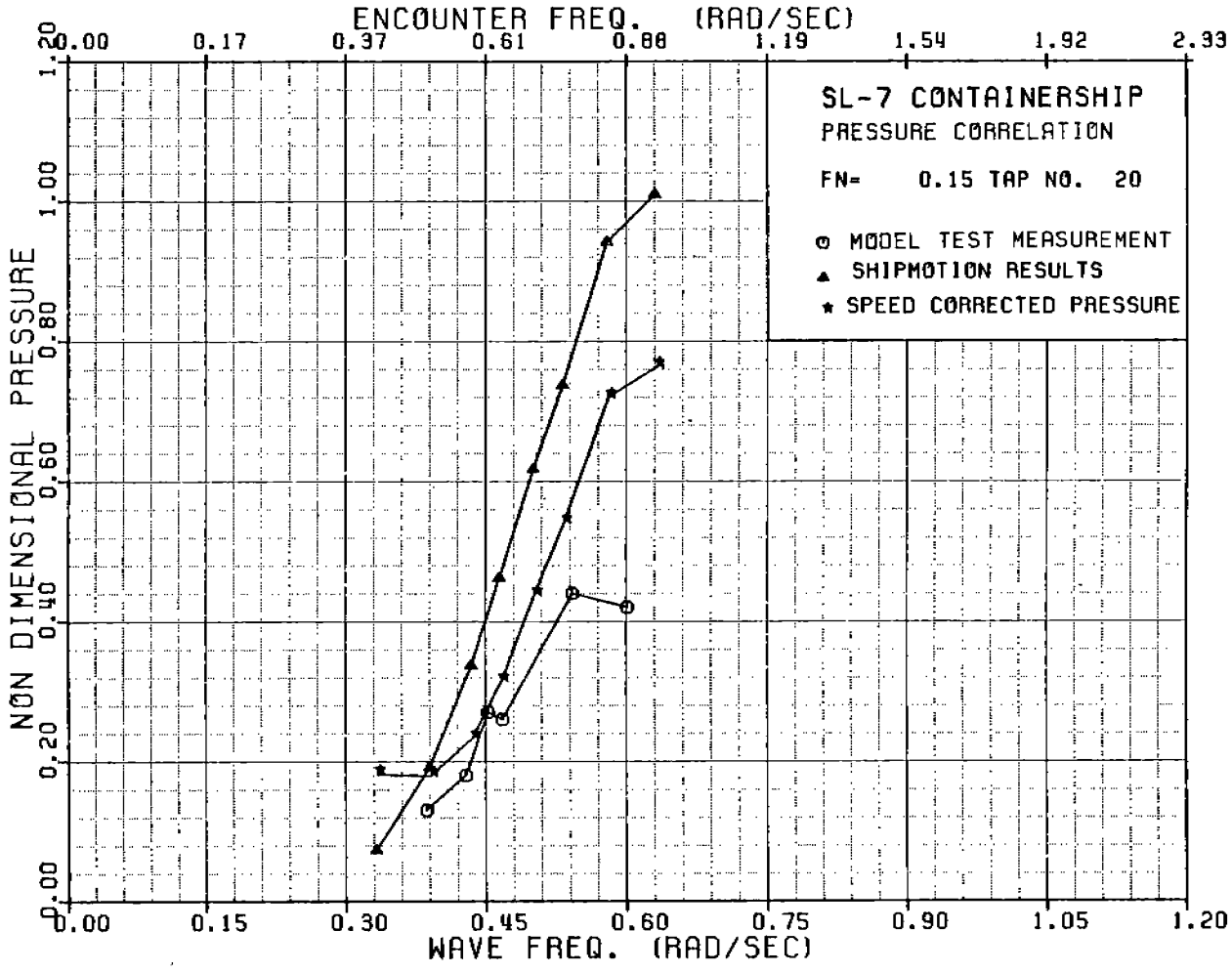

FIGURE A-60 SL-7 NONDIMENSIONAL PRESSURE AT TAP 20, FN= 0.15

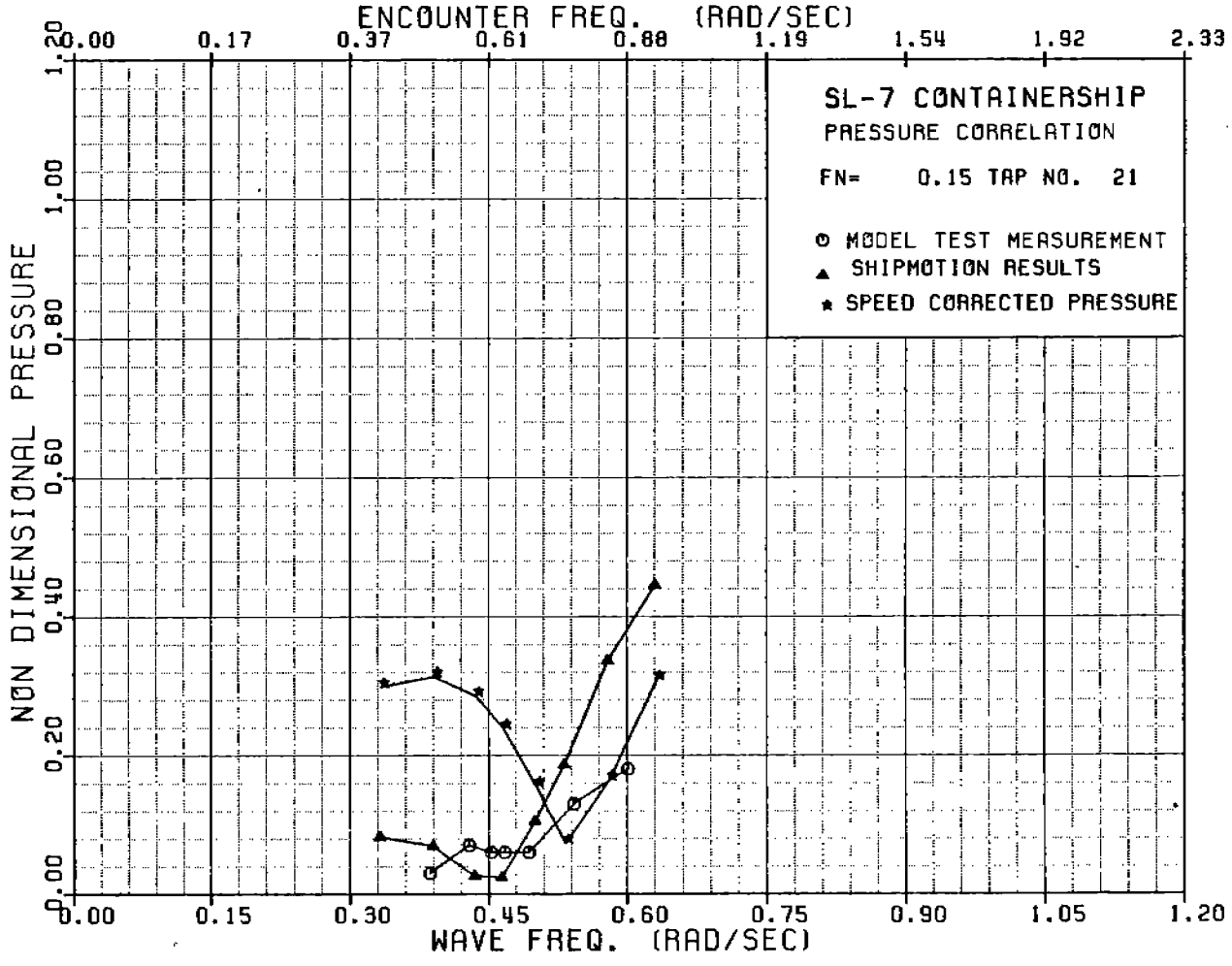

FIGURE A-61 SL-7 NONDIMENSIONAL PRESSURE AT TAP 21, FN=0.15

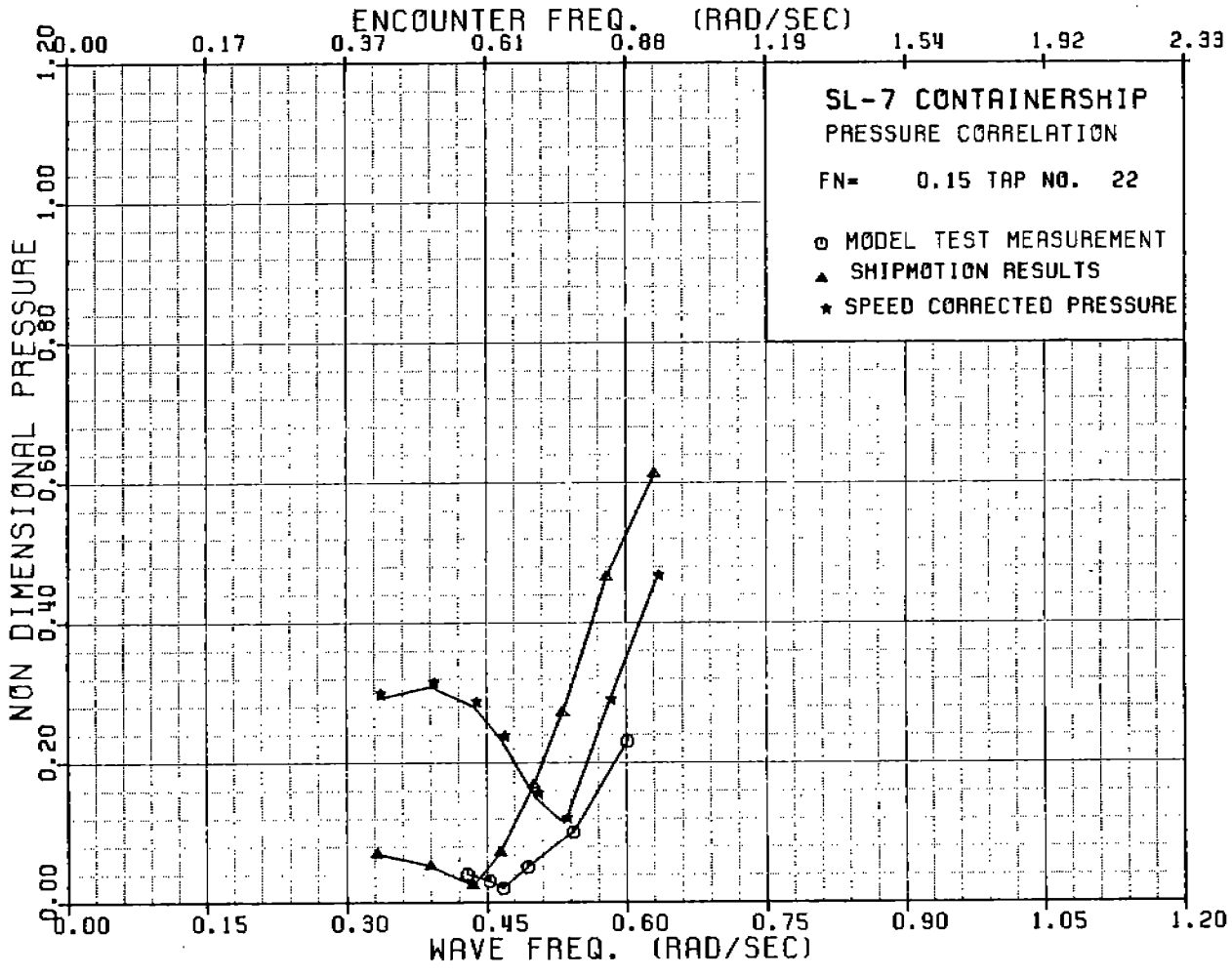

FIGURE A-62 SL-7 NONDIMENSIONAL PRESSURE AT TAP 22, FN=0.15

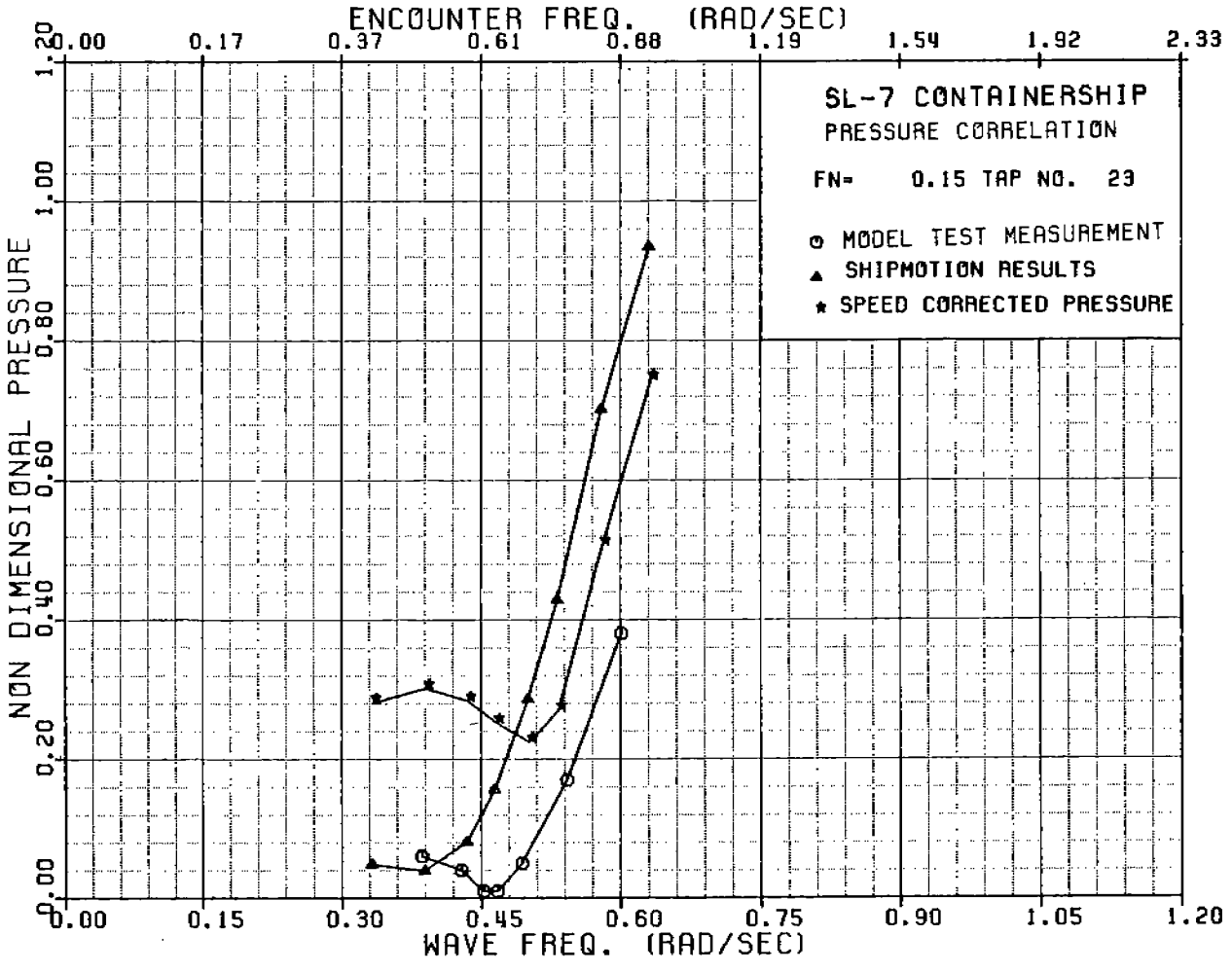

FIGURE A-63 SL-7 NONDIMENSIONAL PRESSURE AT TAP 23, FN=0.15

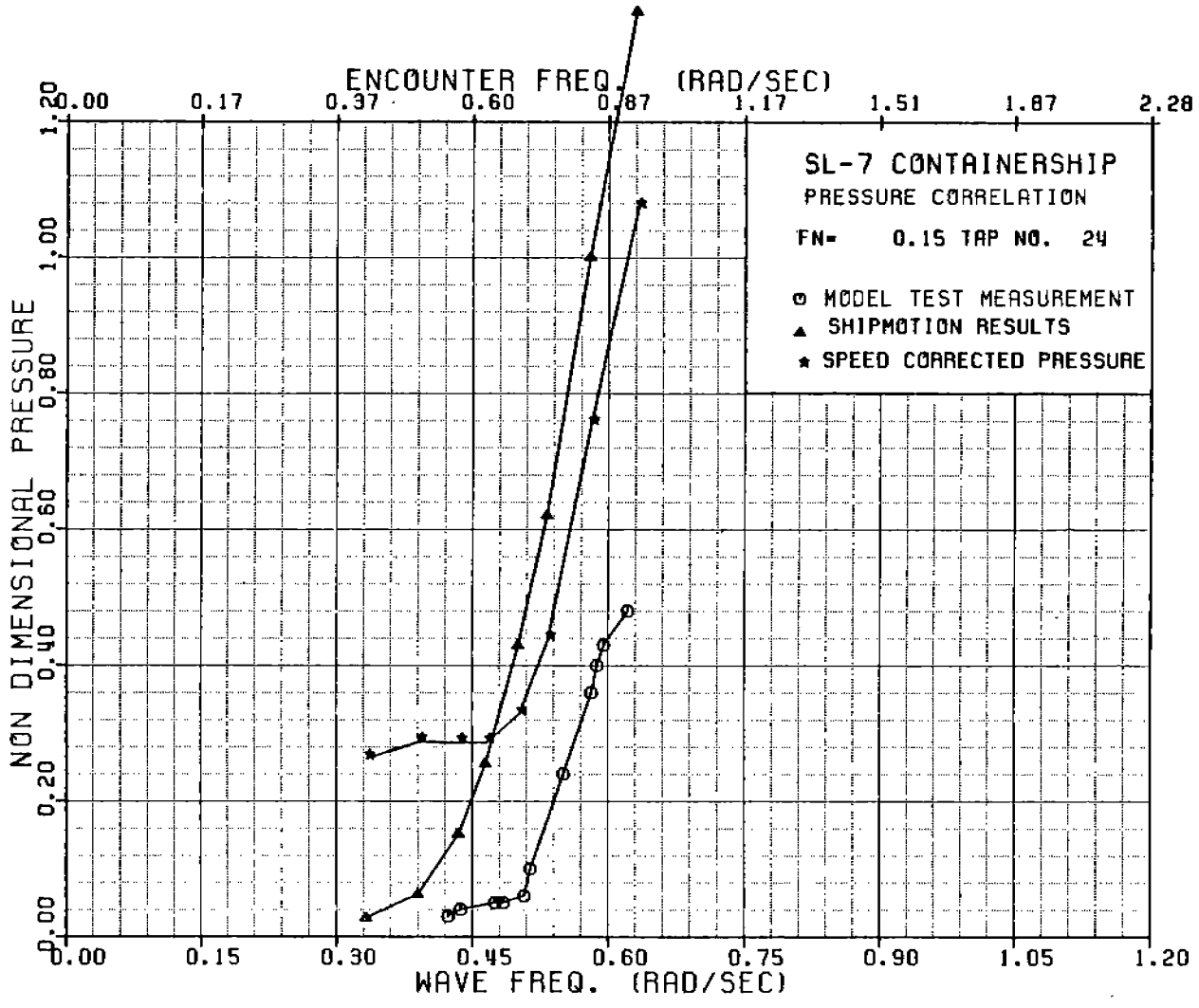

FIGURE A-64 SL-7 NONDIMENSIONAL PRESSURE AT TAP 24, FN=0.15

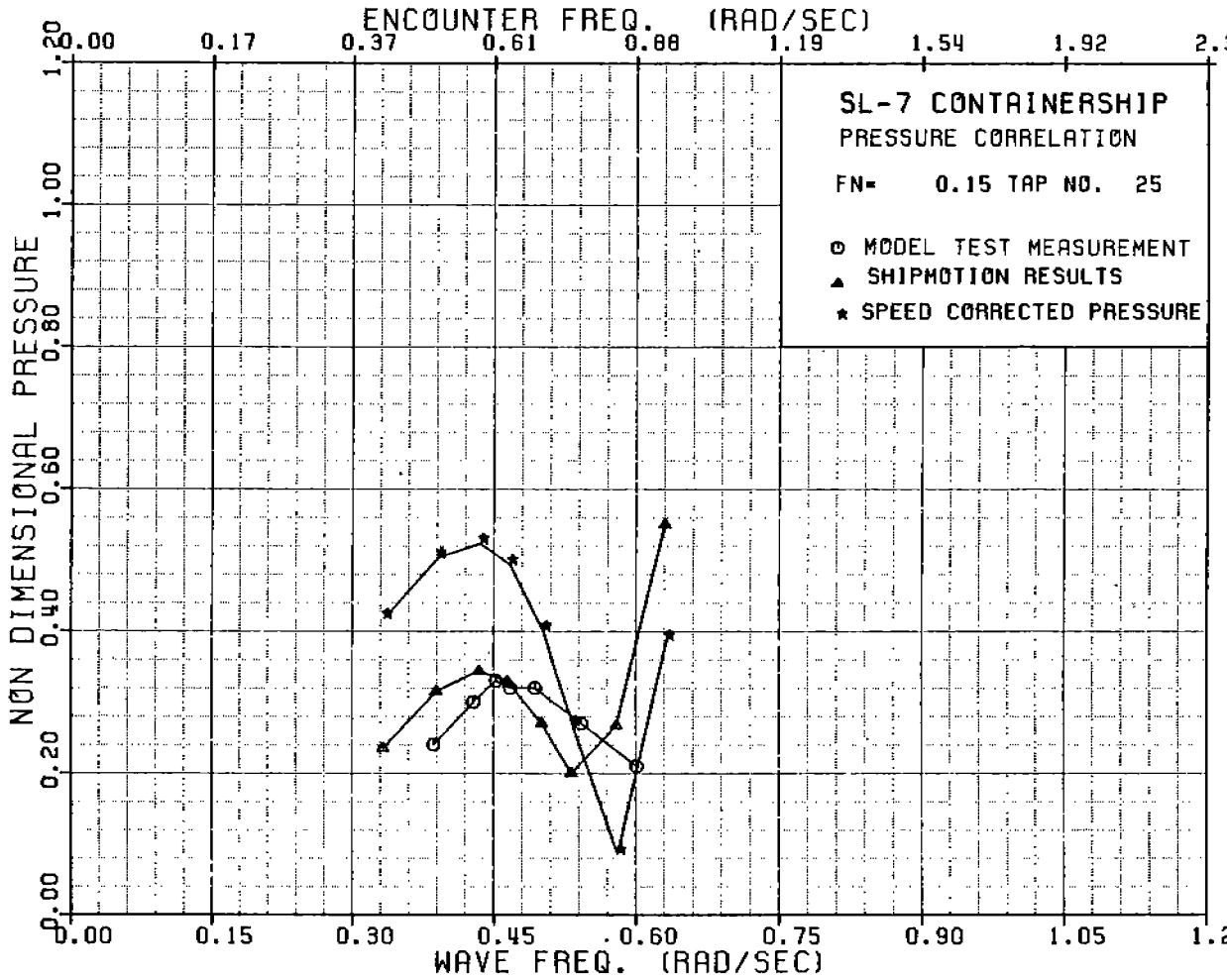

FIGURE A-65 SL-7 NONDIMENSIONAL PRESSURE AT TAP 25, FN=0.

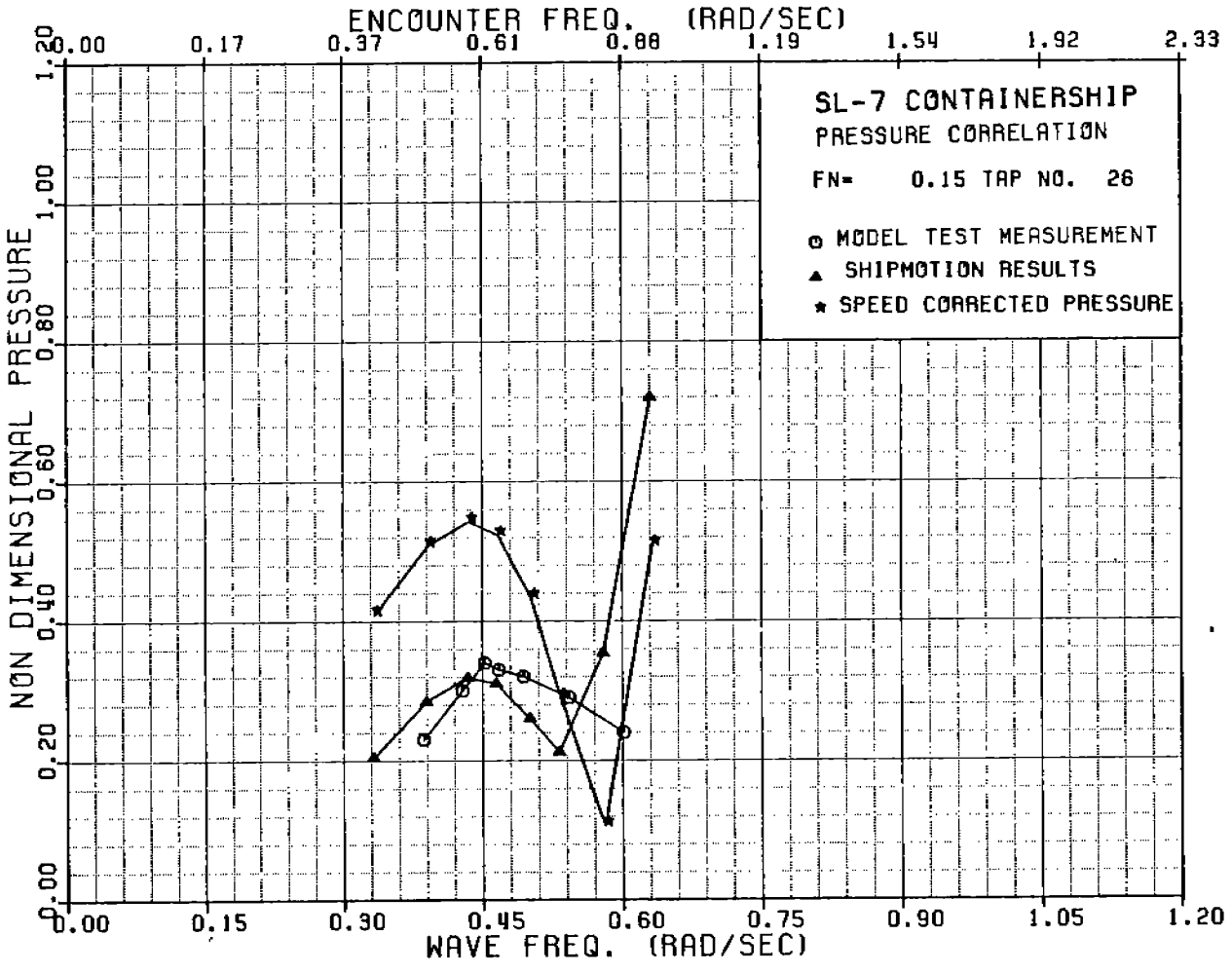

FIGURE A-66 SL-7 NONDIMENSIONAL PRESSURE AT TAP 26, FN=0.15

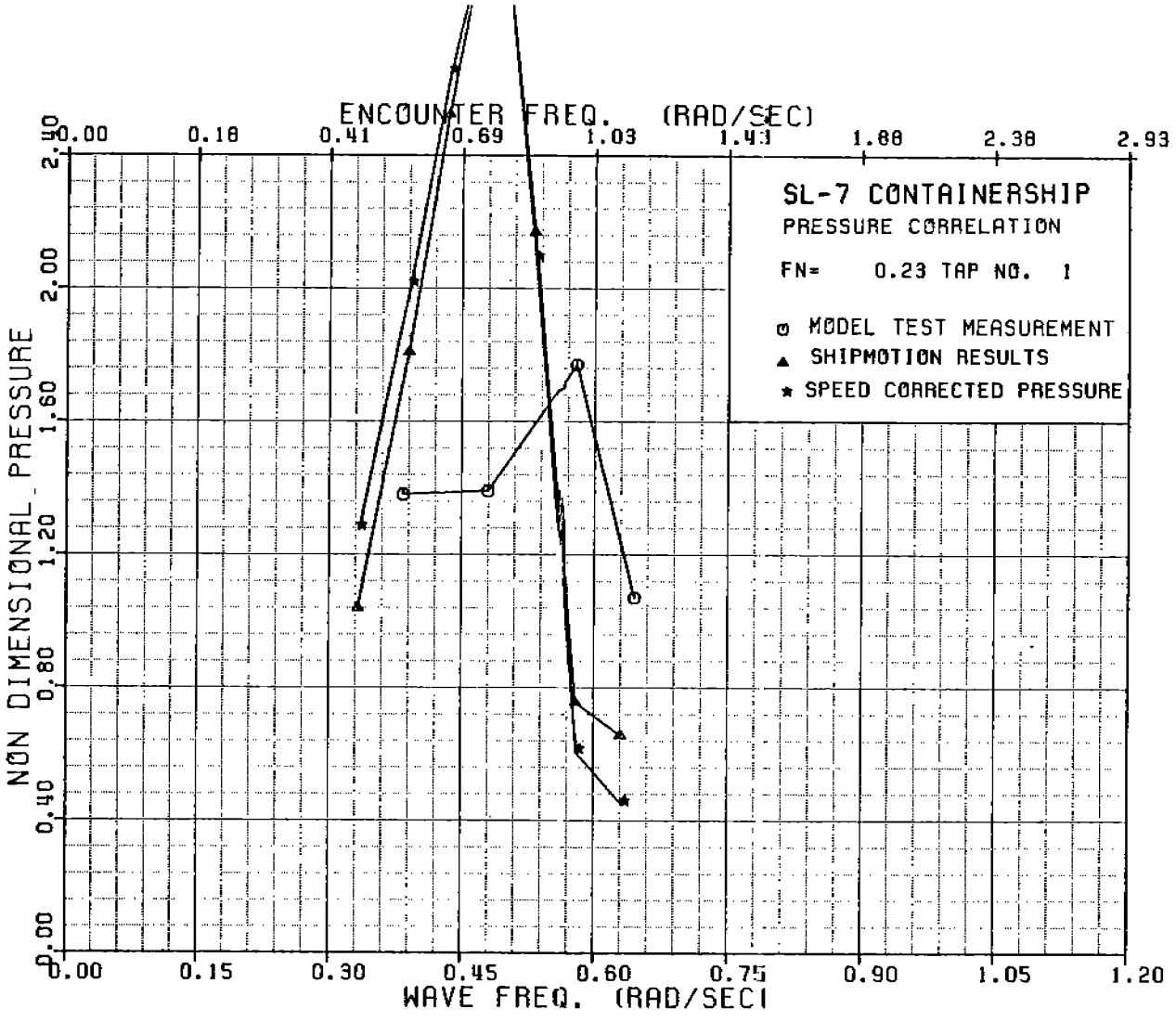

FIGURE A-67 SL-7 NONDIMENSIONAL PRESSURE AT TAP 1 , FN=0.23

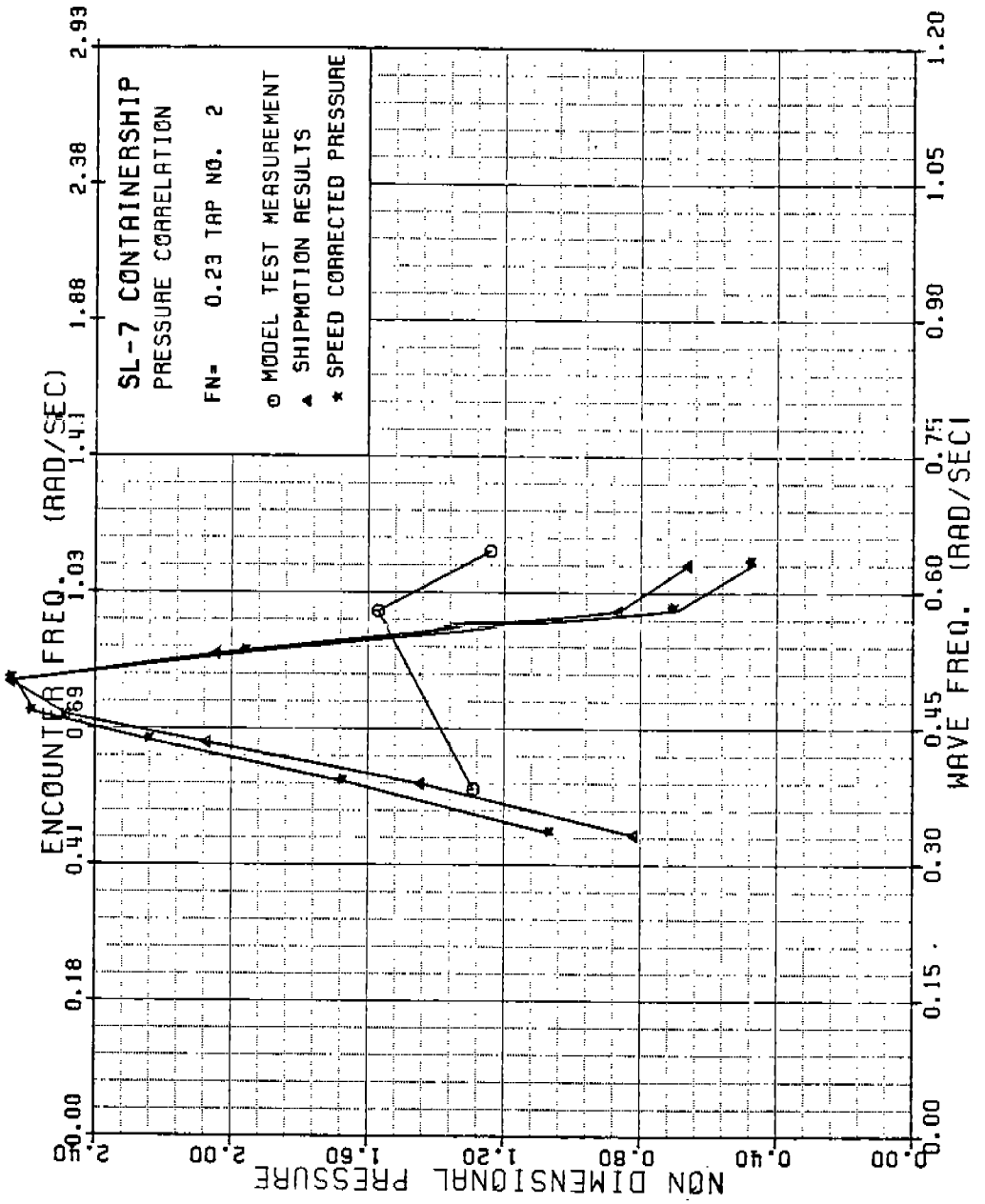

FIGURE A-68 SL-7 NONDIMENSIONAL PRESSURE AT TAP 2 , FN=0.23

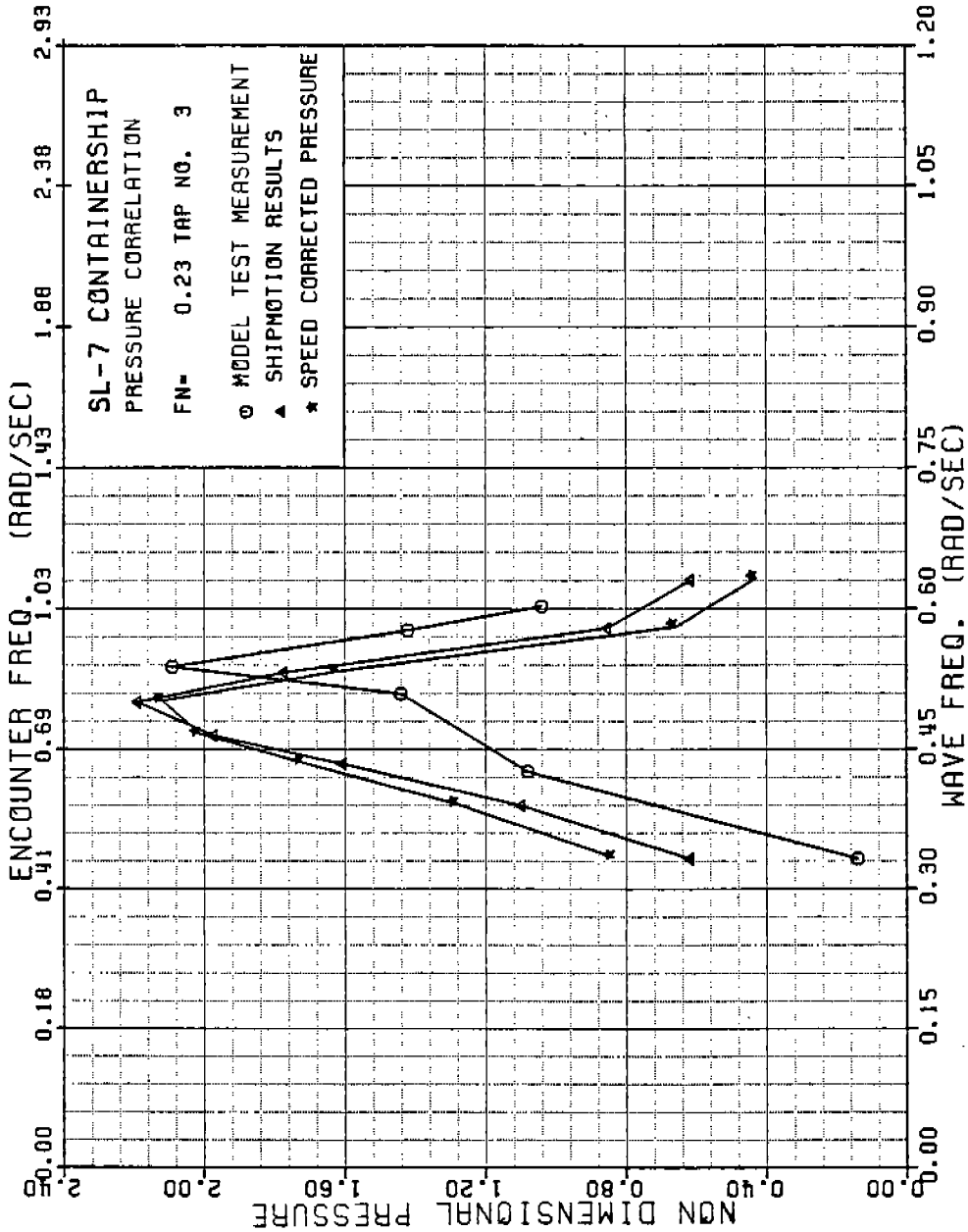

FIGURE A-69 SL-7 NONDIMENSIONAL PRESSURE AT TAP 3 , FN=0.23

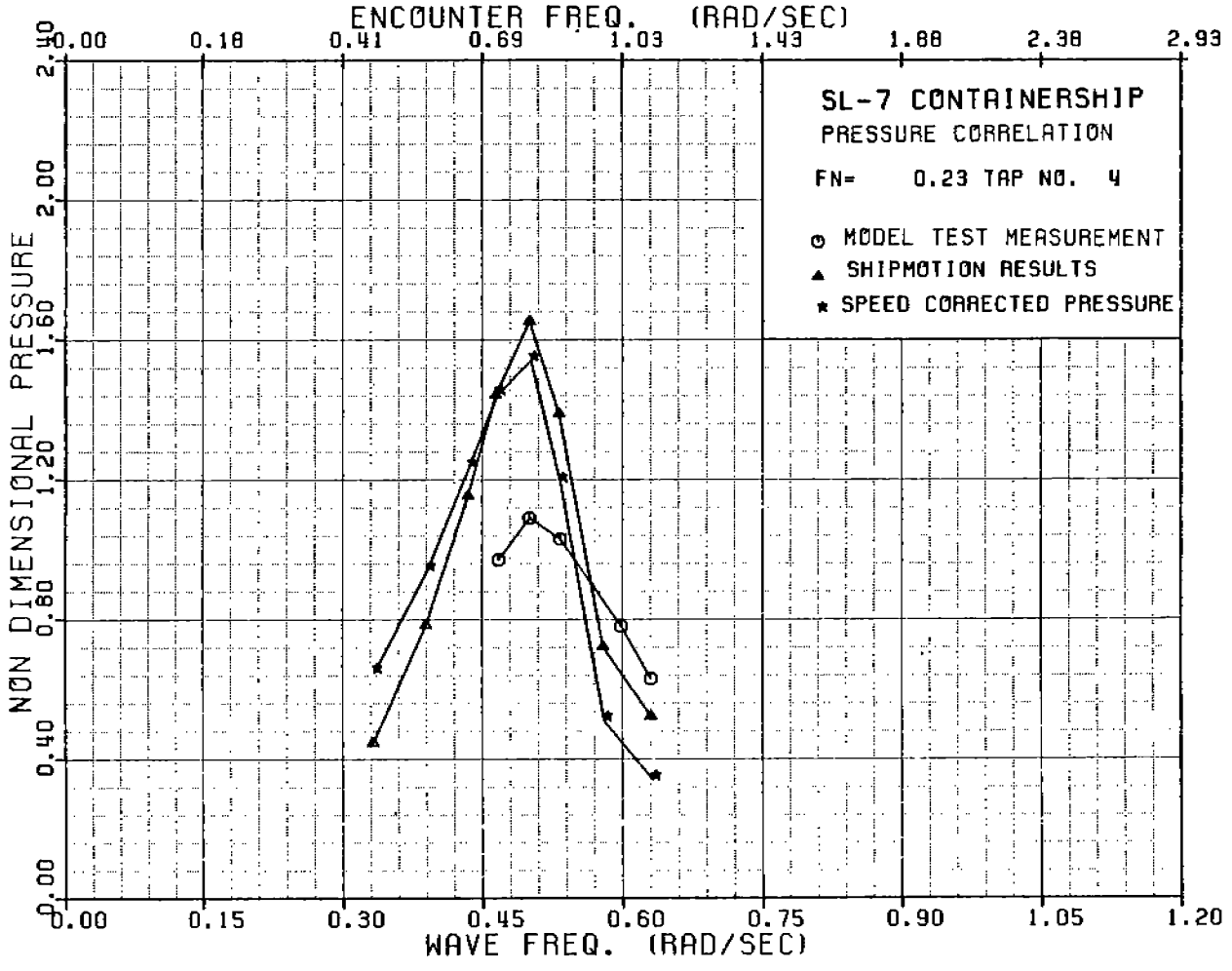

FIGURE A-70 SL-7 NONDIMENSIONAL PRESSURE AT TAP 4 , FN=0.23

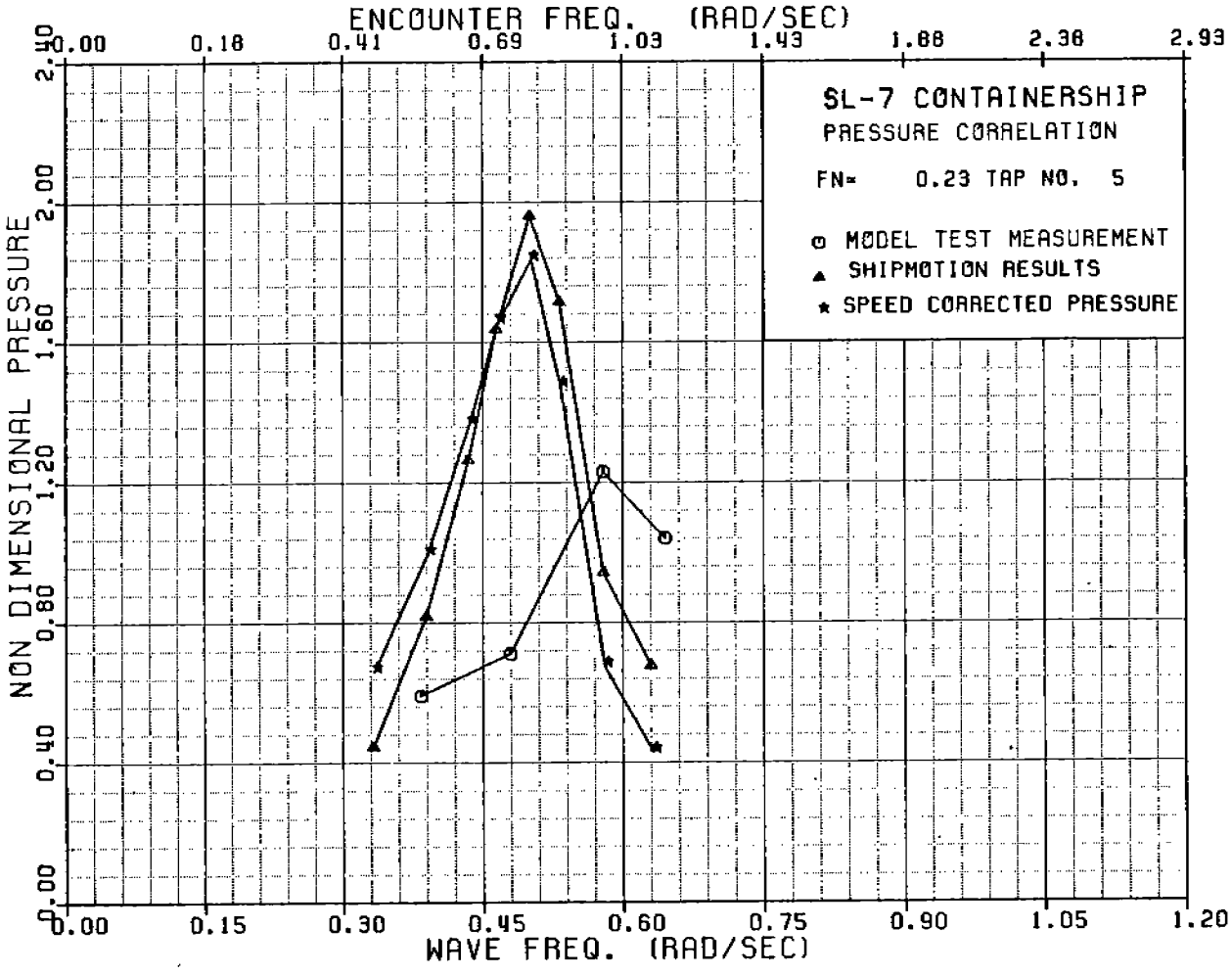

FIGURE A-71 SL-7 NONDIMENSIONAL PRESSURE AT TAP 5 , FN= 0.23

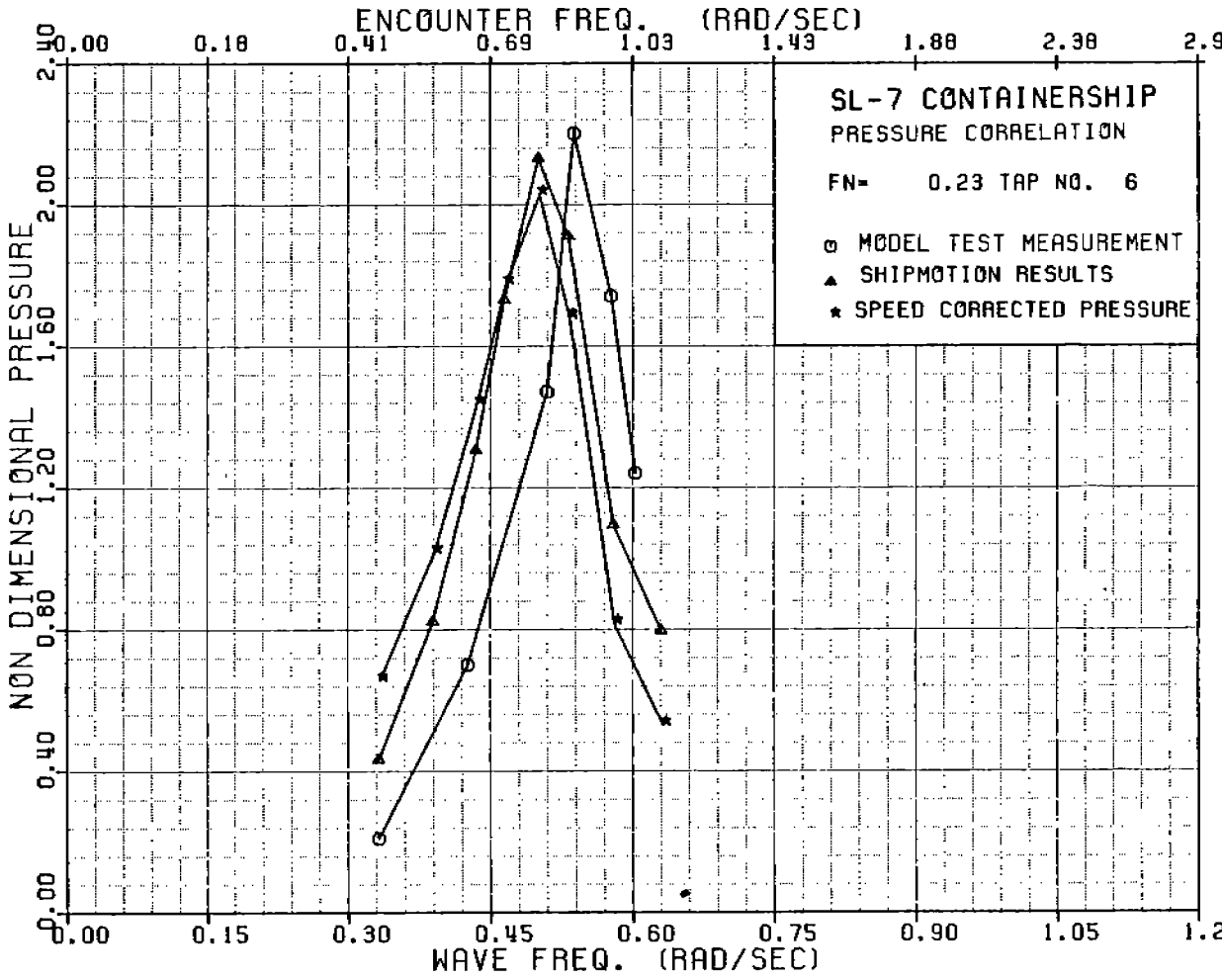

FIGURE A-72 SL-7 NONDIMENSIONAL PRESSURE AT TAP 6 , FN=

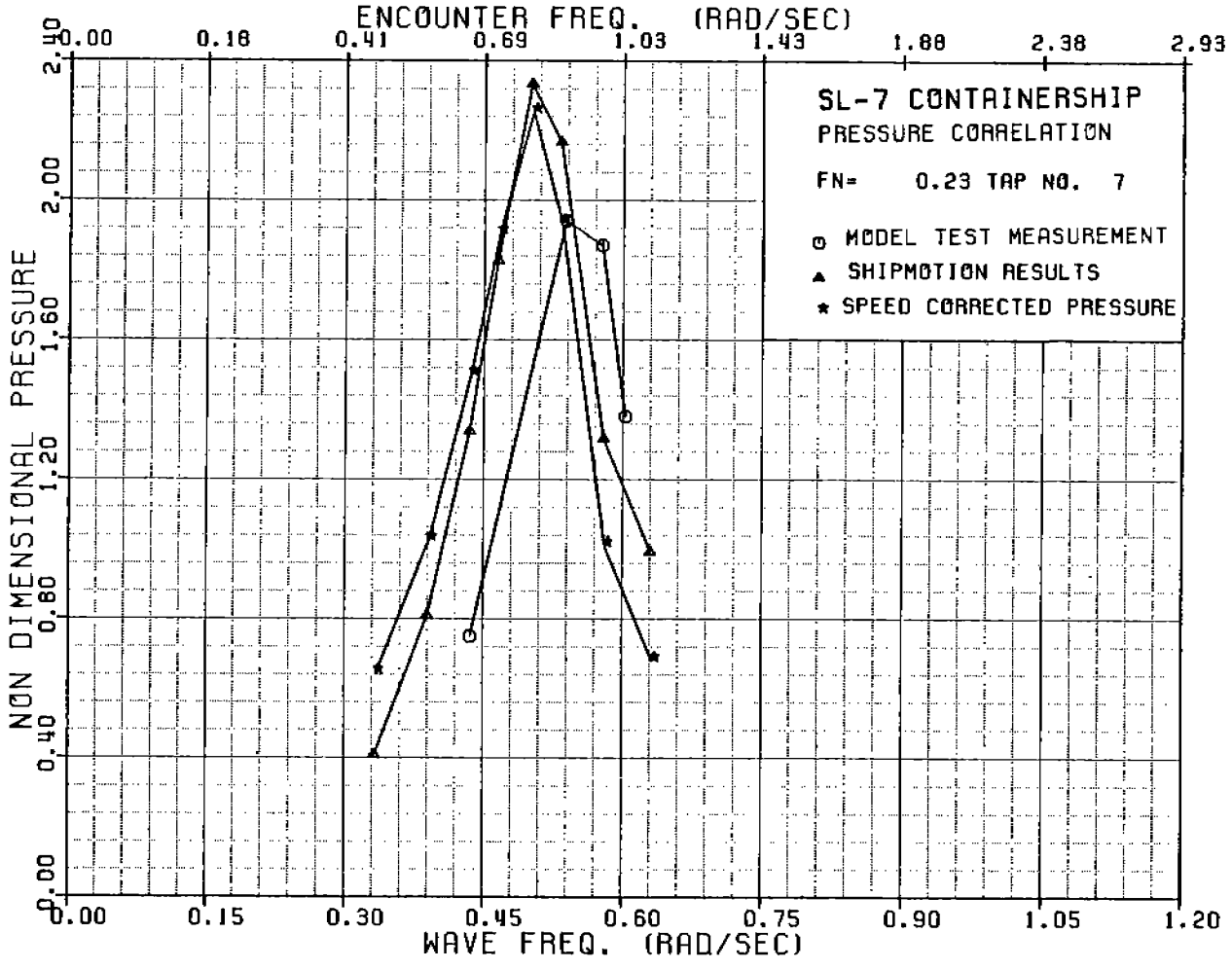

FIGURE A-73 SL-7 NONDIMENSIONAL PRESSURE AT TAP 7 , FN=0.23

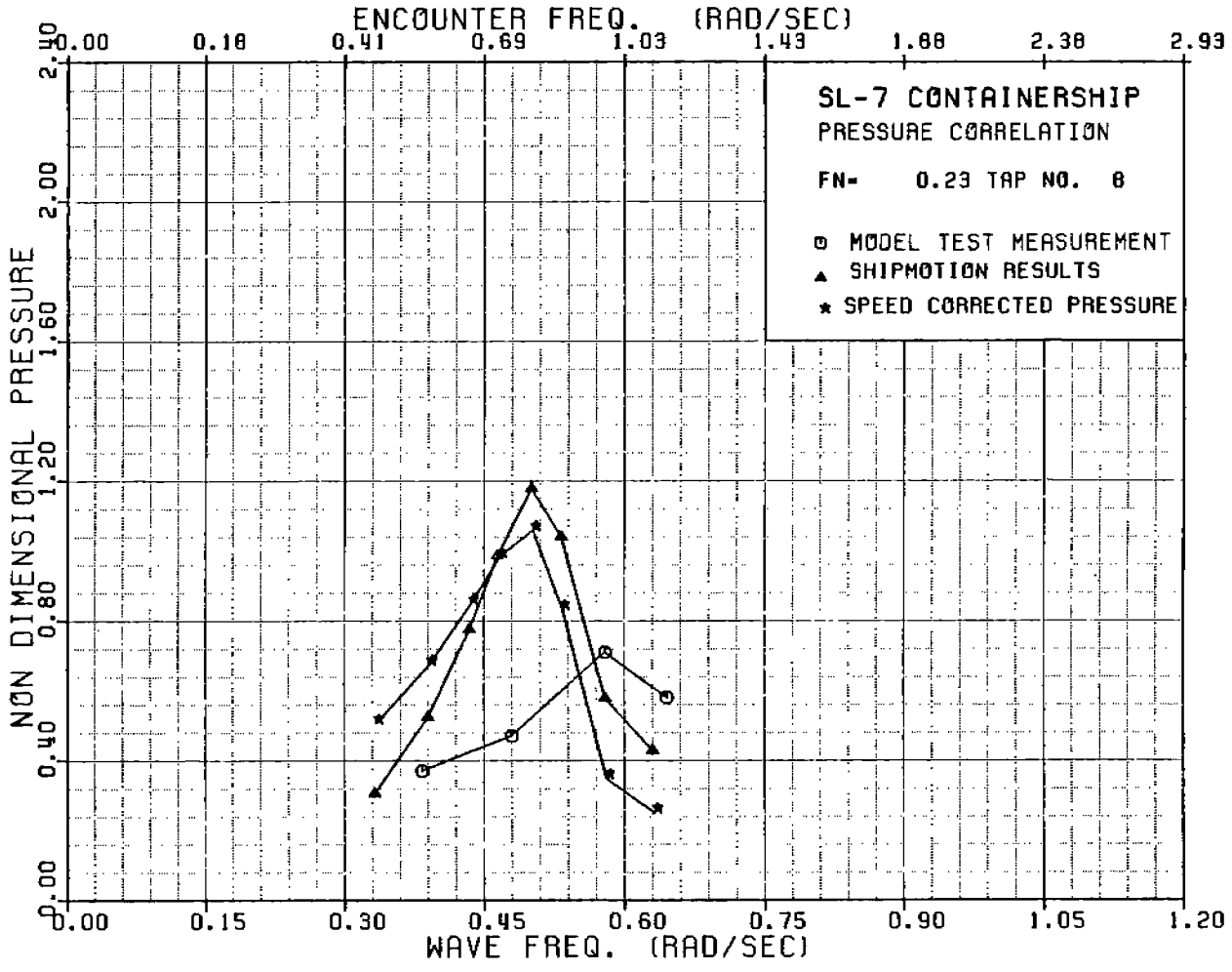

FIGURE A-74 SL-7 NONDIMENSIONAL PRESSURE AT TAP 8 , FN=0.23

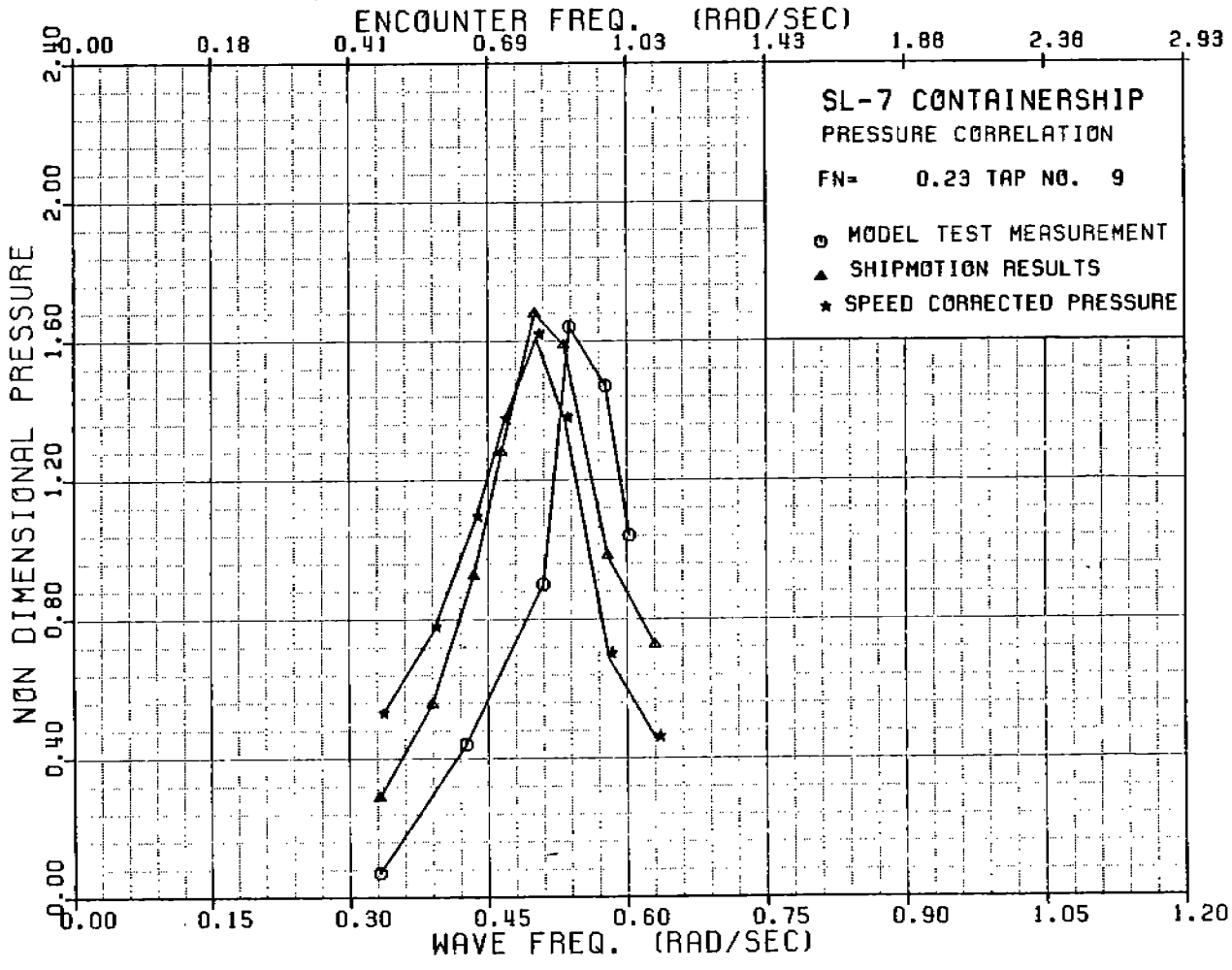

FIGURE A-75 SL-7 NONDIMENSIONAL PRESSURE AT TAP 9 , FN=0.23

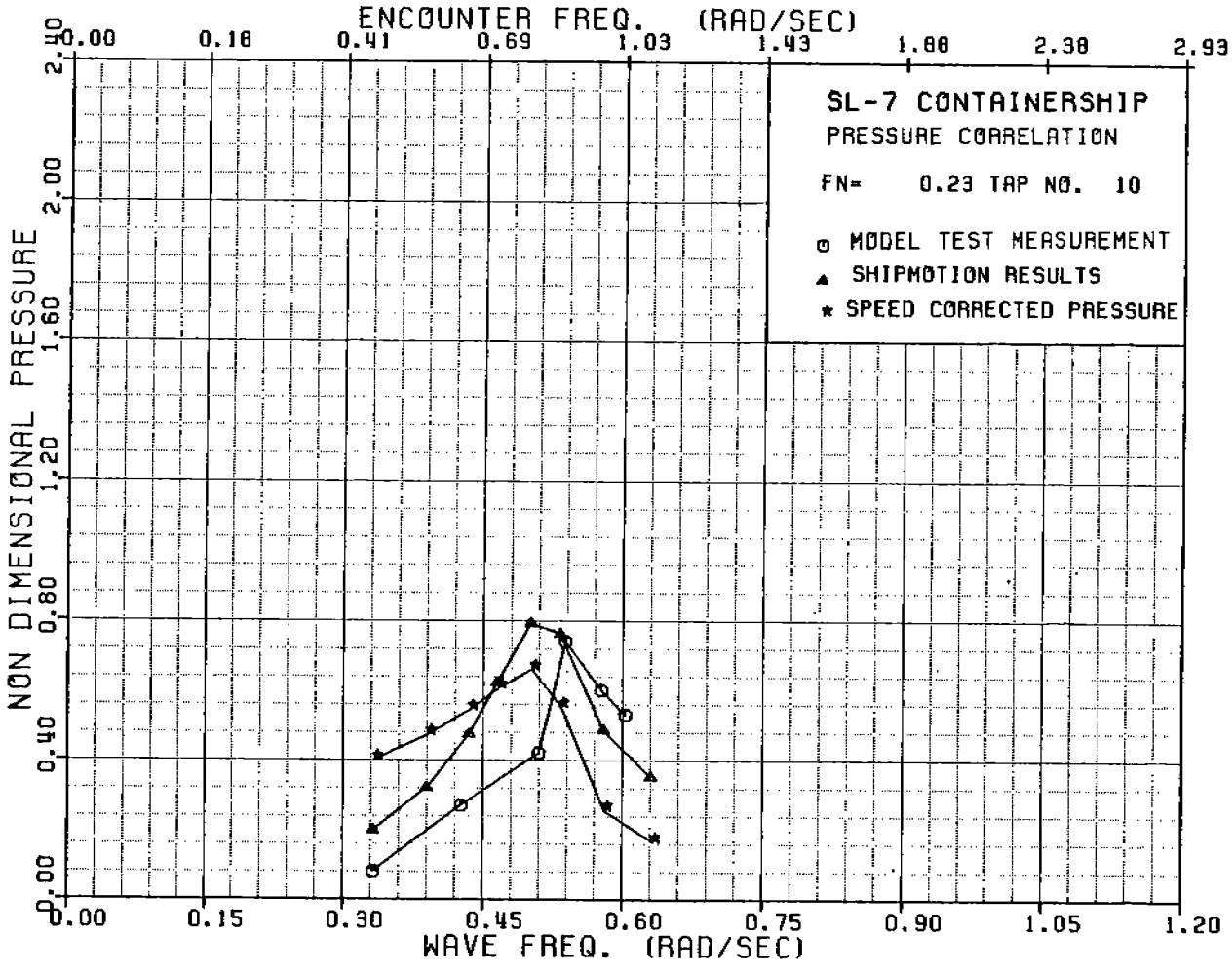

FIGURE A-76 SL-7 NONDIMENSIONAL PRESSURE AT TAP 10, FN=0.23

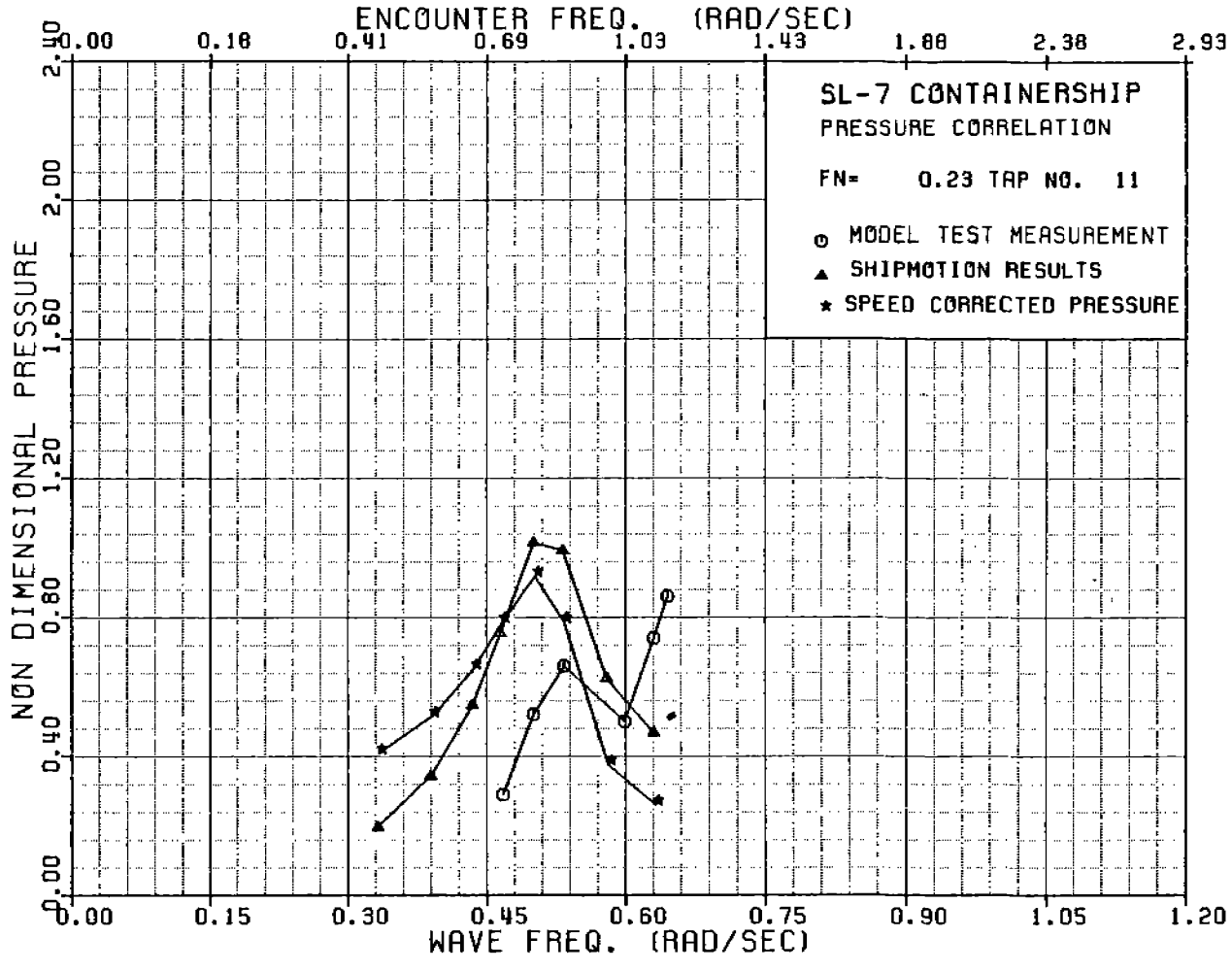

FIGURE A-77 SL-7 NONDIMENSIONAL PRESSURE AT TAP 11, FN=0.23

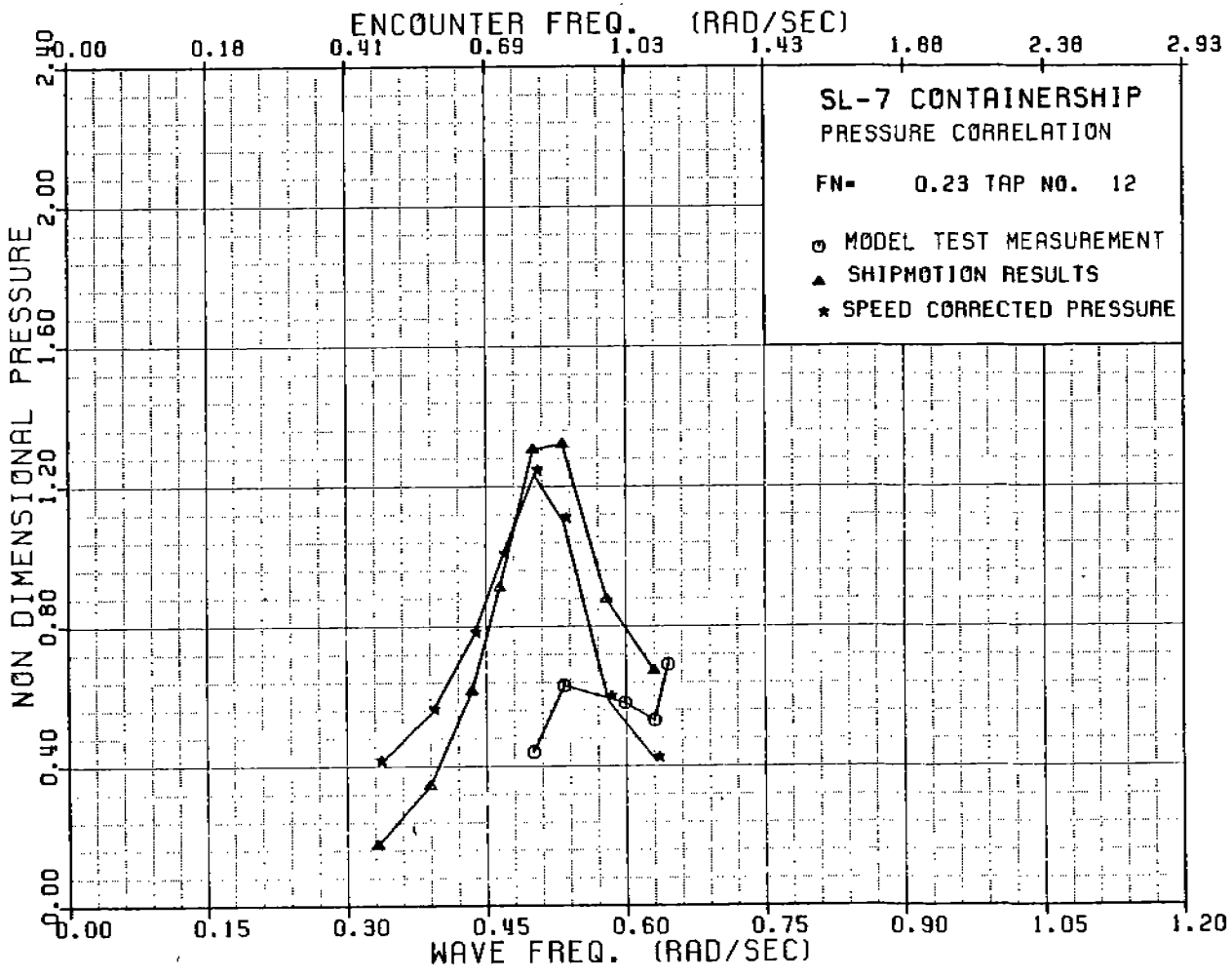

FIGURE A-78 SL-7 NONDIMENSIONAL PRESSURE AT TAP 12, FN=0.23

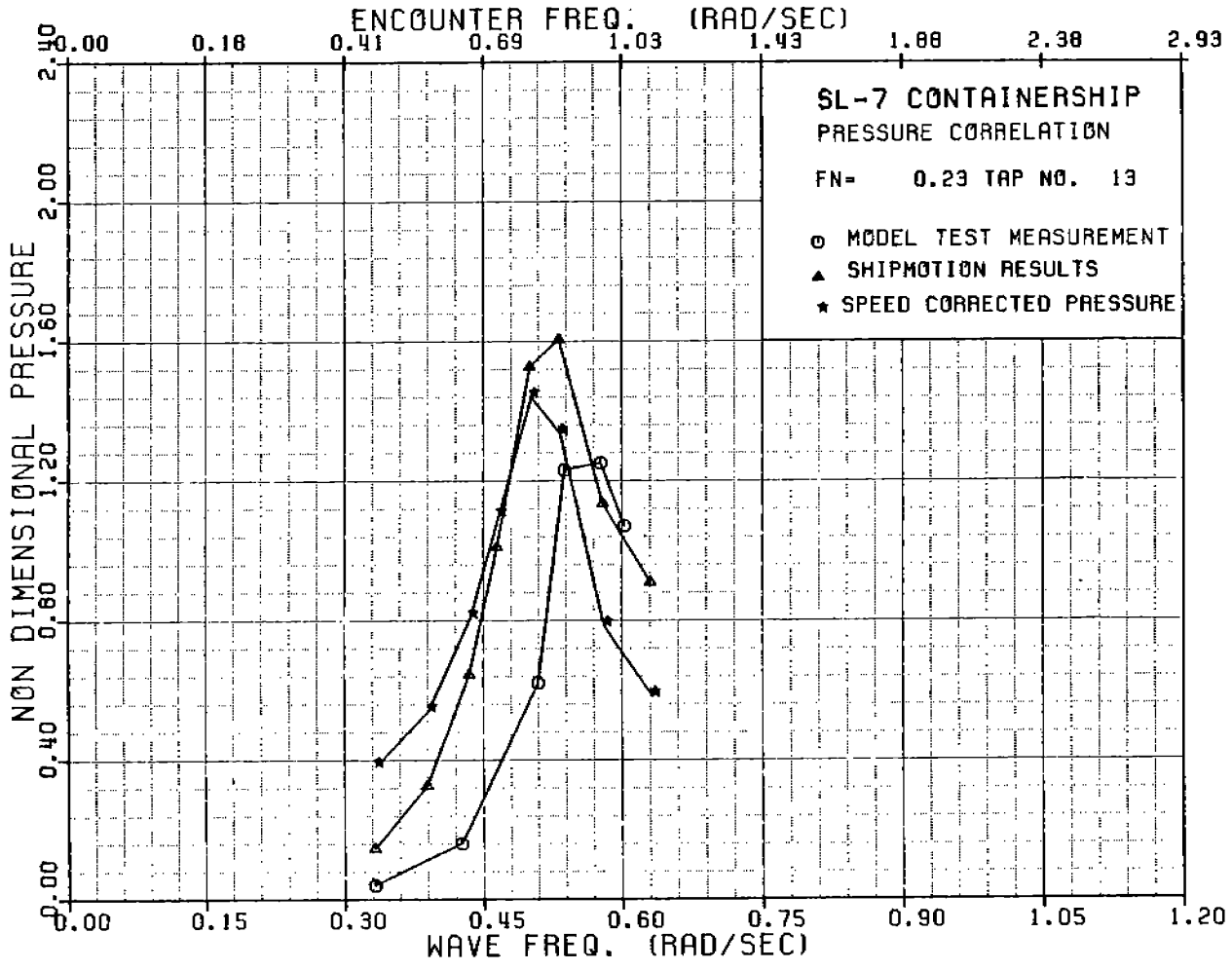

FIGURE A-79 SL-7 NONDIMENSIONAL PRESSURE AT TAP 13, FN=0.23

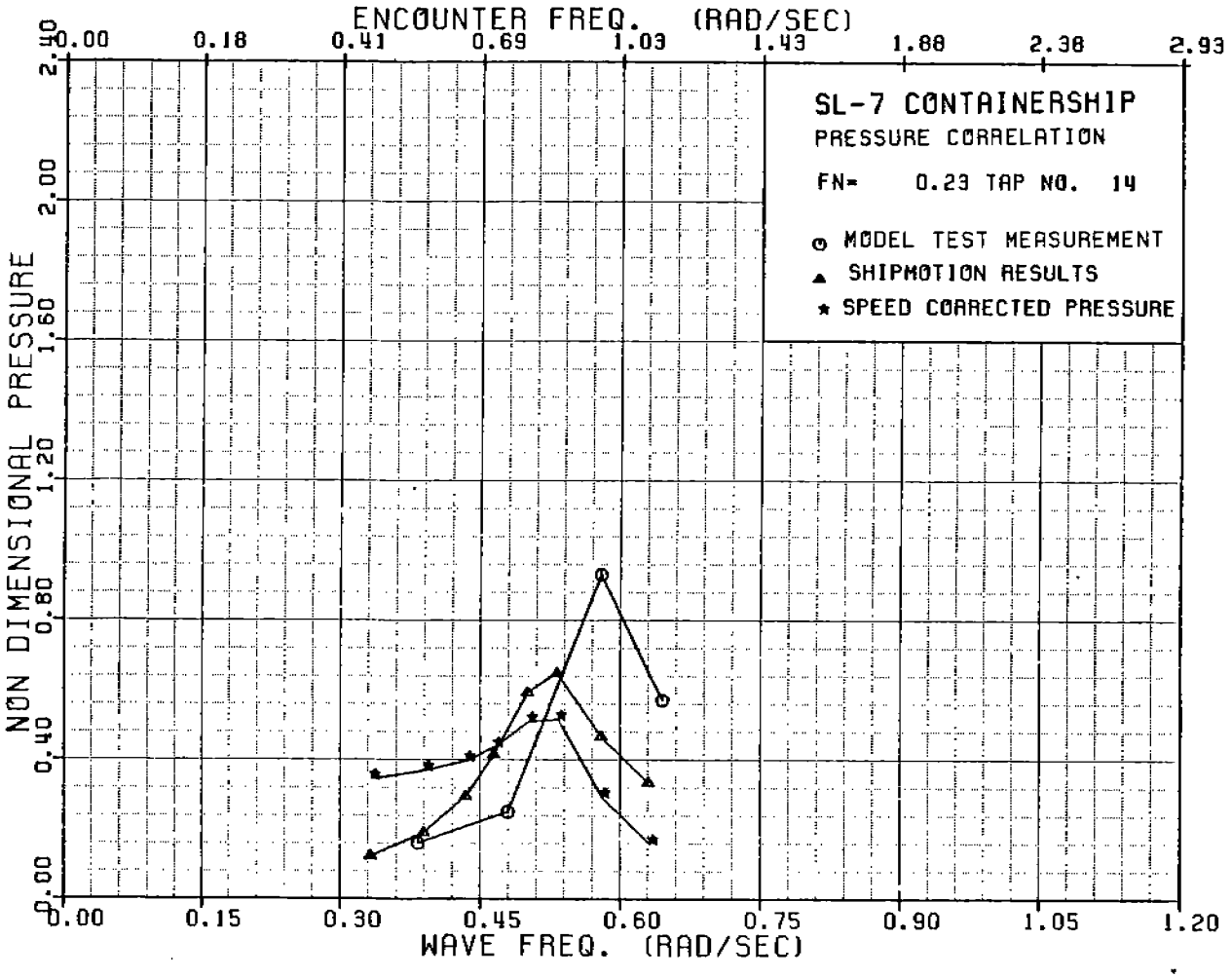

FIGURE A-80 SL-7 NONDIMENSIONAL PRESSURE AT TAP 14, FN=0.23

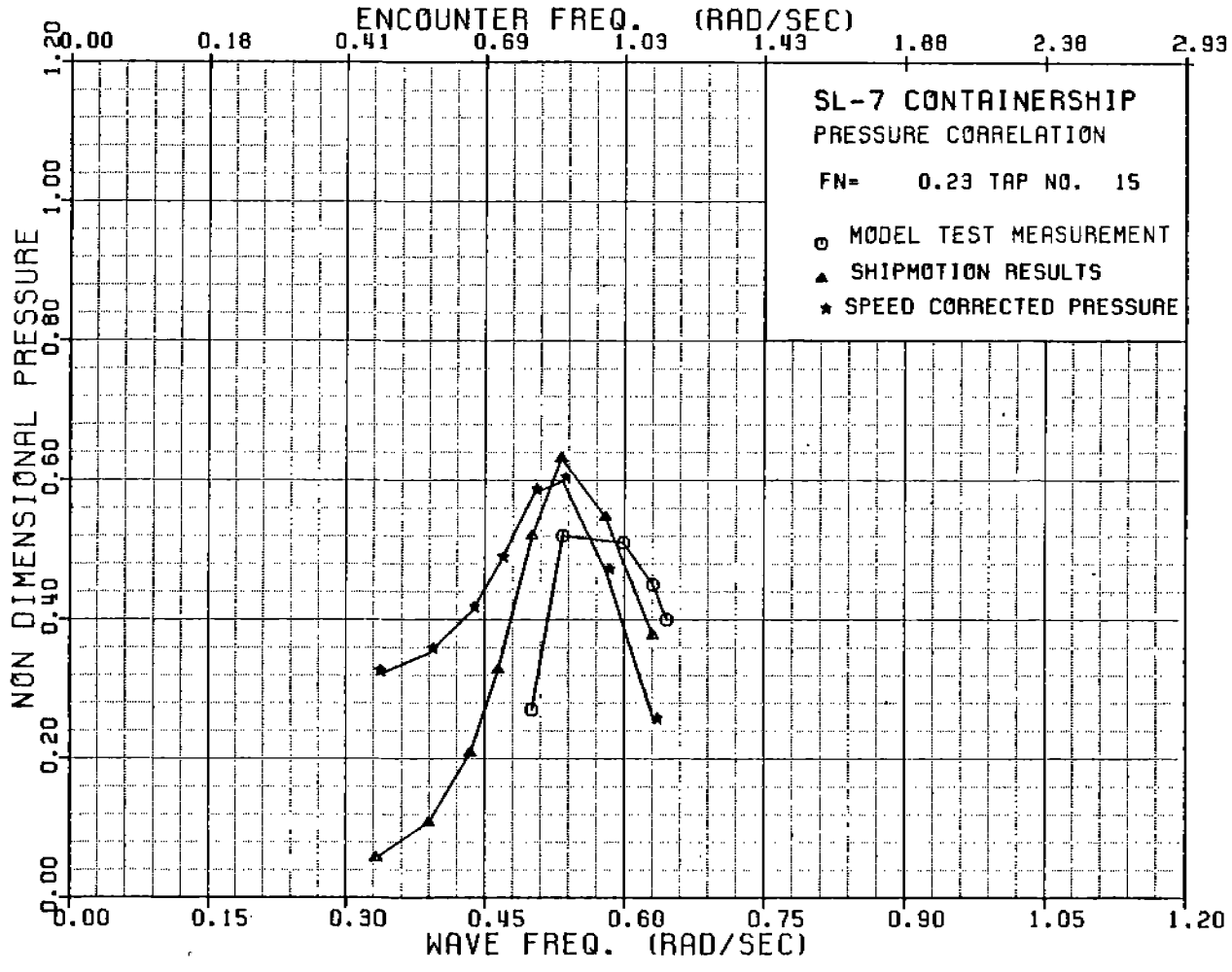

FIGURE A-81 SL-7 NONDIMENSIONAL PRESSURE AT TAP 15, FN=0.23

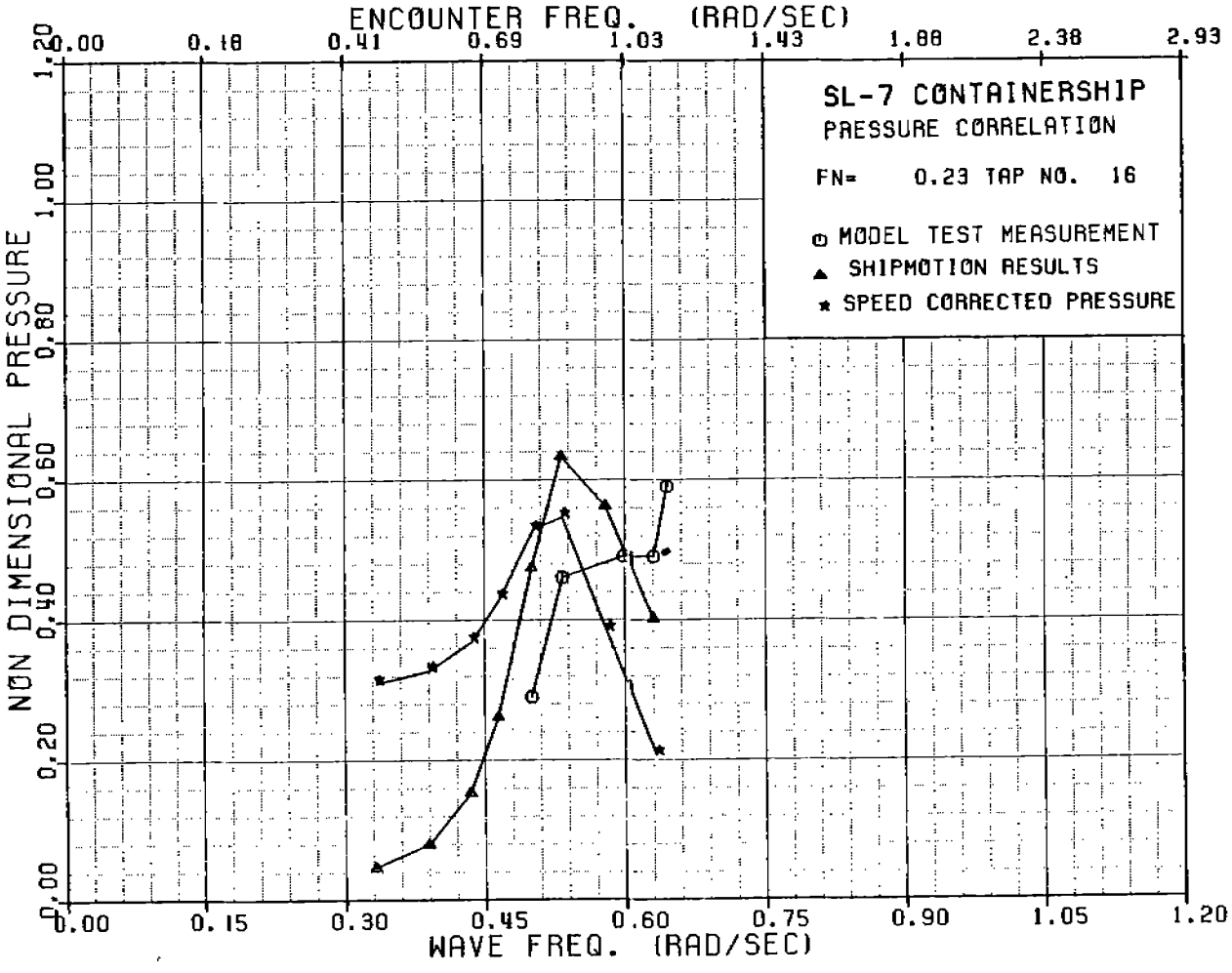

FIGURE A-82 SL-7 NONDIMENSIONAL PRESSURE AT TAP 16, FN=0.23

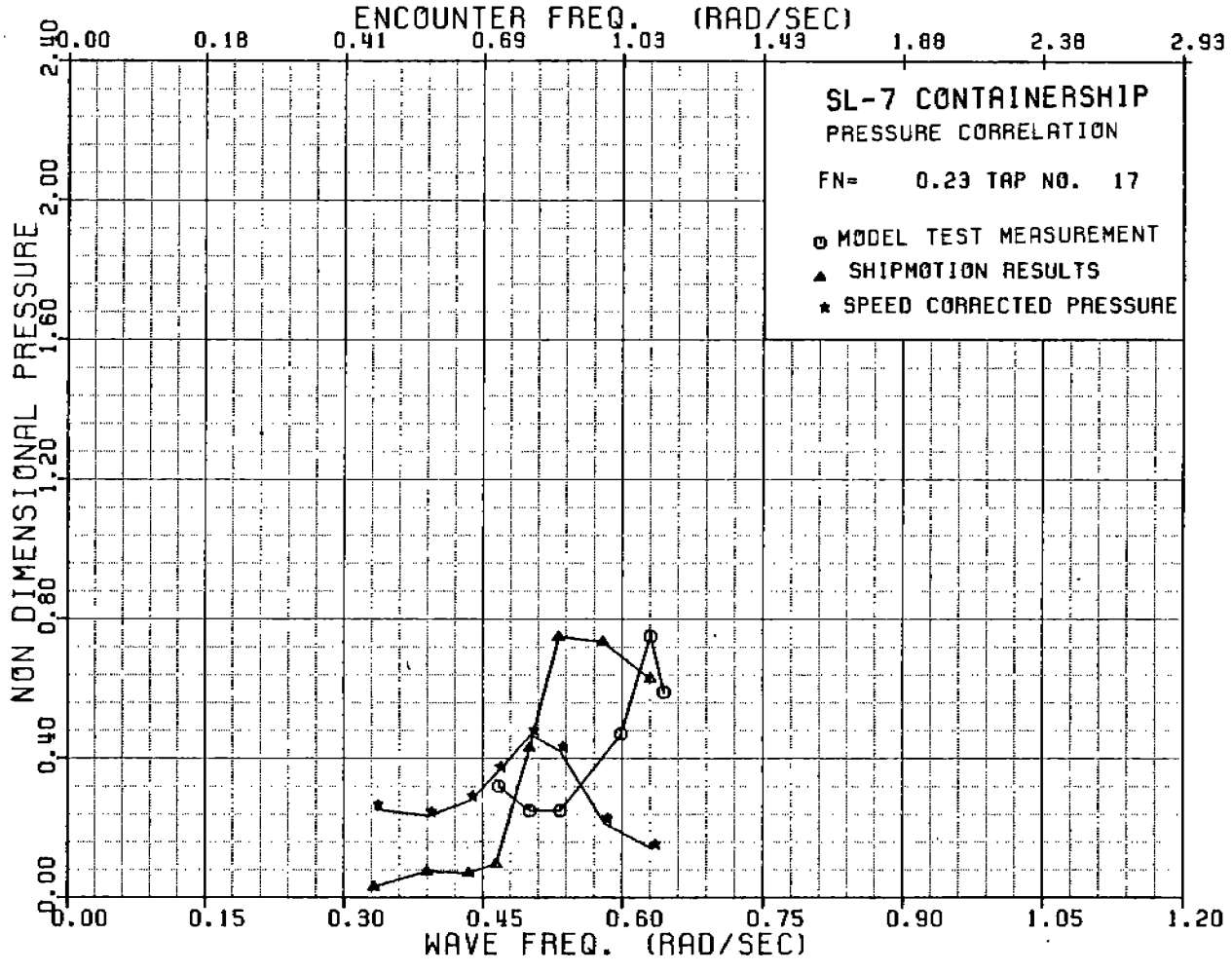

FIGURE A-83 SL-7 NONDIMENSIONAL PRESSURE AT TAP 17, FN=0.23

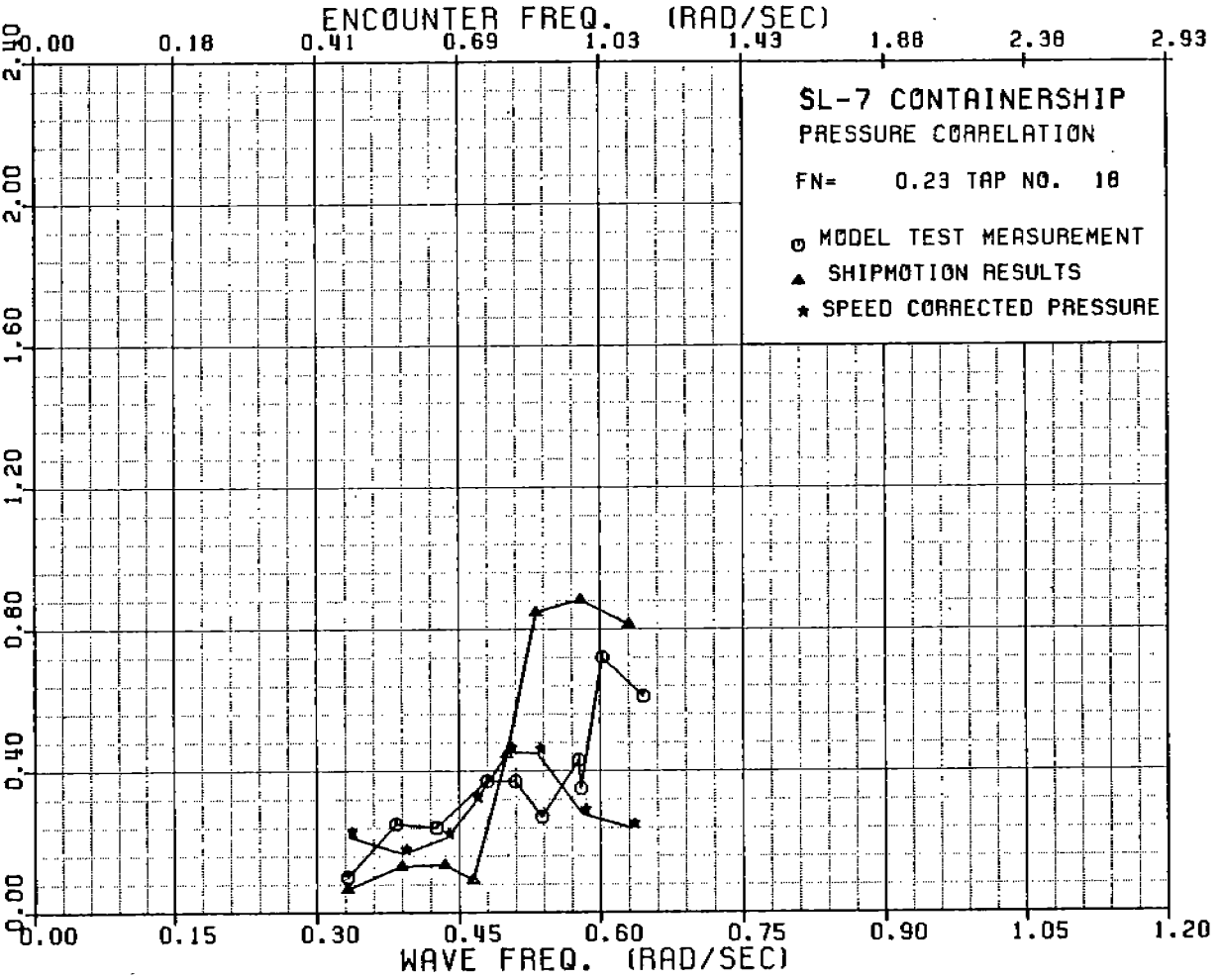

FIGURE A-84 SL-7 NONDIMENSIONAL PRESSURE AT TAP 18, FN= 0.23

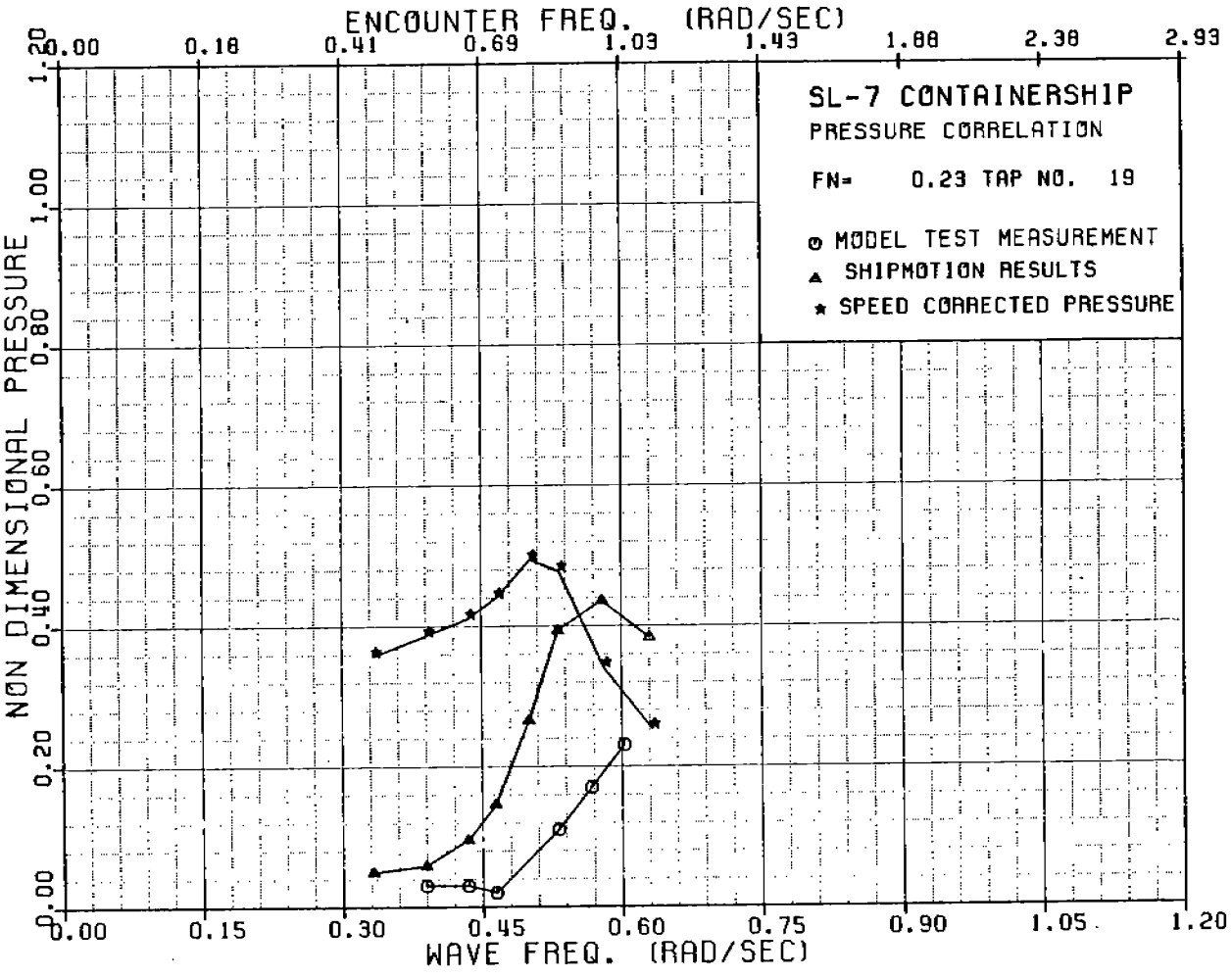

FIGURE A-85 SL-7 NONDIMENSIONAL PRESSURE AT TAP 19, FN=0.23

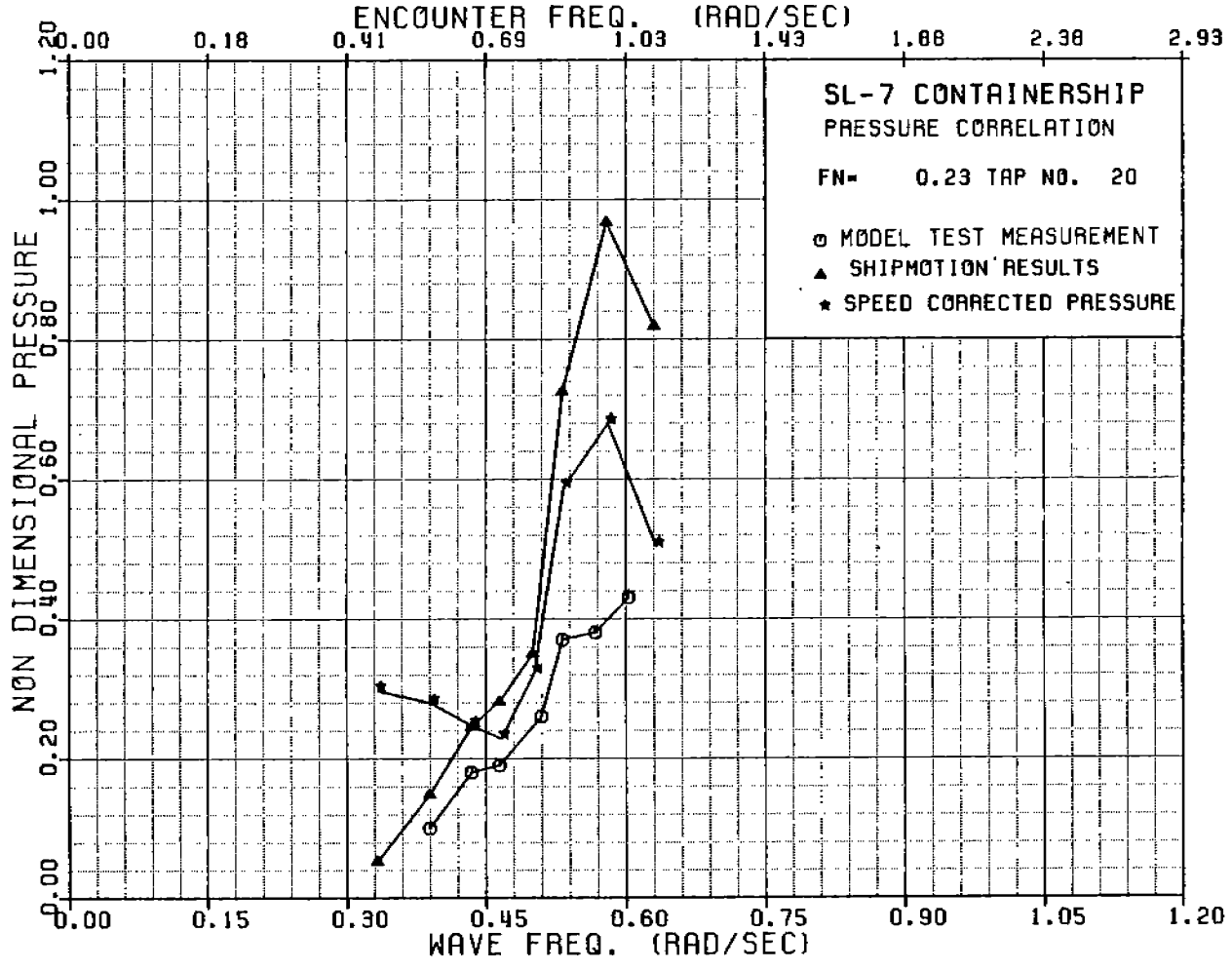

FIGURE A-86 SL-7 NONDIMENSIONAL PRESSURE AT TAP 20, FN=0.23

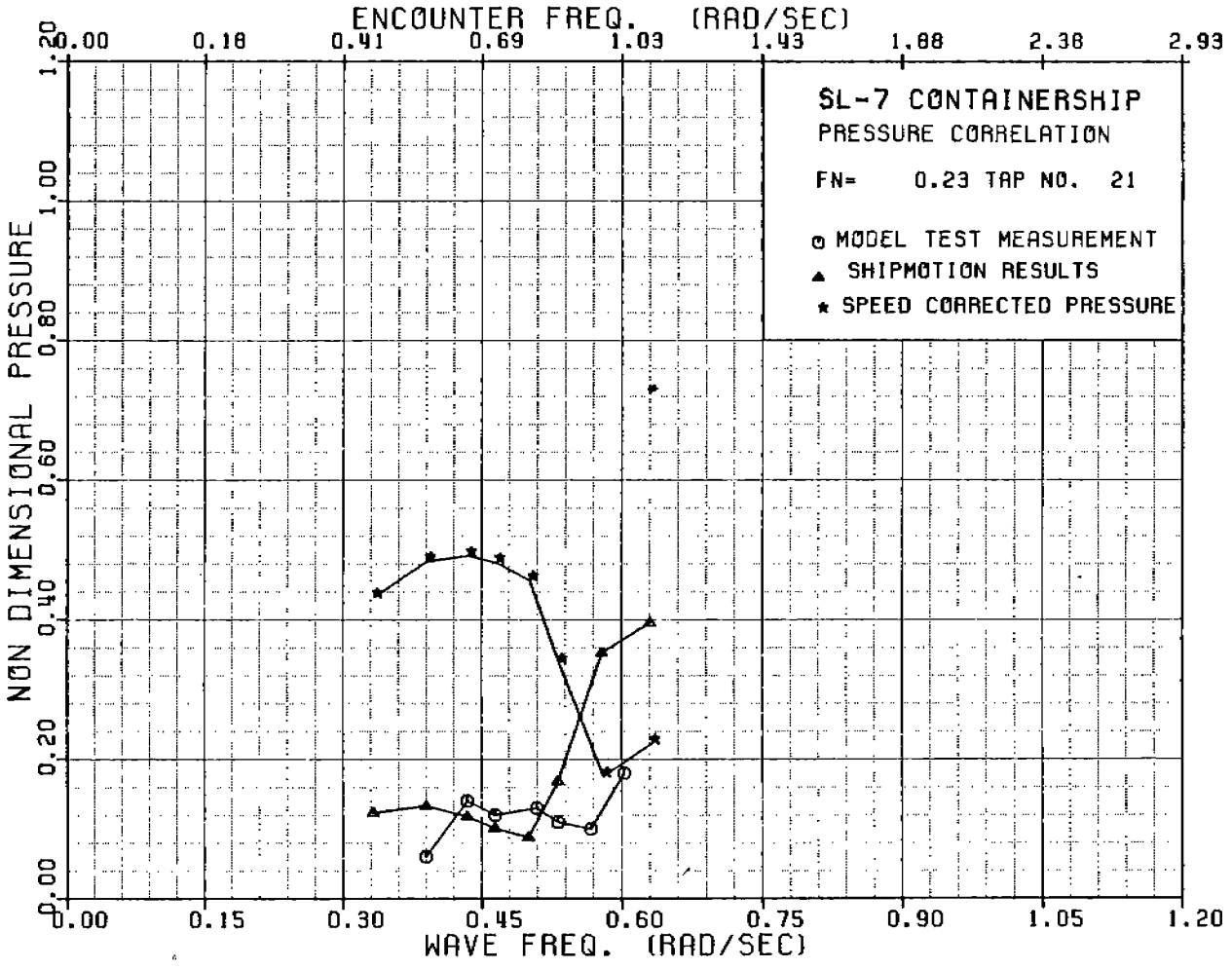

FIGURE A-87 SL-7 NONDIMENSIONAL PRESSURE AT TAP 21, FN= 0.23

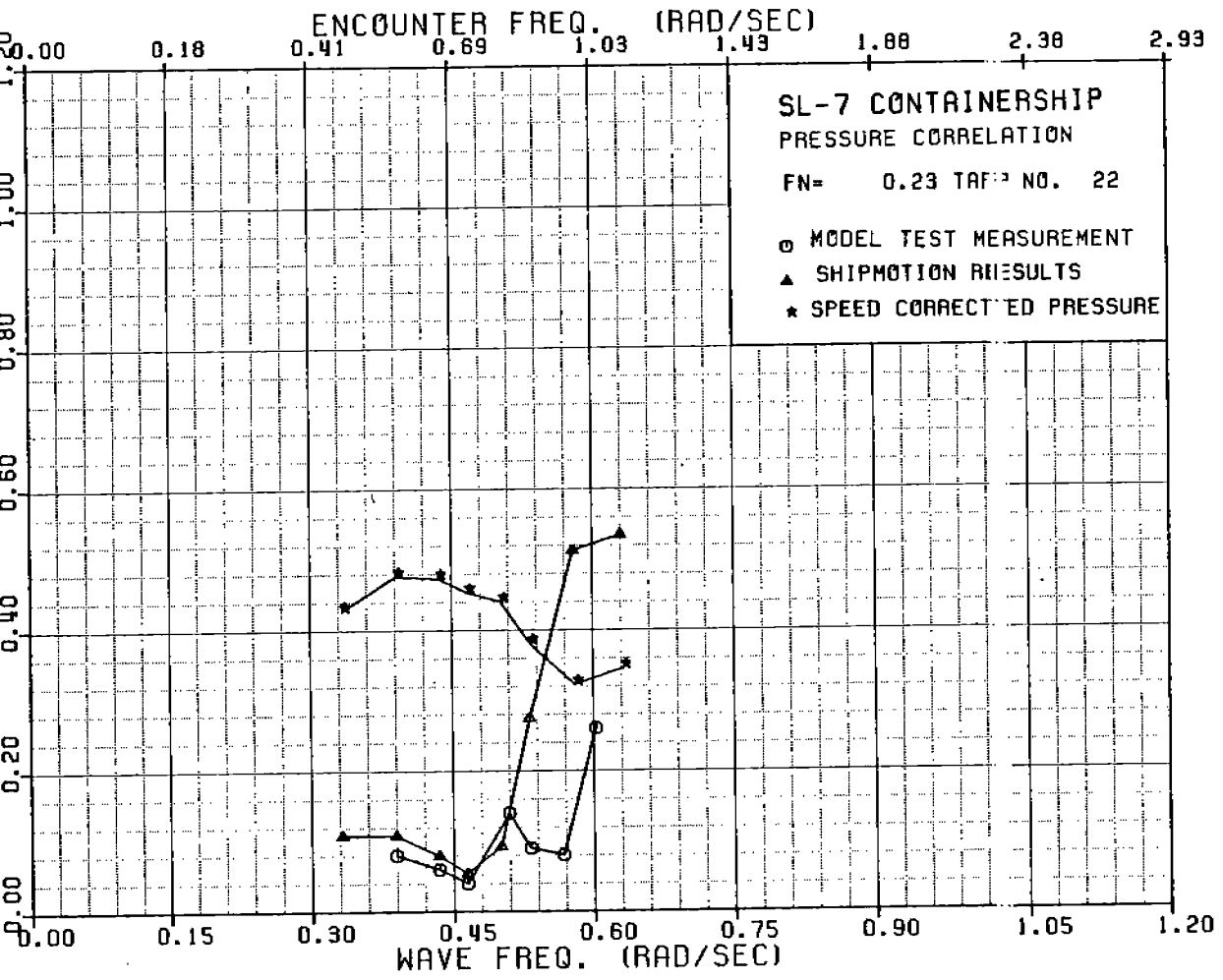

FIGURE A-88 SL-7 NONDIMENSIONAL PRESSURE AT TAP 22, FN=0.23

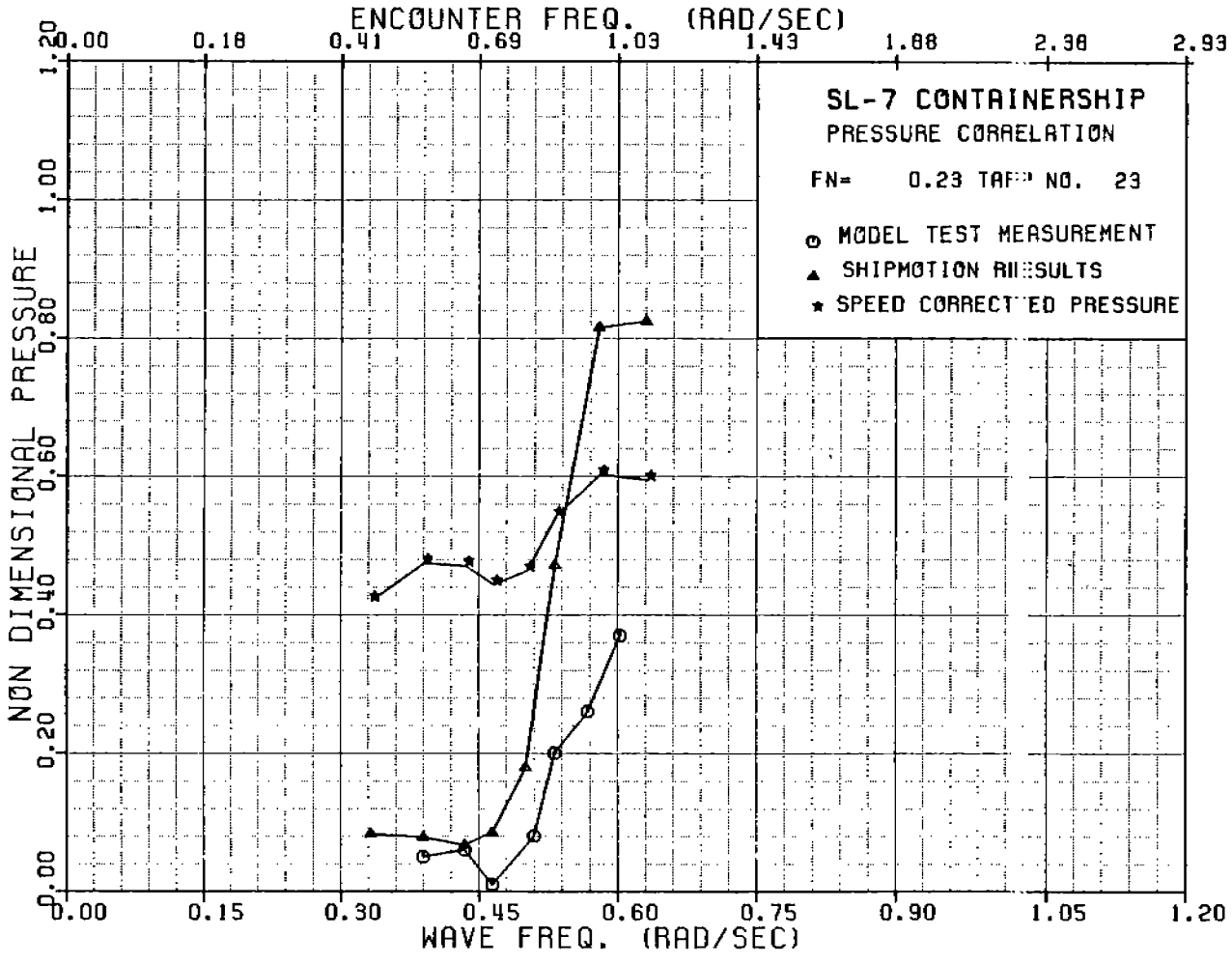

FIGURE A-89 SL-7 NONDIMENSIONAL PRESSURE AT TAP 23, FN= 0.23

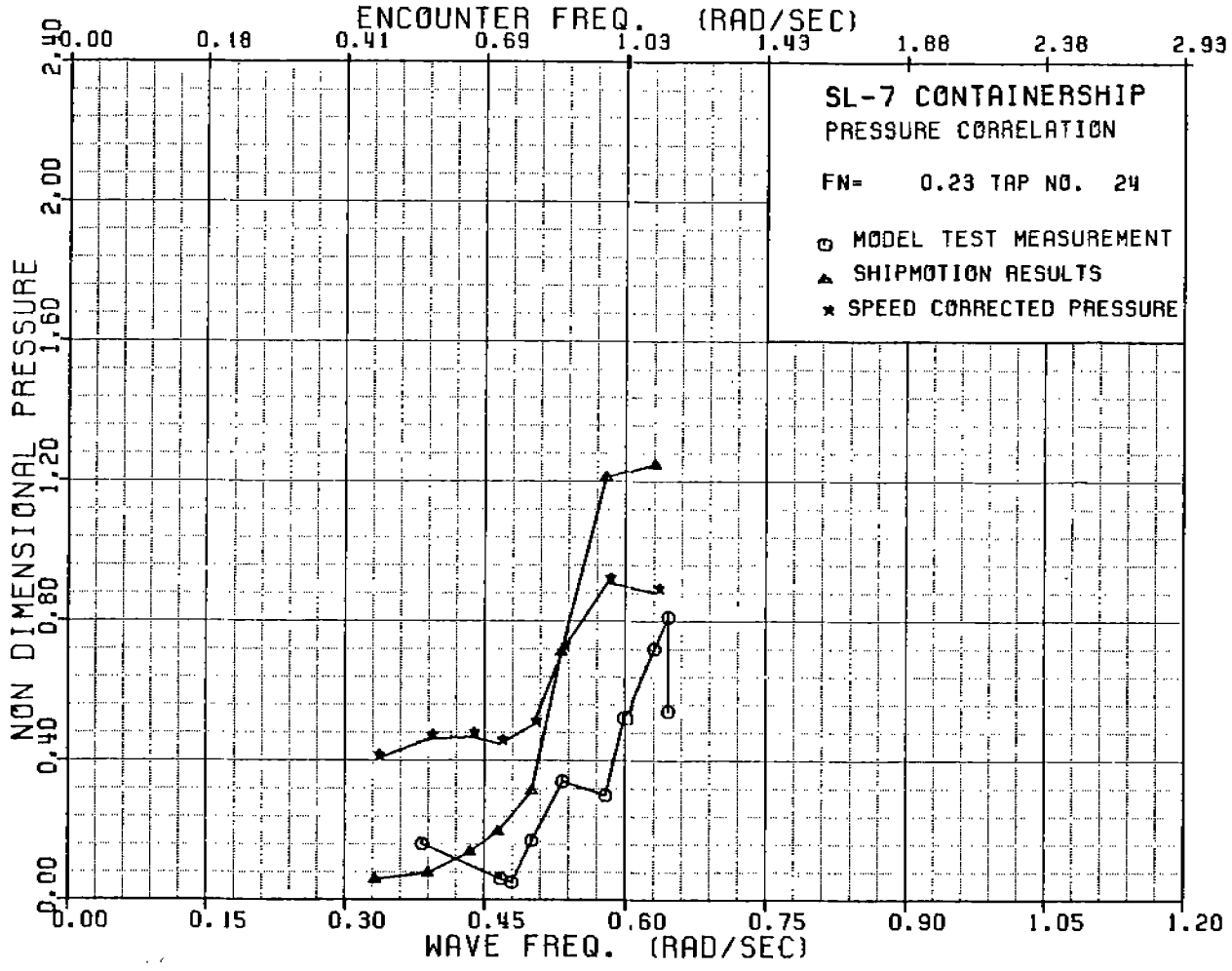

FIGURE A-90 SL-7 NONDIMENSIONAL PRESSURE AT TAP 24, FN=0.23

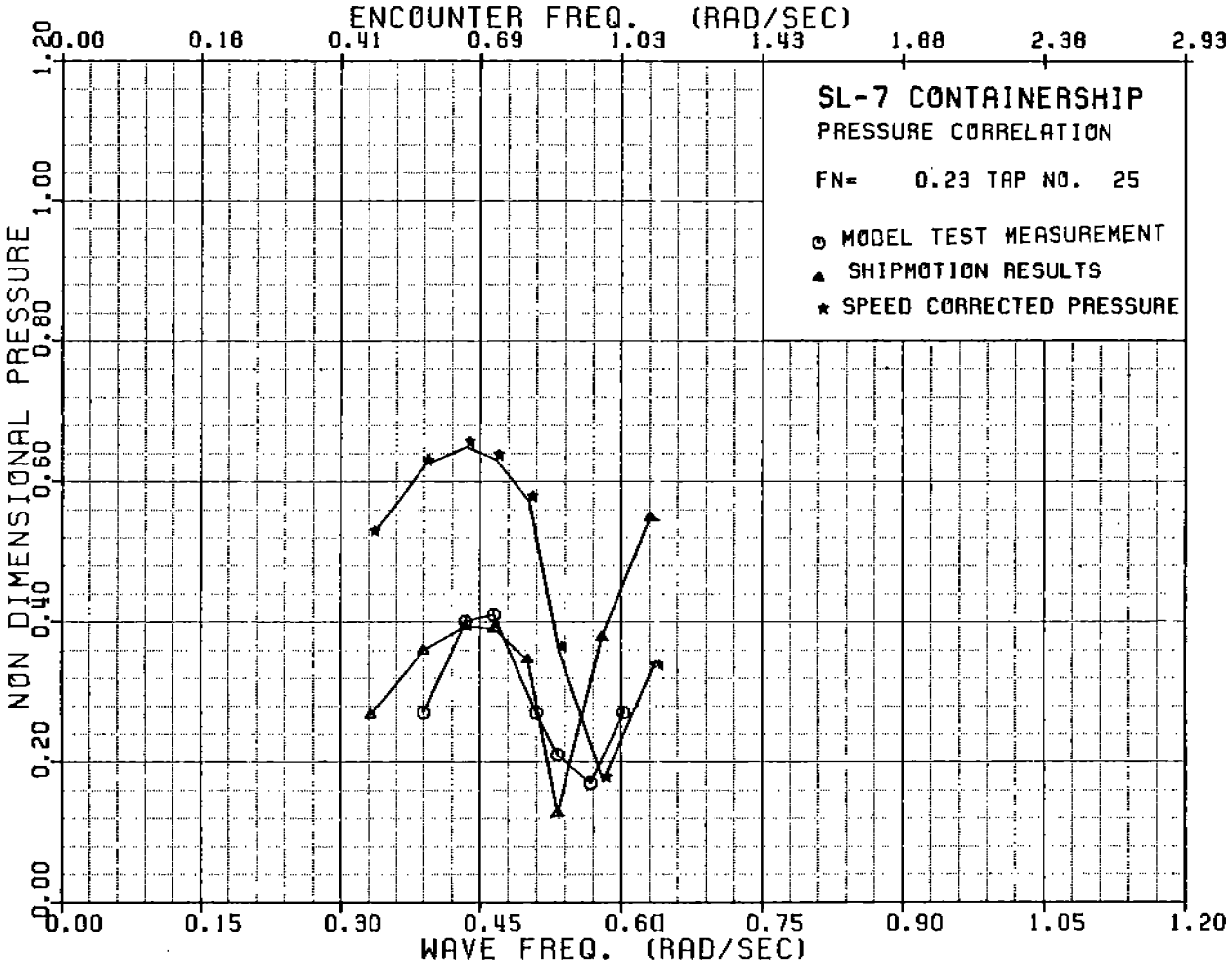

FIGURE A-91 SL-7 NONDIMENSIONAL PRESSURE AT TAP 25, FN= 0.23

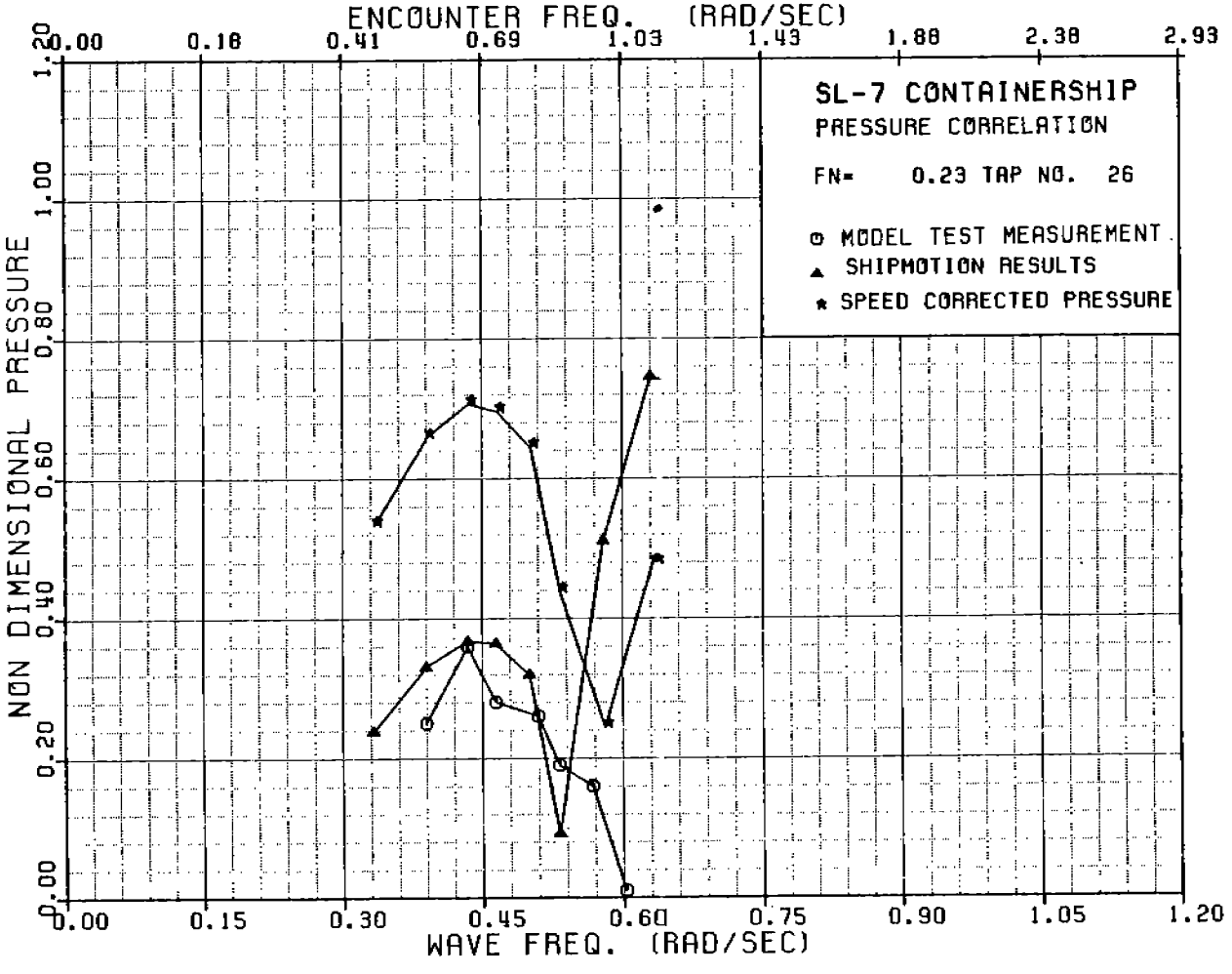

FIGURE A-92 SL-7 NONDIMENSIONAL PRESSURE AT TAP 26, FN=0.23

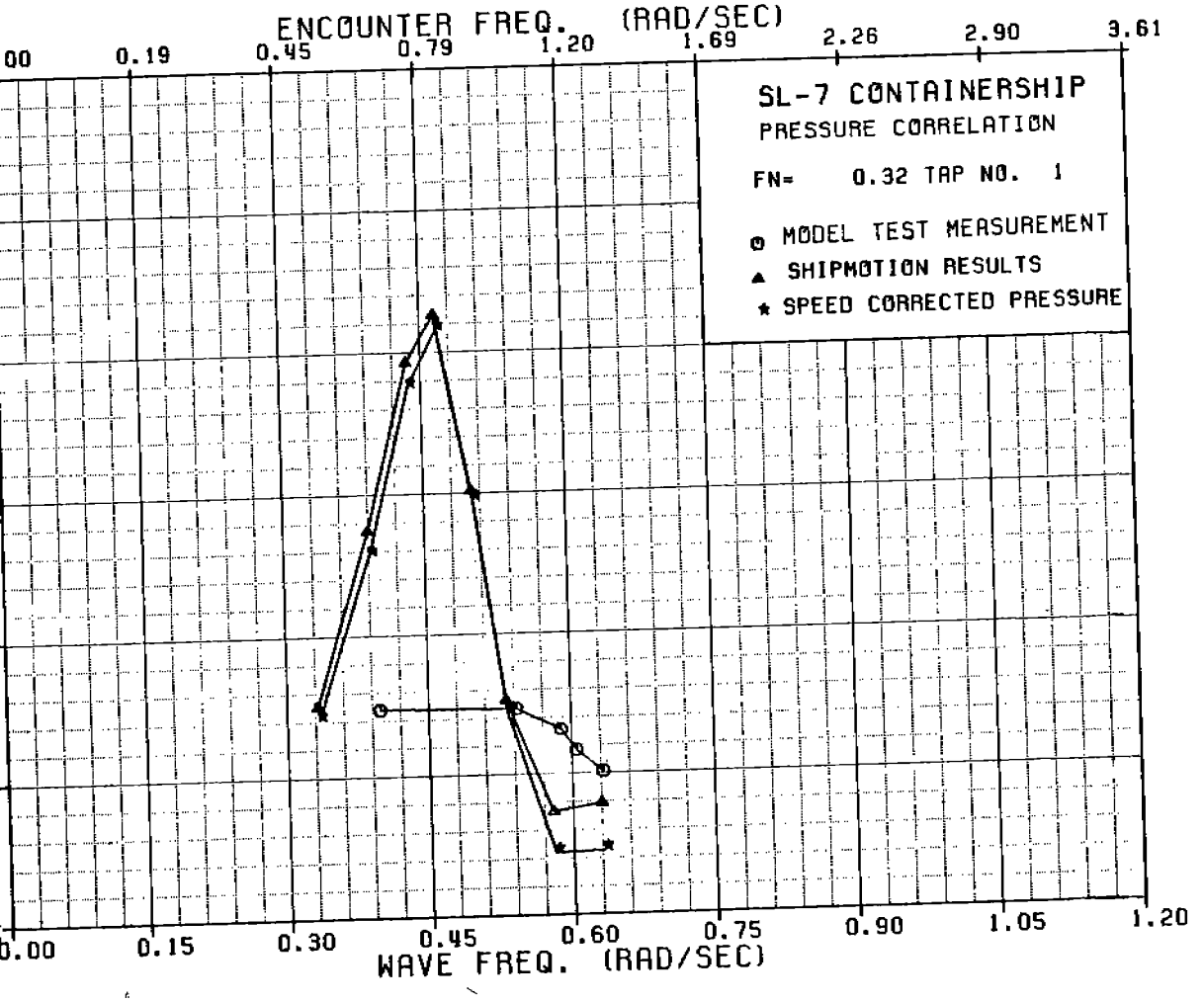

FIGURE A-93 SL-7 NONDIMENSIONAL PRESSURE AT TAP 1 , FN=0.32

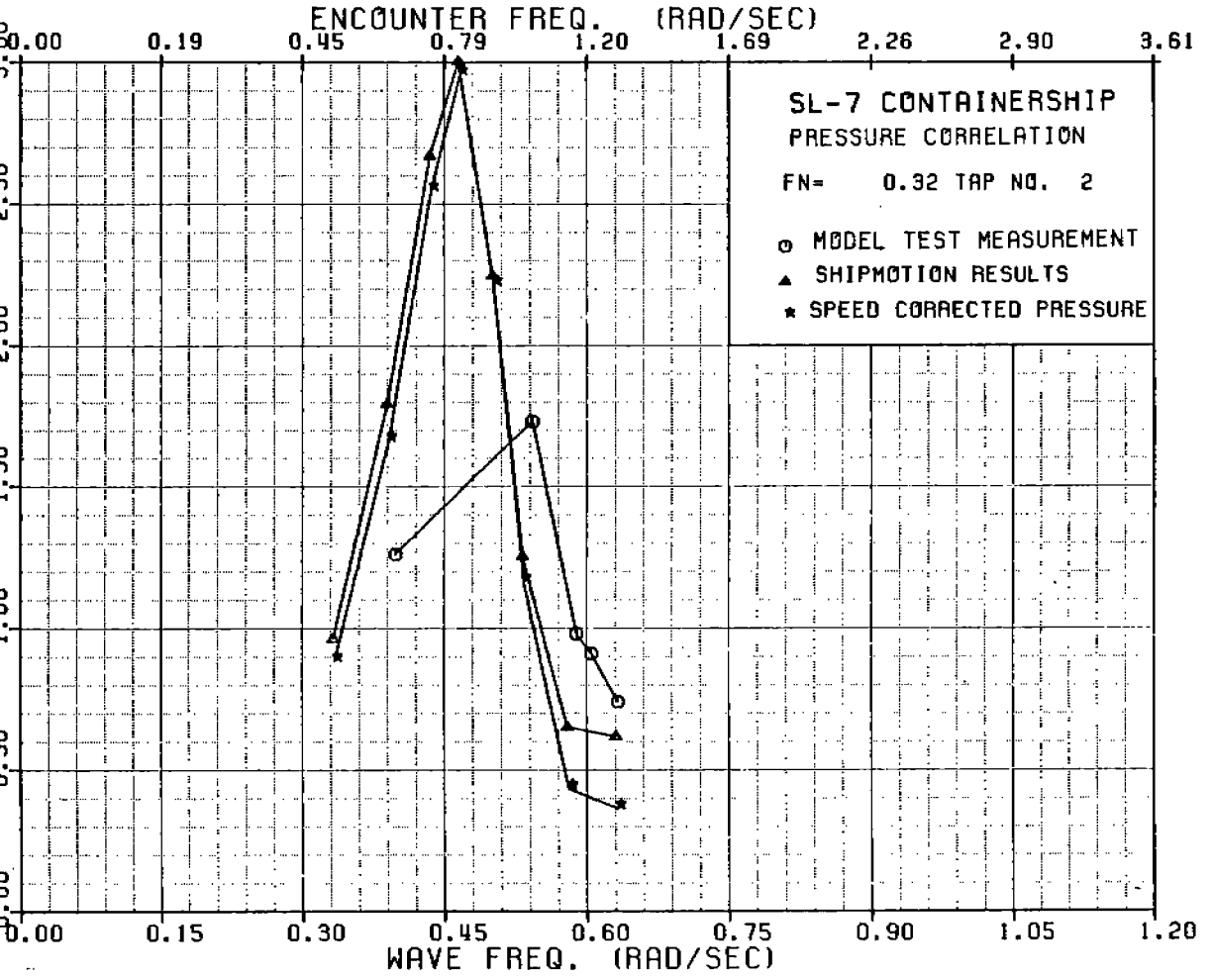

FIGURE A-94 SL-7 NONDIMENSIONAL PRESSURE AT TAP 2 , FN=0.32

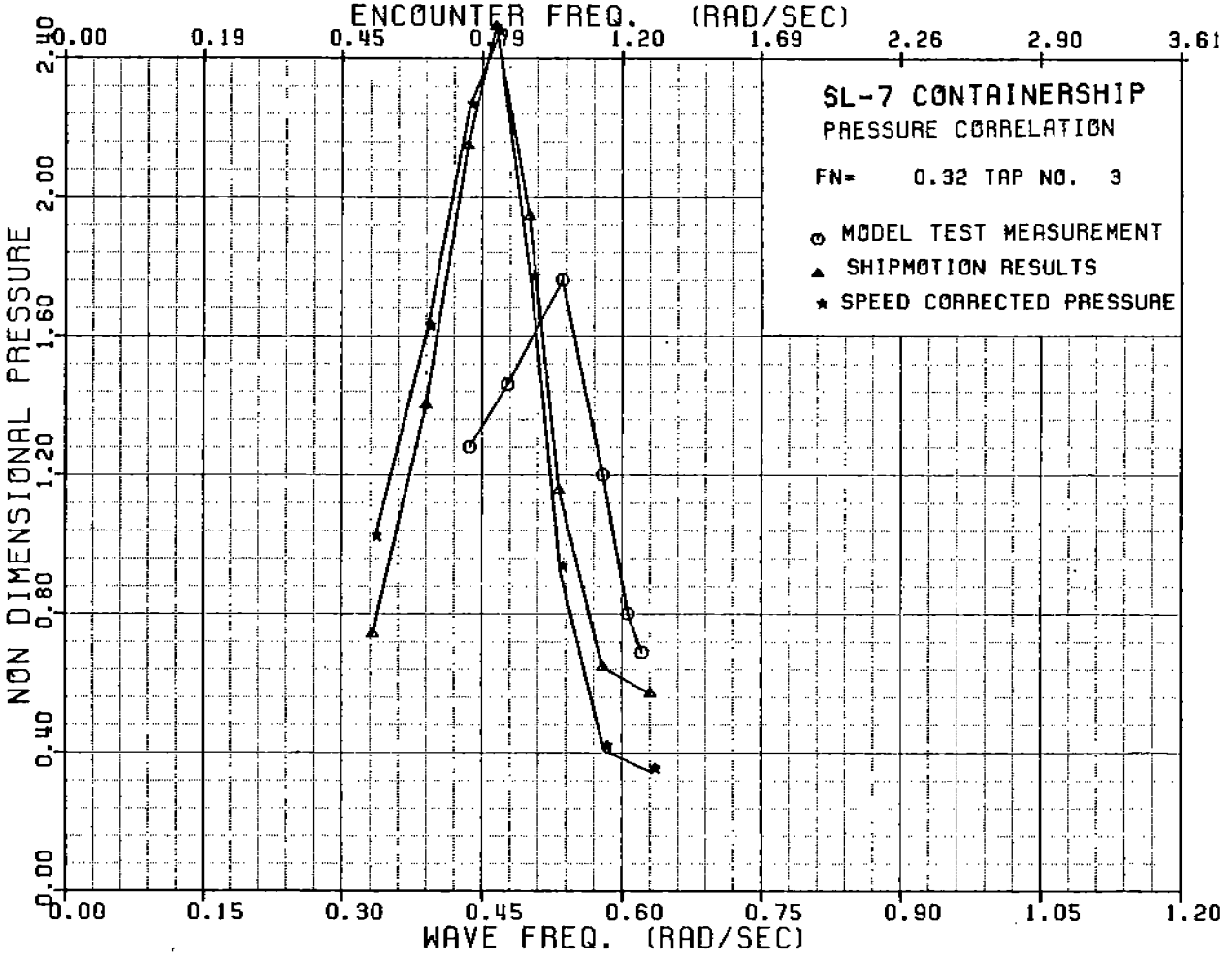

FIGURE A-95 SL-7 NONDIMENSIONAL PRESSURE AT TAP 3 , FN= 0.32

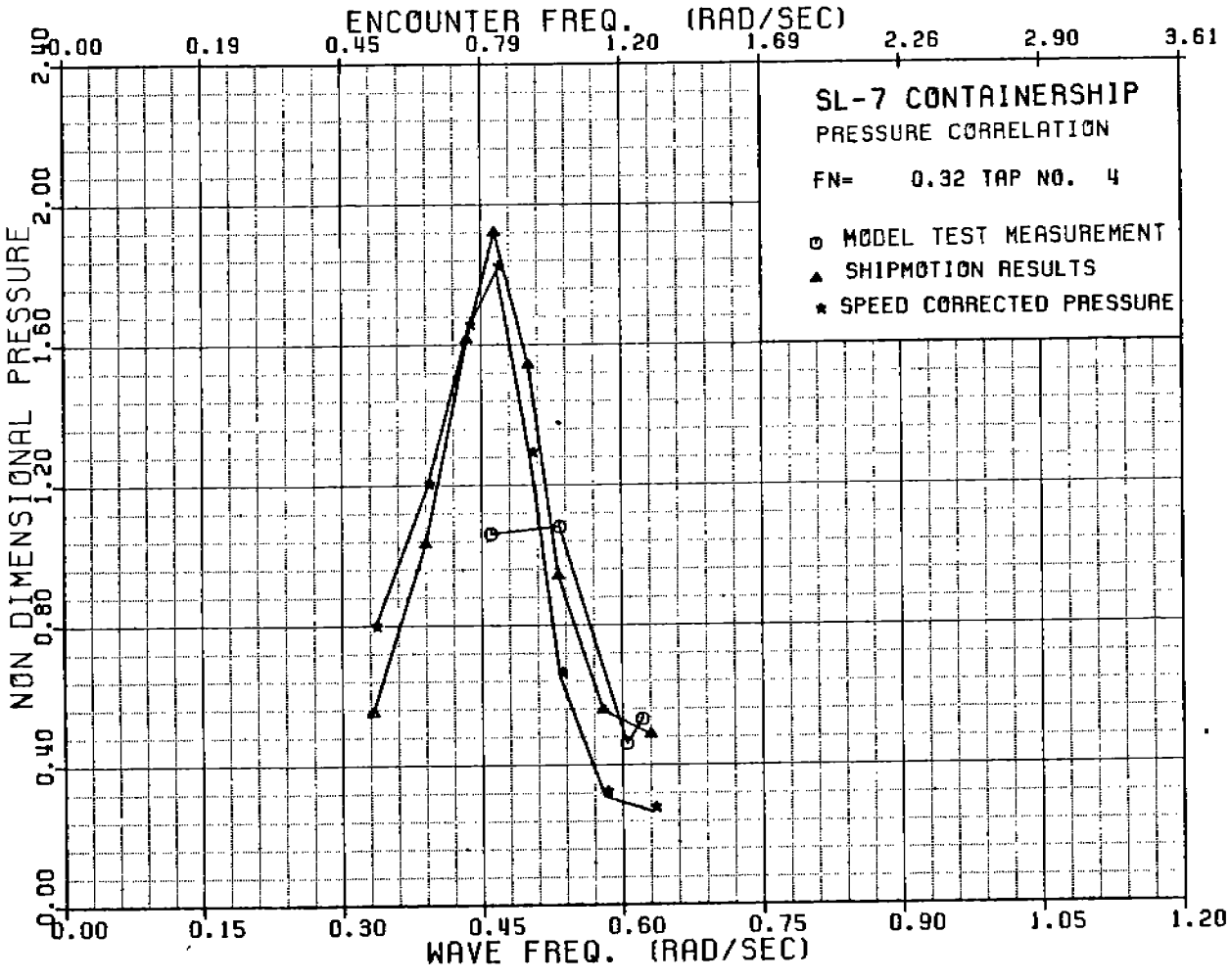

FIGURE A-96 SL-7 NONDIMENSIONAL PRESSURE AT TAP 4 , FN=0.32

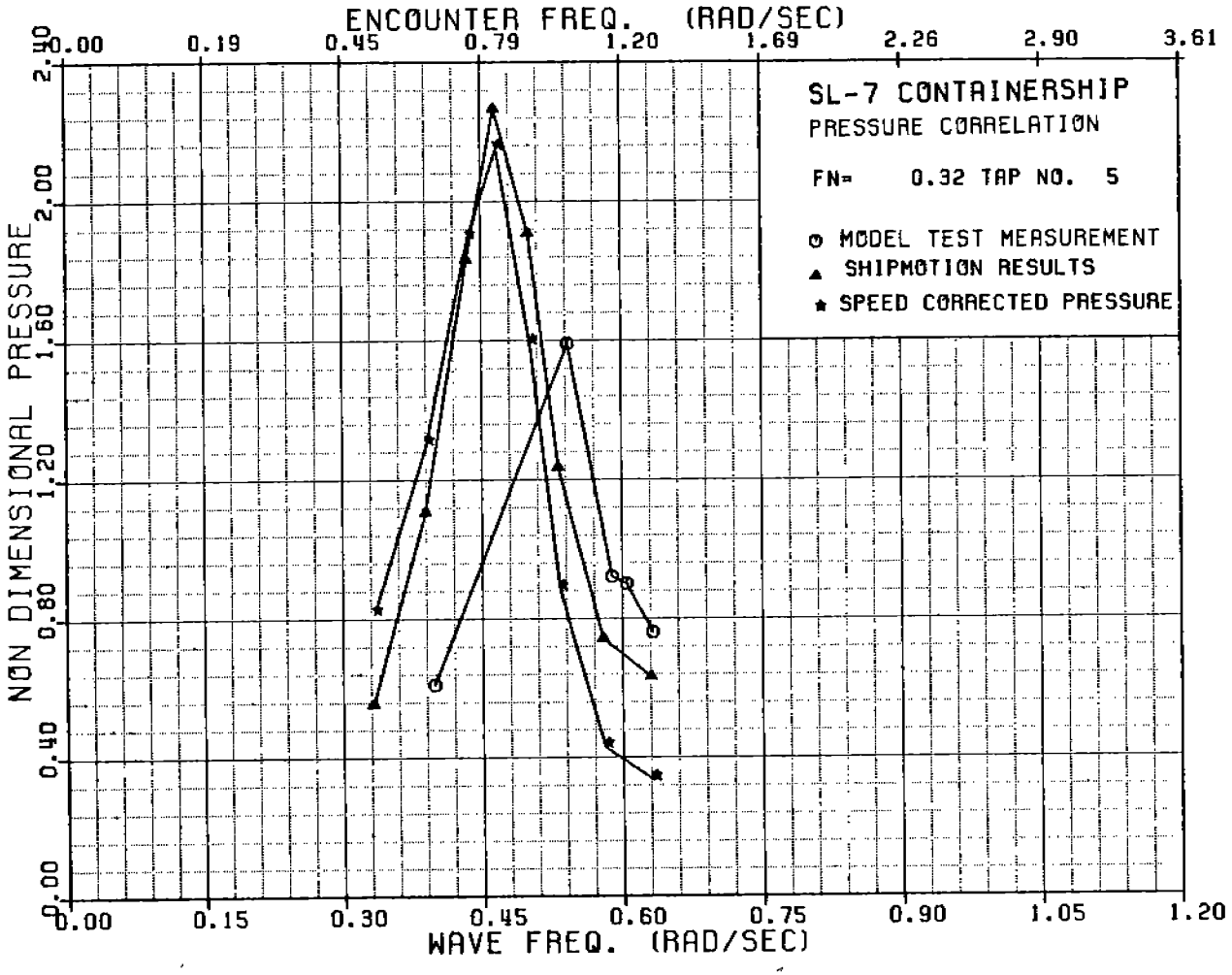

FIGURE A-97 SL-7 NONDIMENSIONAL PRESSURE AT TAP 5 , FN=0.32

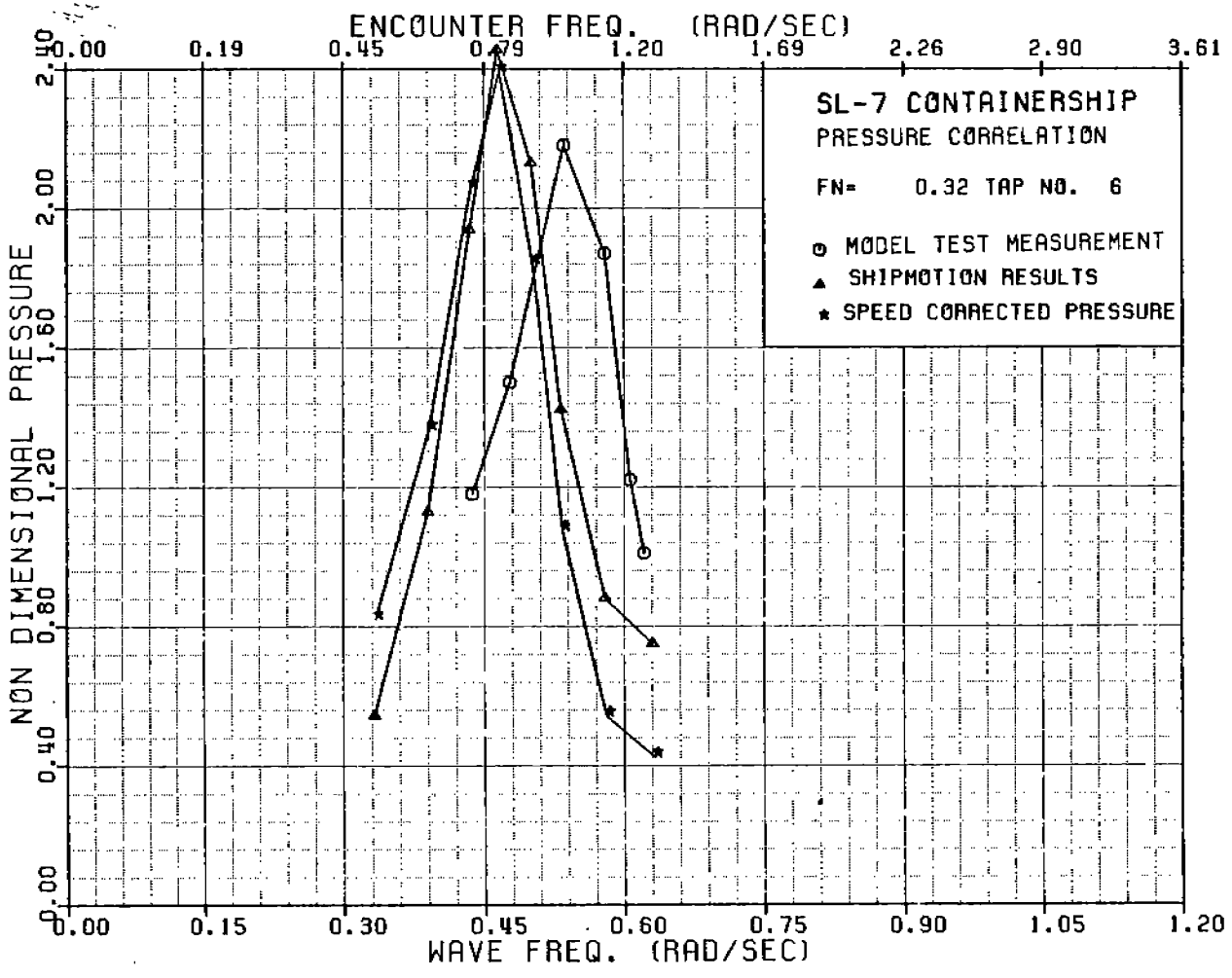

FIGURE A-98 SL-7 NONDIMENSIONAL PRESSURE AT TAP 6 , FN=0.32

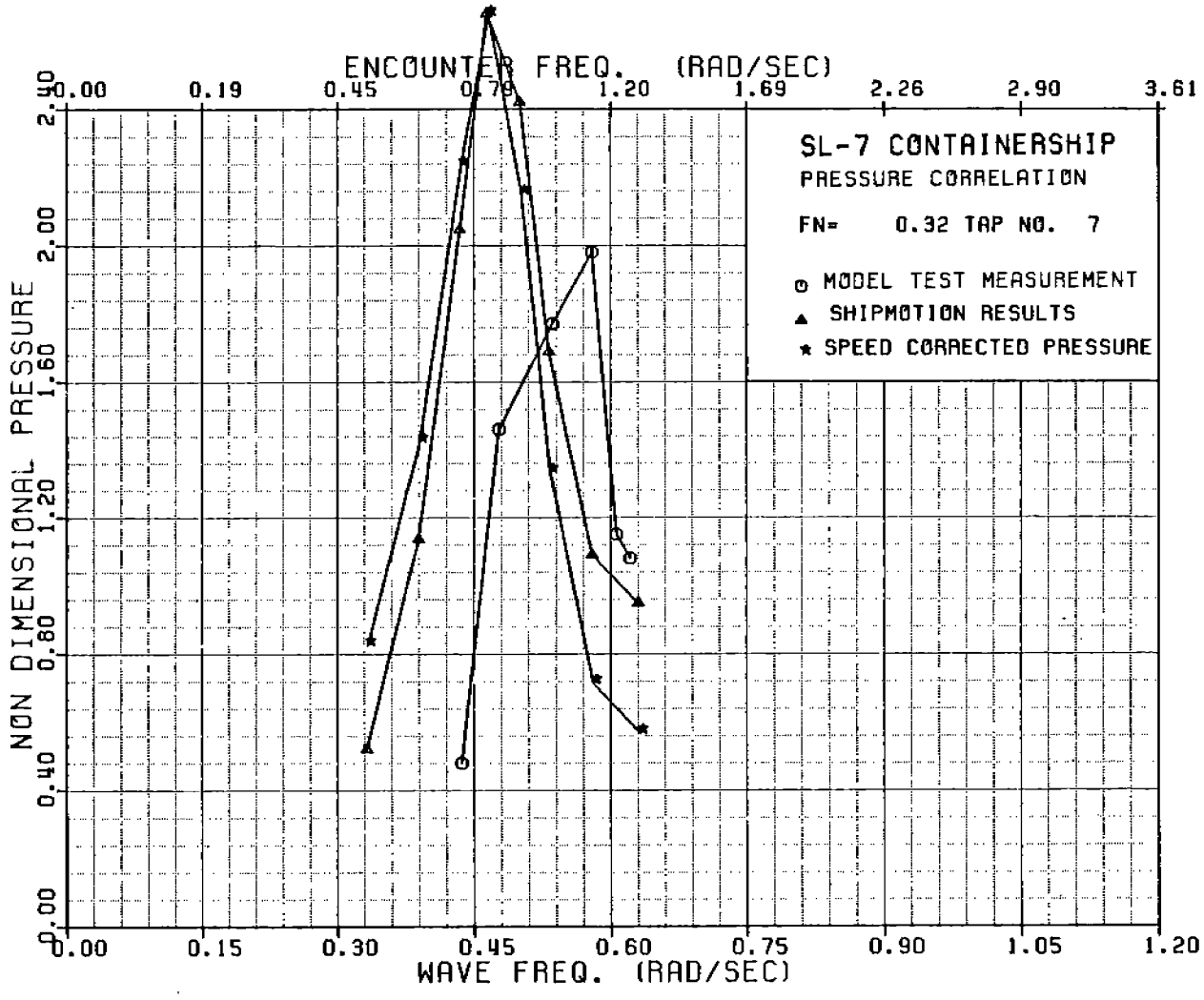

FIGURE A-99 SL-7 NONDIMENSIONAL PRESSURE AT TAP 7 , FN=0.32

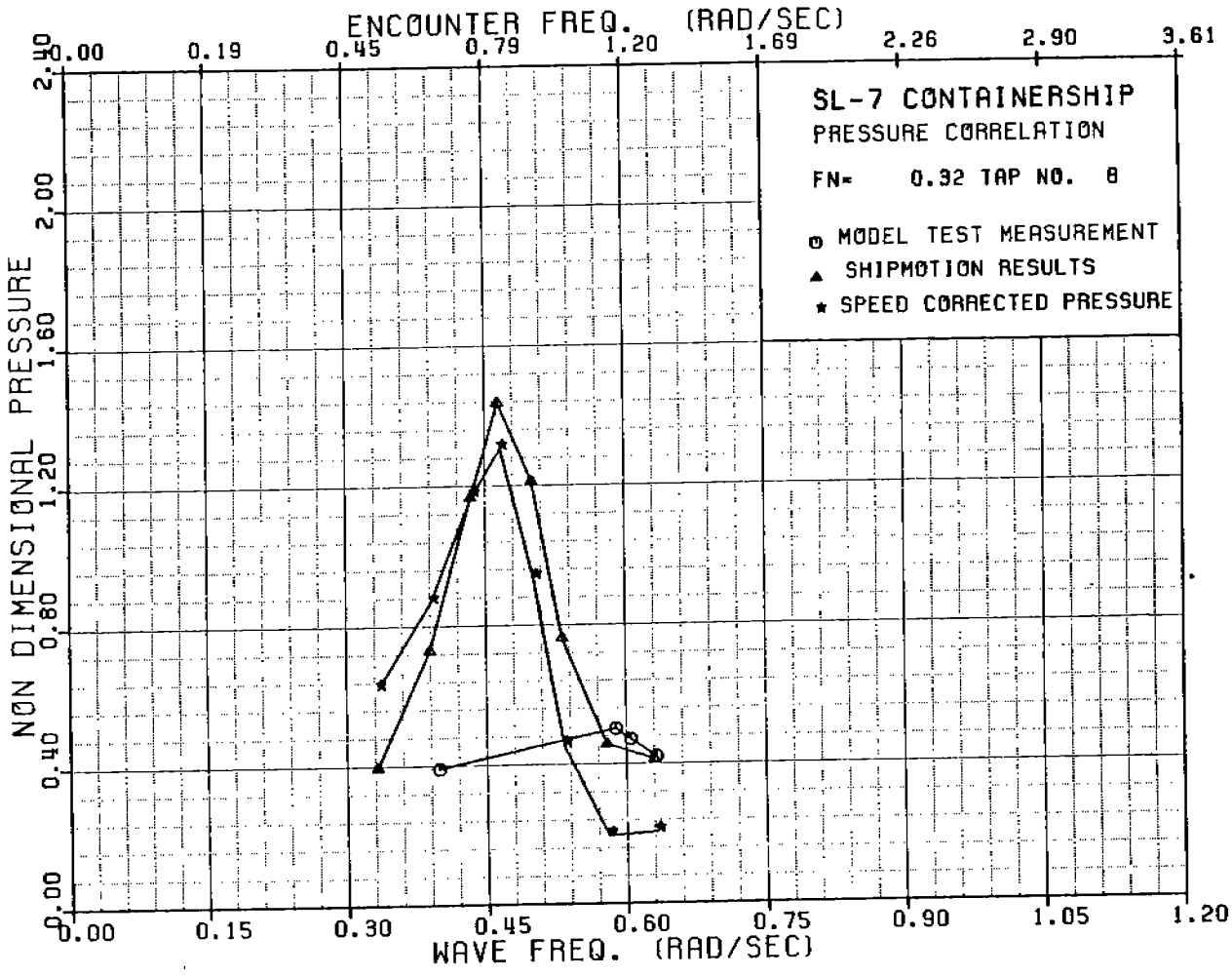

FIGURE A-100 SL-7 NONDIMENSIONAL PRESSURE AT TAP 8 , FN=0.32

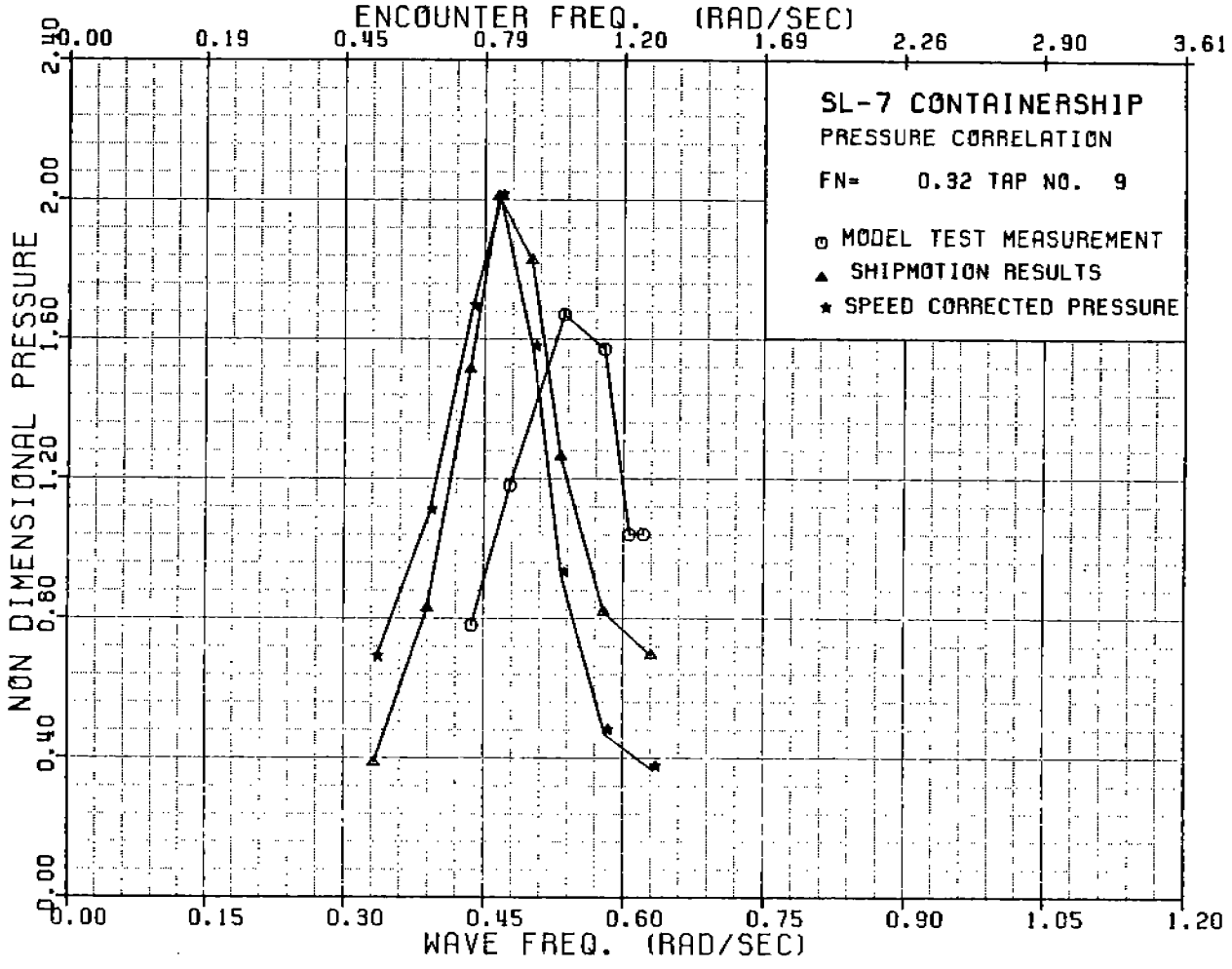

FIGURE A-101 SL-7 NONDIMENSIONAL PRESSURE AT TAP 9 , FN= 0.32

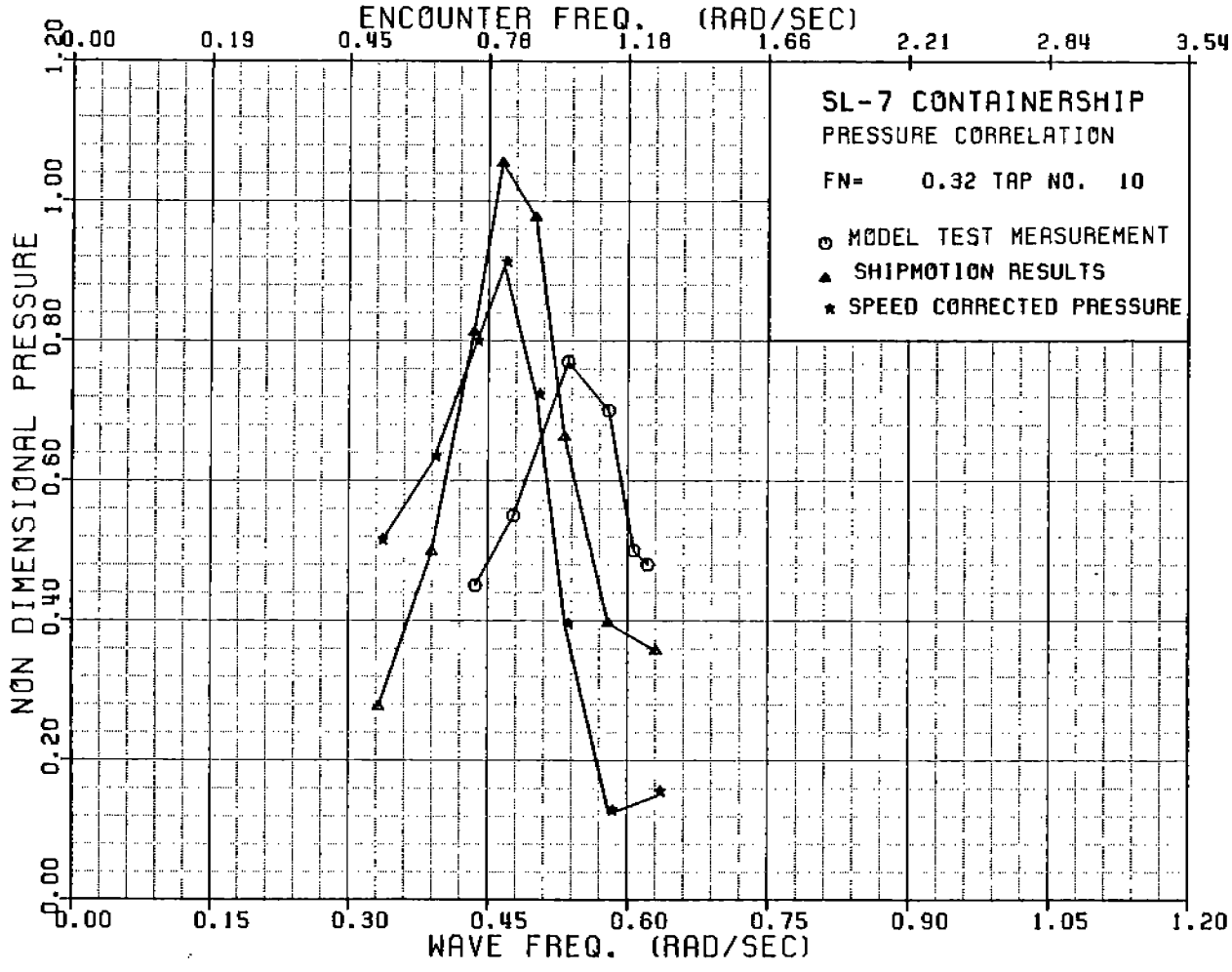

FIGURE A-102 SL-7 NONDIMENSIONAL PRESSURE AT TAP 10, FN= 0.32

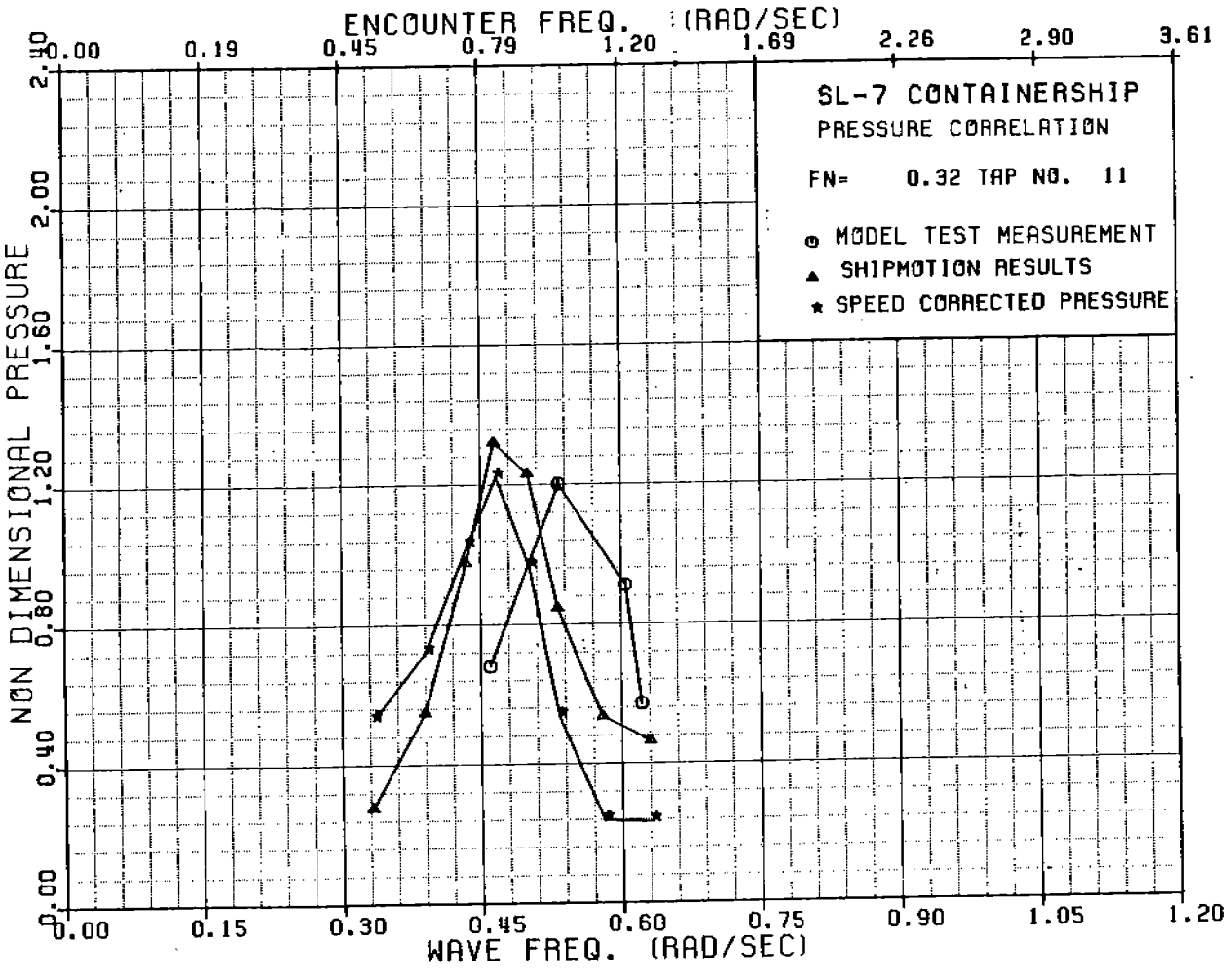

FIGURE A-103 SL-7 NONDIMENSIONAL PRESSURE AT TAP 11, FN= 0.32

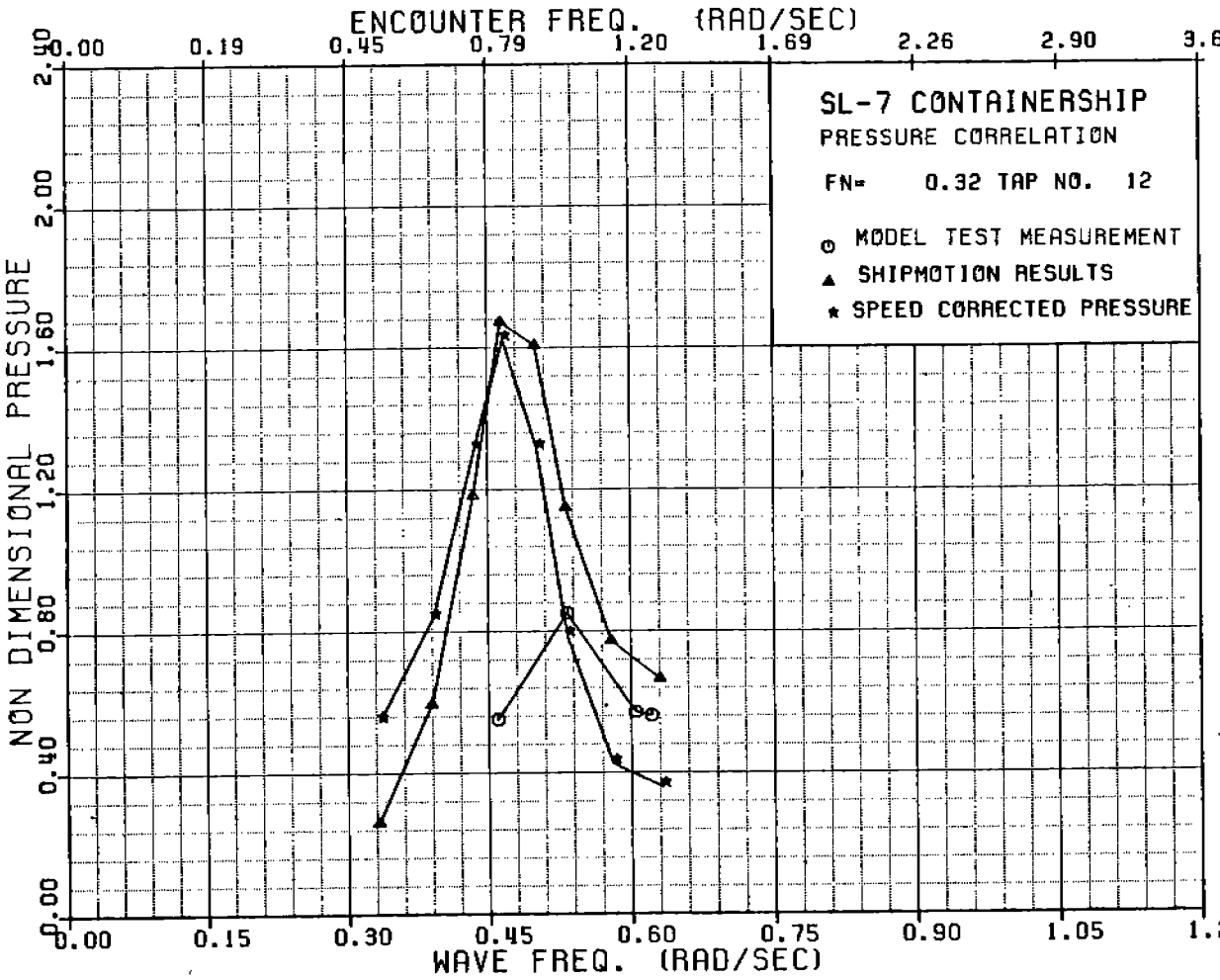

FIGURE A-104 SL-7 NONDIMENSIONAL PRESSURE AT TAP 12, FN=0.32

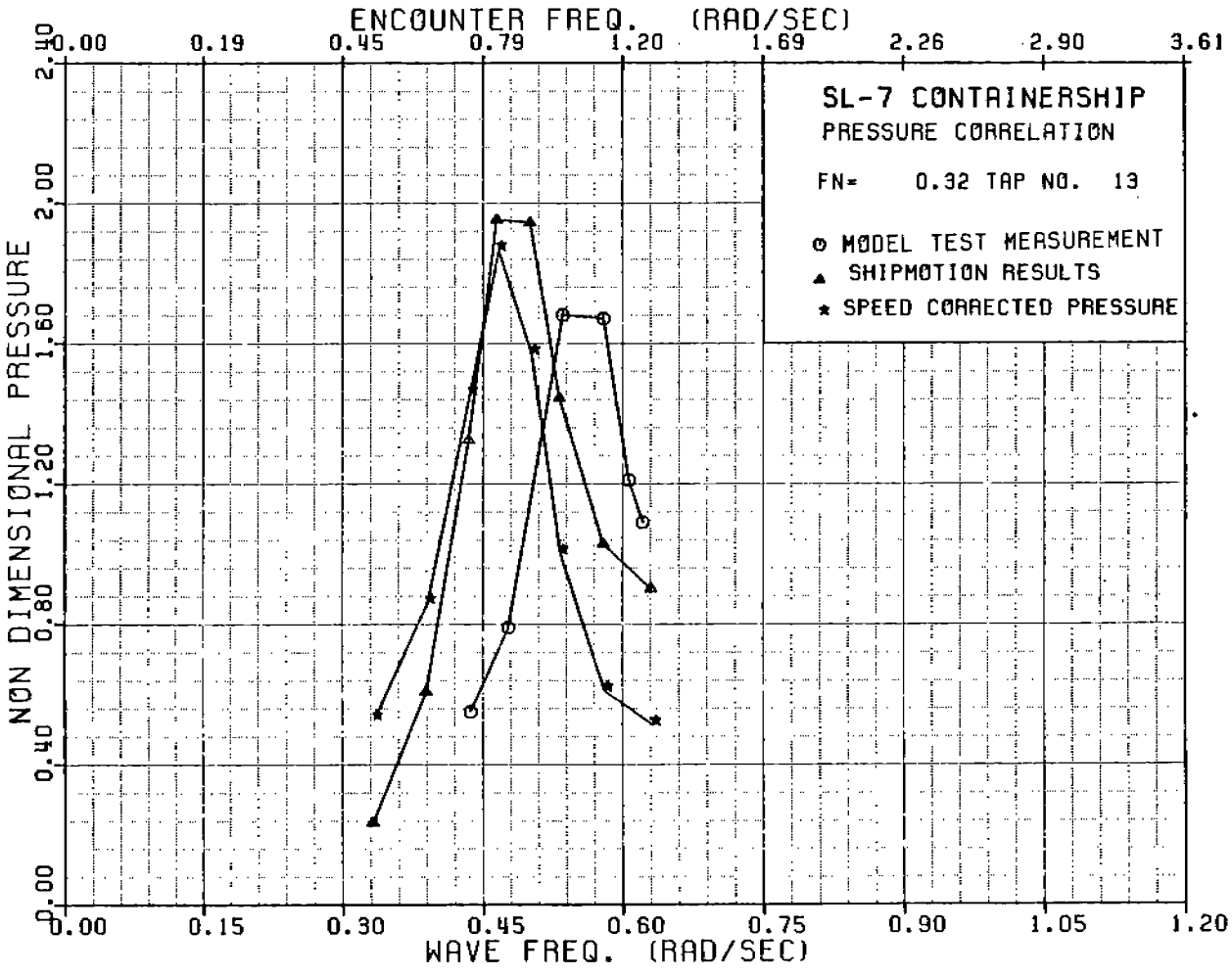

FIGURE A-105 SL-7 NONDIMENSIONAL PRESSURE AT TAP 13, FN=0.32

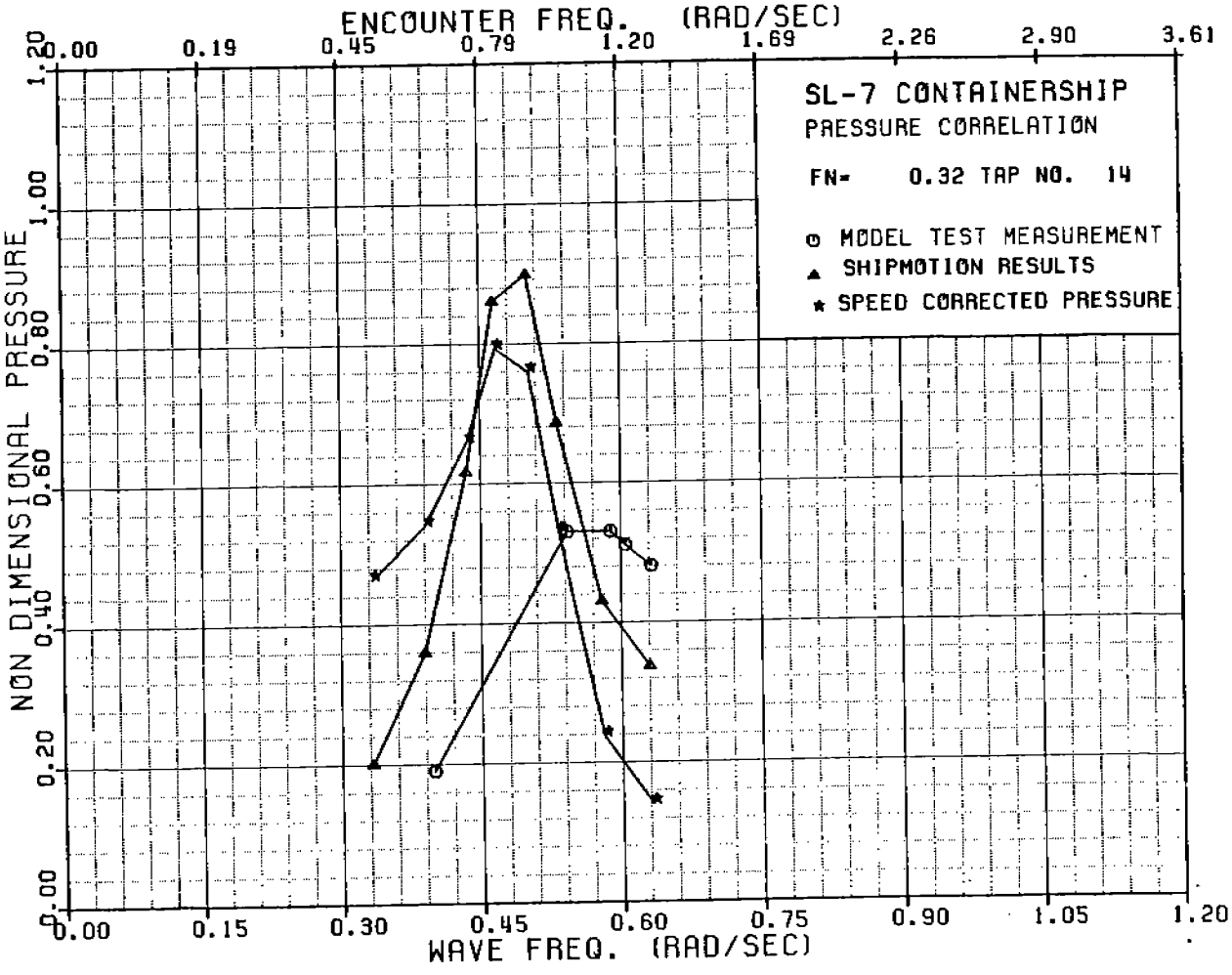

FIGURE A-106 SL-7 NONDIMENSIONAL PRESSURE AT TAP 14, FN=0.32

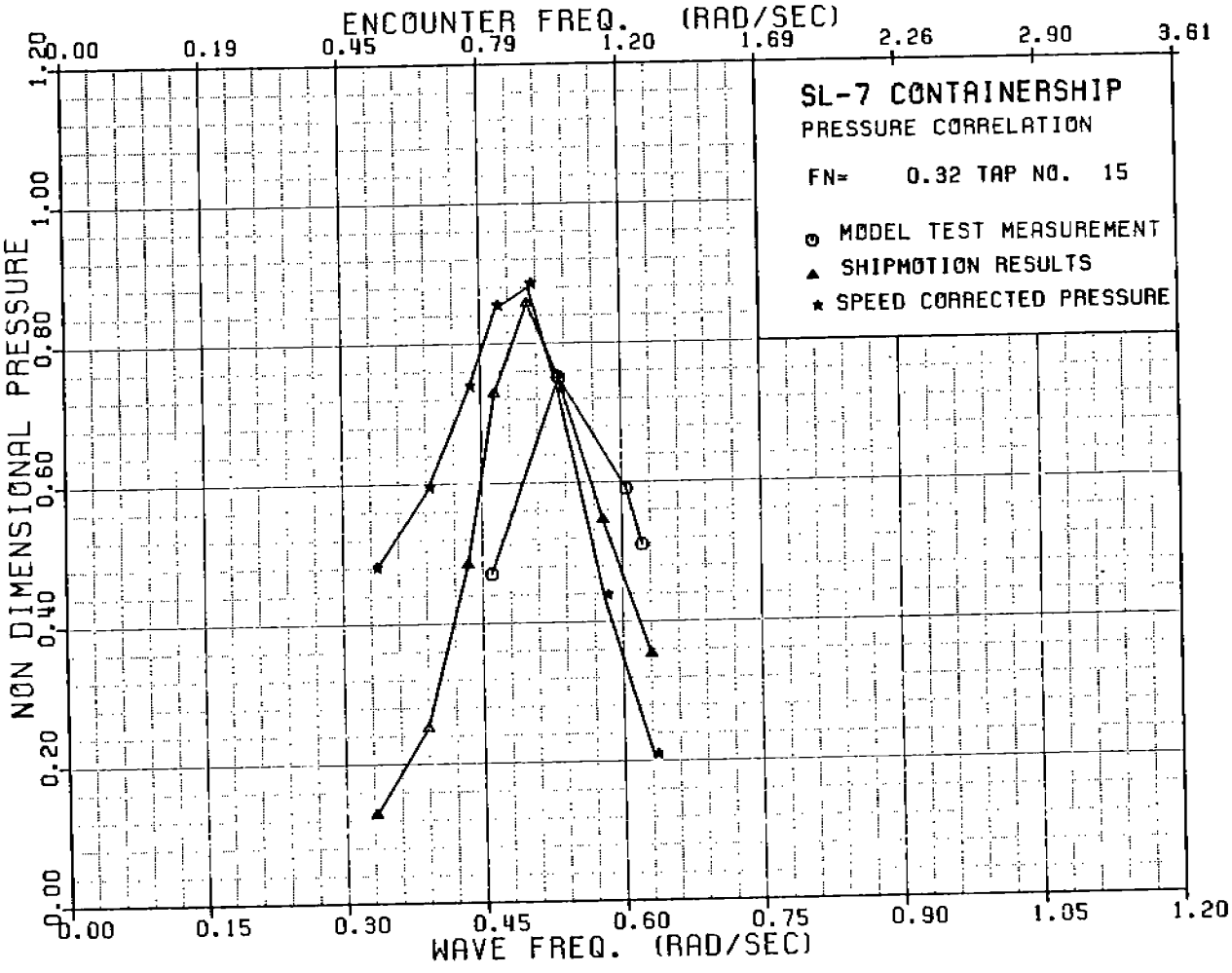

FIGURE A-107 SL-7 NONDIMENSIONAL PRESSURE AT TAP 15, FN=0.32

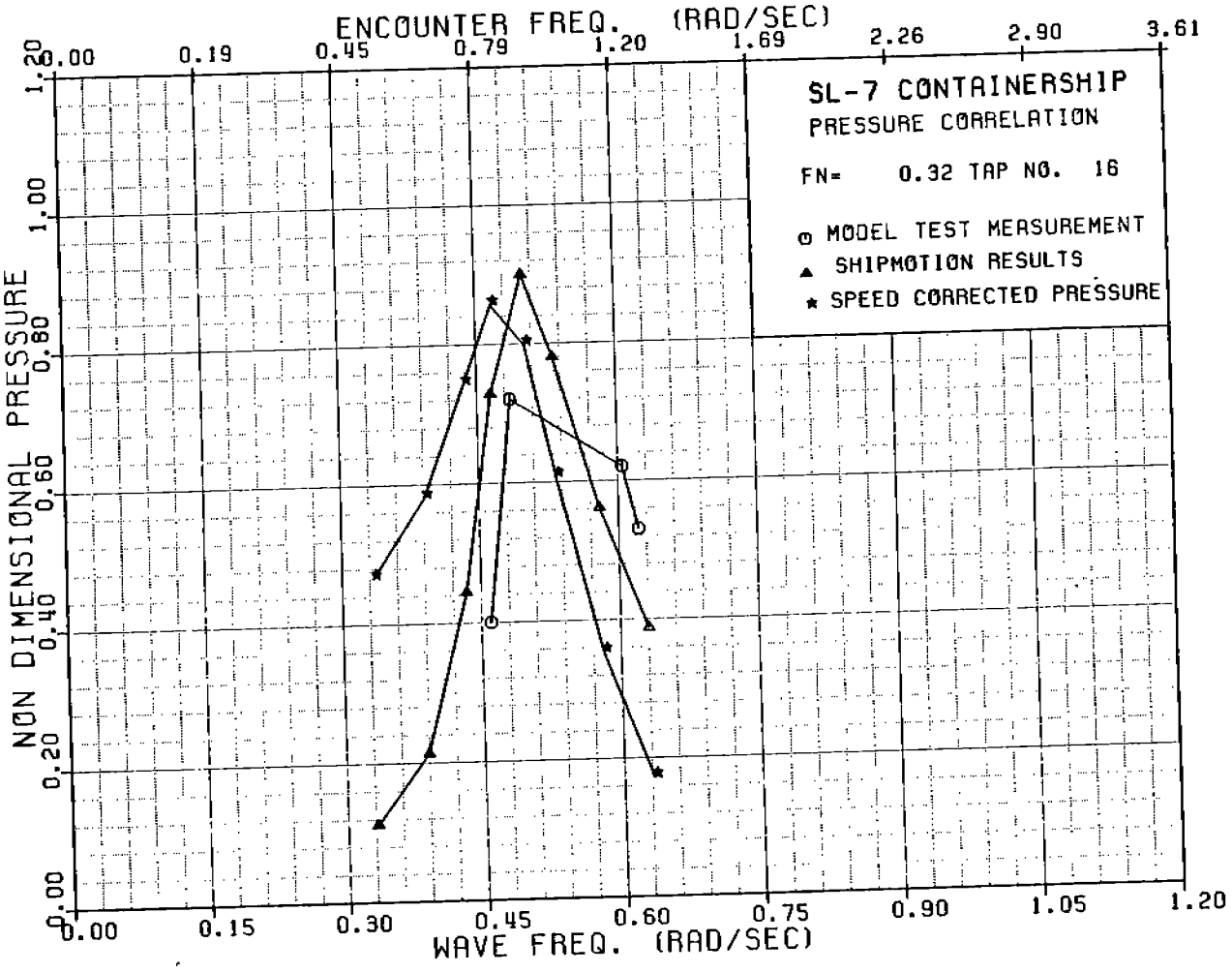

FIGURE A-108 SL-7 NONDIMENSIONAL PRESSURE AT TAP 16, FN=0.32

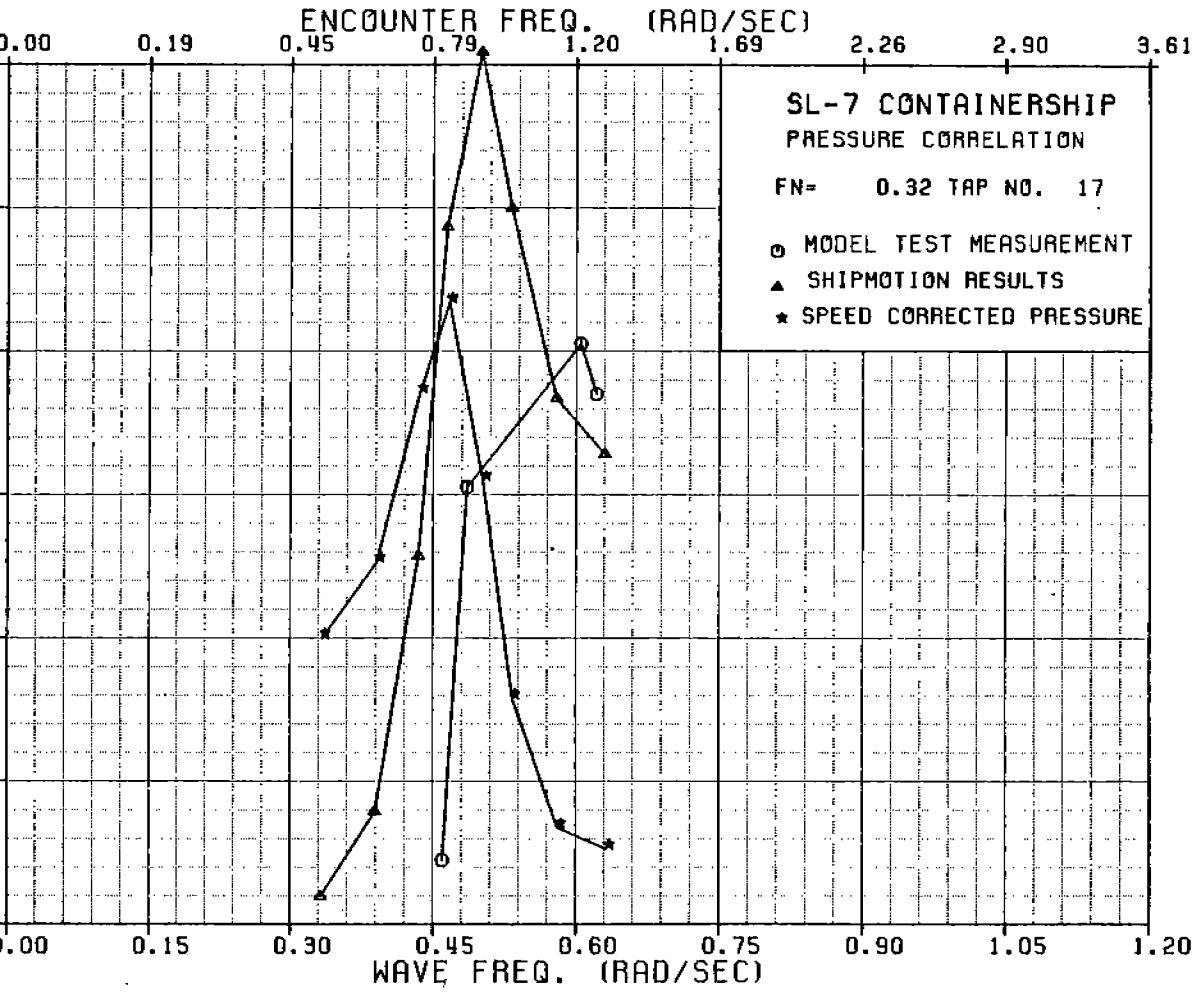

FIGURE A-109 SL-7 NONDIMENSIONAL PRESSURE AT TAP 17, FN=0.32

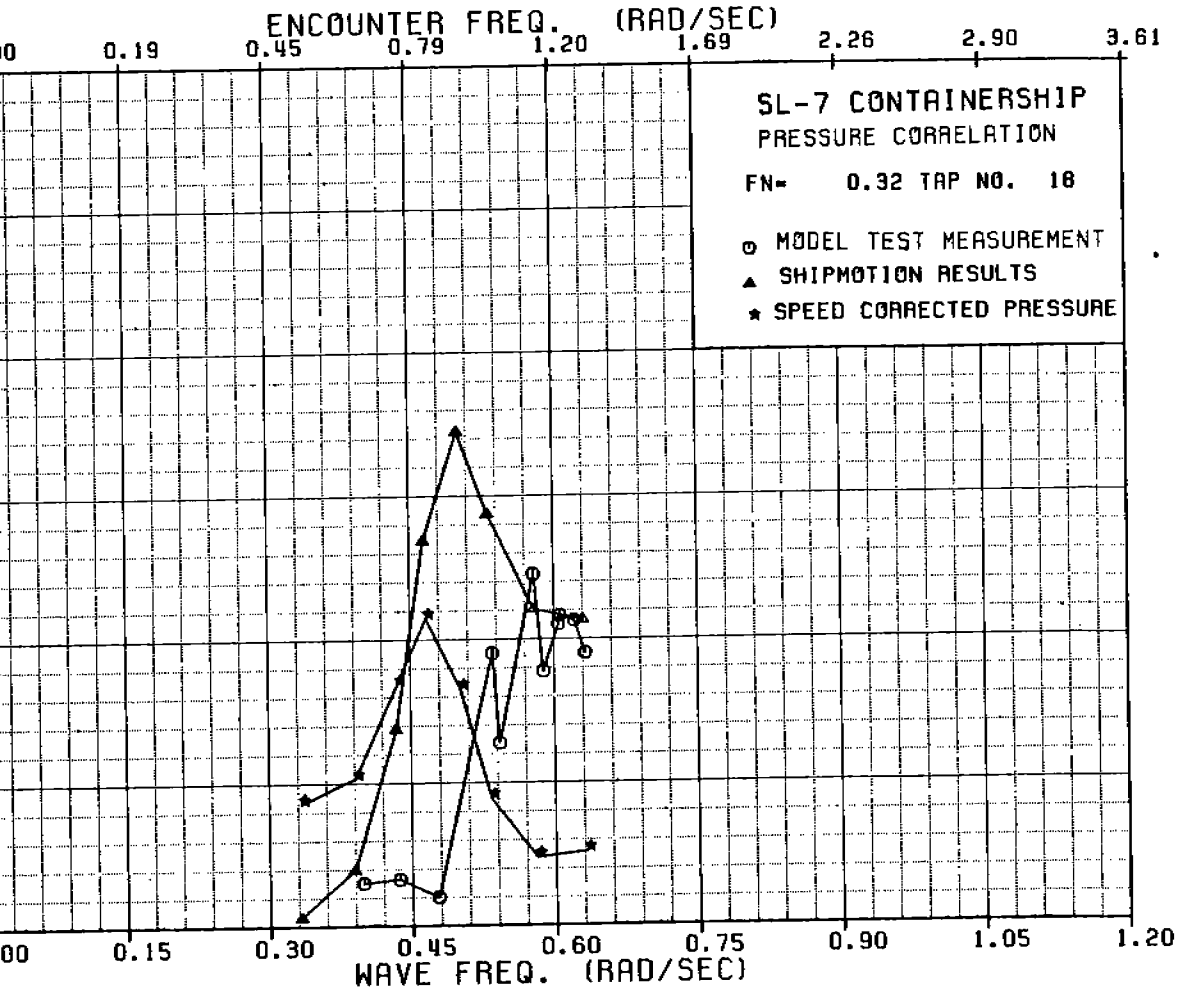

FIGURE A-110 SL-7 NONDIMENSIONAL PRESSURE AT TAP 18, FN=0.32

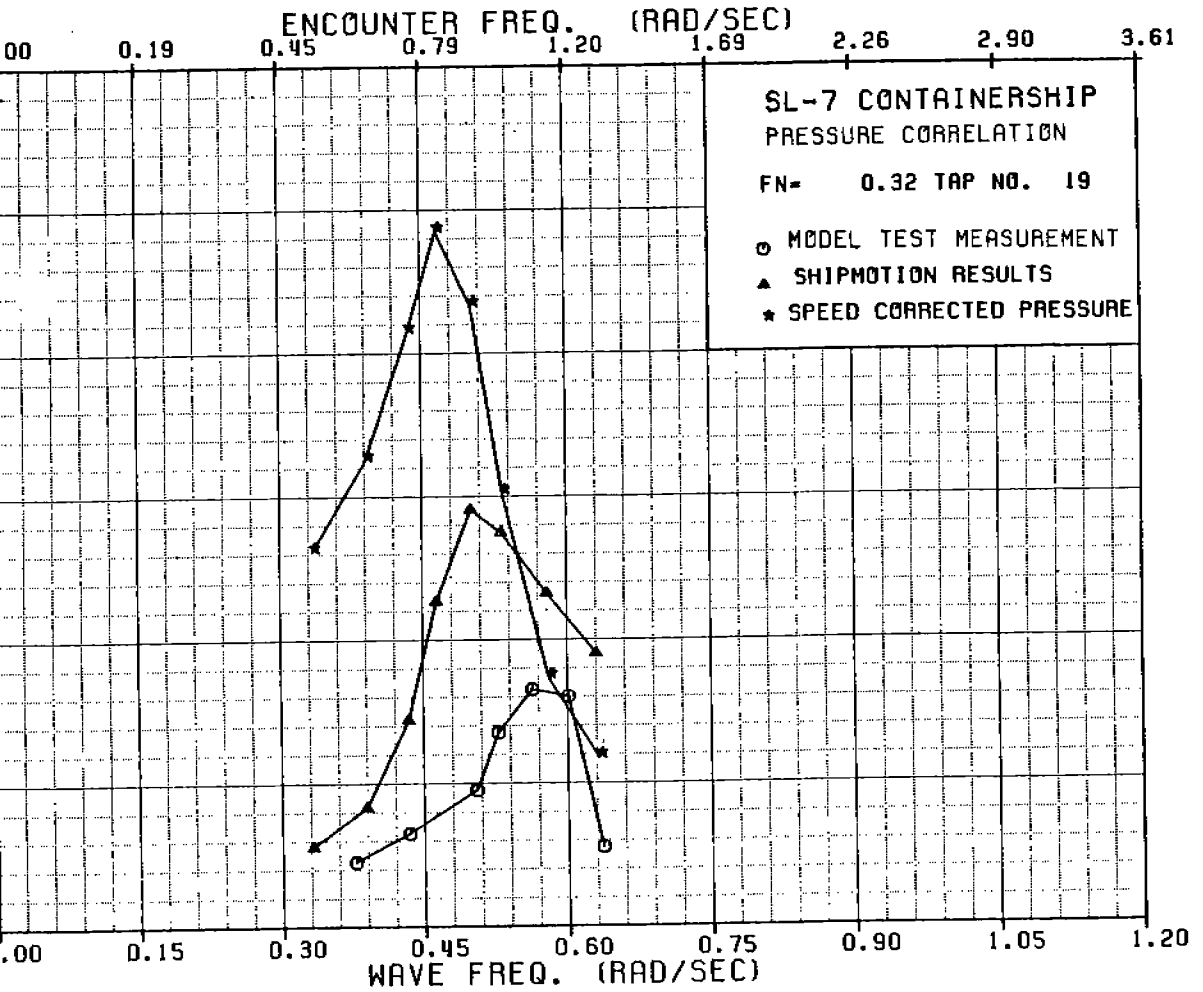

FIGURE A-111 SL-7 NONDIMENSIONAL PRESSURE AT TAP 19, FN=0.32

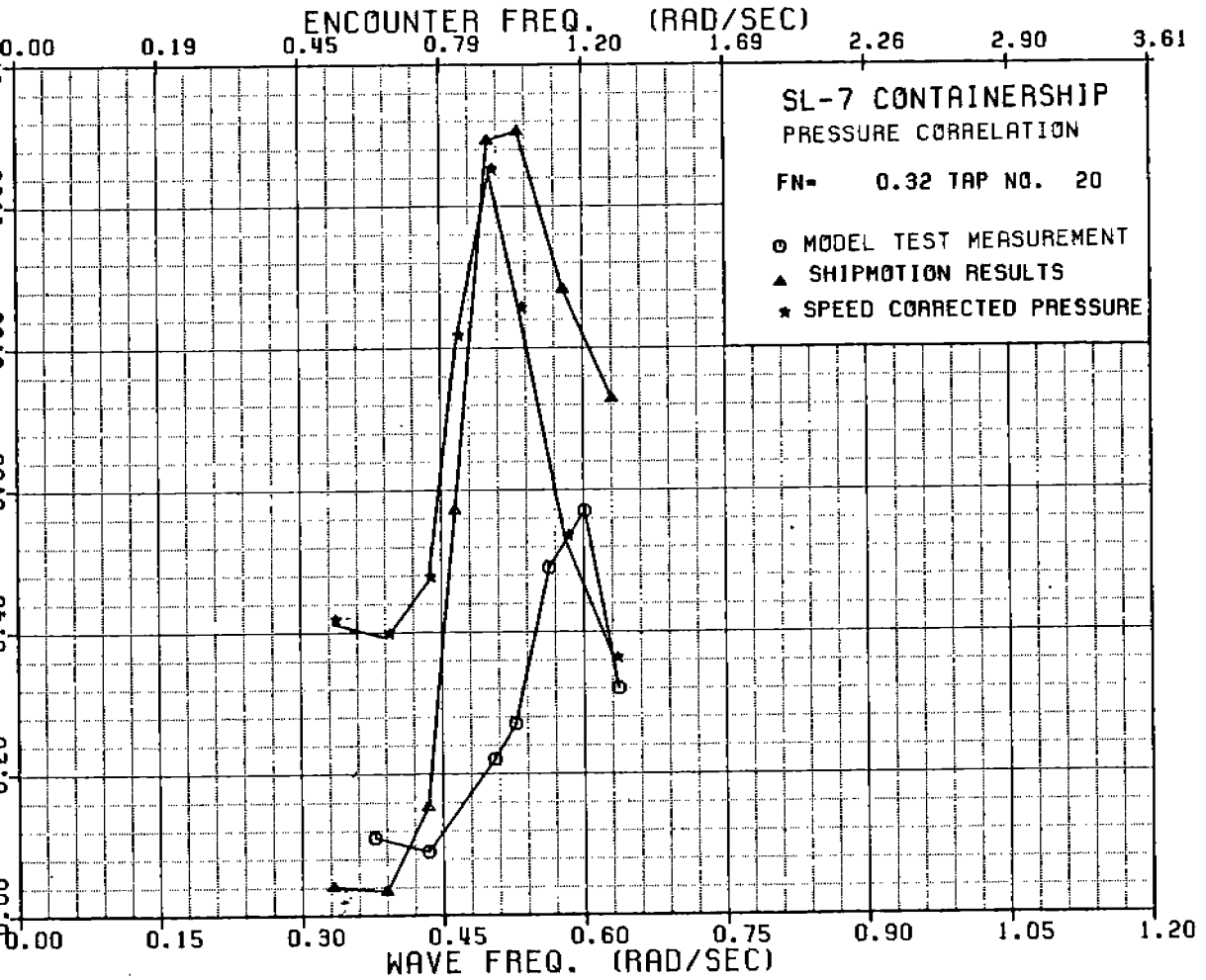

FIGURE A-112 SL-7 NONDIMENSIONAL PRESSURE AT TAP 20, FN=0.32

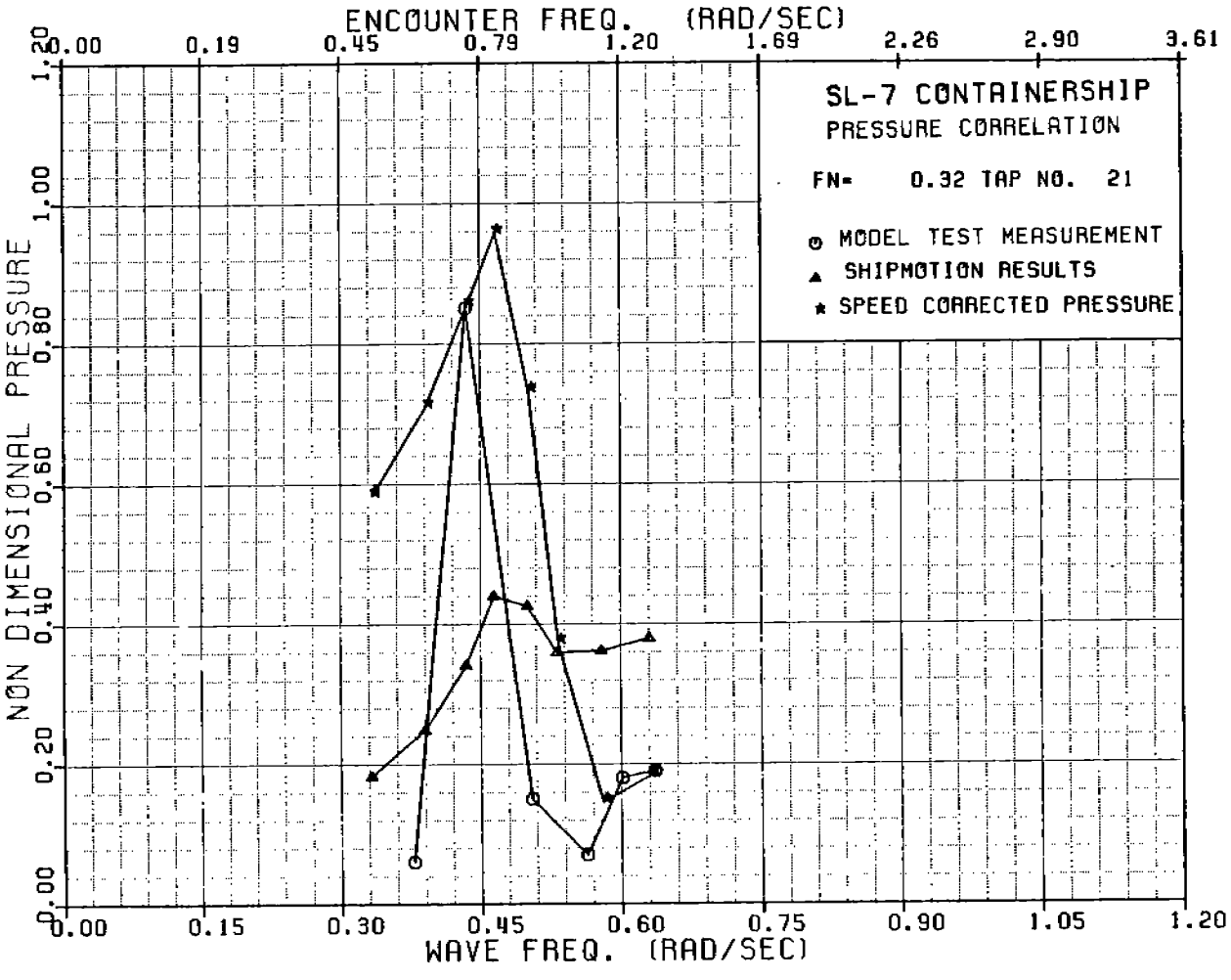

FIGURE A-113 SL-7 NONDIMENSIONAL PRESSURE AT TAP 21, FN=0.32

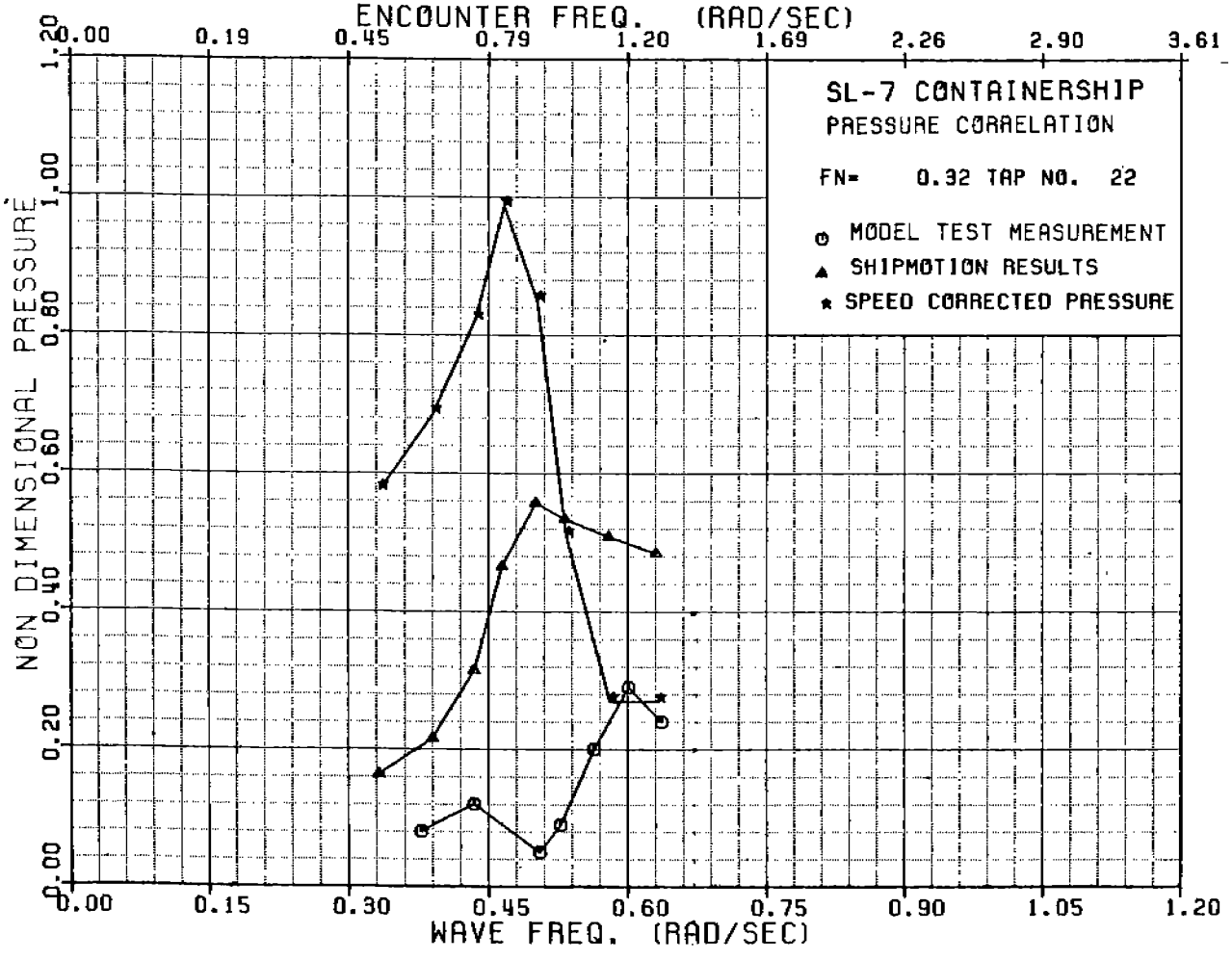

FIGURE A-114 SL-7 NONDIMENSIONAL PRESSURE AT TAP 22, FN 0.32

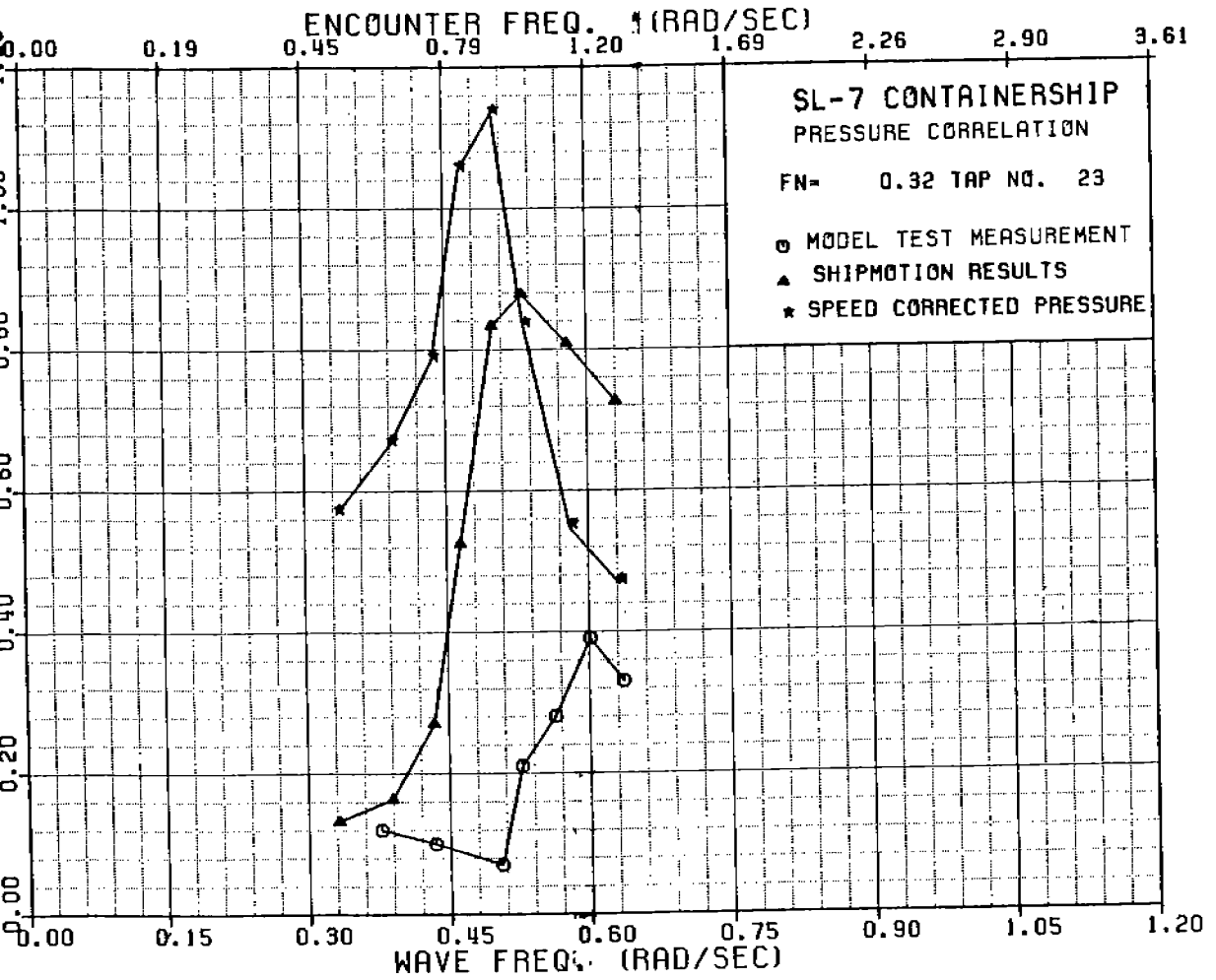

FIGURE A-115 SL-7 NONDIMENSIONAL PRESSURE AT TAP 23, FN=0.32

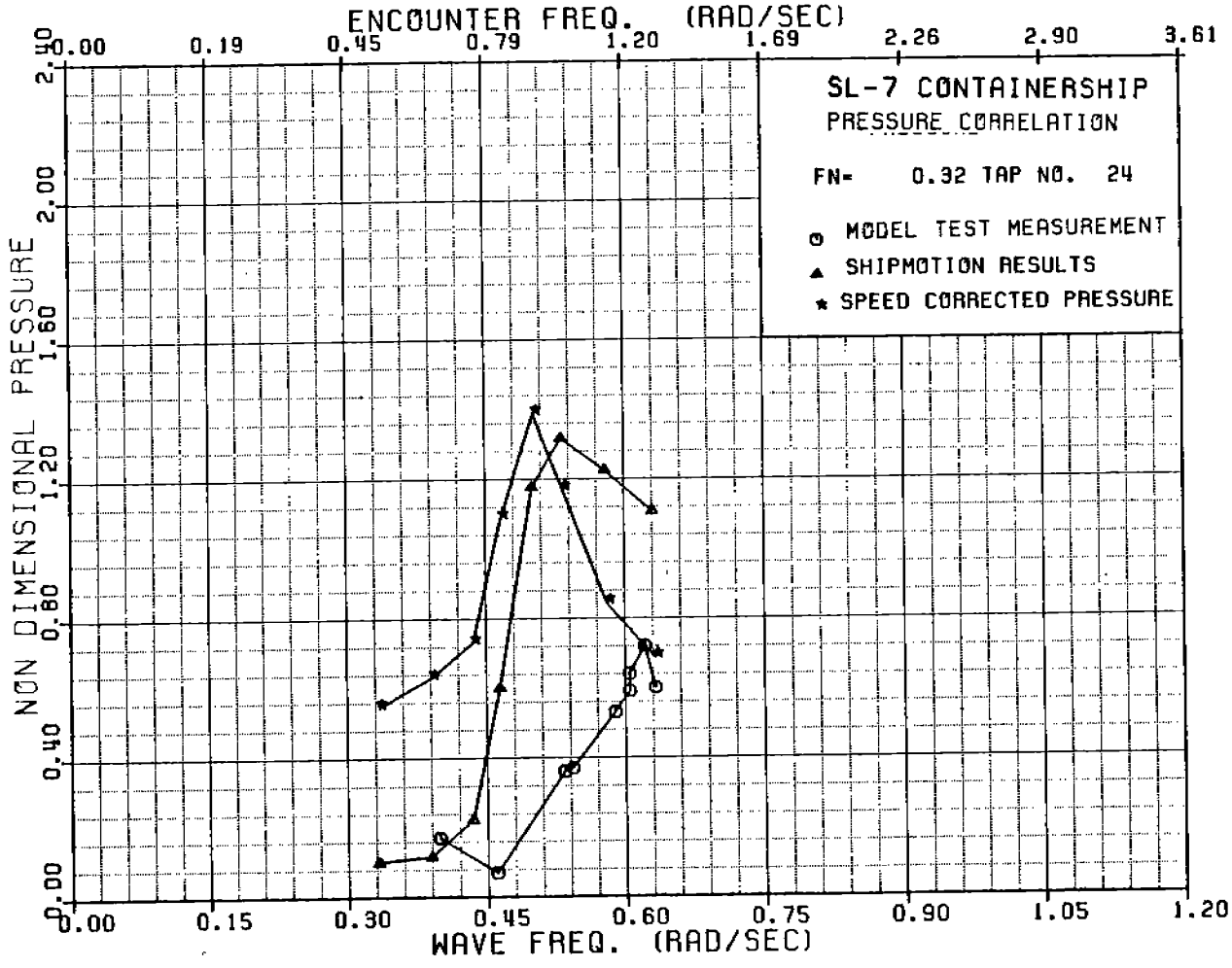

FIGURE A-116 SL-7 NONDIMENSIONAL PRESSURE AT TAP 24, FN=0.32

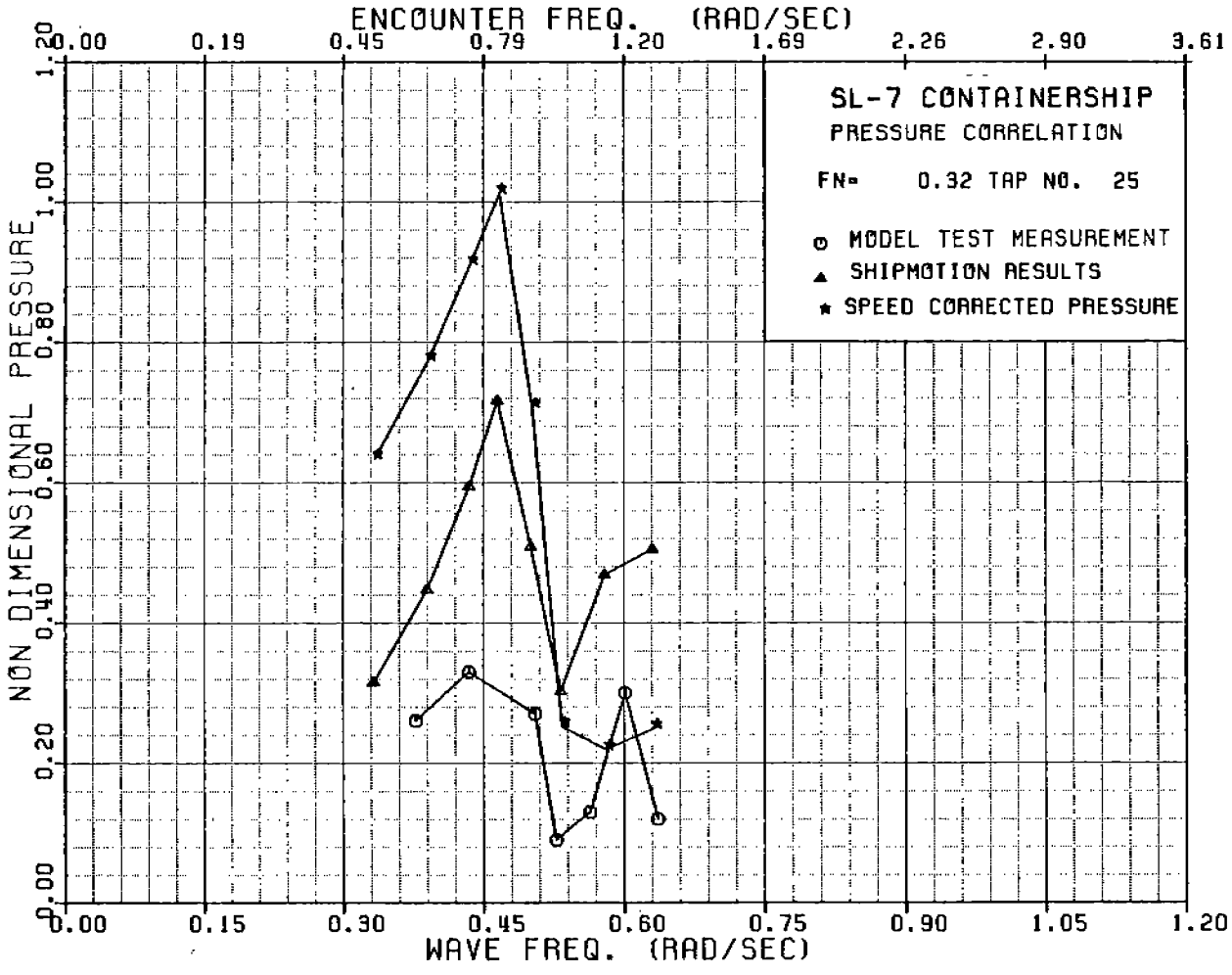

FIGURE A-117 SL-7 NONDIMENSIONAL PRESSURE AT TAP 25, FN=0.32

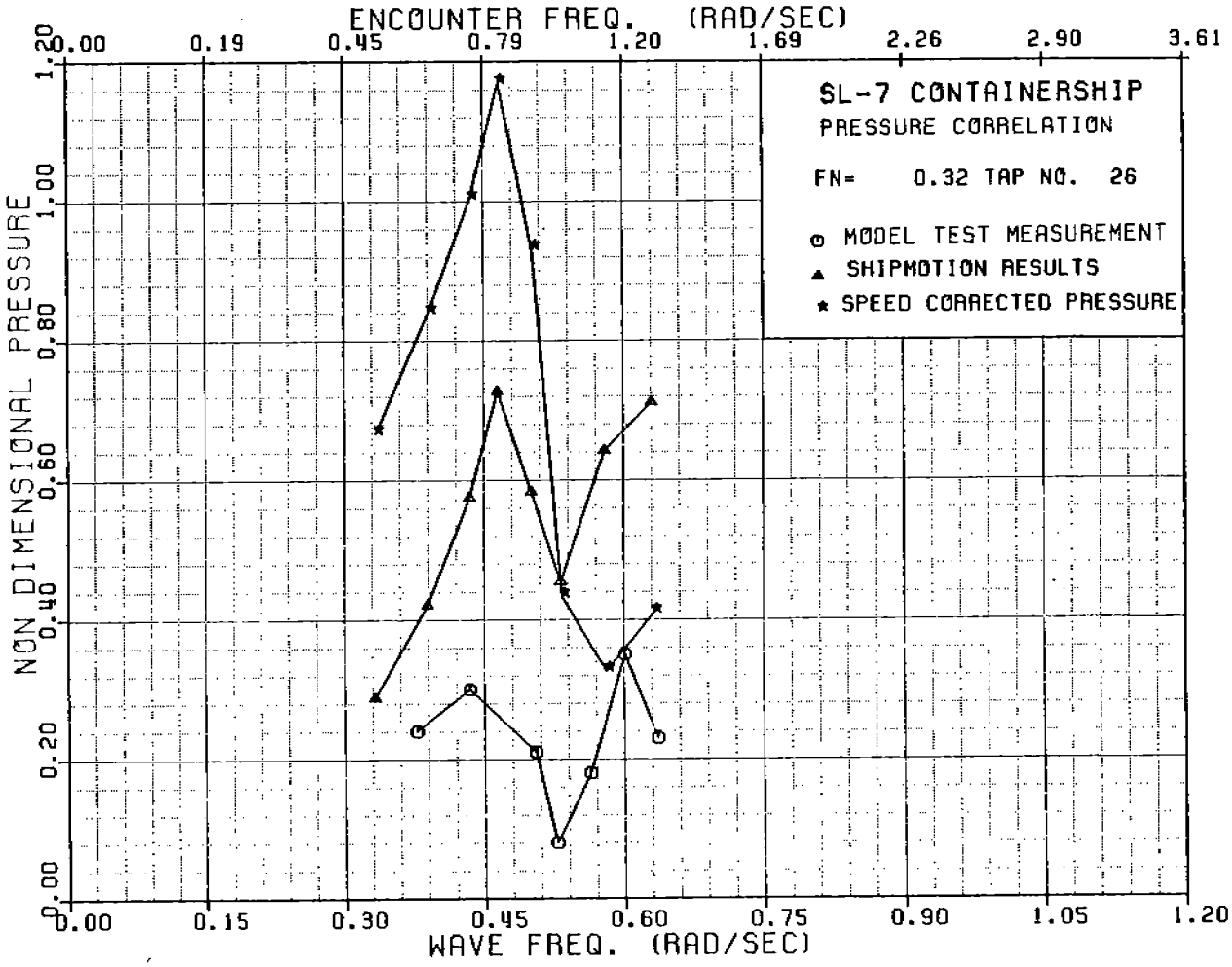

FIGURE A-118 SL-7 NONDIMENSIONAL PRESSURE AT TAP 26, FN=0.32

1¼" TO TRIM

APPENDIX B

M.V. S. J. CORT

MODEL TEST/THEORY CORRELATION PLOTS

1¼" TO BWD

Figs. B-1 to B-24:	S. J. CORT Non-dimensional Pressure, Full Load Condition, F_n = 0.10.
Figs. B-25 to B-48:	S. J. CORT Non-dimensional Pressure, Full Load Condition, F_n = 0.13.
Figs. B-49 to B-58:	S. J. CORT Non-dimensional Pressure, Ballast Condition, F_n = 0.10.
Figs. B-59 to B-68:	S. J. CORT Non-dimensional Pressure, Ballast Condition, F_n = 0.13.

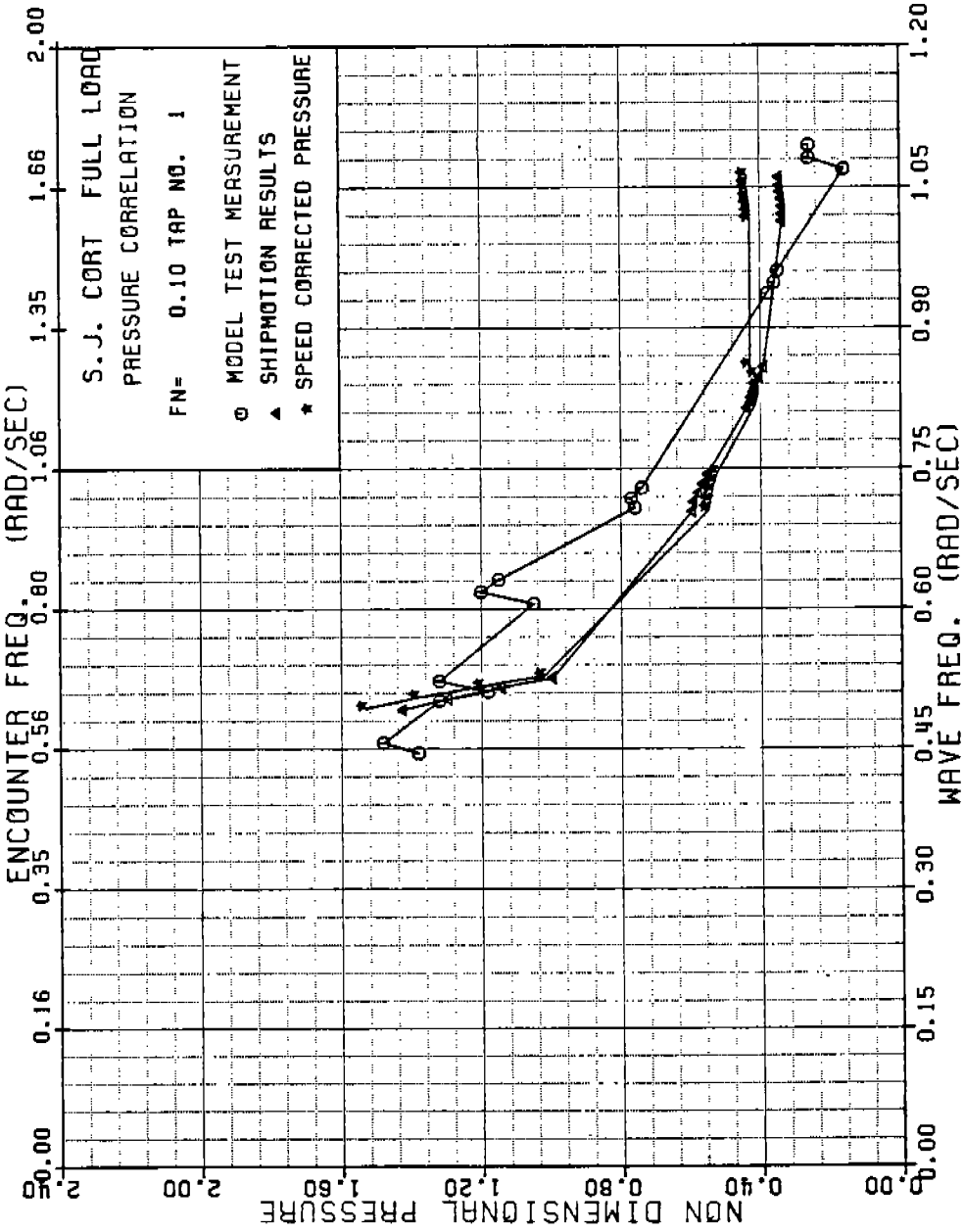

FIGURE B-1 SJ CORT NONDIMENSIONAL PRESSURE . TAP 1 . FN=0.10

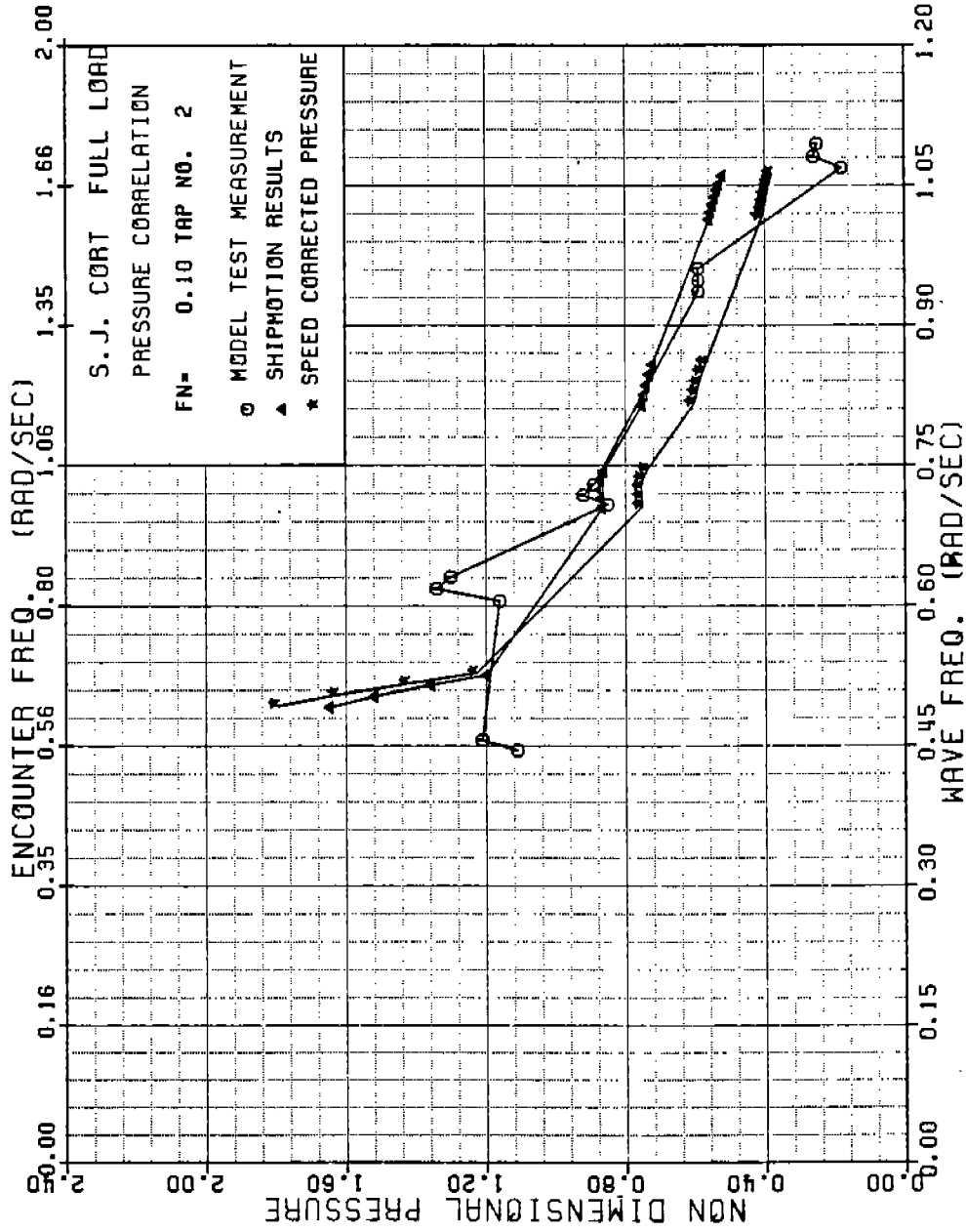

FIGURE B-2 SJ CORT NONDIMENSIONAL PRESSURE , TAP 2 , FN=0.10

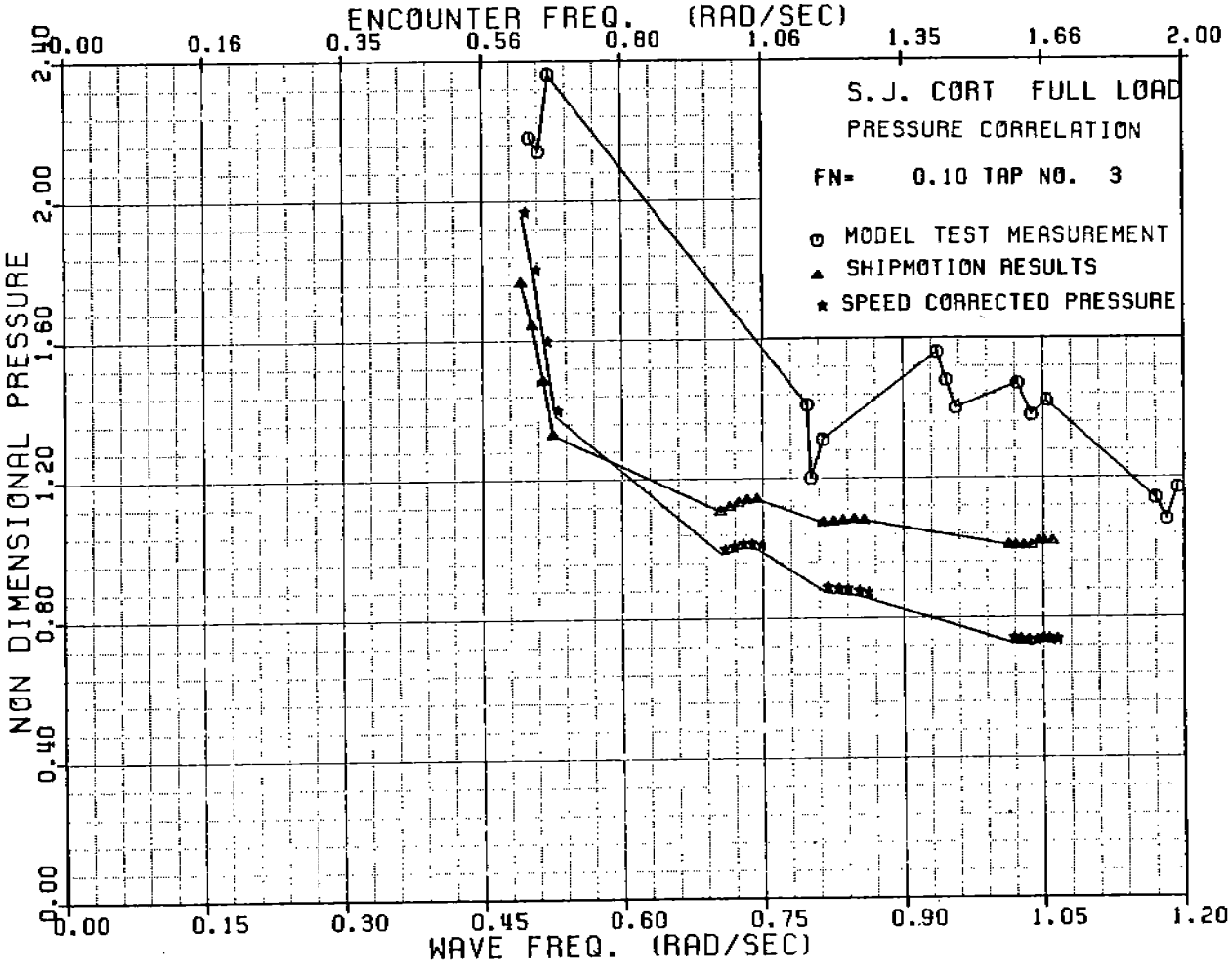

FIGURE B-3 SJ CORT NONDIMENSIONAL PRESSURE , TAP 3 , FN=0.10

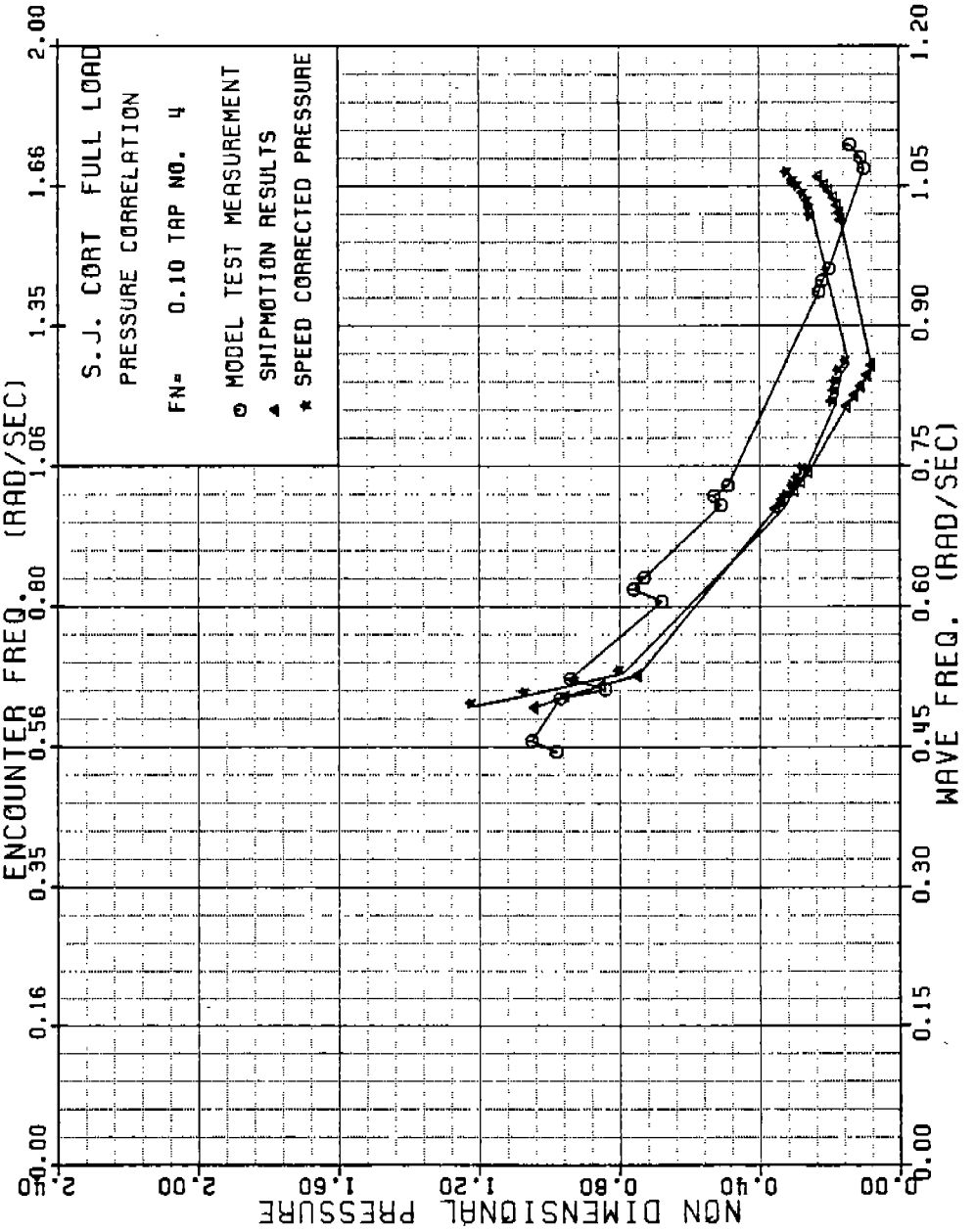

FIGURE B-4 SJ CORT NONDIMENSIONAL PRESSURE , TAP 4 , FN=0.10

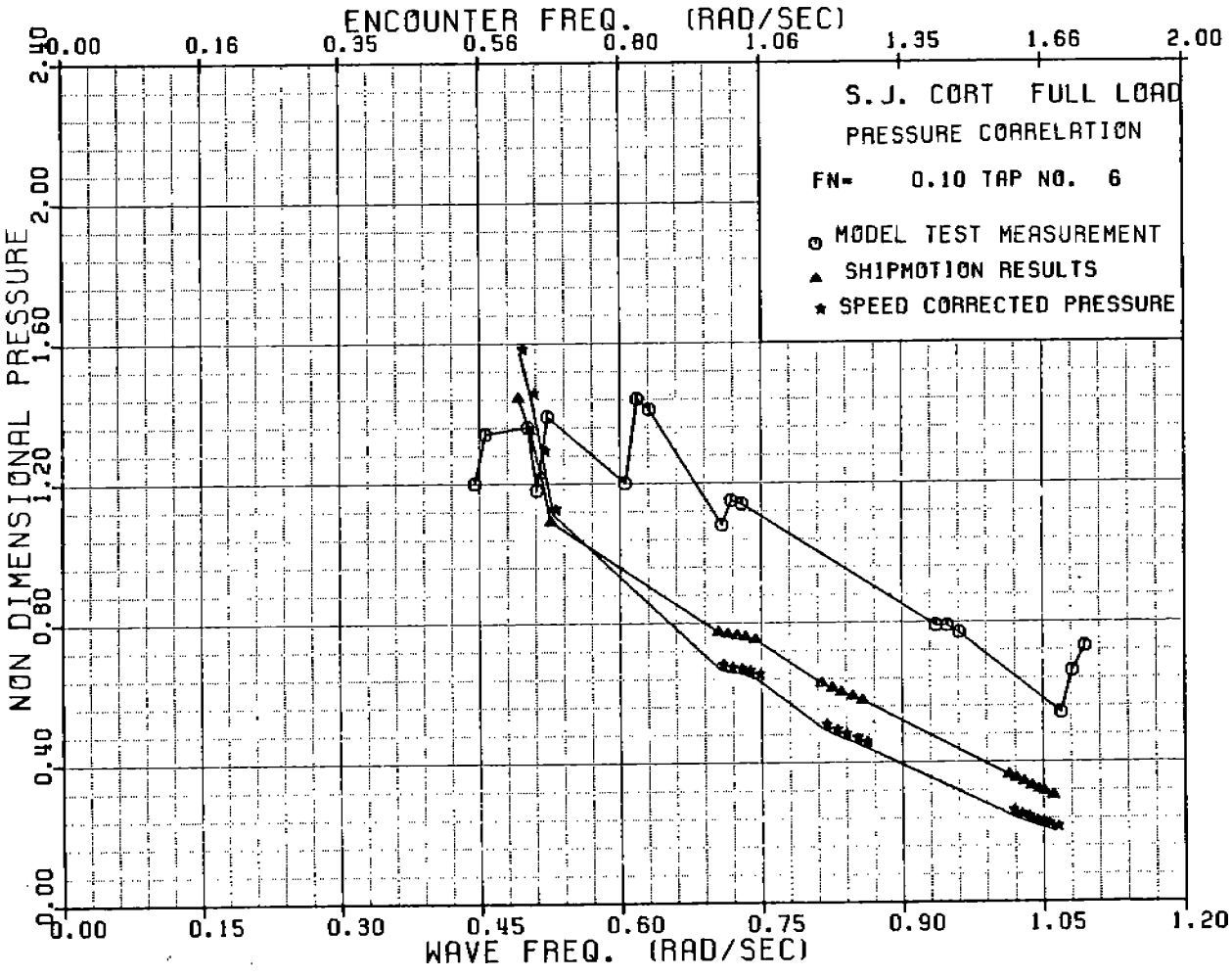

FIGURE B-6 SJ CORT NONDIMENSIONAL PRESSURE , TAP 6 , FN=0.10

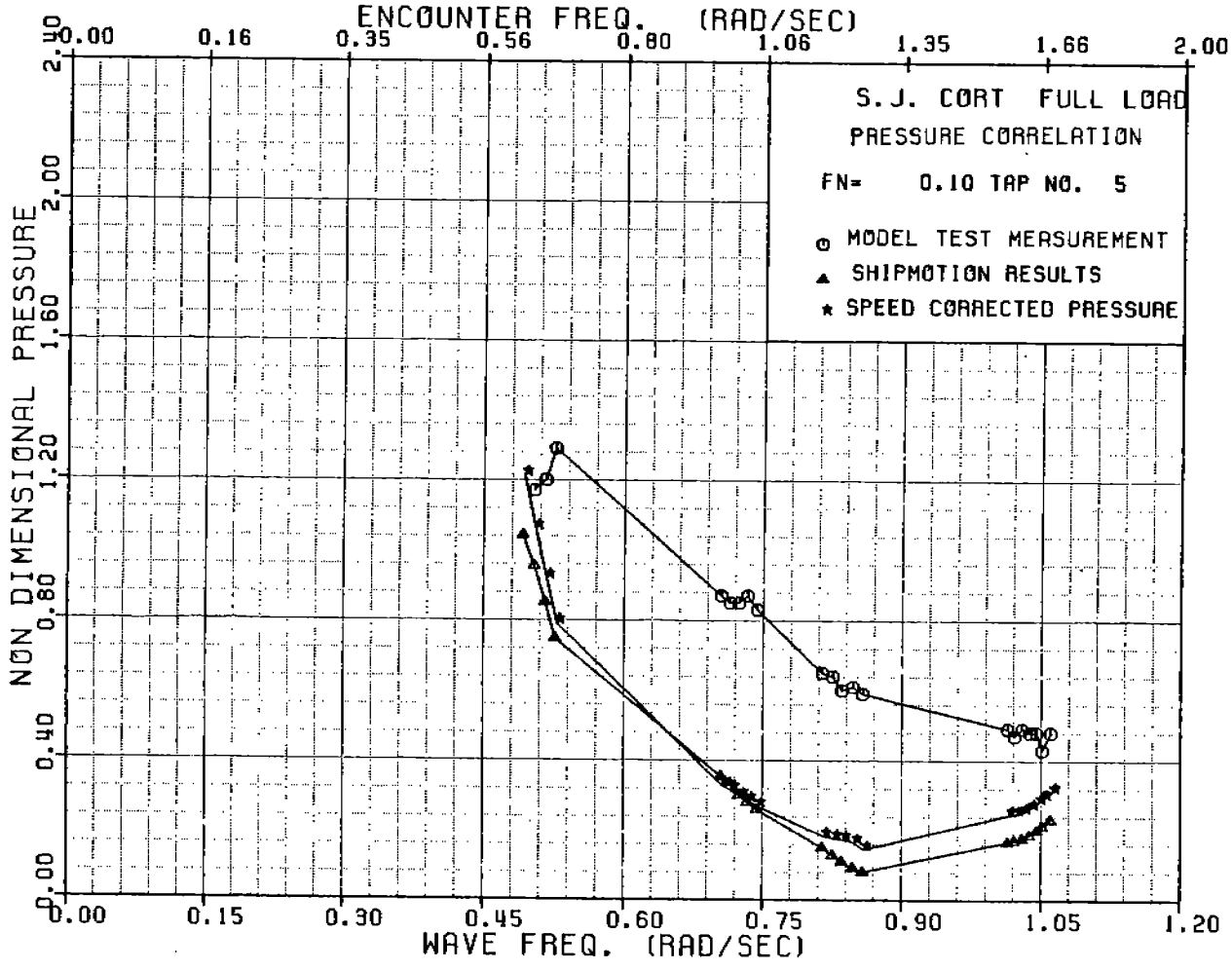

FIGURE B-5 SJ CORT NONDIMENSIONAL PRESSURE , TAP 5 , FN=0.10

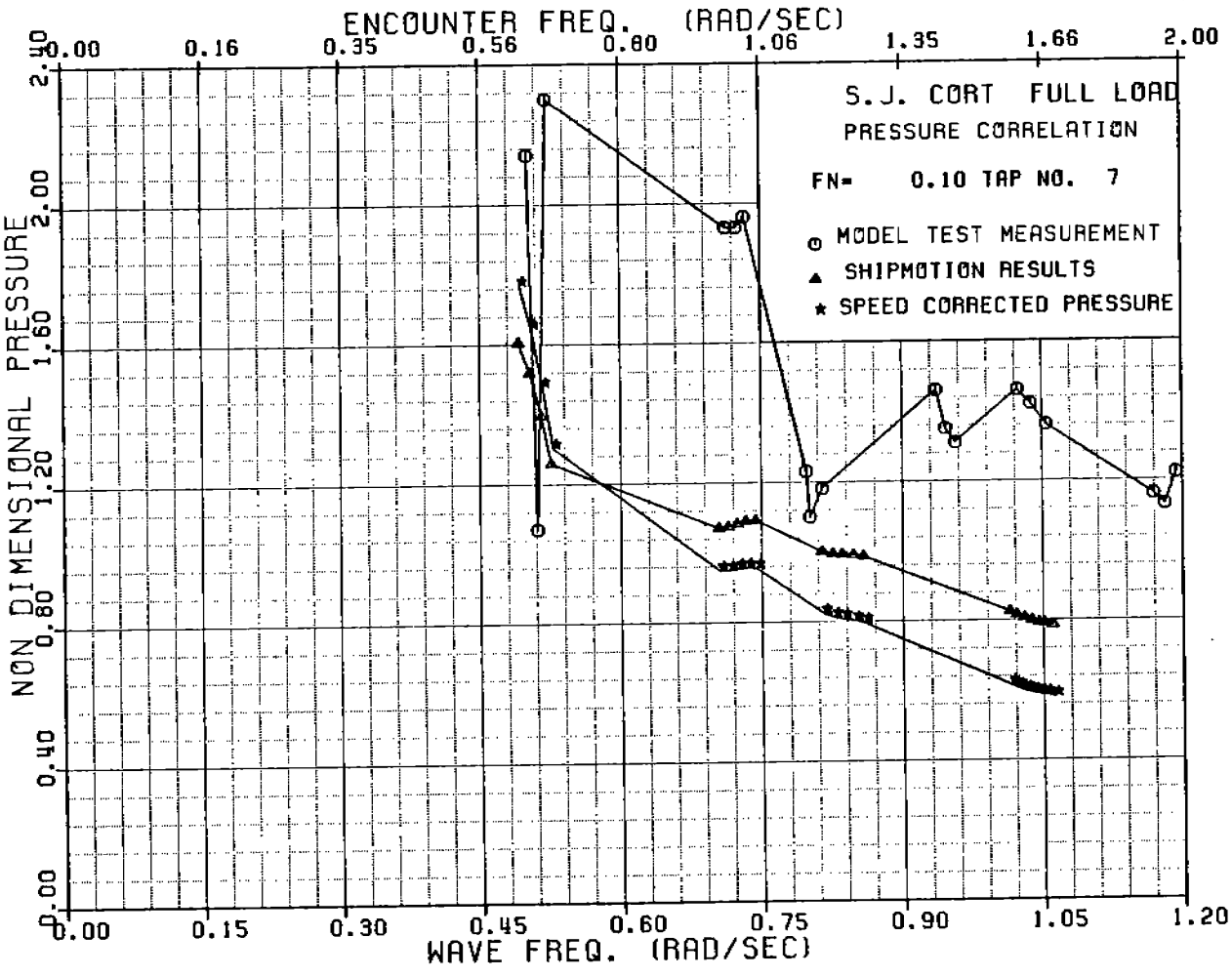

FIGURE B-7 SJ CORT NONDIMENSIONAL PRESSURE , TAP 7 , FN=0.10

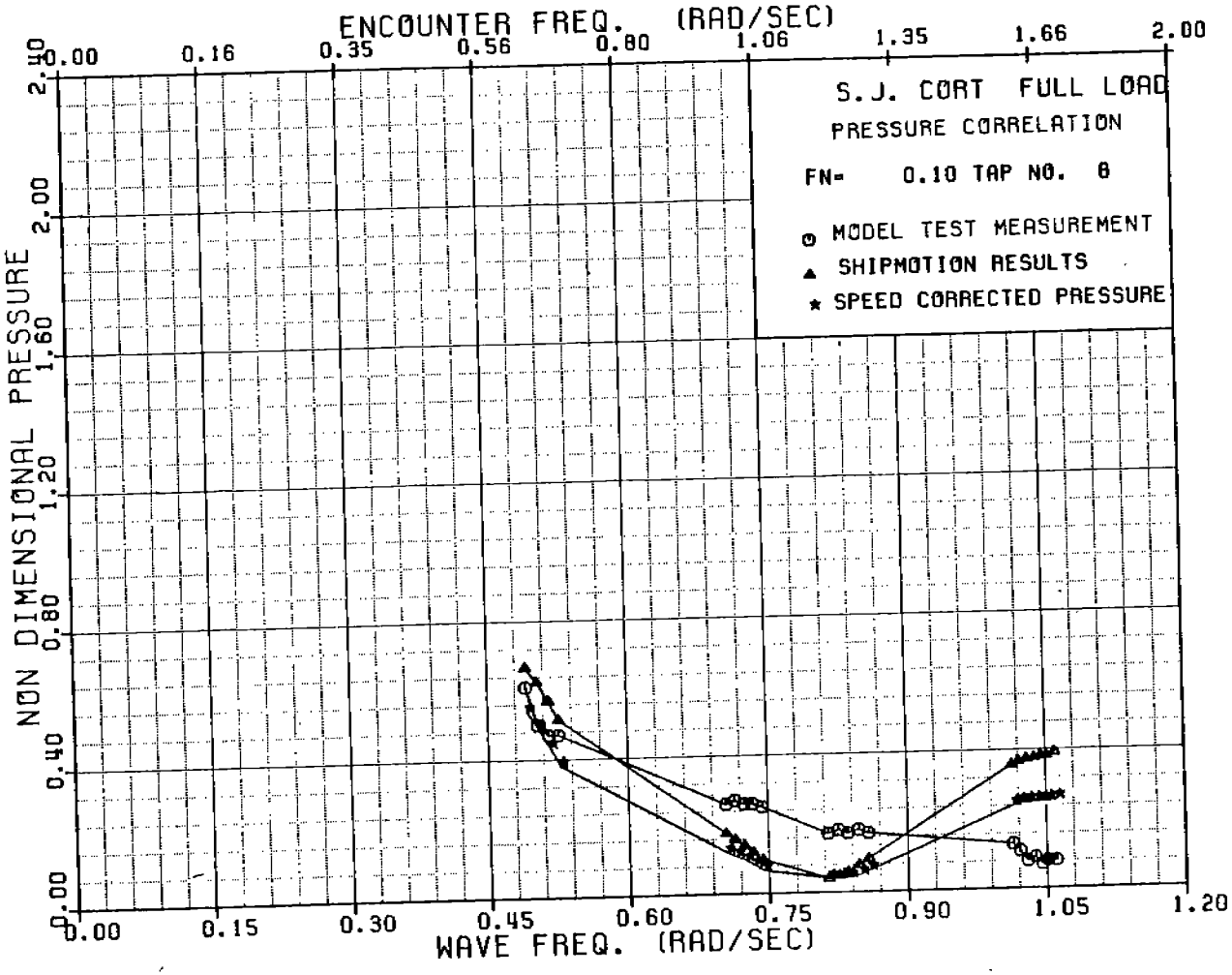

FIGURE B-8 SJ CORT NONDIMENSIONAL PRESSURE , TAP 8 , FN=0.10

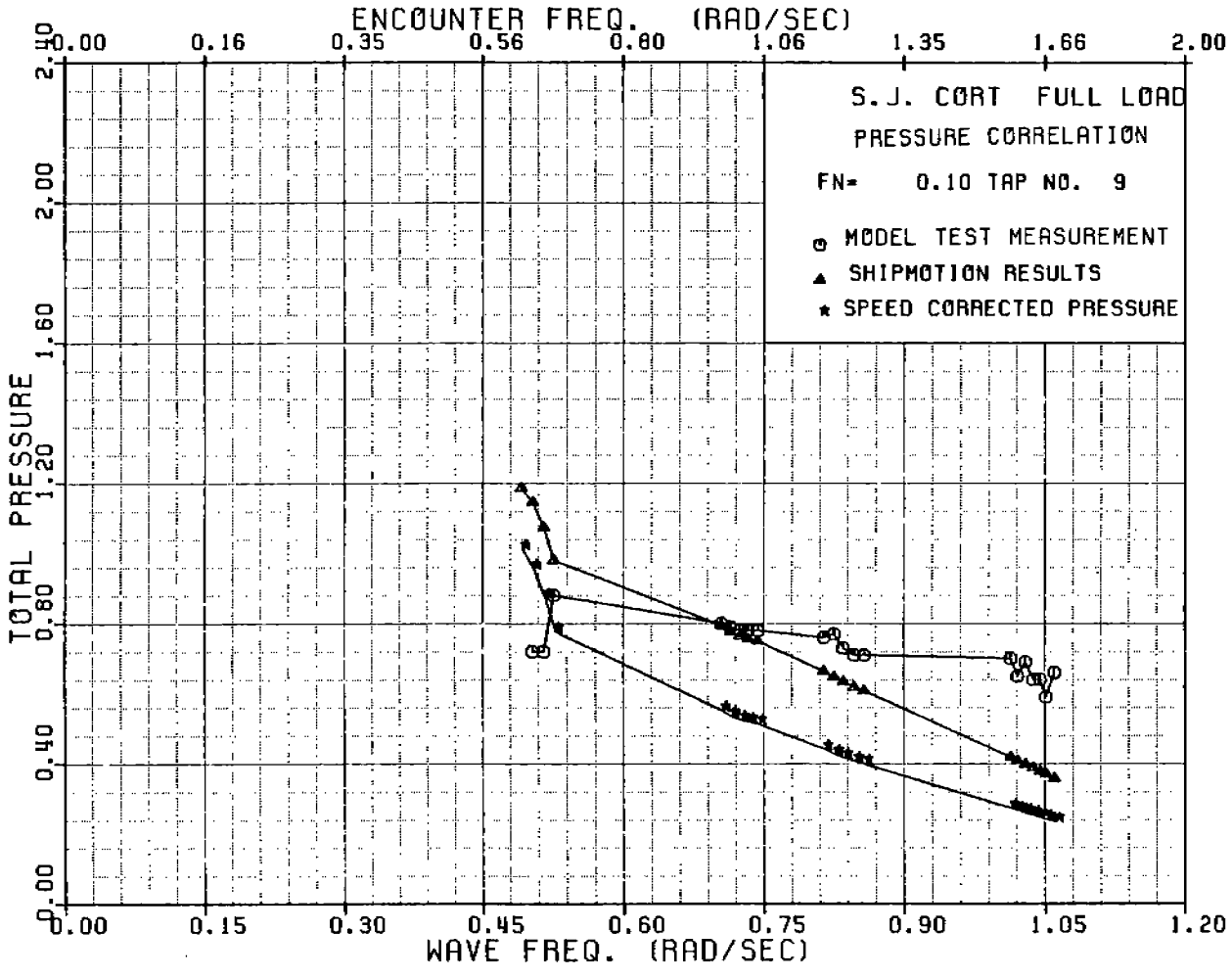

FIGURE B-9 SJ CORT NONDIMENSIONAL PRESSURE , TAP 9 , FN=0.10

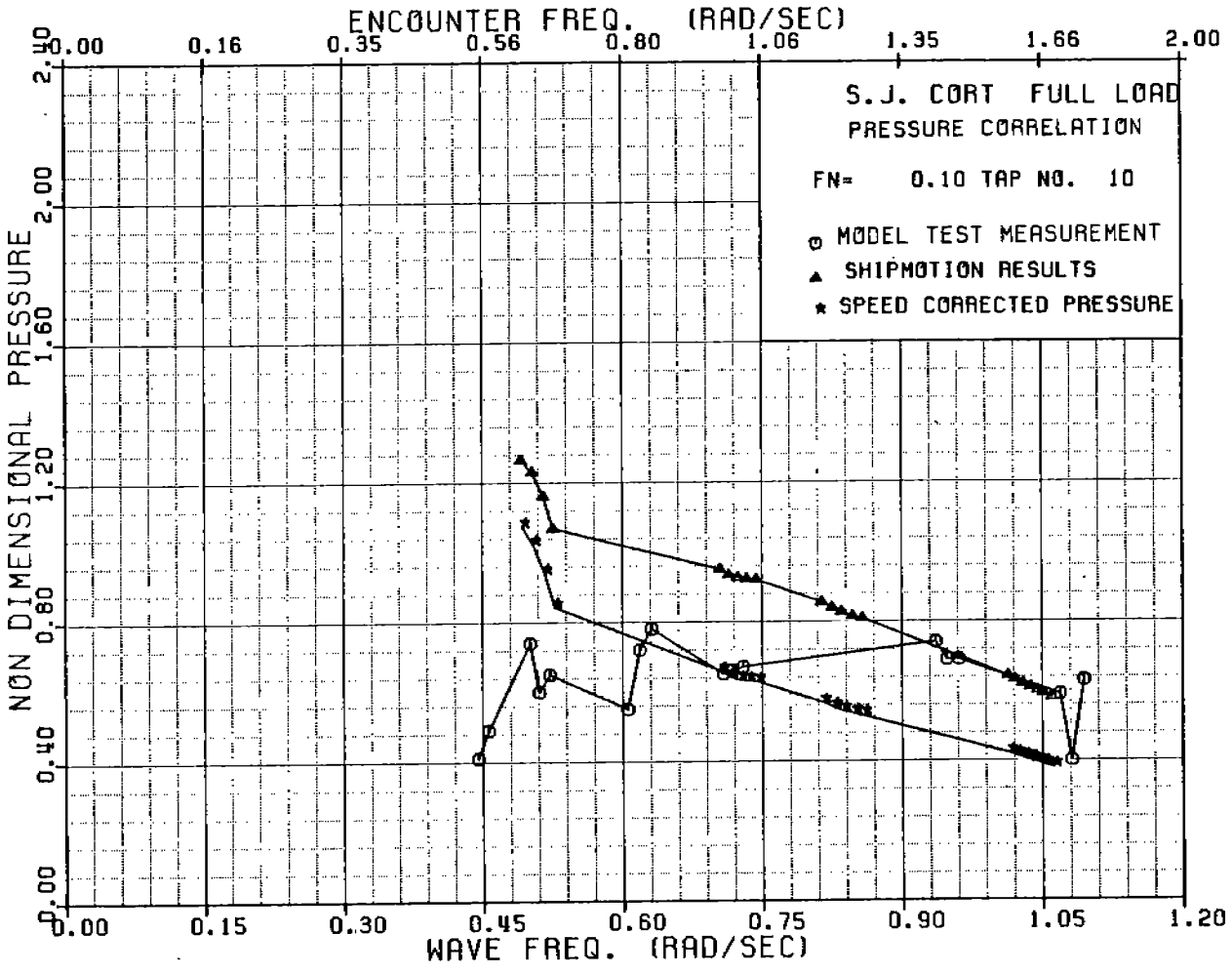

FIGURE B-10 SJ CORT NONDIMENSIONAL PRESSURE , TAP 10, FN=0.10

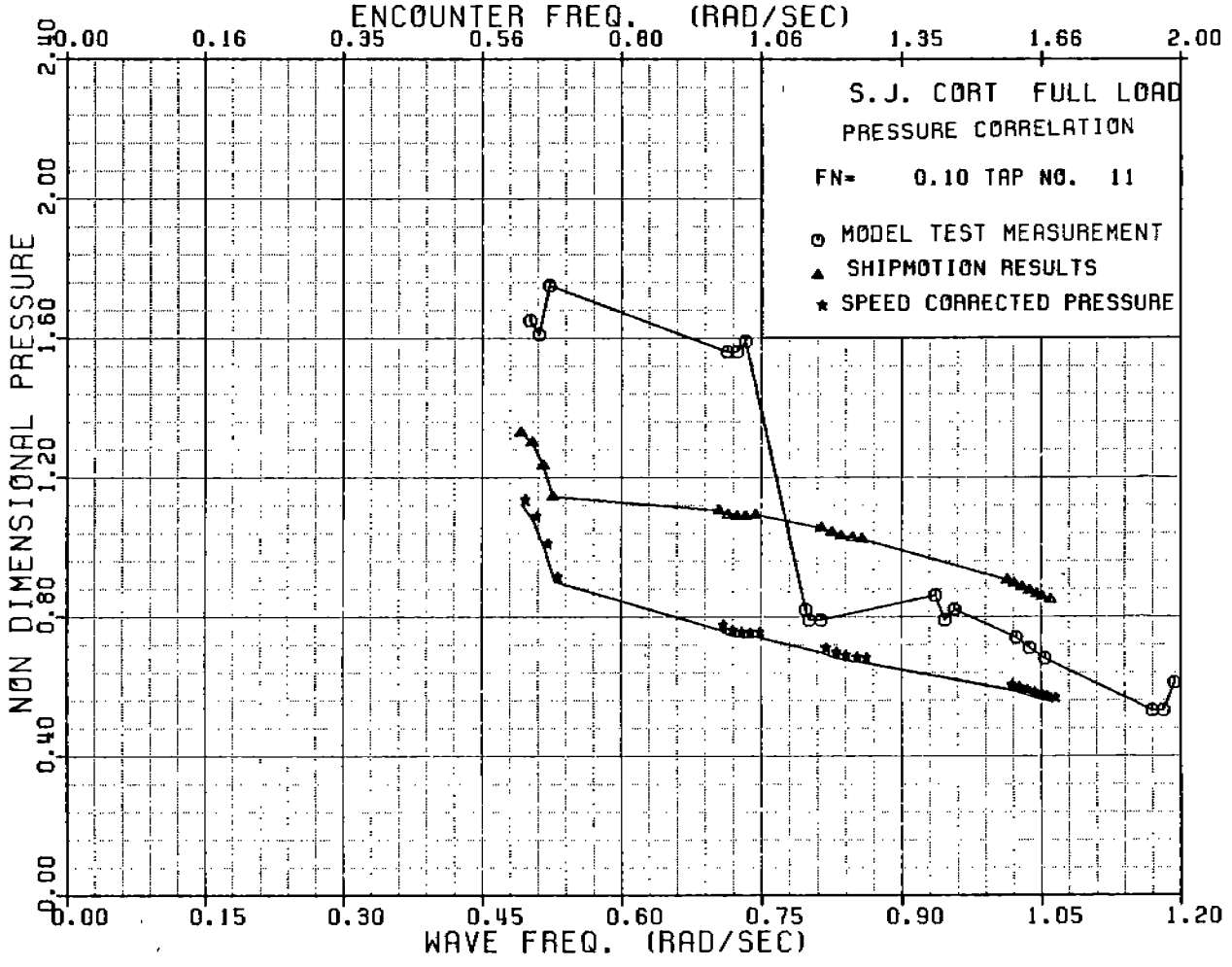

FIGURE B-11 SJ CORT NONDIMENSIONAL PRESSURE , TAP 11, FN=0.10

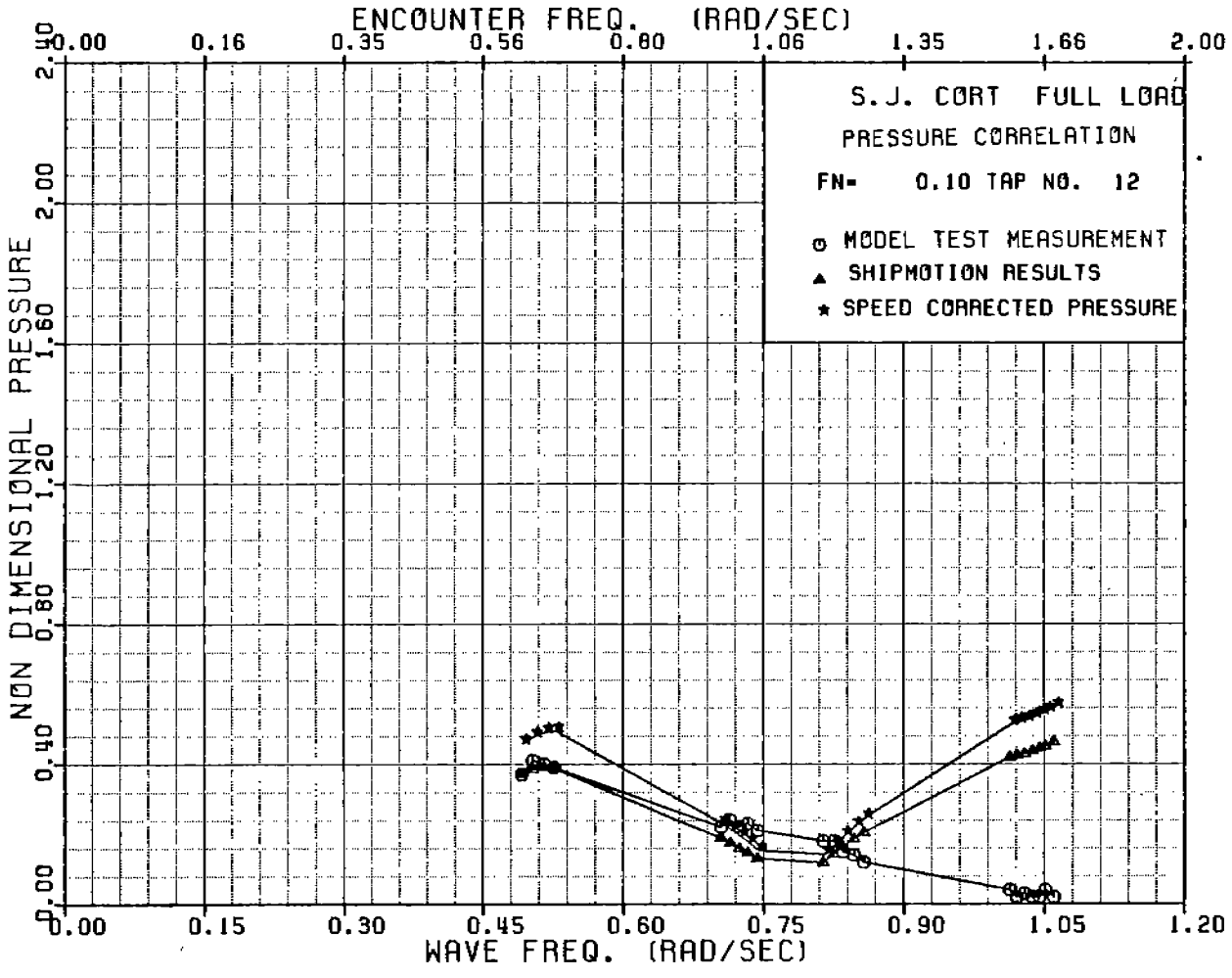

FIGURE B-12 SJ CORT NONDIMENSIONAL PRESSURE , TAP 12, FN=0.10

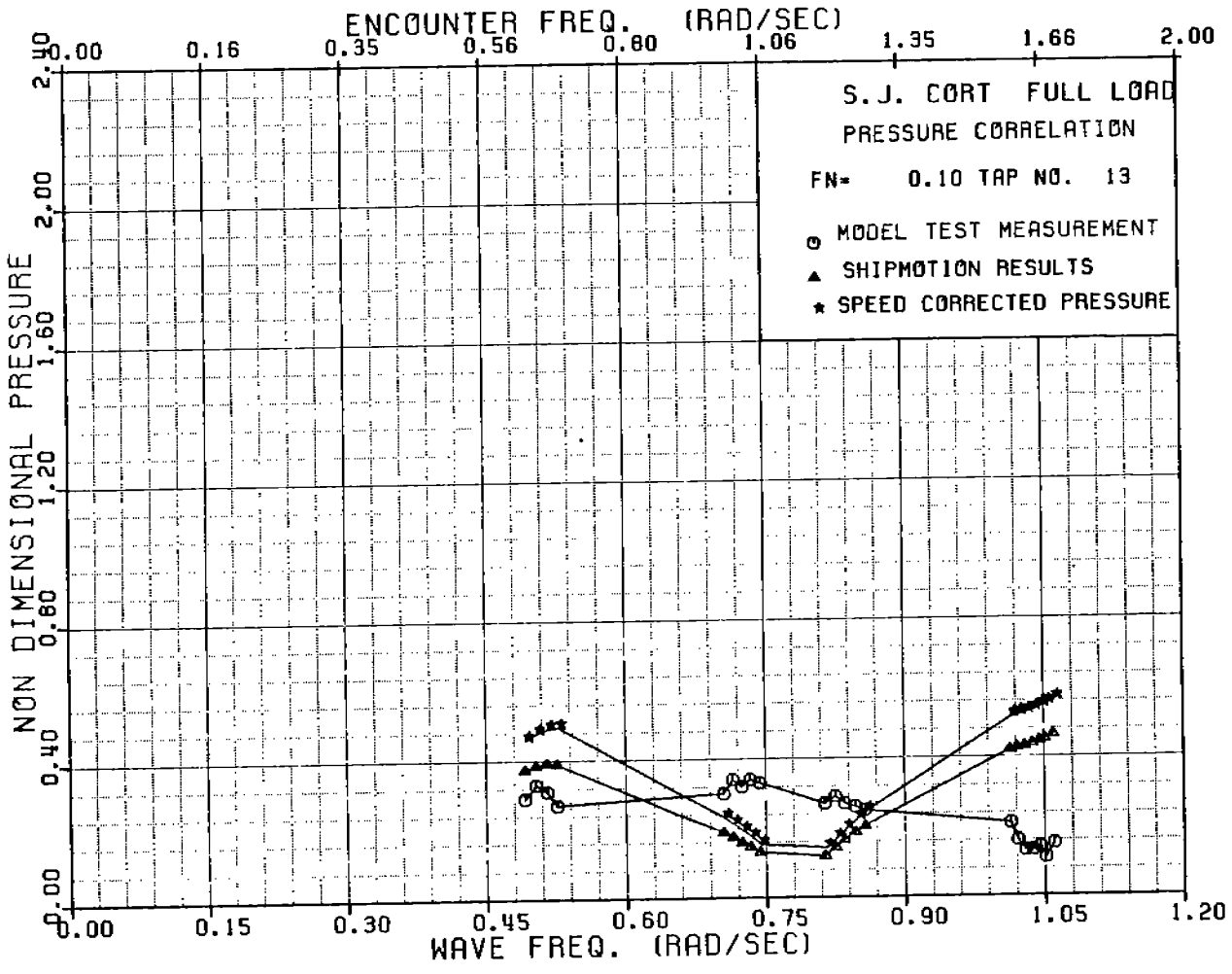

FIGURE B-13 SJ CORT NONDIMENSIONAL PRESSURE , TAP 13, FN=0.10

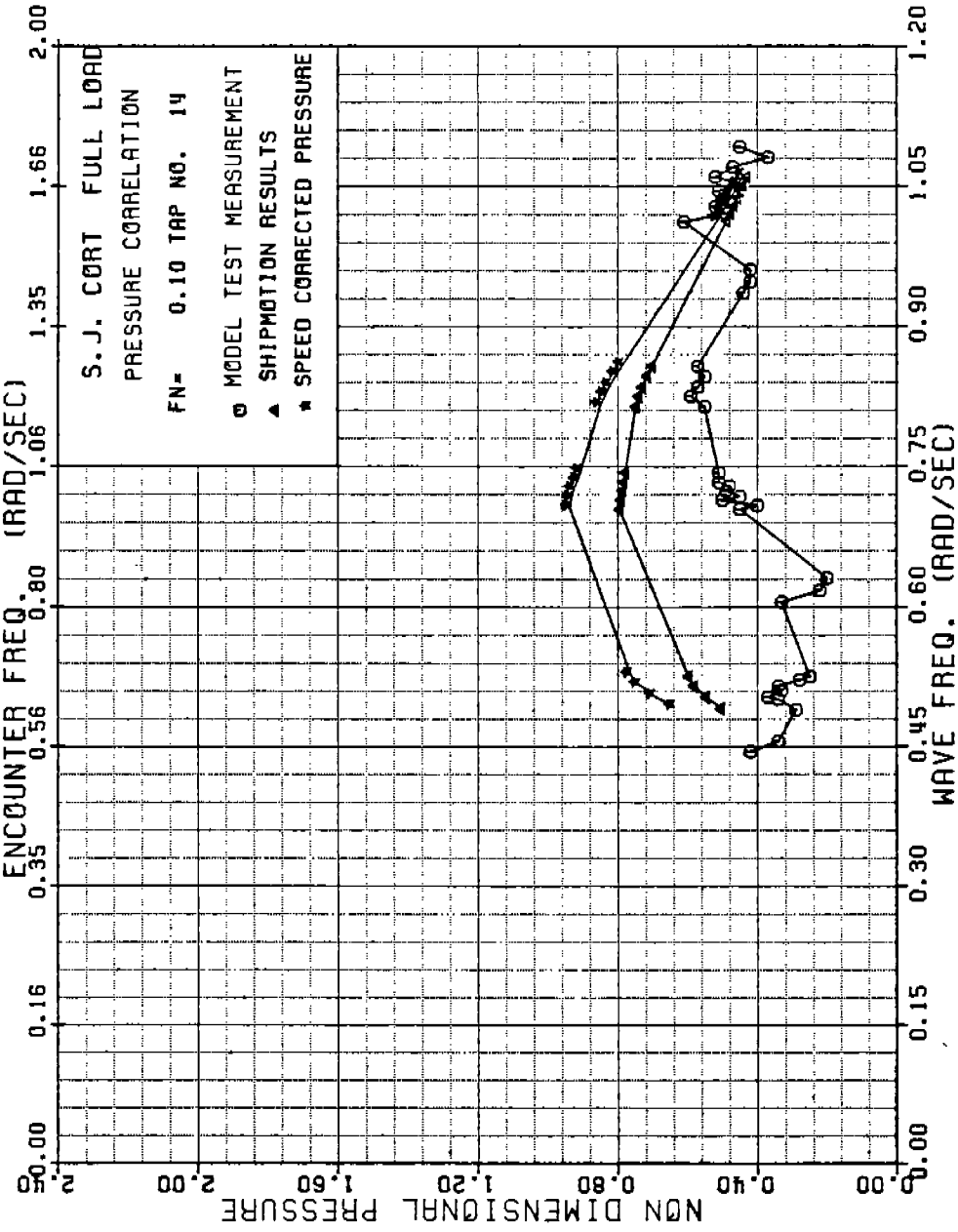

FIGURE B-14 SJ CORT NONDIMENSIONAL PRESSURE , TAP 14, FN=0.10

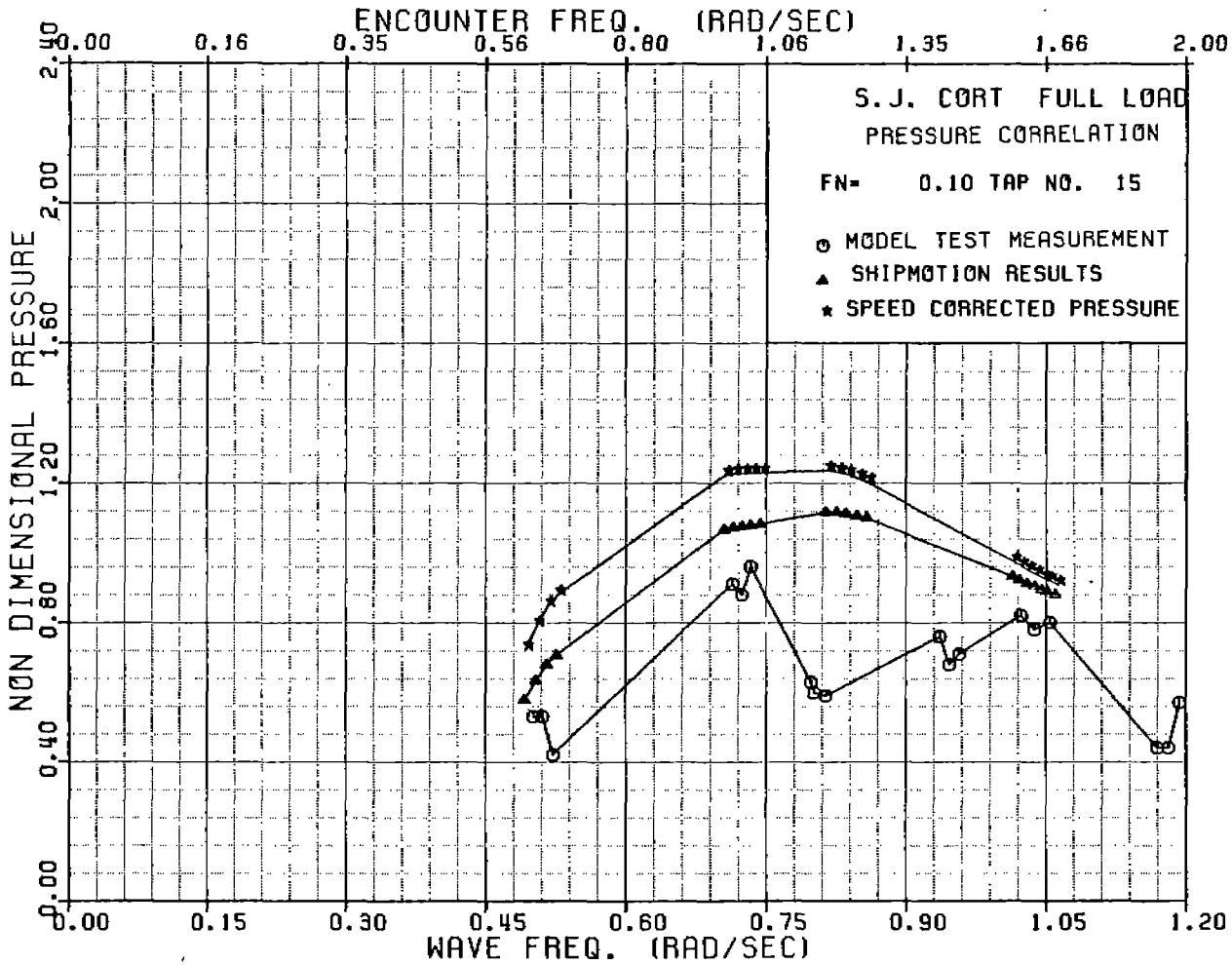

FIGURE B-15 SJ CORT NONDIMENSIONAL PRESSURE , TAP 15, FN=0.10

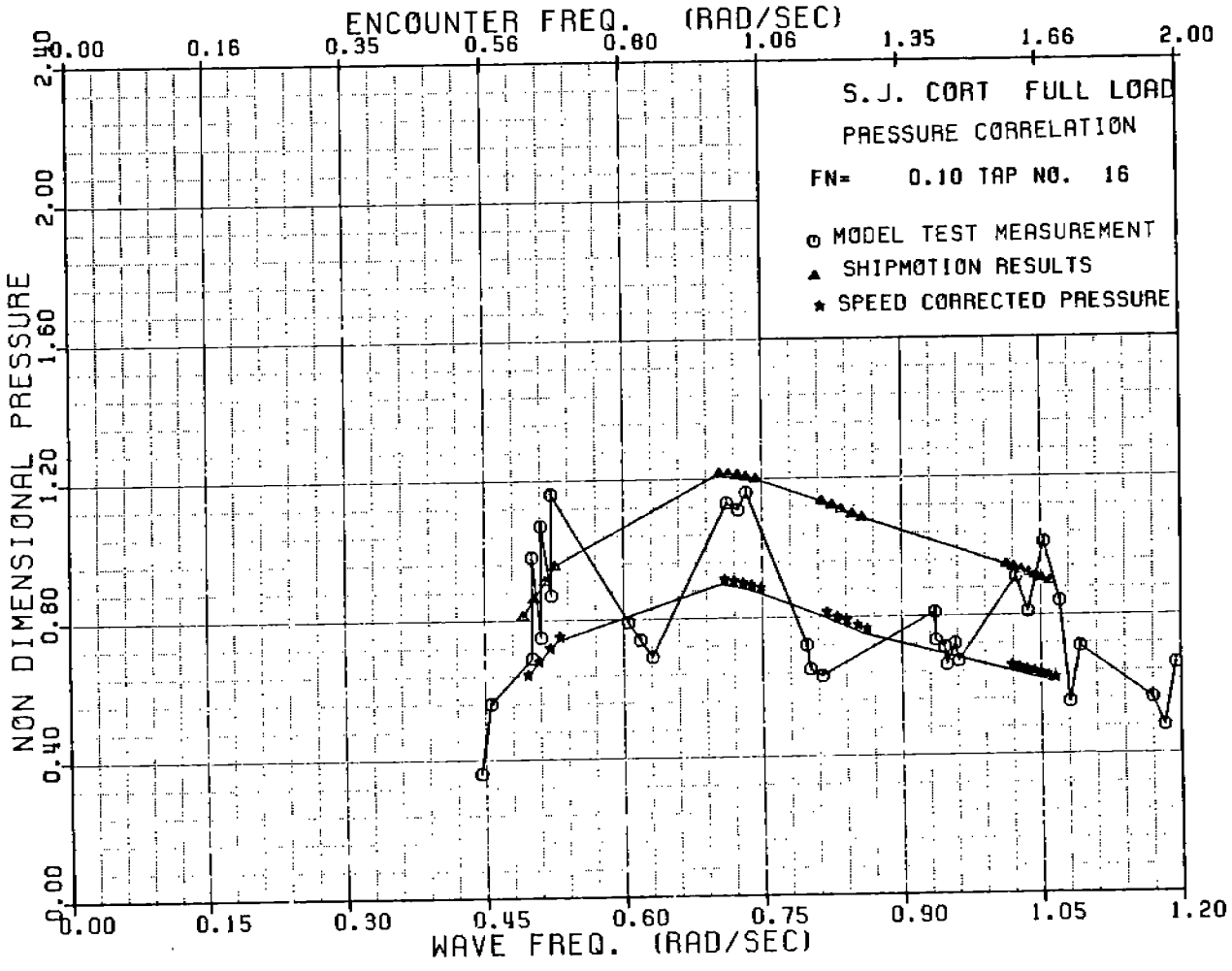

FIGURE B-16 SJ CORT NONDIMENSIONAL PRESSURE , TAP 16, FN=0.10

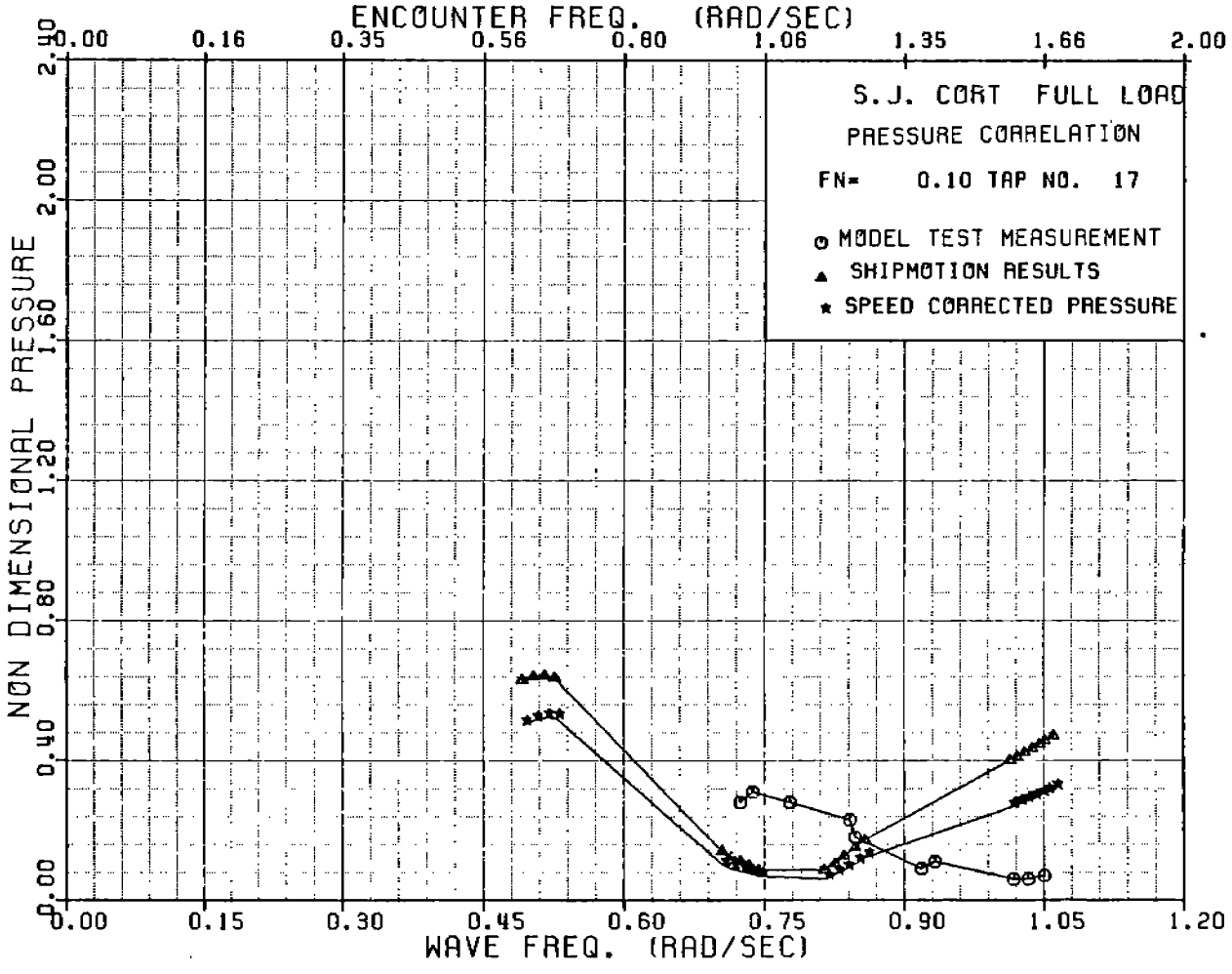

FIGURE B-17 SJ CORT NONDIMENSIONAL PRESSURE , TAP 17, FN=0.10

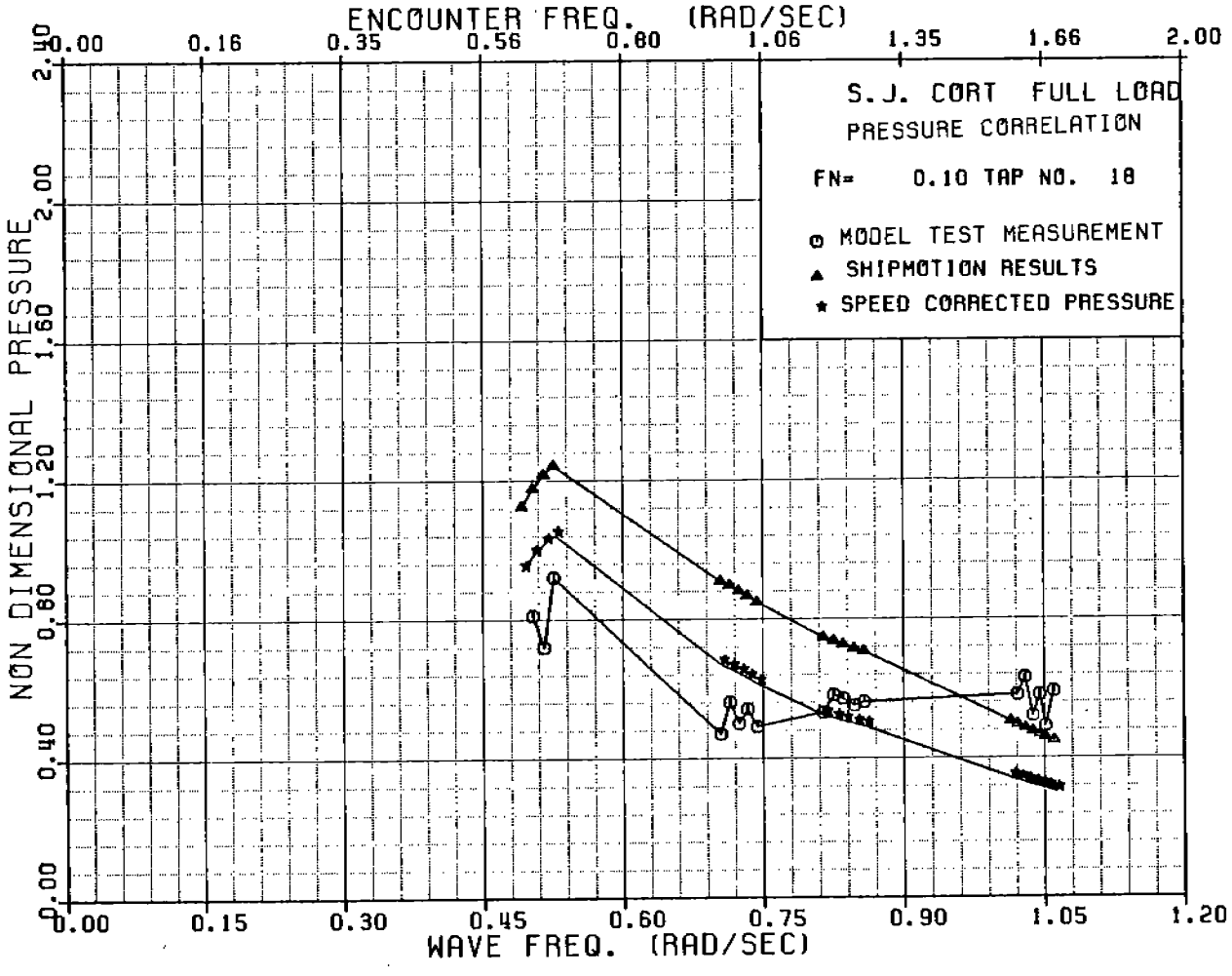

FIGURE B-18 SJ CORT NONDIMENSIONAL PRESSURE , TAP 18, FN=0.10

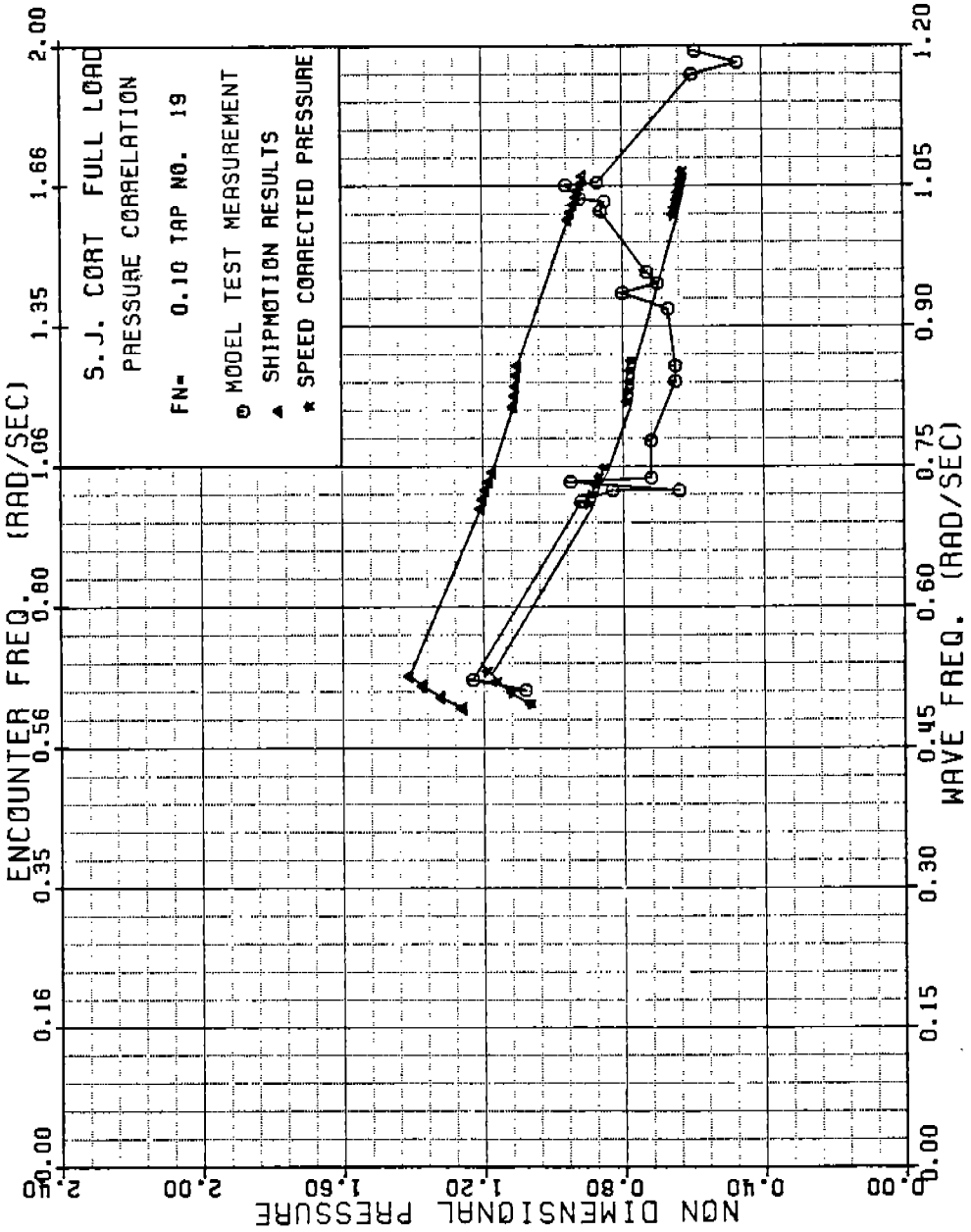

FIGURE B-19 SJ CORT NONDIMENSIONAL PRESSURE , TAP 19, FN=0.10

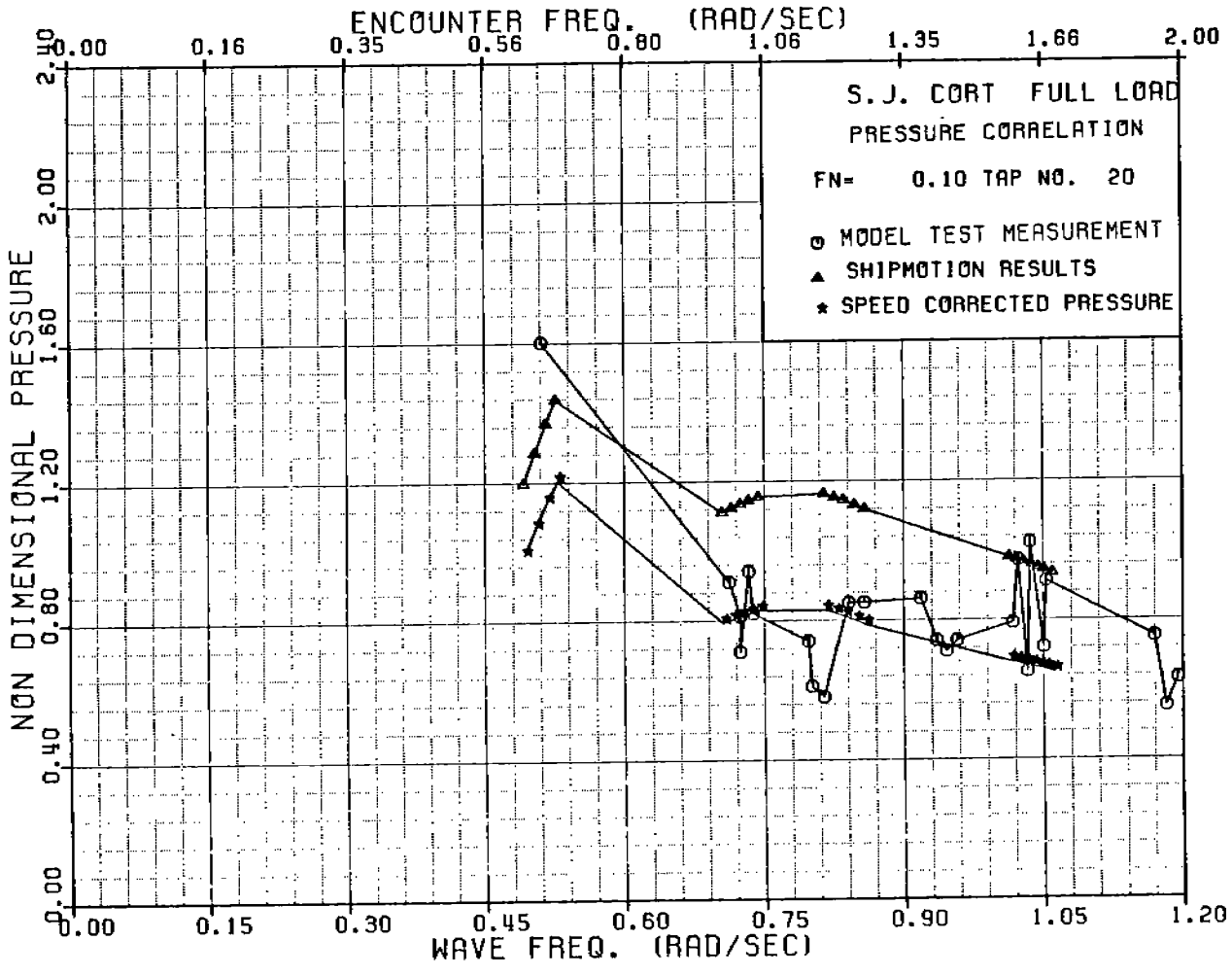

FIGURE B-20 SJ CORT NONDIMENSIONAL PRESSURE , TAP 20, FN=0.10

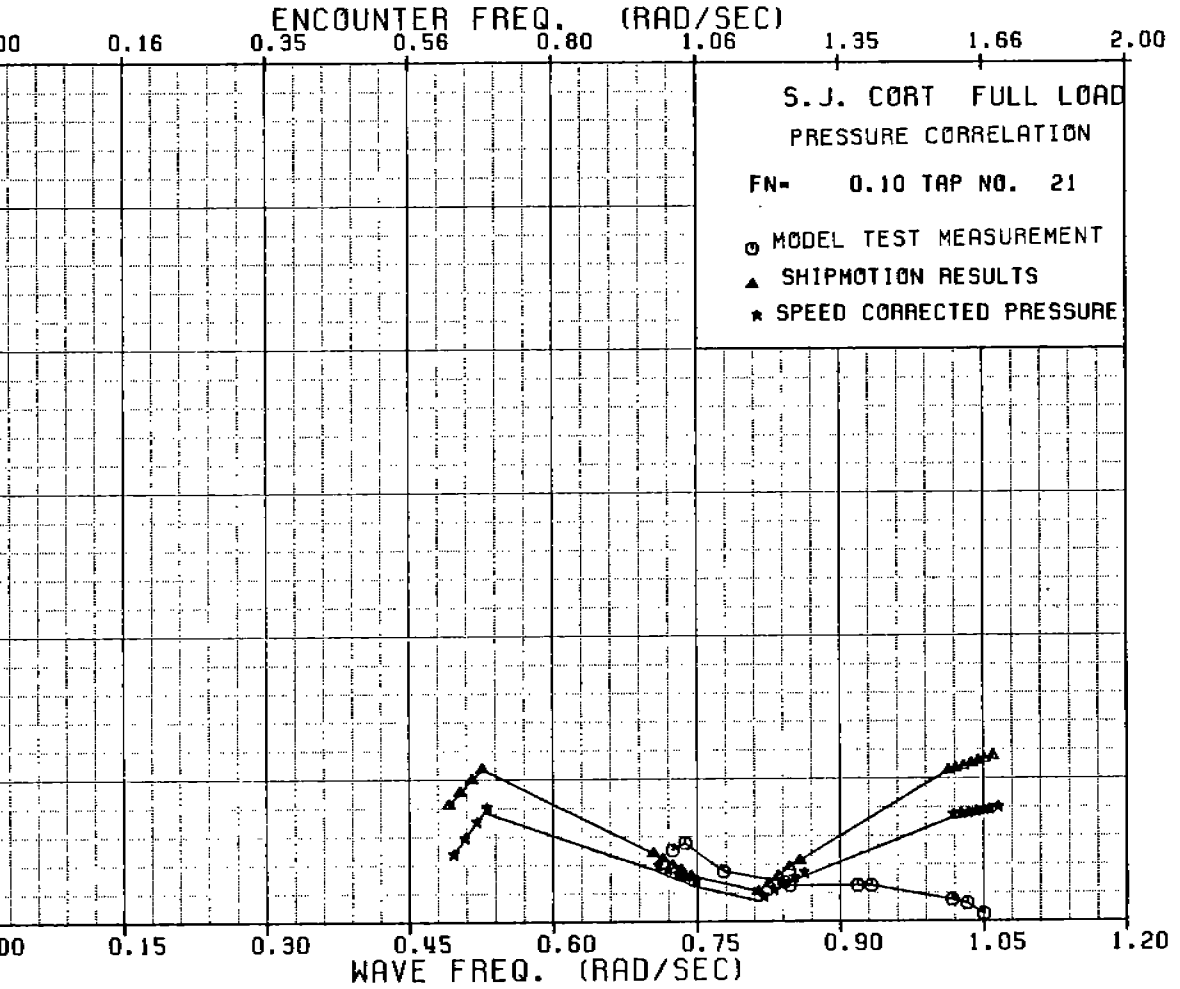

FIGURE B-21 SJ CORT NONDIMENSIONAL PRESSURE , TAP 21, FN=0.10

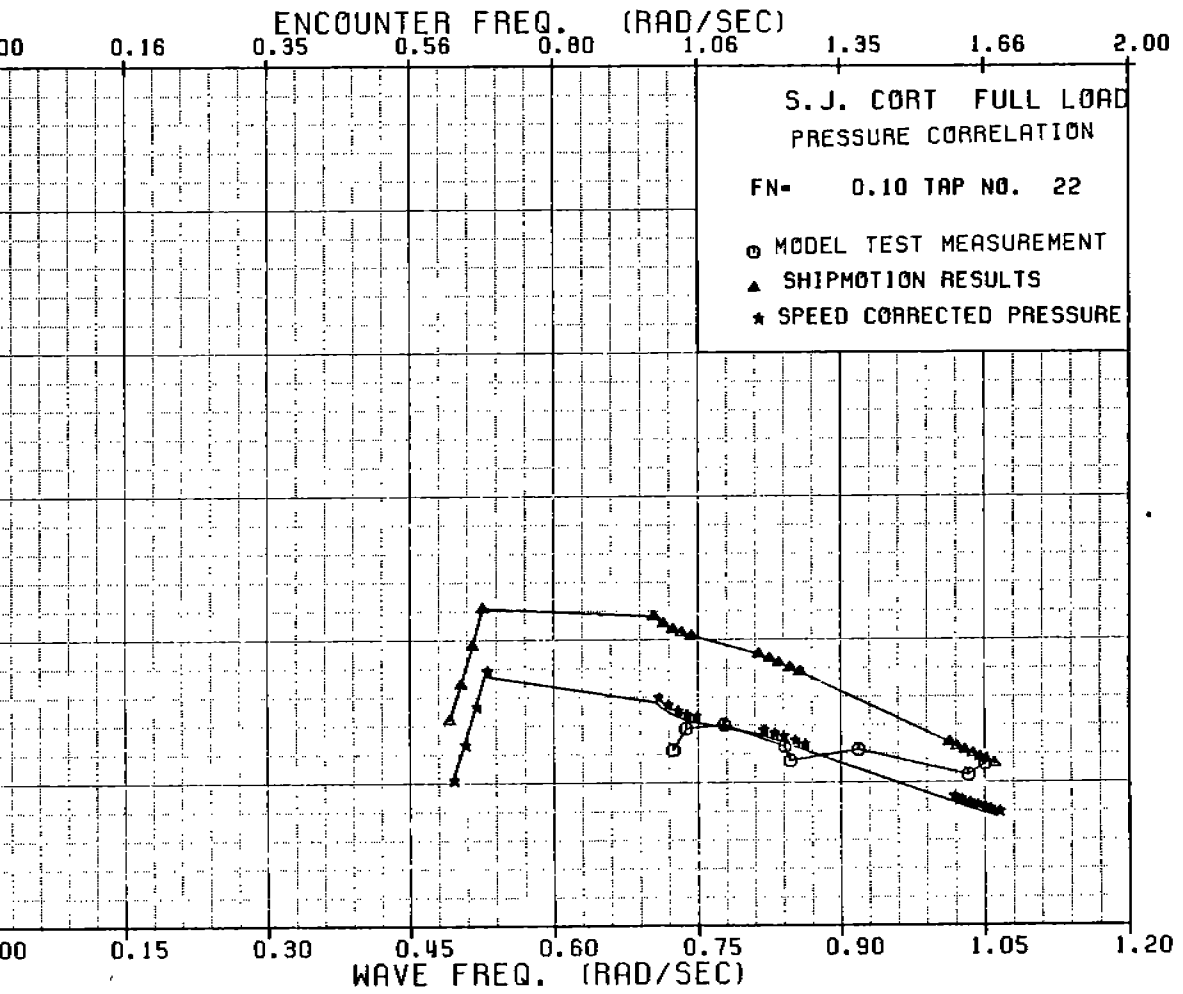

FIGURE B-22 SJ CORT NONDIMENSIONAL PRESSURE , TAP 22, FN=0.10

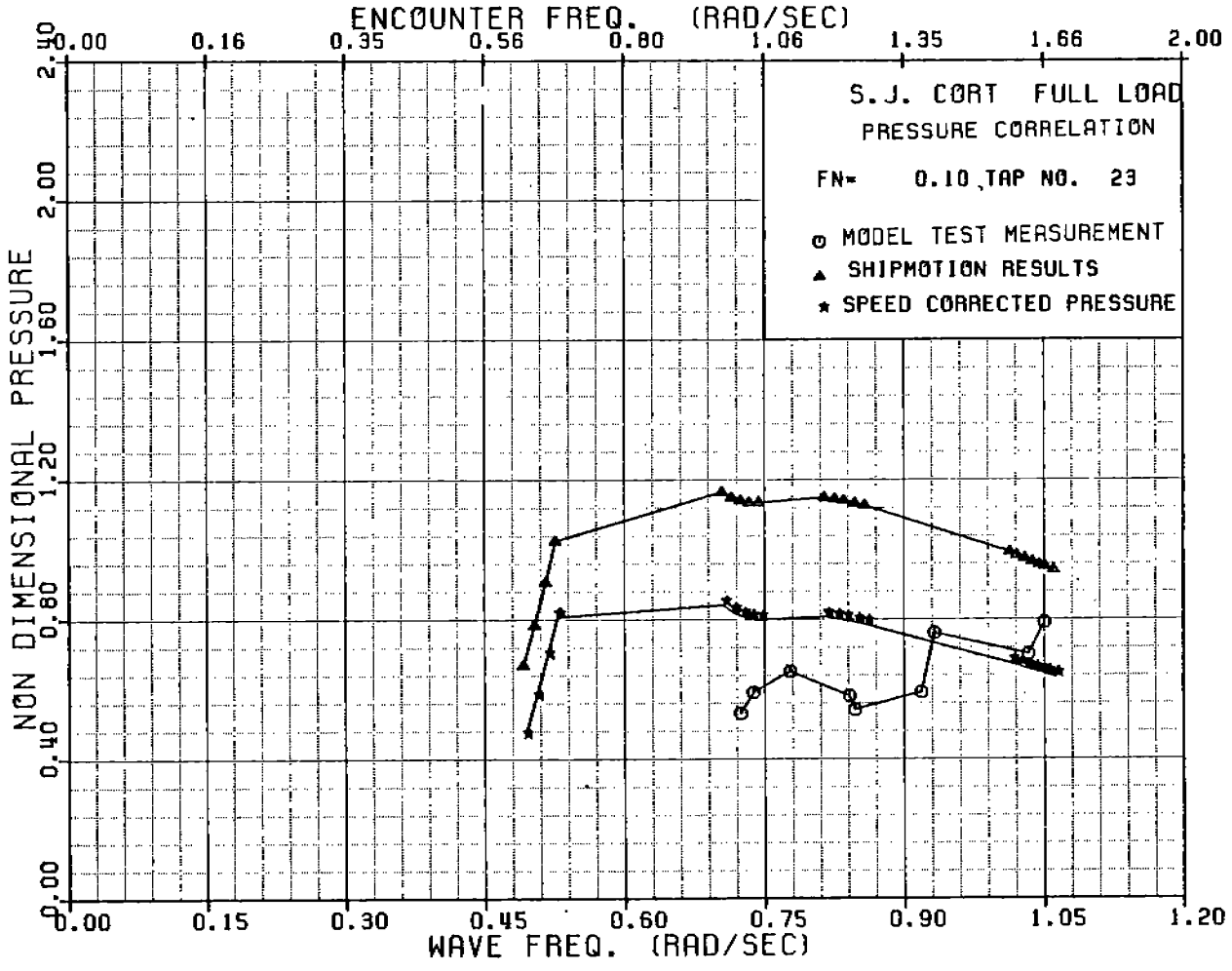

FIGURE B-23 SJ CORT NONDIMENSIONAL PRESSURE , TAP 23, FN=0.10

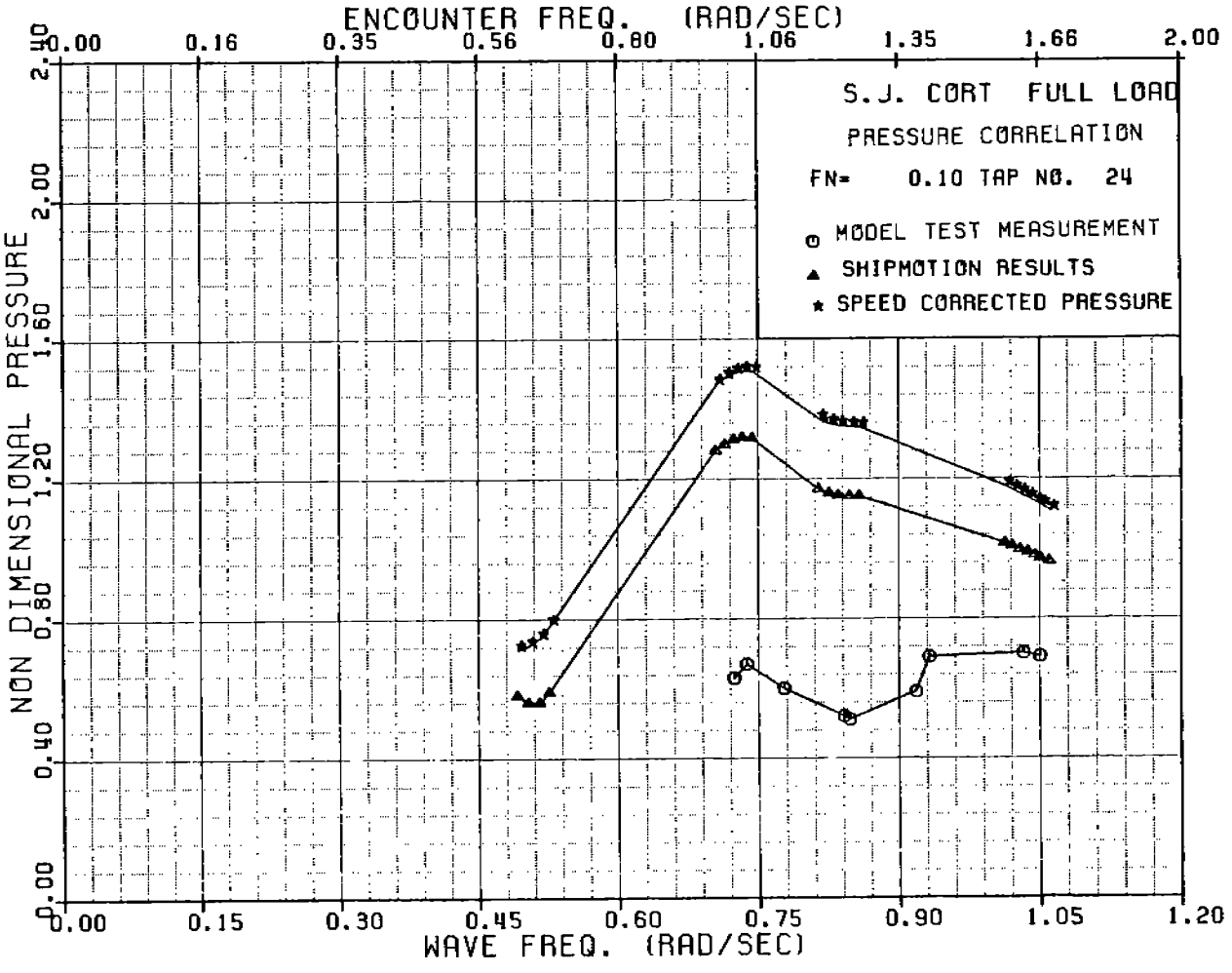

FIGURE B-24 SJ CORT NONDIMENSIONAL PRESSURE , TAP 24, FN=0.10

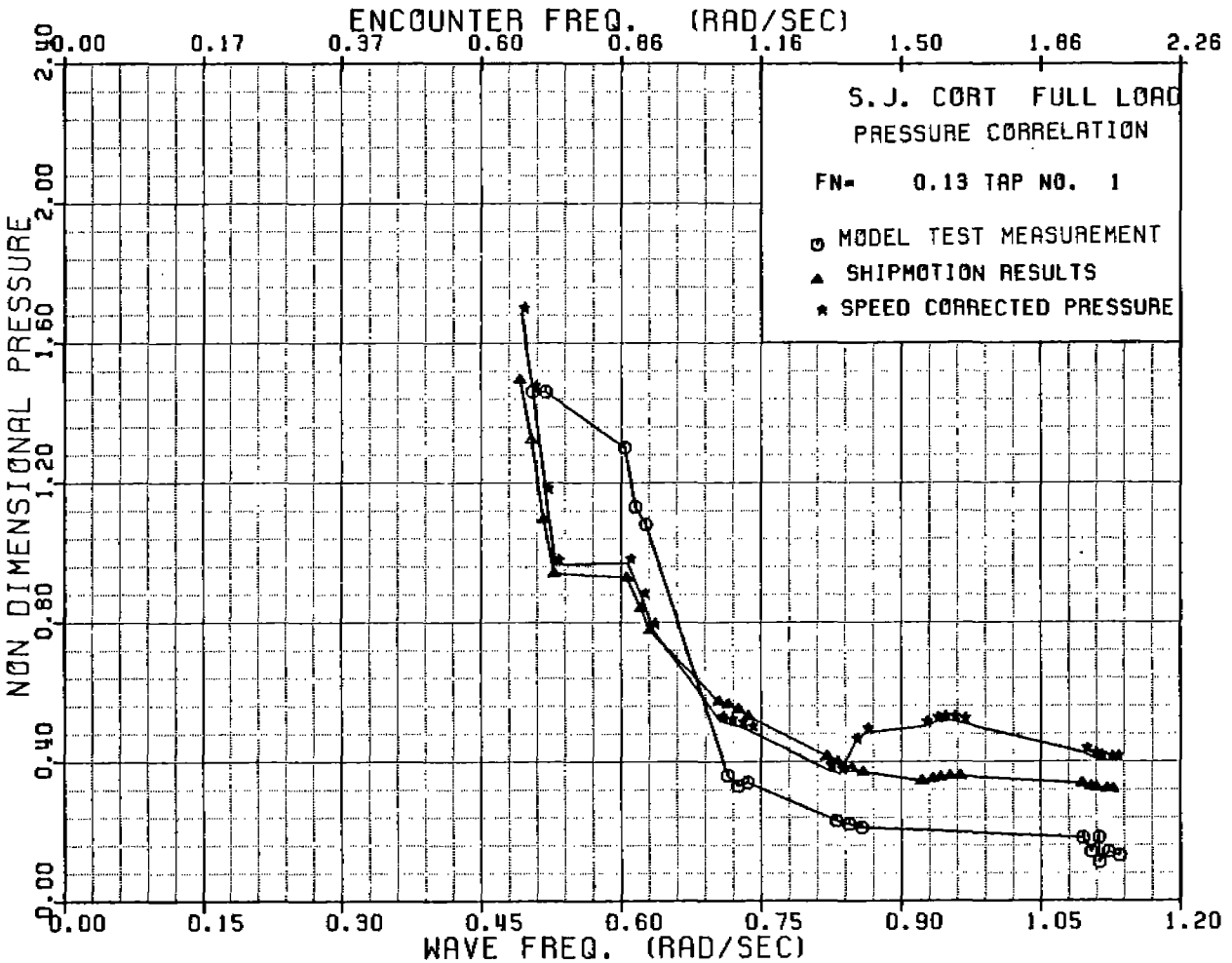

FIGURE B-25 SJ CORT NONDIMENSIONAL PRESSURE , TAP 1 , FN=0.13

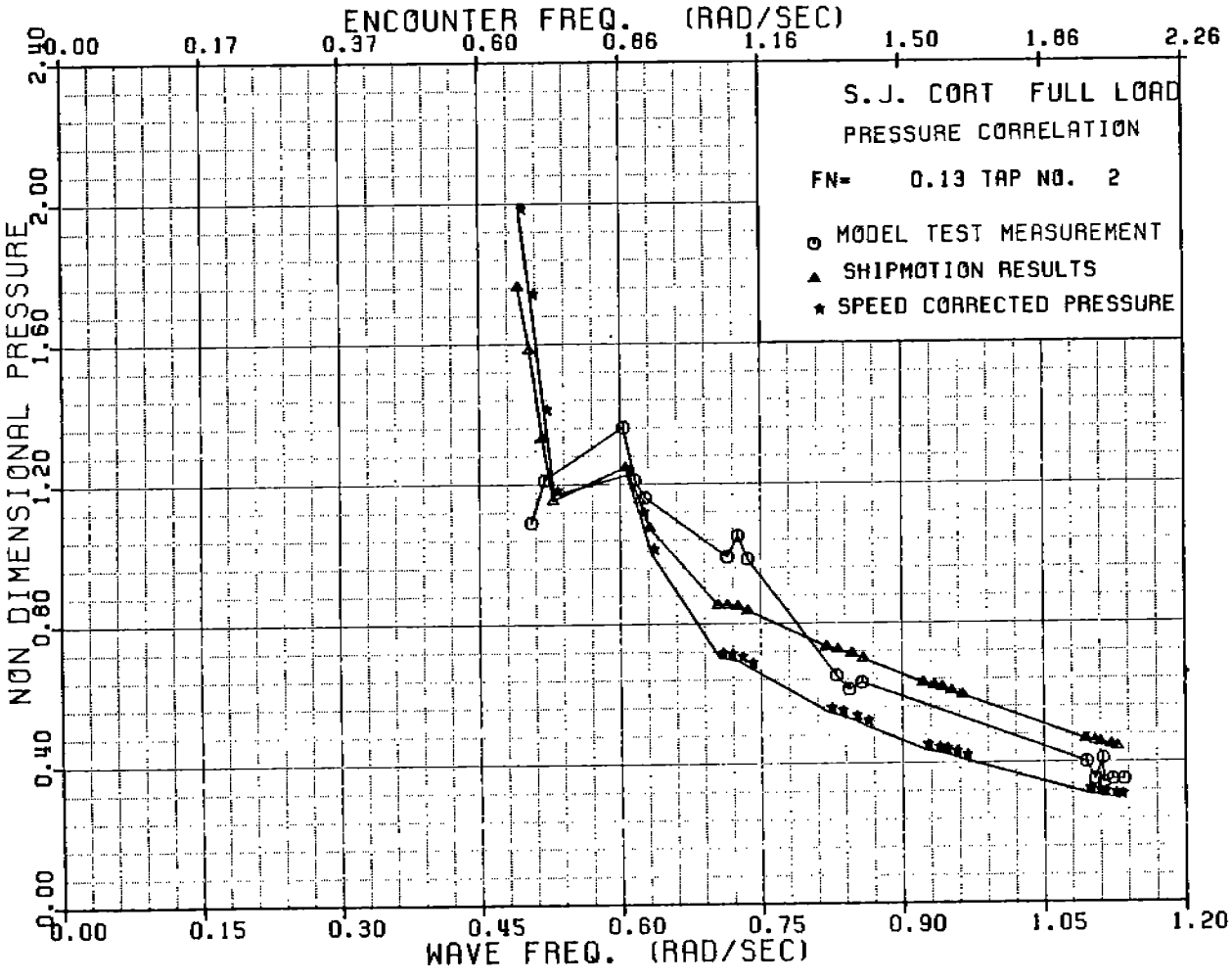

FIGURE B-26 SJ CORT NONDIMENSIONAL PRESSURE , TAP 2 , FN=0.13

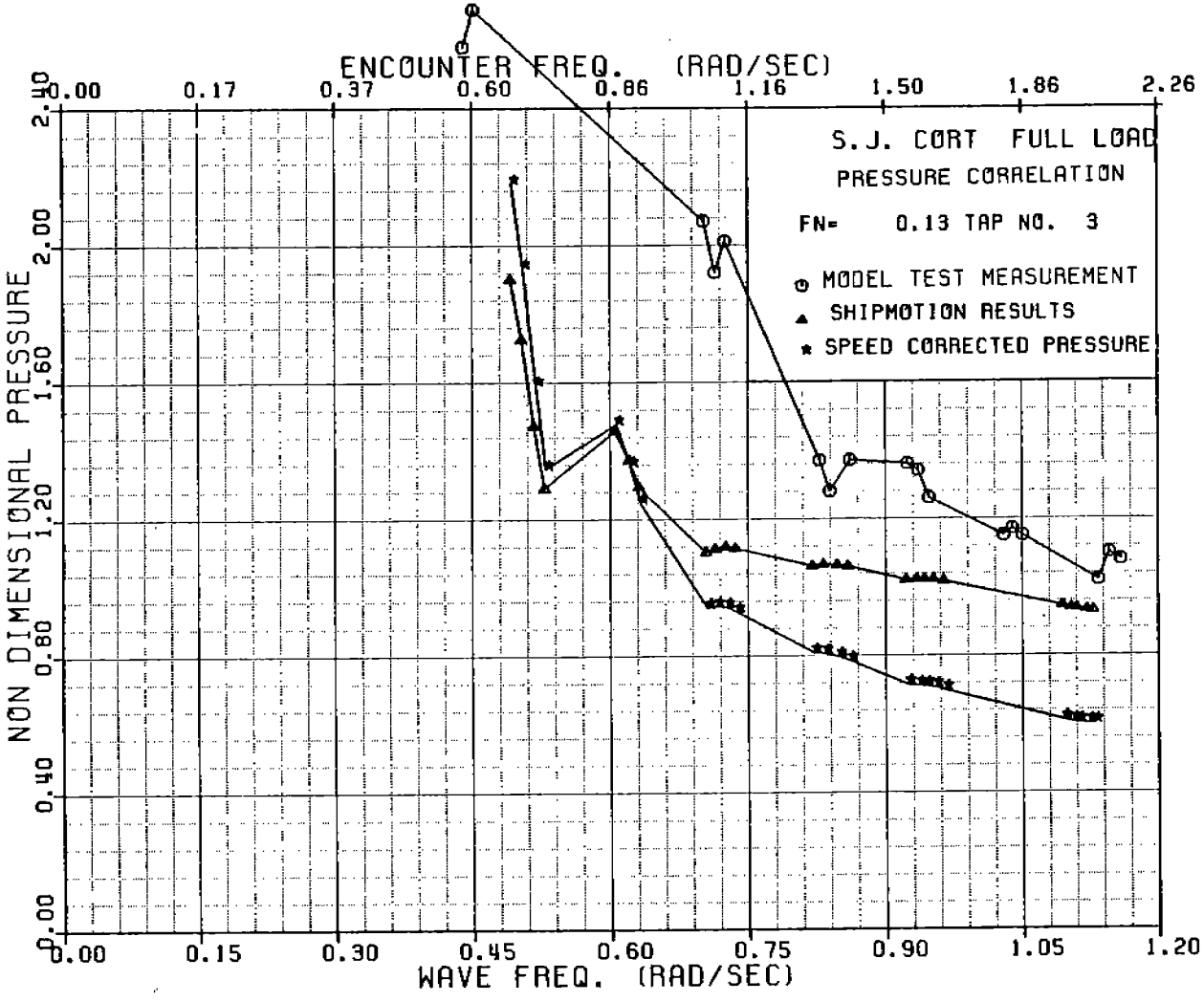

FIGURE B-27 SJ CORT NONDIMENSIONAL PRESSURE , TAP 3 , FN=0.13

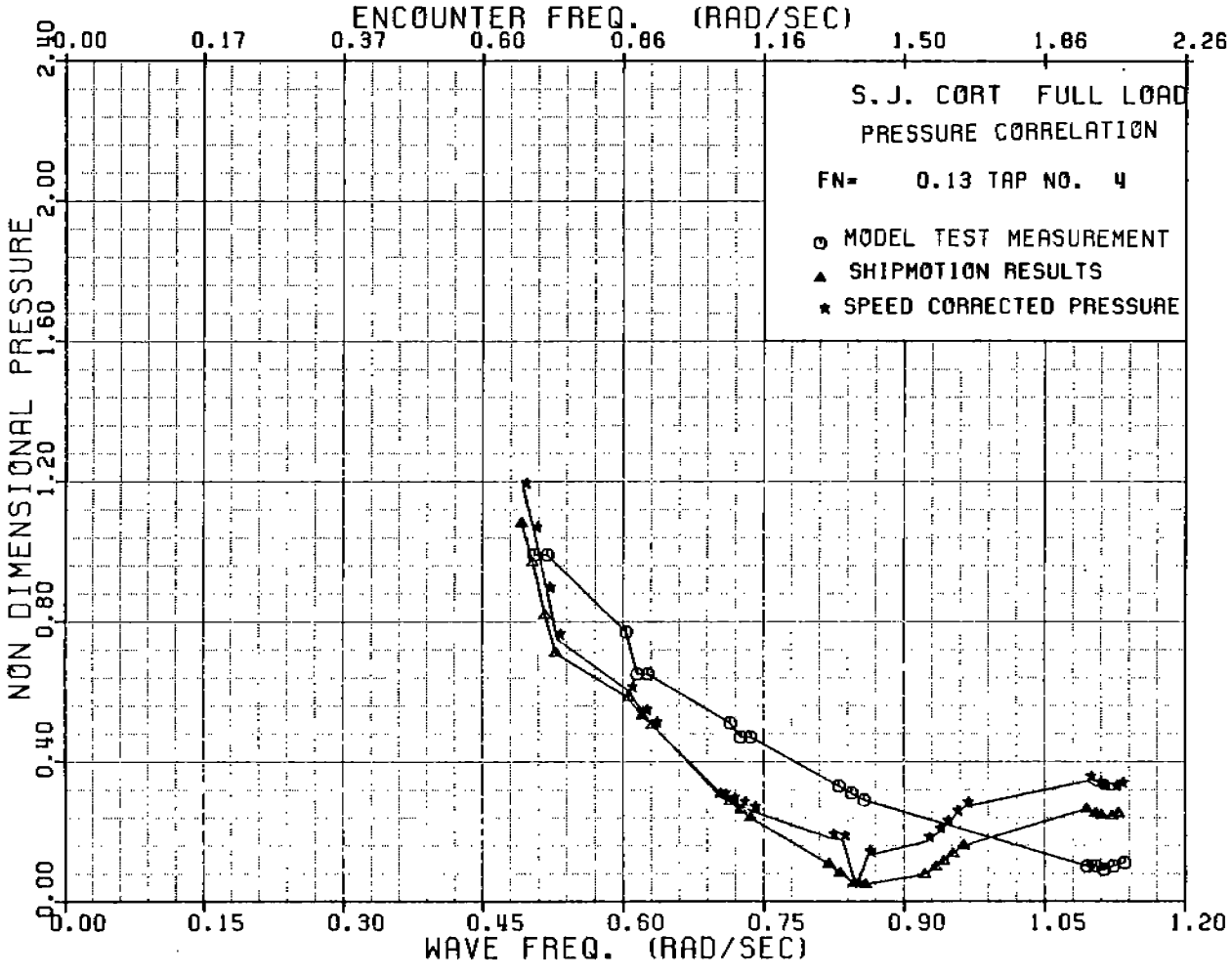

FIGURE B-28 SJ CORT NONDIMENSIONAL PRESSURE , TAP 4 , FN=0.13

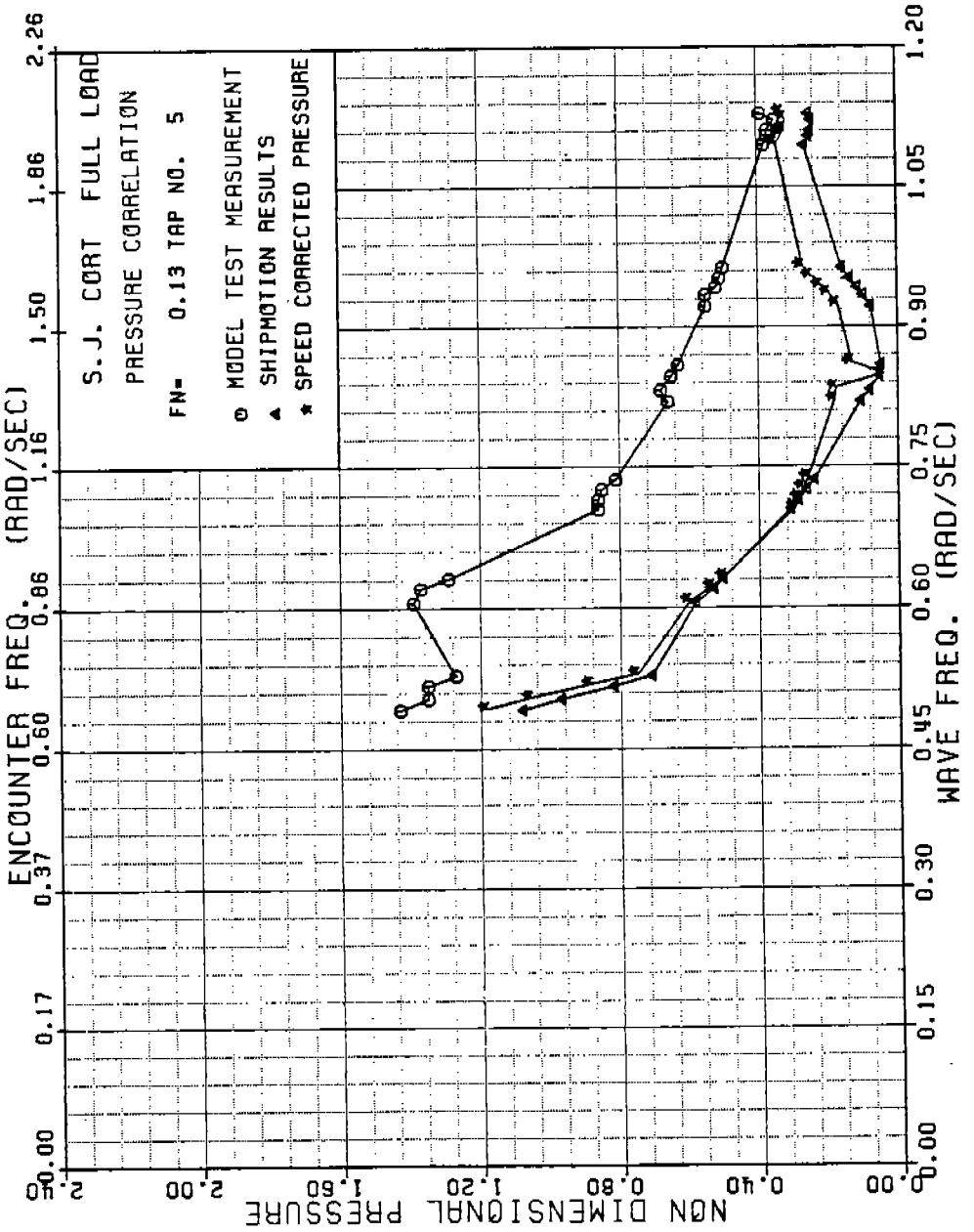

FIGURE B-29 SJ CORT NONDIMENSIONAL PRESSURE , TAP 5 , FN=0.13

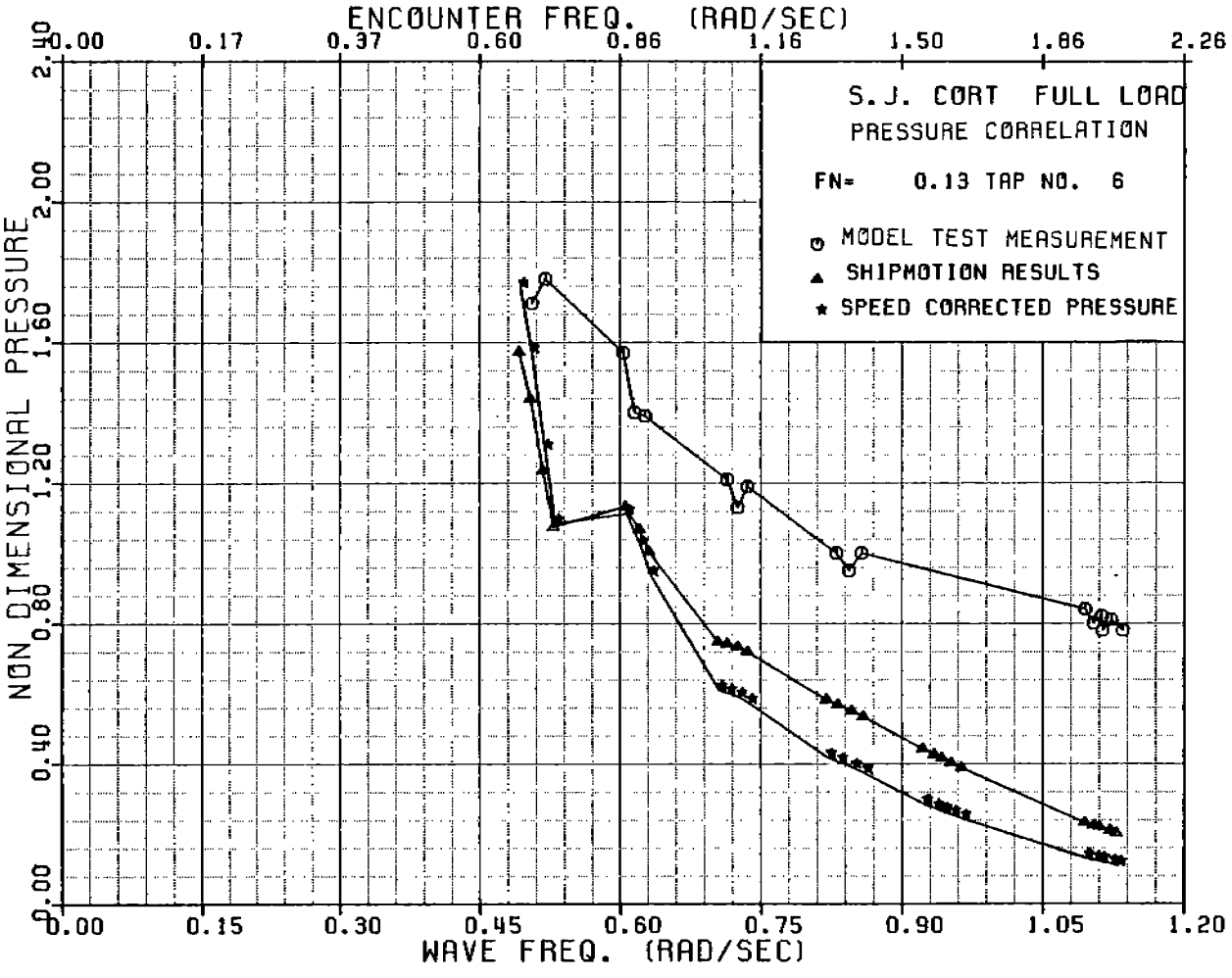

FIGURE B-30 SJ CORT NONDIMENSIONAL PRESSURE , TAP 6 , FN=0.13

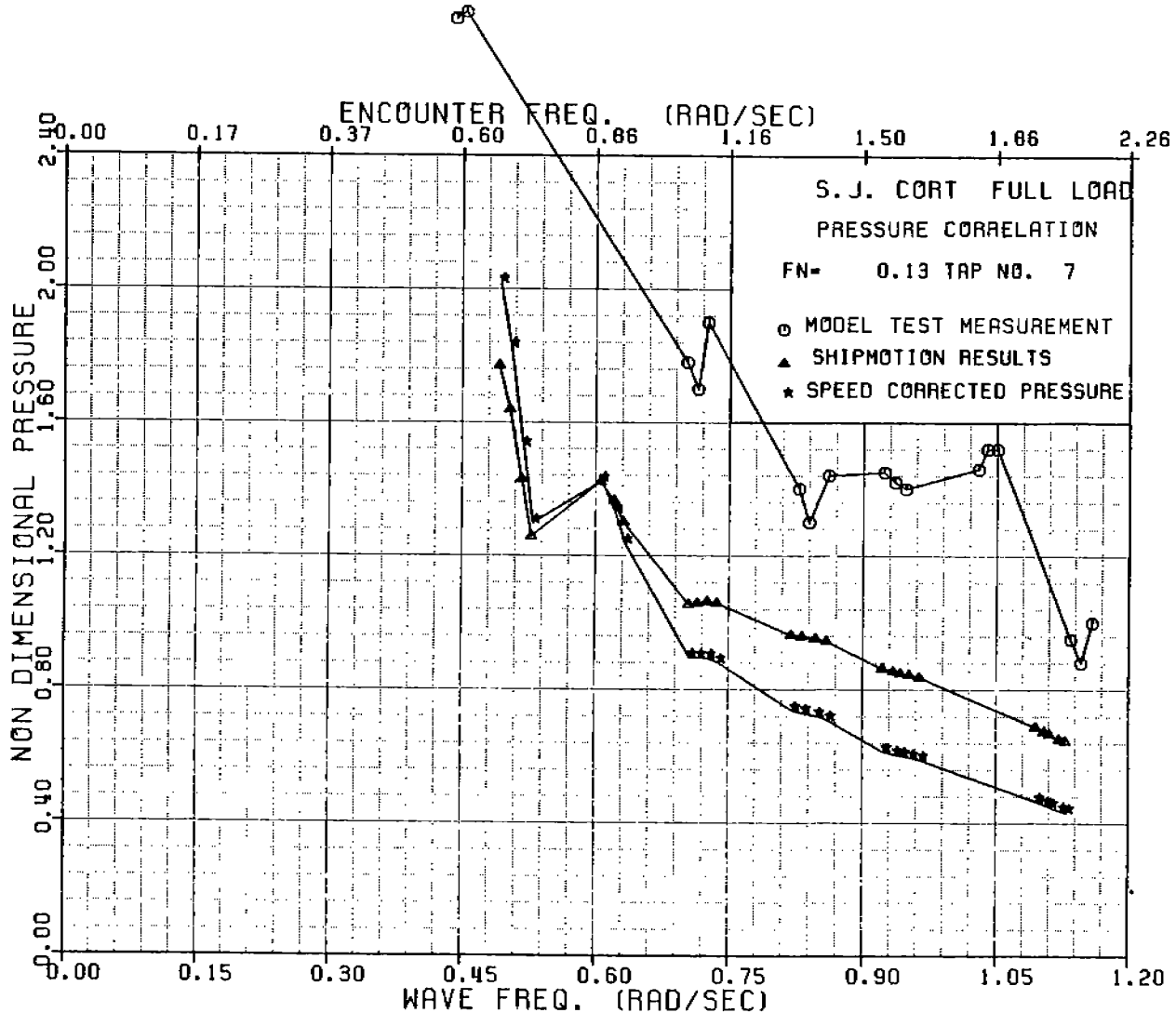

FIGURE B-31 SJ CORT NONDIMENSIONAL PRESSURE , TAP 7 , FN=0.13

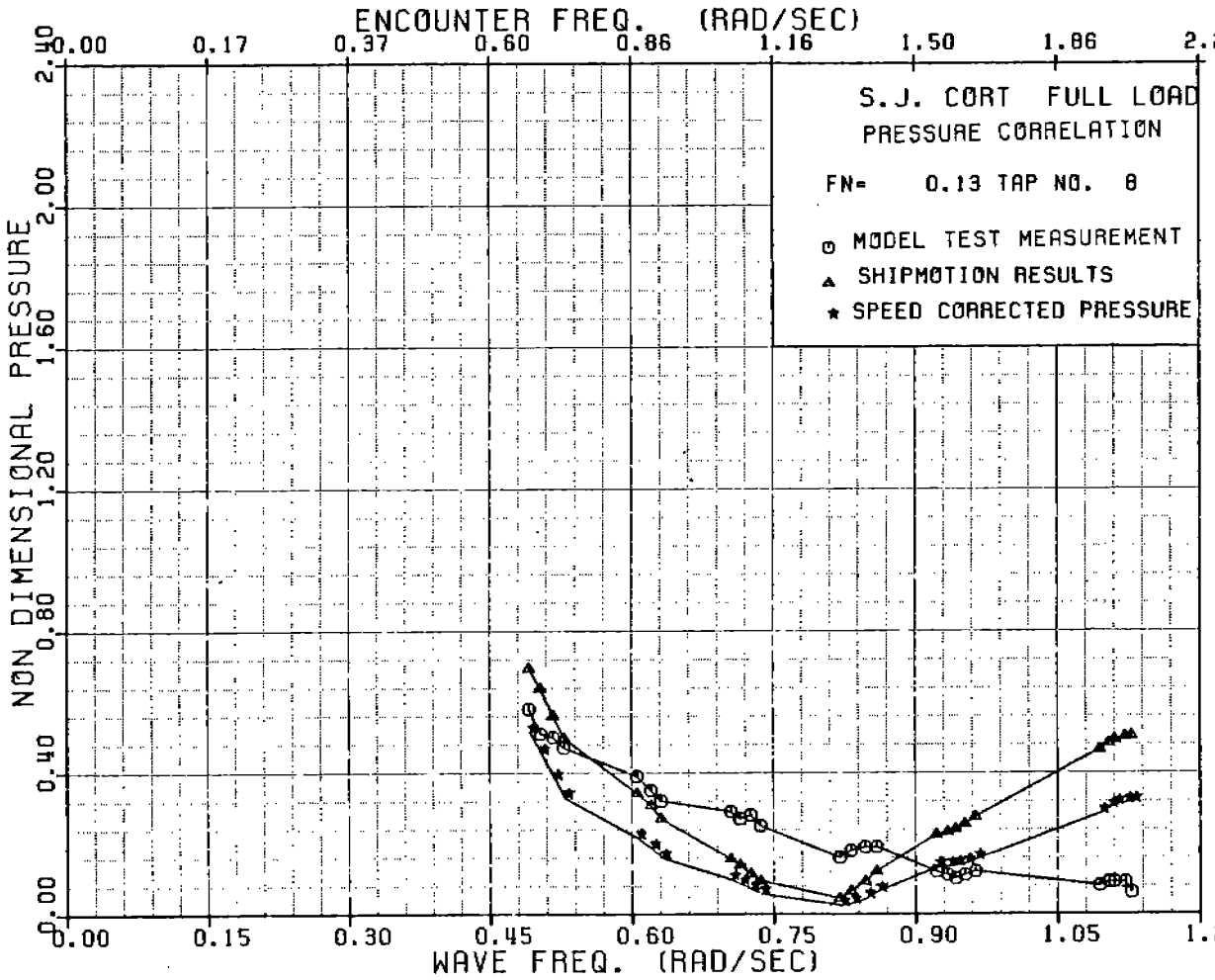

FIGURE B-32 SJ CORT NONDIMENSIONAL PRESSURE , TAP 8 , FN=0.13

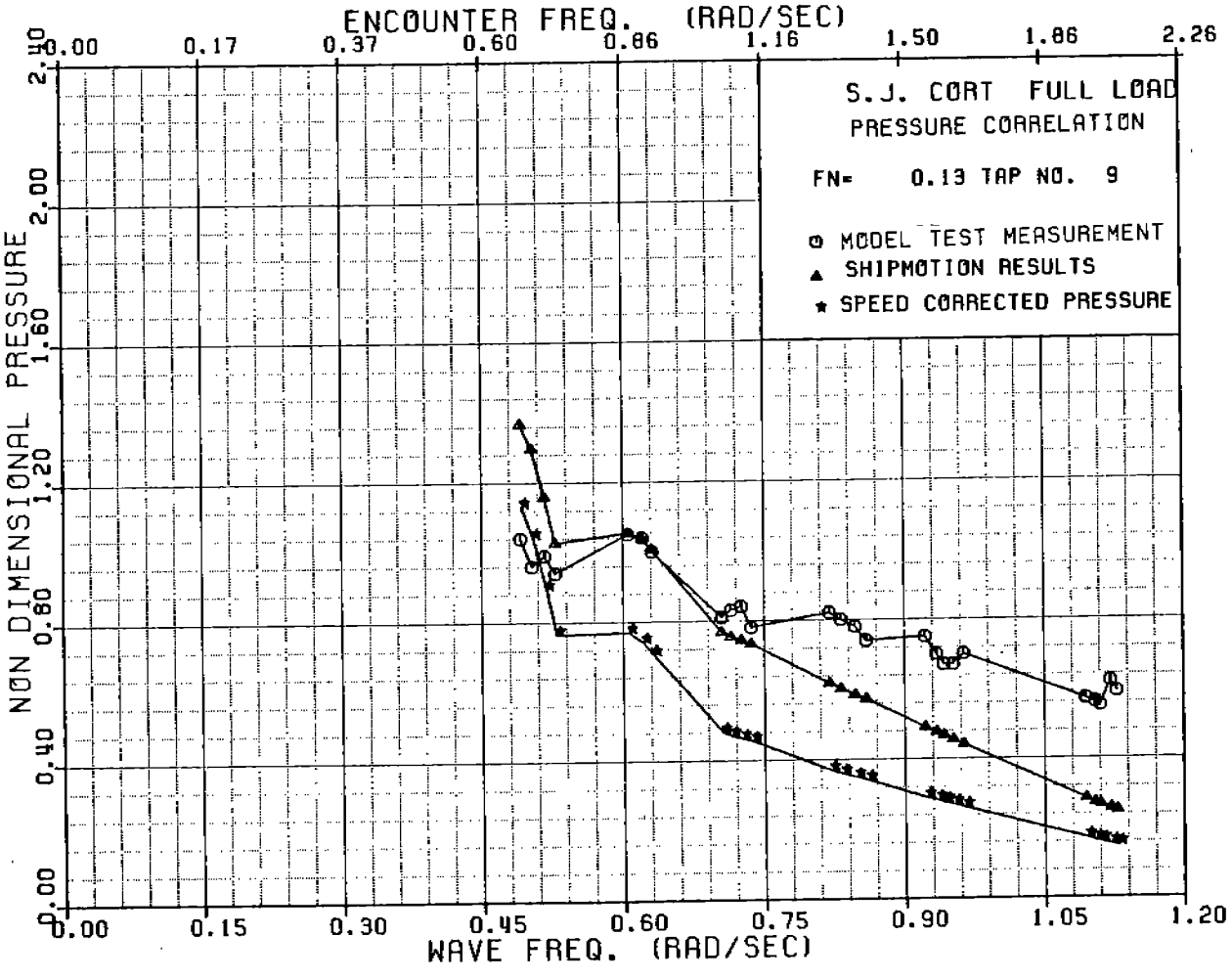

FIGURE B-33 SJ CORT NONDIMENSIONAL PRESSURE , TAP 9 , FN=0.13

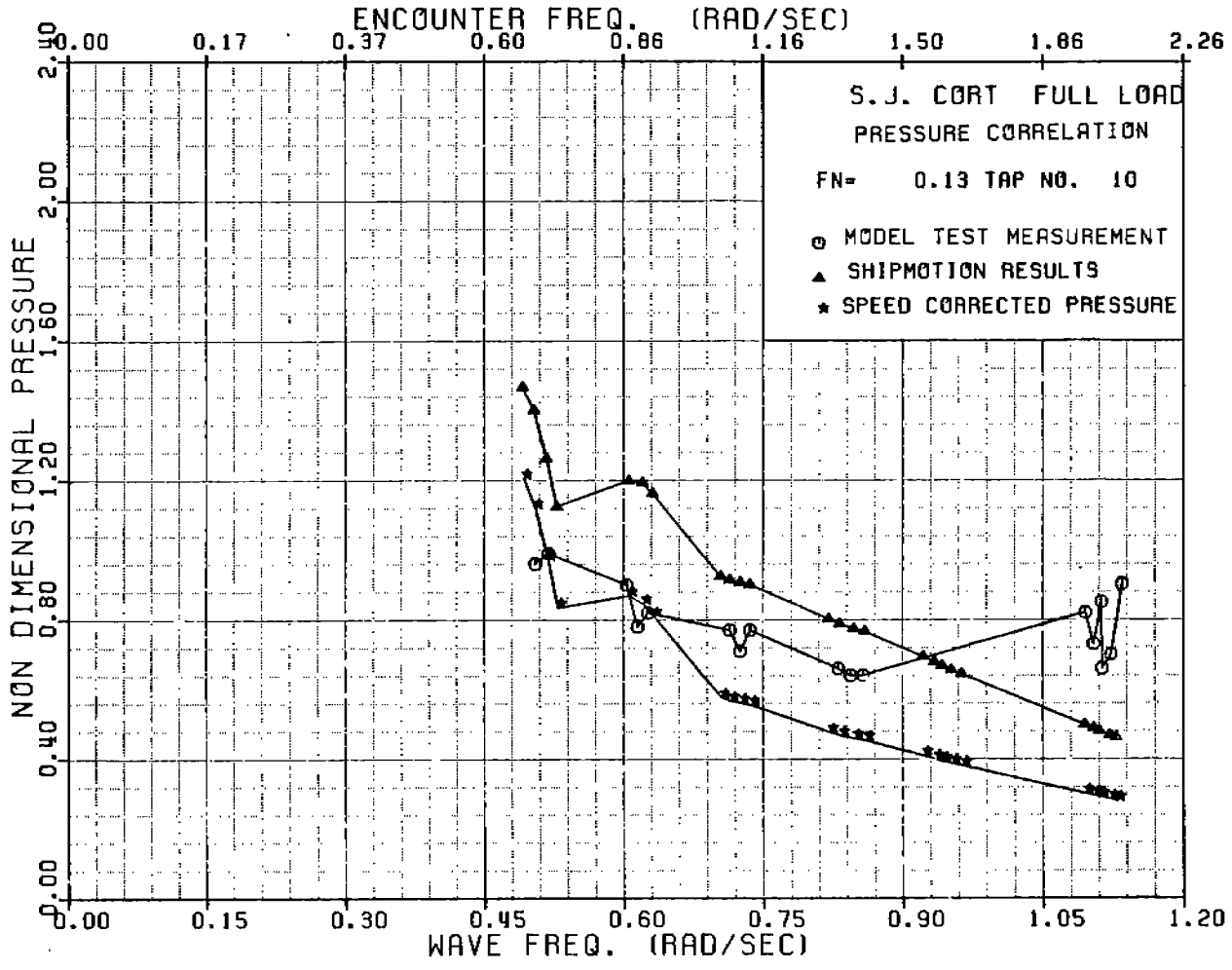

FIGURE B-34 SJ CORT NONDIMENSIONAL PRESSURE , TAP 10, FN=0.13

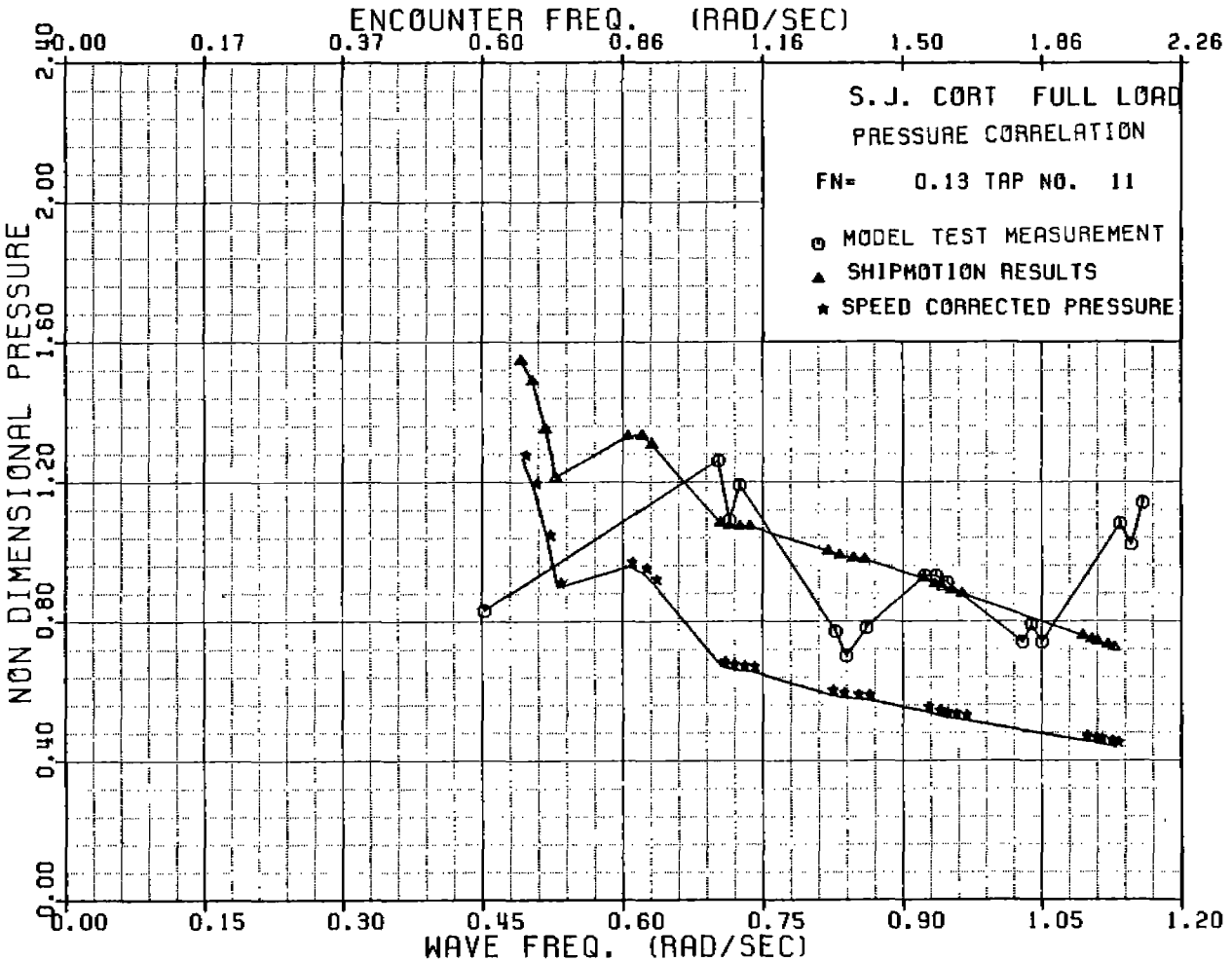

FIGURE B-35 SJ CORT NONDIMENSIONAL PRESSURE , TAP 11, FN=0.13

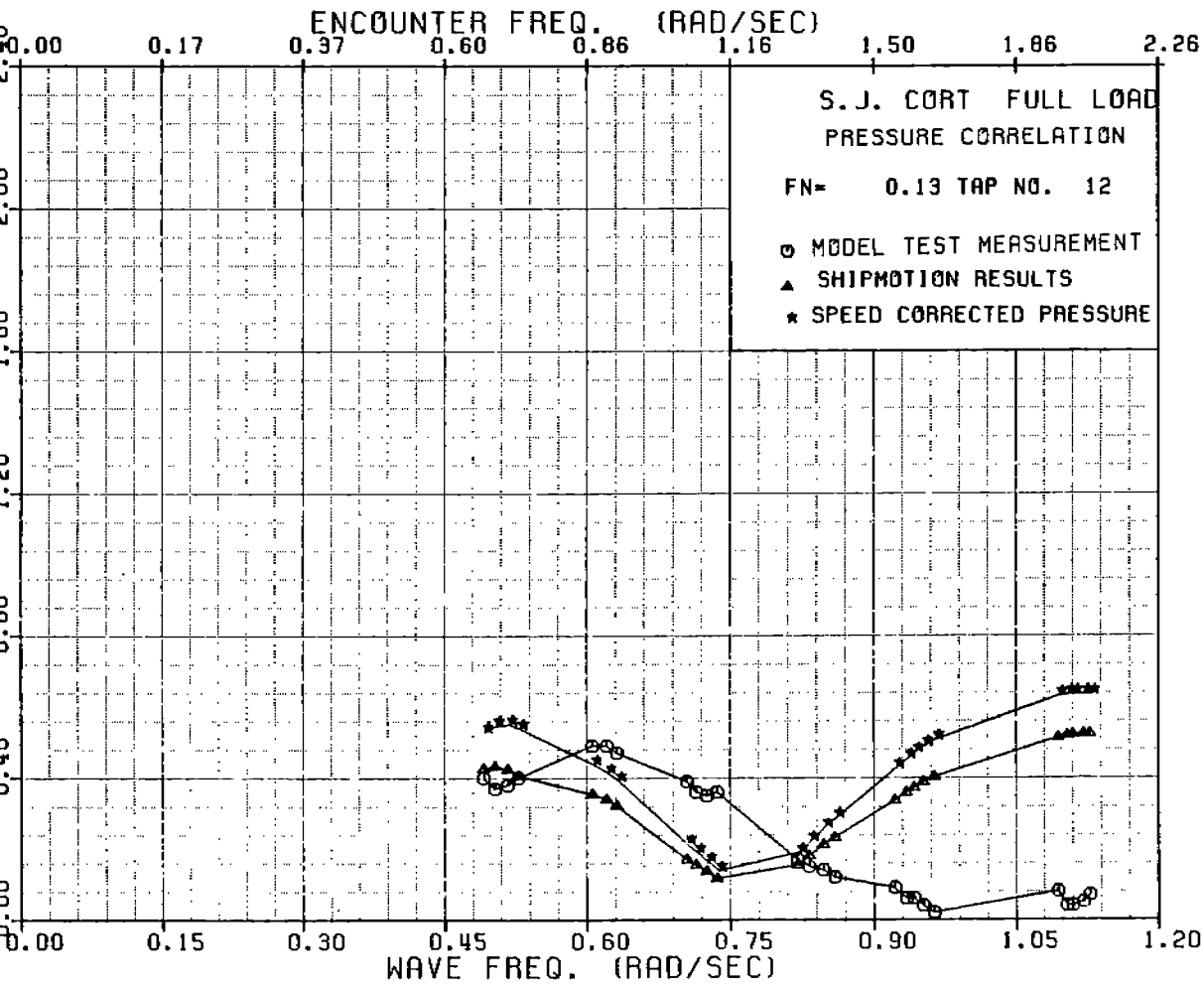

FIGURE B-36 SJ CORT NONDIMENSIONAL PRESSURE , TAP 12, FN=0.13

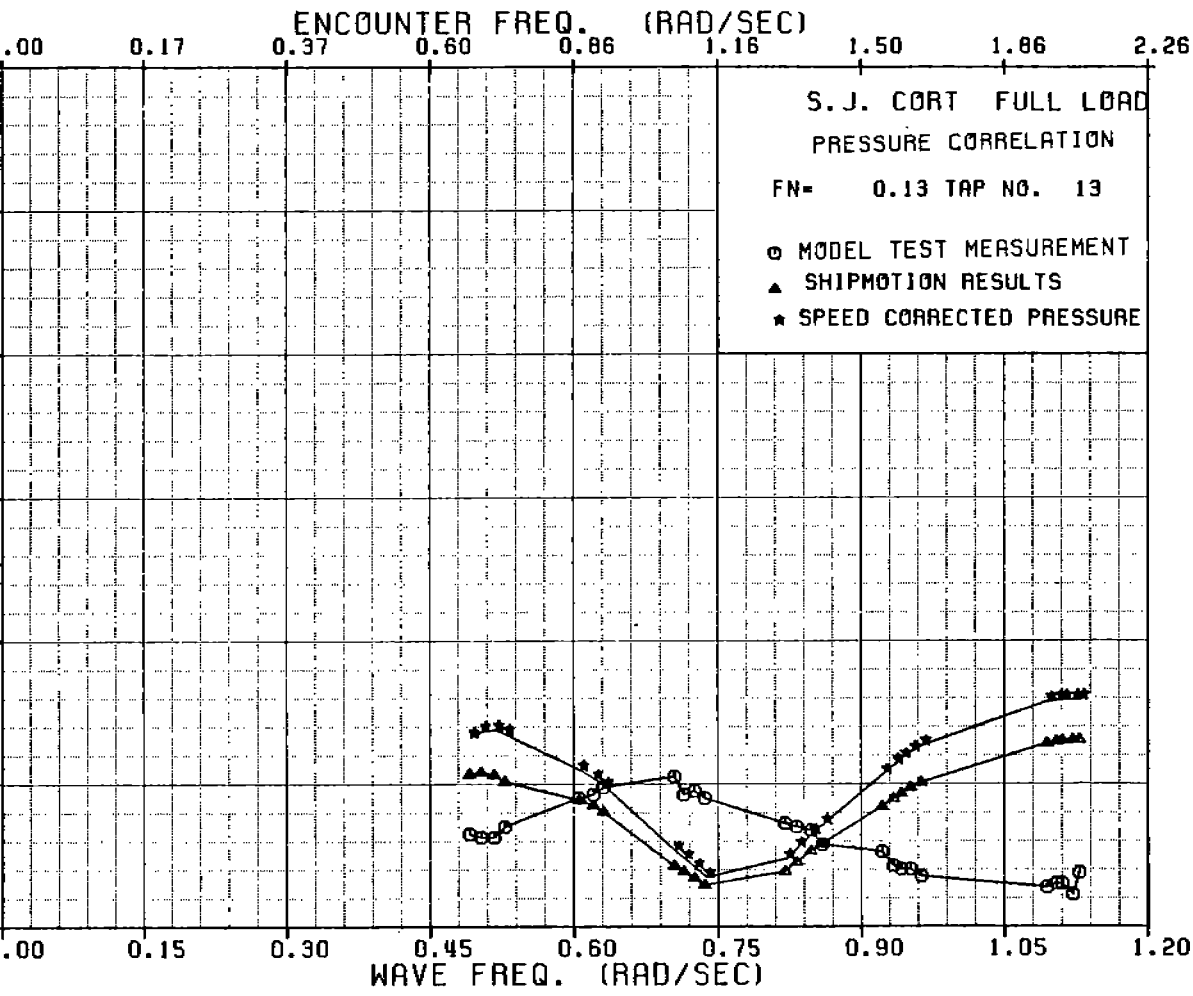

FIGURE B-37 SJ CORT NONDIMENSIONAL PRESSURE , TAP 13, FN=0.13

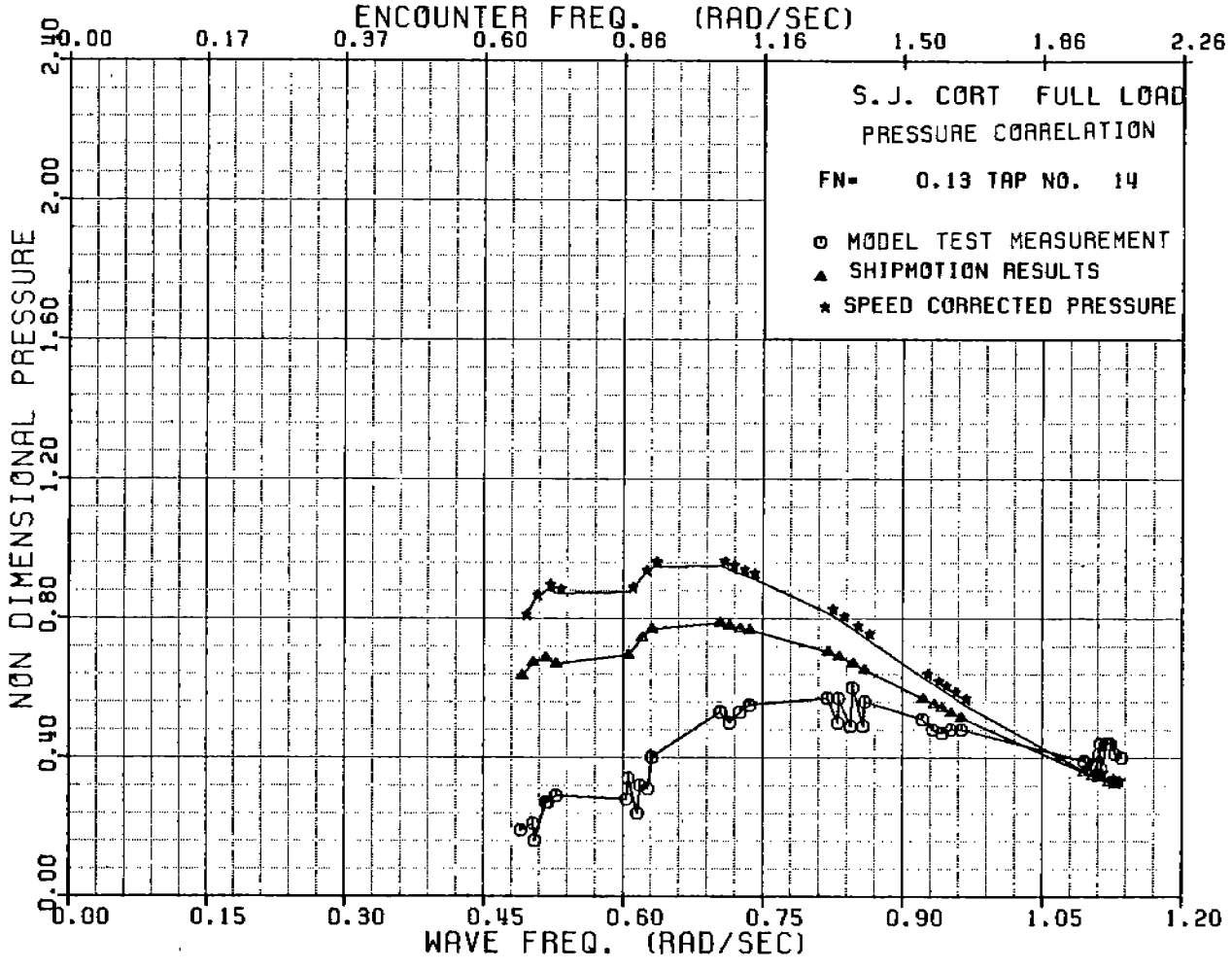

FIGURE B-38 SJ CORT NONDIMENSIONAL PRESSURE , TAP 14, FN=0.13

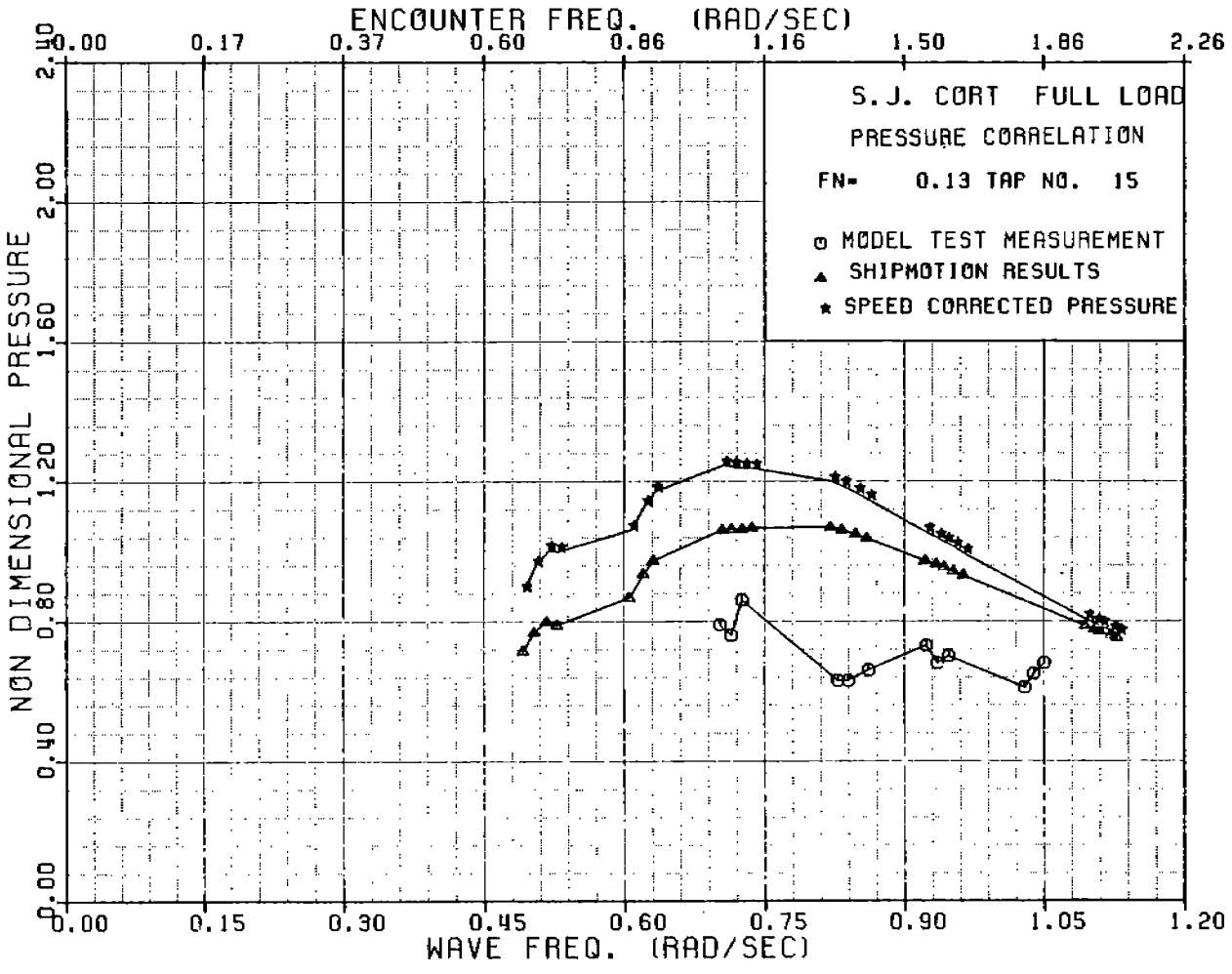

FIGURE B-39 SJ CORT NONDIMENSIONAL PRESSURE , TAP 15, FN=0.13

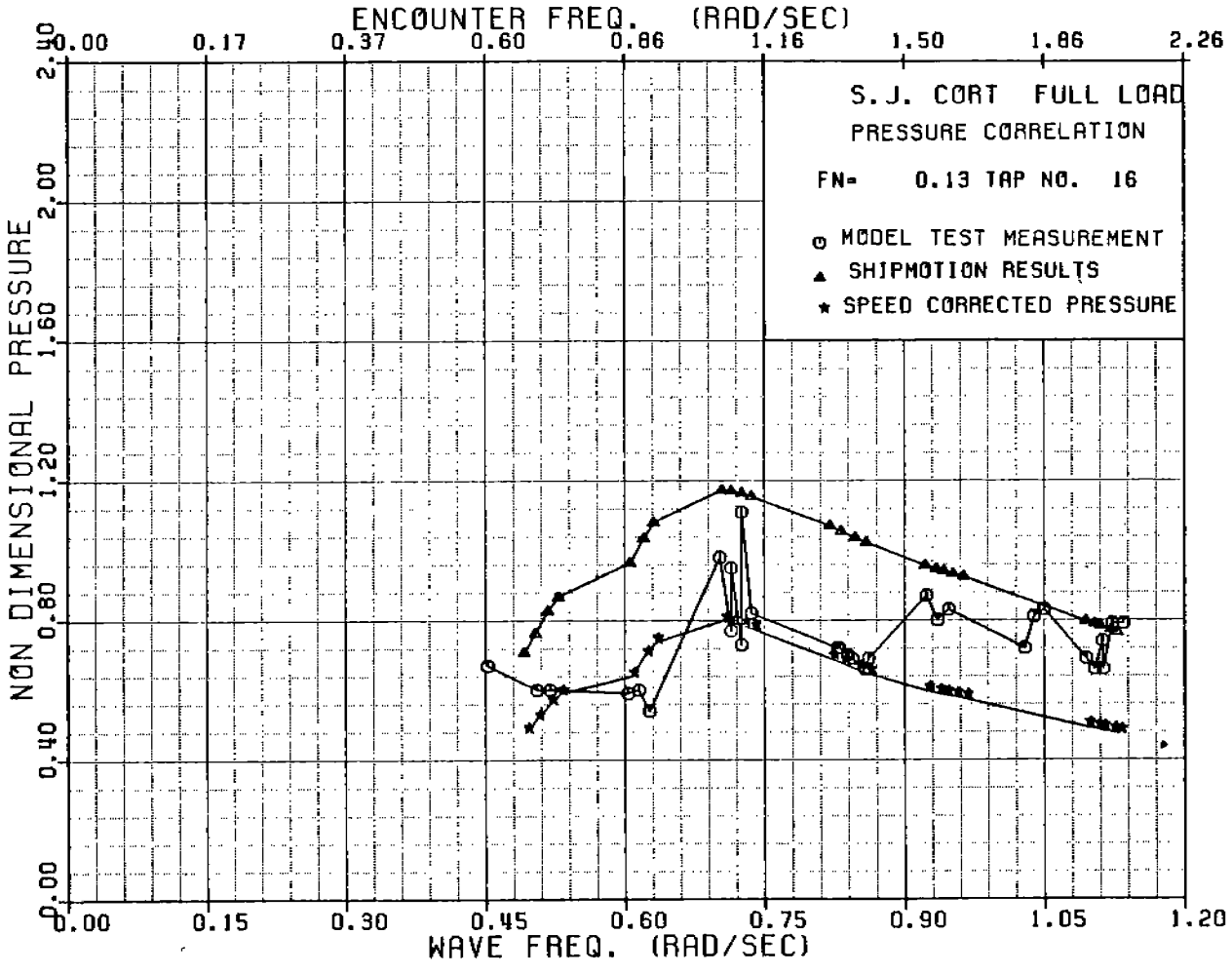

FIGURE B-40 SJ CORT NONDIMENSIONAL PRESSURE , TAP 16, FN=0.13

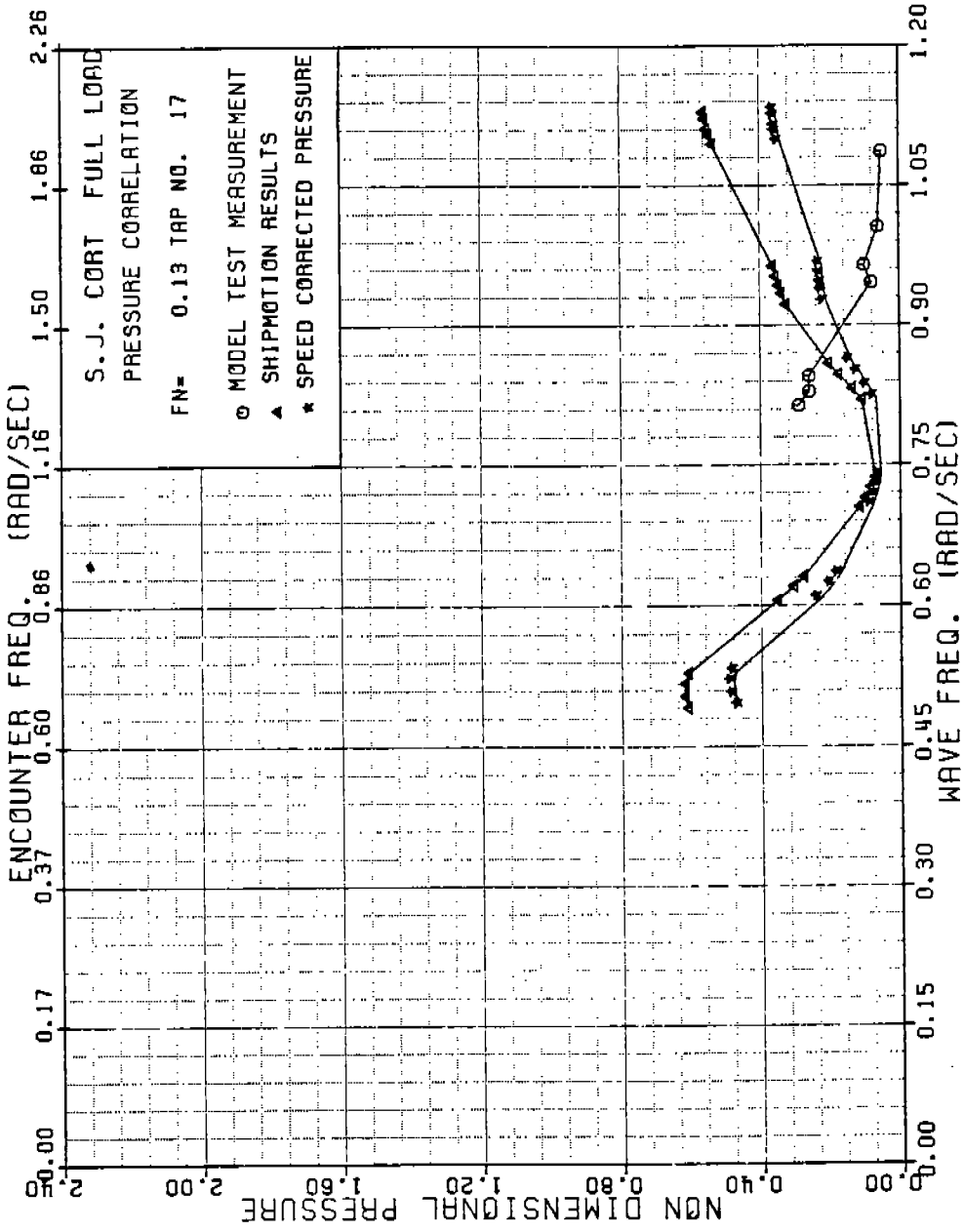

FIGURE B-41 SJ CORT NONDIMENSIONAL PRESSURE , TAP 17, FN=0.13

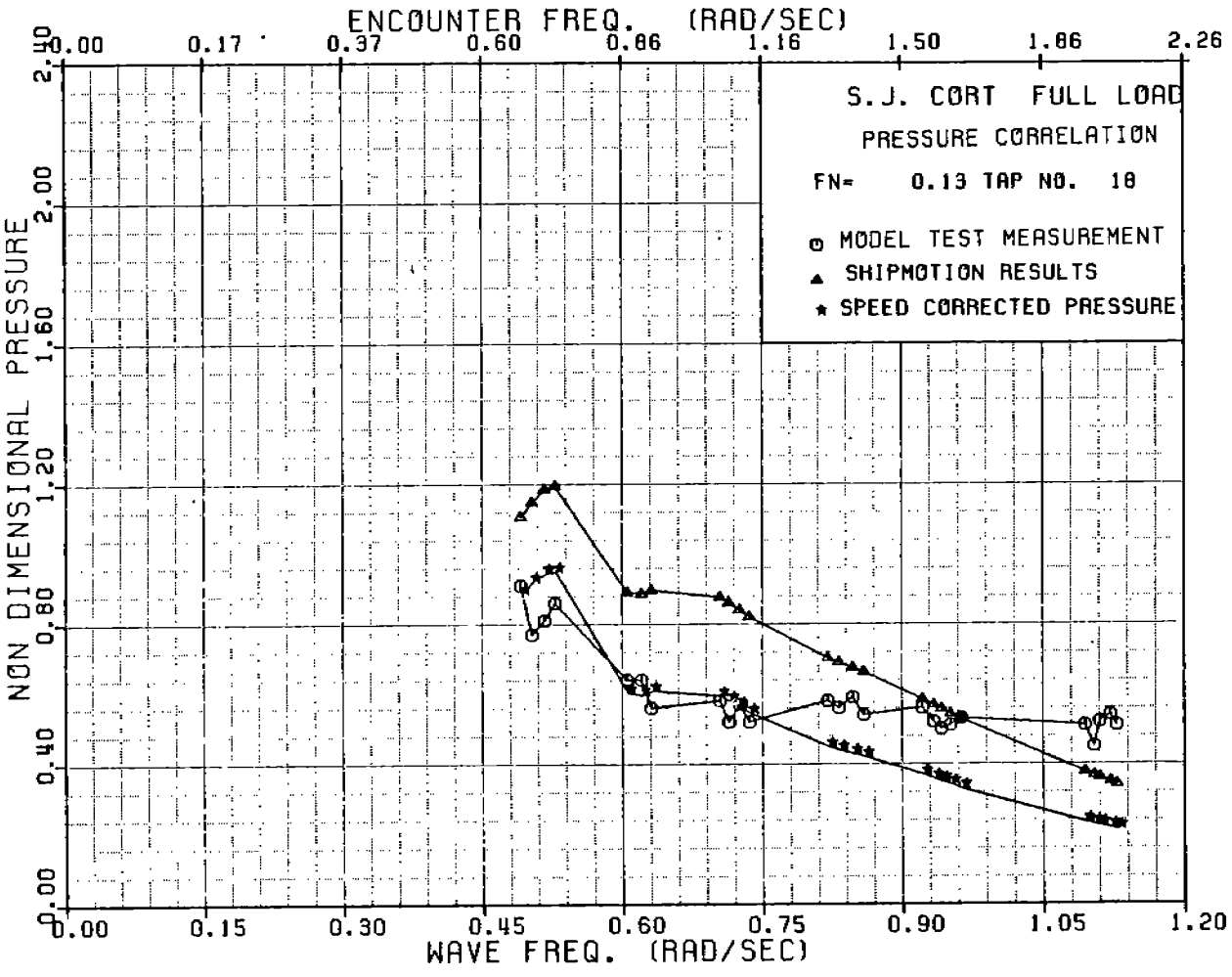

FIGURE B-42 SJ CORT NONDIMENSIONAL PRESSURE , TAP 18, FN=0.13

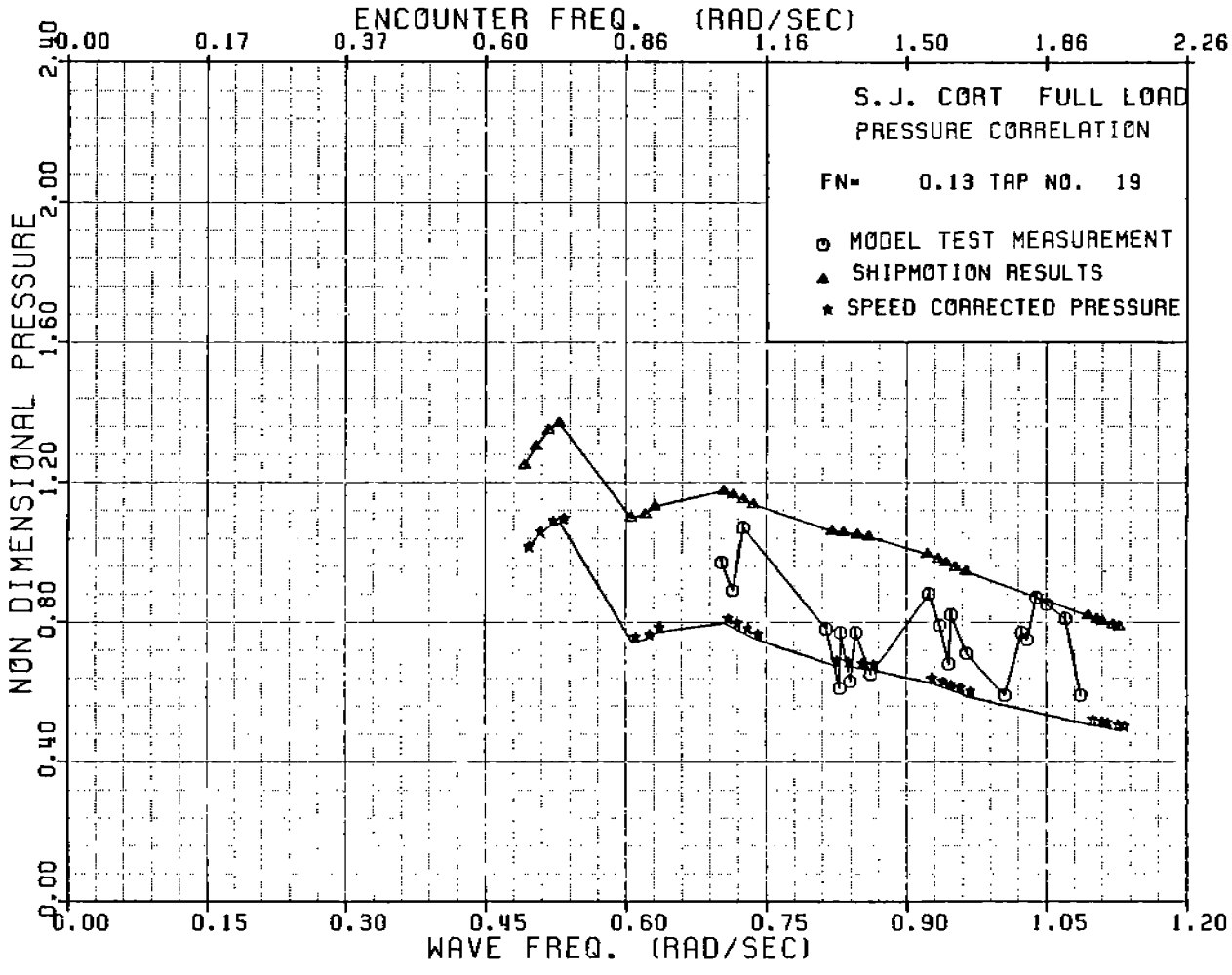

FIGURE B-43 SJ CORT NONDIMENSIONAL PRESSURE , TAP 19, FN=0.13

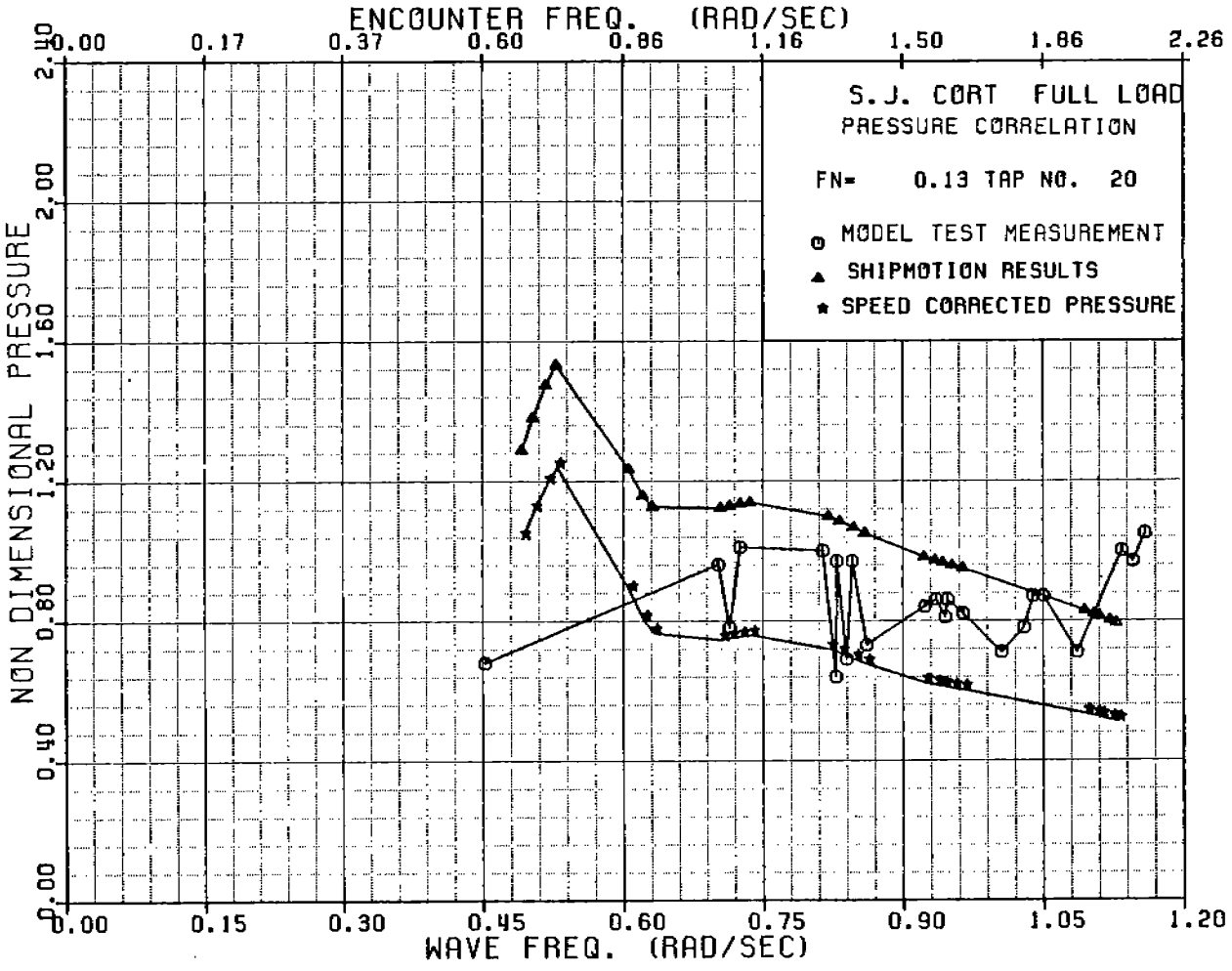

FIGURE B-44 SJ CORT NONDIMENSIONAL PRESSURE , TAP 20, FN=0.13

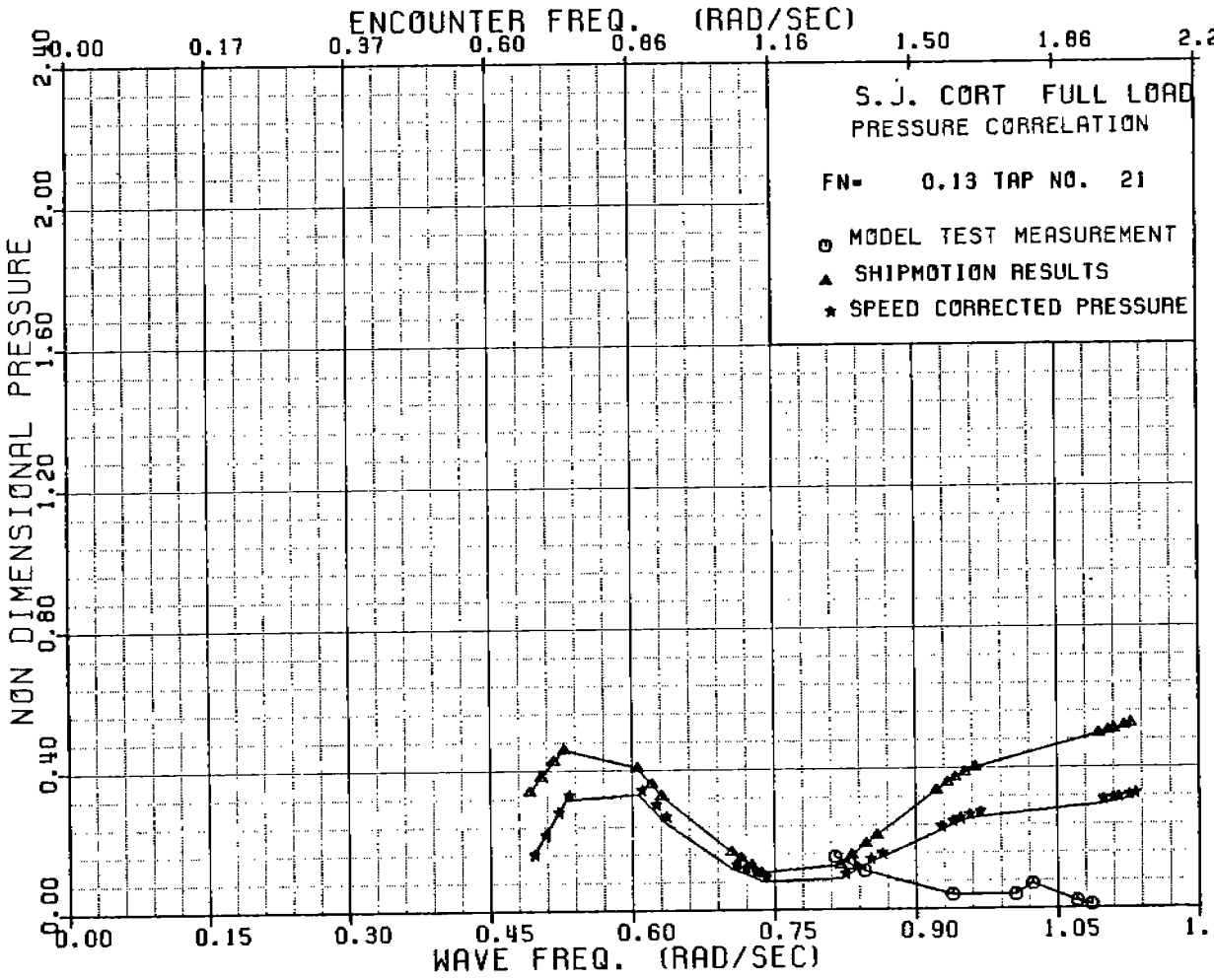

FIGURE B-45 SJ CORT NONDIMENSIONAL PRESSURE , TAP 21, FN=0.13

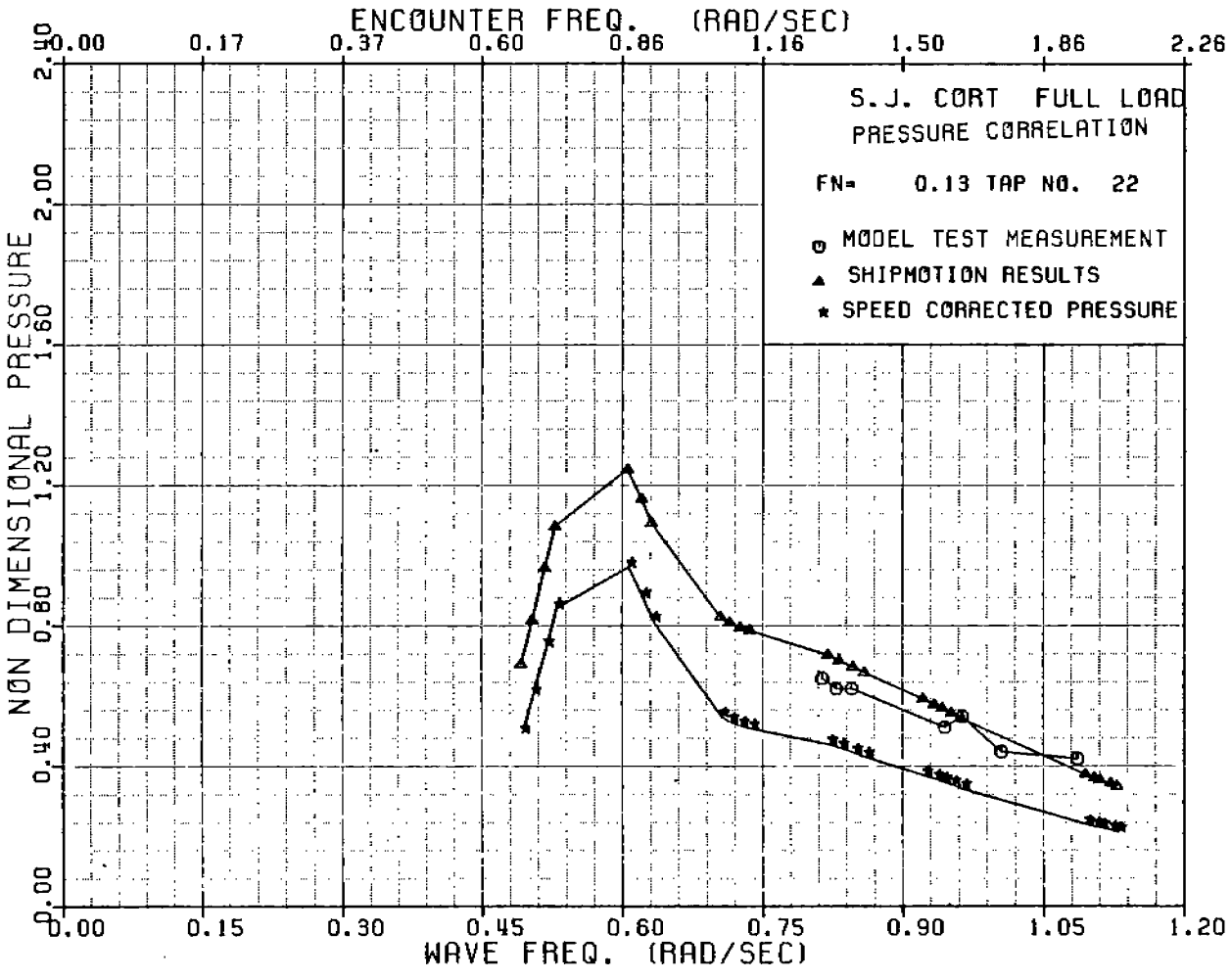

FIGURE B-46 SJ CORT NONDIMENSIONAL PRESSURE , TAP 22, FN=0.13

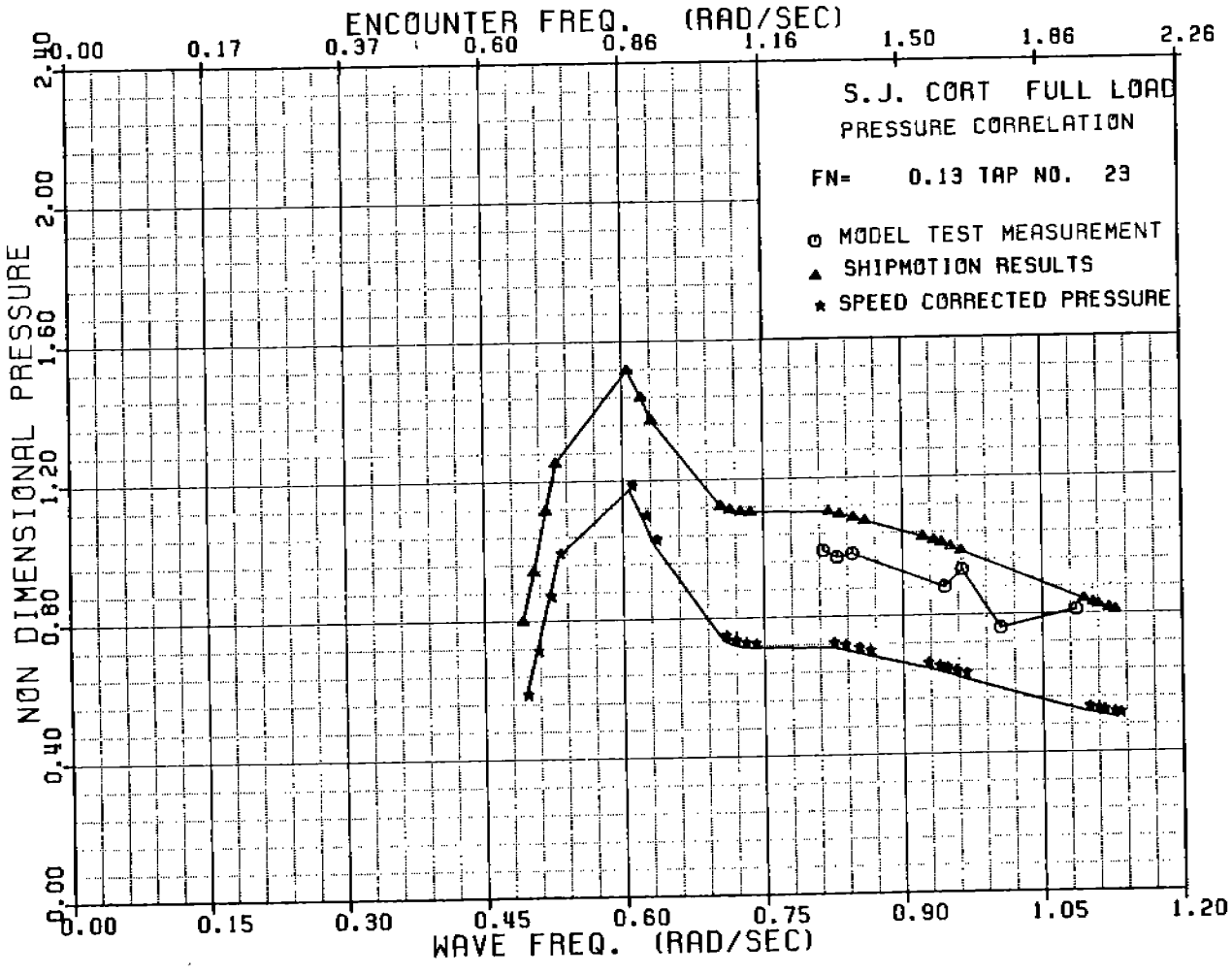

FIGURE B-47 SJ CORT NONDIMENSIONAL PRESSURE , TAP 23, FN=0.13

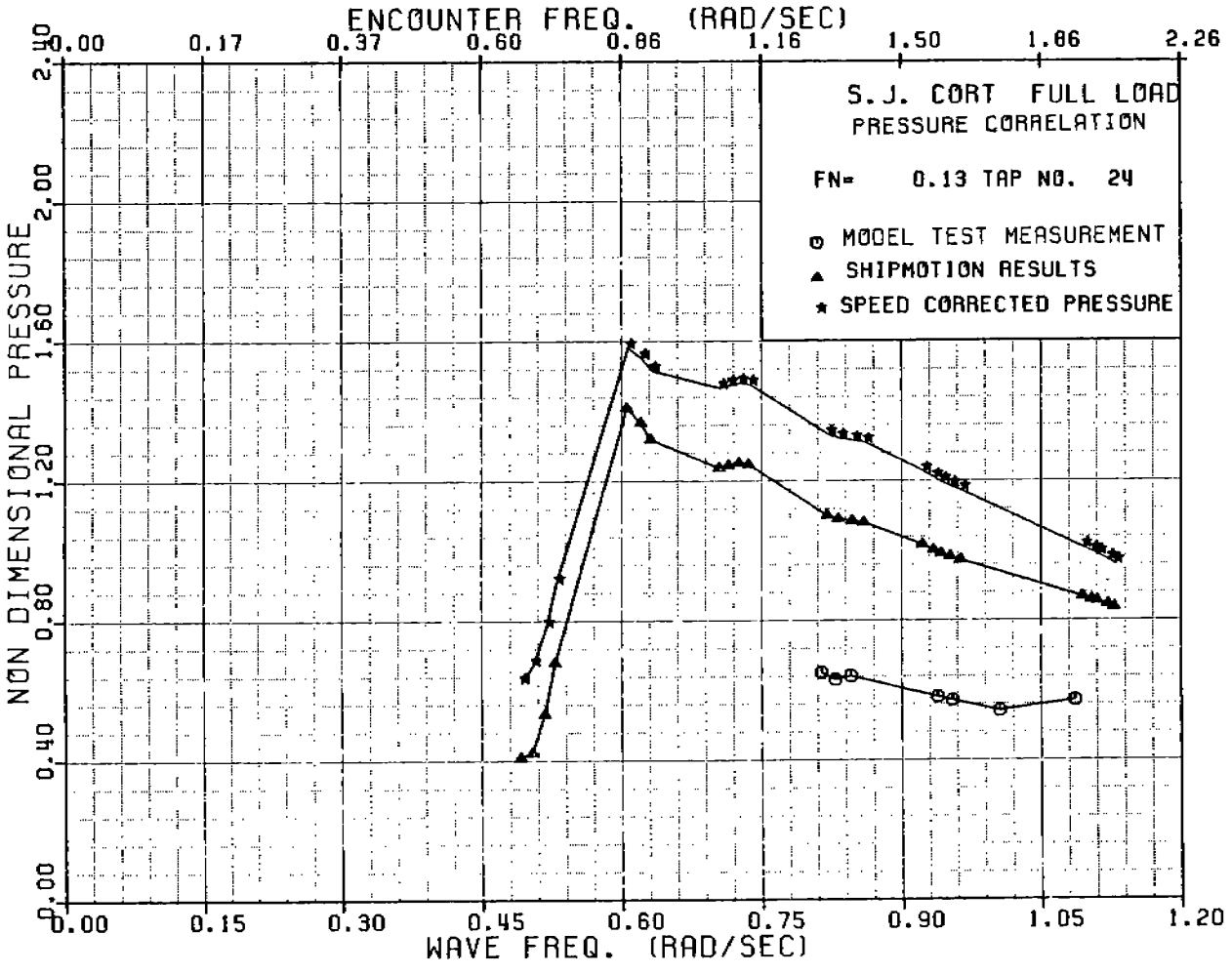

FIGURE B-48 SJ CORT NONDIMENSIONAL PRESSURE , TAP 24, FN=0.13

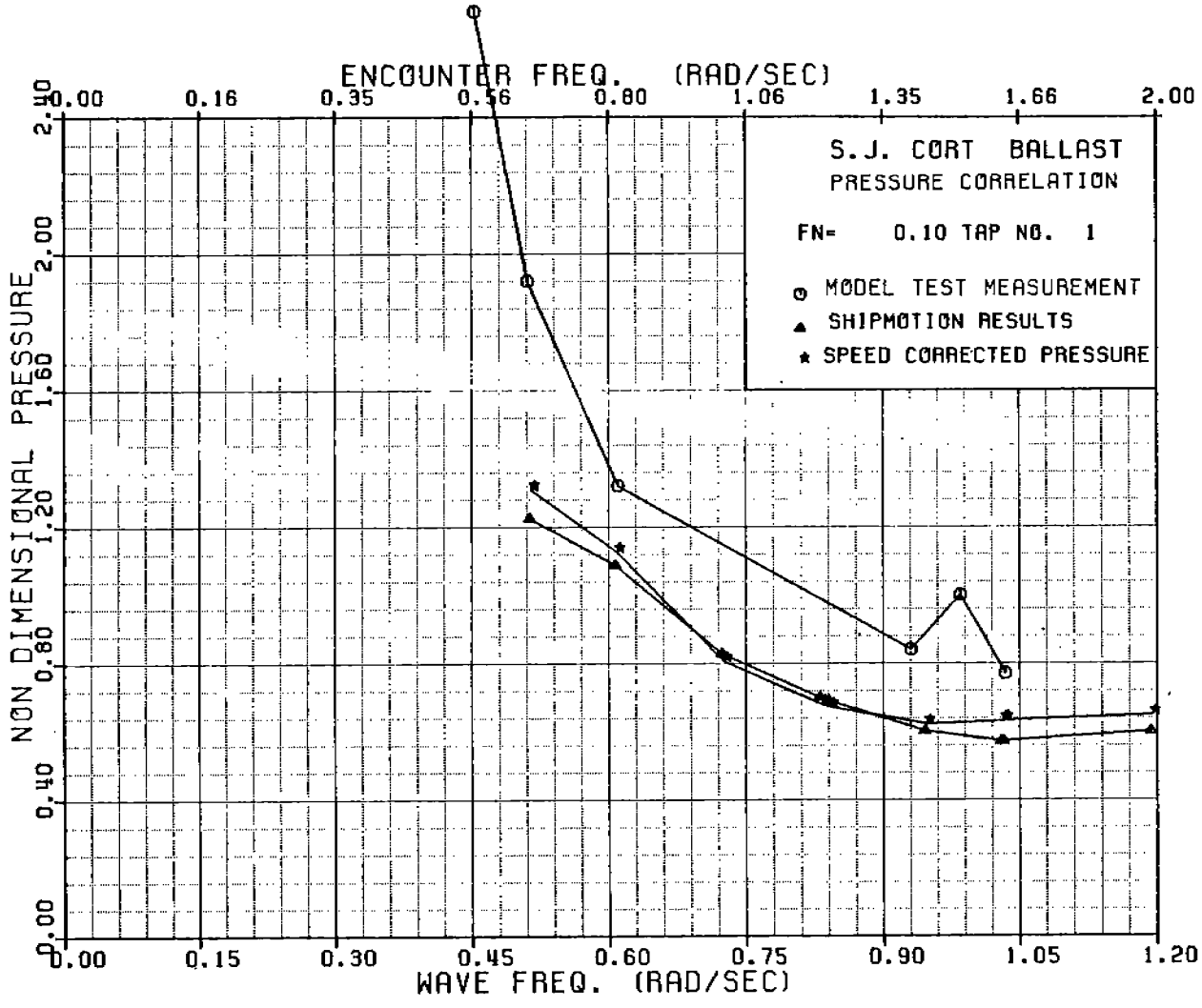

FIGURE B-49 SJ CORT NONDIMENSIONAL PRESSURE , TAP 1 , FN=0.10

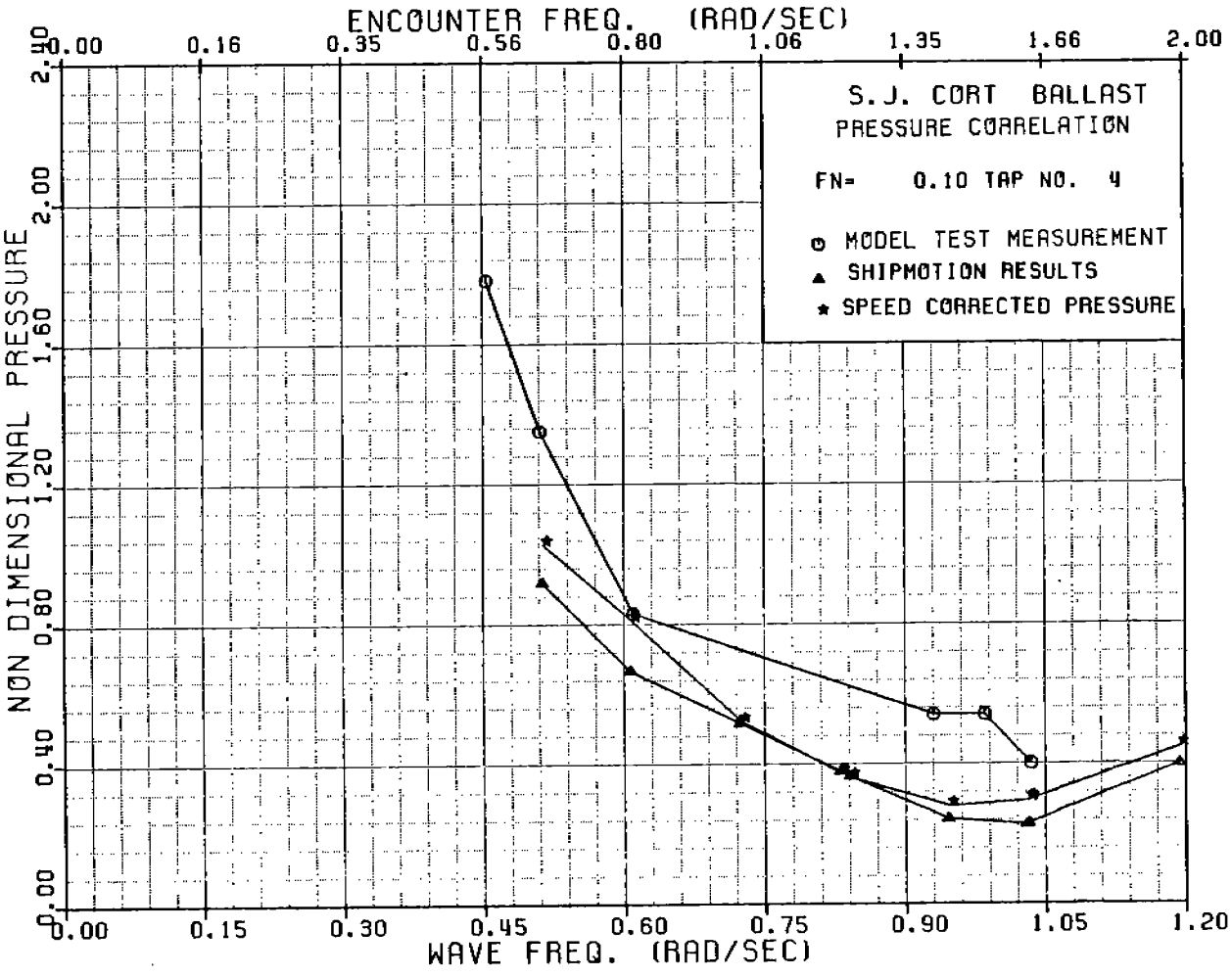

FIGURE B-50 SJ CORT NONDIMENSIONAL PRESSURE , TAP 4 , FN=0.10

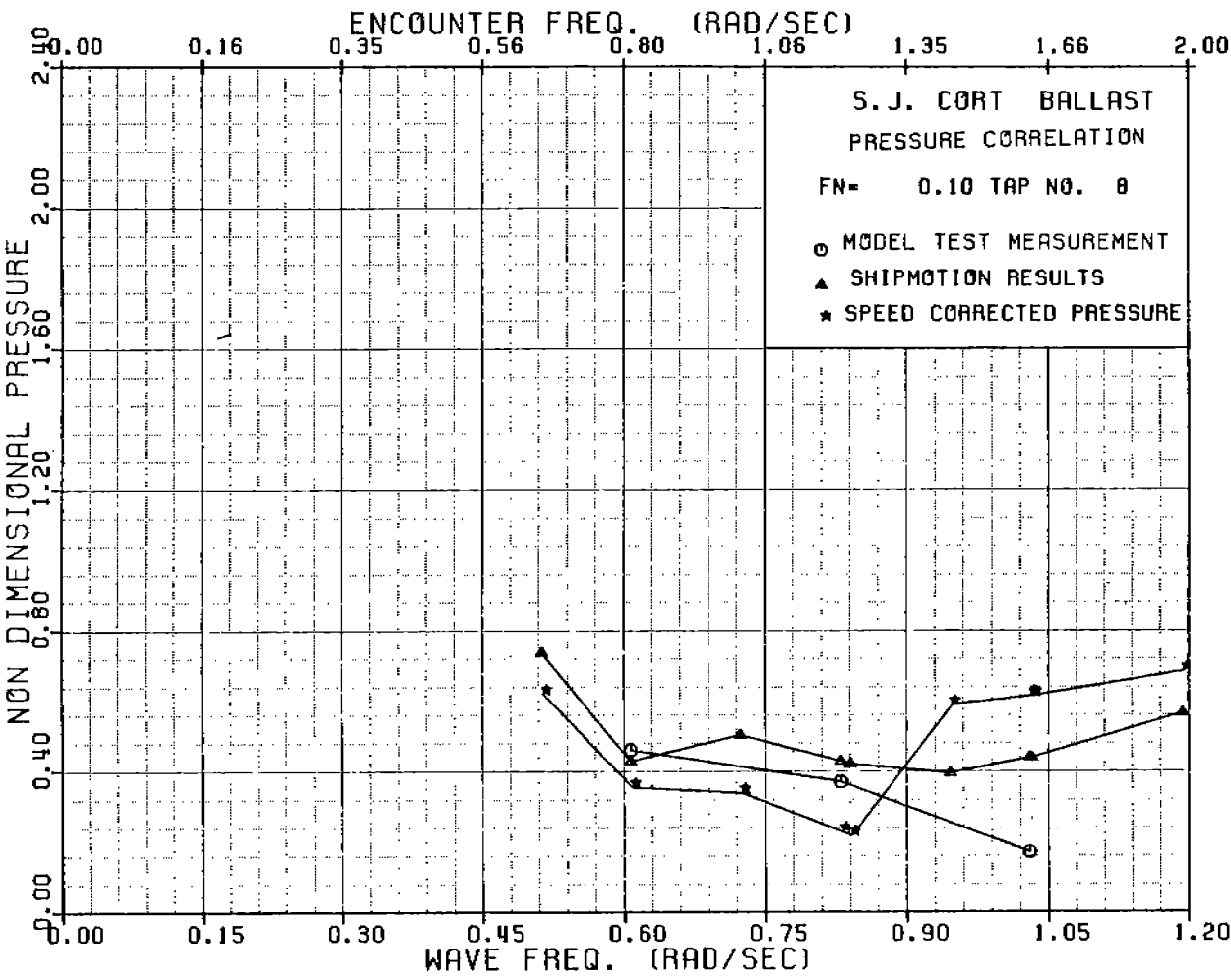

FIGURE B-51 SJ CORT NONDIMENSIONAL PRESSURE , TAP 8 , FN=0.10

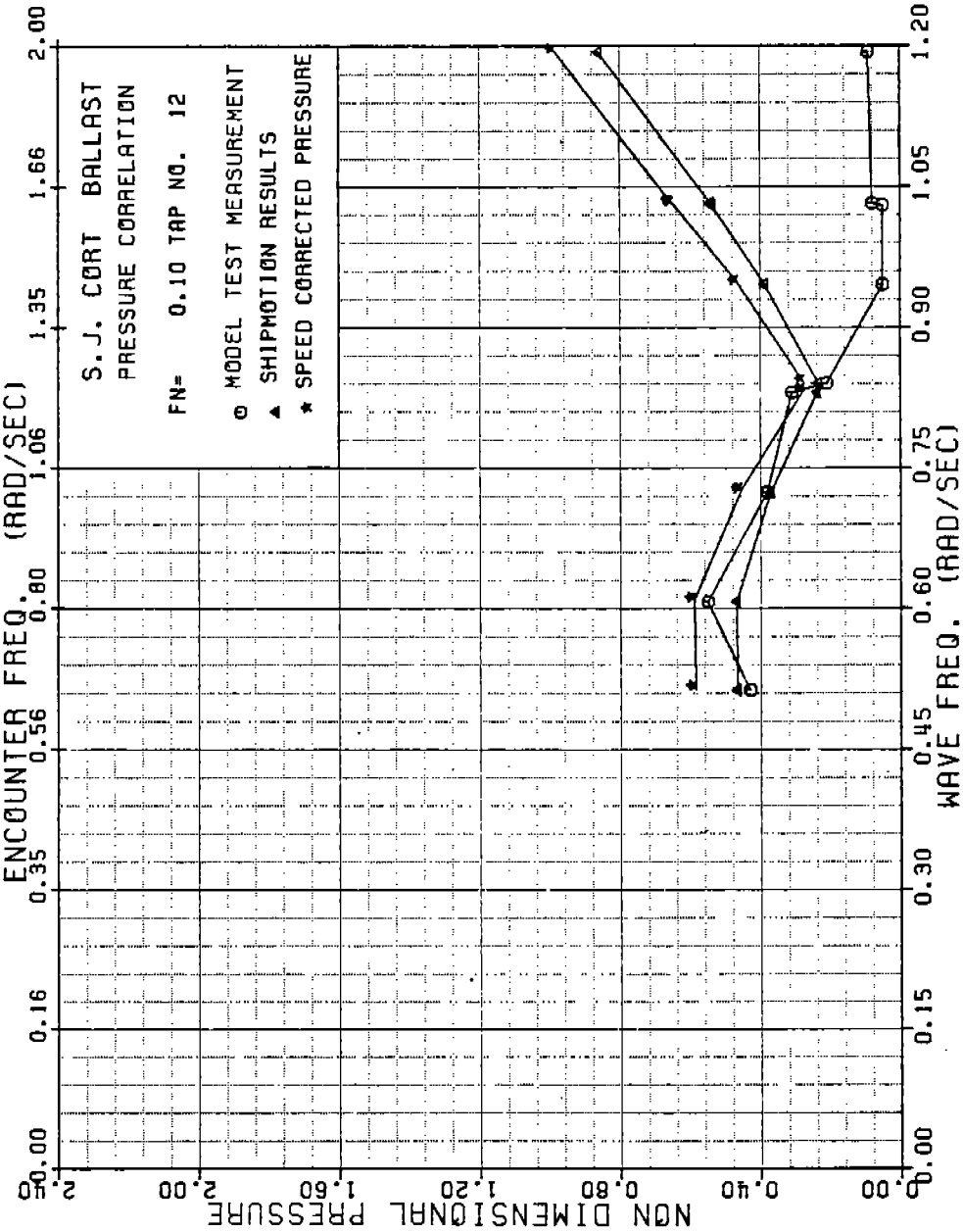

FIGURE B-52 SJ CORT NONDIMENSIONAL PRESSURE , TAP 12, FN=0.10

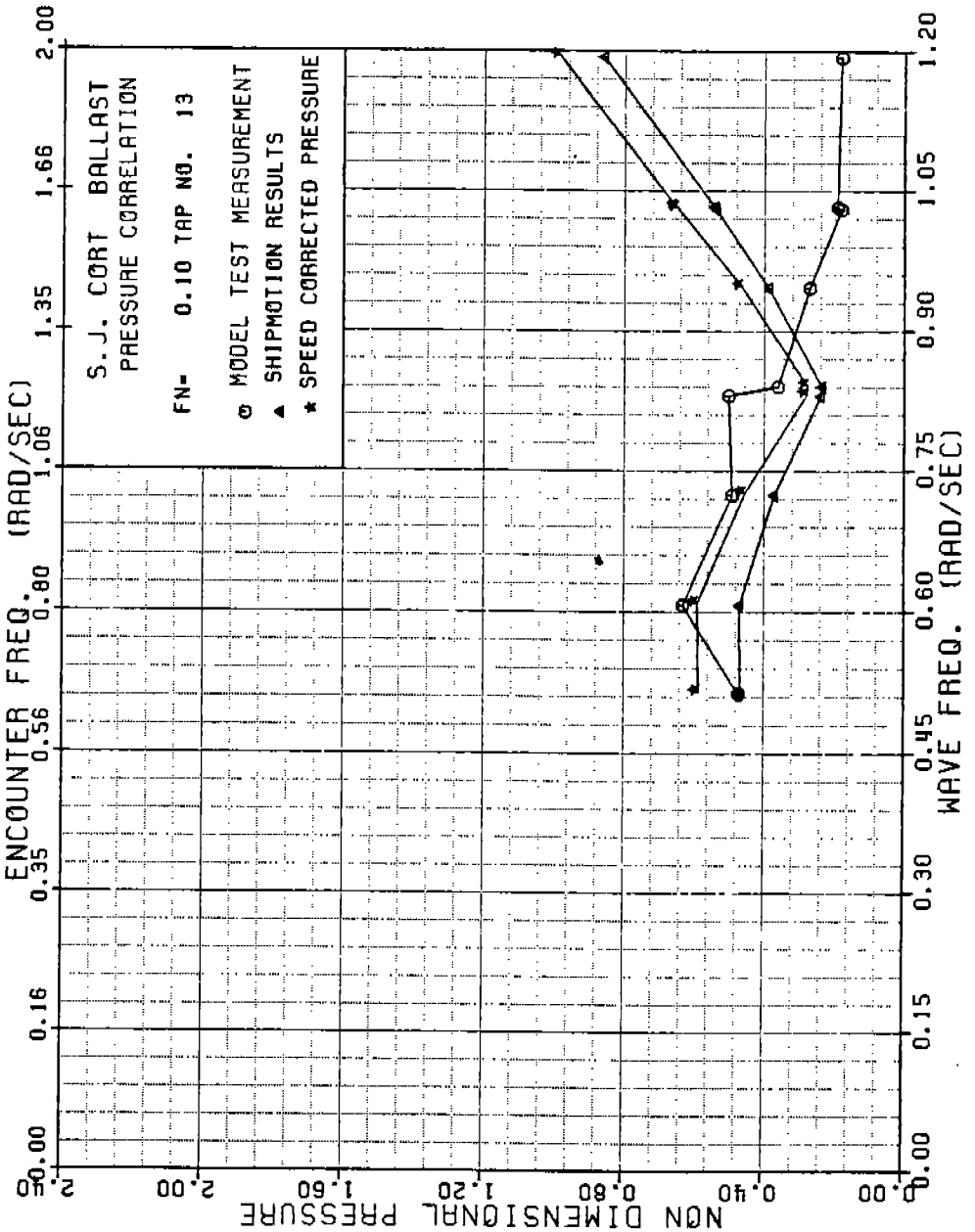

FIGURE B-53 SJ CORT NONDIMENSIONAL PRESSURE , TAP 13, FN=0.10

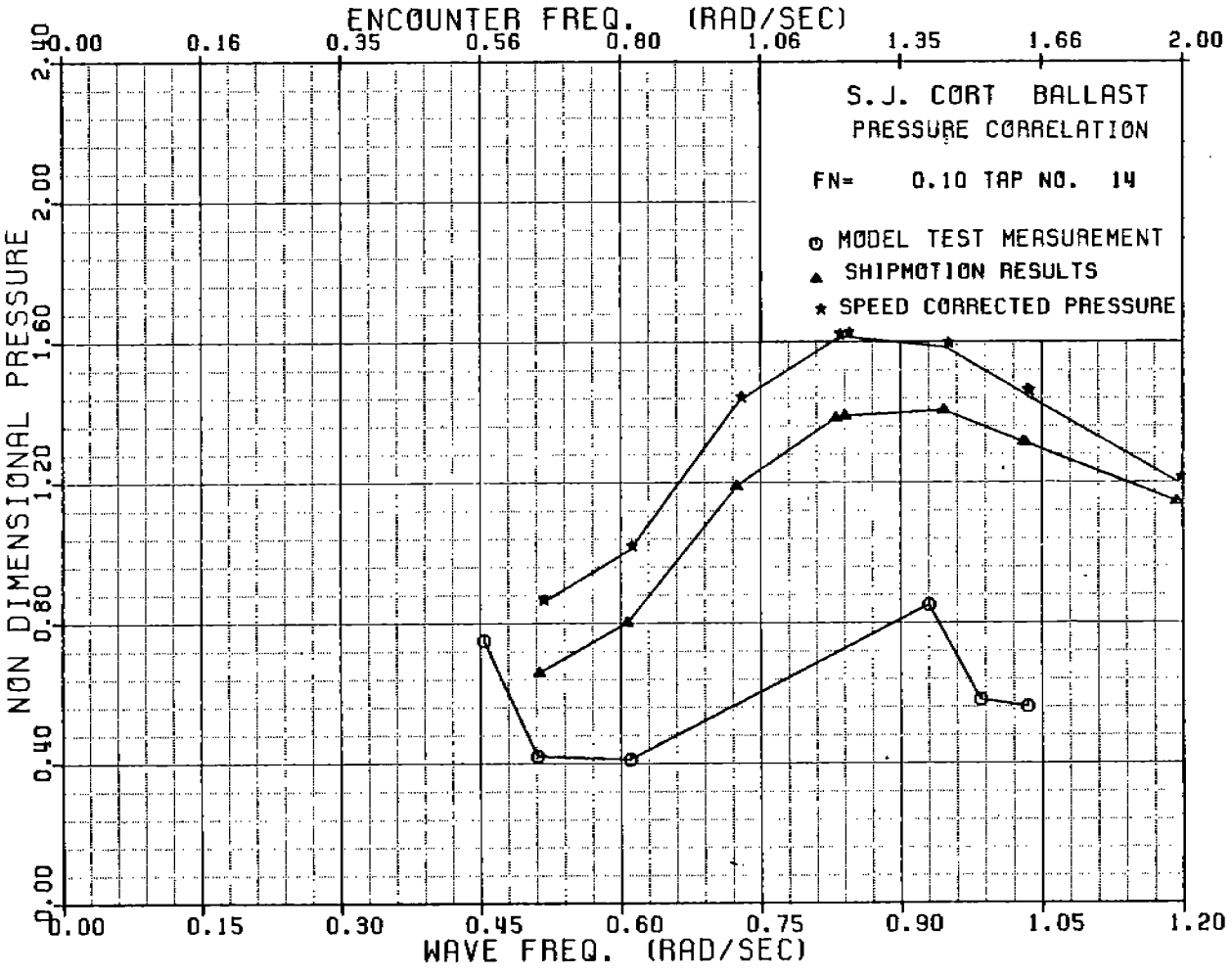

FIGURE B-54 SJ CORT NONDIMENSIONAL PRESSURE , TAP 14, FN=0.10

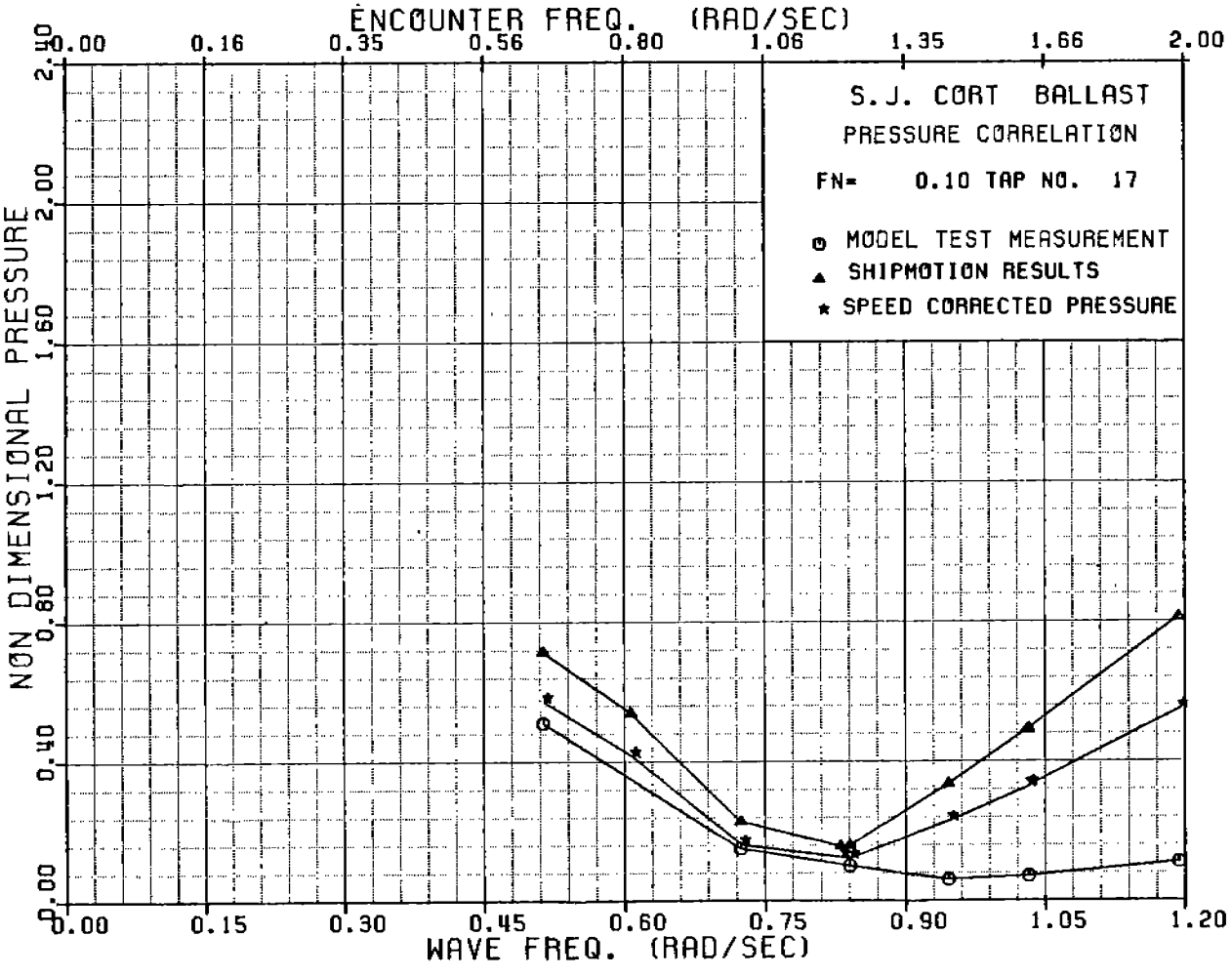

FIGURE B-55 SJ CORT NONDIMENSIONAL PRESSURE , TAP 17, FN=0.10

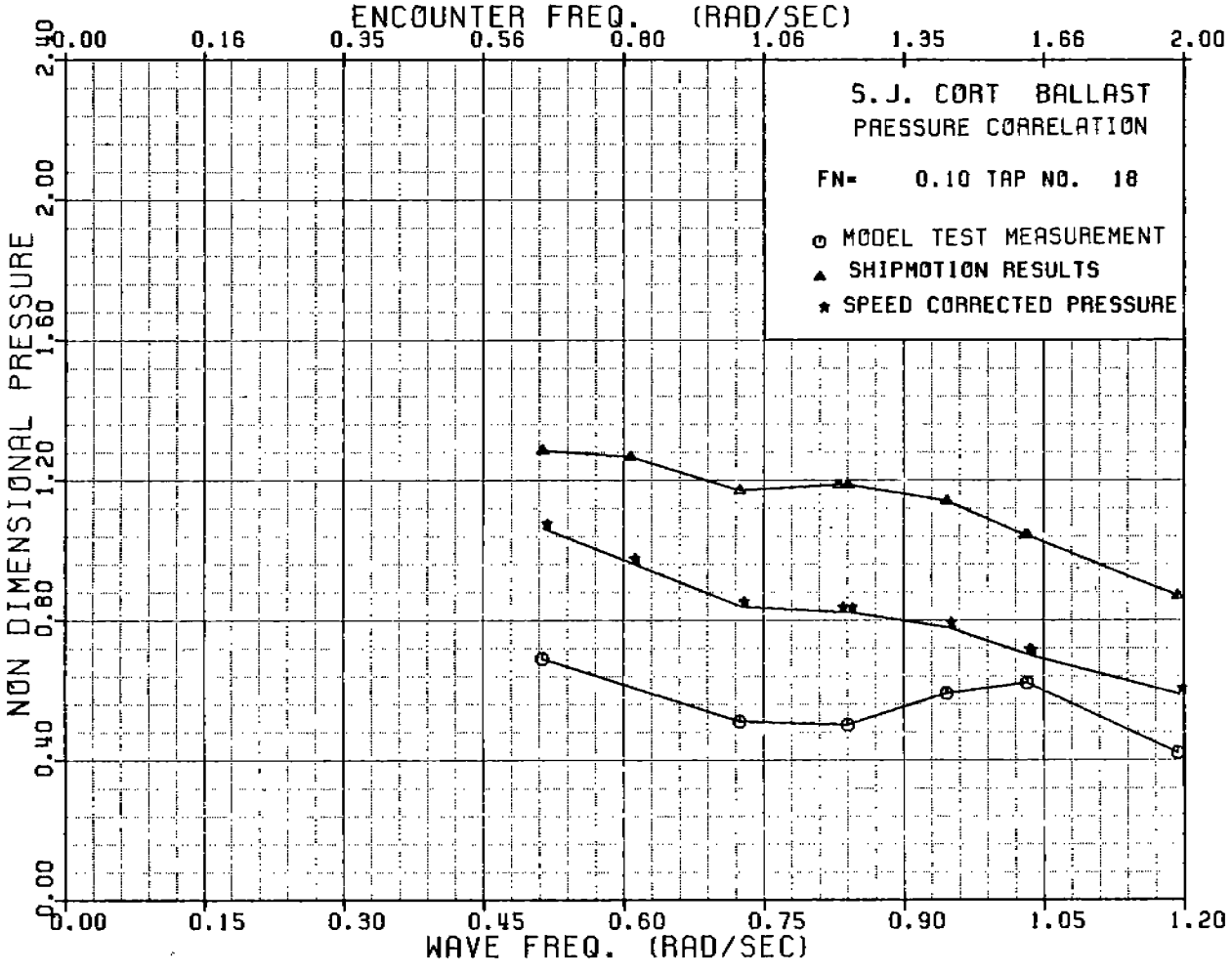

FIGURE B-56 SJ CORT NONDIMENSIONAL PRESSURE , TAP 18, FN=0.10

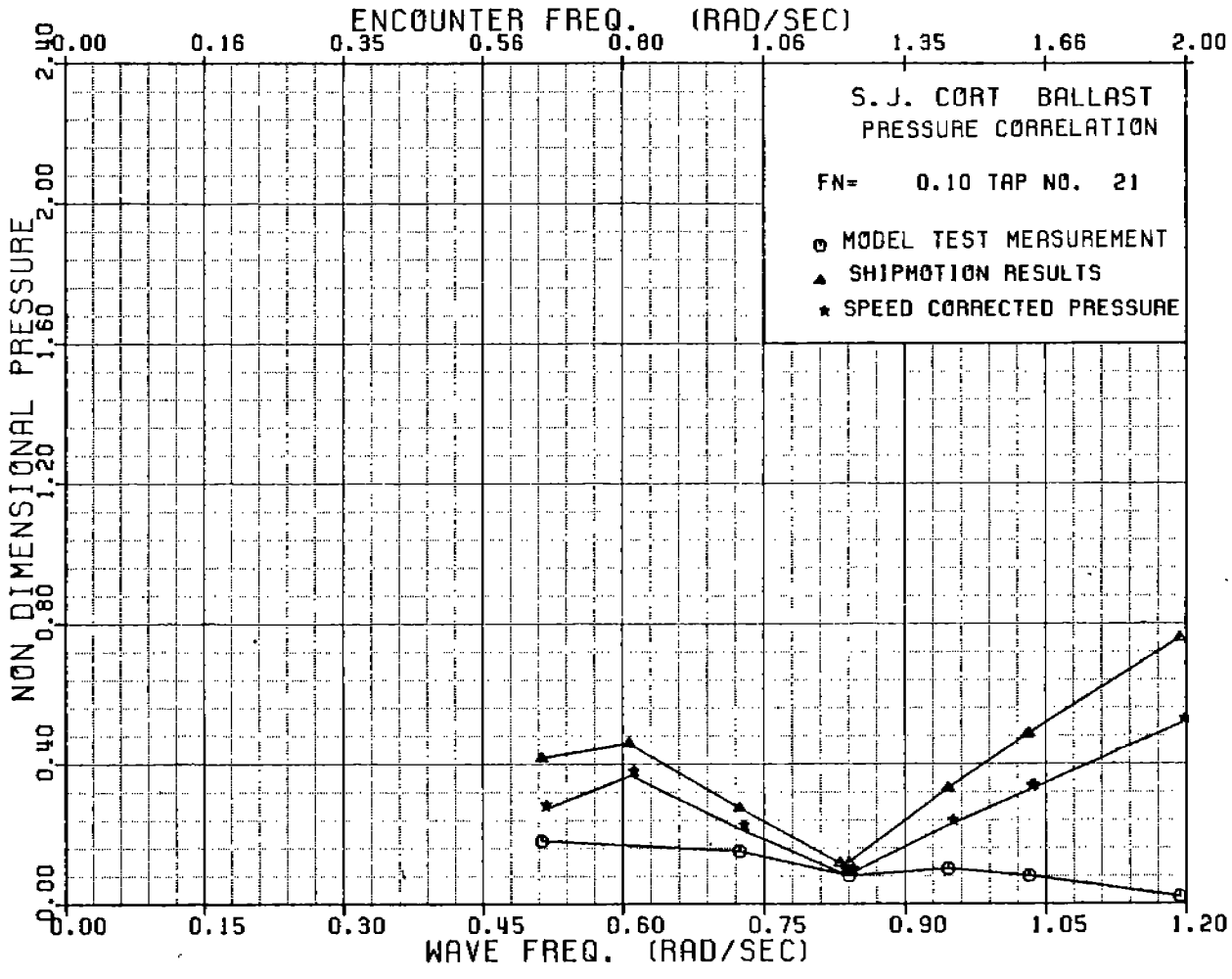

FIGURE B-57 SJ CORT NONDIMENSIONAL PRESSURE , TAP 21, FN=0.10

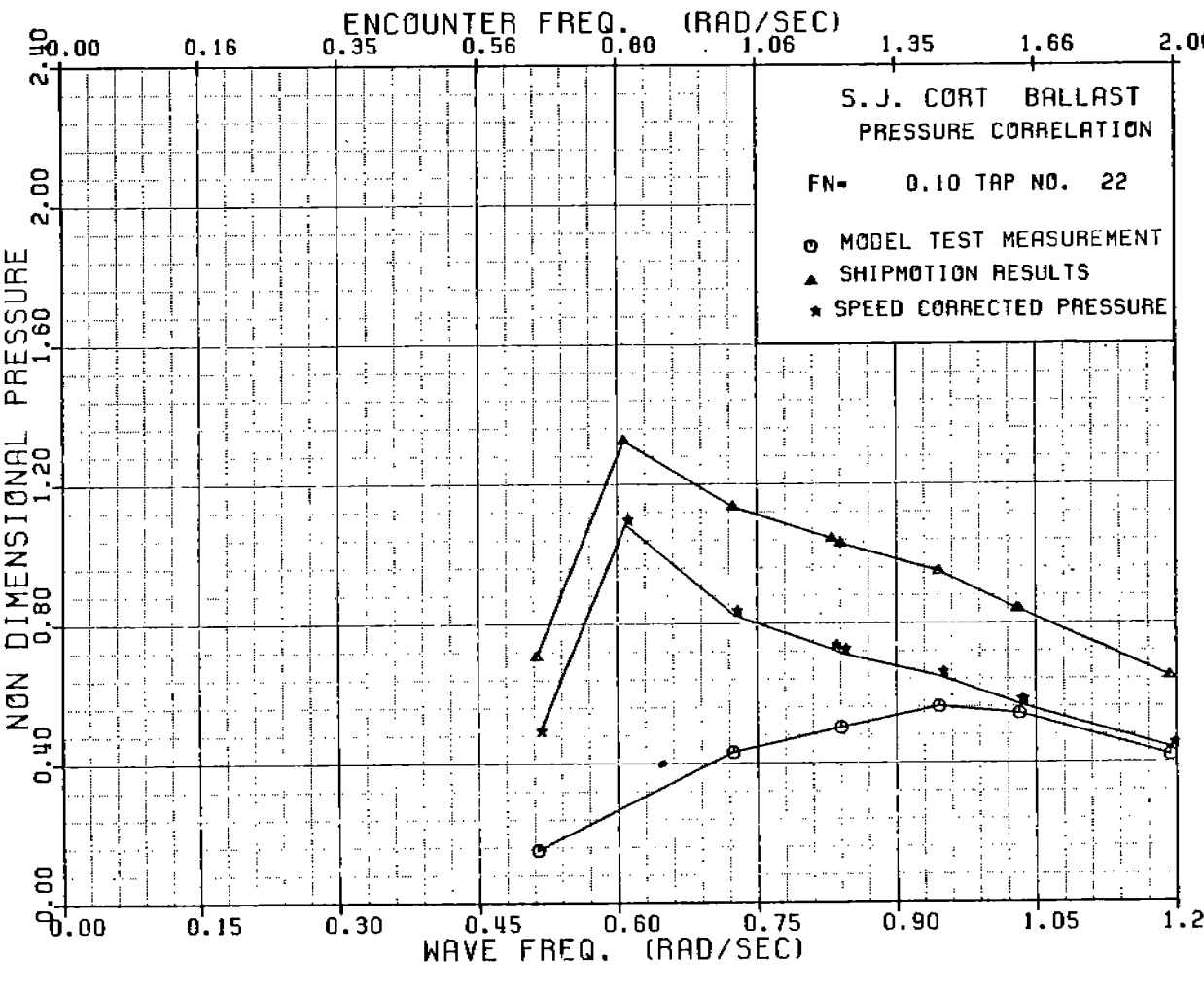

FIGURE B-58 SJ CORT NONDIMENSIONAL PRESSURE , TAP 22, FN=0.10

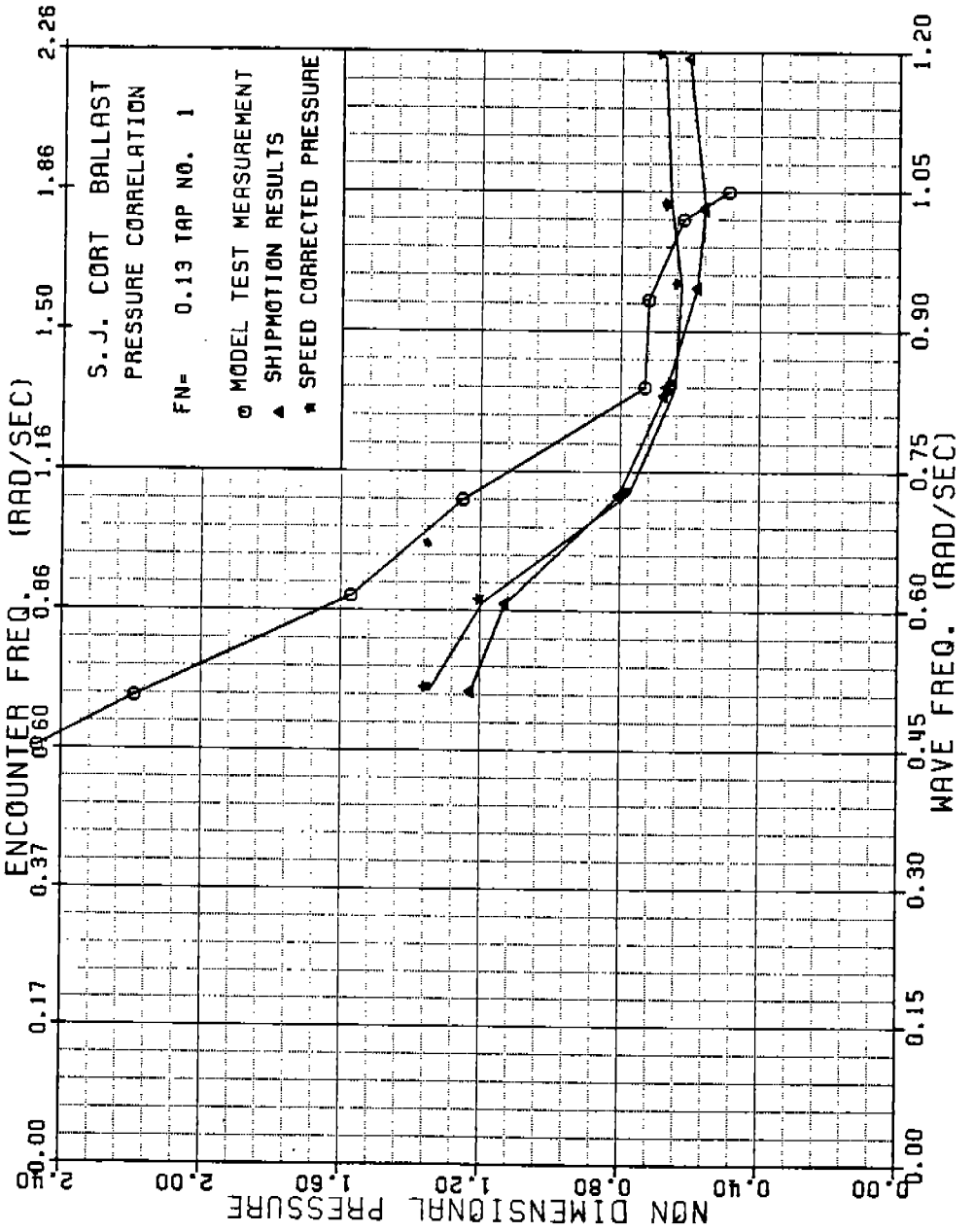

FIGURE B-59 SJ CORT NONDIMENSIONAL PRESSURE , TAP 1 , FN=0.13

(22C)

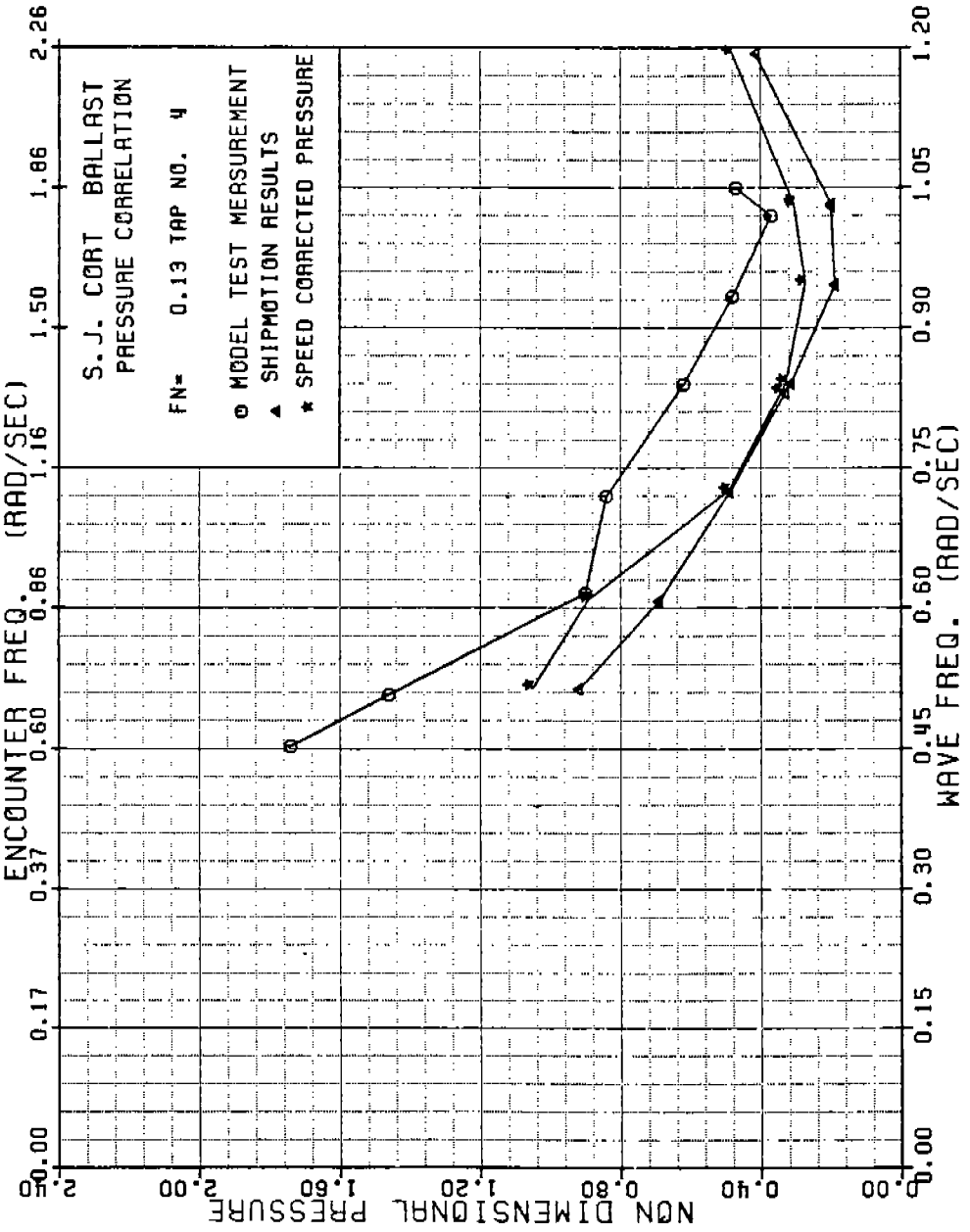

FIGURE B-60 SJ CORT NONDIMENSIONAL PRESSURE , TAP 4 , FN=0.13

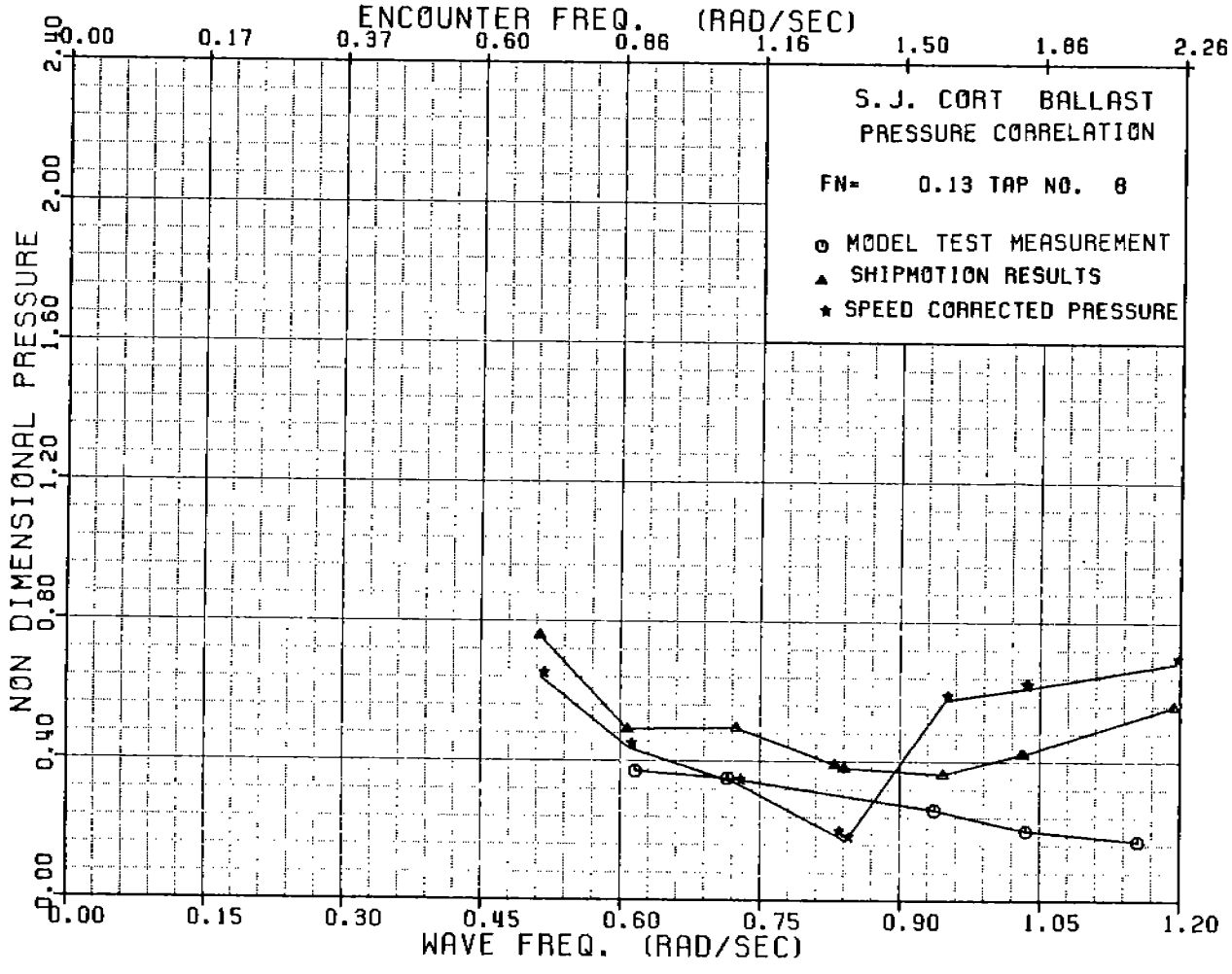

FIGURE B-61 SJ CORT NONDIMENSIONAL PRESSURE , TAP 8 , FN=0.13

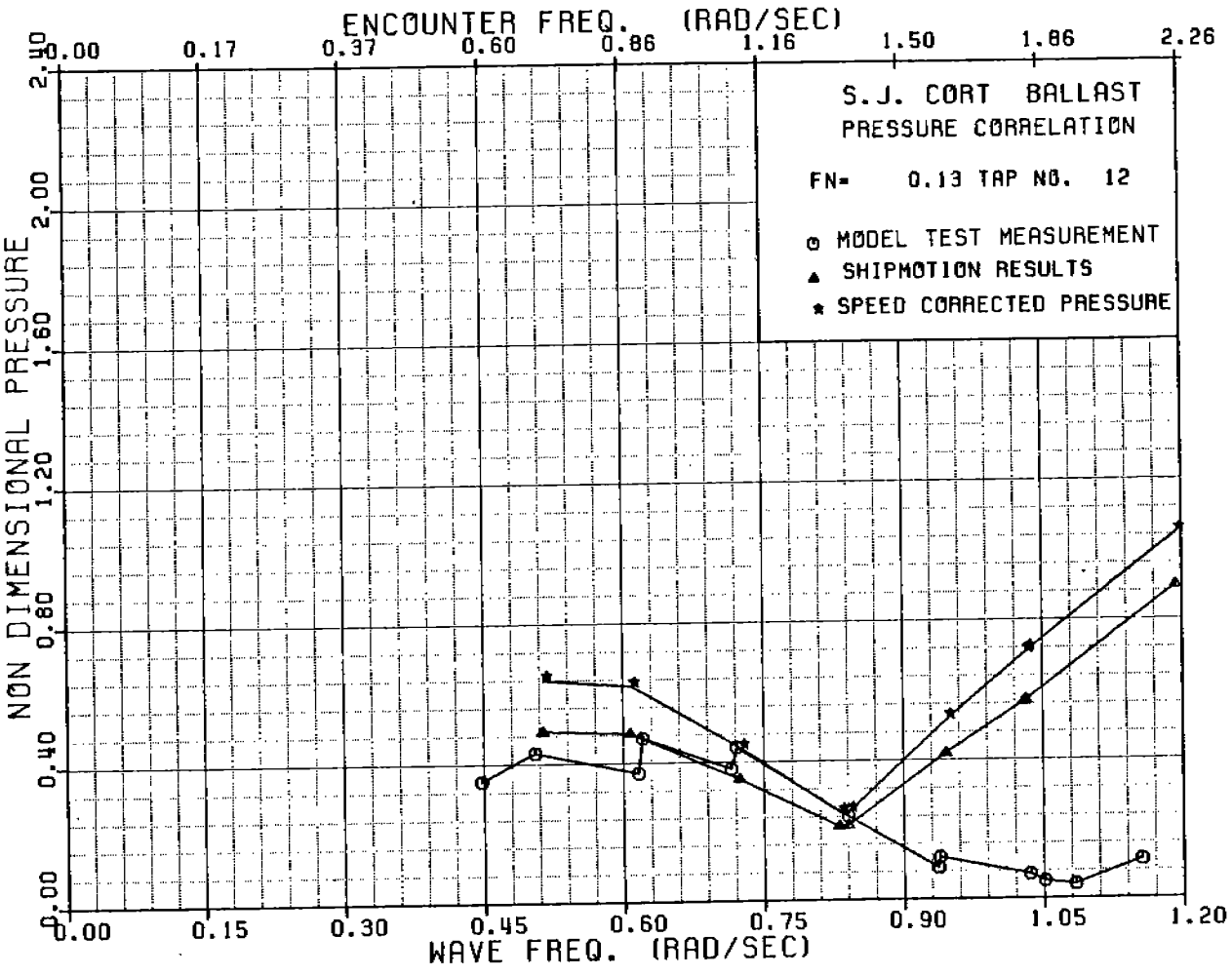

FIGURE B-62 SJ CORT NONDIMENSIONAL PRESSURE , TAP 12, FN=0.13

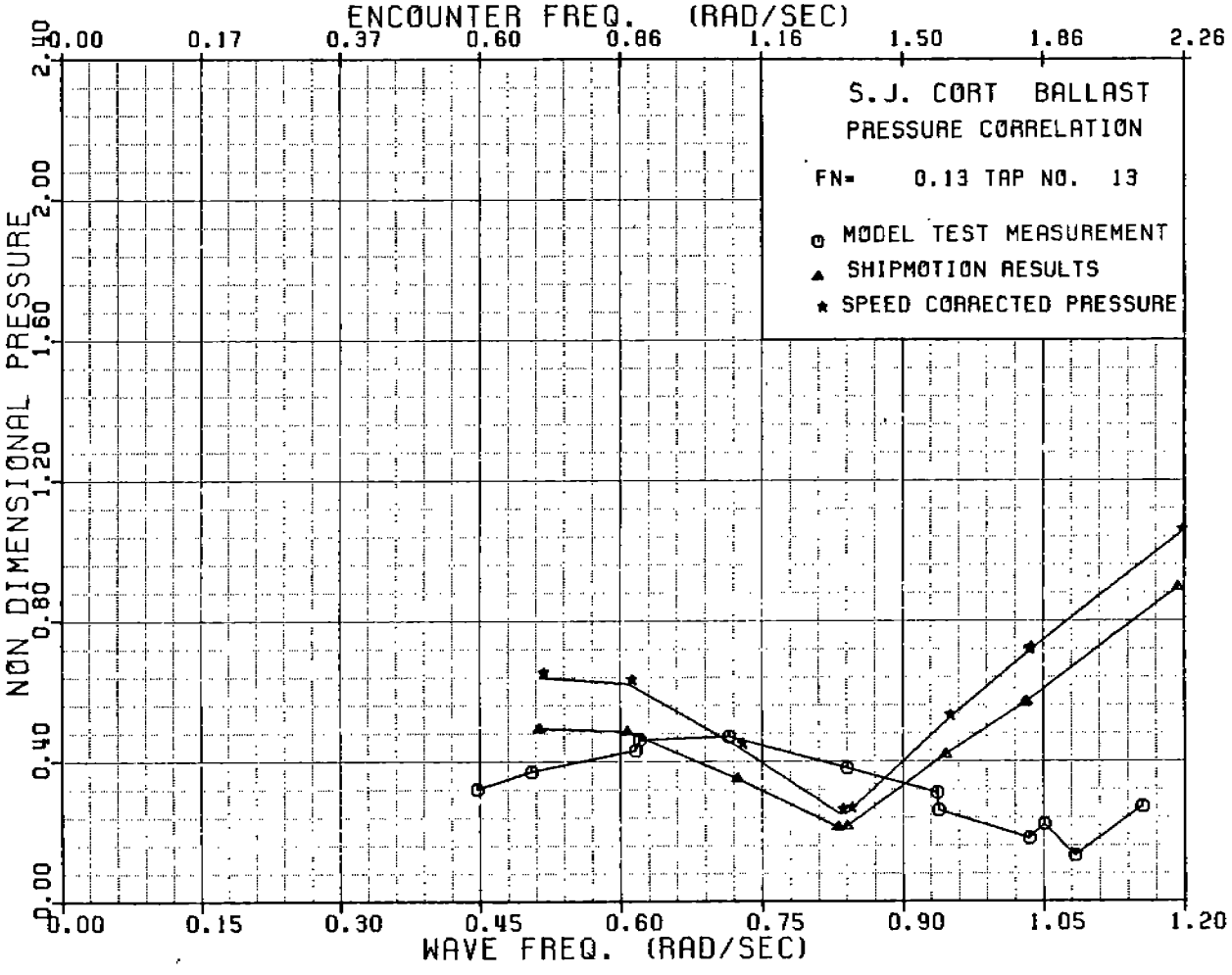

FIGURE B-63 SJ CORT NONDIMENSIONAL PRESSURE , TAP 13, FN=0.13

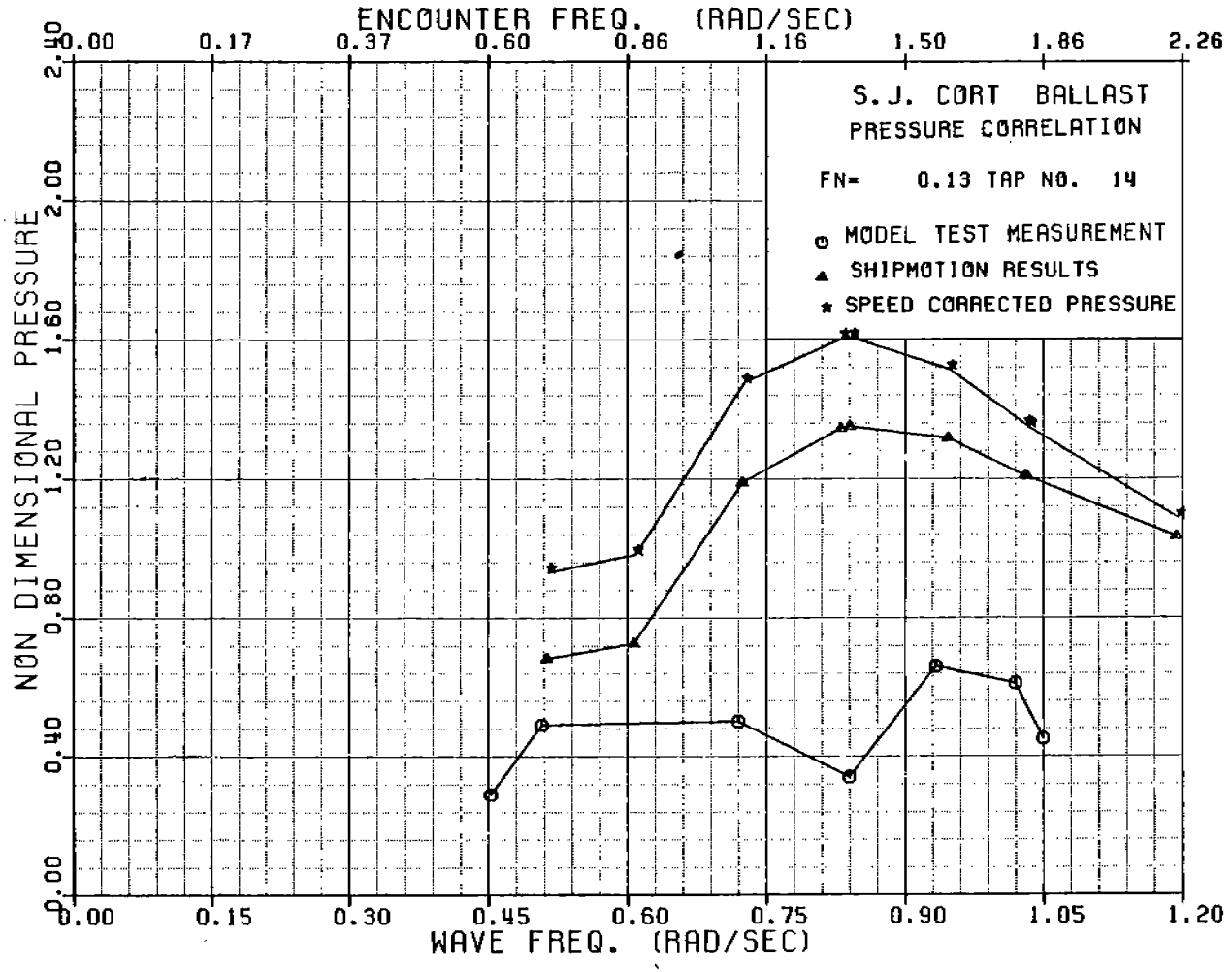

FIGURE B-64 SJ CORT NONDIMENSIONAL PRESSURE , TAP 14, FN=0.13

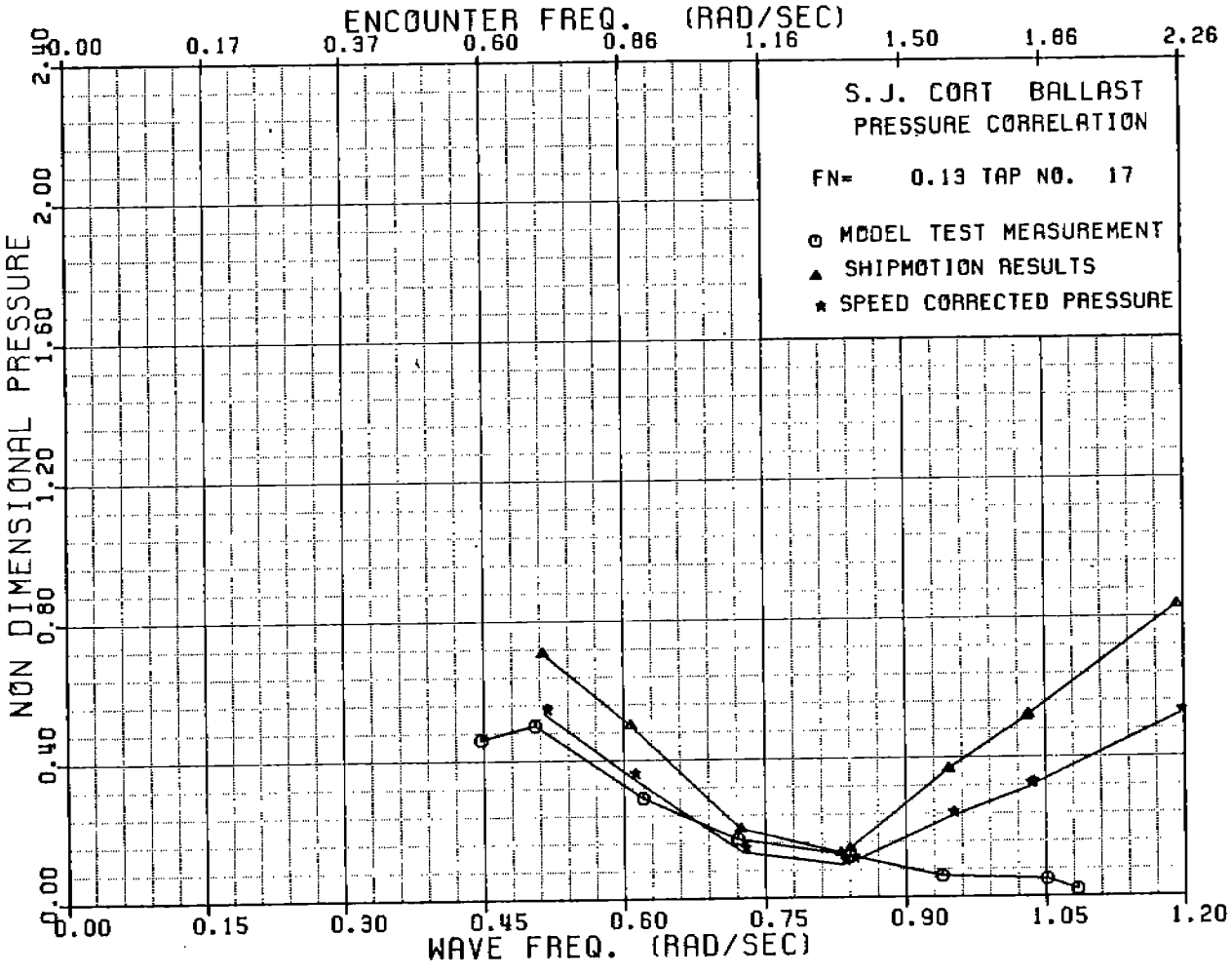

FIGURE B-65 SJ CORT NONDIMENSIONAL PRESSURE , TAP 17, FN=0.13

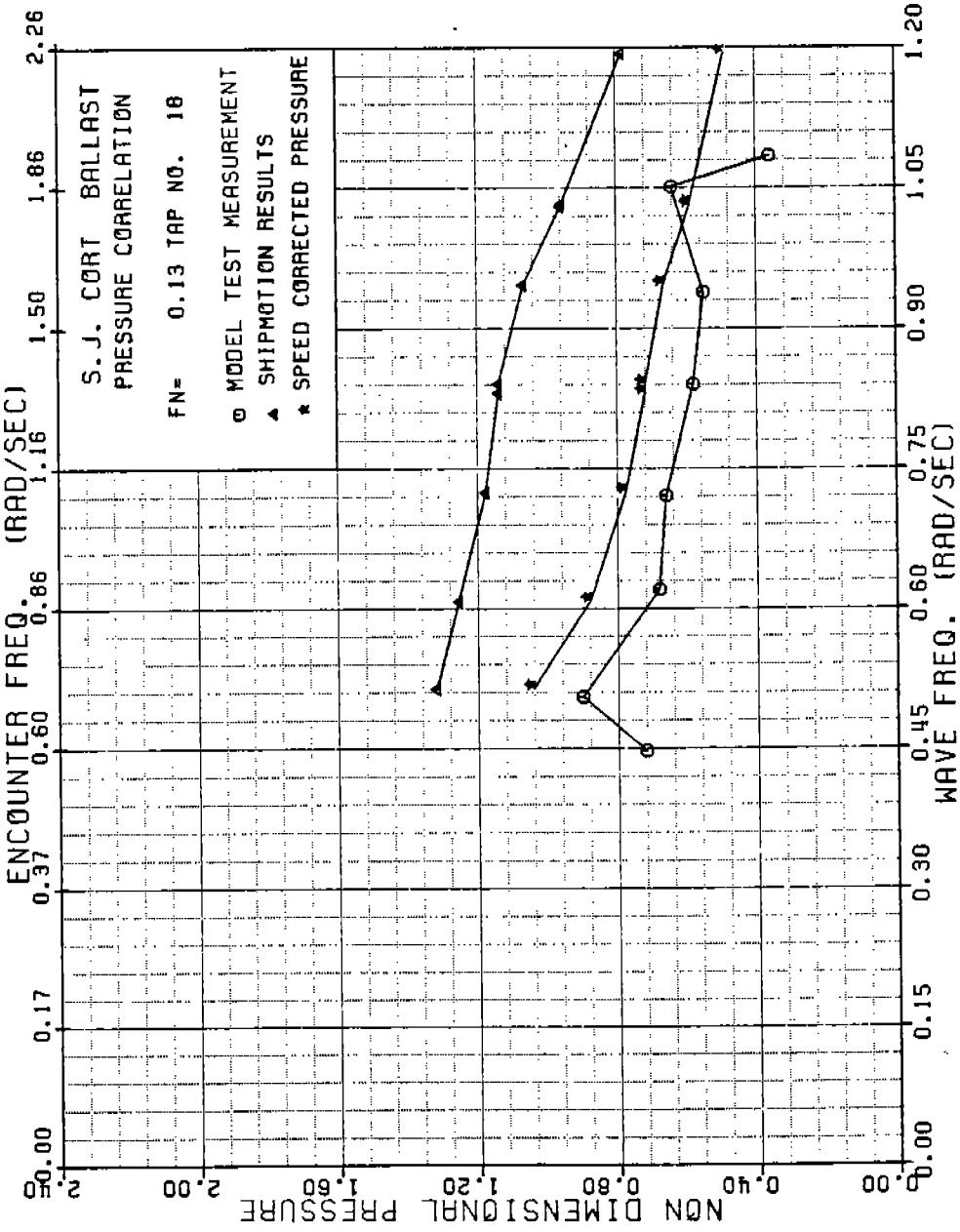

FIGURE B-66 SJ CORT NONDIMENSIONAL PRESSURE , TAP 18, FN=0.13

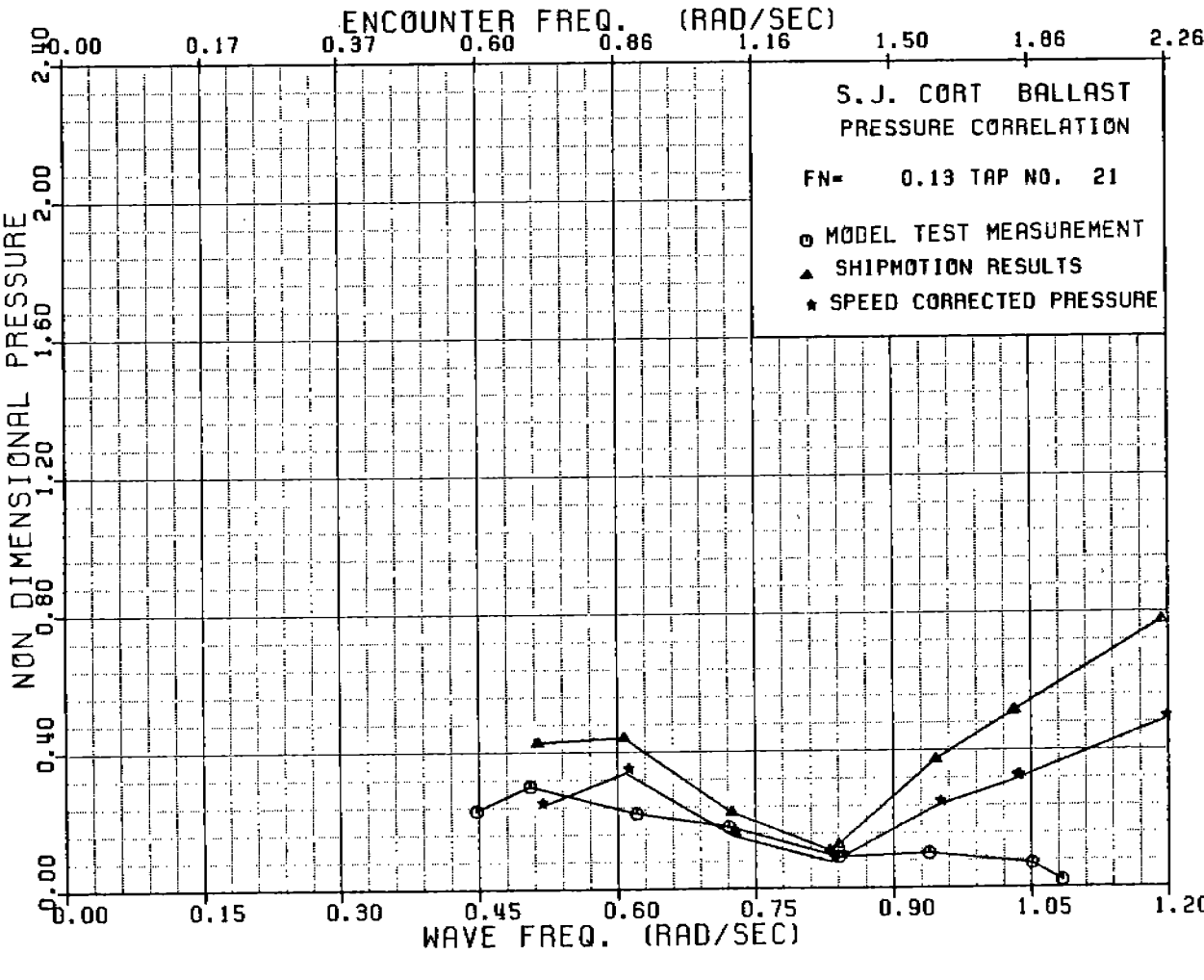

FIGURE B-67 SJ CORT NONDIMENSIONAL PRESSURE , TAP 21, FN=0.13

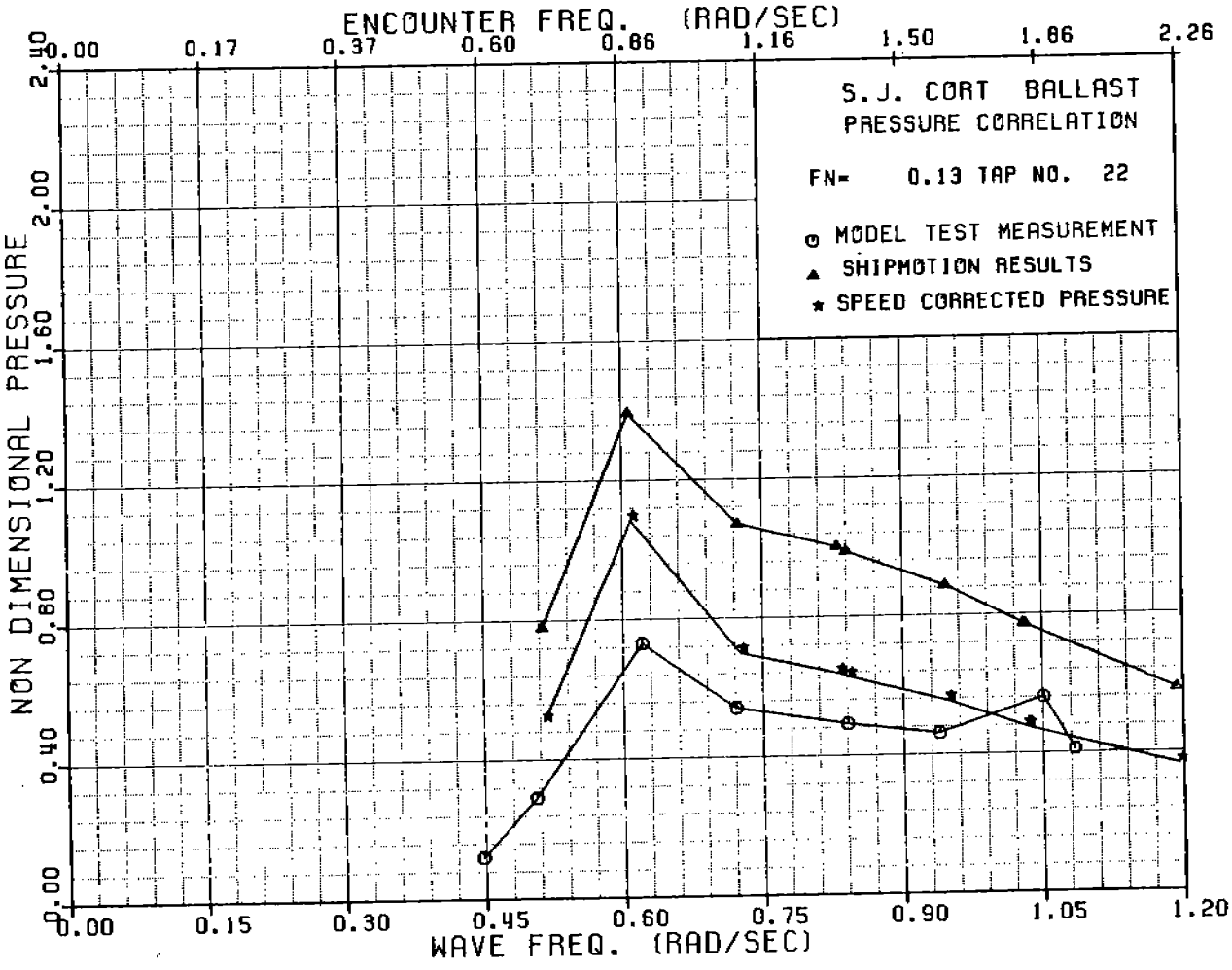

FIGURE B-68 SJ CORT NONDIMENSIONAL PRESSURE , TAP 22, FN=0.13

(1 1/4" TO TRIM)

APPENDIX C

M/V S. J. CORT

FULL-SCALE MEASUREMENT CORRELATION PLOTS

(2 1/4" TO BWD)

Figs. C-1 to C-23: S. J. CORT Wave and Pressure Spectra

Figs. C-24 to C-73: S. J. CORT Pressure Transfer Functions

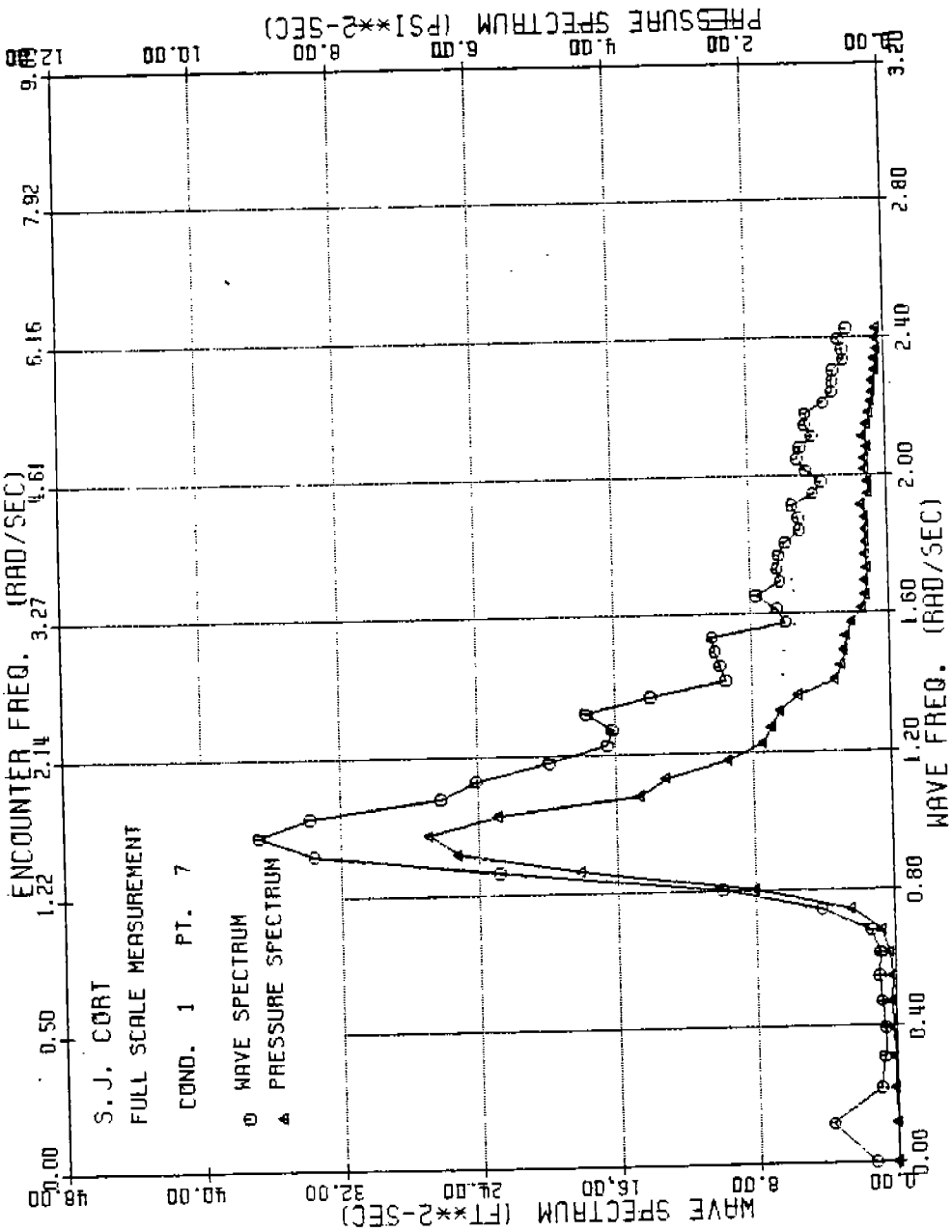

FIGURE C-1: SJ CORT WAVE AND PRESSURE SPECTRA, TAP NO. 7, CONDITION 1

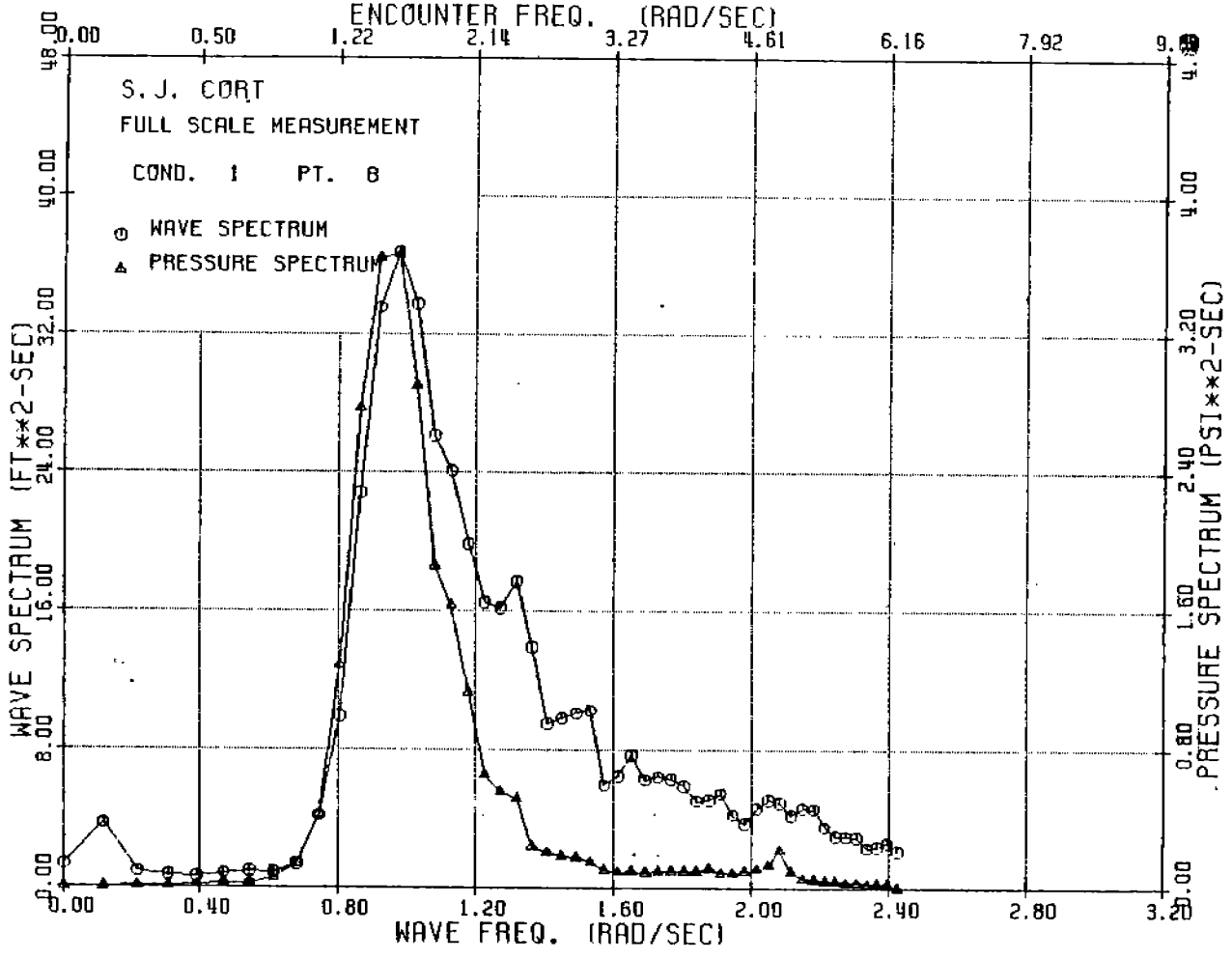

FIGURE C-2: SJ CORT WAVE AND PRESSURE SPECTRA, TAP NO. 8, CONDITION 1

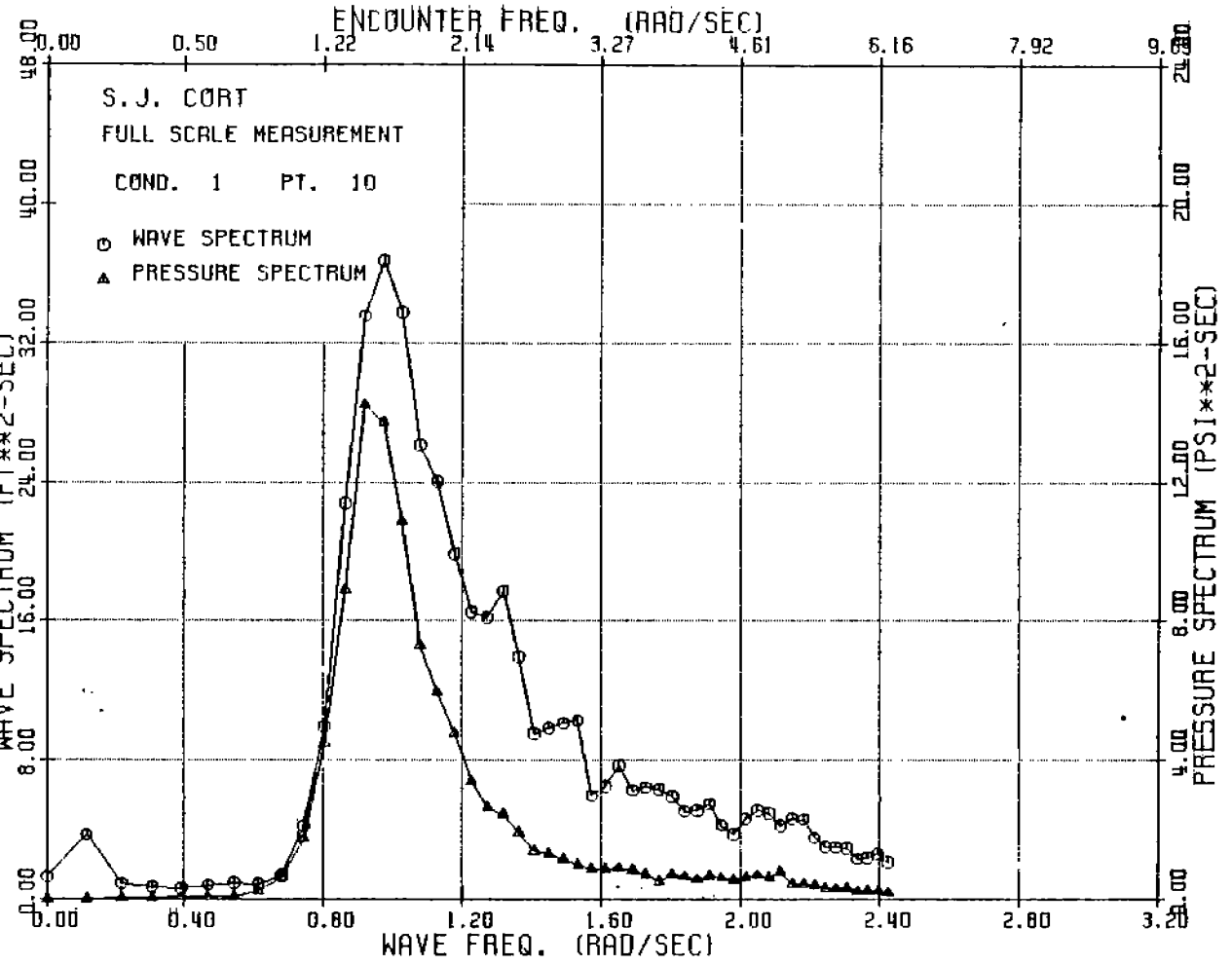

URE C-3: SJ CORT WAVE AND PRESSURE SPECTRA, TAP NO. 10, CONDITION 1

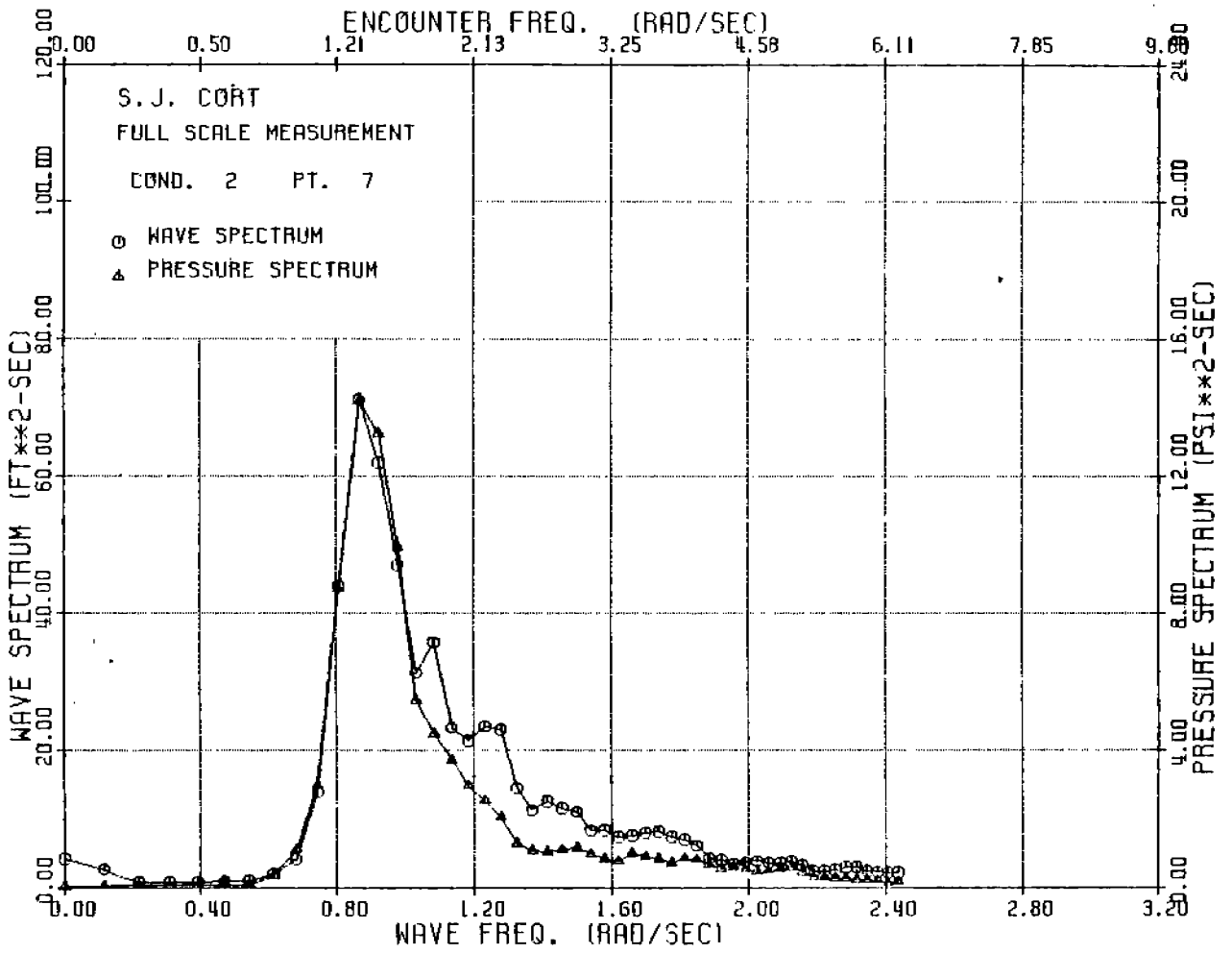

FIGURE C-4: SJ CORT WAVE AND PRESSURE SPECTRA, TAP NO. 7, CONDITION 2

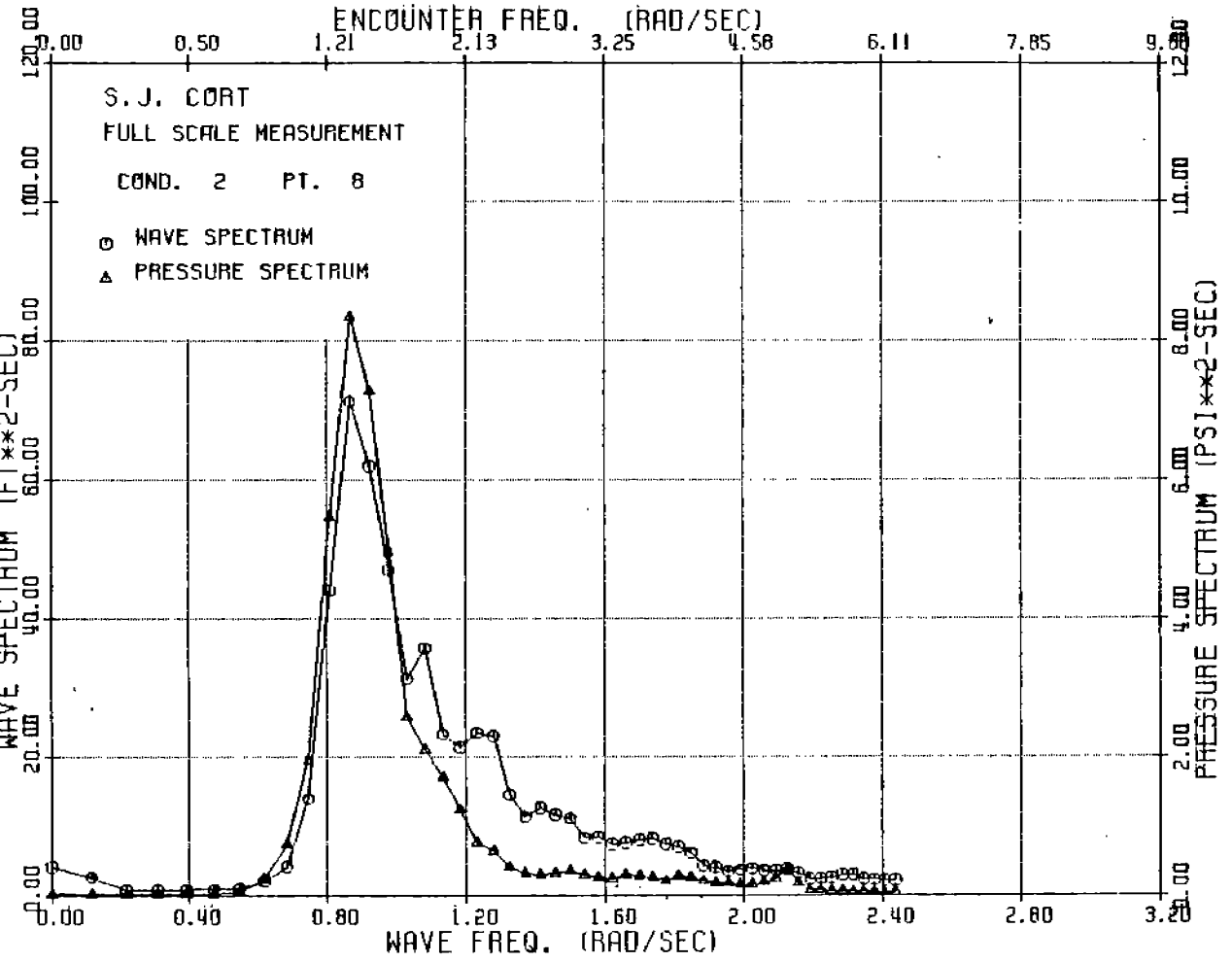

GURE C-5: SJ CORT WAVE AND PRESSURE SPECTRA, TAP NO. 8, CONDITION 2

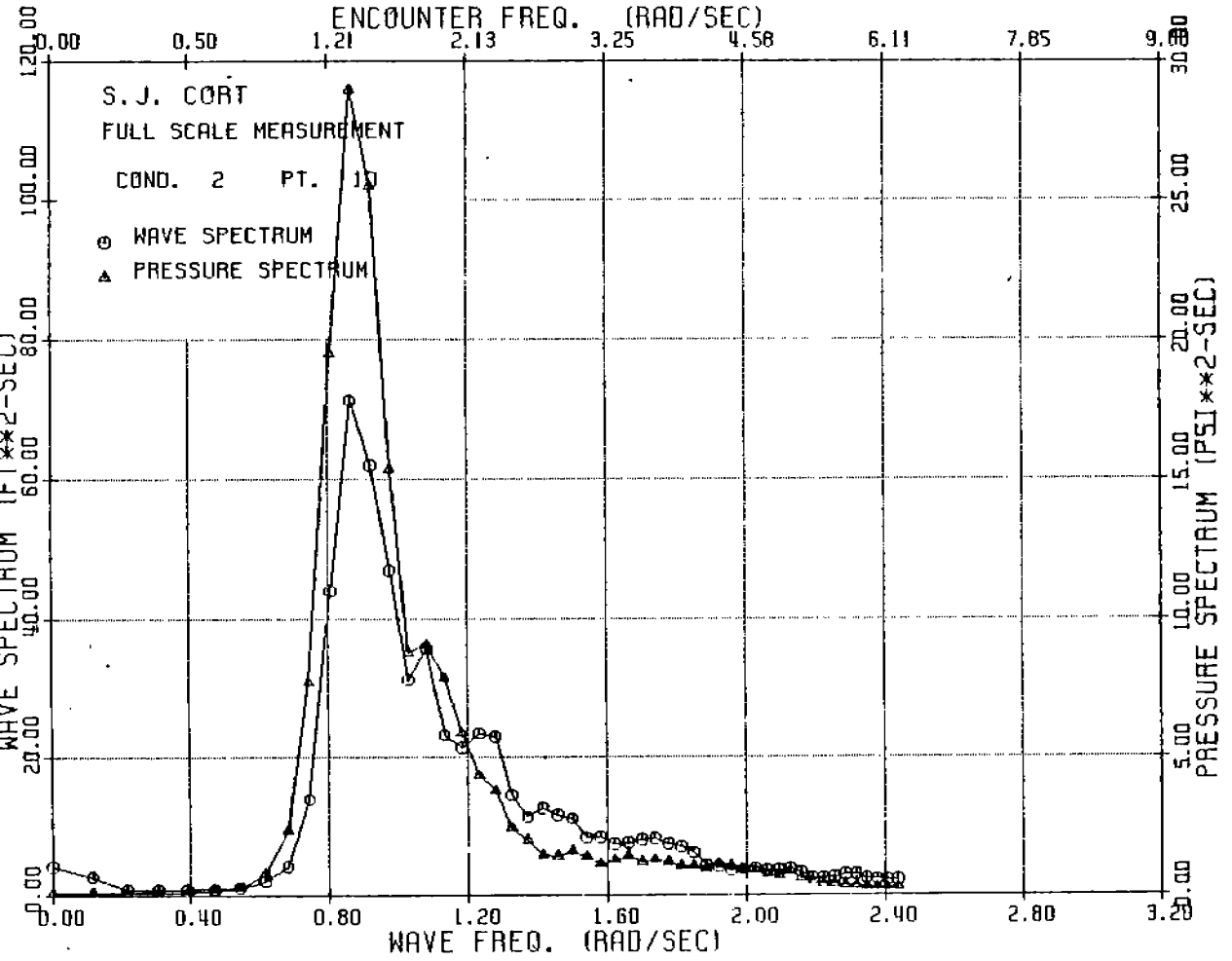

GURE C-6: SJ CORT WAVE AND PRESSURE SPECTRA, TAP NO. 10, CONDITION 2

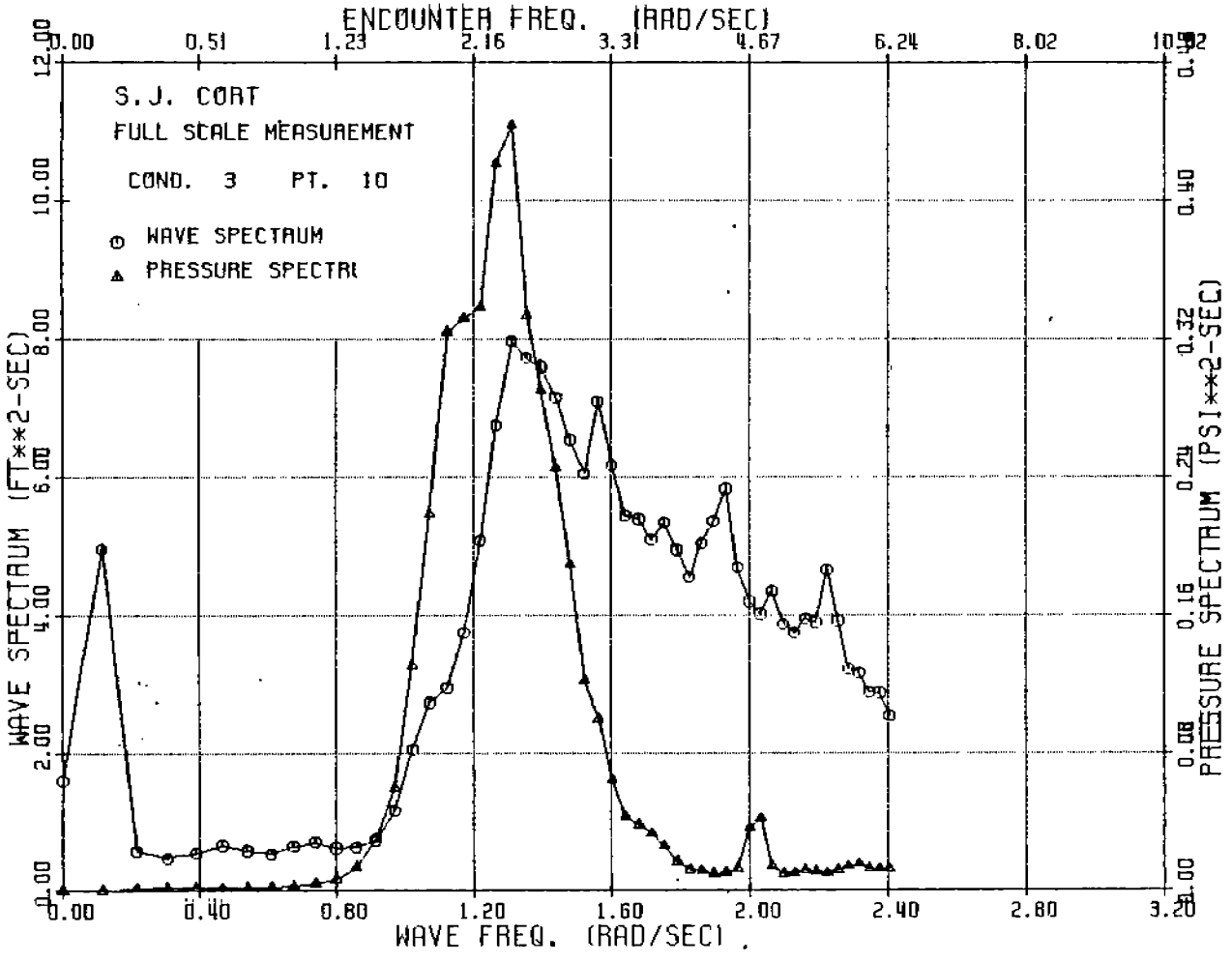

FIGURE C-7: SJ CORT WAVE AND PRESSURE SPECTRA, TAP NO. 10, CONDITION 3

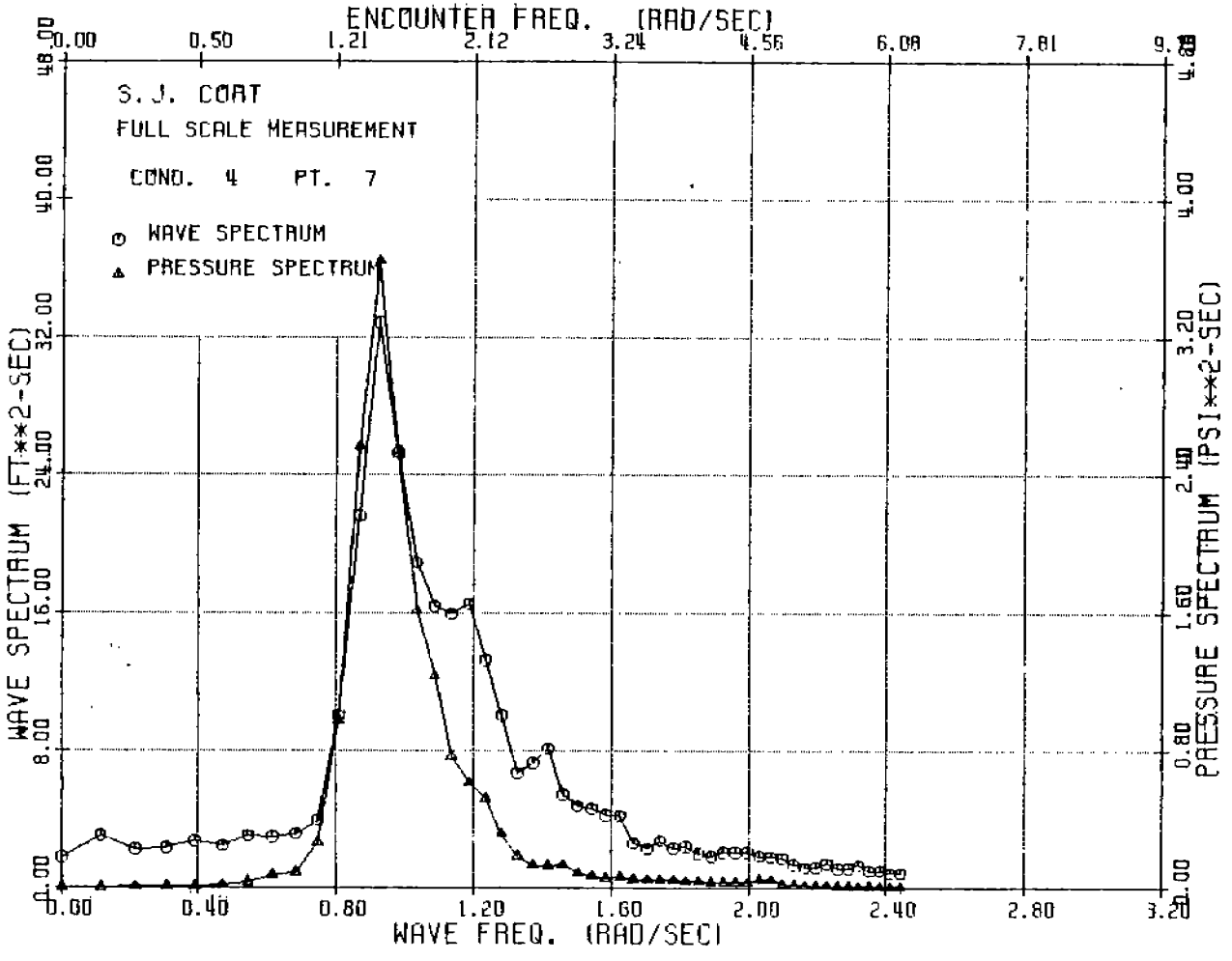

FIGURE C-8: SJ CORT WAVE AND PRESSURE SPECTRA, TAP NO. 7, CONDITION 4

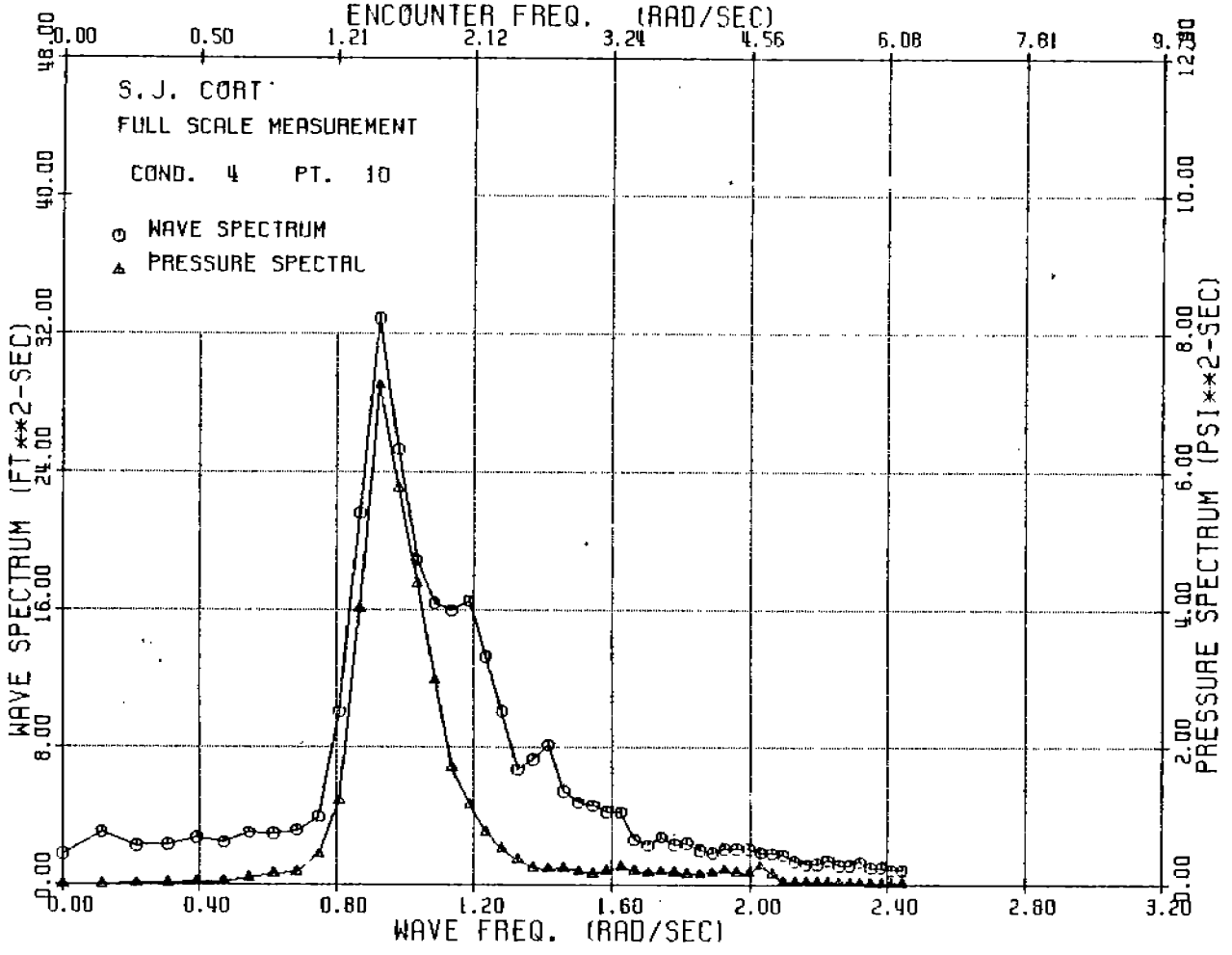

FIGURE C-9: SJ CORT WAVE AND PRESSURE SPECTRA, TAP NO. 10, CONDITION 4

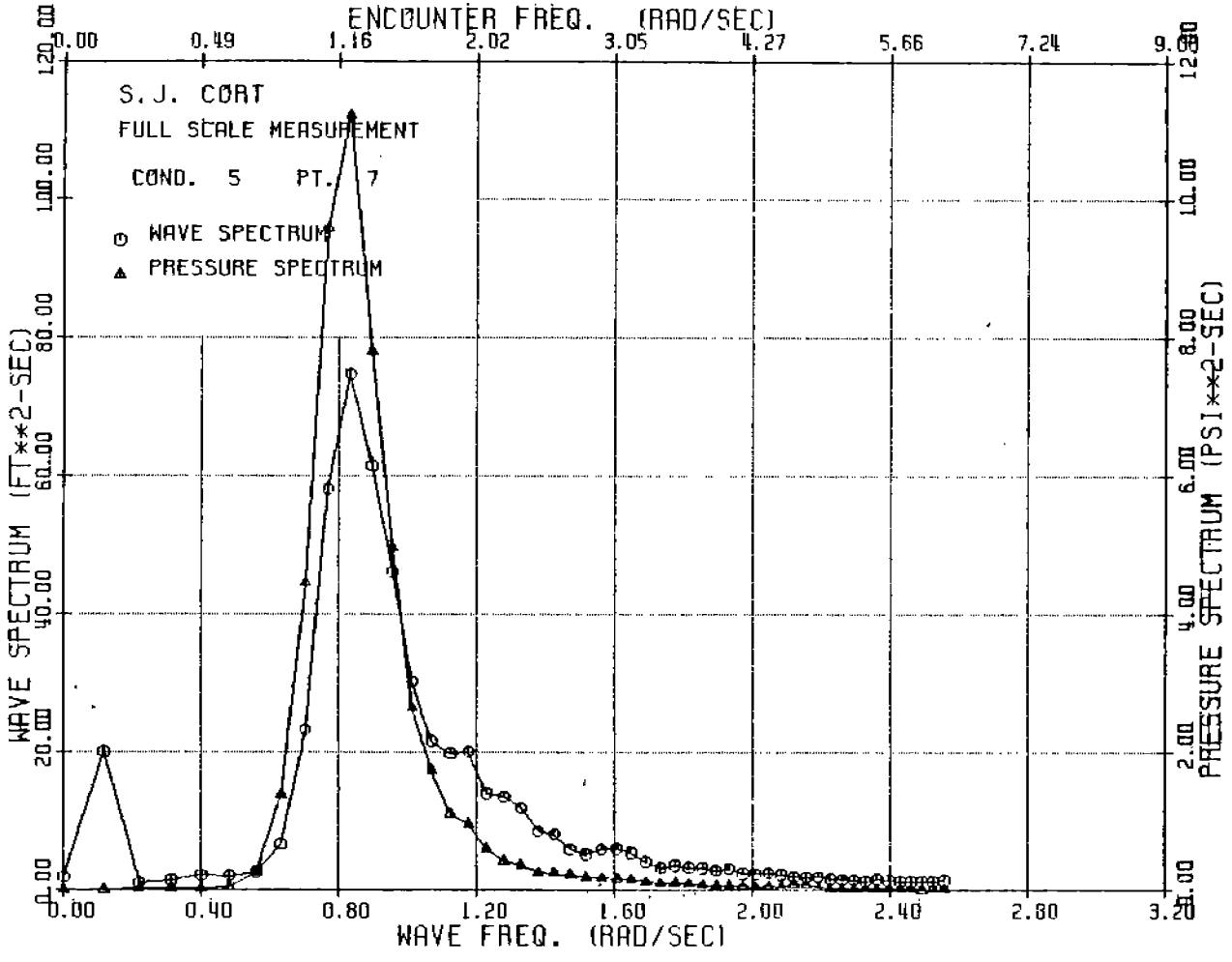

FIGURE C-10: SJ CORT WAVE AND PRESSURE SPECTRA, TAP NO. 7,CONDITION 5

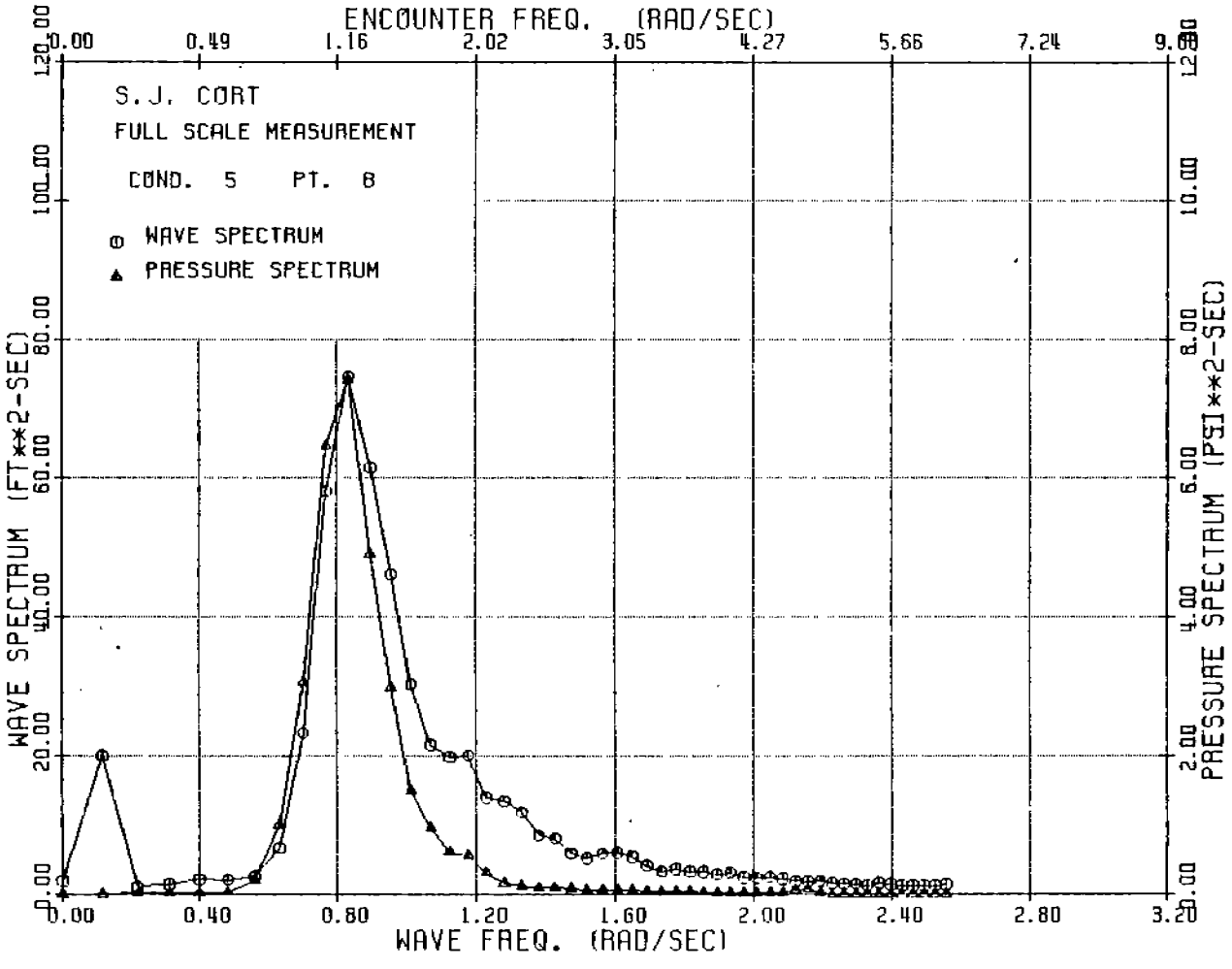

FIGURE C-11: SJ CORT WAVE AND PRESSURE SPECTRA, TAP NO. 8, CONDITION 5

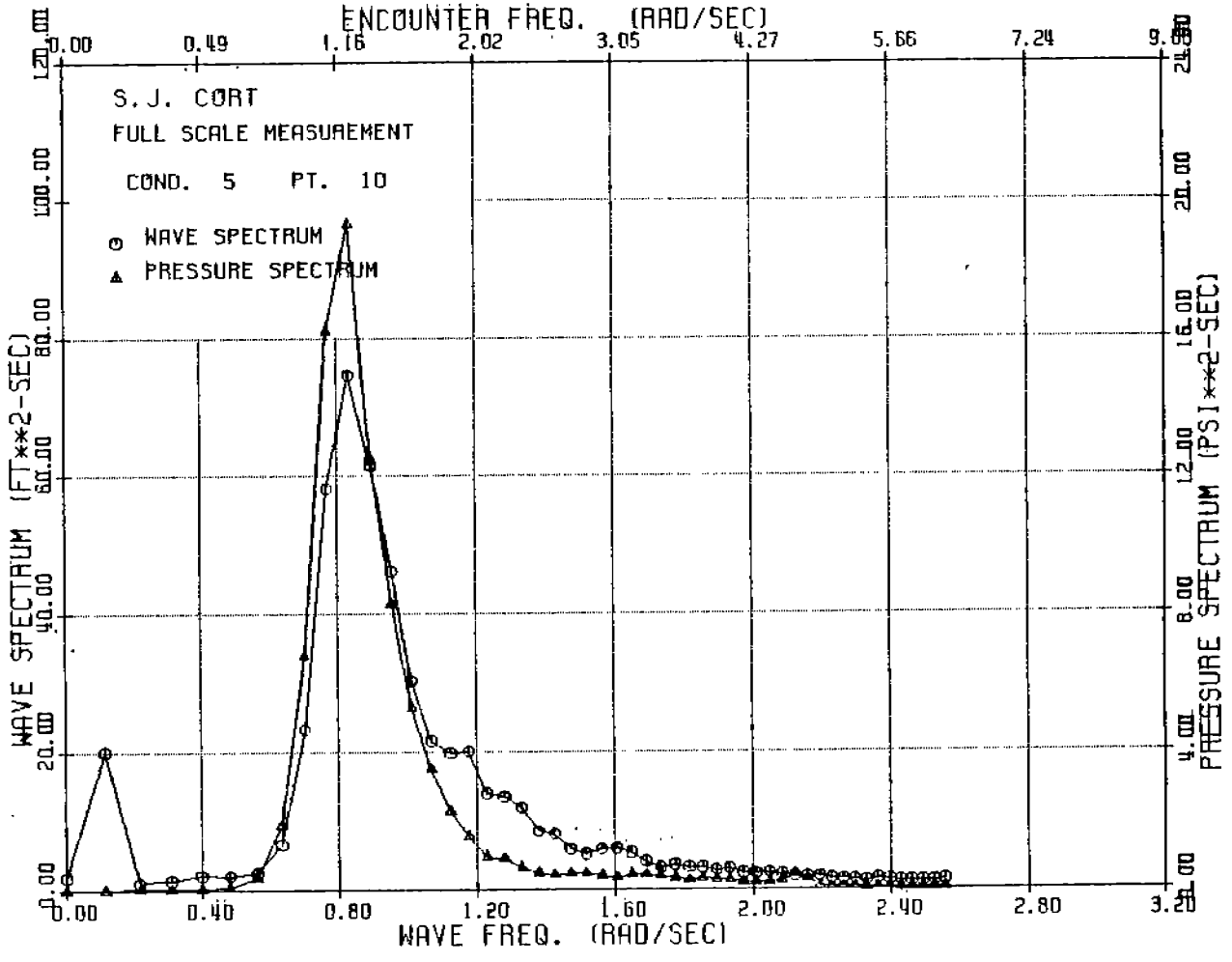

FIGURE C-12: SJ CORT WAVE AND PRESSURE SPECTRA, TAP NO. 10, CONDITION 5

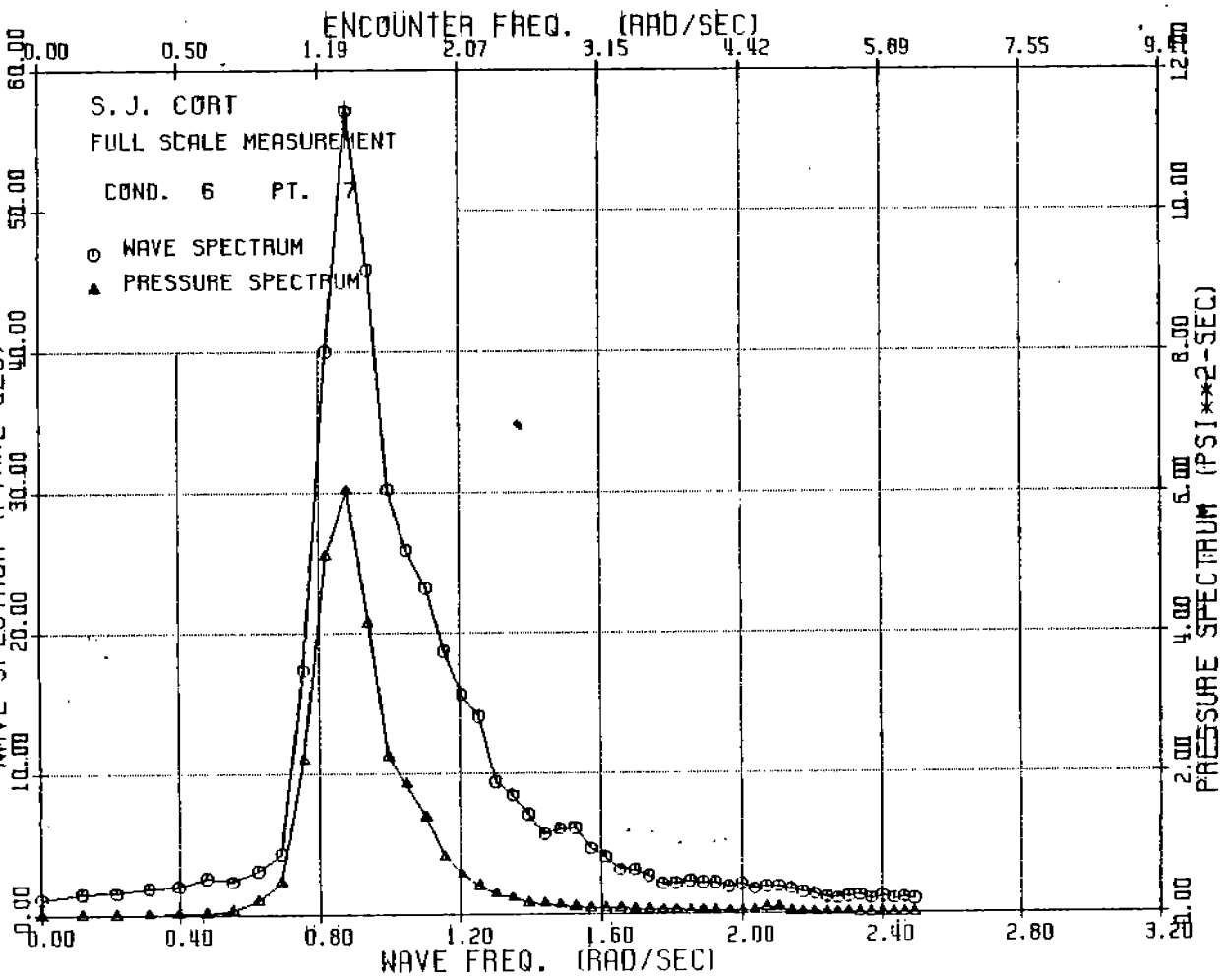

IGURE C-13: SJ CORT WAVE AND PRESSURE SPECTRA, TAP NO. 7, CONDITION 6

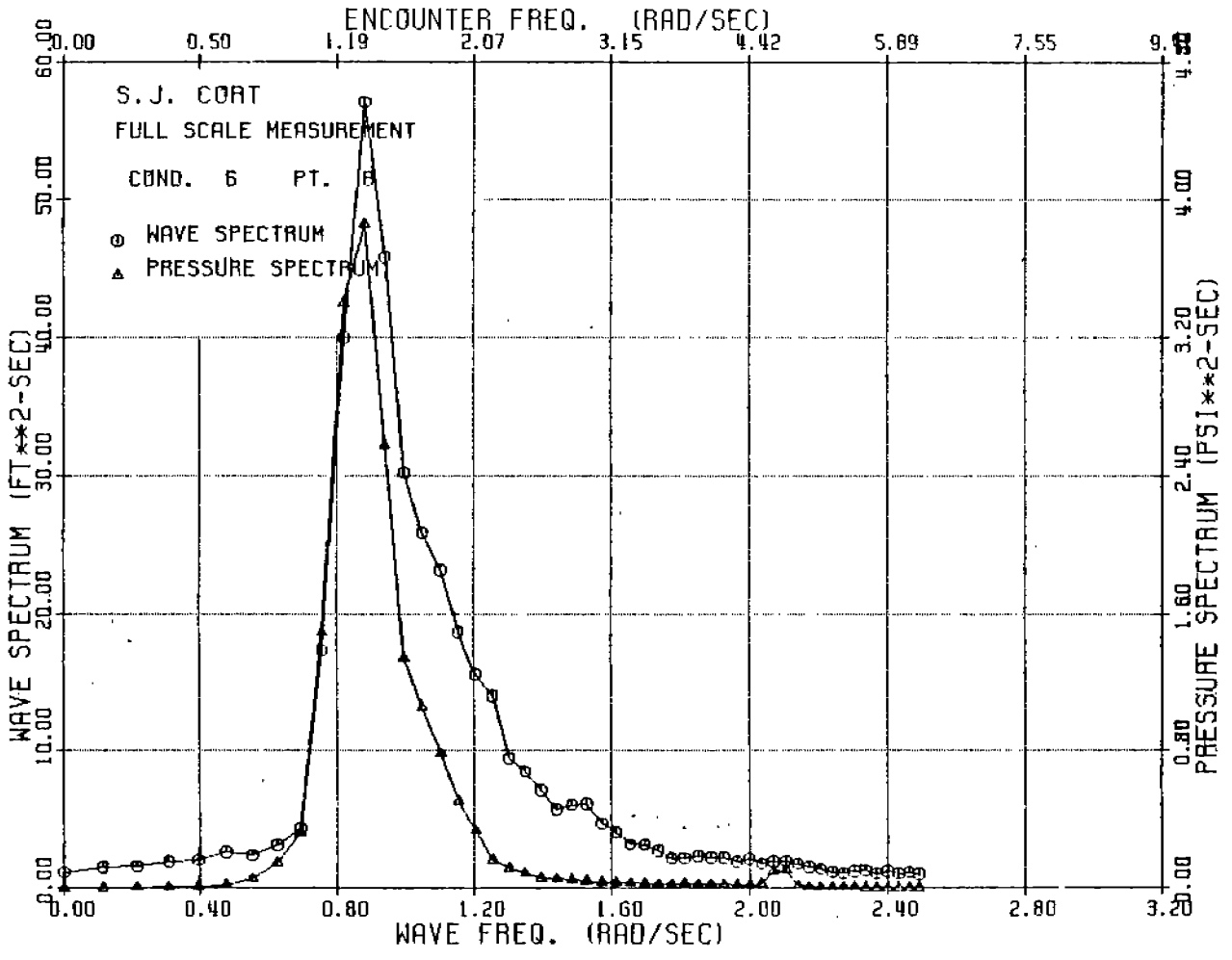

FIGURE C-14: SJ CORT WAVE AND PRESSURE SPECTRA, TAP NO. 8, CONDITION 6

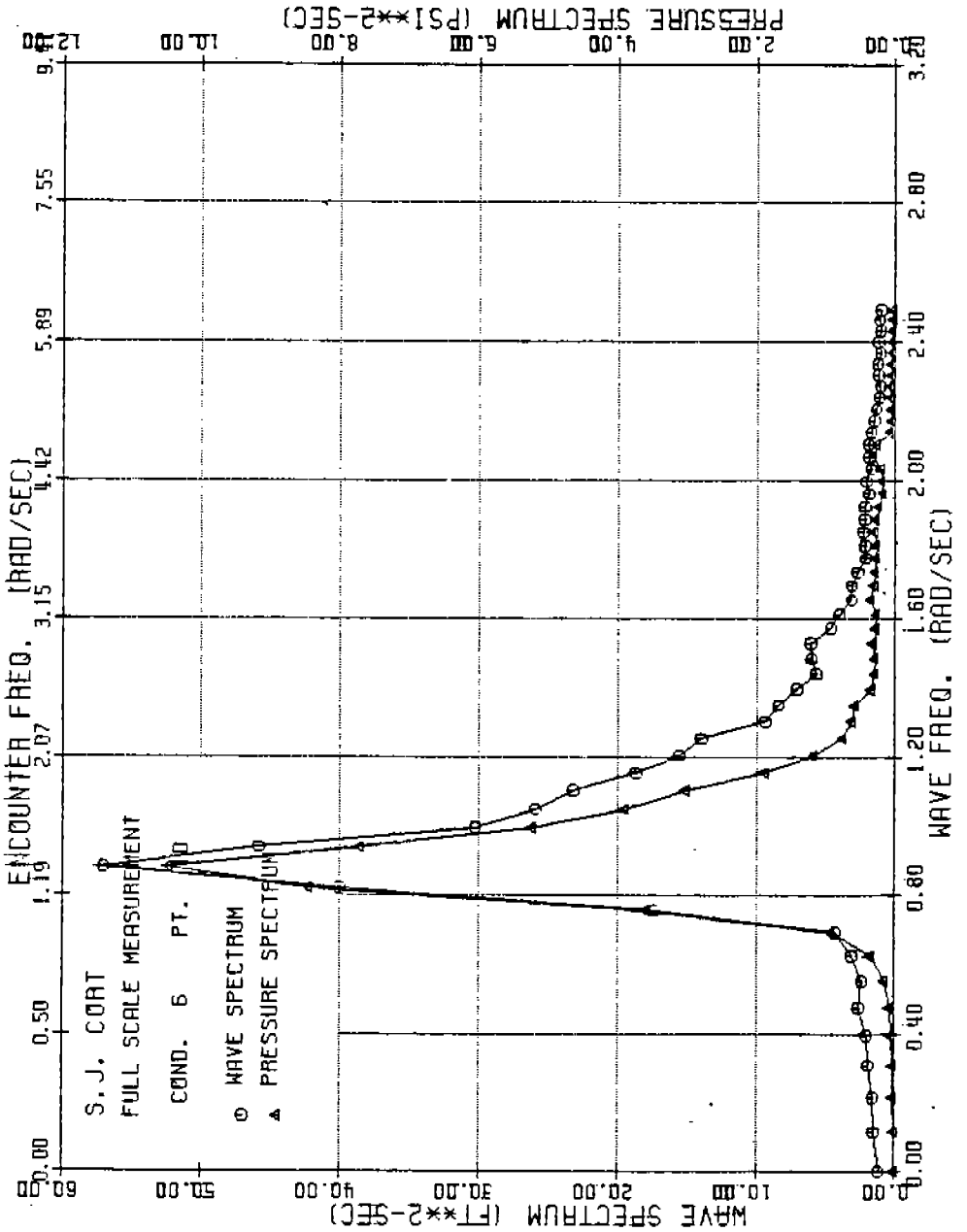

FIGURE C-15: SJ CORT WAVE AND PRESSURE SPECTRA, TAP NO. 10, CONDITION 6

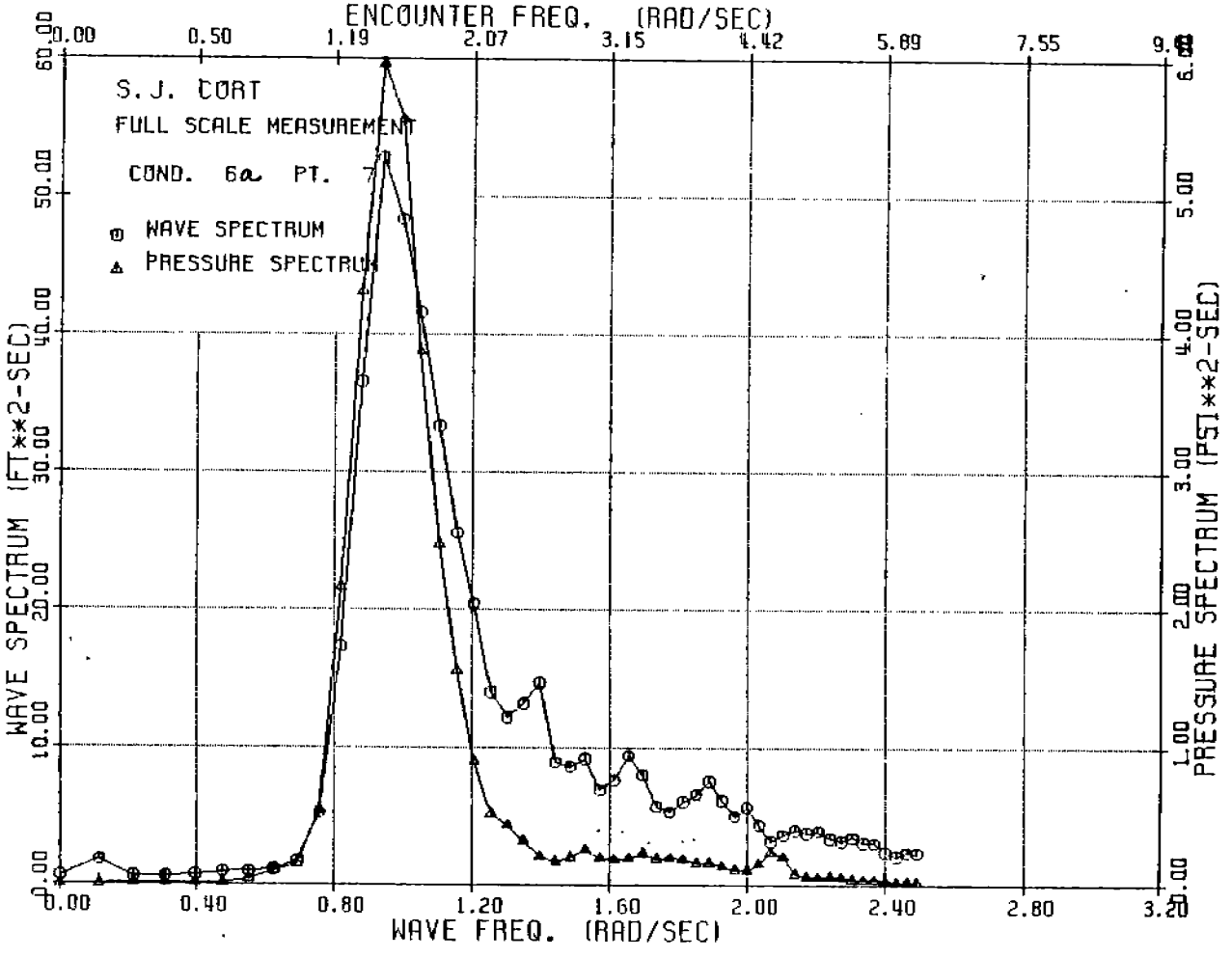

FIGURE C-16: SJ CORT WAVE AND PRESSURE SPECTRA, TAP NO. 7, CONDITION 6a

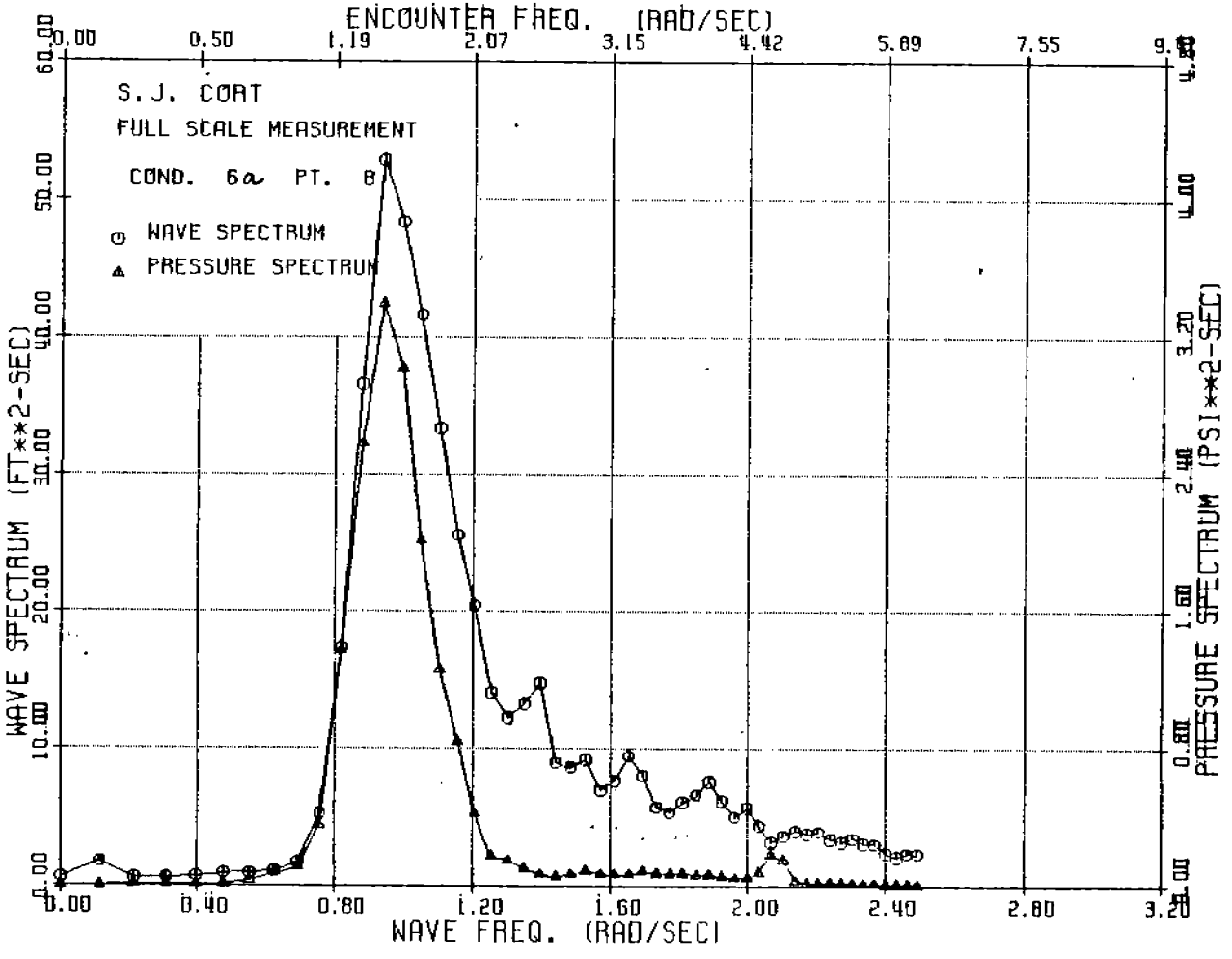

FIGURE C-17: SJ CORT WAVE AND PRESSURE SPECTRA, TAP NO. 8, CONDITION 6a

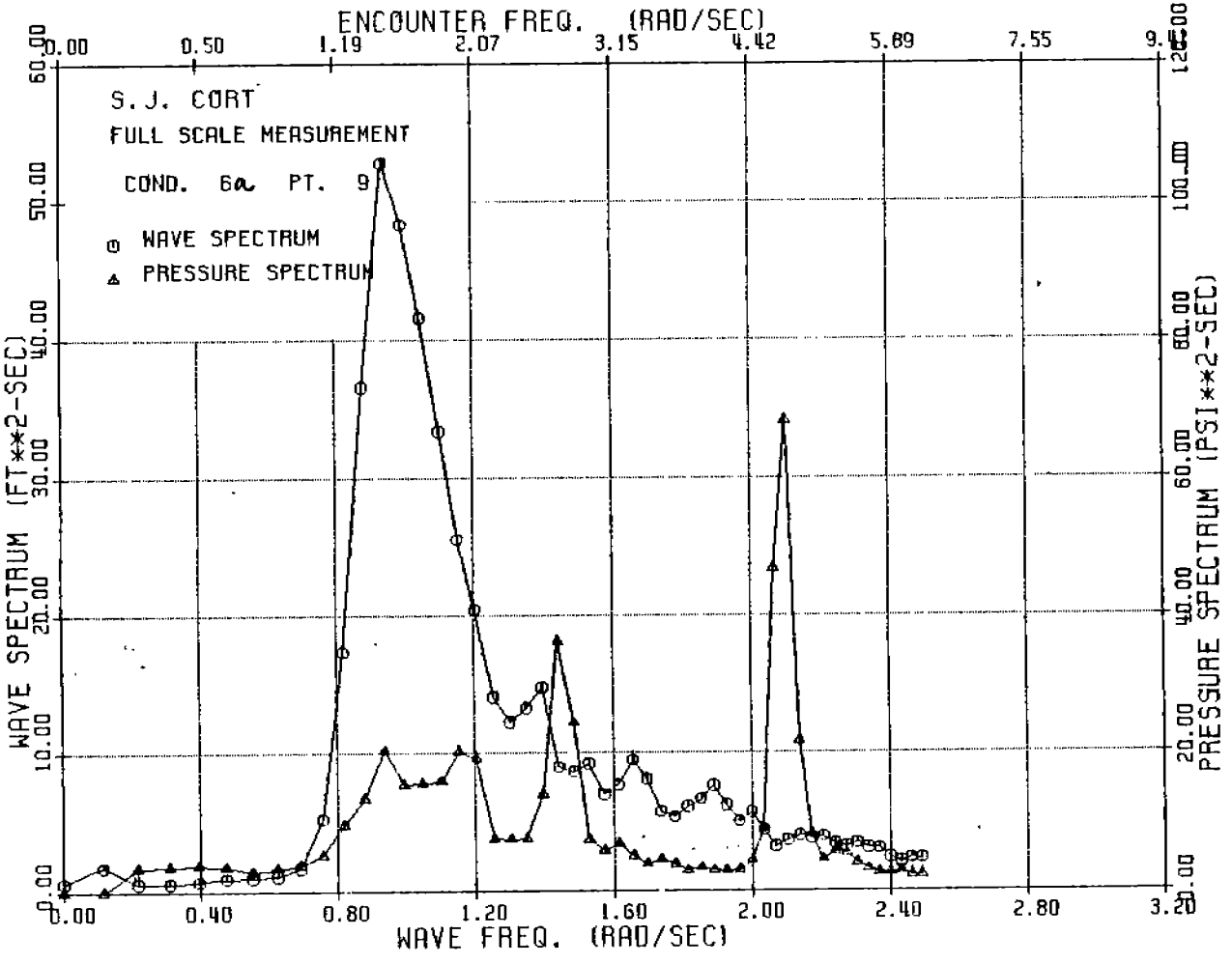

FIGURE C-18: SJ CORT WAVE AND PRESSURE SPECTRA, TAP NO. 9, CONDITION 6a

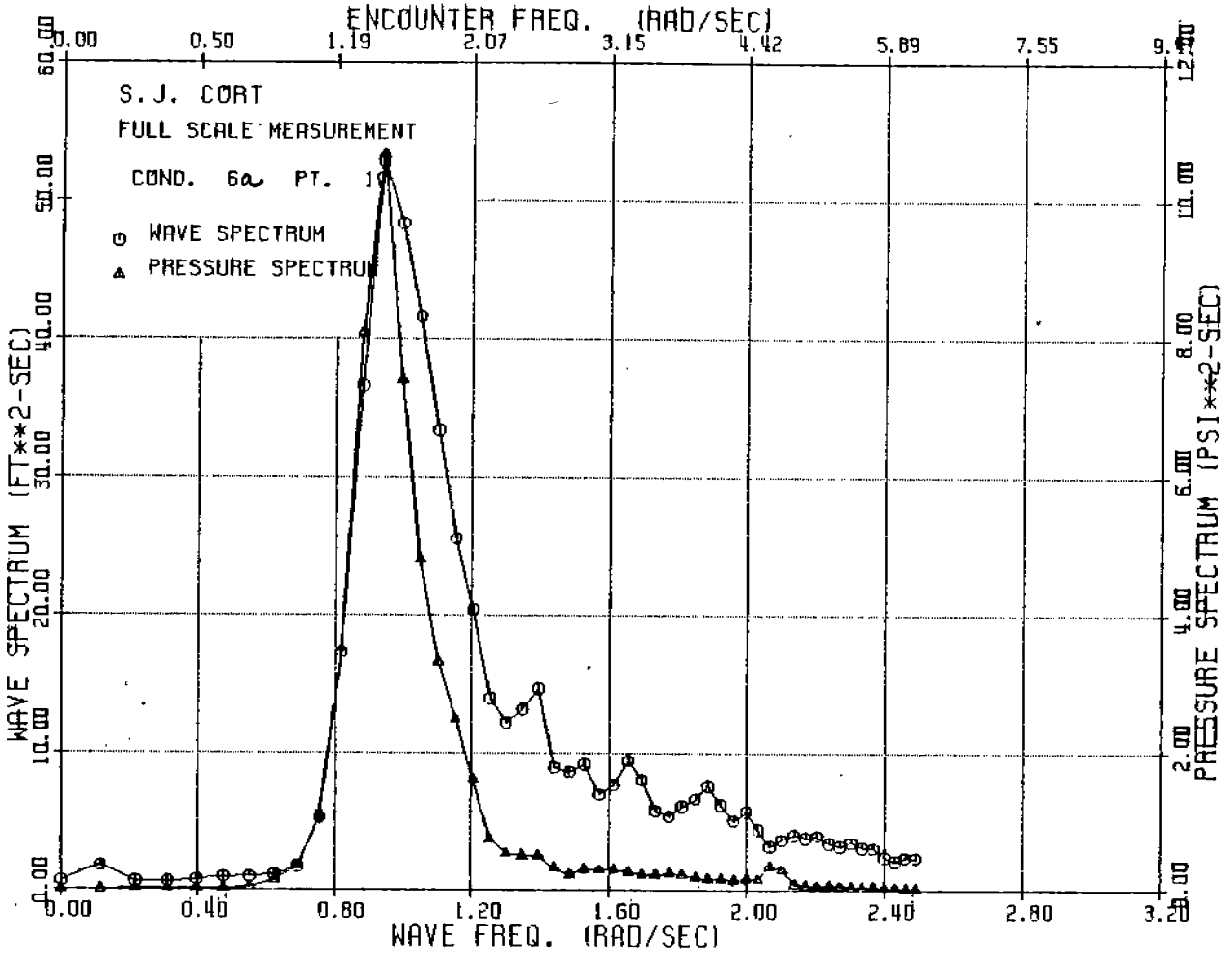

FIGURE C-19: SJ CORT WAVE AND PRESSURE SPECTRA TAP NO. 10, CONDITION 6a

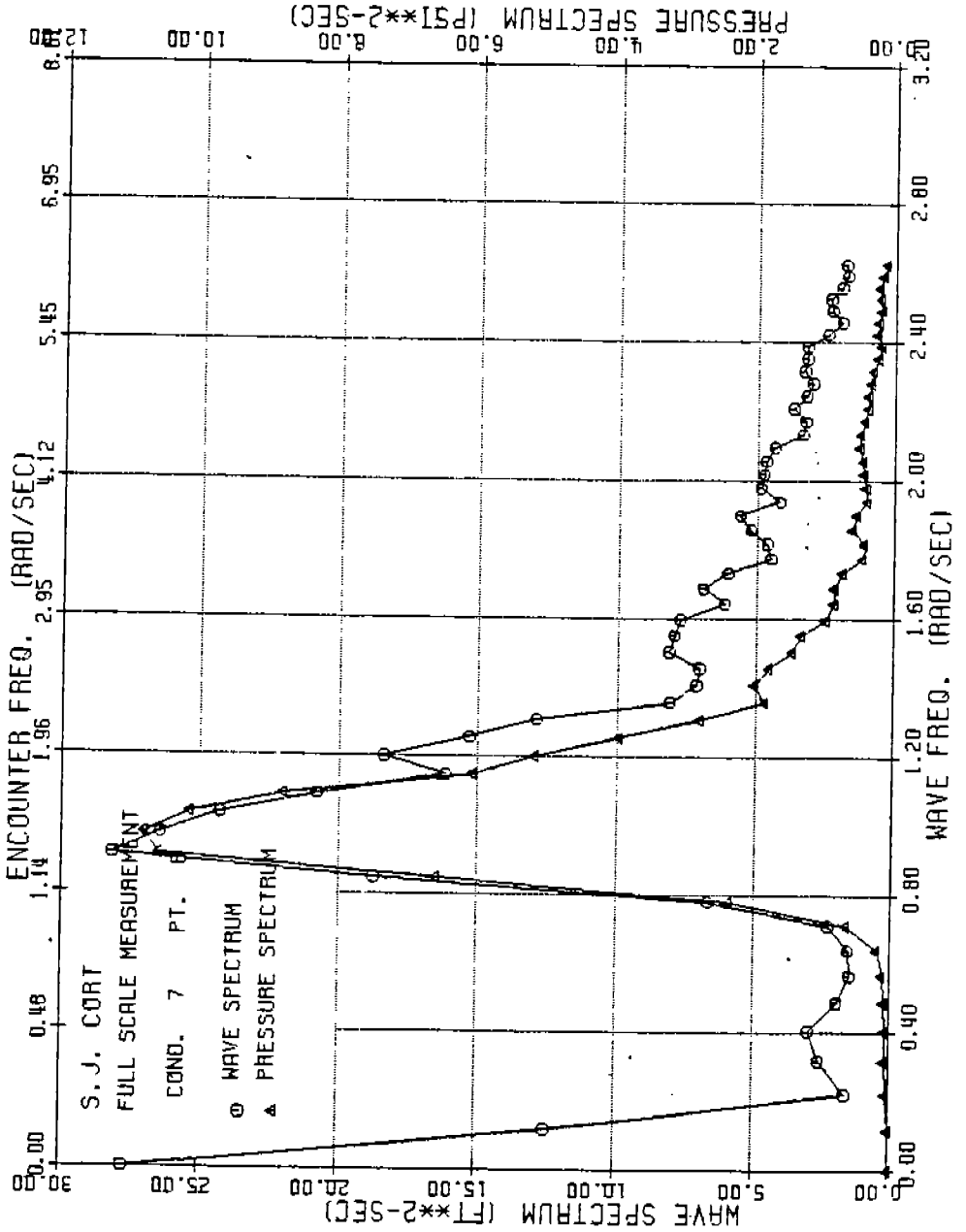

FIGURE C-20: SJ CORT WAVE AND PRESSURE SPECTRA, TAP NO. 6, CONDITION 7

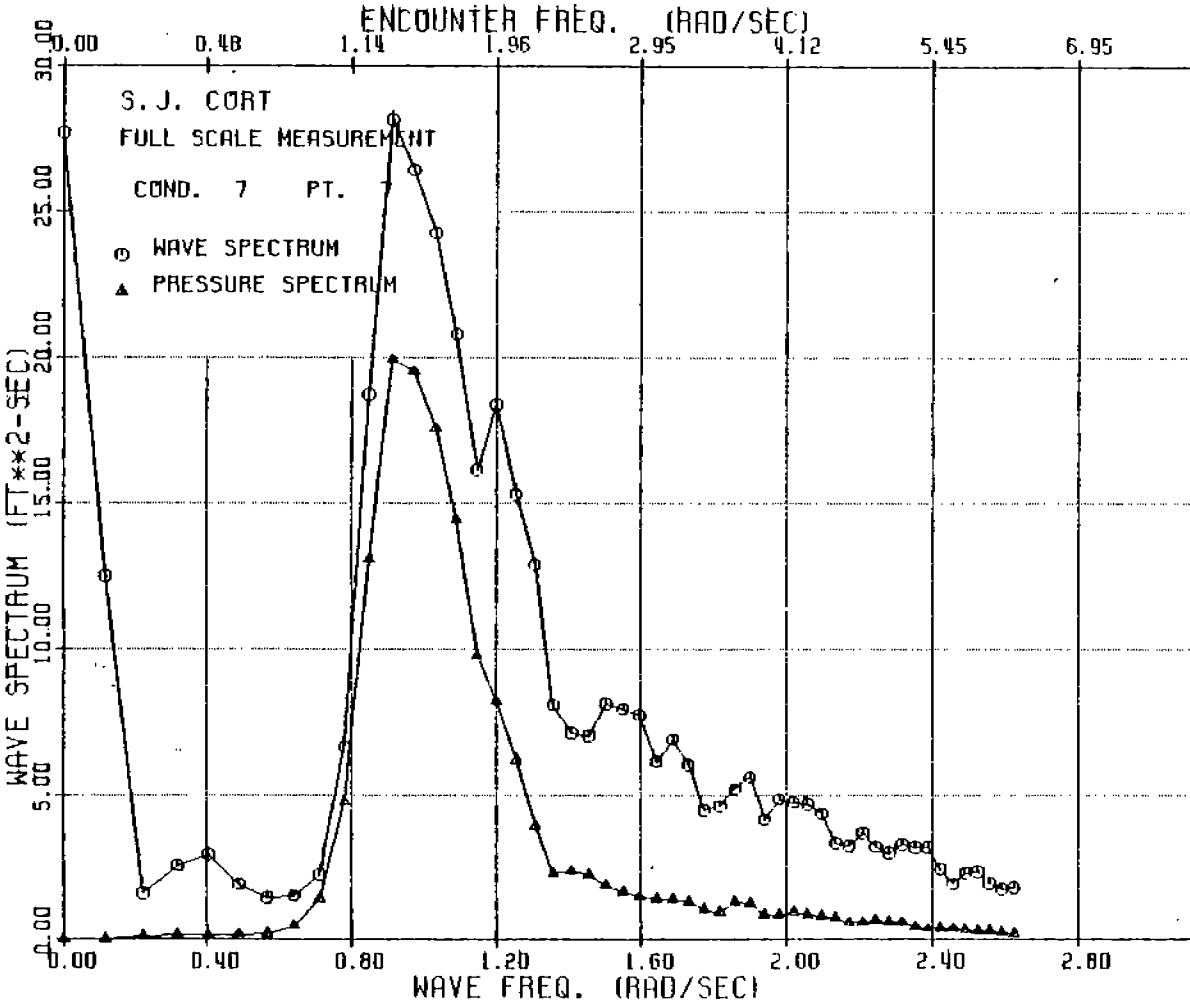

FIGURE C-21: SJ CORT WAVE AND PRESSURE SPECTRA, TAP NO. 7, CONDITIO

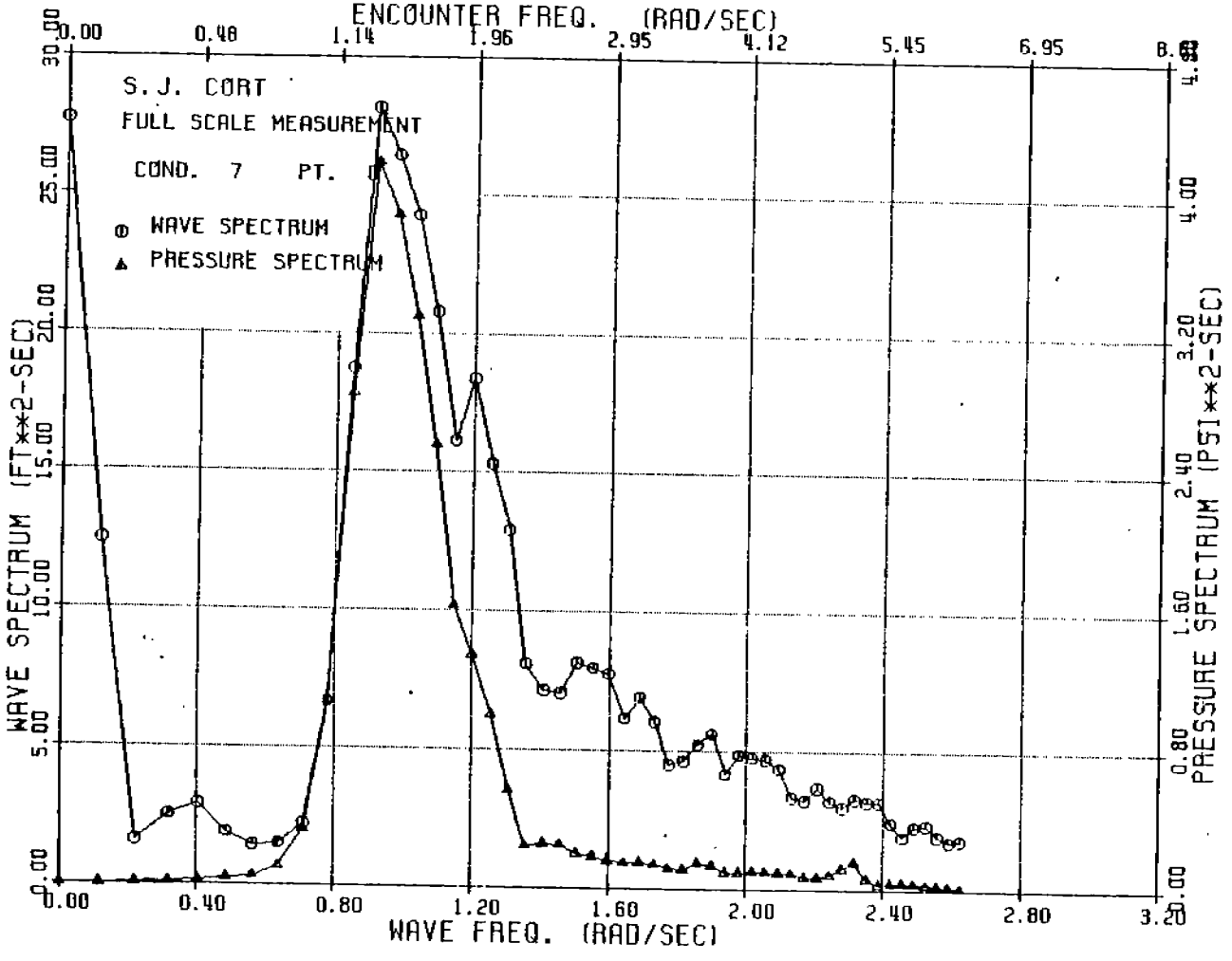

FIGURE C-22: SJ CORT WAVE AND PRESSURE SPECTRA, TAP NO. 8, CONDITION 7

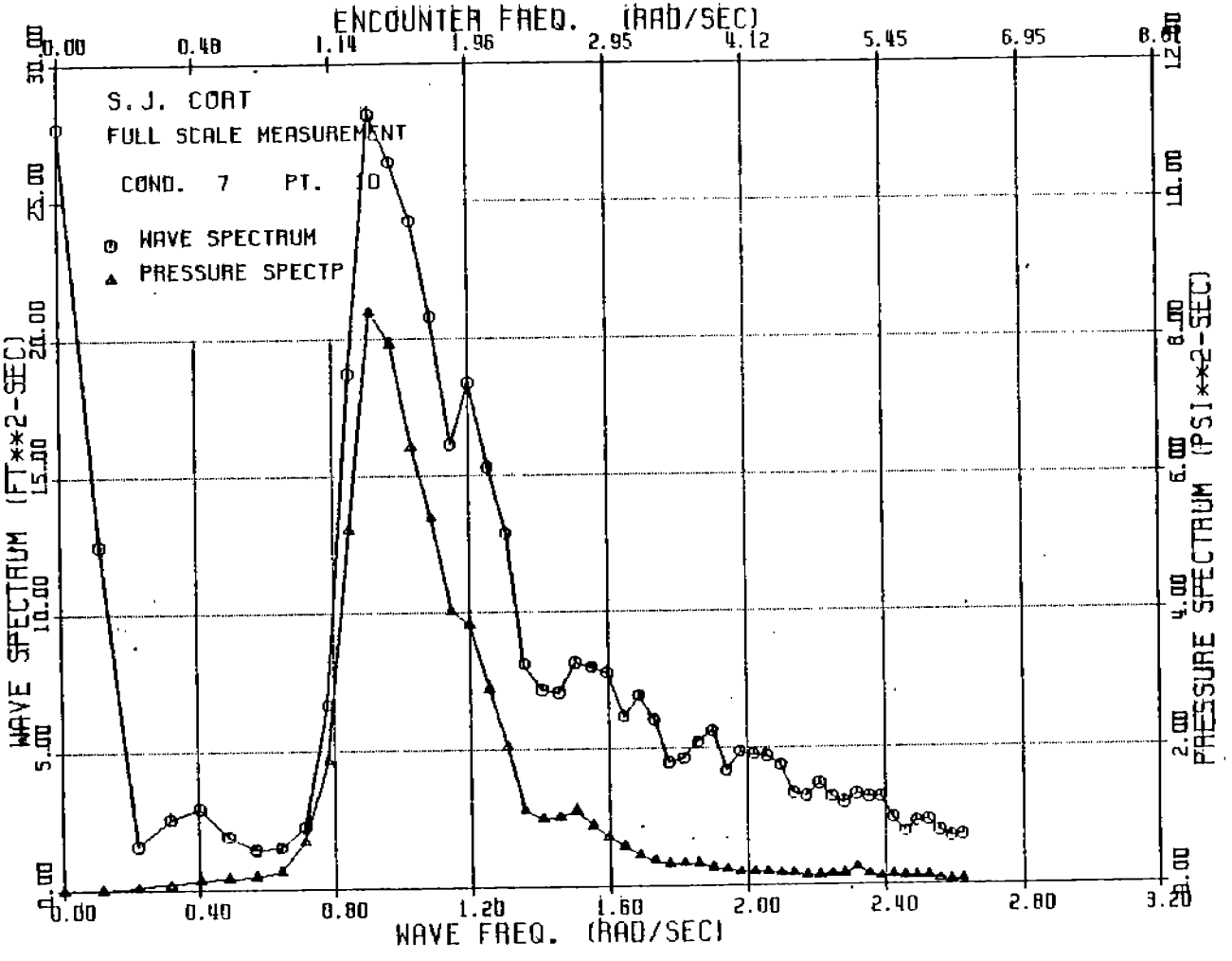

FIGURE C-23: SJ CORT WAVE AND PRESSURE SPECTRA, TAP NO. 10, CONDITION 7

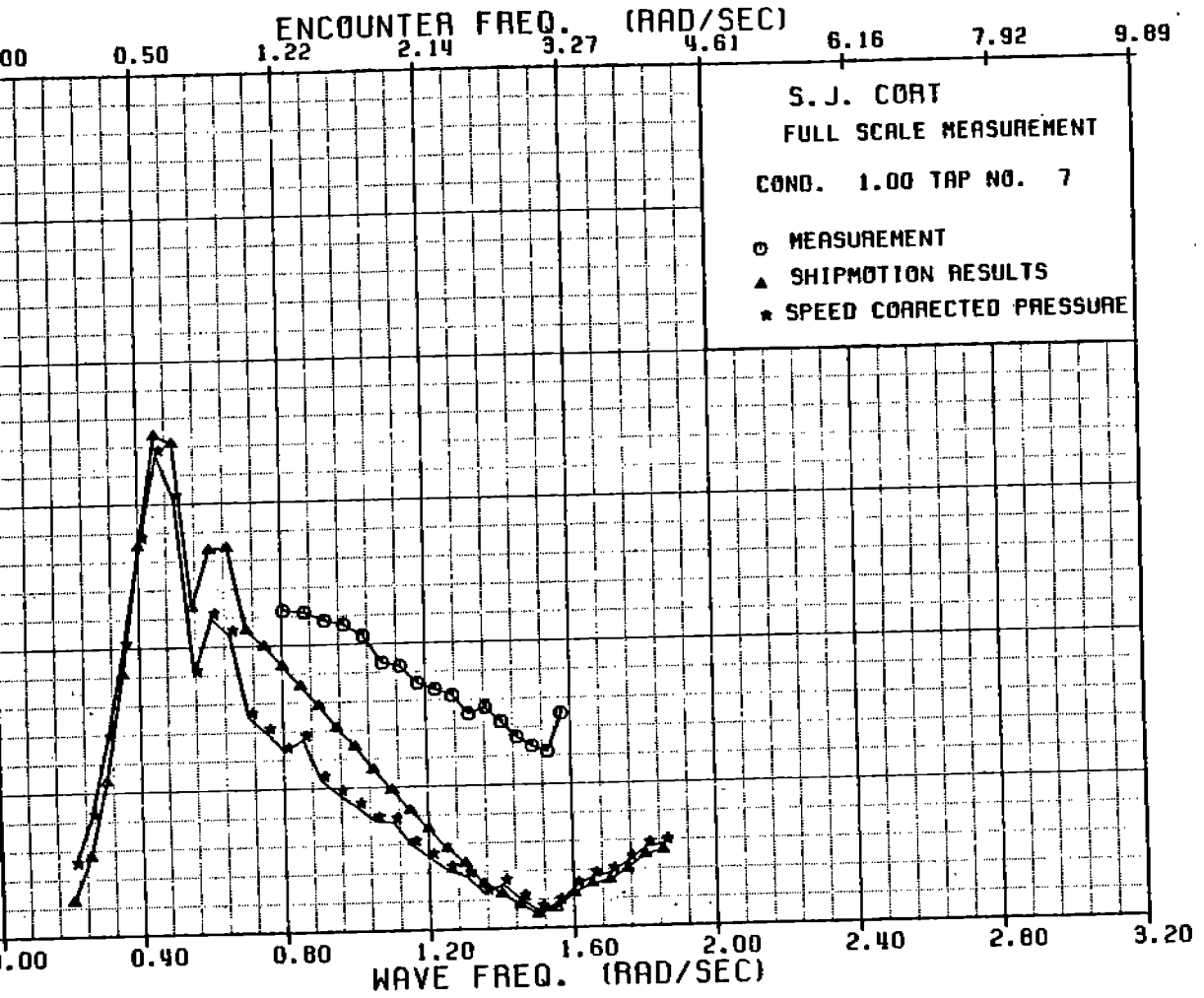

GURE C-24: SJ CORT PRESSURE TRANSFER FUNCTION, TAP NO. 7, CONDITION 1

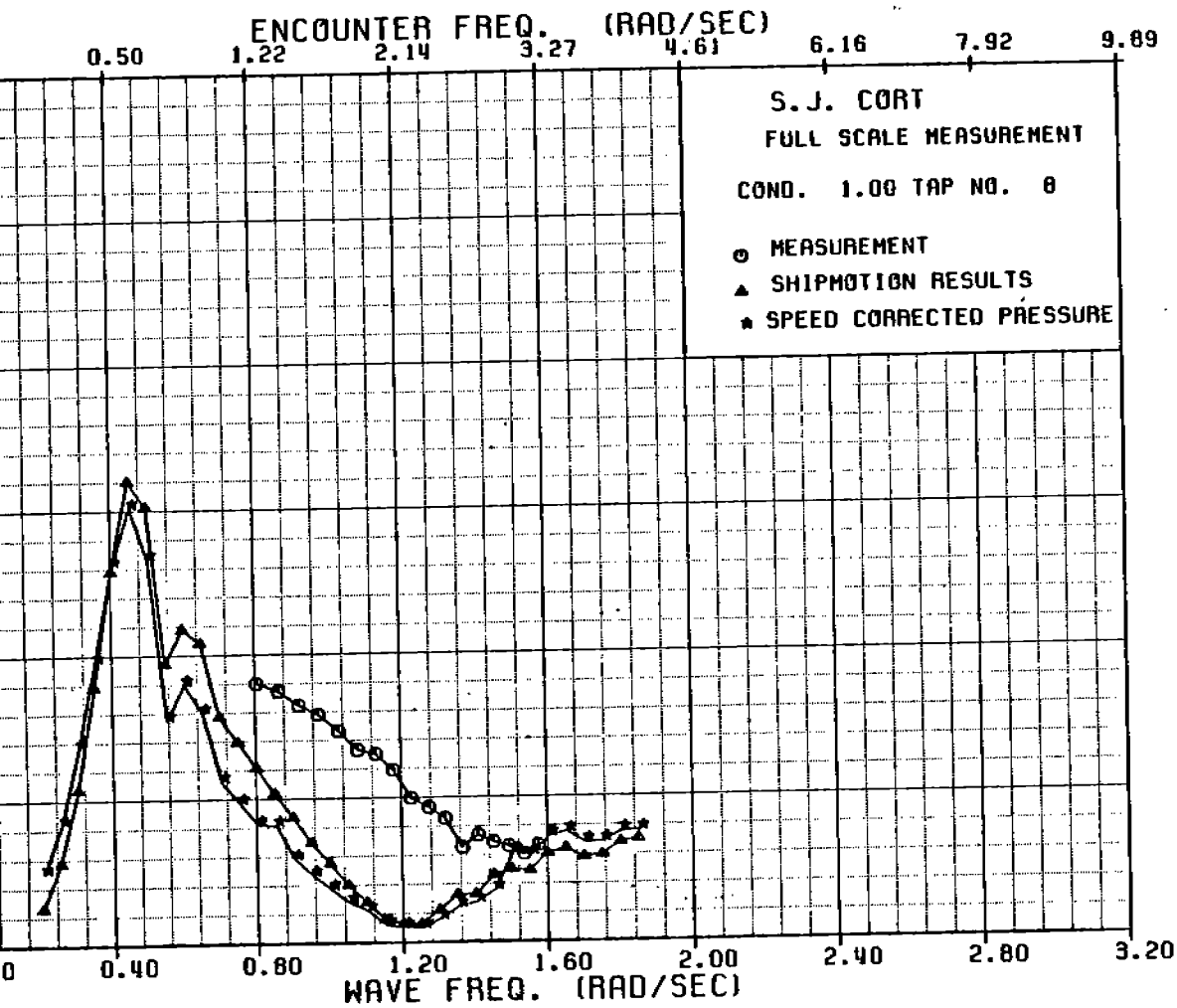

URE C-25: SJ CORT PRESSURE TRANSFER FUNCTION, TAP NO. 8, CONDITION 1

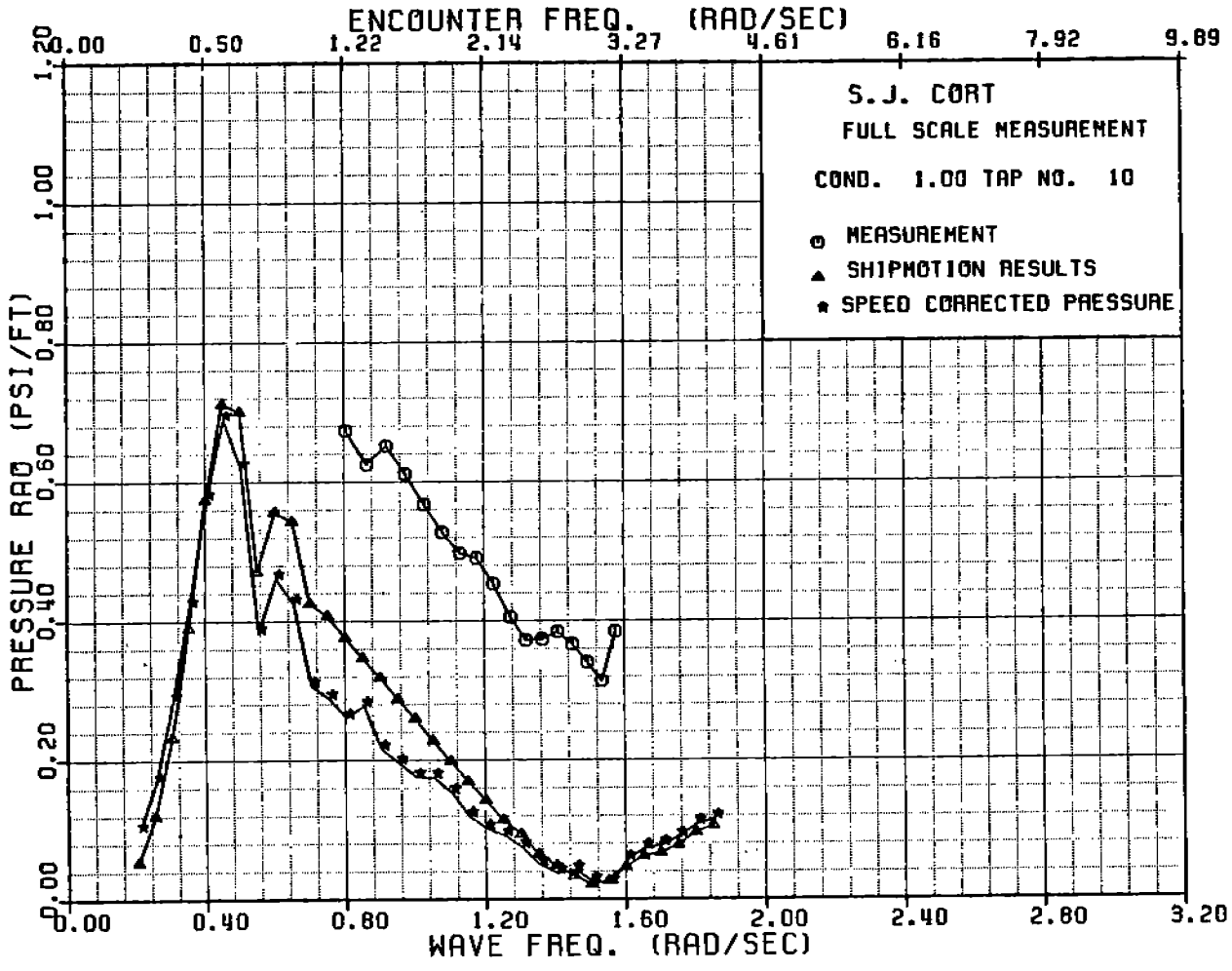

FIGURE C-26: SJ CORT PRESSURE TRANSFER FUNCTION, TAP NO. 10, CONDITION 1

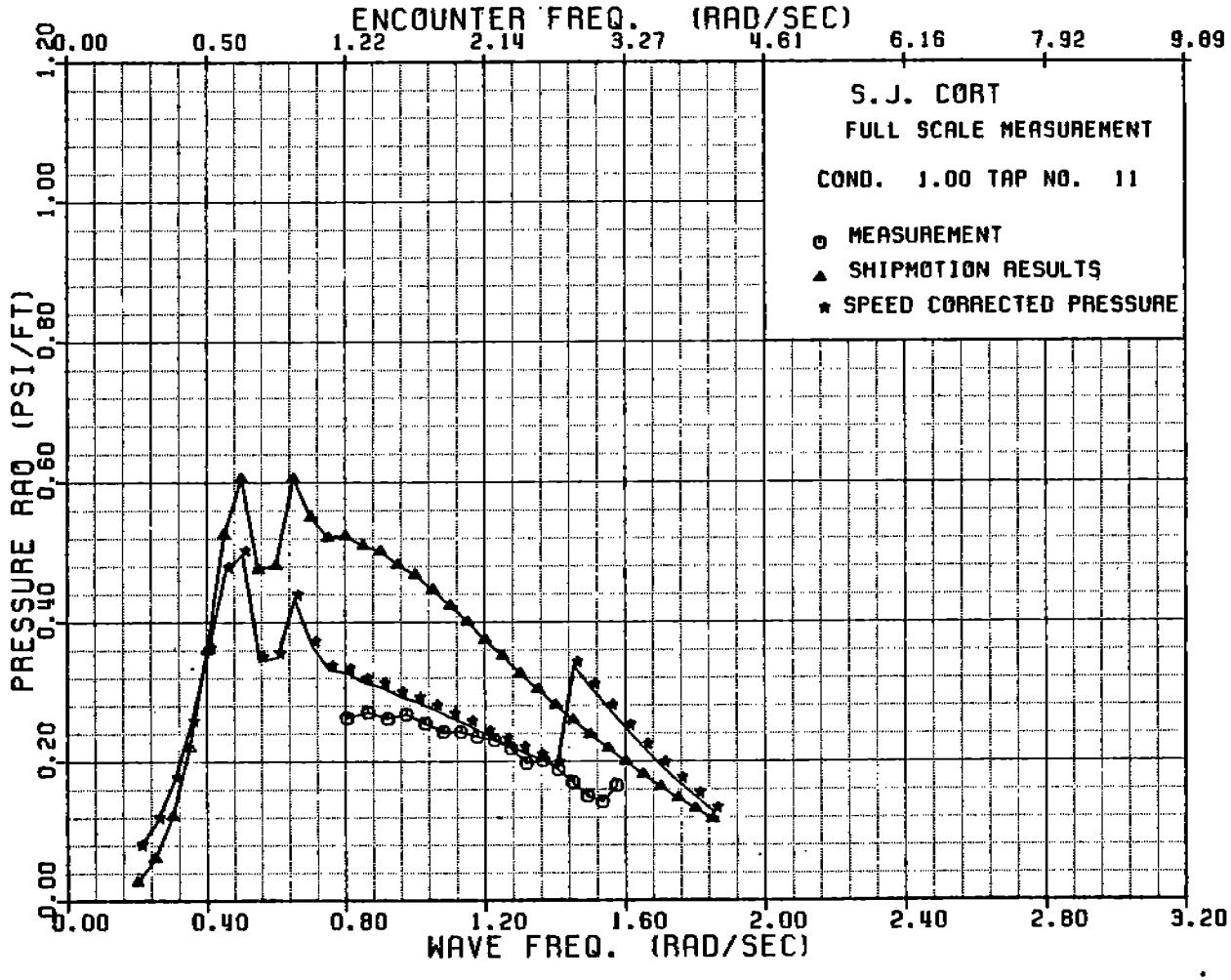

FIGURE C-27: SJ CORT PRESSURE TRANSFER FUNCTION, TAP NO. 11, CONDITION 1

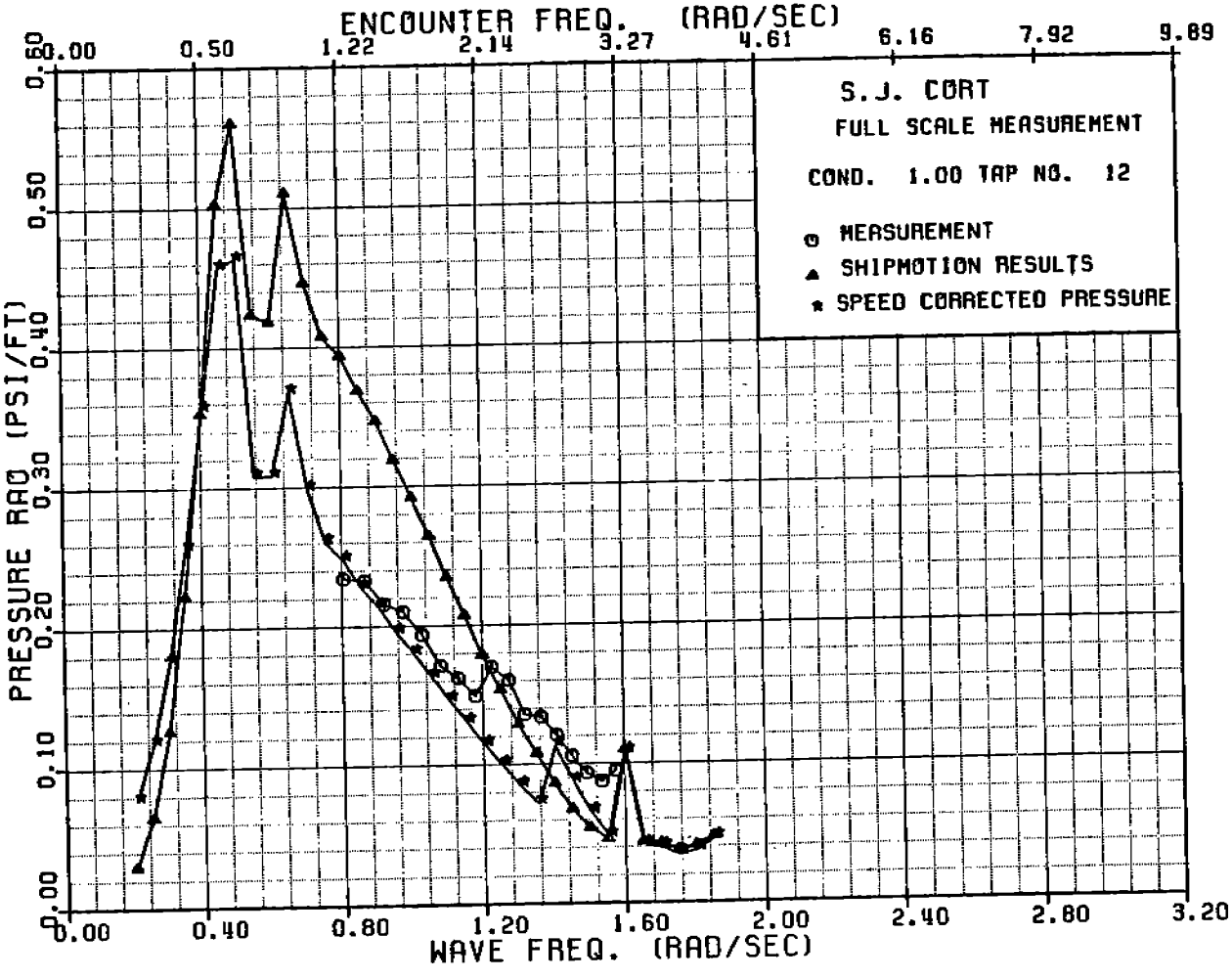

FIGURE C-28: SJ CORT PRESSURE TRANSFER FUNCTION, TAP NO. 12, CONDITION 1

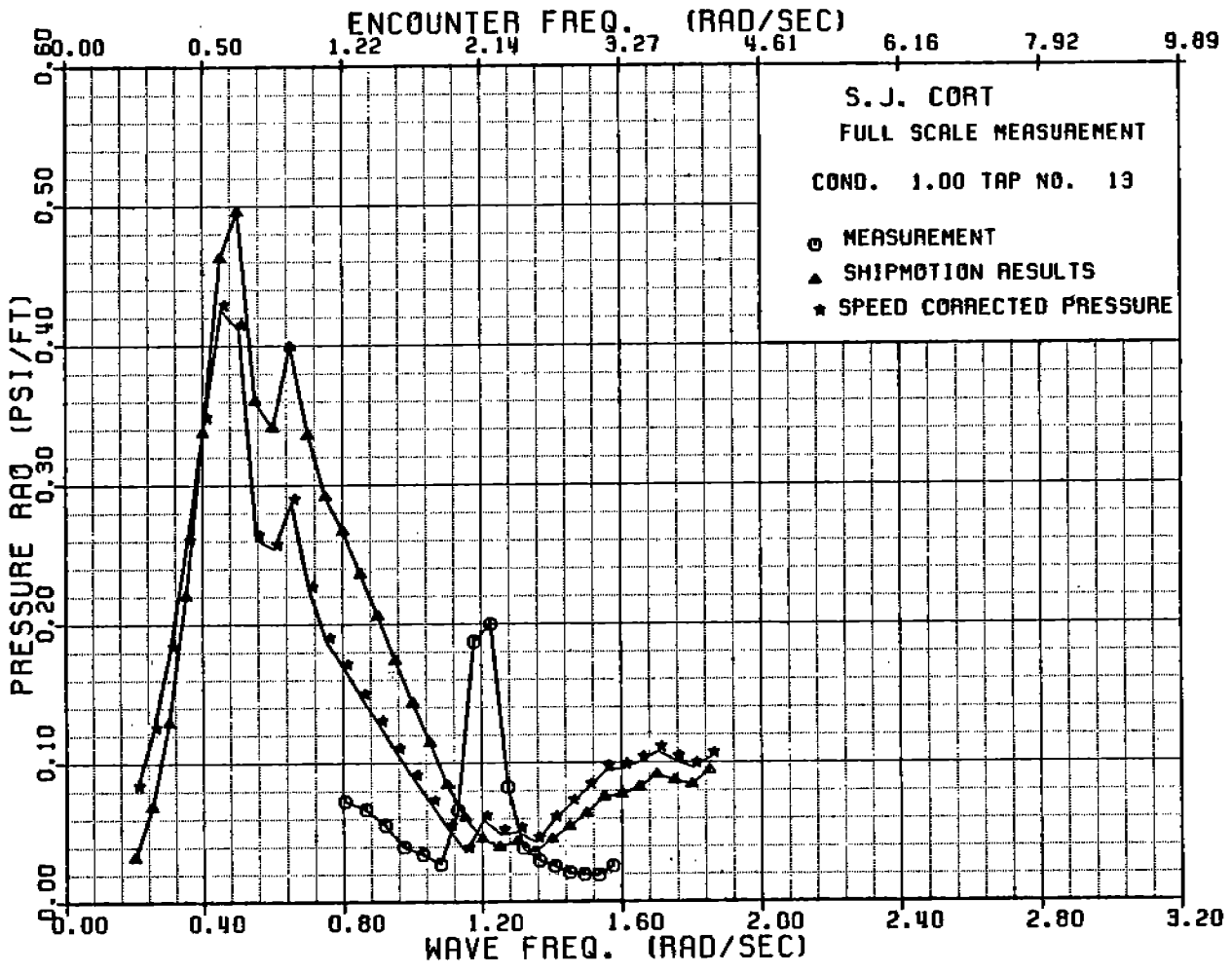

FIGURE C-29: SJ CORT PRESSURE TRANSFER FUNCTION, TAP NO. 13, CONDITION 1

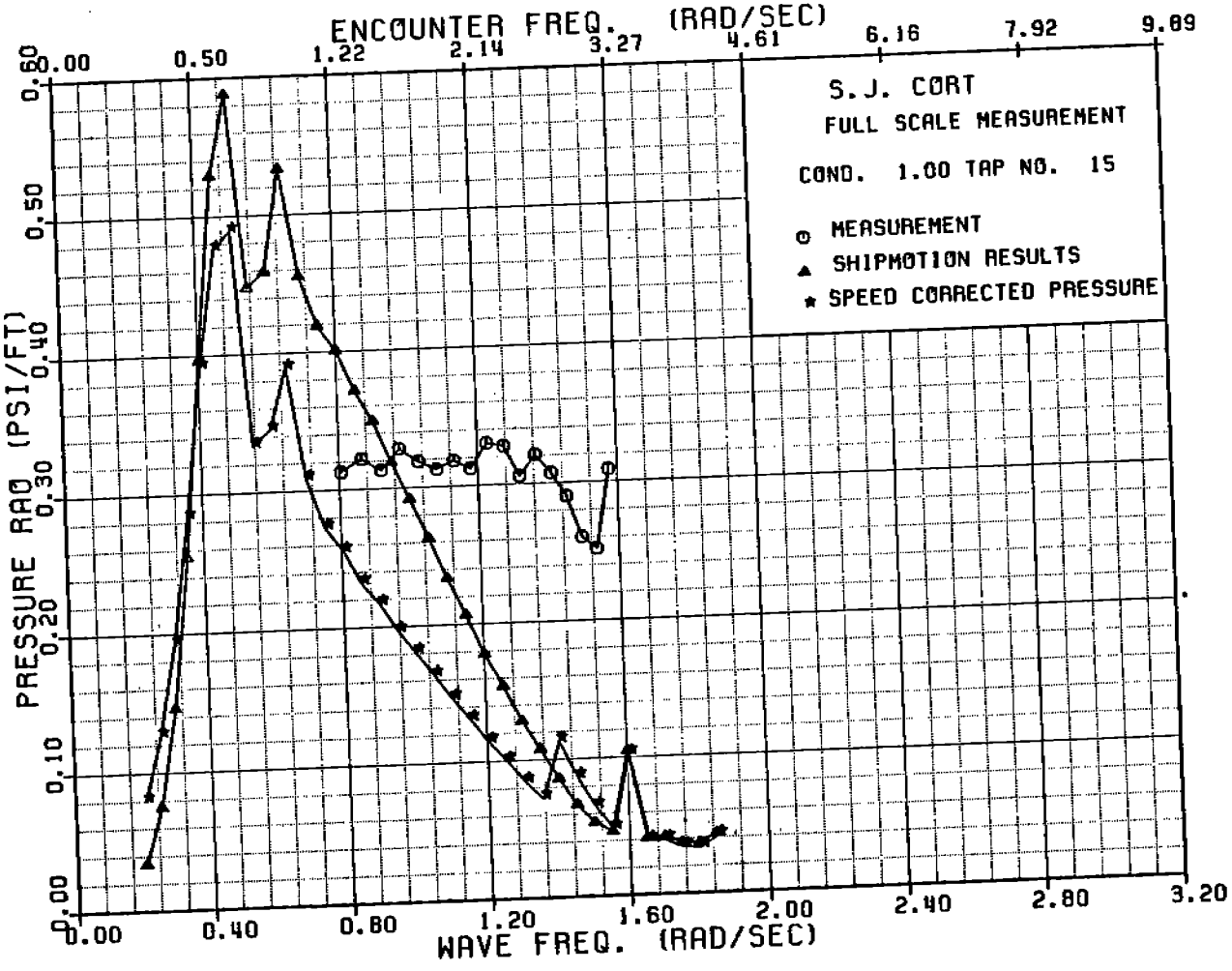

FIGURE C-30: SJ CORT PRESSURE TRANSFER FUNCTION, TAP NO. 15, CONDITION 1

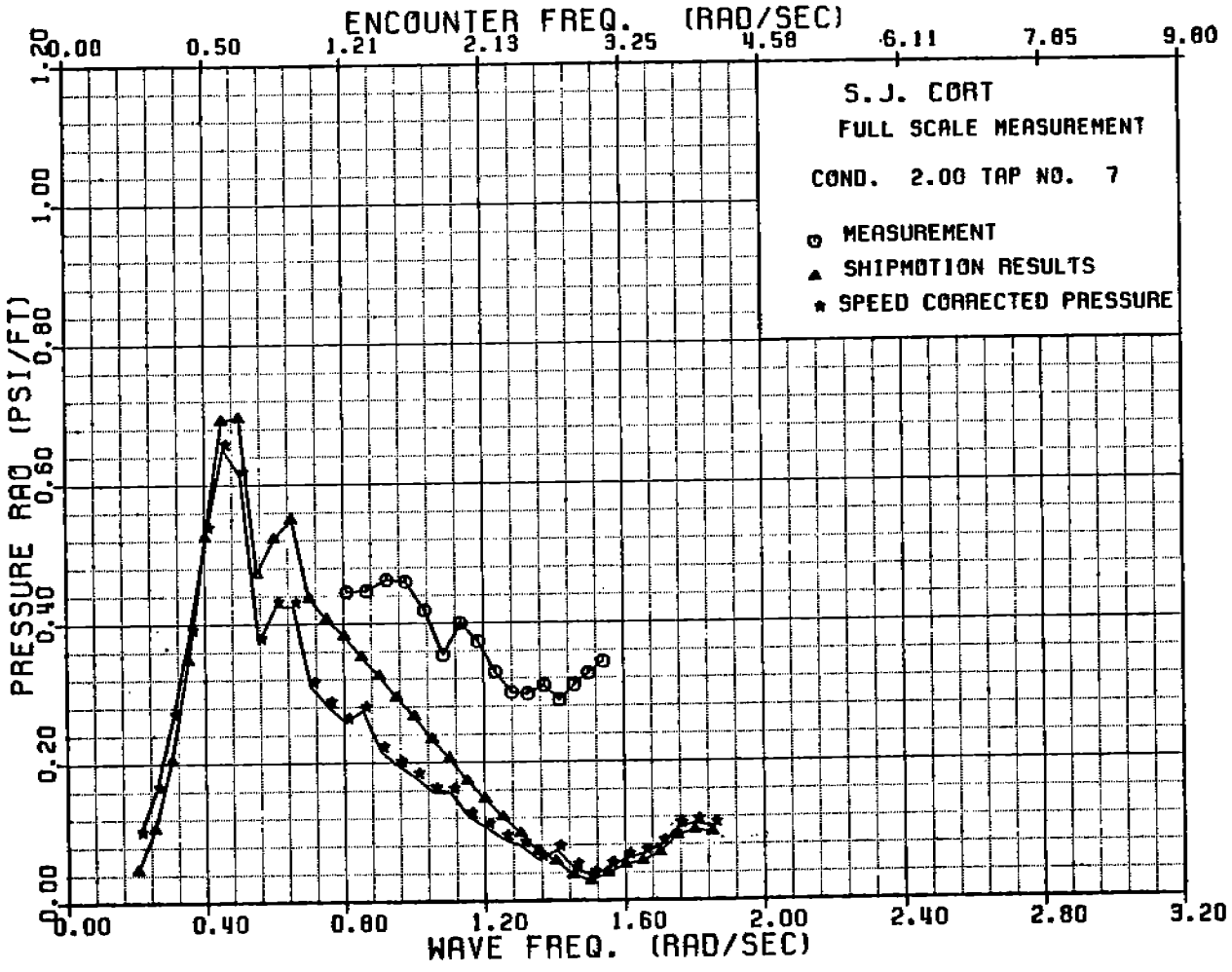

FIGURE C-31: SJ CORT PRESSURE TRANSFER FUNCTION, TAP NO. 7, CONDITION 2

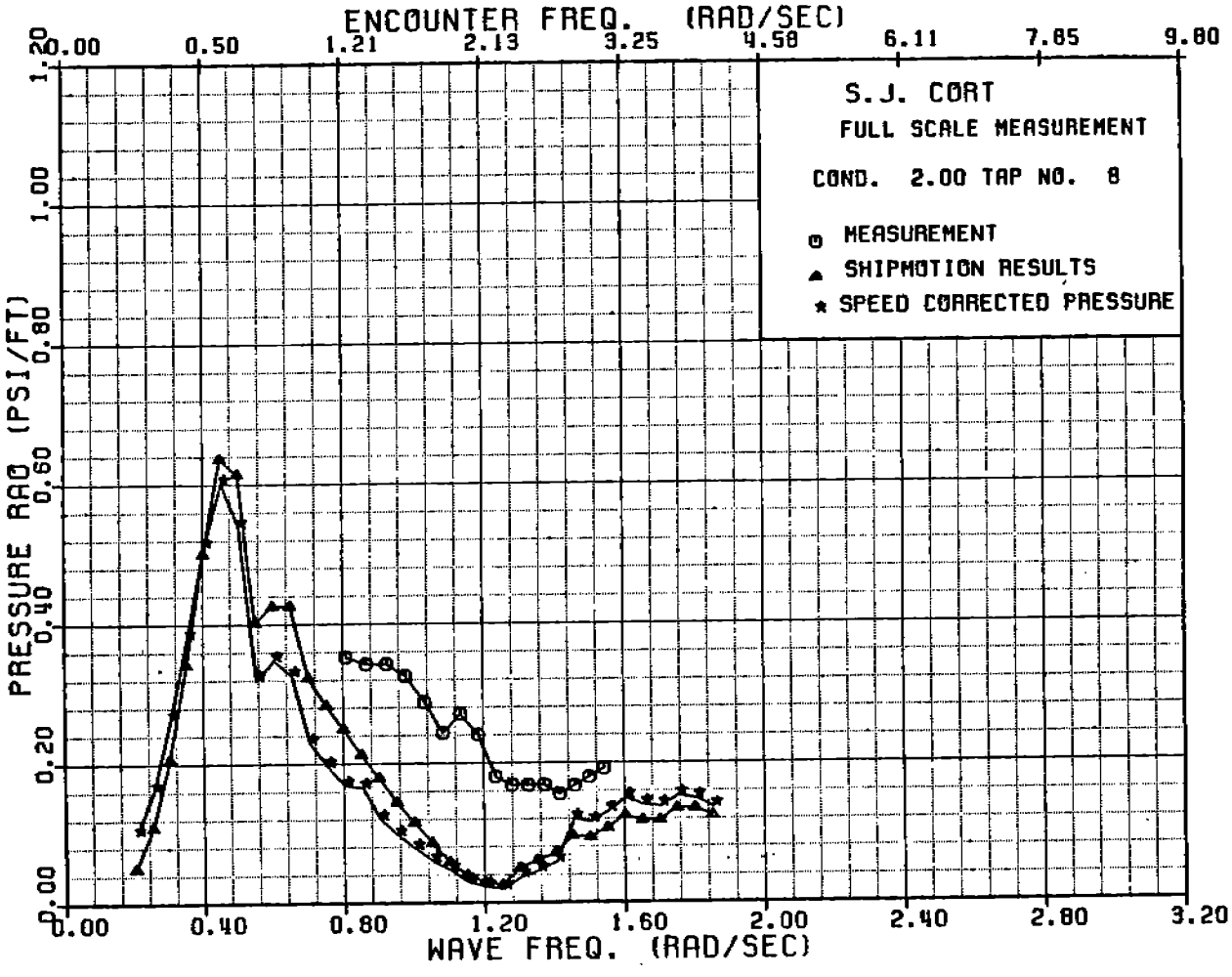

FIGURE C-32: SJ CORT PRESSURE TRANSFER FUNCTION, TAP NO. 8, CONDITION 2

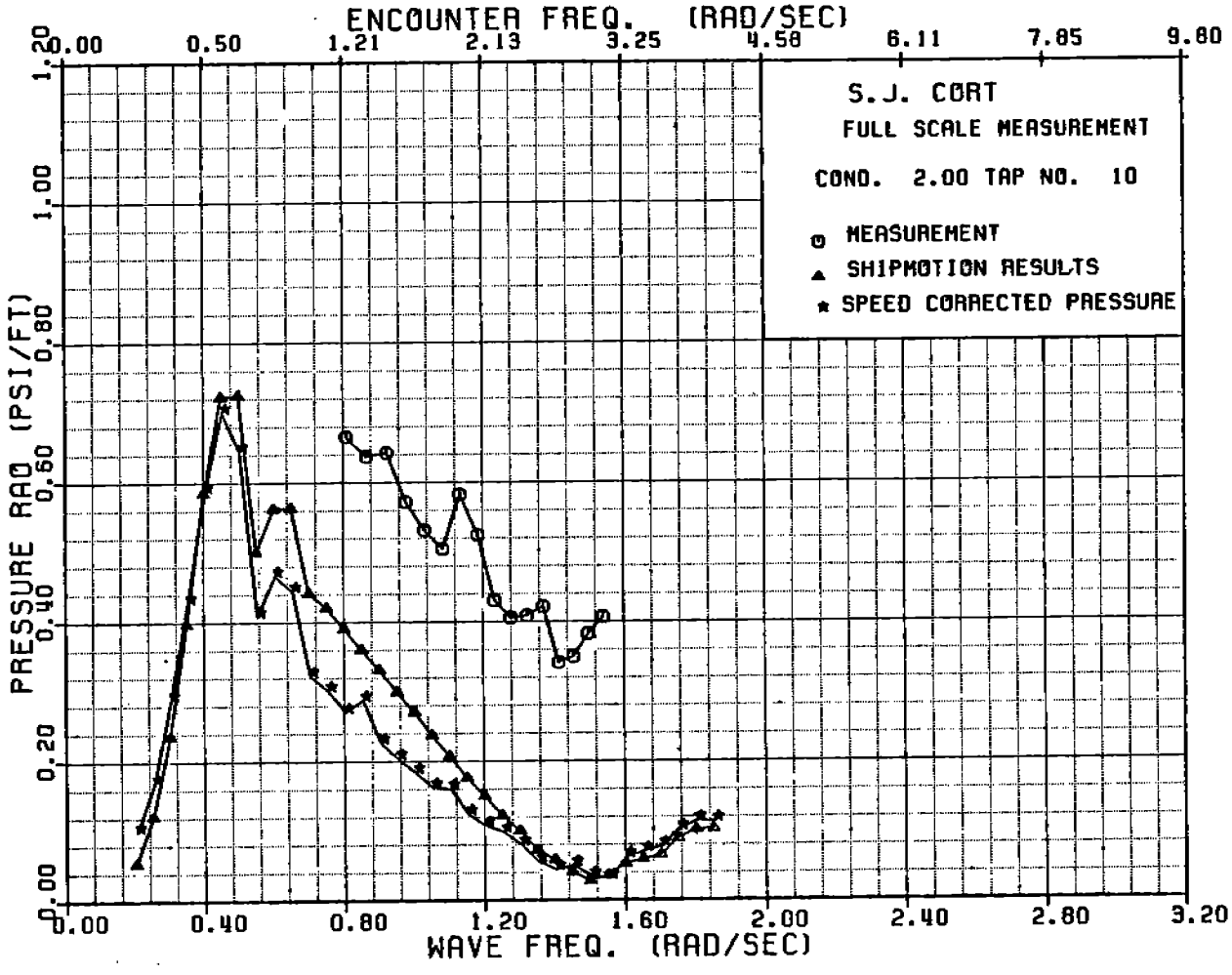

FIGURE C-33: SJ CORT PRESSURE TRANSFER FUNCTION, TAP NO. 10, CONDITION 2

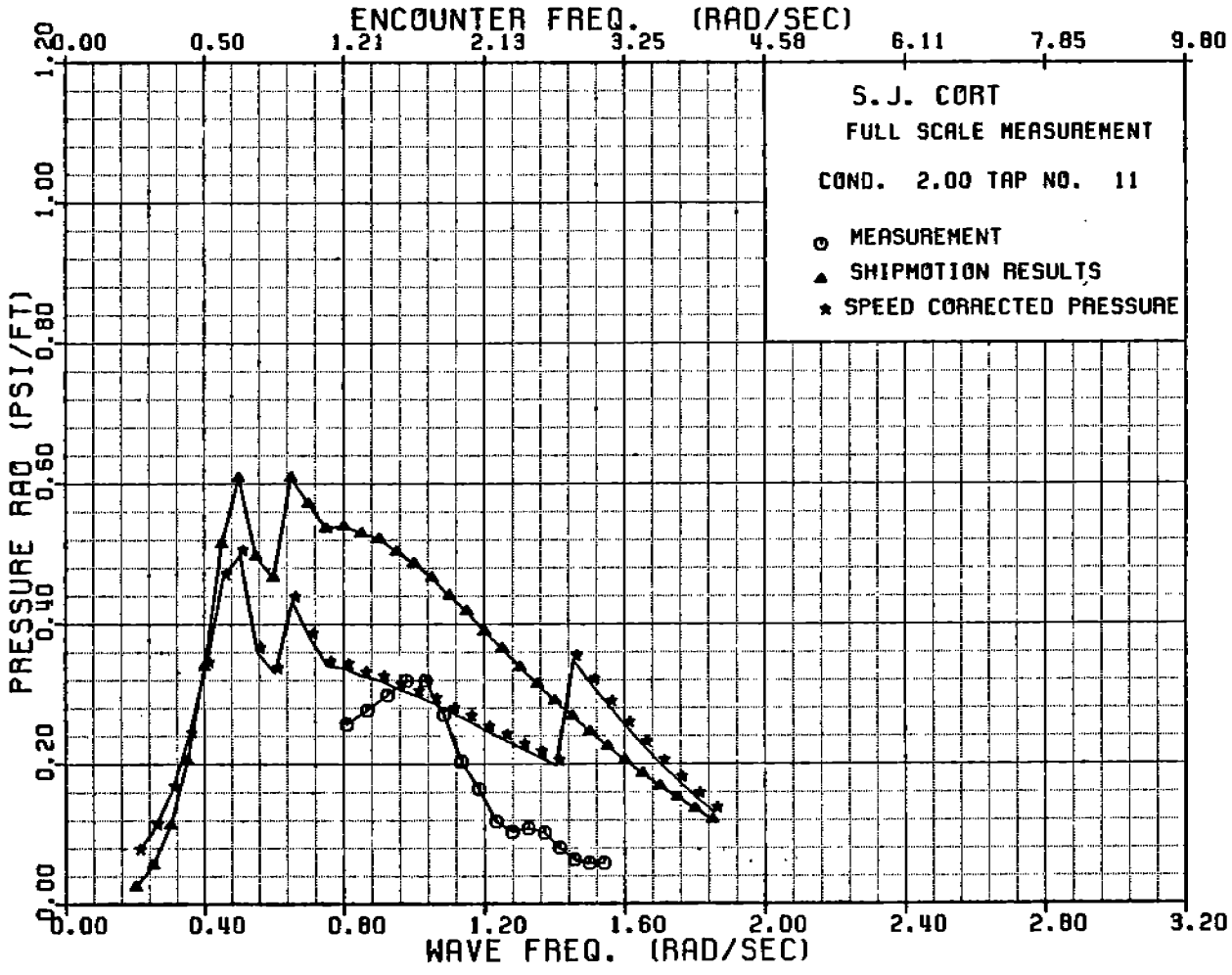

FIGURE C-34: SJ CORT PRESSURE TRANSFER FUNCTION, TAP NO. 11, CONDITION 2

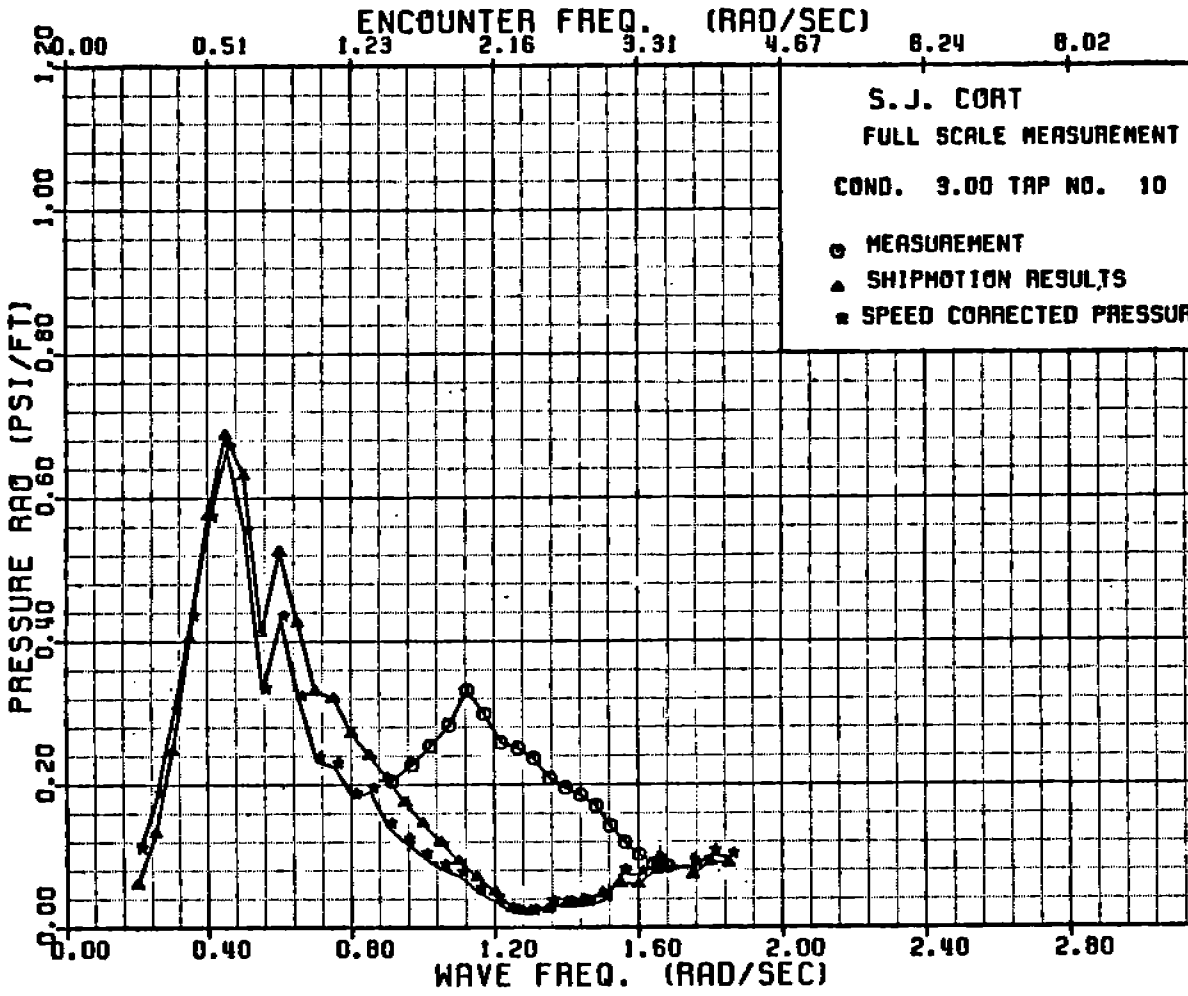

FIGURE C-35: SJ CORT PRESSURE TRANSFER FUNCTION, TAP NO. 10, CONDITI

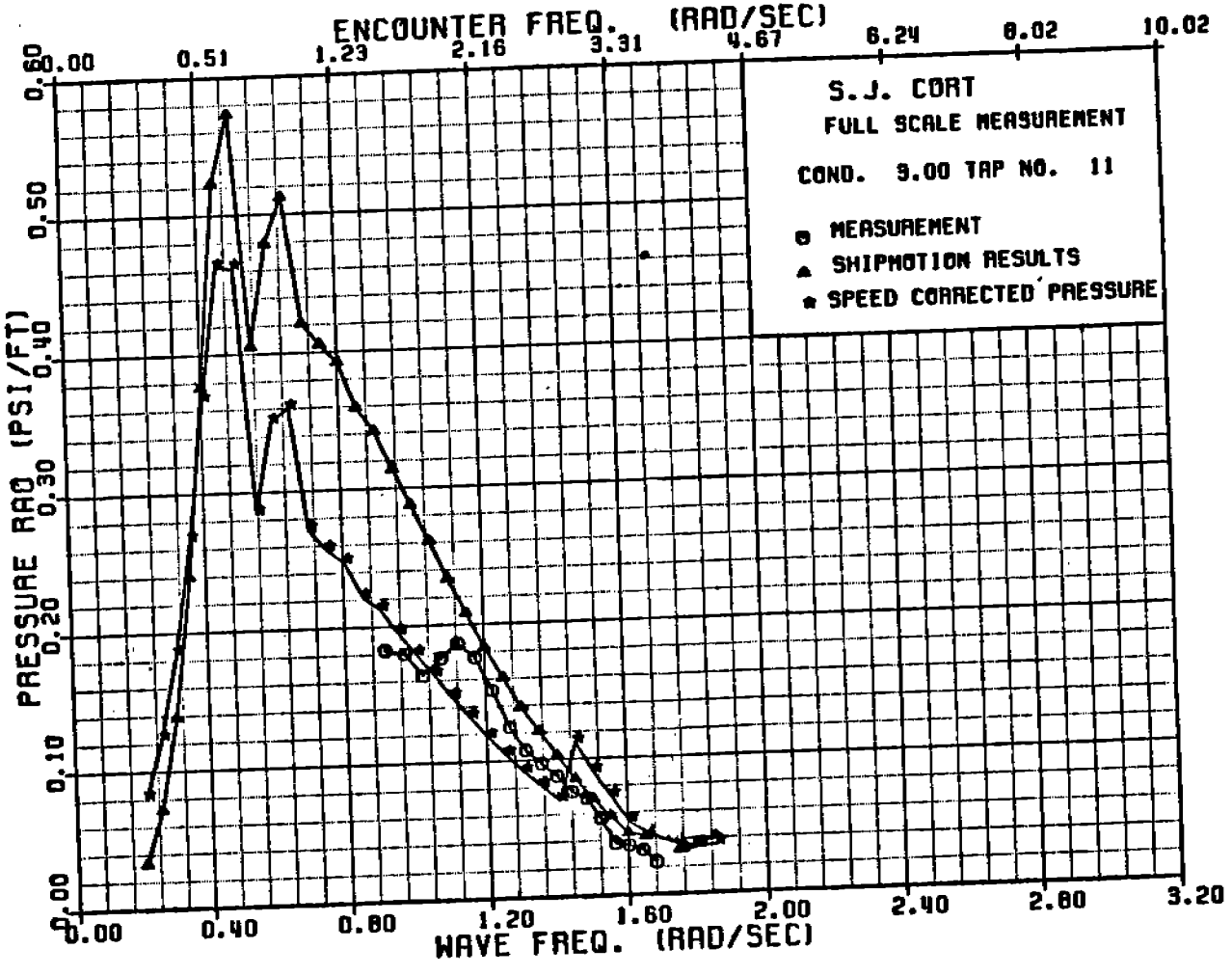

FIGURE C-36: SJ CORT PRESSURE TRANSFER FUNCTION, TAP NO. 11, CONDITION 3

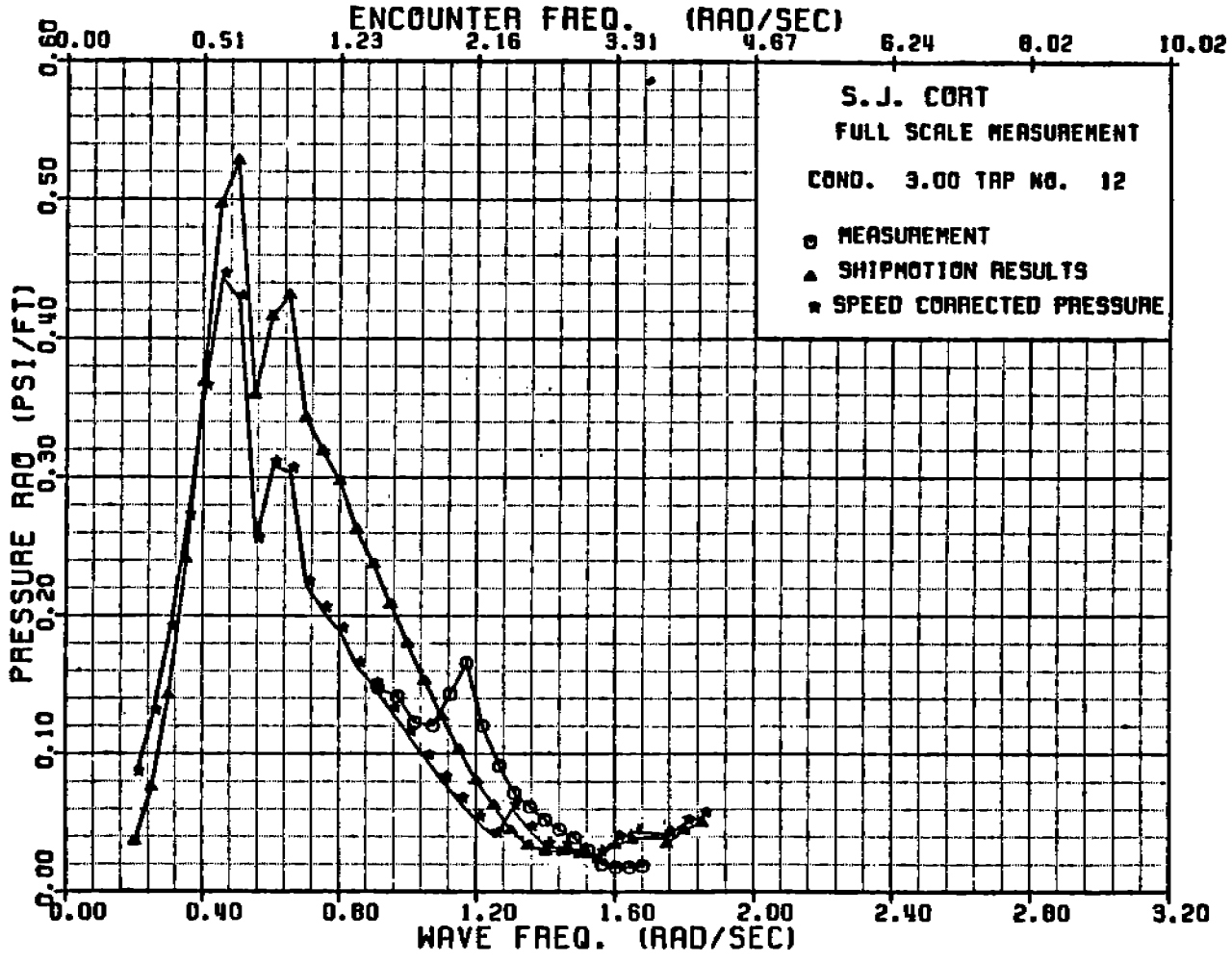

FIGURE C-37: SJ CORT PRESSURE TRANSFER FUNCTION, TAP NO. 12, CONDITION 3

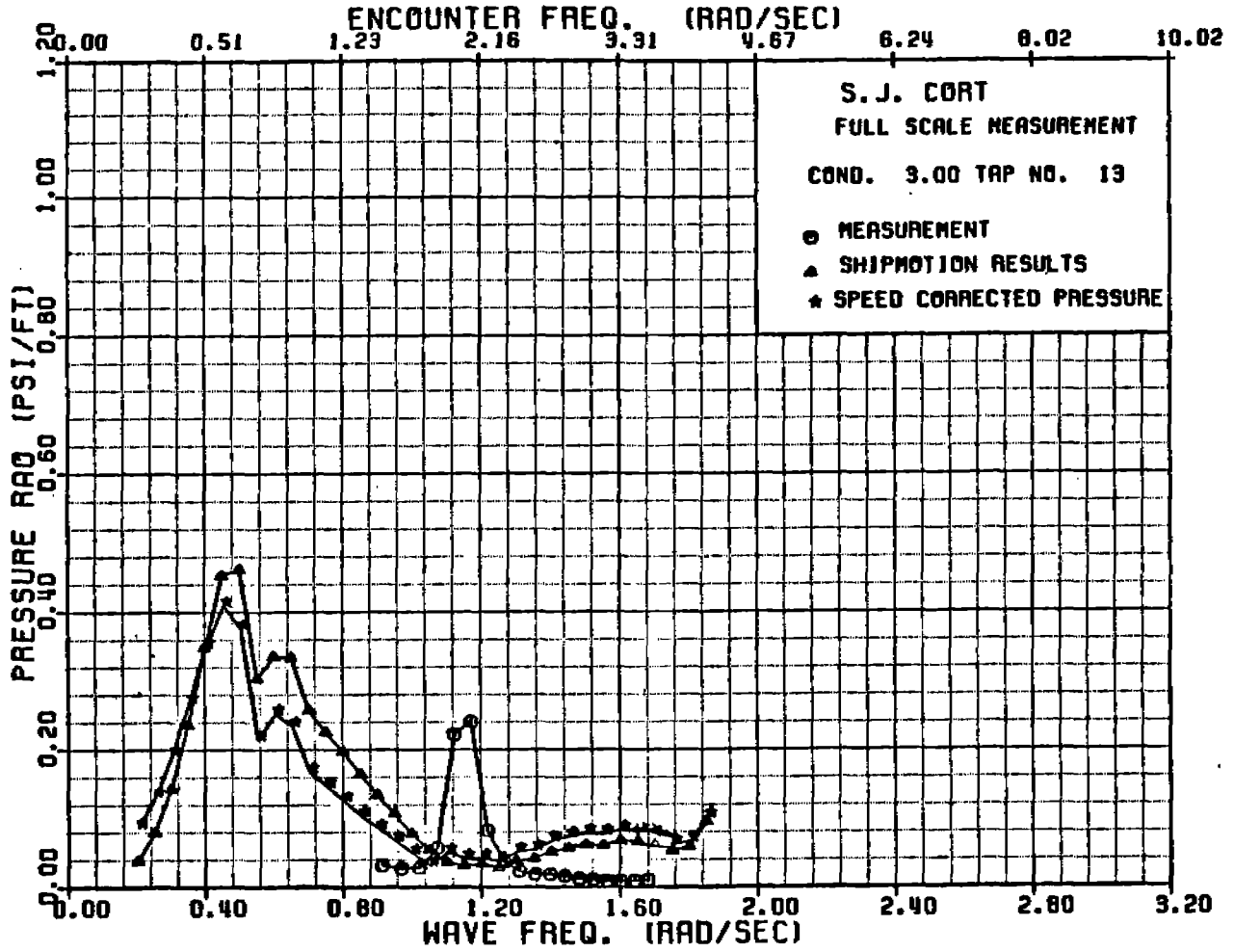

FIGURE C-38: SJ CORT PRESSURE TRANSFER FUNCTION, TAP NO. 13, CONDITION 3

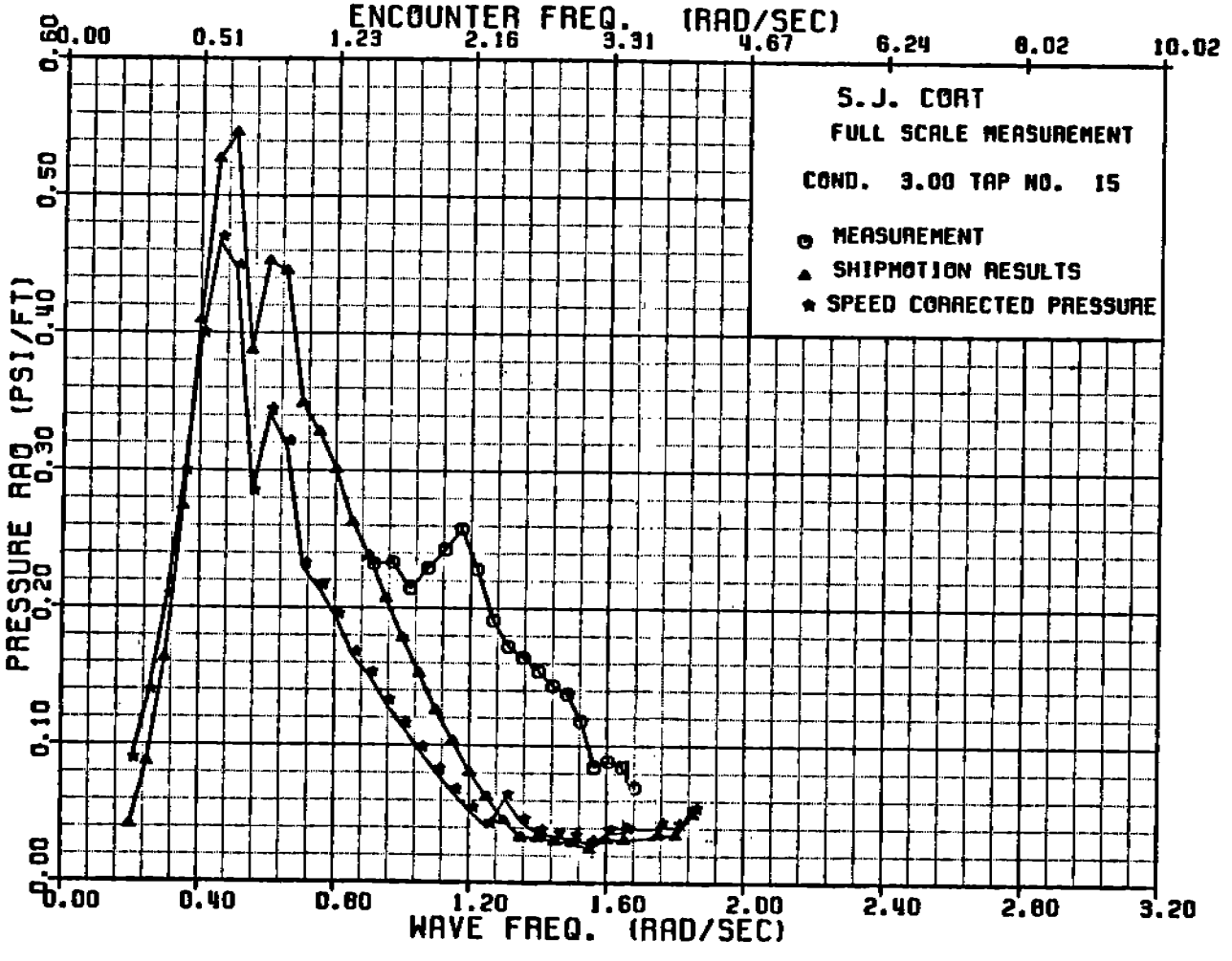

FIGURE C-39: SJ CORT PRESSURE TRANSFER FUNCTION, TAP NO. 15, CONDITION 3

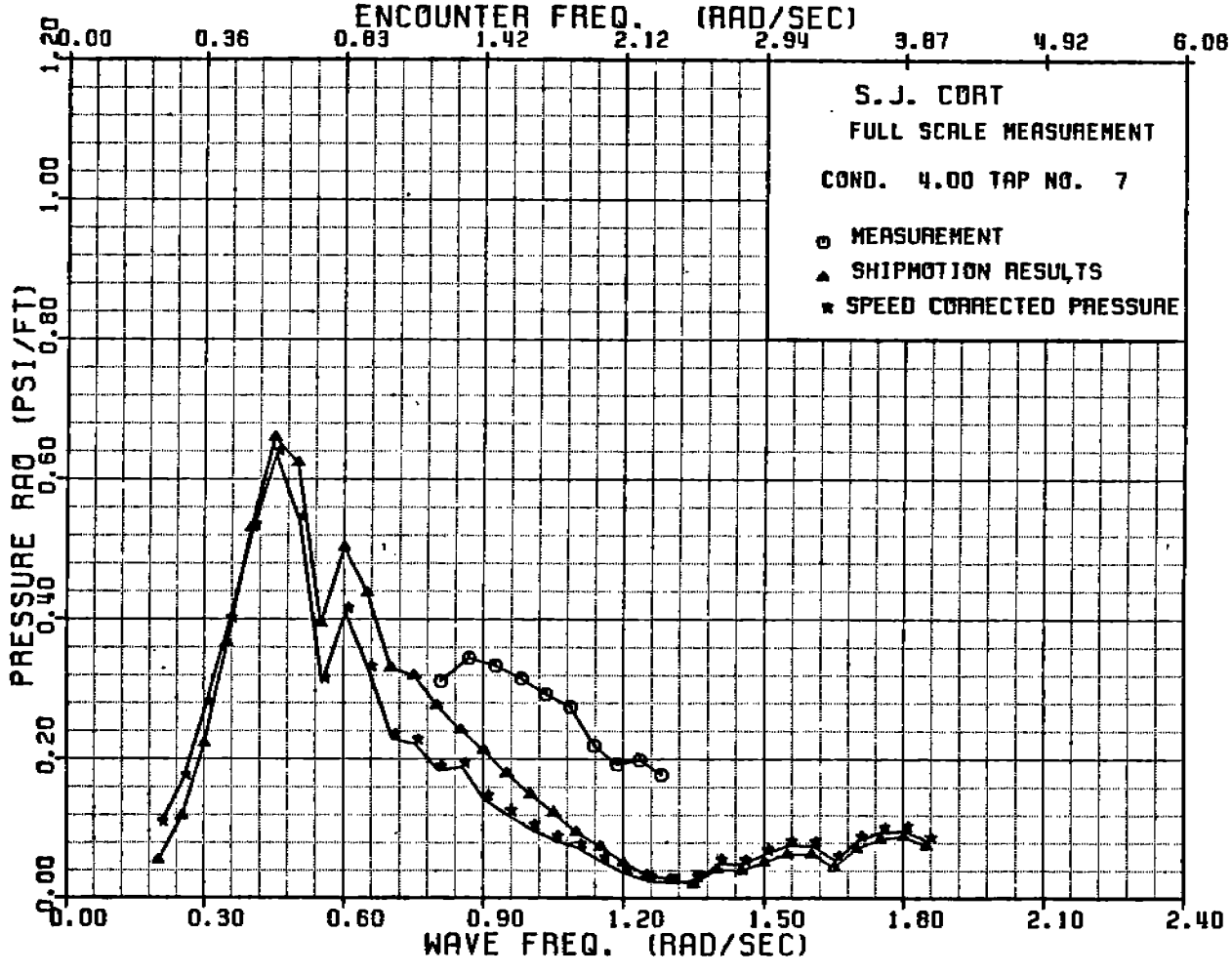

FIGURE C-40: SJ CORT PRESSURE TRANSFER FUNCTION, TAP NO. 7, CONDITION 4

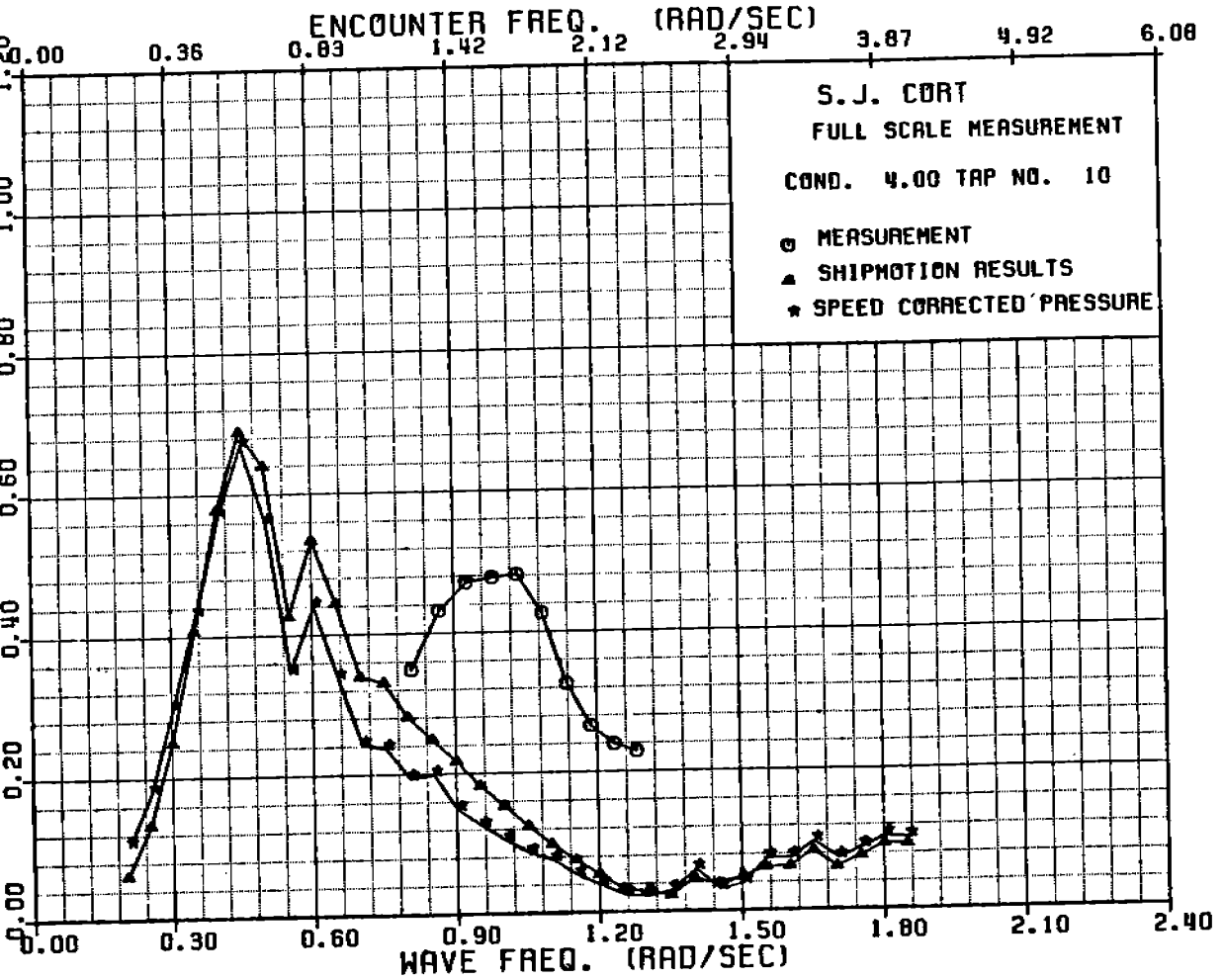

URE C-41: SJ CORT PRESSURE TRANSFER FUNCTION, TAP NO. 10, CONDITION 4

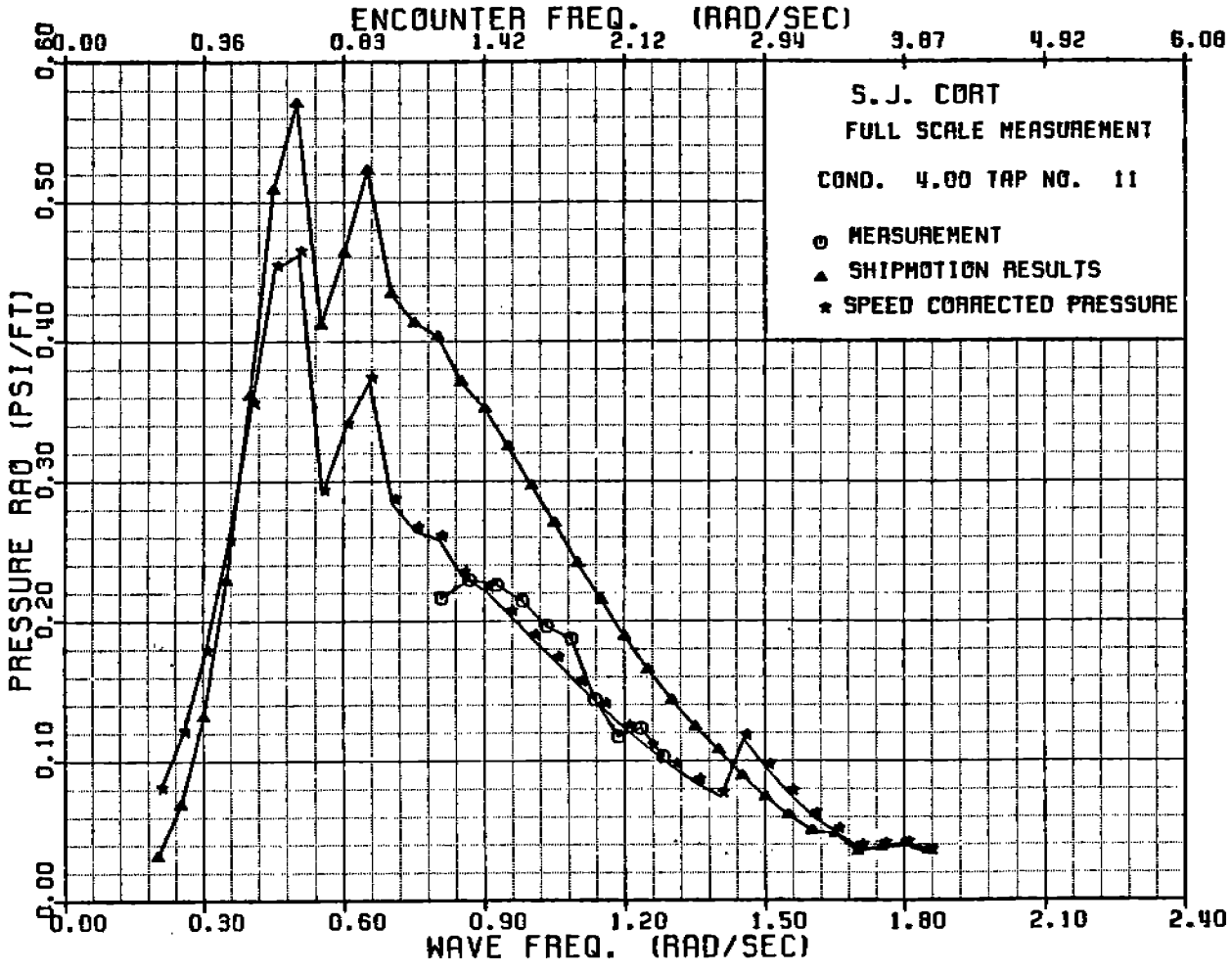

FIGURE C-42: SJ CORT PRESSURE TRANSFER FUNCTION, TAP NO. 11, CONDITION 4

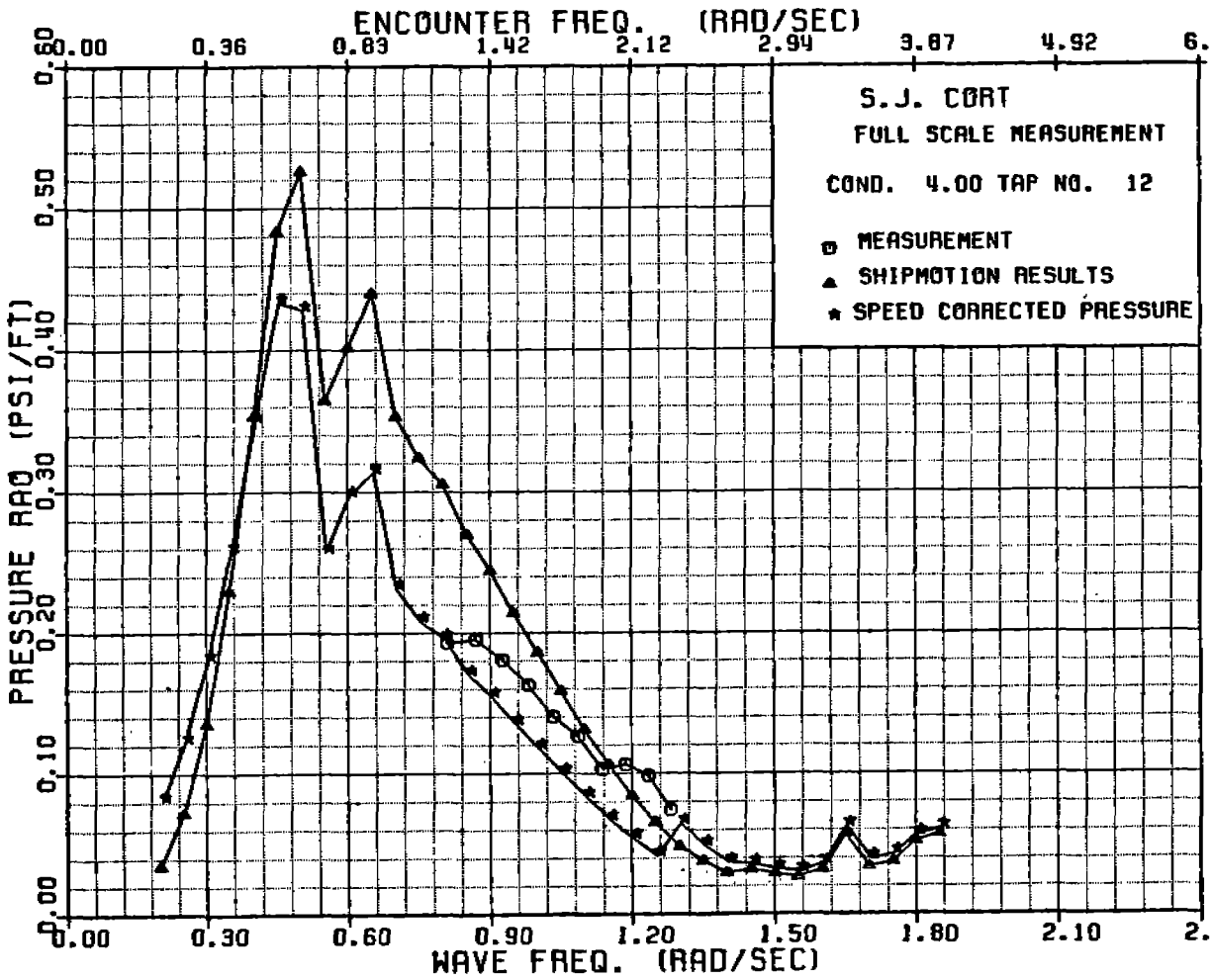

FIGURE C-43: SJ CORT PRESSURE TRANSFER FUNCTION, TAP NO. 12, CONDITION

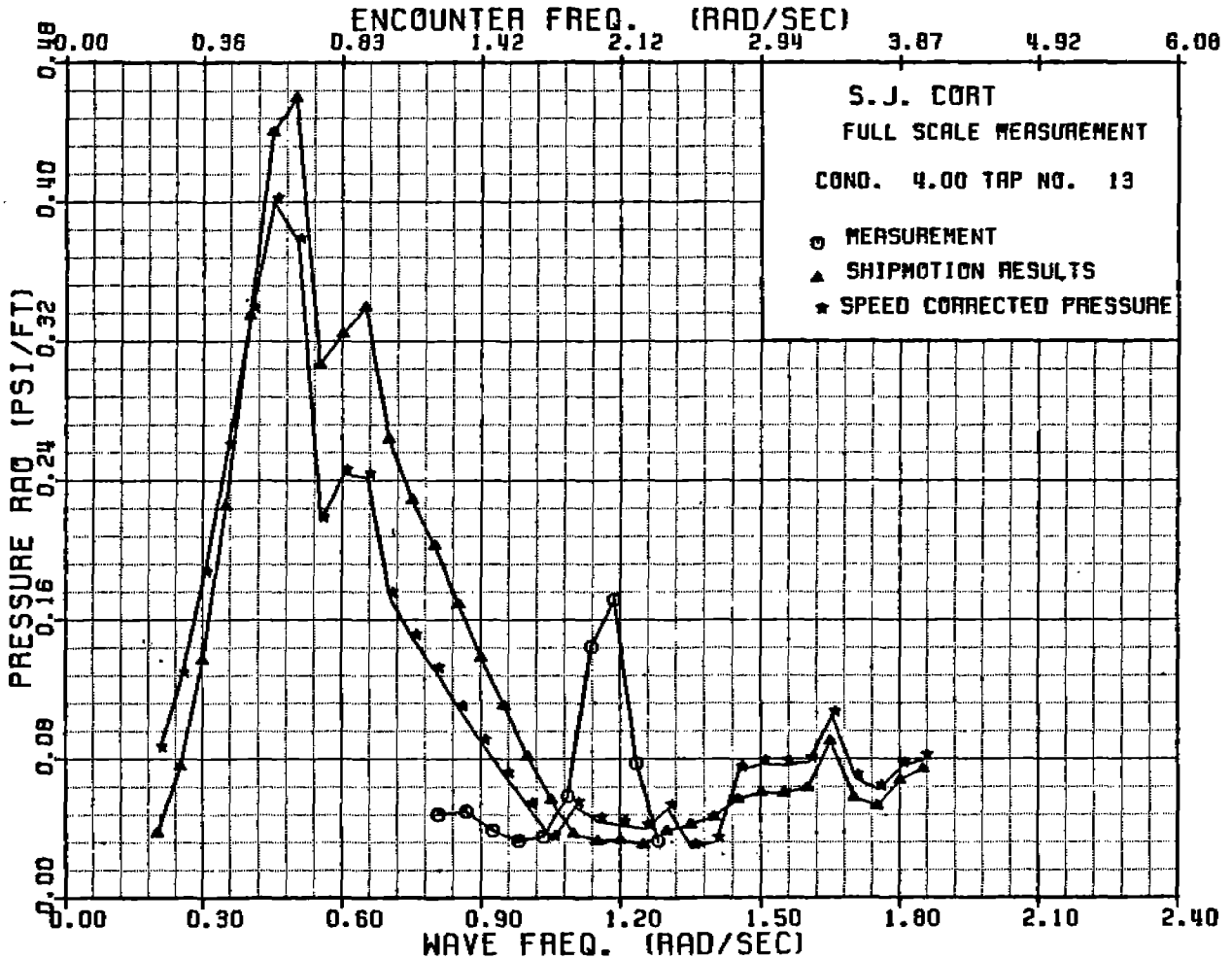

FIGURE C-44: SJ CORT PRESSURE TRANSFER FUNCTION, TAP NO. 13, CONDITION 4

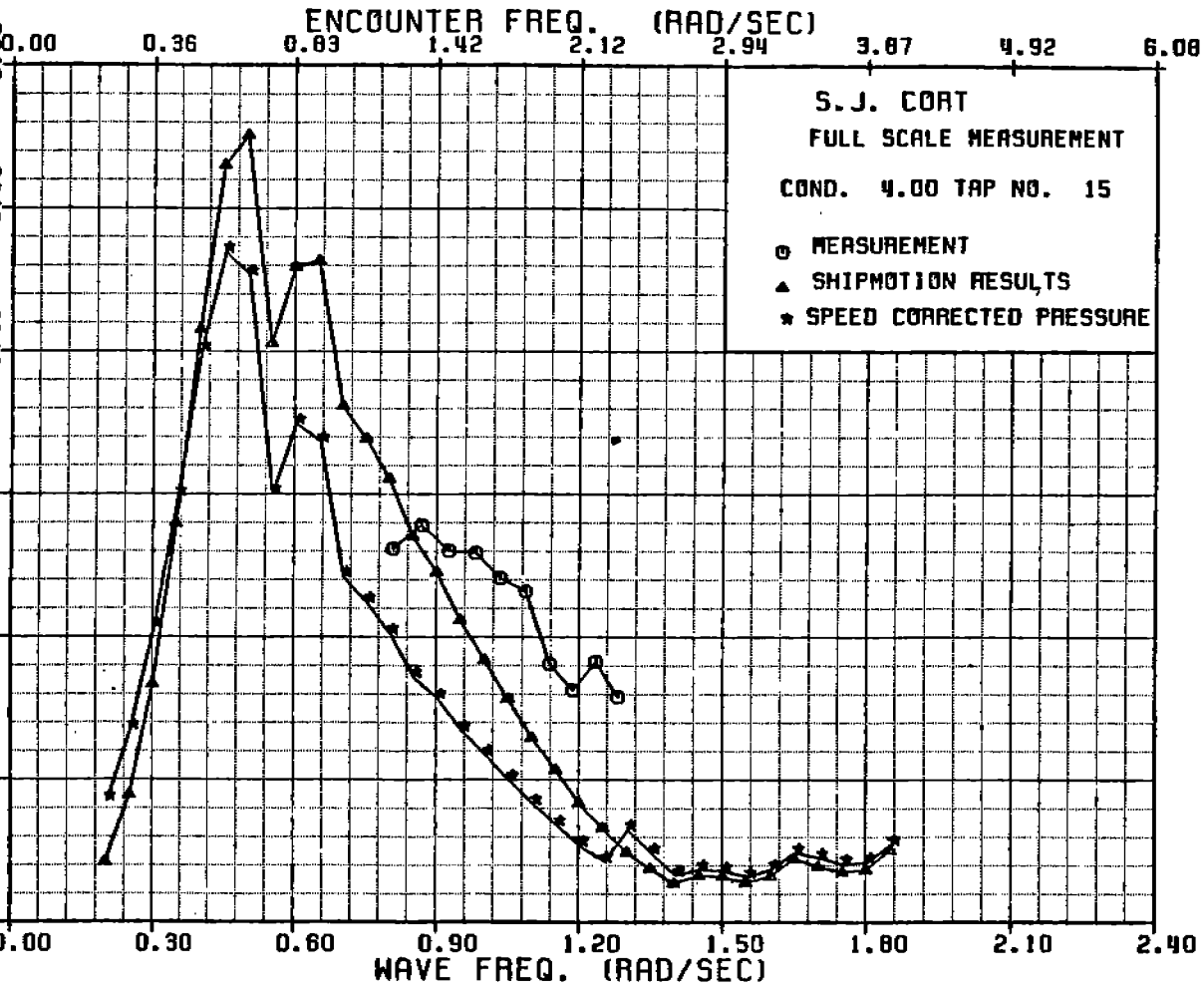

RE C-45: SJ CORT PRESSURE TRANSFER FUNCTION, TAP NO. 15, CONDITION 4

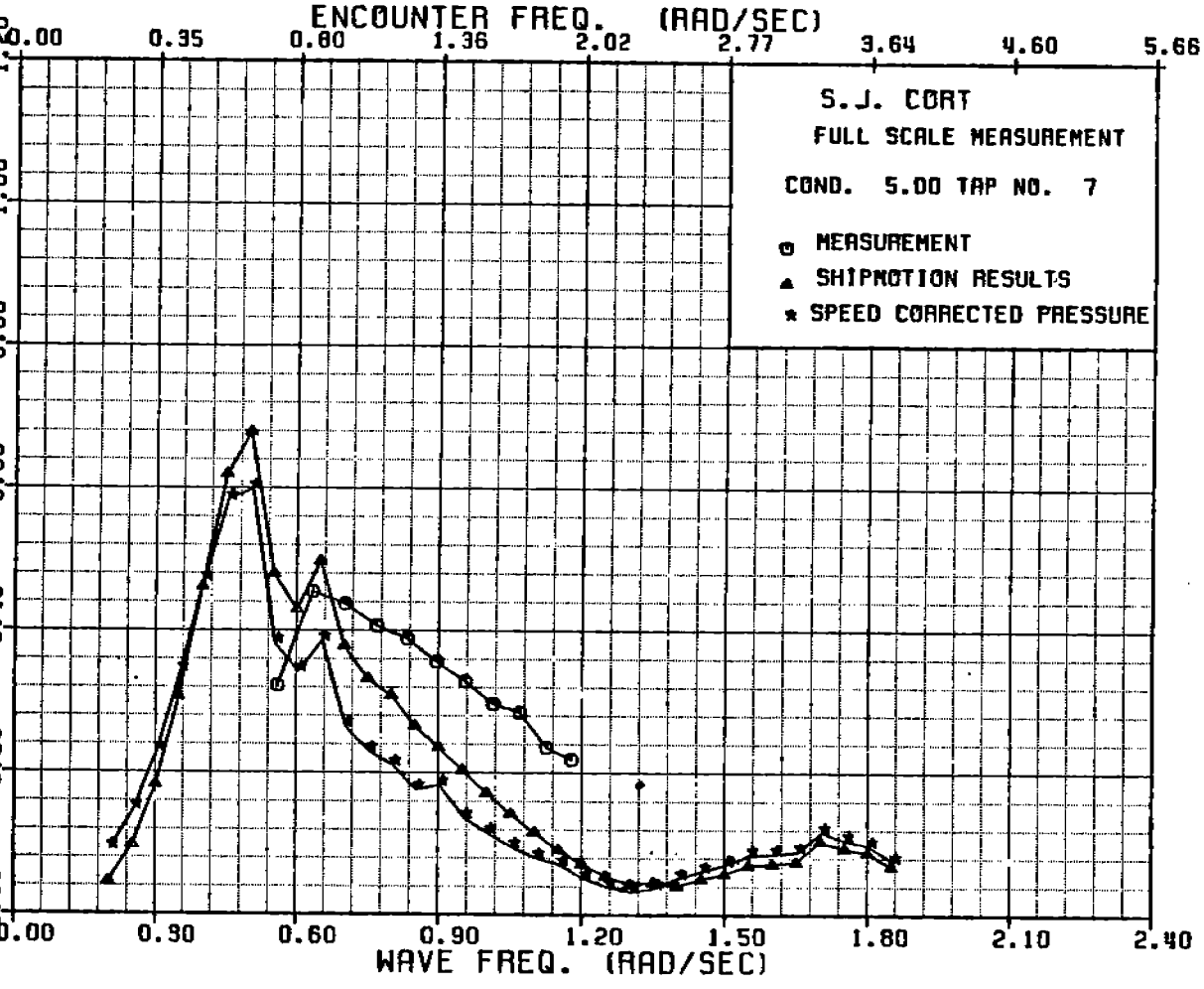

URE C-46: SJ CORT PRESSURE TRANSFER FUNCTION, TAP NO. 7, CONDITION 5

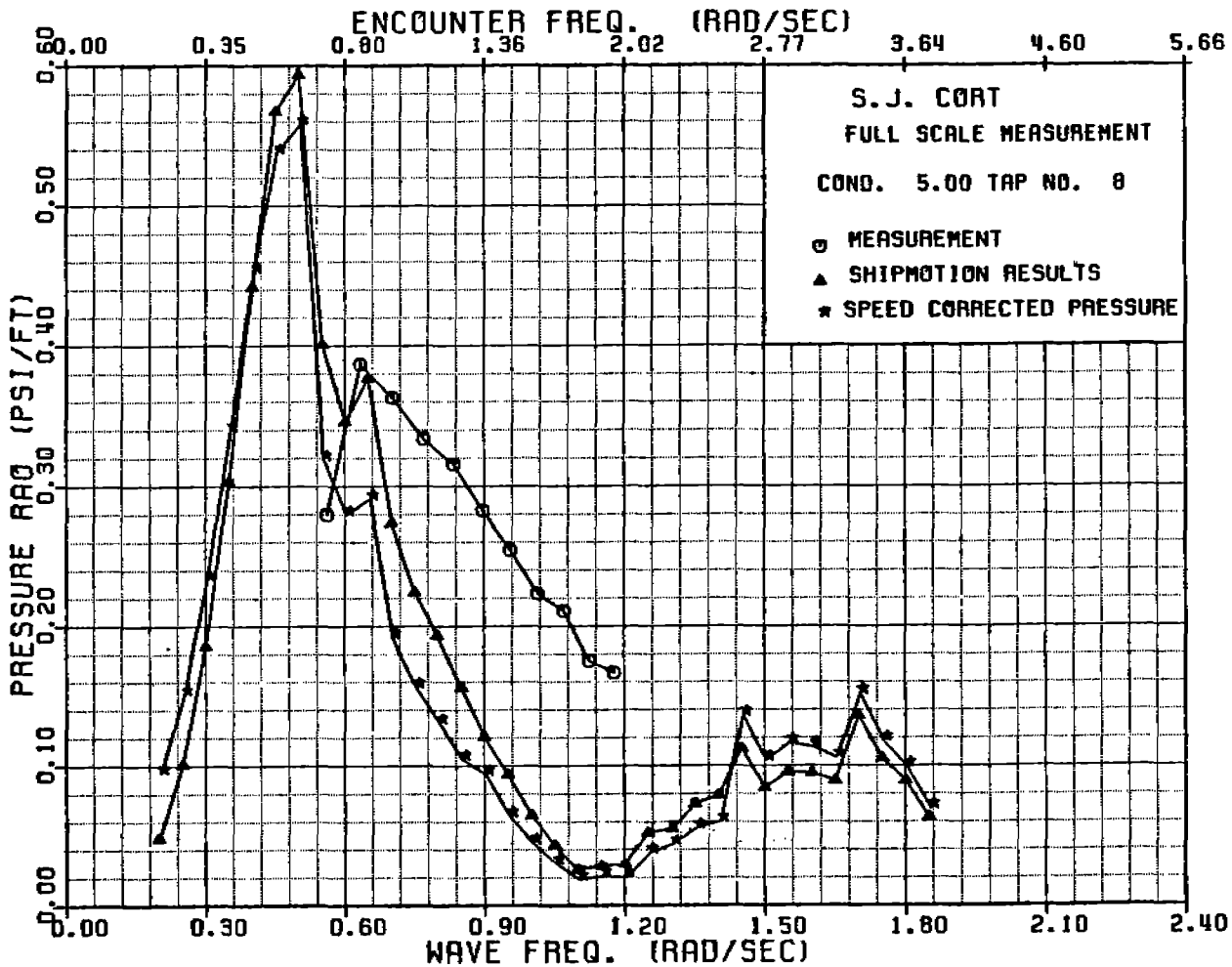

FIGURE C-47: SJ CORT PRESSURE TRANSFER FUNCTION, TAP NO. 8, CONDITION 5

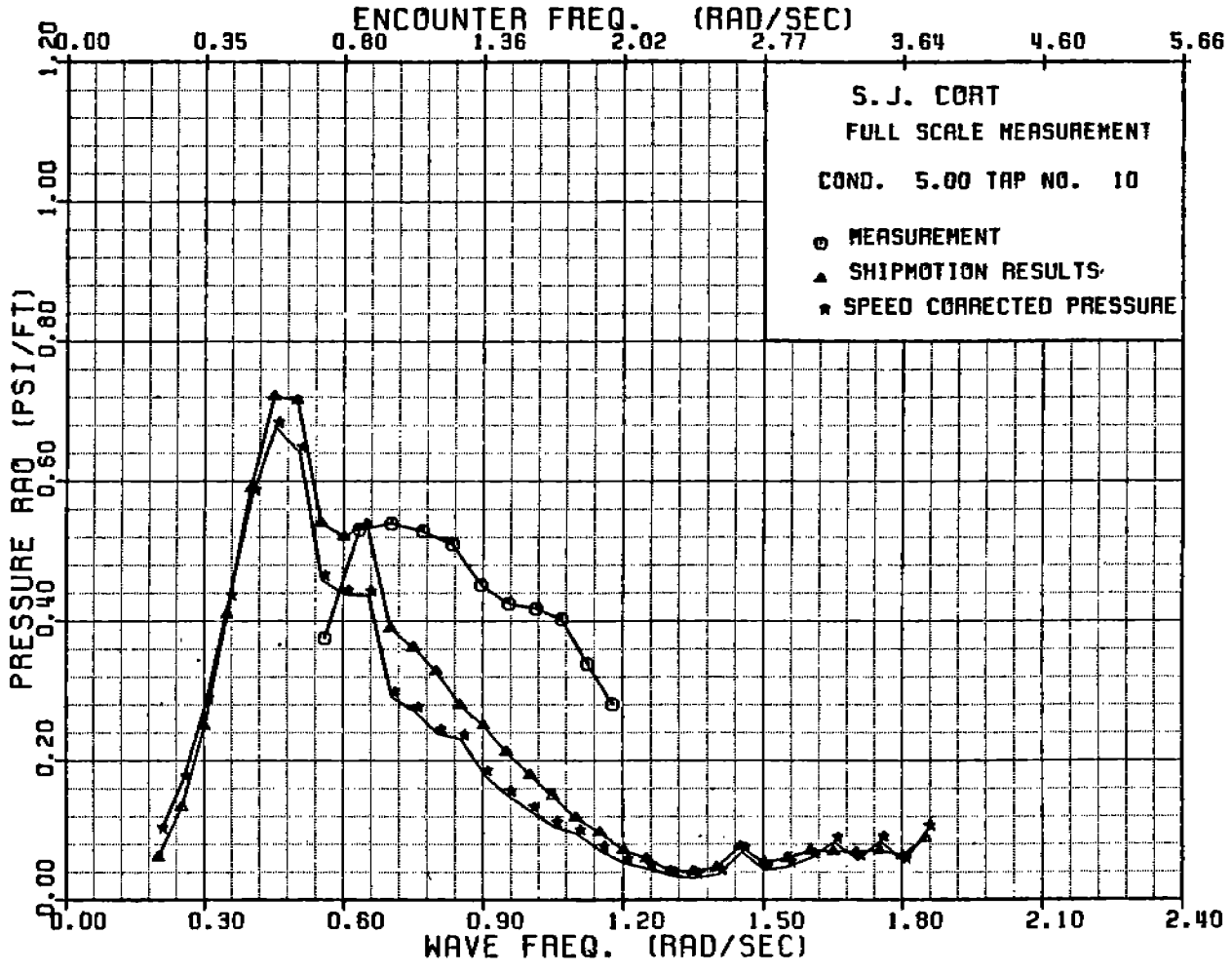

FIGURE C-48: SJ CORT PRESSURE TRANSFER FUNCTION, TAP NO. 10, CONDITION 5

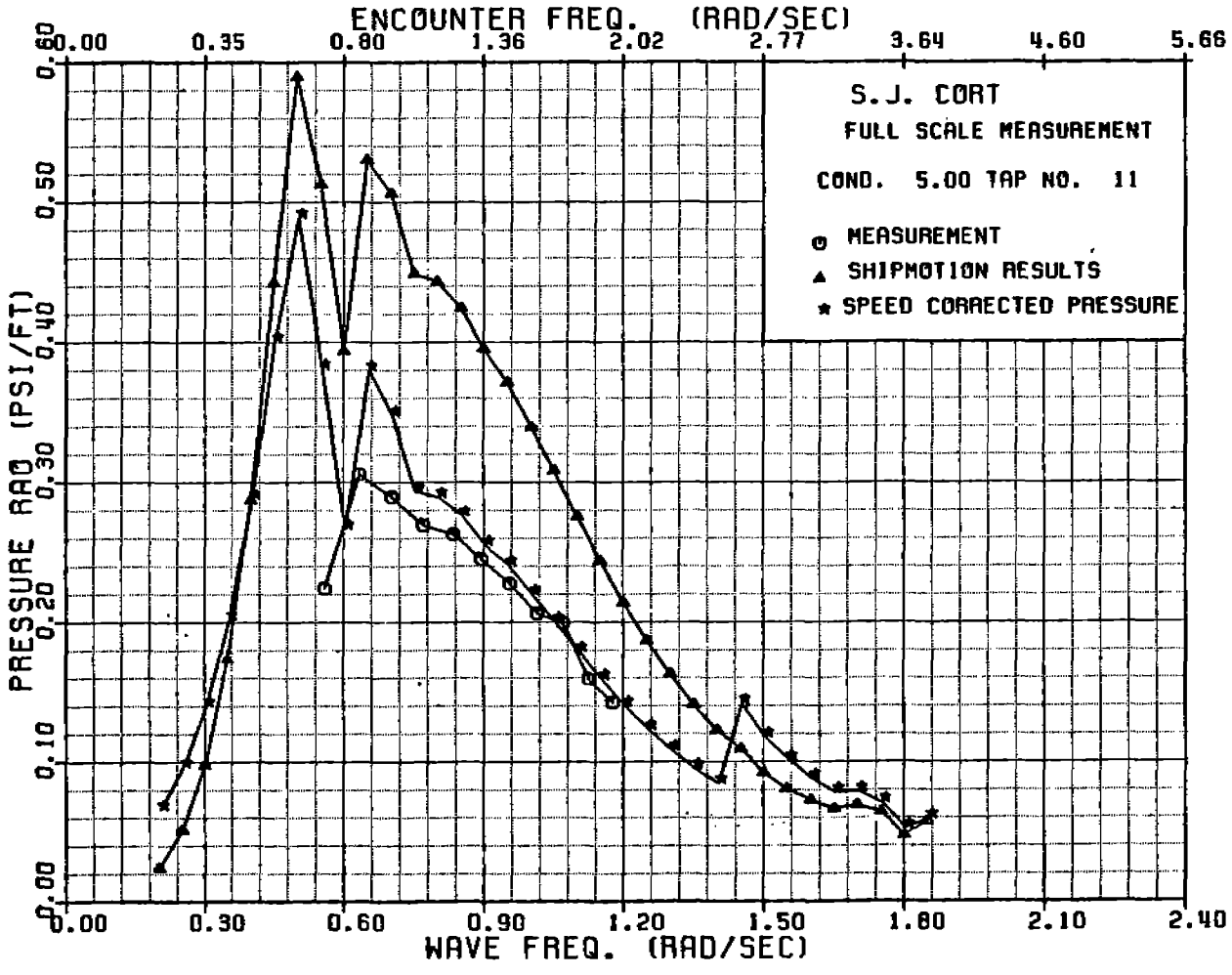

FIGURE C-49: SJ CORT PRESSURE TRANSFER FUNCTION, TAP NO. 11, CONDITION 5

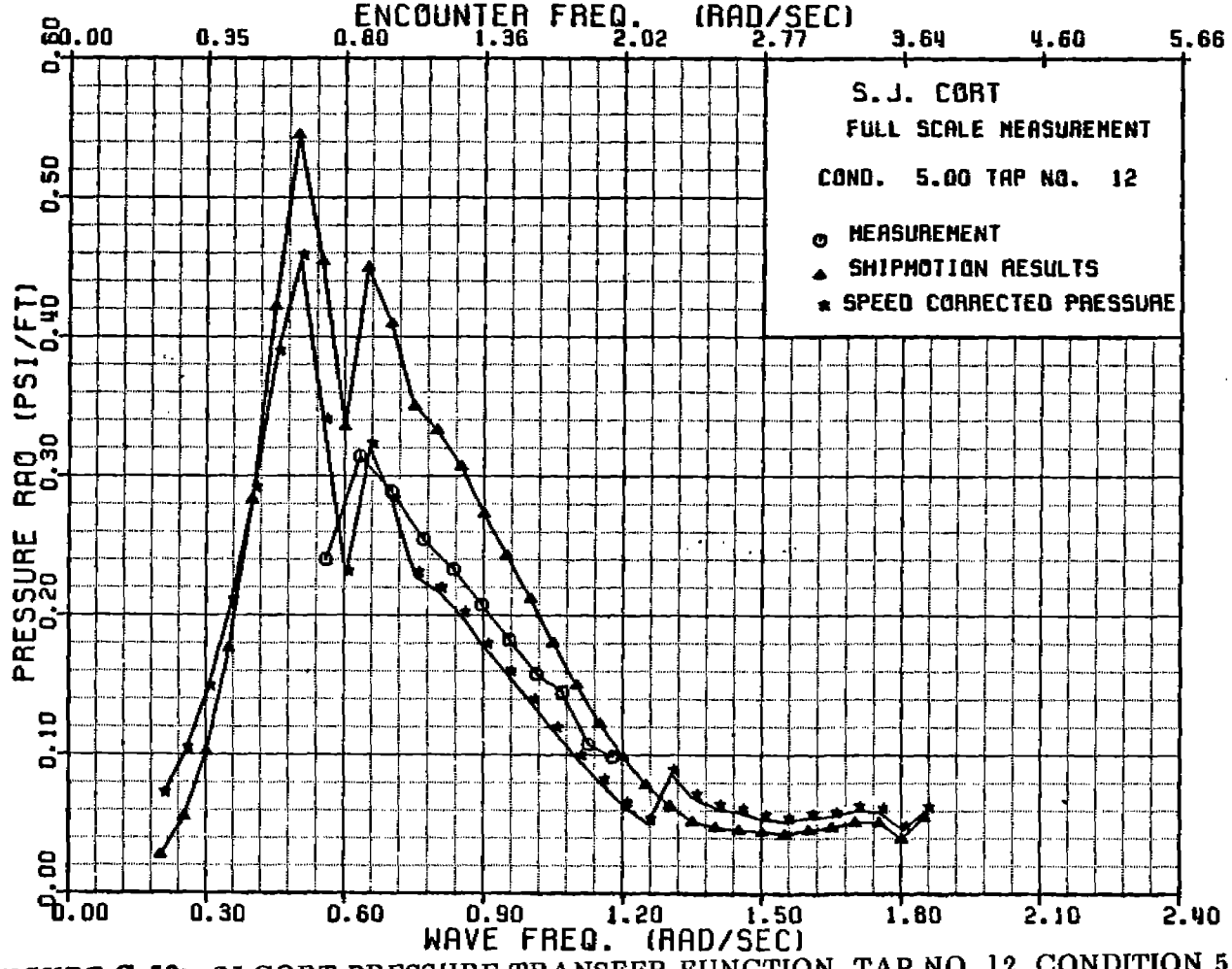

FIGURE C-50: SJ CORT PRESSURE TRANSFER FUNCTION, TAP NO. 12, CONDITION 5

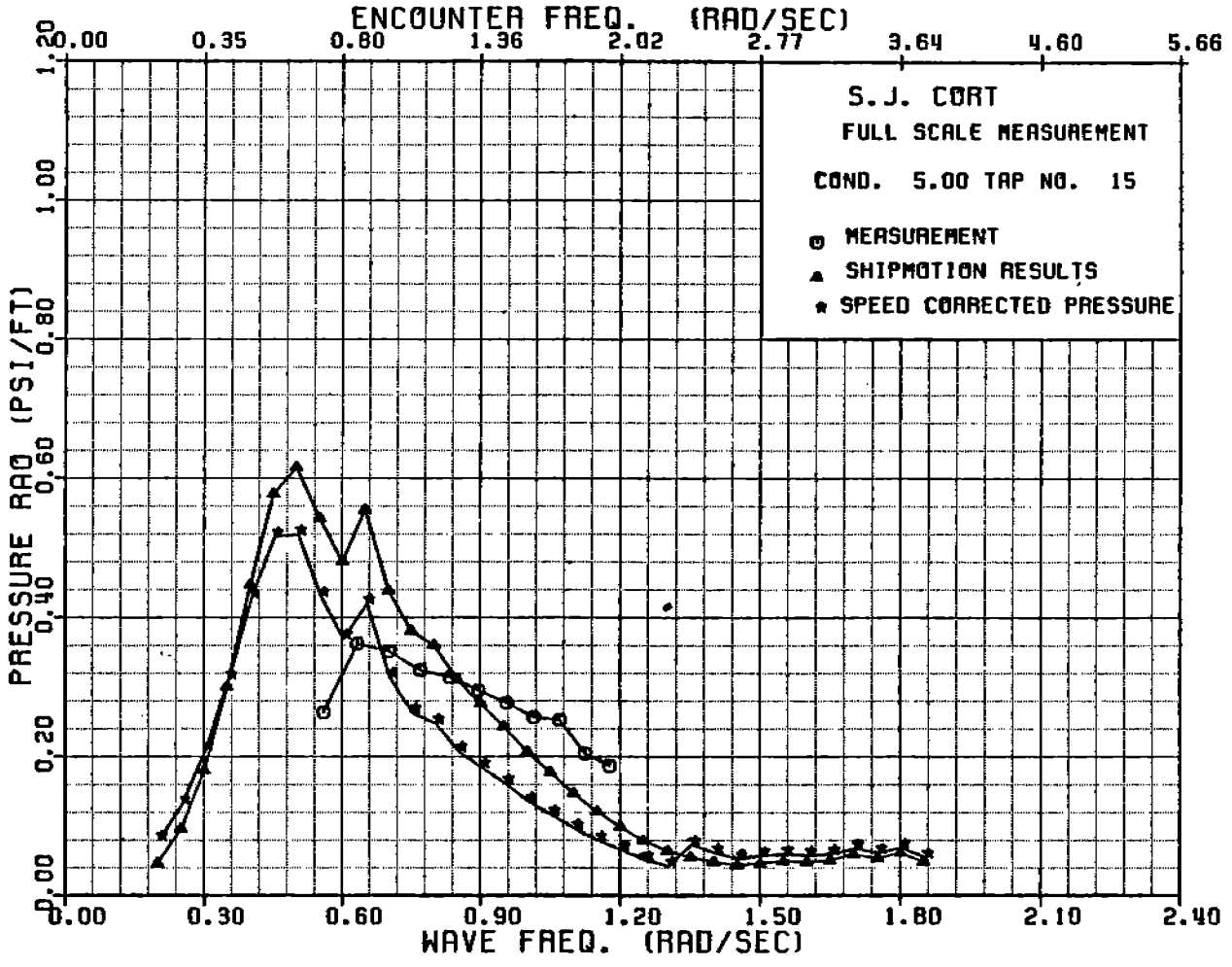

FIGURE C-51: SJ CORT PRESSURE TRANSFER FUNCTION, TAP NO. 15, CONDITION 5

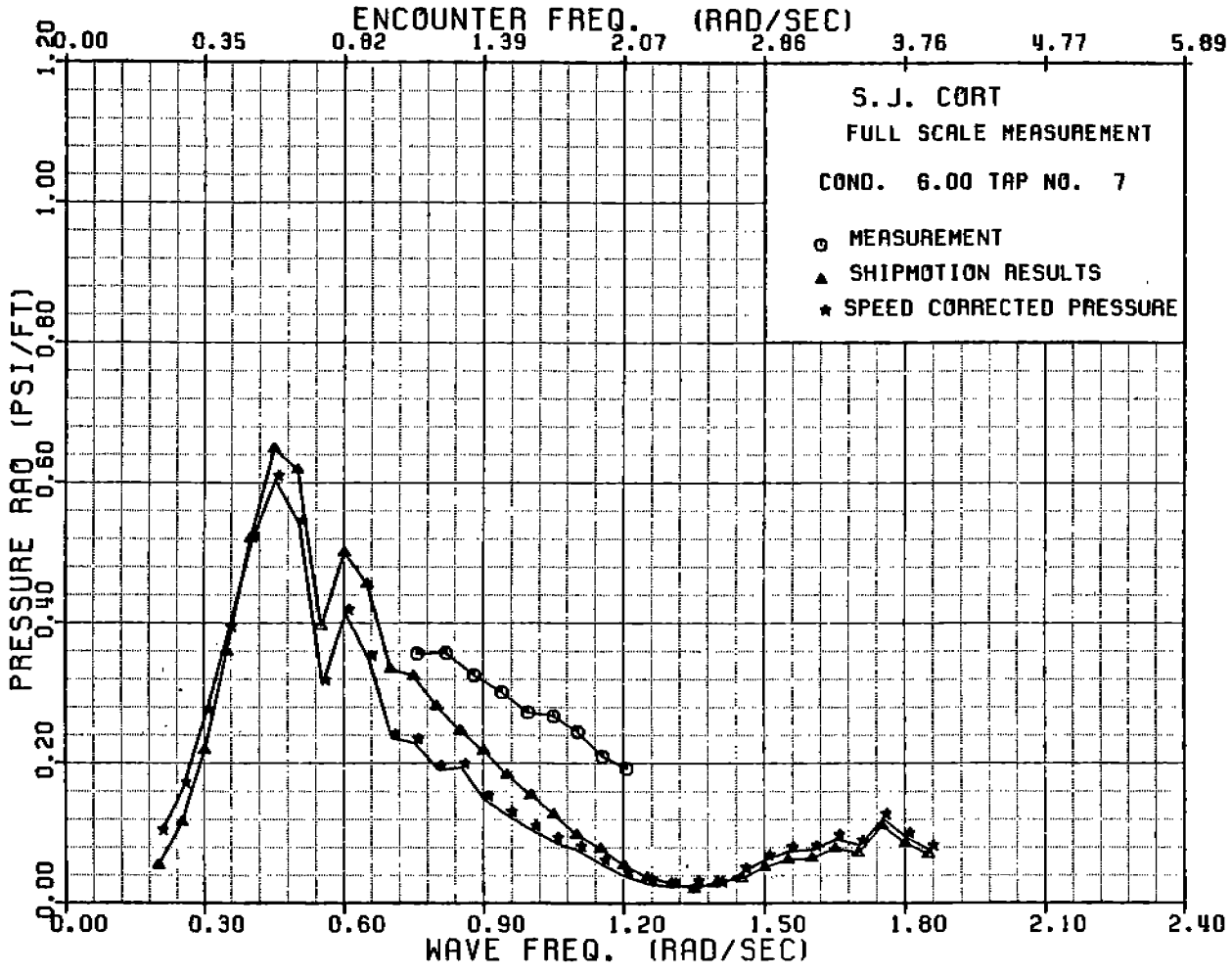

FIGURE C-52: SJ CORT PRESSURE TRANSFER FUNCTION, TAP NO. 7, CONDITION 6

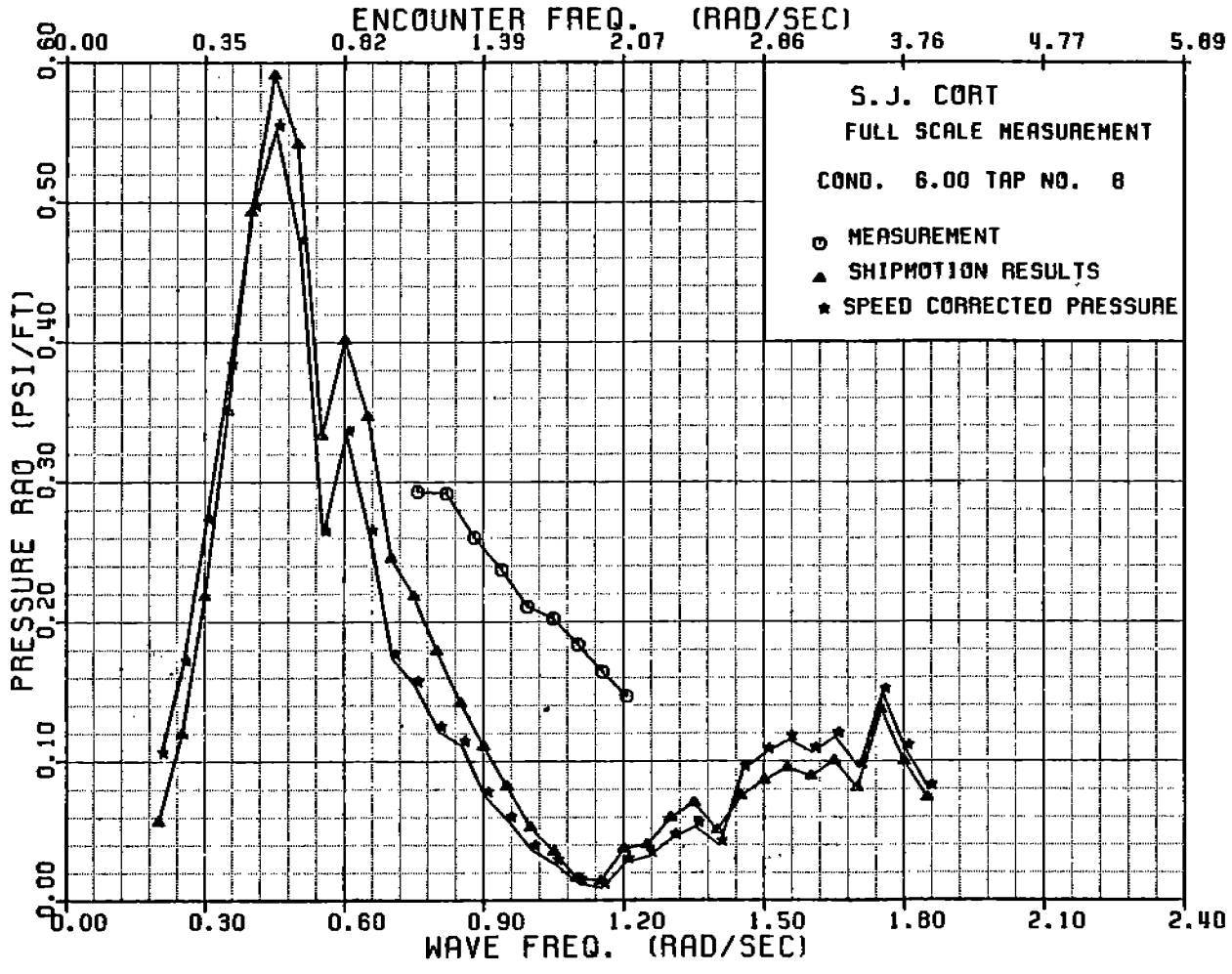

FIGURE C-53: SJ CORT PRESSURE TRANSFER FUNCTION, TAP NO. 8, CONDITION 6

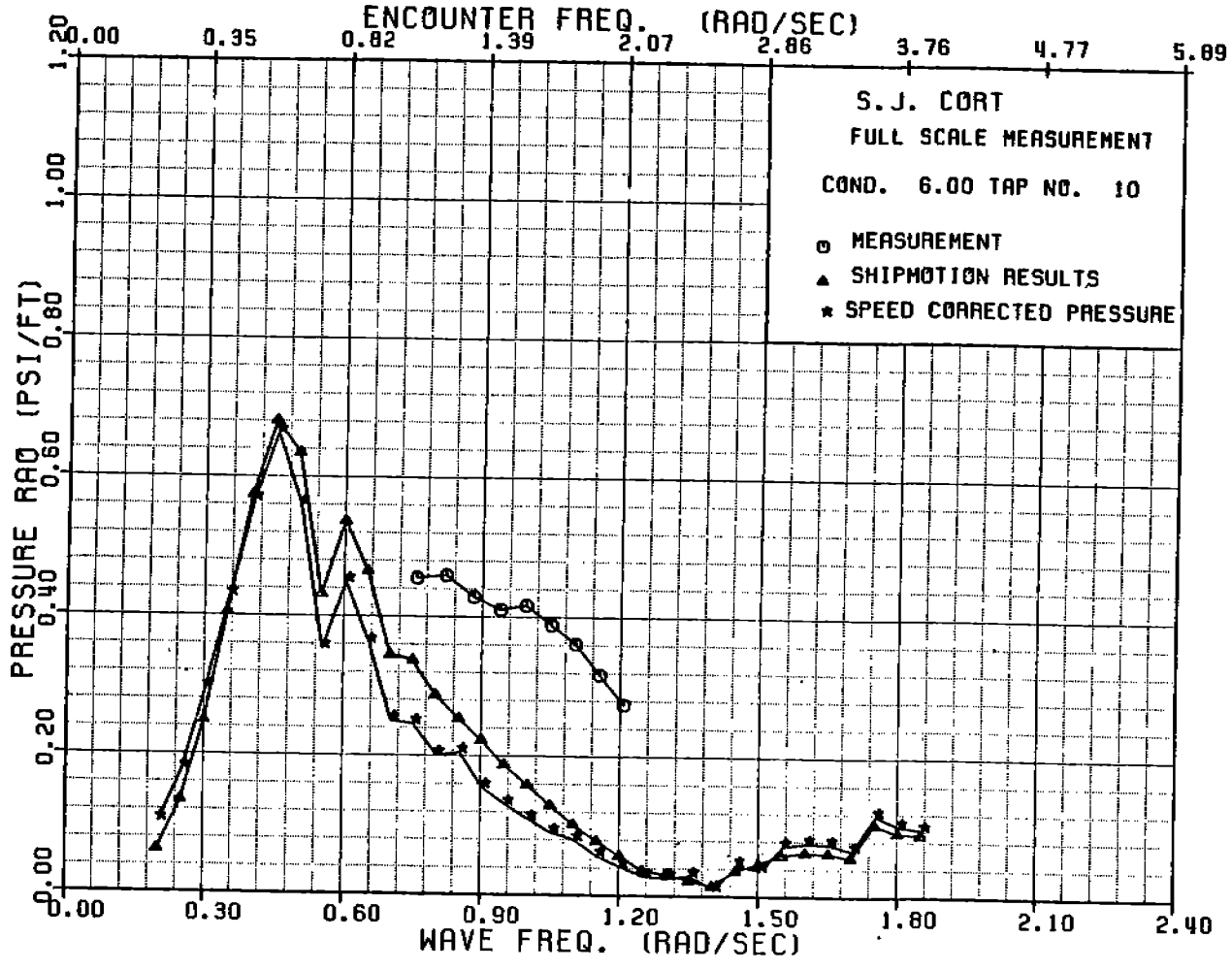

FIGURE C-54: SJ CORT PRESSURE TRANSFER FUNCTION, TAP NO. 10, CONDITION 6

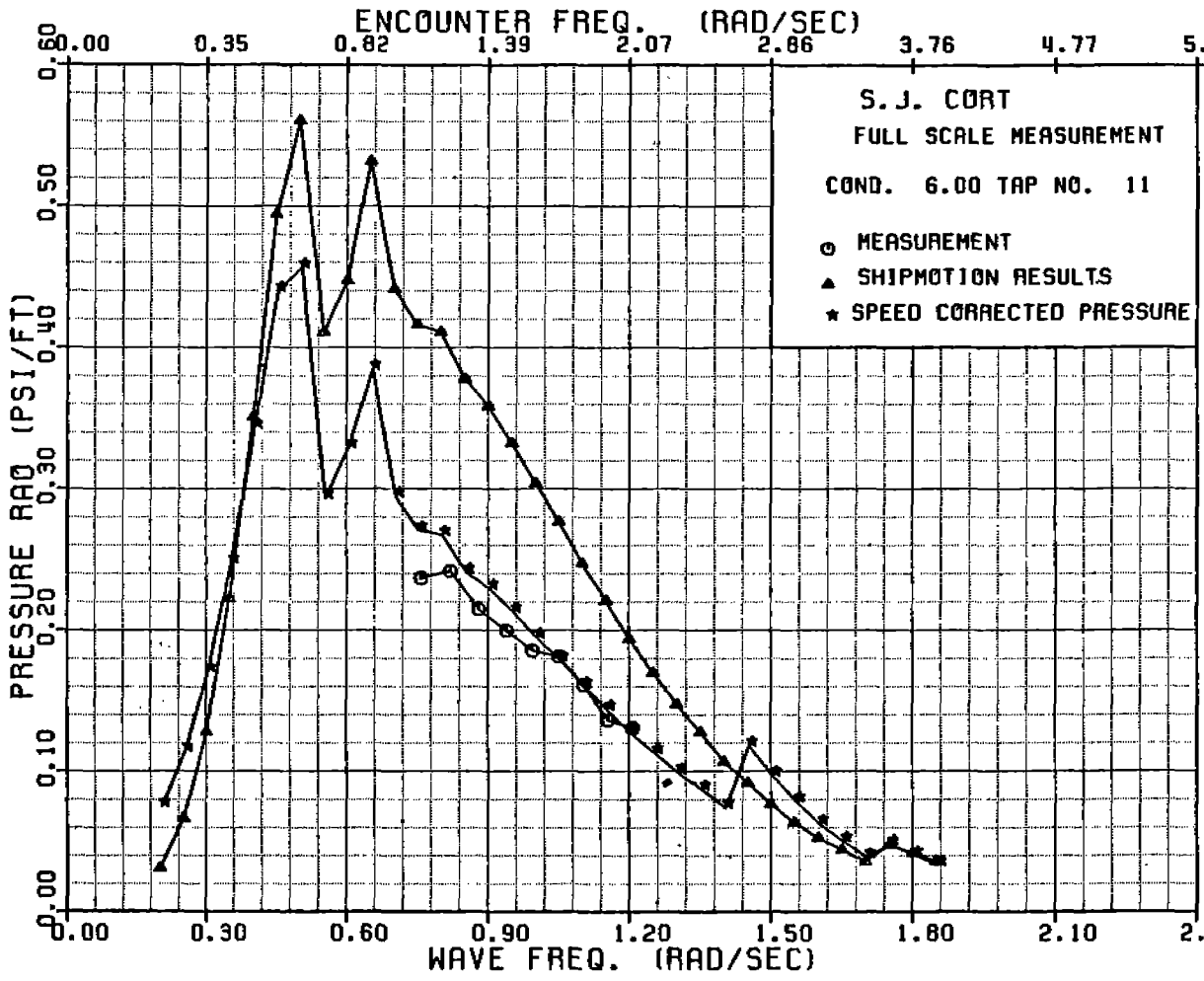

FIGURE C-55: SJ CORT PRESSURE TRANSFER FUNCTION, TAP NO. 11, CONDITION

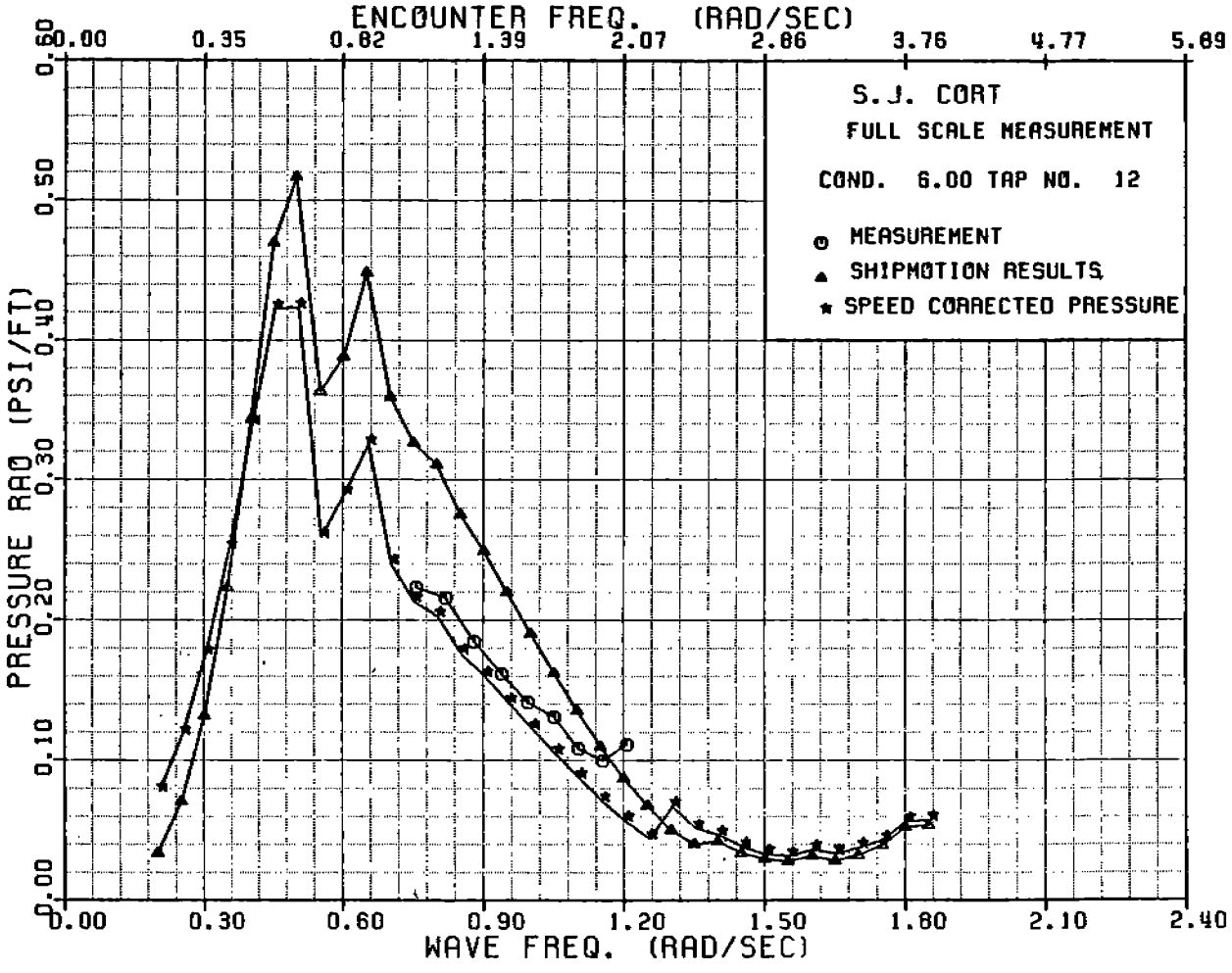

FIGURE C-56: SJ CORT PRESSURE TRANSFER FUNCTION, TAP NO. 12, CONDITION 6

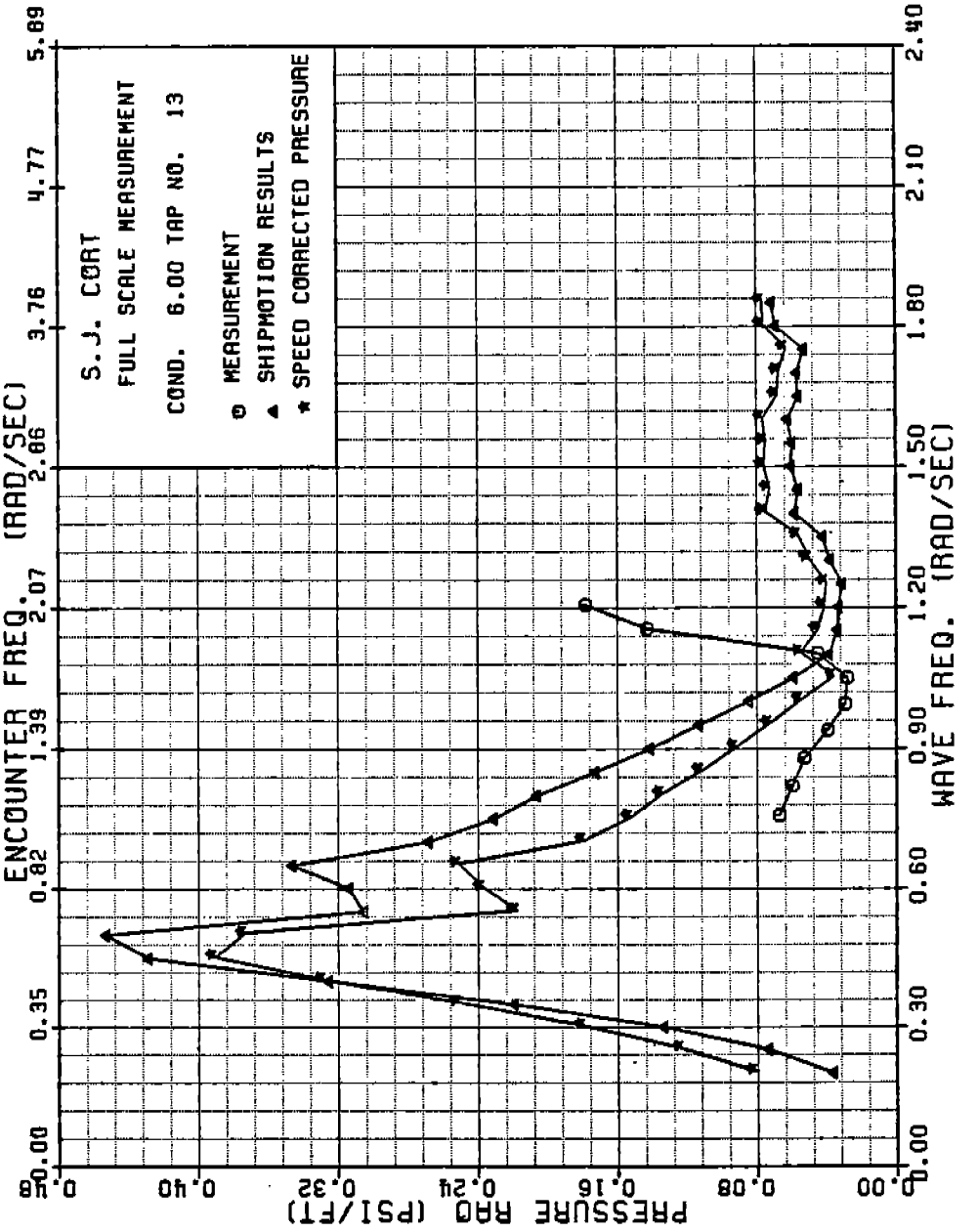

FIGURE C-57: SJ CORT PRESSURE TRANSFER FUNCTION, TAP NO. 13, CONDITION 6

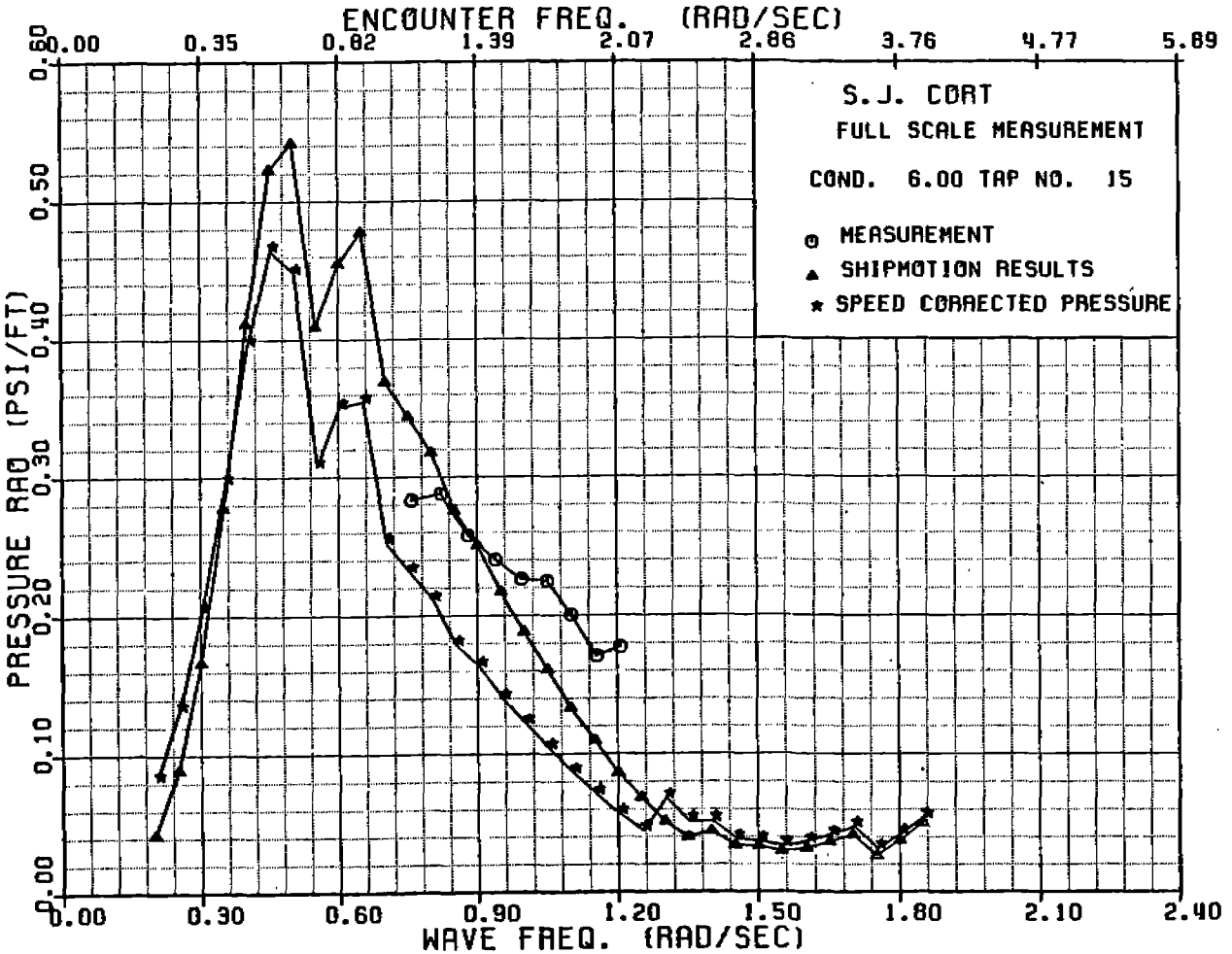

FIGURE C-58: SJ CORT PRESSURE TRANSFER FUNCTION, TAP NO. 15, CONDITION 6

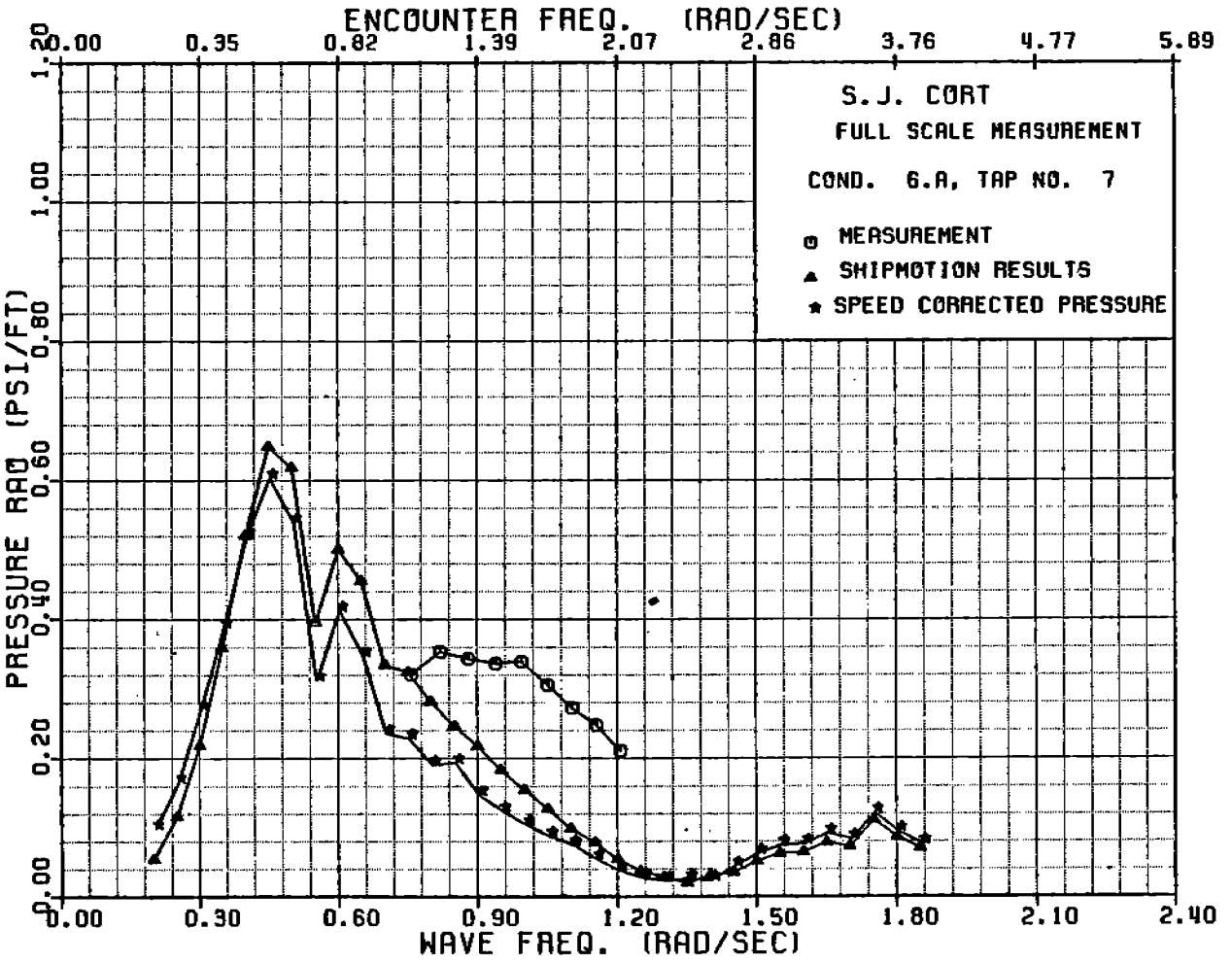

FIGURE C-59: SJ CORT PRESSURE TRANSFER FUNCTION, TAP NO. 7, CONDITION 6a

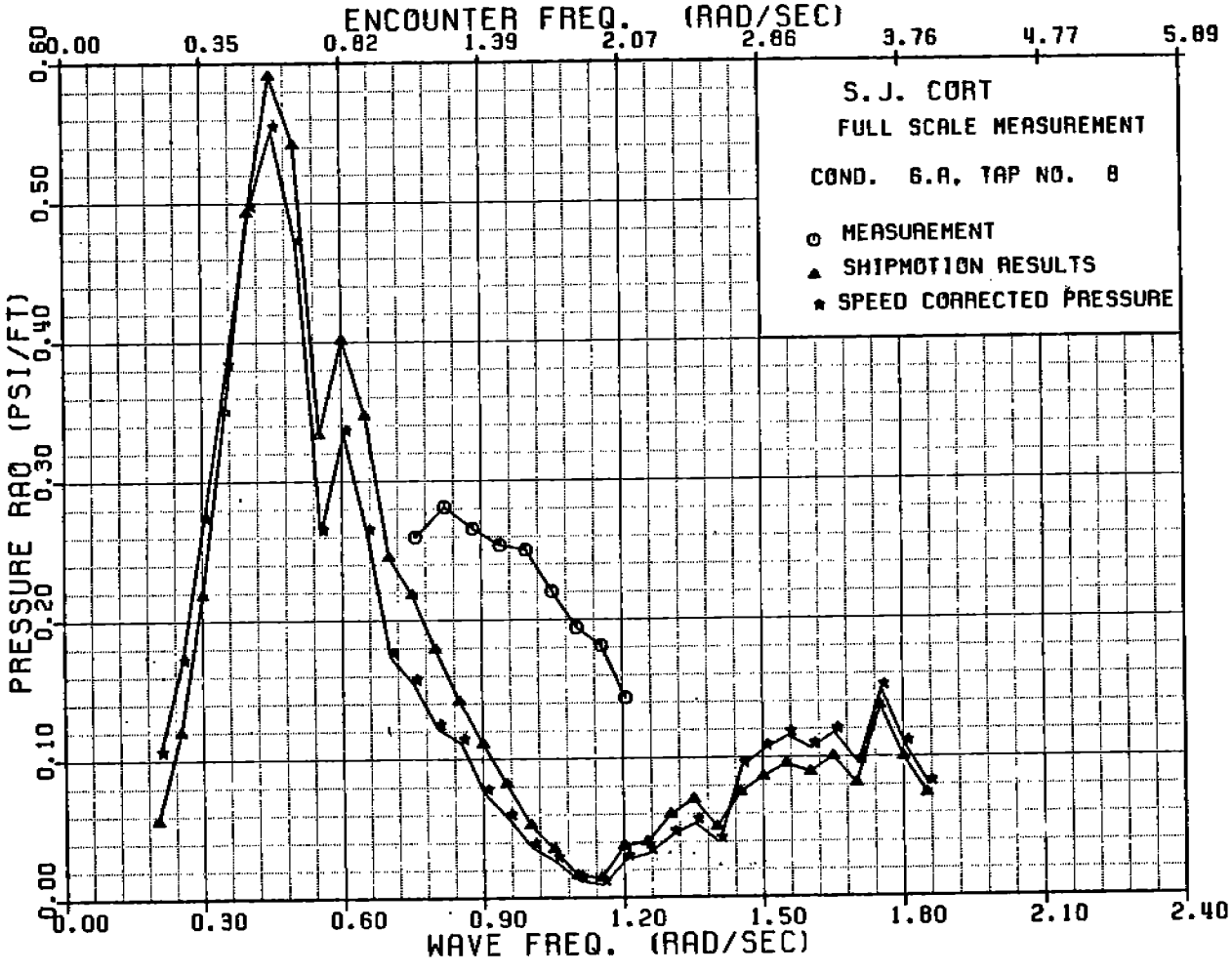

FIGURE C-60: SJ CORT PRESSURE TRANSFER FUNCTION, TAP NO. 8, CONDITION 6a

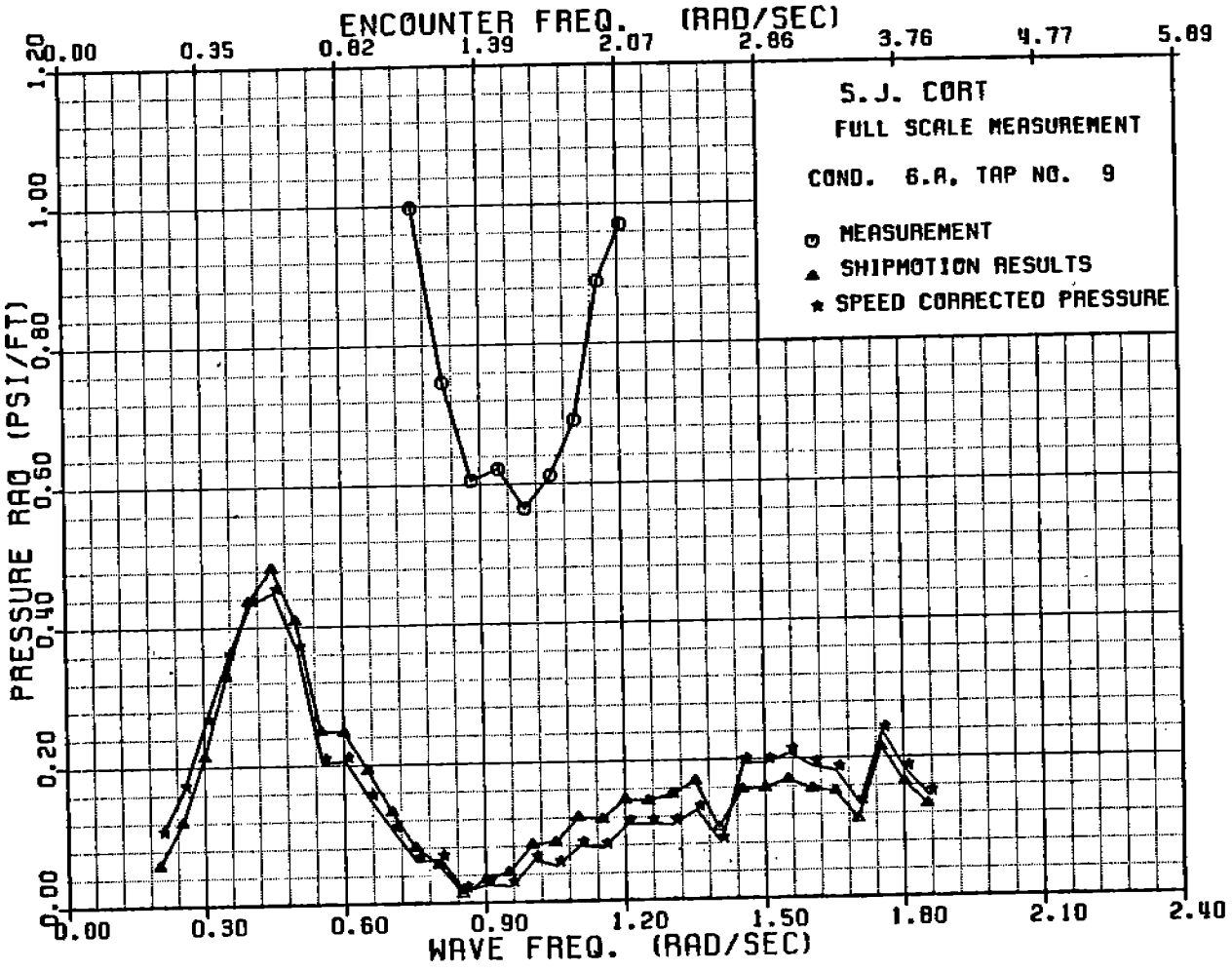

FIGURE C-61: SJ CORT PRESSURE TRANSFER FUNCTION, TAP NO. 9, CONDITION 6a

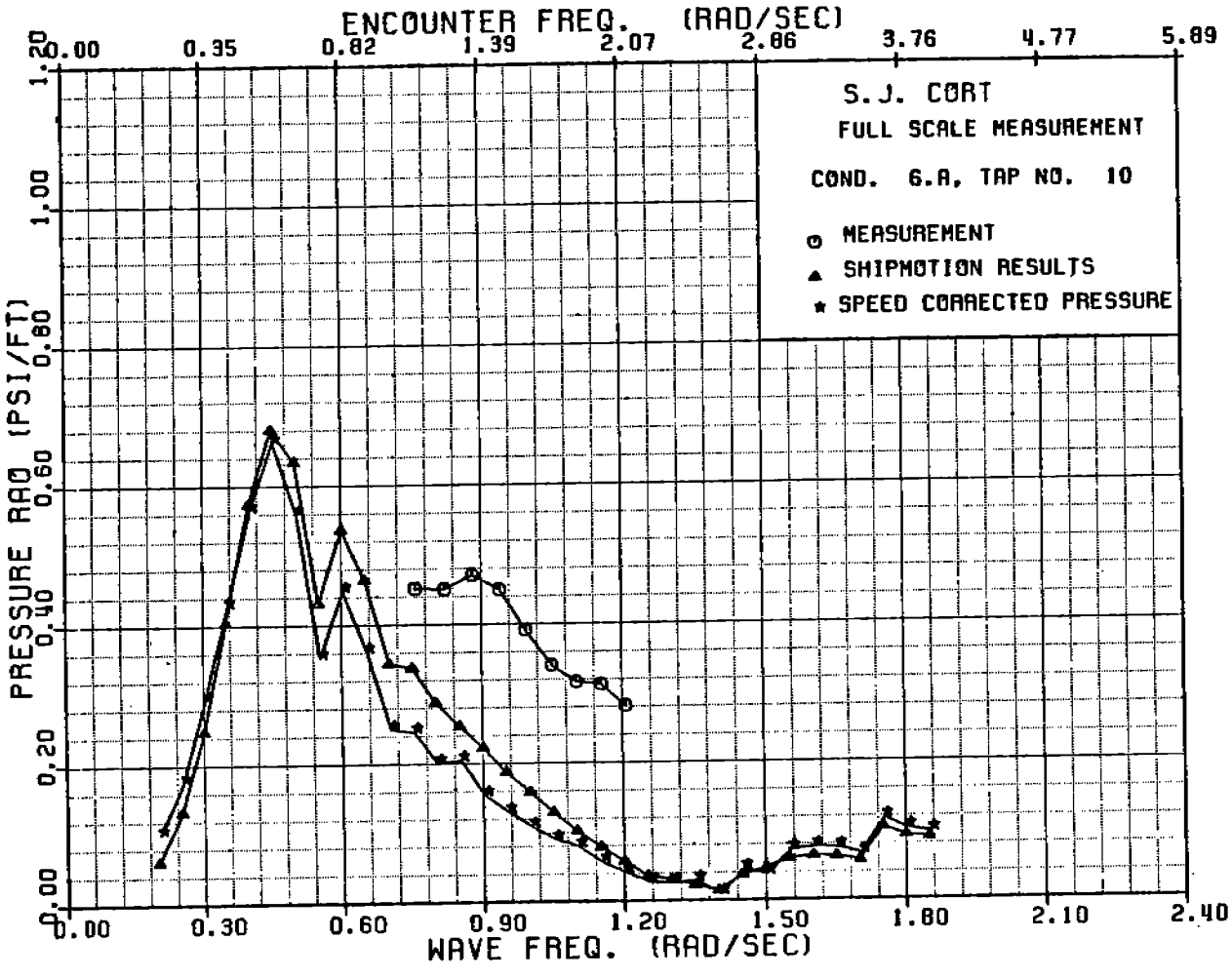

FIGURE C-62: SJ CORT PRESSURE TRANSFER FUNCTION, TAP NO. 10, CONDITION 6a

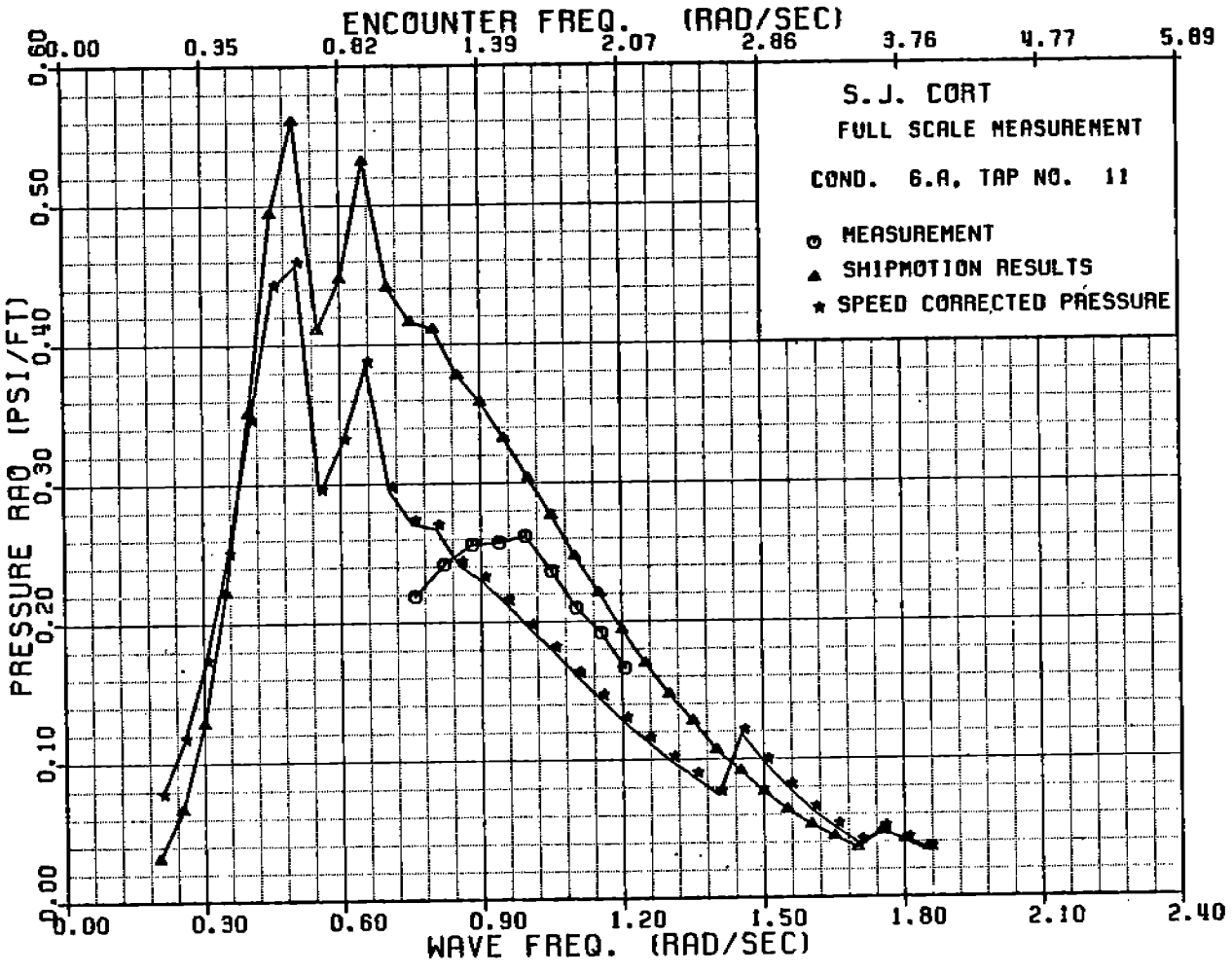

FIGURE C-63: SJ CORT PRESSURE TRANSFER FUNCTION, TAP NO. 11, CONDITION 6a

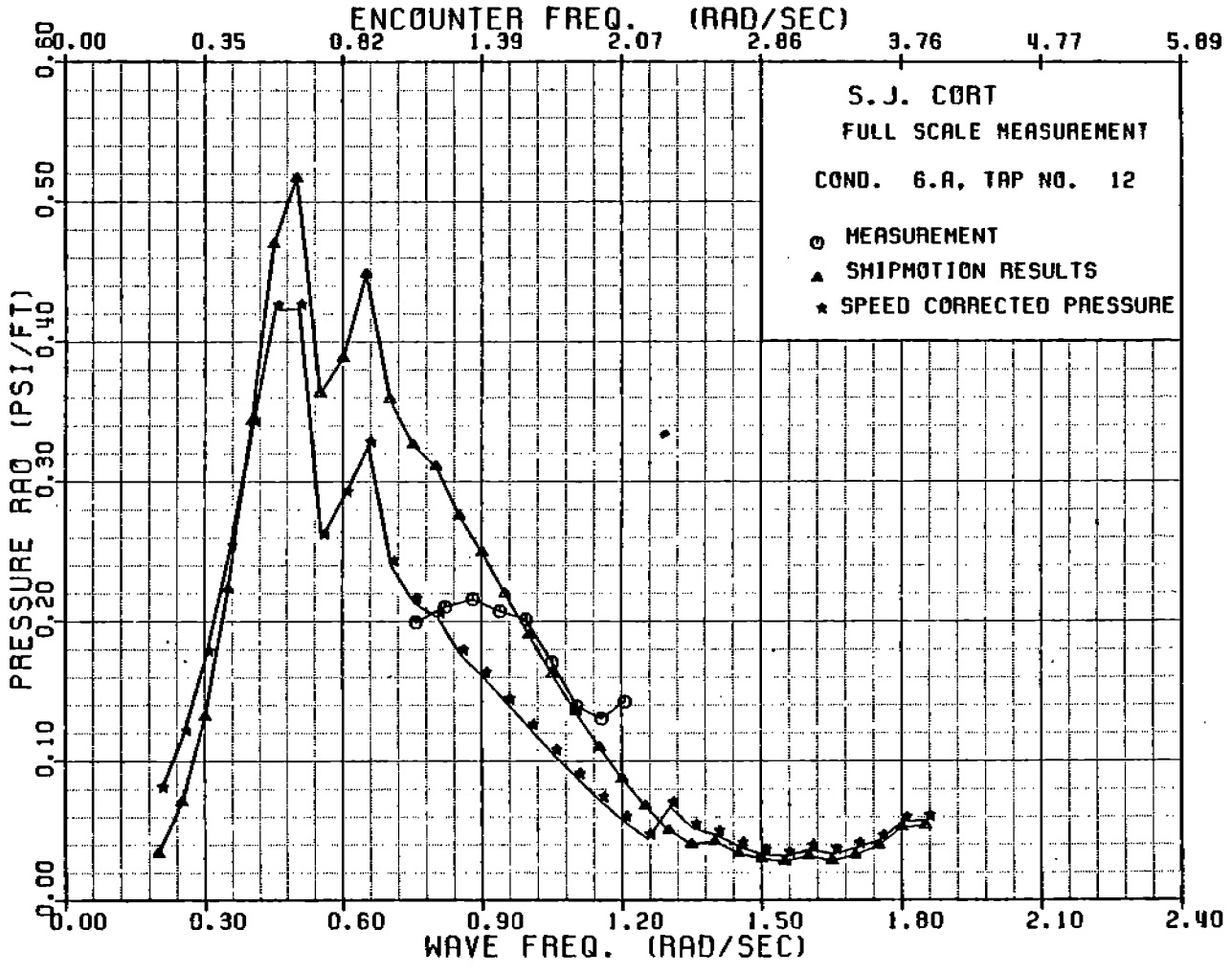

FIGURE C-64: SJ CORT PRESSURE TRANSFER FUNCTION, TAP NO. 12, CONDITION 6a

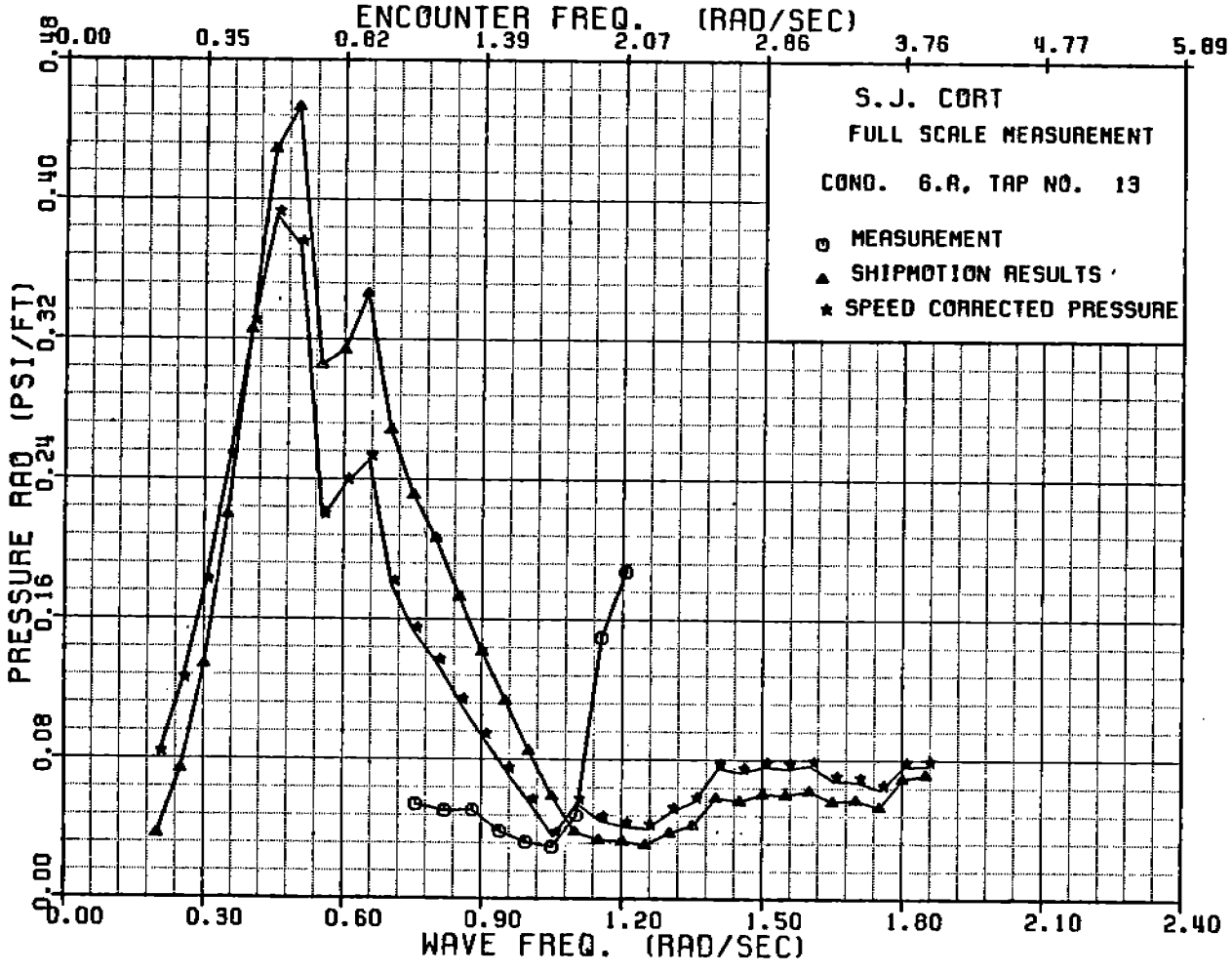

FIGURE C-65: SJ CORT PRESSURE TRANSFER FUNCTION, TAP NO. 13, CONDITION 6a

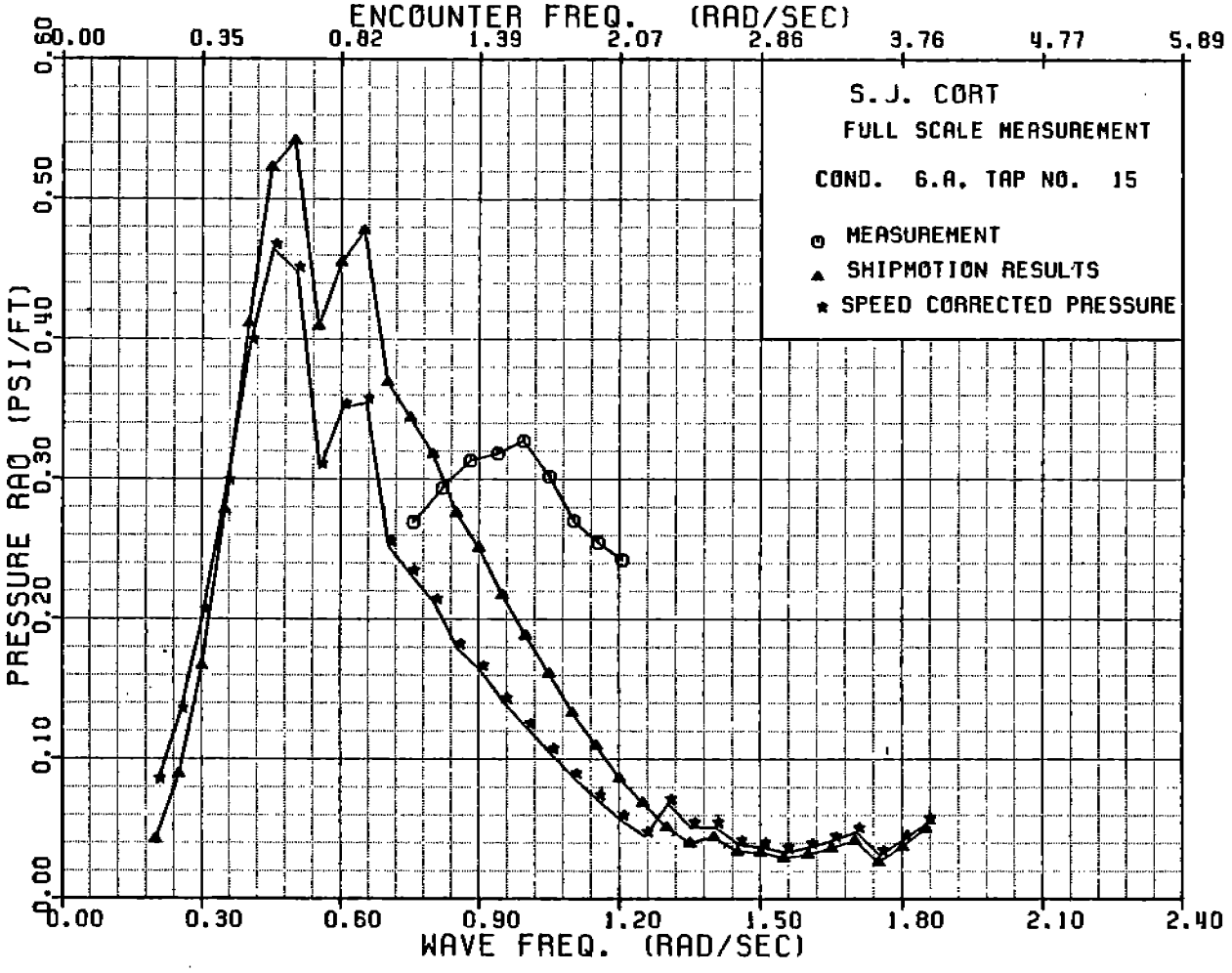

FIGURE C-66: SJ CORT PRESSURE TRANSFER FUNCTION, TAP NO. 15, CONDITION 6a

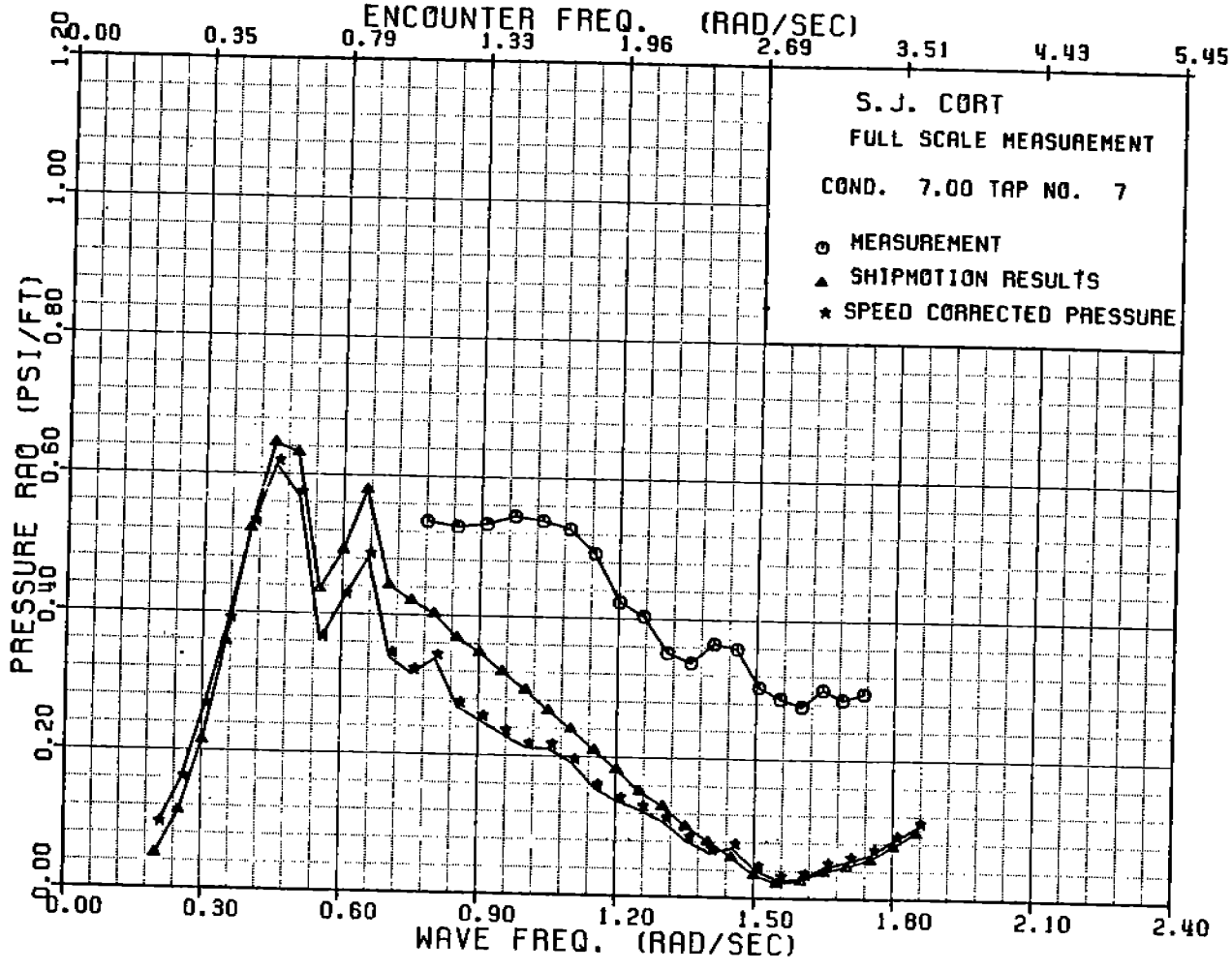

FIGURE C-67: SJ CORT PRESSURE TRANSFER FUNCTION, TAP NO. 7, CONDITION 7

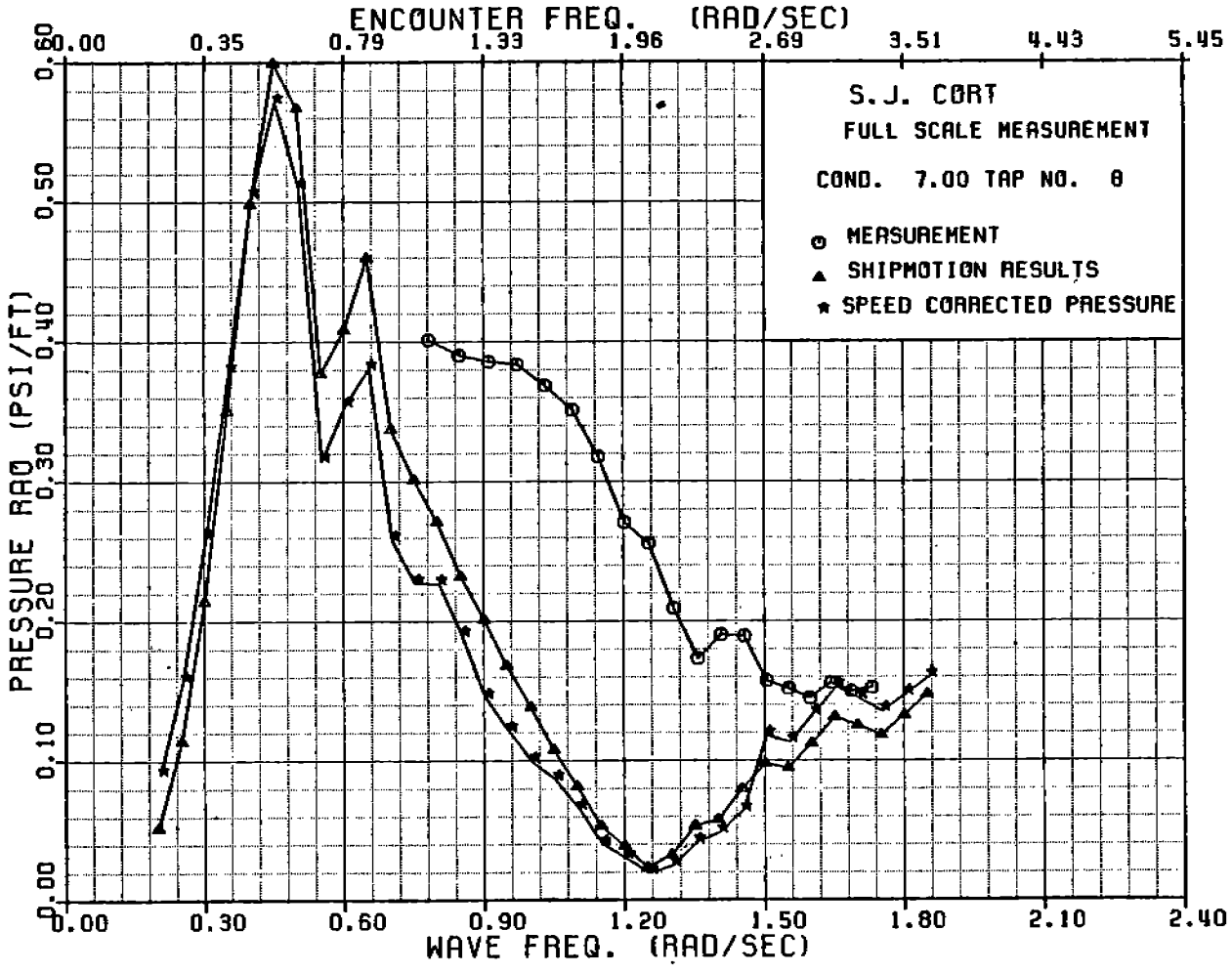

FIGURE C-68: SJ CORT PRESSURE TRANSFER FUNCTION, TAP NO. 8, CONDITION 7

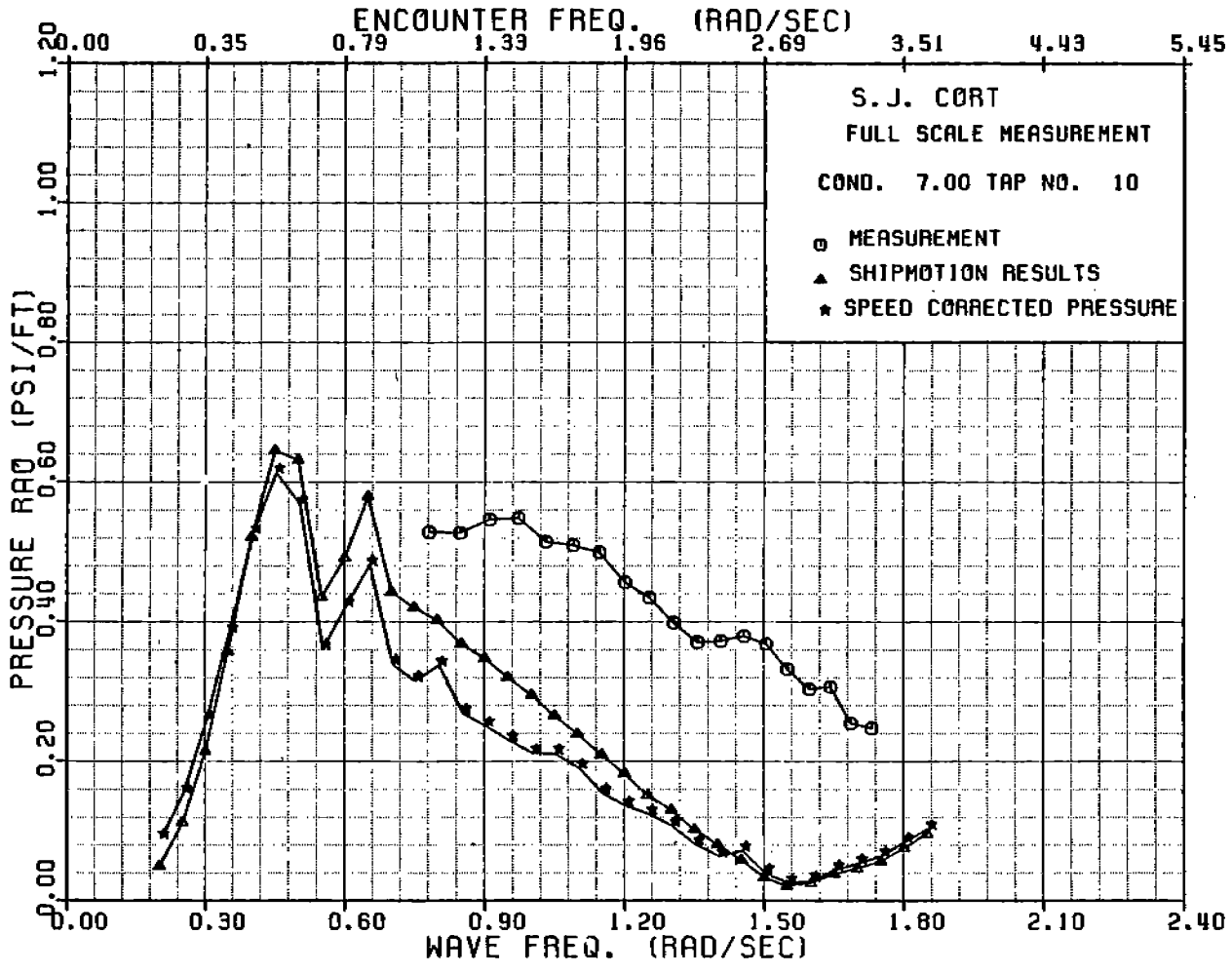

FIGURE C-69: SJ CORT PRESSURE TRANSFER FUNCTION, TAP NO. 10, CONDITION 7

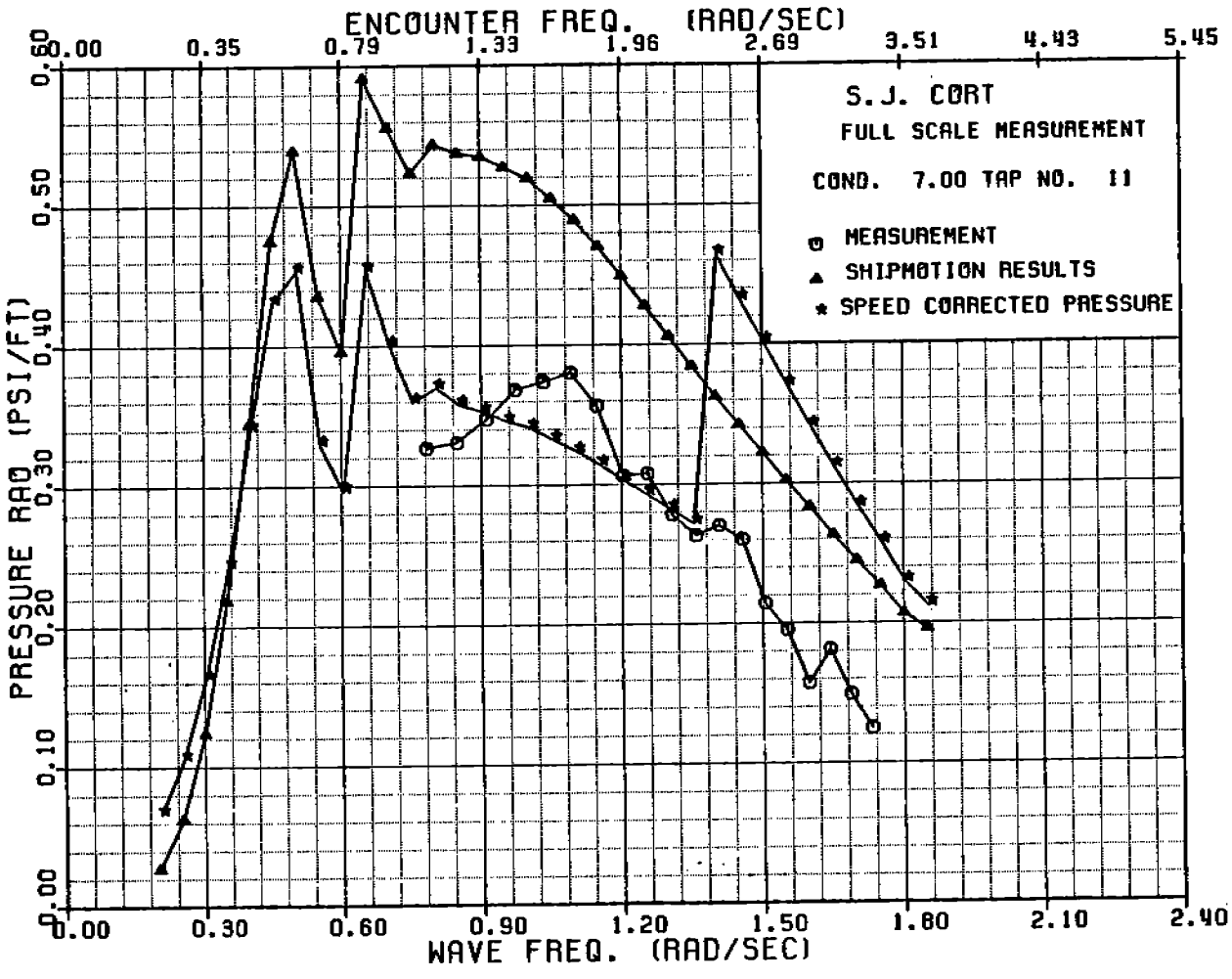

FIGURE C-70: SJ CORT PRESSURE TRANSFER FUNCTION, TAP NO. 11, CONDITION 7

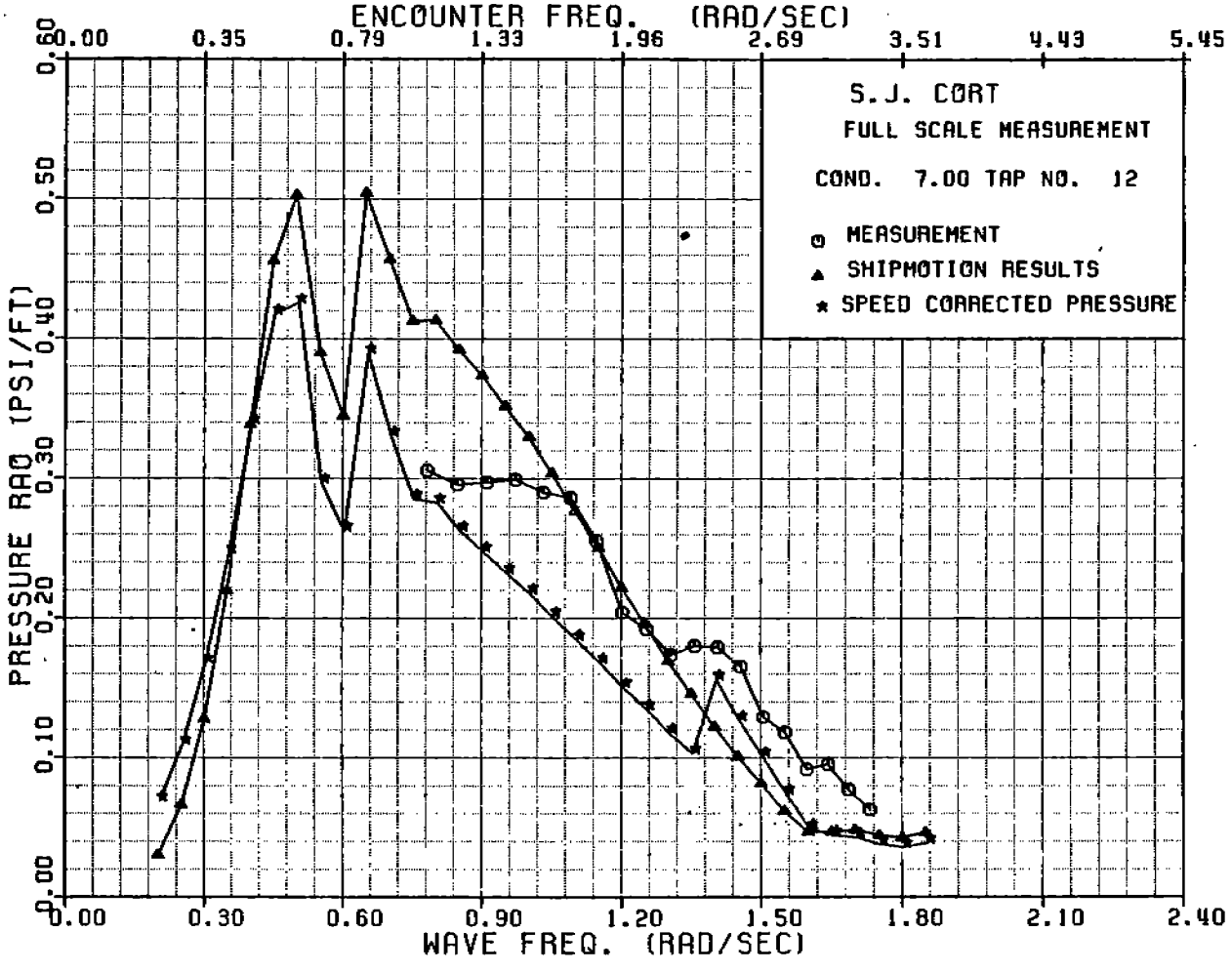

FIGURE C-71: SJ CORT PRESSURE TRANSFER FUNCTION, TAP NO. 12, CONDITION 7

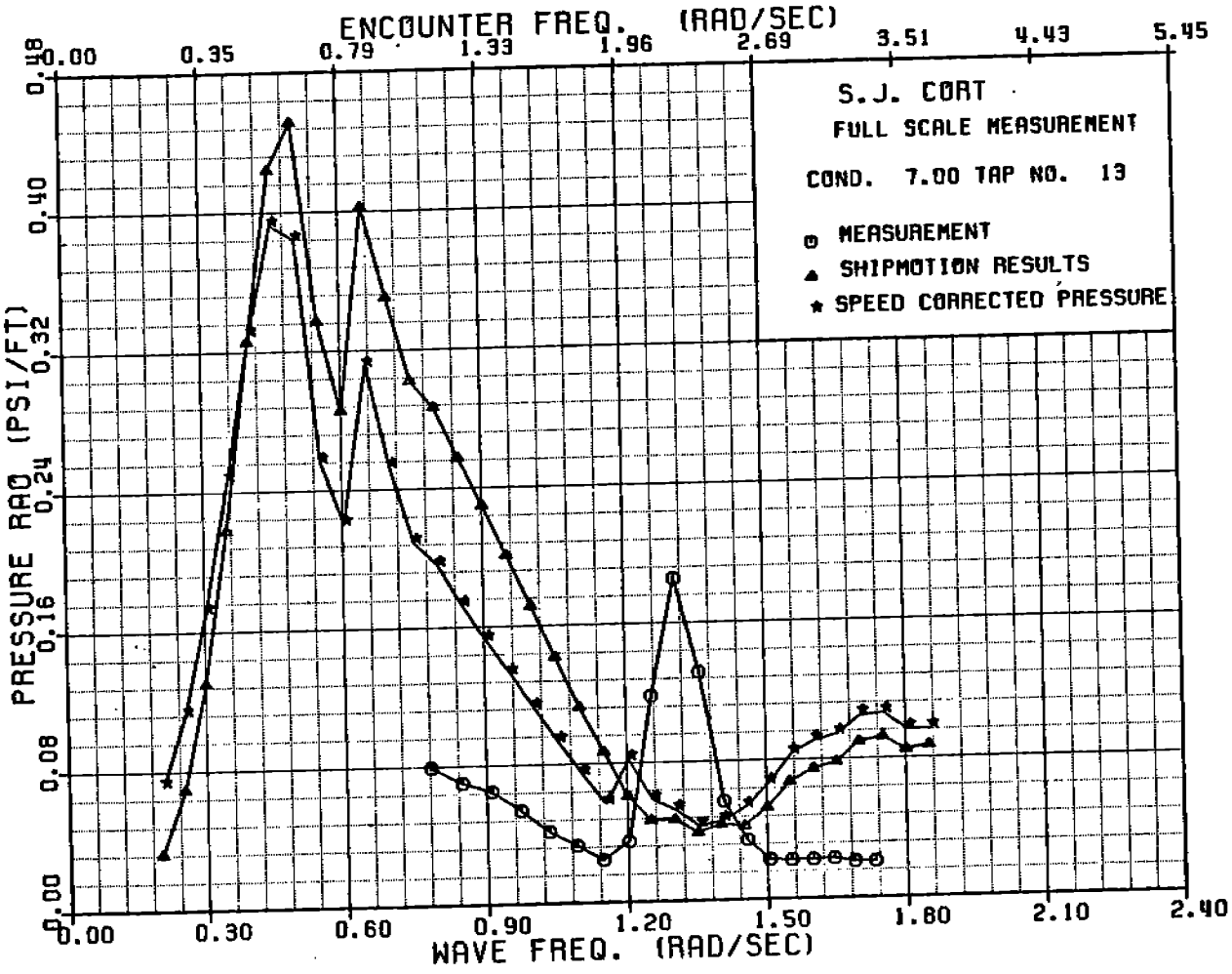

FIGURE C-72: SJ CORT PRESSURE TRANSFER FUNCTION, TAP NO. 13, CONDITION 7

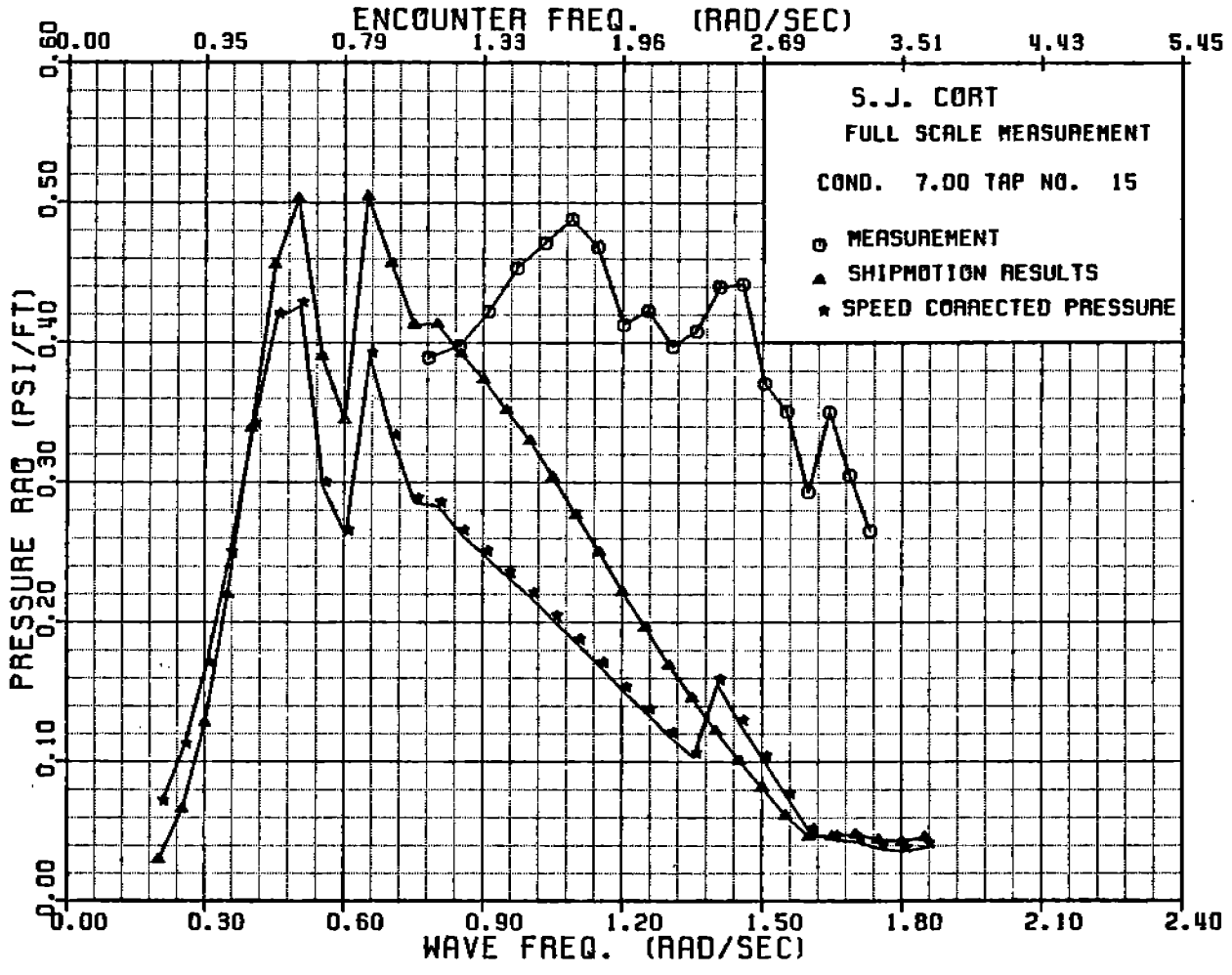

FIGURE C-73: SJ CORT PRESSURE TRANSFER FUNCTION, TAP NO. 15, CONDITION 7